FOREWORD

This report was prepared by the Research and Advanced Development Division, Avco Corporation, Wilmington, Massachusetts under Air Force Contract AF 33(616)-7483. This contract was initiated under Project No. 7381, "Materials Application," Task No. 738101, "Exploratory Design and Protype Development." The work was administered under the direction of the Materials Applications Division, Aeronautical Systems Division, Wright-Patterson Air Force Base, Ohio. L. N. Hjelm was the project engineer in the Air Force Materials Laboratory.

The studies presented began on 11 July 1960 and were concluded on 31 December 1961. Dr. Henryk Hurwicz was the project engineer responsible for the research activity on this project.

Although the studies were administered and conducted mainly by Dr. Henryk Hurwicz and Robert Mascola, other chief contributors and their fields of interest were: J. Brown, T. R. Munson, P. Radkowsky, and R. Grenda, Analytical and Computational Techniques; J. Serpico, J. Newell, and R. Gluck, Thermo-structural Studies; and J. Cordero, Experimental Studies. The authors also wish to acknowledge the assistance of D. Liquornik, H. Spicer, L. Levin, J. Boehringer, R. Spindler, J. Moore and A. Pallone.

This report is the final report and concludes work on contract AF33(616)-7483. The contractor's report number is Avco RAD-TR-62-14.

Work on appendix IV was partly performed under ASD contract. It was published separately as RAD-TR-23, -60, -34 (December 1960). Work on appendix V was sponsored by Air Force contracts AF04(694)-305, -258, -806 and was published as RAD-TR-61-10 (May 1961). Work on appendix VIII was sponsored by Air Force contract AF04(694)-36. Work on appendix IX was sponsored by Air Force contract AF33(616)-7483 and was published separately as RAD-TR-61-35.

ABSTRACT

Pertinent factors affecting the function of thermal protection systems are reviewed with emphasis on glide re-entry applications. Review is made and new information is generated in the areas of : (1) system, material, and design performance criteria needed for evaluation, (2) methods and techniques necessary for experimental and theoretical acquisition of the necessary parameters, (3) correlation of data to present information for the material selection and development effort, and protection system design use, (4) design and development techniques for built-up shield - structure components (vehicle sizing), and (5) basic mechanisms of heat and mass transfer associated with the mode of heat absorption or dissipation and of load carrying and transmission capacity.

Selection of significant parameters for materials and overall thermal protection systems is made. Parametric studies are conducted to provide information for the designer and materials developer for several systems of interest, while correlation methods and techniques are developed. Effort is devoted to the examination of Q* concept for radiation and radiation ablation systems. Experimental techniques and facilities are improved and modified and experiments are conducted to permit meaningful determination of performance criteria needed for materials ranking, and to extend the knowledge of material behavior. A rapid, inexpensive and accurate thermal design method is developed for sizing and parametric studies. Environmental factors and structural effects in the aero-thermo-structural interface are studied. Design and development techniques are established or clarified for initial sizing of the vehicle and methods provided for final design. The dependence of the thermal protection system design on aerodynamic environment for a flight corridor and a range of load carrying substructures is shown, while desirable material characteristics to strive for in material development effort may be deduced from the parametric studies.

Systematic means for material and system selection are provided for radiative system, radiative systems with subsidiary mass transfer (ablation), and for combinations of above systems with forced backface cooling. Forced transpiration system (mass injection) and plastic impregnated matrix are investigated.

This technical documentary report has been reviewed and approved.

W. P. Conrardy

Walter P. Conrardy
Chief, Materials Engineering Branch
Materials Applications Division
AF Materials Laboratory

TABLE OF CONTENTS

TABLE OF CONTENTS (Cont'd)

TABLE OF CONTENTS (Cont'd)

TABLE OF CONTENTS (Concl'd)

Appendices

LIST OF FIGURES

LIST OF FIGURES (Cont'd)

LIST OF FIGURES (Cont'd)

LIST OF FIGURES (Cont'd)

LIST OF FIGURES (Cont'd)

LIST OF FIGURES (Cont'd)

LIST OF FIGURES (Cont'd)

LIST OF FIGURES (Cont'd)

LISTS OF FIGURES (Cont'd)

LIST OF FIGURES (Cont'd)

LIST OF FIGURES (Cont'd)

LIST OF FIGURES (Cont'd)

LIST OF FIGURES (Cont'd)

LIST OF FIGURES (Cont'd)

LIST OF FIGURES (Concl'd)

LIST OF TABLES

LIST OF SYMBOLS

Symbol	
ϵ	**Surface emissivity**
$\bar{\epsilon}$	Modified emissivity factor - dimensionless
η	Transpiration (Blowing Factor)
λ	Constants evaluated for correlation equation (41)
ν_i	Stoichiometric coefficients
ν_j	Stoichiometric coefficients
ν_k	Stoichiometric coefficients
ρ	Density
ρ_s	Density of substructure
σ	Stephan-Boltzmann Radiation Constant
a	Thermal Diffusivity
A_j	Reactant Species
A'	Dimensionless time parameter defined by equation (55)
C_s	Specific heat of load carrying substructure
$C_{j,e}$	Species concentration
H'_g	Time average enthalpy defined by equation (48)
H_c	Effective heat of vaporization of coolant unit
H_e/RT_o	Dimensionless stagnation enthalpy
H_e	Stagnation enthalpy
$(L/D)_{max}$	Maximum lift drag ratio
$L = R$	Thickness of heat shield

LIST OF SYMBOLS (Cont'd)

$[M]_D$	Wall mass loss rate for a diffusion controlled process
$[M]_R$	Wall mass lose rate for a reaction controlled process
Pr	Prandtl Number
Q_c	Total aerodynamic heat input per unit area
Q^*_{eff}	Effective heat capacity of thermal protection system
RT_o	Reference enthalpy = 33.86 Btu/lb
R	Ratio of thermal capacity of heat sink to thermal capacity of substructure
ΔT	Temperature rise
ΔT_{max}	Maximum temperature rise
T_w	Temperature at surface (wall) of heat shield
T_A	Ablation temperature
$T_i = T_o$	Initial temperature
$\Delta T_R = \Delta T_b$	Backface temperature rise
$\Delta T_{R(max)}$	Maximum backface temperature rise
T_{RAD}	Surface radiation equilibrium temperature
T'_s	Equivalent surface temperature defined by equation (54)
$\Delta T'_M$	Mean temperature of heat shield
V	Velocity
W'	Approximate weight per unit area defined by equation (56)
W_A	Weight ablation rate per unit area
W_A	Weight ablated per unit area
W_c	Weight per unit area of required coolant

LIST OF SYMBOLS (Cont'd)

$\dot{W}_c$	Coolant consumption rate per unit area
W_{ins}	Weight per unit area of non ablating heat shield
$W_x = \rho_x$	Space coordinate based on weight
$W_T = \rho L_T$	Total weight per unit area of thermal protection system
W_s	Weight per unit area of heat shield
a	Constants evaluated for correlation, equation (41)
b	Constants evaluated for correlation, equation (41)
c	Constants evaluated for correlation, equation (41)
C_p	Specific heat
C_s	Specific heat of substructure
d	Constants evaluated for correlation, equation (41)
e	Constants evaluated for correlation, equation (41)
g	Graitational constant
h_v	Heat of vaporization of heat shield
h_w	Enthalpy of air at wall conditions
h'_w	Equivalent wall enthalpy defined by equation (51)
k	Thermal conductivity
k_s	Thermal conductivity of load carrying substructure
l	Thickness of substructure
m	Rate of mass loss from heat shield
q_c	Cold wall aerodynamic heat rate
$q_{c(max)}$	Maximum cold wall aerodynamic heat rate

LIST OF SYMBOLS (Concl'd)

q_o	Hot wall aerodynamic heat rate
q_{or}	Hot wall aerodynamic heat rate corrected for radiation losses
q_t^*	Instantaneous heat of ablation
q_c'	Transformed heating rate defined by equation (47)
$\dot{s}$	Linear recession rate of heat shield
s	Total recession of heat shield
t	Time
t_f	Impact time of the re-entry vehicle
t_e	End of critical aerodynamic heating
t_1	Adjusted initial time of heating defined by equation (46)
x	Space coordinate based on distance

I. INTRODUCTION*

Current interest in space exploration has created a need for lightweight vehicles capable of safely transporting manned and unmanned payloads on missions involving orbital and sub-orbital flight. These missions involve exposure to a hyperthermal environment in which severe heating and loading conditions are imposed on the vehicle. As a result, a thermal protection system must be provided to prevent damage to the load carrying structure.

The technical disciplines involved in the design of these systems involve a fusion of the sciences of materials, structures, mechanics, ballistics, aerodynamics, and thermodynamics. It is the purpose of the present study to give careful consideration to the interaction of materials, structures, and environmental parameters affecting the design of thermal protection systems for such vehicles.

One of the principal factors influencing the design is the heating and loading environment encountered during the re-entry phase of the flight. The decision which initially must be made is either to integrate the thermal protection system with a load carrying substructure, or to permit the latter to provide its own thermal protection. This decision depends upon a combination of the re-entry environment and the particular design criteria which are to be satisfied. To satisfy the mission objectives and the design criteria, the thermal protection system depends heavily on the selection of appropriate materials for the heat shield and on the selection of the most efficient mode of heat dissipation. This selection has to be compatible with the structural concept selected for the load carrying function as well, and should afford a certain degree of flexibility in the operational corridor of the overall system.

Since the final design of a thermal protection system depends on the interaction of several material, environmental, and vehicle design factors, importance of an integrated system approach considering all these factors cannot be overemphasized. The selection of materials or the determination of material requirements should be based on an approach that will permit the design of an efficient system. The design cannot be optimized from every point of view since a compromise must usually be reached between the various conflicting requirements. It is thus impossible to speak of a universal** best system or material and it is equally difficult to find a single "best" criterion for rating system performance.

Thermal protection systems associated with ballistic re-entry have received the most attention during the past decade, and information associated with their performance is plentiful. The materials development efforts, design methods, experimental techniques, and theoretical studies reported in the literature of the above period are naturally centered around this application. Such information, however, is widely scattered and not always accessible. In addition, it is often difficult to evaluate the merits and completeness of this information for use in other applications.

*Manscript released by the authors June 1962 for publication as an RTD Technical Documentary Report.

**Universal is meant here as applying to all missions, applications, vehicle types, and thermal protection systems.

The present contract was let to investigate the performance and rating of various thermal protection systems (TPS) for missions not limited to ballistic reentry, and thus to supply tools (methods and techniques) for material development orientation and TPS design. The broad objectives of the studies conducted under this contract were the following:

1. Review and correlation of information on thermal protection systems including a review of the literature and survey of experimental facilities to ascertain the state-of-the-art with respect to:

   a. Systems applicability to a broad range of flight applications;

   b. Evaluation and correlation methods used to determine system performance, especially the so-called Q* approach;

   c. Availability of information applicable to TPS designs for specific flight regimes mutually agreed upon by ASD and the contractor (described below).

2. Generation of new information for evaluation of system performance in a specific flight regime (described below) where such information is not available or cannot be meaningfully extrapolated including:

   a. Development of correlation procedures and design techniques for use as a guide in material selection and development;

   b. Analysis of various concepts and parameters by which thermal protective systems are rated, particular emphasis to be given to validity of Q* concept;

   c. Generation of data necessary to perform above analysis, where these data are not available elsewhere;

   d. Assessment of adequacy of current experimental techniques for ranking materials and built-up configuration;

   e. Evaluation of data gathered and generated with respect to applicability toward design of system tailored to the specific regime described below.

3. Development of thermal protection systems design techniques applicable to the specific application described below. This included determination of the following:

   a. Environmental effects and aero-thermodynamic structural interface;

b. Design methods;

c. Requirements for materials development efforts.

Studies outlined aimed thus to evaluate systematically the presently available thermal protection techniques, to determine necessary thermal and physical property data on materials and composites and to develop, if possible, a simplified method of evaluating thermal protective characteristics of materials and material systems.

To accomplish the above objectives, the program was divided into three phases. A fourth follow-up phase of fabrication and tests of models and representative components was to be planned for but, per se, is outside the scope of this study.

To best satisfy the above objectives, it was decided to limit the scope of the program to the flight regimes, applications, and systems listed below.

1. Thermal flux loads from 15 to 75 Btu/ft^2-sec,

2. Pulse duration from 5 minutes to several hours,

3. Equilibrium surface temperatures from 1800° to 3000°F,

4. Applications:

   a. Re-entry glide vehicle,

   b. Ballistic satellite,

5. Thermal protection systems:

   a. Radiation systems (with and without backface cooling),

   b. Radiation system with subsidiary mass transfer cooling (ablative plastics; ceramic matrix with filler),

   c. Forced transpiration systems.

6. Design studies:

   a. Vehicle components (nose cap, leading edge, and part of fuselage),

   b. Two representative protection systems,

   c. Three trajectories defining the flight corridor.

7. Materials:

Material property and characteristic ranges reasonably expected of attainment within the state-of-the-art up to 1965.

The information on the environment was to be supplied by the Contracting Agency and use of relatively well-known materials was considered for proof testing purposes. No effort on actual development of either new materials was to be expended nor actual vehicle design performed, as the methods and techniques were emphasized.

The limits imposed above were considered flexible and extensions were allowed, provided other phases of the program did not suffer.

The work on determination of performance criteria for a build-up material system was afforded a significant effort. The "Q* concept" validation associated with it was defined as investigation rather than verification. The term "Q* concept" was taken to mean any performance criterion capable of discriminating between materials and/or systems and applicable to their ranking.

The selection of actual applications and systems was motivated by the current interest in them and the lack of information useful for sizing and evaluation.

Since relatively little attention has been given to the flux range of 15 to 75 Btu/sq-ft-sec for the relatively long durations quoted above, this program concentrated on design parameters for this area. A number of thermal design approaches were considered such as (1) use of materials of lower long time temperature capabilities by taking advantage of heat-sink properties, (2) low-temperature ablative cooling of certain structural components, (3) transpiration cooling of the surface or liquid cooling of the substructure, (4) use of an exterior surface as a heat shield and a load carrying substructure which has been insulated and/or cooled, and (5) combination of any four to produce an efficient lightweight structure. These design approaches were suggested and were not considered restrictive.

In the course of the studies conducted under this program, it was found necessary to generate much original information to establish materials requirements for particular applications and to develop methods and techniques for facilitating the design of thermal protective systems. This conclusion was reached after a careful review of design information and techniques published in the literature and a survey of existing test facilities. The appendices to this report include summaries of background information on materials behavior, environment, and thermo-structural considerations acquired from other sources (especially if these were conducted concurrently with this program) in addition to information generated under this contract to fill essential gaps in knowledge. This was done to present a complete and up-to-date picture of the present state-of-the-art concerning the thermal protection systems design for the application defined above.

II. CURRENT KNOWLEDGE

A. GENERAL REVIEW

Various degrees of thermal protection are required by payloads and/or load carrying structures of vehicles re-entering from space. In many cases, it is sufficient to separate the payload from the structure by an intermediate blanket of light-weight insulating material and to permit the structure to operate at elevated temperatures. The design criteria imposed on a system known as hr structures are essentially the allowable operating temperatures based on st tural considerations, and the system as such does not require additional thermal protection. However, for more severe conditions these design limits may be exceeded and an additional protective system or shield is required either to assure the integrity of the structure or to protect the payload. The limits for such systems must now be defined in terms of thermal and structural considerations of the protection system as well as the load carrying structure. This introduces shield material parameters into consideration. At first glance, it appears reasonable to evaluate the shield performance on the basis of its thermal properties and characteristics alone. Mechanical properties may be evaluated but not really considered in material selection as long as they meet "minimum" requirements as a separate member. Such a procedure shifts the emphasis in the system design from strength analysis criteria to one based on thermal analysis. In fact, however, these criteria cannot be separated without suffering serious consequences in the system design. Equally necessary is the consideration of the environment when a thermo-structural analysis of the thermal protection system is conducted. The results of the integrated system analysis will, on the other hand, indicate to the designer the areas and conditions allowing for separate analyses of the system components, and those where the interactions enter.

It is obvious from the outset that because of the wide spectrum of conditions, no single design criterion will suffice. A logical subdivision of the task is required, and a criterion of design "goodness" as general as possible is needed. Once this is achieved, specialized criteria for a given area may be devised which may offer a better resolution for comparison purposes, and may be easier to verify experimentally. Since an experimental verification (if feasible) is the "crowning" of the analysis, the specialized criteria may be important.

1. Environment

Although the methods used for the environment definition are beyond the scope of the program, the environment itself is of paramount importance for thermal protection as it determines the requirements for eventual material selection.

The flight paths of bodies which eventually re-enter the atmosphere and require protective systems vary from high-speed ballistic missiles and re-entering satellites to gliding and lifting vehicles. The re-entry velocities and angles, and the duration of the re-entry cycle may vary from seconds to hours. The requirements for the protection systems are thus quite diversified, and each application may call for a tailor-made system. The stability of the body and its motions (oscillations, roll, angle of attack, etc.) may in turn impose additional restrictions.

The aerodynamic shape selected for the application determines the pressure, shear, and heating distribution which in turn govern the material selection for the protection system and thus must be known to the designer.

The above factors and the resulting magnitude and duration of the aerodynamic heating pulse are some of the more significant parameters for the thermal protection design.

The external and internal loads determine the structural thickness, bonding, and shield strength requirement, thus directly affecting the heat capacity of the system and often the resistance to the heat flow. The allowable structure temperature based on the loading history is one of the limiting design factors for the heat-shield designer. Depending on the class of vehicles and their environment, different design parameters assume significant roles. The determination of their relative importance is one of the first tasks in the evaluation of any thermal protection system.

For various classes of flight vehicles, some of the more important environmental conditions for heat shield and material selection are given in figure 1. It should be emphasized that the boundary of the vehicle regimes in these figures are not rigid, and only represent typical regions of flight conditions. Also the numbers are essentially the maximum expected values. Thus when considering an actual vehicle configuration, such quantities as the heating rate may be reduced considerably on certain portions of the vehicle.

It is not generally possible to classify the aerodynamic heating environment by a set of characteristic vehicle parameters and the initial conditions. Only in the case of ballistic and constant L/D re-entry is such a classification possible. Most other vehicles have some control capability and thus may experience an infinite variety of aerodynamic heating and loading within the somewhat arbitrary bounds of the entire system.

In Table I some of the more significant flight parameters are tabulated showing their relative effects upon the aerodynamic heating and loading parameters. From this table it may be seen that for certain types of heat

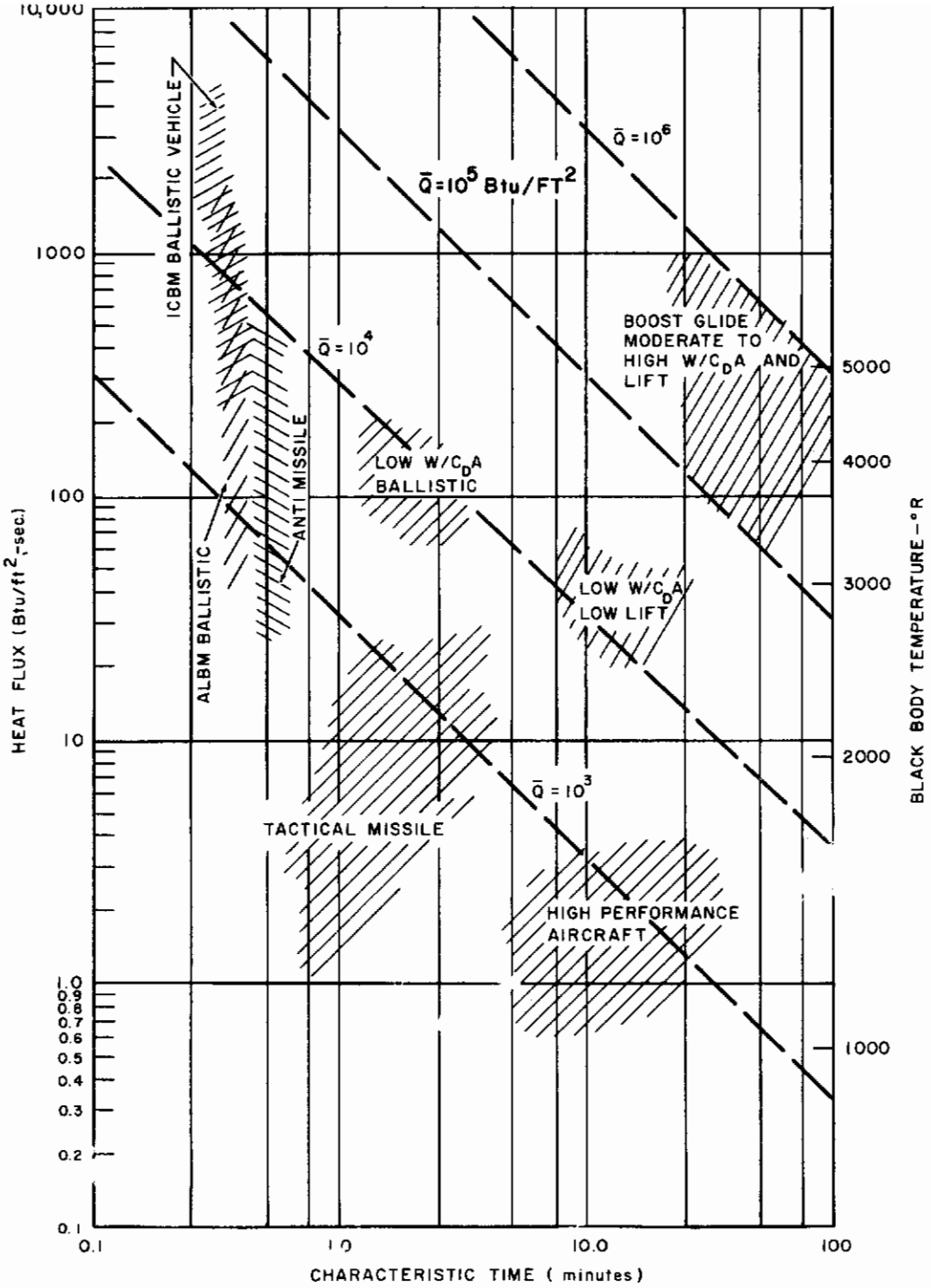

Figure 1 TYPICAL MAXIMUM HEAT INPUT RANGES FOR VARIOUS FLIGHT VEHICLES

TABLE 1

SIGNIFICANT FLIGHT PARAMETER RELATIONSHIPS

Heating Parameters	Trajectory Parameters: V_e (Velocity)	γ_e (Angle)	W/C_DA (Ballistic Coefficient)	W/C_LA (Lift Coefficient)	Thrust
Ballistic Vehicles					
H/RT_o (enthalpy)	+	-	0	-	-
P (Pressure)	+	+	+	-	-
q (heating rate)	+	+	+	-	-
Q (integrated heat input)	+	+	+	-	-
t (time)	0	+	+	-	-
$dq/dt = \dot{q}$	0	+	+	-	-
$\dot{v}$ (acceleration	0	+	0	-	-
Lifting Re-entry					
H/RT_o	+	-	0	0	-
P	+	0	+	+	-
q	+	+	+	+	-
Q	+	0	+	+	-
t	+	0	+	+	-
$\ddot{q}$	0	+	0	0	-
$\dot{v}$	0	+	+	+	-
Boost Glide					
H/RT_o	-	-	0	+	+
P	-	-	0	+	0
q	-	-	0	+	+
Q	-	-	0	+	+
t	-	-	0	+	+
$\ddot{q}$	-	-	0	0	+
$\dot{v}$	-	-	0	0	+
Small Missiles and Aircraft					
H/RT_o	-	-	-	-	+
P	-	-	-	-	+
q	-	-	-	-	+
Q	-	-	-	-	+
t	-	-	-	-	+
$\ddot{q}$	-	-	-	-	+
$\dot{v}$	-	-	-	-	+

CODE

\+ Significant Effect
0 Slight Effect
\- No Significance
Subscript e denotes re-entry

protection, a generalized, systematic parametric study would be quite out of the question at this time. Thus, the more immediate approach will be to define the bounds of the missions within certain classes of vehicles. A limited parametric study within these bounds would follow for materials and thermal protection systems of interest as indicated by the study.

2. Thermal Protection System

Thermal protection system as defined in Appendix I consists of a material system (shield and load carrying member) operating on given heat dissipation principle. The modes of heat dissipation utilized in various protection systems have been divided in the literature (Refs. 1 and 2) into two basic types: absorptive and radiative according to the predominant physical mechanism of absorption or rejection of incident energy. The operating principles, advantages and limitations of such systems (radiation shields, heat sinks, ablation shields, and other internal cooling or transpiration mechanism) as presented in the literature are reviewed in the following sections of the report as well as the inherent problems associated with the design and integration of a material system with the vehicle structural concepts and its environment.

The interaction of thermal and structural components in the thermal protection systems under consideration should be studied in several major areas. These involve both favorable and unfavorable interactions. The former category includes the heat-shield contribution to total load carrying ability and the structural contribution to the thermal capacity. The latter category is largely associated with thermal stress problems.

The maximum structural temperature determination can be made on a weight basis by trading off the increase in structural weight associated with the elevated temperature fall-off in mechanical properties against the decrease in heat-shield requirements associated with increased structural temperatures. Such trade-offs, selection of optimum structural temperatures, are affected to varying degrees by thermal stresses.

The principal thermal stress problems are associated with the steep temperature gradients through the thickness of a heat shield. Such stresses should be studied on a variable mechanical and thermal property, thermoelastic computer program. The aims are to determine stress limitations on heat-shield design and weight effect of structure-shield interaction.

The understanding of the physical process and its proper mathematical formulation for prospective materials leads to the determination of the significant material and system parameters useful in performance evaluation. The differences in aerothermodynamic environment and its transient nature may indicate in gross manner the choices of cooling mode; however,

a study is required to stipulate specific thermodynamic measurement criteria for each system and/or application. The literature discussed below indicated some of the important parameters and methods of system evaluation. Other parameters and their relations were determined in the course of the study to provide a better basis for material development, evaluation, and selection. Improved and simplified correlation methods, as well as design calculation techniques had to be developed to broaden the range of parameters considered.

Particular attention was given to experimental and analytical attempts to establish an overall performance criterion (so-called Q^* concept) applicable for material and system ranking and possibly directly applicable to vehicle design. The experimental techniques and correlation methods employed in the field were surveyed to establish the validity and the extent of the concept applicability.

3. Thermostructural Design Aspects

The heat shield and backup structure portion of a space and/or re-entry vehicle provides the means for balancing loads applied between the payload and the external forces. The prime purpose of the heat shield is to keep the backup structure at a temperature consistent with its load carrying ability. The design requirements must be accomplished with the lowest possible structural weight compatible with the design environments and a high degree of reliability. The structure of most vehicles is made up of an assembly of stiffened or unstiffened shells, plates, longerons, and fittings which are designed for the extreme load and temperature environments that can exist between delivery from the factory and until its intended mission is accomplished.

For design purposes, the complete mission can be divided into design periods; i.e., ground handling, booster flight, ballistic or propelled flight, and landing. In each of these periods, design criteria must be formulated. The pre-flight problems are usually not considered as design requirements (special care is taken to insure that these loads are less than flight loads); however, much of the analysis presented herein is applicable. The booster flight loadings are generally made up of the aerodynamic loads, the interaction loadings between the vehicle and the booster any loads that may be introduced by the guidance commands, and finally the loads induced by the separation of the vehicle from the booster. A large class of design problems during both ballistic and propelled flight arise from environmental conditions that result in problems where incompatibility of materials is involved. For instance, during the booster flight, the vehicle may be heated sufficiently so that materials with different mechanical and physical characteristics could fail due to thermal stresses. Similarly, certain materials with sufficient exposure in a space

environment could decompose or become brittle and could fracture under the thermally induced cyclic loading associated with a space environment. This latter one would probably make the thermal protection system ineffective, evenif the vehicle did not fail before attempting re-entry.

The landing problems have to be considered and these generally fall into two categories: hard and soft landings. Hard landings generally are required for missiles that have a fuzing system to set off a bomb. A soft landing may be required for a manned vehicle or the landing of delicate instruments. A soft landing could be accomplished by a glider-type vehicle or by mechanical means, such as air bags, parachutes, compactible materials, etc.

As can be seen many interrelated parameters must be considered in addition to the weight, cost, scheduling, manufacturing, and other functional requirements. Hence, from the outset, basic criteria will have to be established for the study of a vehicle so that it will meet the requirements of the system.

Generally this means that an initial sizing is made of a vehicle from weight, shape, materials, thermal compatibility, and load-carrying path considerations. After this has been done, the other factors are brought in and successive iterations are made until a satisfactory compromise that fulfills the requirements of the system is achieved. This generally does not end up with the lightest and most reliable vehicle, but provides a trend toward an optimization of the overall systems from cost,scheduling, environment materials, etc. considerations.

It is not the purpose of this study to go into detailed structural design analyses. The intent is to give some information for initial material structural sizing of vehicles and follow-on design studies for refining material structural composites determined by the heat shield and backup structure (if any).

The above discussion indicates in a general sense the type of information looked for in the review of the state-of-the-art. Specific surveys are given in the following sections. Furthermore, in Appendix I q* terminology and some other pertinent definitions used in the report are given to avoid confusion resulting from non-uniform practice noticed in the literature.

B. SYSTEMS AND APPLICATIONS

During the initial phase of this contract a literature search was conducted to obtain information on thermal protection system performance, mechanisms, and design procedures in an effort to determine the state-of-the-art. The existing data would then be categorized and hopefully correlated using either existing methods or those developed during the study program.

As a result a bibliography was compiled (see Appendix II) and kept up to date as new data appeared in the literature. It is clear that as of the early stage of this program, the design of re-entry vehicles using heat sinks and ablation shields had been extensively covered in literature, while very little had been done with radiative and forced or natural convection systems. Available literature on transpiration systems was limited to the effects on heating of injecting a coolant into the boundary layer and very little had been done concerning the engineering aspects of the overall transpiration system which includes porous materials and coolant storage along with associated weights. As a result of the lack of data in the above stated areas, detailed studies of the more promising systems for low heat flux and long durations were later carried out.

A more detailed review of the state-of-the-art of the various thermal protection systems is given below.

1. Heat Sinks

Heat sinks are useful for an application where the heat pulse is of a relatively short duration and overall system reliability is essential. It is possible to design a vehicle utilizing the heat-sink principle under relatively straightforward procedures using ordinary one- and two-dimensional heat transfer analysis.

A number of factors affect the design of a heat sink type of system. Among the most important are the following: allowable weight, magnitude of the total heat input, magnitude of the heat rate, and materials properties such as thermal conductivity, specific heat, density, and melting point. It was found that single materials subject to a given heat pulse may be correlated readily by a generalized relationship (Ref. 2),

$$\frac{Q_c}{\Delta T}\sqrt{\frac{1}{k\rho C_p}} = F\left(L\sqrt{\frac{1}{\alpha}}\right) , \qquad (1)$$

where

Q_c = total heat input per unit surface area,

ΔT = surface temperature rise,

k = thermal conductivity,

ρ = density,

c_p = specific heat,

L = slab (heat shield) thickness,

α = thermal diffusivity.

The above functional relationship shown in figure 2 is typical of a low-performance ($W/C_DA = 100$) re-entry vehicle and shows a correlation of actual heat-sink materials. A more general correlation which includes substructure effects is presented in figure 3 in terms of non-dimensional weight and heat input. Plots similar to this for re-entry vehicles having higher performance could be made; however, the number of materials suitable for heat sink usage diminishes rapidly as either the total heat input or heat flux increases. Thus non-melting heat sinks are inherently limited in their application. Almost entirely, the incident aerodynamic heating is passed onto the heat sink surface. As the sink surface increases in temperature the driving force of convective heating decreases; but for practical materials, the possible "hot wall" reduction rarely will exceed 10 to 20 percent for a typical ballistic missile re-entry trajectory. The heat reduction due to radiation from the heat sink surface is also very small.

To obtain a minimum weight design, it is necessary to optimize based on melting temperature, specific heat, density, and degree of safety. A simplified heat sink design procedure may be derived from reference 3 to supply the designing engineers with preliminary temperature data. This has been done by substituting a simple sinusoidal function (that is, a half sine wave) for the actual re-entry heating cycle and determining the transient temperatures in the heat shield. The data are then presented in either tabular or graphical form in terms of standard dimensionless heat-conduction parameters, so that a wide range of the physical variables are included.

A preliminary design of the vehicle may be easily obtained with a very small effort using graphs and tables of reference 3. It is not intended that this study be used for final design, but rather to reduce the amount of work

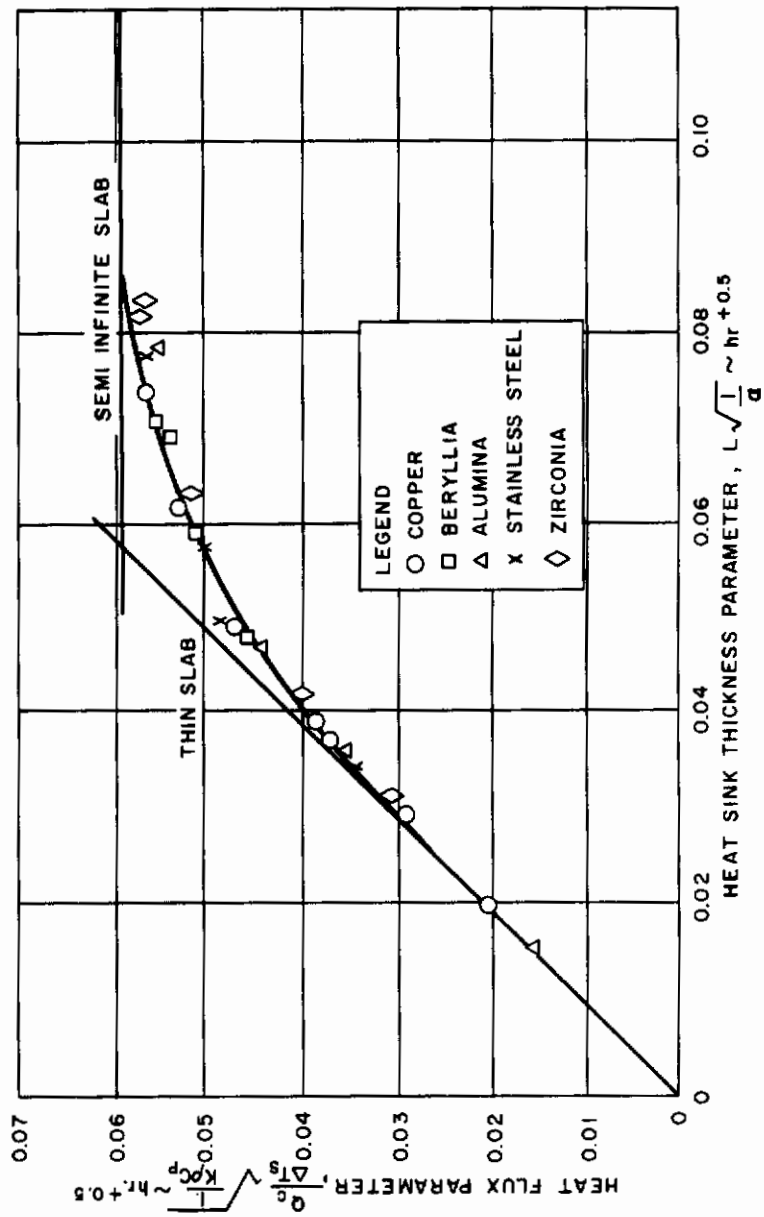

Figure 2 GENERALIZED HEAT INPUT AND SHELL THICKNESS RELATIONSHIP

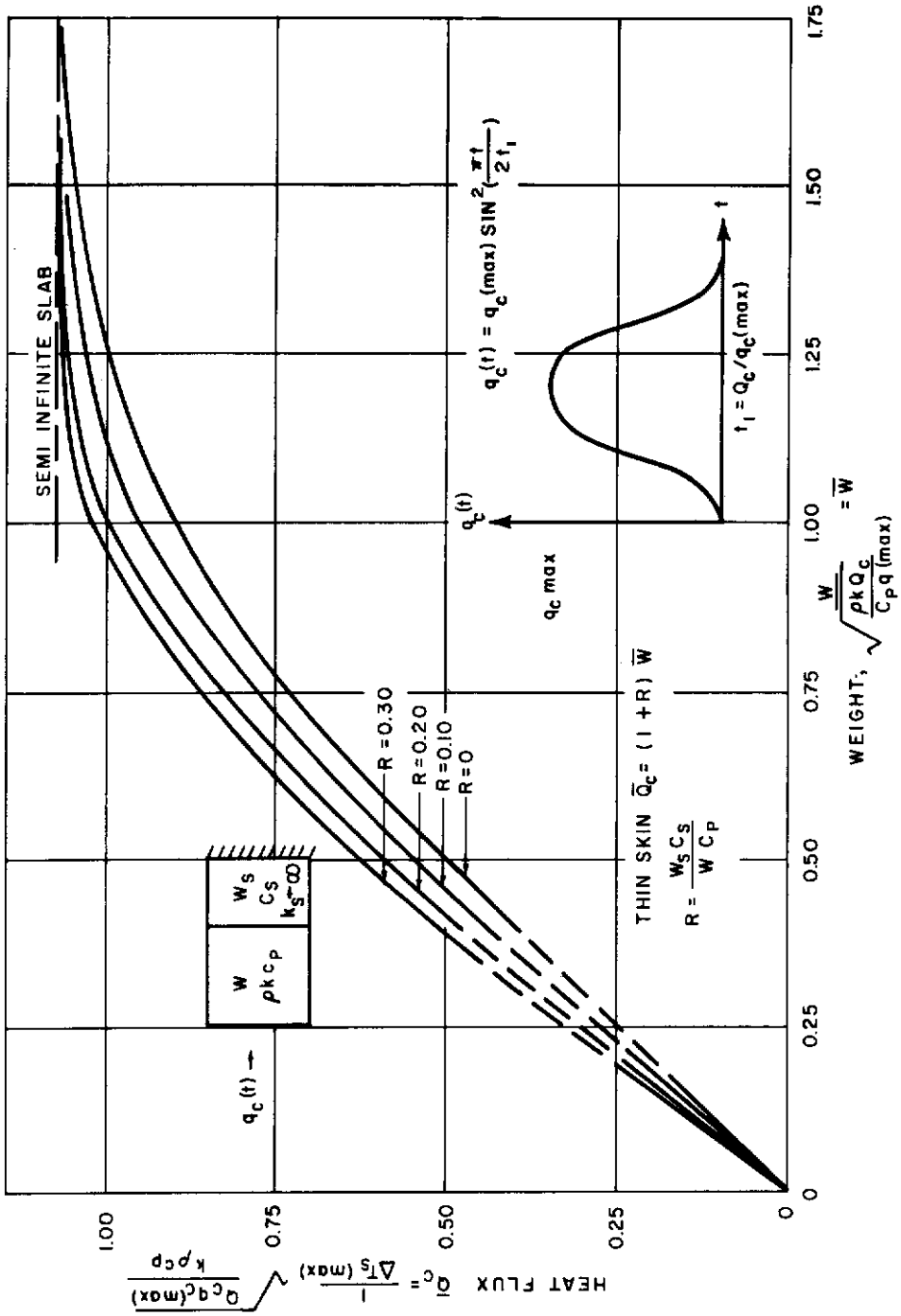

Figure 3 EFFECT OF SUBSTRUCTURE (W_s), HEAT FLUX (Q_c) AND PROPERTIES ($k, \rho, C_p, \Delta T_s$ (MAX)) ON HEAT SINK WEIGHT ($\bar{W}$)

involved in finalizing by supplying reasonable estimates. An actual final design must account for temperature-dependent thermal properties and "hot" wall reduction of heat flux, and is best done using digital or analog computers. The accuracy of design calculations is always of primary concern, and appropriate studies should be conducted to determine the reliability of calculation procedures and material property effects (Ref 4).

From the data available in the literature (Refs. 3 to 5), it was rather apparent that the heat sink systems do not look promising for the extended duration of heat flux and that effort would be concentrated on other systems. The heat sink principles, however, are of importance in all other systems when a residual heat-sink effect is present.

2. Radiative Systems

The design of a thermal protection system which employs heat transfer by radiation for the principal means of dissipating aerodynamic heat involves a variety of approaches. These approaches are in essence alternatives for controlling the high surface temperatures inherent in a radiative system and for protecting any payload within the structure. It will be desirable to discuss the various types of radiative systems in more detail since they offer promise for application in the areas of glide vehicle or long duration re-entry. A comprehensive discussion of radiative systems is given in reference 1 which discusses material requirements as well. One of the first questions to be answered concerning a radiative system is whether or not the load carrying structure will be allowed to be at or near the radiation equilibrium temperature. Should the answer be affirmative, the hot structure may be used. Schematically, this type of system may appear as in figure 4a. Such structures have been considered for the application of interest,and information is available in the literature (Refs. 6 and 7). Although there is no protection weight since the load carrying structure acts as the emitter, the system weight must also include the weight if any, of insulation required to protect the payload. For a given convective input, the surface temperature is determined by a balance between this flux and the radiative losses. Control of the temperature for this relatively simple arrangement is not easily accomplished and is seriously limited. Surface emissivity may be increased by oxidizing the outer surface or by properly coating the material to reduce the surface temperature. Emissivity values ranging from 0.85 to 0.95 may be obtained by allowing the surface to oxidize. The only other way to reduce surface temperature is to polish the inner surface thus making it as highly reflective as possible.

The single advantage of this type of system is its lack of dependence upon mechanical systems. Thus reliability of the entire vehicle is increased.

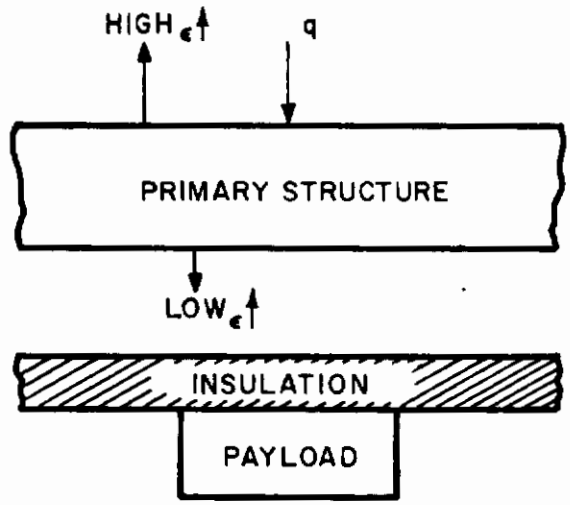

(a) HOT STRUCTURE

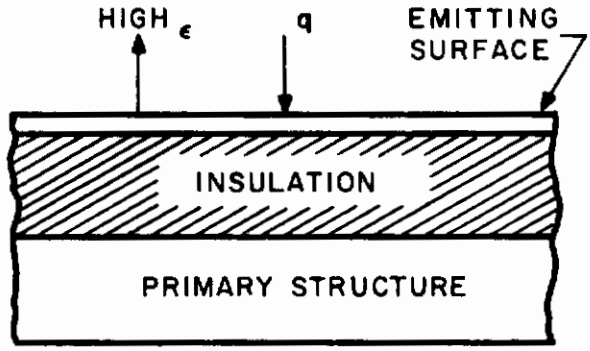

(b) RADIATION SHIELD WITH INSULATED LOAD CARRYING STRUCTURE

Figure 4 RADIATION SHIELDING AND COOLING SYSTEMS

Definite limits exist in the heating conditions which an unprotected hot structure can tolerate. For example, the maximum long time heating rate is 20 Btu/ft^2-sec and the maximum short time total heating is about 2500 Btu/ft^2 for conventional structural materials. (Actual value is dependent on heat flux time history and permissible structural weights.) Various studies have shown that unprotected hot structures are most efficient when the total heating is low enough that aluminum, magnesium, or in some cases titanium can be employed without reaching excessive temperatures or when the total heating is very large, but the maximum heating rate is less than 20 Btu/ft^2-sec. The use of higher temperature tolerance and strength materials will increase the above limits.

The chief disadvantage of hot structures in addition to the heat flux limitations discussed above, lies in the large thermal stresses that are invariably associated with high skin temperatures and cool internal members. Another disadvantage is the existence of hot structural members in contact with temperature sensitive elements or in cockpit or electronic compartment areas. The surface characteristics of the high-temperature structural materials become critical in their selection for the application.

Because of the disadvantage of hot structures, protective-heat shields of radiative type or utilizing mass transfer principles are being considered for glide vehicle application. For such cases the operating structural temperatures may still be elevated. The temperature allowables are then defined on bonding considerations, overall efficiency of the shield-structure system as well as based on the structure integrity.

This alternate approach includes a variety of specific designs all of which may be termed radiation shields. Figure 4b illustrates one type of radiation shield. The surface may be in the form of a thin metallic sheet or a coating on the insulation, the purpose being to attain the desired high surface emissivity. In this particular situation the insulation must perform two functions. It must not only provide sufficient resistance to the flow of heat back to the structure, it must also be capable of withstanding the aerodynamic forces. The primary structure is maintained at some controlled or selected temperature. Any heat penetrating the insulation is absorbed by means of the heat capacity of the structure. If an excessive amount of heat penetrates the insulation, a coolant may be employed to dissipate the excess.

The most evident advantage of a radiation shield over a hot structure is that for the former, the load-carrying function is separated from the thermal function. The thermal protection provided by the insulation for the primary structure may also be adequate protection for the payload.

Restrictions on the applications of radiation shields lie mainly in the limits imposed upon insulation materials or temperature tolerance of a surface skin (or coating). The insulation chosen should be the lightest one that will meet the temperature and strength requirements imposed upon it. Space limitations must also be considered, however. Although a material may satisfy weight, temperature, and strength specifications, it may not fulfill the volume requirement.

The third general approach to the design of radiative systems is that of conducting or radiating the aerodynamic heat from regions of intense heating to regions of low heating. For situations in which severe localized heating exists this type of system appears advantageous, since temperature gradients in the primary structure are minimized or eliminated. This type of design necessitates the use of a highly conductive surface material. This high conductivity may introduce some difficulty because it will tend to increase the temperature of the insulation unless it is directional. Any one of the systems discussed above could be employed for the situation of local heating.

Even though (and perhaps because) the non-ablating systems described above are relatively simple in their thermal mechanism, there was little information available in the open literature which related the performance of radiation system to thermal, environment, material properties, and design criteria. This was to be expected since at the initiation of this study program most thermal protection studies were made for ballistic missiles utilizing ablation. However, with the subsequent interest in manned and glide re-entry, investigation of radiation systems was necessary and a major effort was deployed under this contract to generate performance data for the low flux - long duration thermal environment. This was deemed necessary because of the transient environment precluding the use of steady state or equilibrium criteria.

3. Ablative Systems

Ablative thermal protection systems have been a subject of most numerous studies and reviews because of the interest in this mode of protection during the last decade, and because of the complexity of the process. This system discussed here will be mostly from the point of view of methodology application to glide vehicle re-entry.

a. Ablation With Surface Mass Transfer Only

In this type of ablation process $m = \dot{s}\rho_o$ and no reactions in depth (beyond the recession line) occur; however, chemical reactions in the boundary layer should be taken into account. In nature, such process rarely occurs, but sublimation, instantaneously swept liquid

from the solid surface, or vaporization at liquid-gas interface (all with or without combustion in the boundary layer) may be treated fairly rigorously under such idealizations provided input functions (surface temperature-pressure relations, transpiration, and/or combustion) are properly treated. Some of the other processes may be treated in this fashion provided equivalent characteristics are obtained from exact analyses or carefully controlled experiments, and if energy equation includes sink (source) terms. Caution should be exercised in a priori assumptions concerning equivalency, as even then computed recession rates and temperature distributions may not be accurate while mass loss is fairly well approximated. In addition, the agreement with experiments may be expected for only a limited range of conditions. This is especially true for conditions where a large (relative to the removed) depth below the surface is activated.

Ablation with simple (or no) combustion effects,a case of essentially simple evaporation or sublimation, was thoroughly reviewed with appropriate references (Refs. 8, 9) which will not be repeated here; it also has been treated since, as a special case of sublimer in references 10, 11, and 12. Teflon is thought by some to behave in this fashion with some increase in heating due to combustion in the boundary layer. An extremely high viscosity glass or graphite under favorable conditions may sublime. Low viscosity melting glass under high shear may be swept rapidly and thus its ablation might be treated in this manner. The mathematical model used, e. g. references 13 and 14, in this case follows as the simple one-dimensional heat equation:

$$\rho C_P \frac{\partial T}{\partial t} = \frac{\partial}{\partial x}\left(k \frac{\partial T}{\partial x}\right) \quad s(t) < x < L \quad , \tag{2}$$

with boundary conditions:

$$-k \left.\frac{\partial T}{\partial x}\right|_{x=s} = q_o(t) - \sigma \epsilon T^4 - \rho \dot{s} [h_v + \eta(H_e - h_w)] = q_{or} - m[h_v + \eta(H_g - h_w)] \tag{3}$$

$$\left.\begin{aligned} \dot{s}(t) &= 0 \text{ for } T(s,t) < T_m \\ \dot{s}(t) &\geq 0 \text{ for } T(s,t) = T_m \end{aligned}\right\} \tag{4}$$

$$\left.\frac{\partial T}{\partial x}\right|_{x=L} = 0 \quad , \tag{5}$$

and initial condition:

$$T = T_o \Big|_{t=o} \tag{6}$$

The instantaneous effective heat of ablation is

$$q_t^* = \frac{q_{or}}{m} = C_p (T_w - T_o) + h_v + \eta (H_e - h_w) \quad , \tag{7}$$

where h_v may be thought of as combined heat of melting, vaporization, and also including combustion or internal reaction effects (if not accounted for otherwise), and η is the transpiration coefficient. The mechanics of use of this formulation depend on the degree of sophistication of the solution and input philosophy. The "cold wall" aerodynamic heat flux (q_c) is successively reduced to its "hot wall" (q_o) value, transpiration blocking reduces it to q_i, and radiation emission to q_{ir} which then is the input to the gas-solid (or liquid) interface unless combustion takes place which then has to be added in the heat balance. If effective heat of ablation concept is used, the heat of combustion may be subtracted in the h_v term to modify the combined heat of ablation. A relationship of $\dot{s} = f(T_w)$ is necessary and assumes in the simplest form a constant T_w.

The present treatments of the problem (Refs. 10, 11, 13 to 21) advance the state-of-the-art by providing solutions and/or computational programs* for a transient ablation analysis with arbitrary heat inputs. Radiative inputs are included and coupled with the internal (conduction and radiative) energy transport in reference 53 while previously only quasi-steady-state solutions were available. The latter are useful for understanding the basic process but their a priori use is questionable for actual engineering application to an overall heat protection system.

Parametric studies based on the approximate as well as rigorous methods were conducted in references 9, 15 to 24, and are applicable to the surface mass transfer phenomena. They shed a useful light on the aero-thermodynamics of re-entry ablation for various environmental conditions and applications. The trends discerned during parametric studies are useful in orienting the materials development effort as they indicate the "desirability" of materials parameters for given environment. An example of application of the method to selection of materials for re-entry environments is given in references 8, 9, 16, 23 and 24, and illustrates the changing requirement for material with the application. Most of these references indicate the mathematical simulation procedure.

*In some references it is not clear whether or not the authors have programmed their solutions; often it is difficult to determine the method by which the results were computed.

Attempts to correlate ablation materials performance using analysis similar to that given above by equations (2) to (7) according to the thermal properties and environment have been made by several authors (Refs. 19 to 24), in addition to the efforts by Avco RAD described elsewhere. Although some very definite and useful trends have been indicated for particular thermal environments and thermal properties, no well-defined (or generally accepted) figure of merit has been established which would enable a designer to select a particular material for a given thermal environment and design criterion. A major difficulty is that the number of variables involved is very large making a complete correlation a difficult task. A generalized correlation would have to relate the weight required for successful re-entry with:

1) The aero-thermodynamic environment; i. e., heating rate versus time and altitude, total heat input and altitude versus time and other trajectory parameters,

2) Thermal properties and characteristics of the materials; i. e., conductivity, density, specific heat, emissivity, ablation temperature, and heat of ablation (as a function of the aero-thermodynamic environment), and

3) Design criteria; e. g. limiting backface temperature.

The general analytical solution for an ablation shield including the above variables is not available. Some specific solutions do exist for heat conduction and ablation in solid shields, assuming the effective aerodynamic heating varies inversely with time or that the ablation rate varies inversely proportional to the remaining material (Refs. 25 and 26).

Such assumptions render these solutions of little practical engineering value in design although they do have value in checking numerical solutions. Approximate solutions of a semi-analytical nature have been developed for ablation and heat conduction for arbitrary heating rate profiles, and are very useful for quick engineering estimates of temperatures and ablation rates. However, no closed form approximate analytic solutions exist which are comparable to present numerical solutions in generality and accuracy. Even with the use of high-speed computers and numerical techniques, excessive data generation would be required to correlate useful design data which would include all the necessary variables and their interactions. It is not surprising then that data presented in the literature are very limited. Furthermore, attempts to correlate all the existing data are complicated by lack of precise definition and of complete statement of assumptions and methods used in obtaining data.

As an indication of the type of data available in the literature, several limited correlation attempts are reviewed here. First, consider an ablation thermal protection system consisting of only the ablation material itself. The material is initially at some specified temperature and is heated on one face by some prescribed heating rate. At some temperature, the material begins to ablate and loses mass depending on its thermal properties and characteristics. When the heating becomes sufficiently small, ablation stops and heat is conducted through the slab. It is necessary to find the weight required to limit the back face to some prescribed level. An example of the resulting correlation is shown in figures 5 and 6 which indicate the dependency of weight on ablation temperature, heat of ablation, conductivity-density product for fixed values of total heat input, maximum heating rate, initial temperature, and maximum backface temperatures. It should be noted that although useful trends are indicated, the correlation between weight required and material properties for fixed heating and design conditions is limited since, it would require a large amount of calculation to vary all parameters over a broad range and present a general correlation. Another limited correlation attempt is shown in figure 7, where materials are evaluated rather than material properties. Here, a wide range of aerodynamic environments (ICBM, IRBM, satellites, etc.), is considered for a few materials, and the results are given in terms of weight required to keep 0.0725-inch of aluminum to a limit of 600°F. Notice that this analysis includes a structural member while the example cited above does not. The assumed geometry further complicates comparing and correlating available data. It would appear that were all of these available limited parametric studies compiled, the data could be reduced to a common denominator. The difficulty in an attempt of such a correlation is that data have been obtained by widely different methods. Assumptions range from a steady-state ablation temperature profile, linear temperature profile, to constant heat inputs which are referenced to various surface temperatures. In many cases, it is not clear how the data have been obtained or what assumptions are made.

Several attempts have been made to correlate ablation materials according to thermal properties and environment. To simplify the analysis and generalize the correlation, a basic assumption is sometimes made that the time-varying heat flux may be replaced by an average constant square-wave input of characteristic duration. This assumption has been checked by some of the authors (Ref. 20), and accuracies for estimating required weights have been made by comparing results using both constant and variable heat-flux profiles with the same total heat input. Errors due to this assumption have been shown to be relatively small for application where high percentage of the total heat load

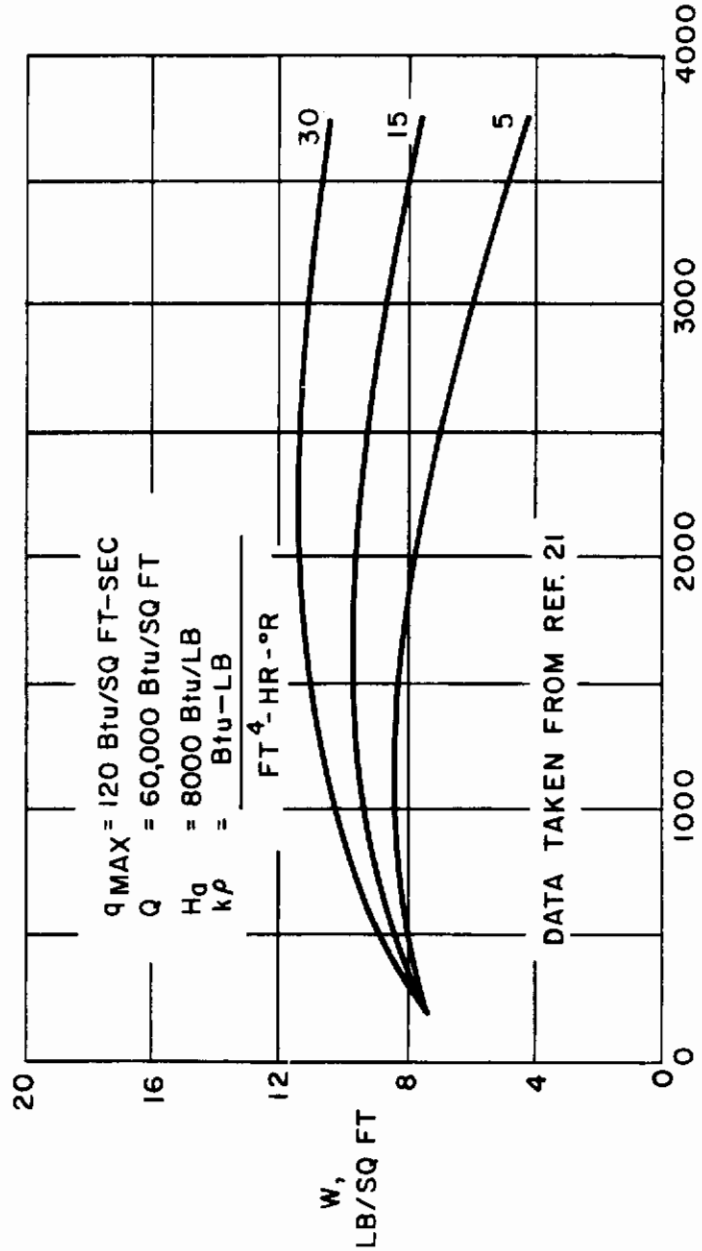

Figure 5 EFFECT OF DENSITY-CONDUCTIVITY PRODUCT ON THERMAL PROTECTION SYSTEM WEIGHT

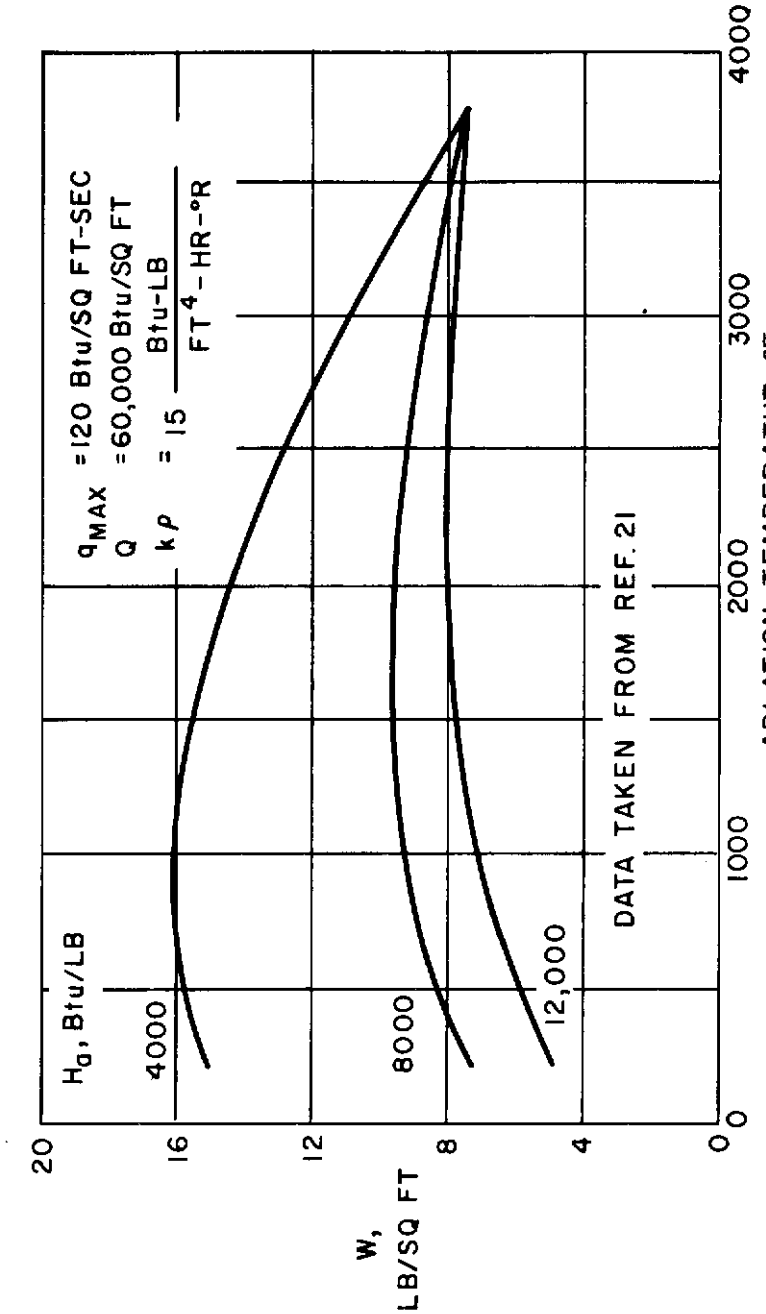

Figure 6 EFFECT OF HEAT OF ABLATION ON THERMAL PROTECTION SYSTEM WEIGHT

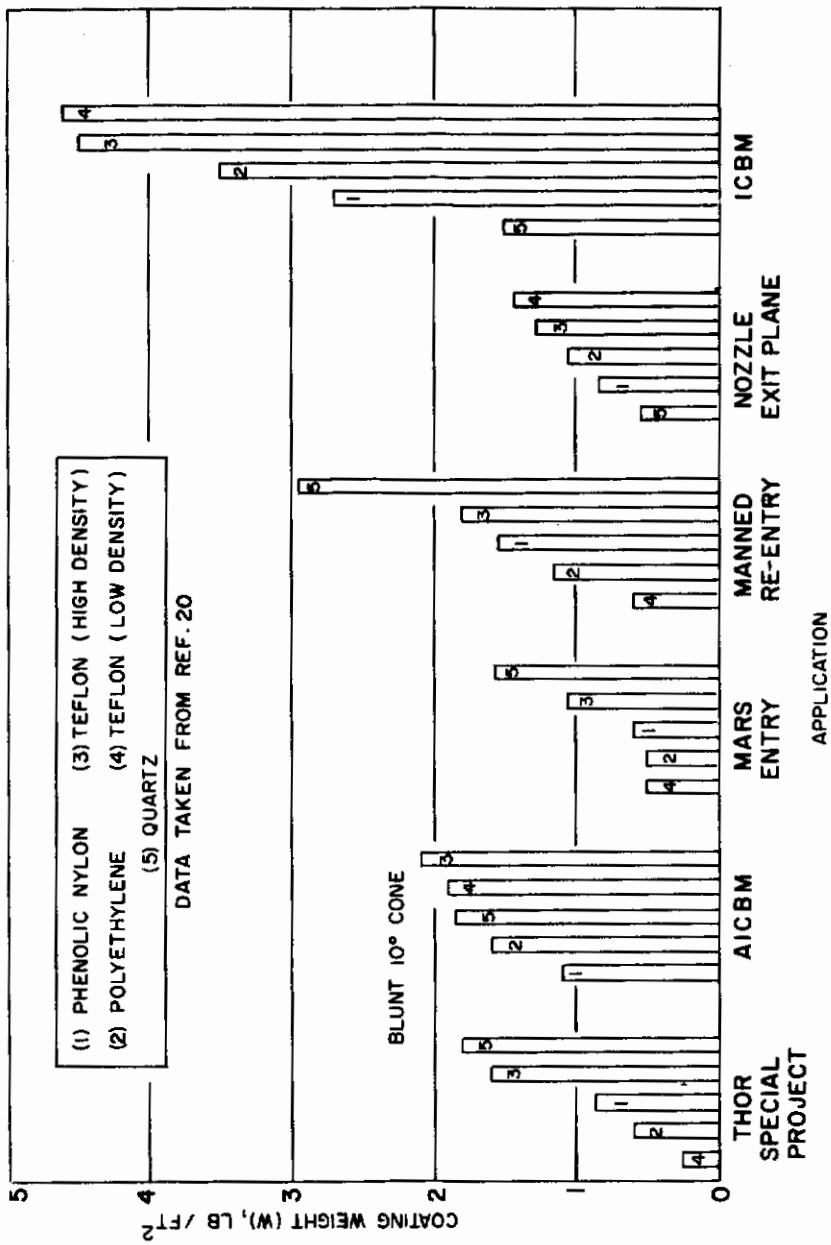

Figure 7 COMPARISON OF PROTECTIVE COATING MATERIALS

is absorbed by ablation. Still, the error may become unacceptable when a significant transfer of energy by conduction is present. However, no general rule for accuracy is available, and errors should be determined for particular applications.

The apparent advantage of using a constant heat-flux profile is that the environmental parameters are extremely simplified and it becomes possible to construct a set of material selection charts for a wide range of material properties, aero-thermodynamic environments, and design limitations (backface temperature). However, it becomes extremely important to define exactly what is meant by aero-thermodynamic environment. There are basically two approaches for correlating material performance with aero-thermodynamics. First, this type of correlation might be based on a "cold wall" heat flux, $q_c(t)$. This is the heat flux to a wall at some reference temperature such as 300°K. For a given aero-thermodynamic environment, q_c is independent of material properties (and mass injection), making it a worthwhile reference parameter. Alternatively, the correlation might be based on an effective heat flux, i.e., the heat flux q_{or} to the "hot wall" at the actual temperature level during flight. This effective flux,

$$q_{or} = q_c \left[1 - \frac{H_w}{H_s}\right] - \sigma \epsilon T_w^4 \quad , \tag{8}$$

is the heat flux to a "hot wall" including radiation loss from the surface, and depends on material properties, making direct comparisons of heat flux and material performance slightly more difficult. Still another reference heat flux used is that to a wall at the ablation temperature and further corrected for shielding (mass injection), i.e.,

$$q_{ref} = q_{or} - \eta \rho \dot{s} \ (H_s - H_w). \tag{9}$$

Unless it is assumed that steady-state ablation occurs, it is difficult to evaluate a priori, the heat reduction due to shielding, i.e., the mass flow rate, $\rho \dot{s}$ is not known. It is easier to consider $\eta(H_s - H_w)$ as part of the heat of ablation, and then, determine temperature and mass loss rate.

The review of methods and criteria used in interpretation and correlation of thermal protection systems performance and comparison of the evaluation techniques clearly indicated that no "best" technique was available. Furthermore, an insufficient number of flight applications of the low flux - long duration have been investigated in the literature to assess validity of the presently used criteria. It is indicated

thus that a very serious effort will have to be applied in later studies of Phases Two and Three to such data for regimes of interest. In this respect a technical report on the thermal protection of satellites with "cold wall" ablation was compiled under this contract from data generated at Avco RAD under other Air Force contracts and is included in Appendix IV.

b. Ablation With Decomposition in Depth

In the cases of ablation discussed previously, the assumption of $m = \dot{s}\rho_o$ was made and justified for practical purposes for some materials classes. Approximate methods were developed and used on the same principle for materials which actually decompose in depth, and in many cases (e. g. teflon) the ablation (mass loss) behavior was accurately determined while recession rates and temperature profiles were distorted. No experimental data were available in the literature up to date to confirm or discredit the latter statement. Some recent experimental data will be shown in Appendix VI to confirm it. In any case, for the surface recession (including liquid layer) theories, only the temperature, viscosity, and radiant flux gradients have been considered assuming that the sub-surface regions display an invariant density, and furthermore that temperature gradient is not affected by the internal reactions. The effects of these reactions were assigned to heat of ablation - a boundary type of value. In fact, very few actual materials except silica would approach such idealized surface process. Pure and reinforced plastics, whether the reinforcement is of organic or inorganic nature will display some decomposition in depth and a density gradient in depth may be expected.

The nature of these materials is such that the assumption of $m = \dot{s}\rho_o$ may not be made except for quasi-steady-state and other means of analysis accounting for the density and temperature gradient are needed. In addition, for the case of fragile char layers formed or when mechanical erosion occurs, mechanism of removal other than physico-chemical phenomena has to be established. Otherwise evaporative liquid layer formation (if any) or chemically reactive boundaries have to be considered together with the internal decomposition reactions. A complete treatment would include radiative (internal and external) transport in a transient manner for arbitrary heat flux function, and should pertain to materials which ablate:

1) Without char formation (e. g. teflon),

2) With formation of char which is immediately removed without build-up (e. g. some epoxy versamides),

3) With formation of fragile char which is removed after a build-up of finite thickness (e. g. nylon-phenolics),

4) With formation of stable char building up a finite thickness but not removed mechanically during period of interest (e. g. refrasil-phenolics),

5) Ceramics impregnated with plastics where only plastic component ablates, and

6) Other composites where only one component ablates.

This array of ablation processes presents a formidable task to analyze and simplifications have to be made to obtain a calculable solution.

A comprehensive review of the ablation literature up to 1962 is given in reference 27; however, most of the references discussed there were not available while major efforts were expended during this program, and thus could not be utilized. Appendix V treats the general problem in detail, and specific attempts on solution of problems associated with category (6) above are given in Appendix VI.

The "in depths" ablation problems were considered of particular interest for glide re-entry, as the use of plastics capable of ablation for a basically radiative protection system was considered promising.

c. Ablation With Gas Boundary Chemical Reactions and Gas-Surface Interactions

Some consideration of secondary reactions in the boundary layer is often given by a simplification resulting in increase in the heat flux to the surface. In this section, chemical reactions controlling the ablation mechanism at the surface will be discussed. Three investigations merit particular interest, (references 28 to 30). The latter two references pertain to flight applications, while reference 28 is of particular interest for propulsion devices such as rocket nozzles and combustion chambers.

Consider the laminar flow of a reacting gas mixture over a two-dimensional or axisymmetric solid surface which sustains a heterogeneous reaction with one or several of the free-stream constituents. * Assuming that the Prandtl and Lewis numbers are unity and all of the species have equal gas phase diffusion coefficients, Lees (Ref. 31) has demonstrated that the presence of chemical reactions in the boundary layer is reflected only in the species concentrations at the wall

* discussion which will follow is equally valid for turbulent boundary layers if Reynolds Analogy is invoked.

and the variation of the transport properties across this layer. Under these conditions the stagnation enthalpy and species concentrations are linearly related everywhere in the boundary layer if they are constant at the wall and at the outer edge, independent of pressure gradient.

Investigating a class of heterogenous reactions between n gas-phase reactant species A_j and a given wall material A_i which produce m gaseous products A_k, it is proposed that:

$$\nu_i A_i(s) + \sum_{j=1}^{n} \nu_j A_j(g) \rightarrow \sum_{k=1}^{m} \nu_k A_k (g) \quad , \tag{10}$$

where ν_i, ν_j, and ν_k are the appropriate stoichoimetric coefficients. Postulating, in addition to the previous assumptions (i.e., $Pr = 1$, etc.), that Ficks law adequately describes the diffusion velocities and there are no chemical reactions within the boundary layer, one arrives at the following simple relation for the total ablation rate:

$$m = \frac{\rho_e u_e C_h \left(\sum_j \phi_j (C_{j,e} - C_{j,w}) \right)}{1 - \sum_j \phi_j C_{j,w}} \quad , \tag{11}$$

where

$$\phi_j = \frac{\nu_i M_i}{\nu_j M_j} \quad .$$

Note that if reactions involving the species A_j do occur within the boundary layer, their influence on the concentrations $C_{j,w}$ must be presented explicitly (Ref. 30).

In the past, the limiting case of a diffusion controlled surface reaction (i.e., $C_{j,w} = 0$) received the attention of most investigators (Refs. 32 through 37) because of its analytical simplicity. In general, however, the rate of surface material removal will depend on the true surface kinetics, and the more recent studies have included this effect. For example, Nolan and Scala (Ref. 29) incorporated surface kinetics in their calculations for the ablation rate of graphite leading edges on a hypersonic lifting vehicle. These authors assume that this ablation rate is inversely proportional to the "diffusional resistance" plus the

"chemical resistance." That is, if $[m]_D$ is the wall mass loss rate obtained by assuming a diffusion controlled surface reaction and $[m]_R$ is that dictated by the true heterogeneous kinetics along, i.e., $c_{j,w} = c_{j,e}$, then it is proposed (Ref. 29) that:

$$m = \frac{1}{\frac{1}{[m]_D} + \frac{1}{[m]_R}} \qquad (12)$$

However, equation (12) will only yield the correct results when the surface reaction happens to correspond to either a diffusion controlled reaction, i.e., $[m]_R >> [m]_D$, or a kinetic rate controlled reaction, i.e., $[m]_D >> [m]_R$.

Invoking, for both laminar and turbulent boundary layers, the previously mentioned assumptions which led to equation (11) (but excluding the frozen boundary layer postulate), Bartlett (Ref. 28) chose to neglect pressure gradient effects and then utilize the resulting linearity between the species concentrations and the velocity. He was able to compute the species concentrations at the ablator surface, while including both vaporization and an arbitrary number of reactions in the boundary layer, by assuming an equilibrium composition at this surface. That is, by just listing all gaseous and condensed species which may be present at the gas-solid interface, the equilibrium composition at the local surface temperature and pressure is obtained by minimizing the free energy of the mixture. Although the actual heterogeneous kinetics cannot be consistently employed with the equilibrium composition constraint, Bartlett's approach should be very useful for computing the ablation rates of rocket nozzle liners, since the pertinent heterogeneous reactions, let alone the kinetics, are often unknown a priori.

Choosing to leave the surface chemistry as general as possible by simplifying the aerodynamics, Moore and Zlotnick (Ref. 30) constructed an analytical model which included both a free-stream with few reactants and a surface for which the heterogeneous kinetics were relatively well understood, that is, a carbon body re-entering the Earth's atmosphere. Making the now familiar assumptions which lead to a linear relationship between species concentrations and stagnation enthalpy, these authors presented a scheme for calculating the ablation rate of carbon which involves only the graphical solution of two algebraic equations. Calculations are presented for a blunted slender body having a flight Mach number of 15 at an altitude of 100,000 feet, and a most interesting result is that the ablation rate of a non-porous carbon surface approaches the reaction rate controlled limit, this rate being less than the diffusion controlled value by a factor 10 to 10^4 (depending on the geometry and location on the body).

Of interest is the comparison with experimental data reported in reference 38; however, the detail of the experiment was not available to this author at the date of writing. The reference indicates that a computer program was devised and may be used in conjunction with other thermodynamic programs for evaluation of materials for propulsion devices.

It is noted again that very few experimental data exist in the literature for comparison with theory. Reference 39 reports turbulent ablation data of carbon, a combustible sublimer, in oxygen-nitrogen mixture in good agreement with theory (Ref. 40), and notes increase in ablation rates and equilibrium temperatures with pressure and oxygen concentration which is in qualitative agreement for stagnation mass transfer with Scala in reference 9. Similar effects were observed for stagnation region in reference 41 for nylon-phenolic materials. Since for the glider application, relatively little material removal would be predicted (Refs 29 and 30), it was not deemed necessary to apply exact analysis for the trend evaluations. No further investigation of the problem was made in the course of the program.

4. Double-Wall Cooling

A great deal of effort has been expended by various manufacturers (Refs. 42 and 43) on this system of structure cooling and it offers promise in association with the above thermal protection systems. The merits of this system will be evaluated in the course of this program by appropriate simulation of the boundary conditions.

Double-wall (or water-wall) construction is a design approach for maintaining air frames subjected to severe aerodynamic heating to acceptable temperature levels. It consists of an outer aero-thermodynamic covering, which is the aerodynamic surface and which dissipates most of the aerodynamic heating by re-radiation and/or ablation. Under the covering is a layer of insulation and/or radiation shields which prevents nearly all of the heat from reaching the load carrying structure. Attached or adjacent to this structure is a supply of water which absorbs the heat that has been transmitted through the insulation. The water maintains the structure to temperatures less than 200°F.

Double-wall construction can only be usefully employed under certain flight conditions. It is most beneficial when the exposure to aerodynamic heating is of moderate length (5 minutes to 2 hours) and when the heating rates are moderate (ideally an order of magnitude less than for ICBM re-entry). Double-wall construction is of particular merit when the vehicle is reusable. The outer covering can be of several forms: an ablation material, a metal, or a ceramic, depending upon the peak heating experienced during

the flight. Ablation materials are thought applicable when the exposure times are fairly short and the peak heating fairly large, while a metal covering is most applicable when the peak heatings are fairly low (10 to 20 Btu/ft^2-sec) but occur for a longer duration. Ceramic materials are useful as an outer covering in the in-between areas. The maximum temperature for both the metal and ceramic coverings can be approximately estimated by setting the radiation heat flux to the peak heat input.

If the covering is made of a metal or ceramic, it must be designed so as to allow thermal expansion without failure. This is usually accomplished by making the outer covering in small panels. The panels are supported to the load carrying structure by a system of supports which not only maintain the panels in the proper position but also minimize conduction to the structure. Many different support designs presently exist; examples are one support in the center, or supports at the four corners, and line supports running axially.

The insulation between the outer covering and the structure is ideally a light weight, high temperature insulant. Since the times of exposure are generally long, the significant parameter is $\rho k/C_p$. Because fibrous insulants have both low density and low conductivity, and because they are easy to install, they make logical choices for double-wall. The insulation must be picked in consideration of the maximum temperature experienced by the outer covering with which it may be in contact. Again there exists fibrous insulants with short time capabilities to 3000°F.

The water which cools the load carrying structure can be supplied in a passive or active system. An example of a passive system is one where the water is contained in a wick material which is placed next to the load carrying structure. Problems with this system are in maintaining contact with the structure, in venting the steam overboard, space requirements, long time storage, and large g forces. An active system implies tubes attached or integral to the structure, which are connected to a pump and heat exchanger. An open or closed system can be used between the tubes and heat exchanger. If the tubes are not integral to the structure, they must be in good thermal contact. This is accomplished by means of a potting compound. Present thinking favors integral tubes. Analysis has shown tube diameters of approximately 1/8-inch are both feasible and desirable and tube spacings between 4 and 6 inches are realistic.

The advantages of double-wall are that it permits conventional structural design techniques, conventional materials, and conventional construction. It is suited for skin stringer and sandwich construction, employing aluminum as a basic material. Another advantage of double-wall construction is that, for the flight regions discussed above, it may show a weight saving over a hot structure or a pure ablation-insulation approach. Double-wall

also is advantageous in that it maintains internal compartments to acceptable temperature limits without any additional provisions. Since the load carrying structure never attains high temperatures and since the outer covering may not carry loads, double-wall is ideally suited for applications where many flights are envisioned.

One disadvantage of double-wall is that the outer surface in all probability will be far from smooth. The outer surface must also be carefully designed to prevent flutter. Another disadvantage is that the system contains useless weight in the form of a wick material and unuseable water or tubes, water, pumps, and heat exchanger and boiler must be designed in space applications for zero-g effects while, for a wick type, vacuum flight may not be acceptable. Finally, questions arise as to the reliability of this system. At this time no reasonable answer is known to this question. Extensive ground tests have been performed which show the system to be entirely feasible, but flight tests with this type of construction have not yet been accomplished.

5. Transpiration

Transpirative thermal protection systems are based upon the injection of mass into a boundary layer, a process which reduces the heat transfer rate through two mechanisms:

a. Absorbing energy within the boundary layer, and

b. Thickening the boundary layer so that gradients normal to the surface become less steep.

Additional cooling may result as the injected fluid passes through the hot skin material.

Significant parameters in the design of a transpirative system include the choice of an injection fluid, the injection geometry, and the nature of the heated surface (skin material).

Prior to this contract, analytical investigations of transpiration dealt primarily with the parameters of the transpiration mechanism. Such analyses as references 44 and 45 indicate that, for purposes of transpiration, the most important gas thermal property is the specific heat at constant pressure. Normally a large specific heat is desirable. The transpiration gas should also have a small Schmidt number (high binary diffusivity) and a large Prandtl number (large ratio of thermal diffusivity to momentum diffusivity). Although the latter two values are less important than the specific heat, a sufficiently large Schmidt number reduces the importance of the specific heat.

In reference 46, it was reported that too large a transpired momentum flux produces a "spike" which pierces the boundary layer. As a result, the normal heating is felt at the base of the spike and the major portion of the transpired mass flow is wasted. This phenomenon coupled with structural problems determines the practical limits of the transpiration system structure. That is, for structural reasons, it is not desirable to have an entire outer skin made of a porous material. Therefore, some areas must be protected by transpiration through other areas, but the spike effect must also be avoided.

6. Thermostructural Problems

The literature search made brought to light previous work done in this field, even though the result of the search is not too promising. Although considerable work has been done on optimization of structures at room temperature and some work has been done at elevated temperatures, little effort is evident to include the effects of thermal stress and creep. Reference 47 combines the effect of axial load, thermal stress, and creep on flat plates. References 48 and 49 present a method of creep stress analysis for thin walled closed sections. Neither of these structures are directly applicable, and work is underway to indicate the extent that the latter references must be modified to be useful in this program. If these modifications are extensive, it may be necessary to either develop new analytical methods, or to introduce simplifying assumptions to utilize the published work without extensive modification.

A number of useful references concerned with thermostructural problems, fabrication, and problems associated with protection of surfaces against oxidation and corrosion are compiled in reference 6.

The literature survey showed that considerable work had been performed on optimization of structures subjected to elevated temperatures for relatively long periods of time. Under these conditions the secondary, constant rate, creep deformations predominate. Most of the work had been conducted using the simplifying assumptions that both stress and temperature remain constant and the secondary phase of creep was of such duration that the primary stage could be neglected. It was further assumed that a uniaxial state of stress existed and to achieve this, structures were idealized as sandwiches in which the facings were subjected to a pure membrane stress and the core remained unstressed. Further, most of the work published dealt with idealized columns, and little work had been performed on other structural elements.

Very little data was available concerning face wrinkling of sandwich structures of cylinders and cones and, therefore, it was decided to establish an analytical procedure for this as the first major objective.

C. SURVEY OF EXPERIMENTAL FACILITIES SUITABLE FOR THE SIMULATION OF GLIDE-TYPE RE-ENTRY VEHICLES

The conditions associated with long duration, low heat flux re-entry are discussed below and the types of experimental facilities suitable for realistic simulation of full-scale vehicles are described. One type of experimental facility is very well suited for the desired purpose and a representative example is described in detail. At the present time, several such installations are in an advanced stage of development. Other experimental techniques which yield meaningful data with partial simulation of full-scale conditions are described briefly.

1. Simulation Parameters

a. Altitude

The full-scale vehicle will effectively re-enter the Earth's atmosphere at 400,000 feet. Significant aerodynamic effects will occur in the altitude range down to 300,000 feet but, broadly speaking, the heating effects will be negligible. Much more noticeable heat transfer effects will occur below 300,000 feet; however, the vehicle may spend a significant proportion of the total re-entry time between 200,000 and 300,000 feet while it is maneuvering onto the desired final re-entry flight path. Therefore, it is important that the experimental facility should be able to simulate pressures corresponding to altitudes up to 300,000 feet at least.

b. Enthalpy and Simulated Velocity

The velocity of the vehicle may be simulated by producing tests at the correct enthalpy value H/RT_o. The effective velocity V is then obtained from

$$V^2 = 2gJ\,RT_o\left(\frac{H_e}{RT_o}\right) \quad . \tag{13}$$

The high enthalpy (high simulated velocity) facilities may be divided into two types; those with ultra-short running times (of the order of milliseconds) such as the shock tunnels and hotshots, and those with moderate (seconds) to essentially continuous (up to 60 minutes) running times typified by the various types of plasma arc-driven wind tunnels and the wave superheater facility.

c. Mach Number

The Mach number of the vehicle should be simulated if possible so that the correct local flow conditions exist along the surface of the vehicle at several characteristic lengths back from the nose.

d. Scale

Portions of the full-scale vehicle (for example, a complete built-up leading edge section), might be tested in a relatively small facility. On the other hand, exact scale models of the full-scale vehicle may be tested on the Reynolds analogy basis used in conventional wind tunnels. This latter approach is not meaningful when chemical reactions and non-equilibrium effects are present in the airstream and/or at the surface of the vehicle. It is much more satisfactory to test material specimens in elementary rigs (e.g., a turbulent pipe apparatus) for preliminary screening purposes and then to conduct careful detailed experiments on chosen materials with close simulation of full-scale conditions.

e. Time

Clearly the ideal re-entry vehicle facility should simulate the exact real-time variation of heat flux and total integrated heat input to the vehicle, together with the appropriate altitude variation.

2. Selection of Suitable Facility

The requirements outlined in the previous section clearly indicate that all the ultra-short duration facilities are unsuitable for materials testing of any kind. However, shock tunnels (Ref. 50) can give extremely accurate heat transfer rates as a function of the correct altitude, correct simulated velocity, Mach number, and enthalpy. This information can be of use in some cases. The majority of other facilities cannot reach the required maximum enthalpy and simulated velocity values. The only correct simulated parameters in rocket or ramjet exhaust tests are the heat flux (and possibly, the pressures and shear stresses). Enthalpy levels and flow Mach numbers are quite low. They do, however, operate for fairly long time periods and hence are of use in the present context.

The NASA Ames Atmosphere Entry Simulator (Ref. 51) is an ingenious experimental facility but the scale of the model is so small that it is not possible to test structural concepts for built-up models.

The Cornell Aeronautical Laboratory Wave Superheated Wind Tunnel (Ref. 52) is a large-scale facility which will produce complete simulation for altitudes between 110,000 and 180,000 feet in the Mach number range from 7 to 12. At the present time, however, this facility is relatively untried and full operational capability will not be attained until 1962.

The remaining facilities are all driven by plasma jets, normally using air as the working fluid. In these cases the enthalpy levels may be very high

and easily cover the desired range. At present, most of the experimental equipment operates simple splash tests; the jet produced from the arc plasma chamber is allowed to impinge on the model. Very recently, significant strides forward have been taken. The power supplied to the arc and the mass flow of working fluid may be controlled and programmed so as to produce a smooth heat pulse - exactly similar to that experienced by the full-scale vehicle. Certain advanced facilities, using continuous vacuum pumping (rather than the blowdown tunnel principle) are now able to operate with real time simulation for periods of 30 minutes or more. The Mach number simulation has been extended to about M = 4 already and it is feasible to extrapolate current techniques to M = 15 in the next year or so. Thus, these advanced arc facilities give the best simulation of the full-scale glide vehicle yet achieved in the laboratory.

Enthalpy, velocity, pressure, and heat flux may be simulated in real time together with say, variations programmed to duplicate the skipping of the vehicle into and out of the atmosphere.

A review of the existing facilities used for simulating re-entry thermal environments was made to determine which if any could be used in later experimental testing of thermal protection mechanisms. The pertinent characteristic of each facility including gas temperature, heat flux, enthalpy, pressure, flow rates, run duration instrumentation and sample sizes were obtained whenever possible. The information gathered on the experimental facilities has been tabulated in Appendix III. From the available data it was concluded that an arc jet would provide the best simulation of re-entry thermal environments. However, with the exception of the Plasmadyne Air Arc no other facility available at the initial phase of this contract was capable of long duration re-entry simulation and it was originally planned to arrange for testing at this facility. However, during the course of planning the test program, two Avco air arcs, Channel 3 of the 10 mw facility and OVERS (see Appendix III) became operative. Both facilities were used in this program although the major effort was carried by the lower operating cost Channel 3 which is described in detail later in this report.

D. SURVEY OF MATERIALS

The materials used or contemplated for use in thermal protection systems have to display either high temperature tolerance while maintaining their integrity if not the strength. As an alternative they may either provide effective heat capacity through a mass transfer process, or be encased in a high temperature material. The use of a particular material class is closely associated with the mode of heat dissipation employed in the thermal protection system. Many arbitary classifications of materials in groups may be made. A quite acceptable classification is given in reference 1 and will be essentially adhered to here. The usage of materials in various protection systems may be broadly categorized as:

1. Radiation Shields, Hot Structures, and Heat Sinks

   a. Copper-steel-nickel composites,

   b. Beryllium,

   c. Molybdenum,

   d. Tungsten and tungsten composites,

   e. Berrylia, alumina, etc.,

   f. Graphites and pyrolytic graphites with and without coatings,

   g. Liquid lithium - cooled composites,

   h. High-temperature ceramic and refractory metal skins.

2. Radiation Cooling

   a. Graphite and pyrolytic graphite composites,

   b. Solid or foamed ceramics (high thermal conductivity),

   c. Refractory metals,

   d. Metallic plastic fabrics.

3. Mass Transfer (ablation and shields, and transpiration systems)

   a. Silica (glassy) materials,

   b. Reinforced plastics (organic and inorganic reinforcement including salts),

   c. Plastics (charring and non-charring),

   d. Plastic reinforced ceramics and refractory metals,

   e. Reinforced (ductile) ceramic systems including silica magnesia, tantalum carbide and other carbides, nitrides, and oxides,

   f. Graphite, pyrolytic graphite, and graphite reinforced plastics.

4. Insulation

   a. Solid and porous ceramics,

   b. Crystalline glasses,

   c. Reinforced ceramics,

   d. Organo-ceramics,

   e. Vacuum insulation,

   f. Fibrous and powder insulation,

   g. Plastics (reinforced).

The knowledge of the mechanism of heat accommodation for these materials and their thermal and mechanical properties has progressed to various degrees of completeness and accuracy. It is, however, essential when their selection for the system is required. The availability of the material is of equal importance to the designer.

The accumulation of information on material properties and characteristics is a subject of intensive effort by Purdue University (Ref. 53) and Armour Institute (Ref. 54) and as such was not the principal objective in this program. Some typical values have been compiled and are shown in table 2 for orientation purposes. It is nevertheless evident that high-temperture information is not readily available.

In the structural design of re-entry vehicles, it is apparent that a more efficient design could be obtained, from a minimum weight and cost point of view, if quantitative information on the mechanical properties of the heat-shield material, as a function of temperature, load and time could be obtained.

Such information is needed because many vehicles use dissimilar materials either as a composite or attached together in some manner, thus to make the analyses sufficiently general, materials are assumed to be dissimilar. For instance, in re-entry vehicle design, when the thermal protection material (heat shield) is bonded to the load-carrying structure a class of composite structures results. The combined load and temperature environment which occurs at re-entry requires a rigorous analysis of the composite structure for strain compatibility, stress and displacement distribution. In figure 8 the Young's modulus versus temperature of a non-metallic material in tension is given. Most metallic materials over the same temperature range would be almost constant. This implies that for a composite structure using a material with properties given in figure 8 and a metallic material at low temperatures

TABLE 2

PROPERTIES AND CHARACTERISTICS OF MATERIALS FOR THERMAL PROTECTION SYSTEMS

A. RADIATION AND CONDUCTION MECHANISMS (RADIATION SHIELDS, HEAT SINKS, STRUCTURES)

Properties	Beryllium	Molybdenum	Molybdenum +1/2% Ti Alloy	Columbium	Columbium FS-82 (33% Ta, 0.75% Zr)	Graphite	Zirconia ZrO_2	Alumina Al_2O_3	Beryllia BeO	Magnesia MgO
Density, lb/ft^3	116	640	637	535	650	140	363	250	187	218
Specific Heat, (C_p)—Btu/lb-°F	0.45	0.065	0.065	0.07	0.064 -0.089	0.165 at 76°C 0.390 at 1450°C	0.16 25° to 1000°C	77°F-0.185 1341°F-0.292 2241°F-0.303	0.497	30° to 1100°C 0.283
Thermal Conductivity, K~Btu/ft-F-hr	87	70	65	40	40	0.298 (100°C) 0.134 (600°C) 0.105 (1000°C)	1.2 2400°F	2.5	high	3.4
Melting Temperature, °F	2340	4760	4750	4474	4550	6380	4928	3722	4658	5072
Modulus of Elasticity, $\times 10^6$ lb/in.^{2}	42	42	42			Plain 14.0 Impervious 2.2	24.8	54	42.8	12.4
Tensile Strength, $\times 10^3$ lb/in.^{2}	20 to 40	147	85 to 175	48 to 130	100	Plain 0.8 Impervious 2.4	17.9	37	13.8	
Compressive Strength, $\times 10^6$ lb/in.^{2}						Plain 0.0055 Impervious 0.010	0.3025	0.4125	0.1031	
Thermal Expansion Coefficient, $\times 10^{-6}$ in./in./°F	7	3.0	3.0	3.9		7.8	5.0	3.3 to 3.9	25°C to 1260°C 9.2	13.4
Thermal Shock Resistance						very good	fair	good	very good	fair
Resistance to Abrasion						poor	good	good	good	very poor
Coating Req'd										

TABLE 2 (Cont'd)

Properties	Titanium	Aluminum 7075-76	Stainless Steel Type 316	Magnesium HK31A	Titanium Nitride	Steel SAE4340 Contains NiCrMo	Molybdenum +1/2% Titanium	Zirconium	Tungsten	Tantulum
Density, lb/ft^3	282	173.0	492	112	339	489	637	415	1210	1037
Specific Heat, (C_p)~Btu/lb-°F	0.13	0.2045 at 100°F	0.116 (200°F)	0.247	$C_p = 11.9 + 0.91 \times 10^{-3}T - 2.96 \times 10^{5}T^{-2}$ cal/mol°K	0.107	1500°F 0.0712	0.069	0.032	0.036
Thermal Conductivity, K~Btu/ft-°F-hr	9.8	73	8.29 (200°F)	60 (212° to 570°F)	392°F 21.8 1112°F 6.05 2192 4.85	21.6	(1000°F) 62.0	9.6	96	32
Melting Temperature, °F	3140	1186	2250	1195	5342	2740°F (melt) 1000°F (limit)	4748	3355	6152	5425
Modulus of Elasticity, $\times 10^6$ lb/in.^{2}	15	10.4	28	6.1		(25° to 1200°F) 31.5 to 7.3	high	14	50	27
Tensile Strength, $\times 10^3$ lb/in.^{2}	89 to 150	80	80	31		(75° to 1200°F) 198.1 to 138.6	(82° to 4500°F) 112.9 to 0.6	24 to 90	70 to 300	50 to 180
Compressive Strength, $\times 10^6$ lb/in.^{2}										
Thermal Expansion Coefficient, $\times 10^{-6}$ in./in./°F	5.8	13.3	8.9	12.1		(0° to 1200°F) 8.1	(68° to 3000°F) 3.75	3.1	2.2 to 2.9	3.8
Thermal Shock Resistance		good	excellent				excellent			
Resistance to Abrasion						good				

TABLE 2 (Cont'd)

Properties	René 41	Super Alloy A-286	Titanium Carbide	Tungsten Carbide	Zirconium Carbide	Titania	Beryllium Carbide			
Density, lb/ft^3	515	494	307	979	418	260	152			
Specific Heat, (C_p) ~ Btu/lb.-°F	0.16	0.11	0.201			0.166	0.3			
Thermal Conductivity, K ~ Btu/ft.-°F-hr	(1000°C) 10	(100° to 1000°F) 7.4 to 13	9.91	37.9	11.8	3.62 (100°C) 1.83 (1800°C)	1.3			
Melting Temperature, °F	2450 to 2550	2500	5650	5000	6350	3294	3780			
Modulus of Elasticity, x 10^6 lb/in.^{2}	25.0	23.5	51	102.5	49	12.7 to 15.5 (20°C)	45 (20°C)			
Tensile Strength, x 10^3 lb/in.^{2}	168	(1000°F) 132								
Compressive Strength, x 10^6 lb/in.^{2}										
Thermal Expansion Coefficient, x 10^{-6} in./in./°F	7.6	(1000°F) 9.78	(24° to 500°C) 7.42	(20°C to 1930°C) 5.2 to 7.3	(24° to 500°C) 6.73	7.5	10.8			
Thermal Shock Resistance										
Resistance to Abrasion										

TABLE 2 (Cont'd)

B. MASS TRANSFER MECHANISMS (ABLATION, ABLATION-RADIATION, TRANSPIRATION SYSTEMS)

Properties	Teflon	Polymethyl-methacrylate	Nylon Phenolic	Epoxy Versamid		Silica-Epoxy Materials			Honeycomb Reinforced Magnesium Oxide	Refrasil Graphite	Pyrolytic Graphite
				Low Temperature	3000 Series	4000 Series (Low Silica to Resin Ratio)	5000 Series (Low Silica to Resin Ratio)	High Silica to Resin Ratio			
Density, ρ, lb/ft^3	137.0	74.0	75	71	69	72	66 to 73	77	188	95	125
Specific Heat, C_p, Btu/lb-°F	0.22	0.35	0.38	0.44	0.4	0.3	0.31	0.24	0.22	0.3	0.58
Thermal Conductivity, k, Btu/hr-ft-°F	0.15	0.12	0.23	0.13	0.14	0.1	0.11	0.23	5.4	0.25	0.2
Emissivity, ϵ	0.5	0.2	0.9	0.5	0.7	0.6	0.8	0.6	0.9	0.6	0.85
$\rho K/C_p$, lb^2/ft^4-hr	93.4	25.03	45.39	20.97	24.1	24.0	23.4 to 25.9	73.8	4614.0	79.2	190.2
Melting Temperature, °F	1350	1000	5000	1780	3000	4000	5000	4100	5100	4100	6700
Transpiration Coefficient	0.42 0.18	0.43 -	0.7 0.25	0.53 0.15	0.46 -	1.0 -	1.2 -	0.49 -	1.0 -		0.5
Heat of Vaporization, H_v	320	800	1000	260	200	1000	1000	2300	5000	3900	7400
Effective Heat of Ablation (q^*), Btu/lb at H_e/RT_0 = 300 — Laminar (30 sec)	4500	5000	9000	6100	5200	11,200	13,000	6600	14,600	8500	8900
Effective Heat of Ablation (q^*), Btu/lb at H_e/RT_0 = 300 — Turbulent (10 sec)	2300	-	5100	2500	-	-	-	4100	-	4100	-
Coefficient of Thermal Expansion, 10^{-5}/°F, in./in./°F	5.6	5	5	8	8	2 to 3	2.6	5 to 6	0.8 to 1.2	0.2 to 1.4	0.07
Modulus of Elasticity, 10^6 psi	0.06	0.4	0.5	0.3	0.4	0.7	0.7	0.9 to 1.3	4.7	1 to 3	-
Poisson's Ratio	-	-	-	0.3	0.3			0.25	0.19 to 0.26		
Tensile Strength, ksi	1.5 to 3.0	6 to 8	5	4.4	7	3 to 4	3 to 4	3.5	3.8	1.5 to 7.5	1 to 50
Compression Strength, ksi	1.7	11 to 14		8.5					4.2		
Ultimate Strain, percent	100	2 to 7		2 to 5	2.3	0.7	0.7	0.4	0.51	0.6	
Fraction Vaporized, (f)			1.0		1.0		1.0	0.85		0.85	1.0

TABLE 2 (Cont'd)

Properties	Silicon Carbide	Thoria	Carbon	Tantalum Carbide	Silicon Nitride	Fused Quartz SiO_2	Boron Carbide	Stabilized Zirconia ZrO_2 (5% CaO)	Zircon $ZrO_2 SiO_2$	Spinel $MgO Al_2 O_2$	Mullite Porcelain 70% Al_2O_3 27% SiO_2 3% Mo + M_2O	High Alumina Porcelain 90% Al_2O_3 4% SiO_2 1% Mo + M_2O
Density, lb/ft^3	197.8	605	125	903	214	136.0	156	333	293.3	220	175	234
Specific Heat, C_p, Btu/lb-°F	1000°C 0.1216	25°C 0.06	0.168 to 0.387	$C_p = 7.28 + 1.65 \times 10^{-3}T$ cal/mol °K	$C_p = 16.83 + 23.6 \times 10^{-3}T$ cal/mol °K	0.19	0.443	0.12 (20°C) 0.16 (500°C)	0.131	0° to 1042°F	0.25	0.26
Thermal Conductivity, k, Btu/ft-hr-F	5.9 to 10	1.65	1.5	12.8	0.9	0.8	15.7 (20°C)	0.97	0.966	1.2	(100° to 1000°C) 1.7 to 3.45	(100° to 1000°C) 12 to 3.6
Melting Temperature, °F	4892	5486	sublimes 6399°F	6840	3452	3050	4410	4680	4622	3875	1400°F limit	1500°F limit
Modulus of Elasticity, $x 10^6$ lb/in.^{2}	17.0 to 9.5	17.9	plain 1.9 impervious 2.8			10	65 (20°C)	16	24.0	31.7		
Tensile Strength, $x 10^3$ lb/in.^{2}	14		plain 0.9 impervious 1.8			7			12.7	18.6		
Compressive Strength, $x 10^6$ lb/in.^{2}		0.22	plain 0.007 impervious 0.0185		0.72 to 0.92				0.09	0.2475		
Thermal Expansion Coefficient, $x 10^{-6}$ in./in./°F	0° to 1700°C 4.3	25° to 800°C 9.5	500°C 1.5 to 5.5	(20° to 2380°C) 8.2	0.28 1.37	4.5 crystalline and above 600°F	7.2	20° to 700°C 4.9	25° to 800°C 8.5		5.5	7.8
Resistance to Thermal Shock	good	fair	very good		better than most ceramics	excellent (above 600°F) fair (below 600°F			very good	fair		
Resistance to Abrasion	very good	good	good						good	good		

TABLE 2 (Concl'd)

C. INSULATION SYSTEMS

Class	Solid Ceramic									Crystalline Glasses		Reinforced Ceramics		Organo-Ceramics			Fibrous			Powders	
Material	Thorium Oxide ($Th O_2$)	Zirconium Oxide ($Zr O_2$)	Forsterite ($Mg_2 Si O_4$) 31% Porosity	Firebrick	Firebrick	Foamsil	Eccofoam	Alumina Coating (98.6% $Al_2 O_3$)	Zirconia Coating (98% ZrO_2)	Pyroceram 9608	Pyroceram Foam	Aluminum Phosphate Bonded Alumina	Zirconium Phosphate Bonded Zirconia	Min-K	Mark I	Mark II	Aluminum Silicate Fibers (Fiberfrax)	Silica Fibers (Q-felt)	Basalt Volcanic Rock Fibers (Basaltwool)	Diatomaceous Earth Powder	Thin-Skin Vacuum Panel
Density, (ρ), lbs/ft^3	600	363	139	65	29	11	22	200	325	156	14.4	190	242	20	40	30	6	3	5	17.2	15.5
Thermal Conductivity, (k), Btu/hr-ft-°F	1.65 (1800°F)	1.2 (1800°F)	0.97 (1800°F)	0.3 (2000°F)	0.106 (1500°F)	0.154 (900°F)	0.06 (800°F)	1.58 (2000°F)	0.67 (2000°F)	1.13 (70°F)	0.125	0.6 (2400°F)	0.5 (2400°F)	0.022 (1000°F)	0.1	.04	0.25 (1300°F)	0.97 (1400°F)	0.225 (1300°F)	0.074 (1400°F)	0.0025 (49°F)
Specific Heat, (C_p), Btu/lb-°F	0.06	0.16	---	---	---	0.19	0.19	0.3	0.16	0.19	0.19	---	---	0.4	0.3	0.3	---	---	---	---	---
Insulative Performance Parameter, (ρk), Btu-lb/hr-ft^4-°F	990	435	134	19.5	3.07	1.70	1.38	317	216	177	---	114	121	0.45	4	1.2	1.5	0.29	1.13	1.76	0.039
$\rho k/C_p$, $\frac{lb^2}{ft^4-hr}$		2722	---	---	---	8.91	6.94	1053	1360	927	9.4										
Present Temperature Limit, °F	4850	4500	3400	3000	1800	2000	1600	3000	4200	2250	2250	---	---	1.1	13.3	4.0	---	---	---	---	---
Heat Flux Limit, (Q), Btu/sec-ft^2	324	247	90	58	20	25	7	52	192	22	22	3500	4000	2000	2400	2400	2500	2000	1500	2500	1000
Resistance to Thermal Shock (Qualitative)	Poor	Fair	---	---	---	---	---	Excellent	Good	Excellent	---	100	161	15	---	---	23	15	5	12	1
Surface Characteristics	Hard	Hard	Hard	Crumbles Easily	Crumbles Easily	Easily Abraded	Easily Abraded	Hard	Hard	Hard	Easily Abraded	Excellent	Excellent	---	---	---	---	---	---	---	---
												Hard	Hard	Easily Abraded	Hard	Crumbers Easily	Loose Fibers	Loose Fibers	---	Loose Powder	Hard

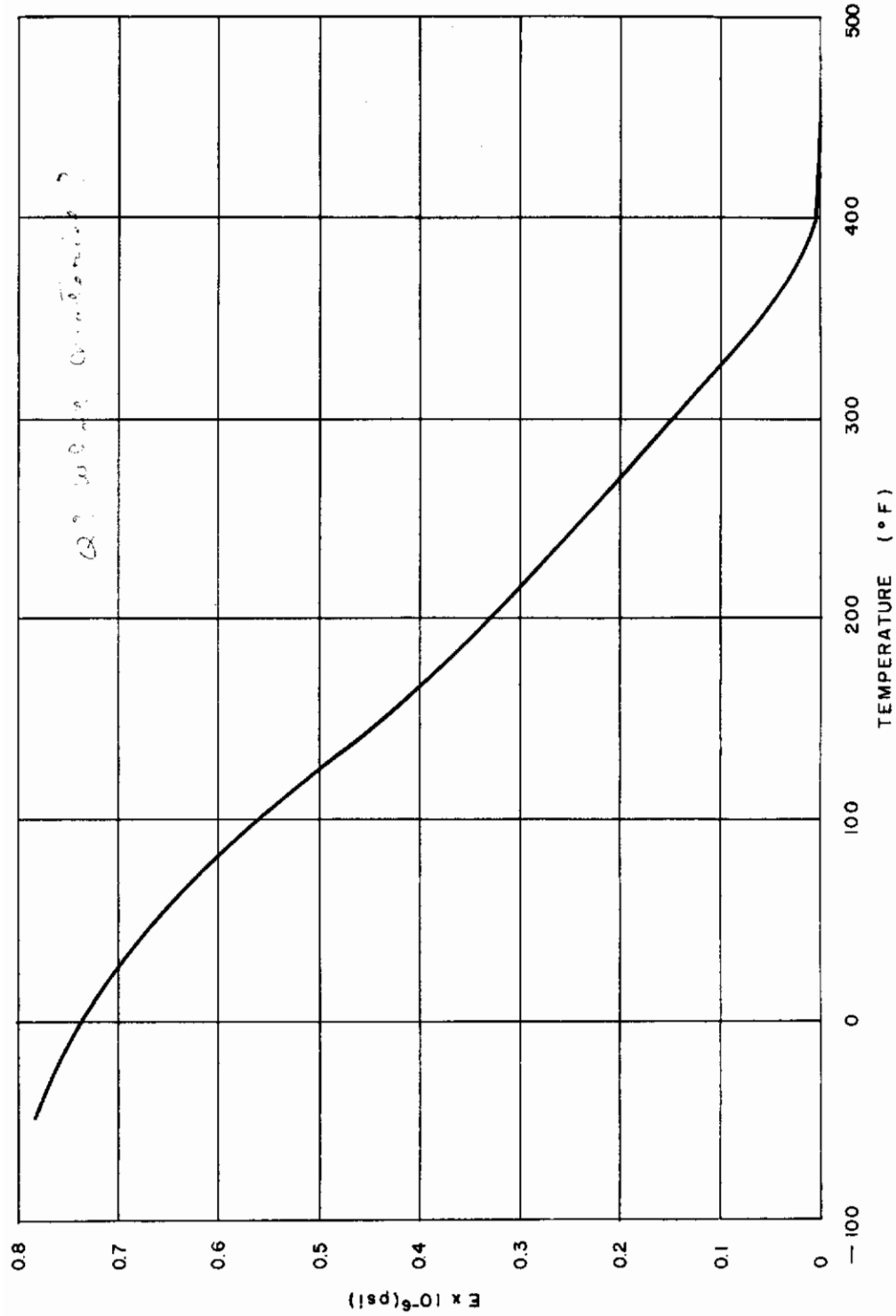

Figure 8 TEMPERATURE DEPENDENCE OF YOUNG'S MODULUS WITH SPECIMENS IN TENSION

of 100°F and less, the load carrying capacity of vehicle would be distributed between the metallic and non-metallic materials. As the temperature increased the metallic portion of the structure would be carrying more and more of the load. Further, it is important to determine the stress and displacements of the two materials separately for they have different coefficients of thermal expansion and, hence, an analyst would want to make sure that they hold together.

In the section on stress-strain analysis in Appendix VII general cross sectional mechanical rigidity properties of multi-layer heat shield back-up structure combinations are given. The values of material properties may vary through the thickness as well as along the surface. Further illustrations are given of how to determine mechanical properties of sandwich-back-up structure heat-shield combination, where the sandwich may have different thickness of face sheets and the core may be a honeycomb, a corrugation, etc.

In view of gaps in the knowledge of material properties the parametric studies performed in the course of the program (Section III. A.) are of particular value. They indicate the degree of sensitivity of system performance to the uncertainty in properties knowledge as well as the significant properties needed in design. This is in addition to providing a guide for material selection and definition of "desirability" of certain characteristics.

The user of the charts should consider the availability of the material or feasibility of its fabrication for an extended forecast range up to 1965, as it is not implied that the range of property variations used in the parametric studies is representative of today's state-of-the-art. Neither is it implied that the materials referred to or tested during the program are best representatives of their class. The use of such materials for study purposes was due either to their availability, or knowledge of their properties helpful in demonstrating methods and techniques.

E. EVALUATION

The review of the state-of-the-art revealed lack of information needed for the thermal protection system design and material development efforts directed towards glide re-entry applications. The search of data available for other regimes (ballistic missile or satellite capsule re-entry) indicated that there is no correlation method available which would permit extrapolation of data to the regime of interest when the very limited data for that regime could be used as end points. Furthermore, the variety of reference or effective heat flux data used without clear definition of the original cold wall flux does not permit correlation of the existing data. Unpublished Avco data for a satellite capsule were correlated in a systematic fashion to provide design and material performance data for that application (Appendix IV).

Only limited parametric studies involving interaction of material environment and design criteria of use in an integrated design approach were published for glider type re-entry. They either cover specific materials or a very narrow range of parameter variation. The more inclusive studies are available for ballistic re-entry. The great majority of studies is done assuming quasi-steady state or makes unverified assumptions which often lead to unpredictable errors.

No simple analytical method for transient heat flow calculations is available for use in evaluation studies or preliminary design purposes greatly curtailing the feasibility of trend determination. Thus, no general parametric studies are available.

The figure of merit or performance criteria used vary all over the field. Those which are used are not proven analytically or experimentally valid. A great many misconceptions exist concerning mechanisms of thermal protection and measures of their evaluation. The performance criteria used or proposed (shown in table 3) do have merits for particular regimes and with proper analysis constitute a good source for selection.

Most information is available in graphical form, which seems to be the more acceptable, because of the number of factors involved in thermal protection design. It may be seen thus that many gaps have to be filled for a proper analytical evaluation of glider re-entry consistent with the objectives and the scope of the program.

The experimental side presents a brighter picture because facilities and techniques used are basically adaptable for the purpose of this program. However, full use of the facilities is not made because with improvement in instrumentation more useful information could be extracted from the test data. The interpretation of the data in the sense of comparison of experiment and theory is far from abundant and not much analytical effort is observed in the establishment of simulation requirements.

Most information on materials is available in the low temperature range, and mostly for ablating systems. The predominance of information concerning various aspects of ablating systems for ballistic re-entry is a feature of the field, as may be apparent from the preceding review. This does not imply the systems desirability (or lack of it) for the regime of interest, but simply reflects the interest in the field.

TABLE 3

SUMMARY OF CRITERIA FOR MATERIAL SELECTION AND PERFORMANCE EVALUATION

Parameter	Definition	Desired Trend	Best Region of Application as a Figure of Merit
Effective Heat of Ablation* q^*	sensible heat + heat of decomposition + mass transfer shielding + shear effects	$\longrightarrow \infty$	High-flux region; i.e., when most of the aerodynamic heating is absorbed by ablation.
$\frac{\rho k}{C_p}$	$\frac{\text{density x conductivity}}{\text{specific heat}}$	$\longrightarrow 0$	This parameter is predominant when no ablation occurs and gives some indication of material performance when the rate at which heat is conducted into the shield is very small compared to the heat radiated away from the surface.
ρk	density x conductivity	$\longrightarrow 0$	Same as above except somewhat less indicative.
T_A	ablation temperature	No general trend. Depends on interaction with other parameters and design criteria	None except as to indicate whether or not ablation will occur.
T_t	backface temperature	Low or as prescribed	A design and comparative criterion for testing.
ϵT_E^4	emissivity x (radiation equilibrium temperature)^4	$\epsilon \rightarrow 1$ depends on interaction with other parameters and design criteria	Short duration, or when heat leakage into system is minimized.
Q^*_{eff}	$\frac{\text{total "cold wall" heat input}}{\text{total required weight of T.P. system for a given backface temperature}}$	$\longrightarrow \infty$	Indicates material (and system) performance in all regions since it is essentially a weight parameter including the interaction of all other variables. Must be calculated based on a knowledge of all material properties and mission environment.
w_t or ρL_t	total required weight of T.P. system	$\longrightarrow 0$	Same as above.

*Also referred to by many other symbols with various heat fluxes as reference.

III. SYSTEMS ANALYSIS

The significance of system parameters, their relationships, and methods of their calculation have to be established prior to any systematic study leading to the evaluation of performance (Section IV) and selection of materials and optimum overall systems (Section V). In this section the significant parameter affecting the performance of several thermal protection systems will be determined first. Secondly, correlation methods will be adapted to establish parametric relationships between them. Thirdly, computational techniques will be developed (or described if already available) to calculate such relationships readily.

A. PARAMETERS

System performance may be described in terms of three parametric groups due to environment, materials, and design requirements. For the purpose of this study the environmental factors are the forcing functions (inputs). Material parameters are divided into properties independent and characteristics depending on the environmental inputs. Furthermore, material performance is defined by its temperature response and ability to accommodate heating and loading within a given weight requirement. Material performance on one hand relates to the operating limits of primary shield material (e.g. surface temperature, erosion or structural integrity) on the other hand, it is related to design criteria associated with the substructure (e.g. limiting backface temperature), with the system (e.g. allowable weight, reusability) or aerodynamic configuration (e.g. external shape change). In most cases all the above criteria have to be considered at one time. Since the number of factors is very large, it is necessary to separate the significant effects from the unimportant ones by analysis of each system and application to facilitate the study of performance and to ascertain the "desirability" of certain material properties and characteristics.

Depending on the material, application, and type of process, some of the parameters are more significant than others. In defining the term "significant" a distinction should be made between the overall thermal protection system and the process itself. Some of the parameters will be significant for both, some, however, although very important for the overall system, may affect the process but little. It was chosen here to consider the significance in terms of the overall system. The term "desirability" bears similar connotation. From the overall system point of view, the effective heat capacity (Q^*_{eff}) should be maximized. This may be achieved by maximizing for instance the ablation efficiency, i.e., absorption of the incident flux in ablative process rather than its conduction into the interior. Thus low conductivity (k) of material is necessary but not sufficient, if the combined heats of ablation or surface temperatures and emissivities were low, and if ablation rates or recession rates were to be minimized. Depending on the environment, various combinations of parameters may be desirable and/or significant.

In respect to "significance" and "desirability" various re-entry applications may differ although the basic analysis of the process is the same.

The modes of heat transfer and applications will largely determine the significance of various parameters. The parameters of the systems considered for the glide re-entry are analysed in the following paragraph.

1. Radiation Shield

Radiation systems are of particular interest for the glide re-entry applications. Systems involving mass transfer are also of interest; however, their mechanism is more complex and considerably more parameters than in radiation shield are involved. The study of the radiation shield is in a sense the first step towards evaluation of more complex mechanisms, as all the parameters significant for radiation will appear in the other system equations.

Starting with a system consisting of a single slab and assuming constant thermal properties, k, ρ, C_p, and ϵ the equations to be considered are:

$$\rho C_p \frac{\partial T}{\partial t} = k \frac{\partial^2 T}{\partial x^2} \quad 0 < x < L, t > 0 \tag{14}$$

$$T(x,0) = T_i = \text{constant initial temperature,} \tag{15}$$

at the heated surface, $x = 0$

$$-k \frac{\partial T}{\partial x} = q_c(t) \left[1 - \frac{h_w / RT_o}{H_e / RT_o} \right] - \sigma \epsilon T^4 \quad . \tag{16}$$

At the backface (cold surface), $x = L$

$$\frac{\partial T}{\partial x} = 0 \text{ (perfectly insulated),} \tag{17}$$

where

$q_c(t)$ = convective heat transfer rate to a cold wall,

$\frac{H_e}{RT_o}$ = dimensionless stagnation enthalpy,

$\frac{h_w}{RT_o}$ = dimensionless enthalpy of air adjacent to the heated surface,

RT_o = a reference enthalpy.

The material parameters involved are thermal conductivity, density, specific heat, and emissivity. The design parameters are the initial temperature, maximum allowable surface and back face temperatures, and the thickness (or weight) required to satisfy these temperature conditions. Cold wall heating and stagnation enthalpy are functions of the reentry trajectory and are initially fixed for the several types of thermal protection systems being considered.

Since the weight of the heat shield is generally of more importance than the thickness, it is convenient to transform the above equations to a weight basis, i.e., setting $W_x = \rho x$ and $W_{ins} = \rho L$,

$$\frac{\partial T}{\partial\left(\frac{\rho k t}{C_p}\right)} = \frac{\partial^2 T}{\partial W_x^2} \quad ; \quad 0 < W_x < W_{ins},\ t > 0 \quad , \tag{18}$$

$$T(W_x,0) = T_i = \text{constant initial temperature.} \tag{19}$$

At the heated surface, $W_x = 0$,

$$-\rho k \frac{\partial T}{\partial W_x} = q_c(t)\left[1 - \frac{h_w/RT_o}{H_e/RT_o}\right] - \sigma\epsilon T^4 \quad , \tag{20}$$

and at the cold face, $W_x = W_{ins}$

$$\frac{\partial T}{\partial W_x} = 0 \quad \text{(perfectly insulated)} \quad . \tag{21}$$

Analyzing the above set of equations it is seen that the material properties density, conductivity, and specific heat enter into the differential equation as $\rho k/C_p$ while the boundary condition at the heated surface includes

only the product ρk. Strictly speaking, the weight depends on the properties ρk and C_p separately and not on the lumped quantity $\rho k/C_p$. However, since radiation is the primary mode of thermal protection in the above model, an analysis of the boundary condition at the heated surface suggests that the heat conducted into the body is very small compared to that radiated away from the surface. If this assumption proves valid for the materials to be used in glider vehicle application, then the heat conducted can be set equal to zero in the boundary condition at the hot face, for the purpose of determination of the significant parametric group. The problem reduces now to:

$$\frac{\partial T}{\partial\left(\frac{\rho k t}{C_p}\right)} = \frac{\partial^2 T}{\partial W_x^2} \quad ; \quad 0 < W_x < W, \; t > 0 \quad , \tag{22}$$

$$T(W_x, 0) = T_i = \text{constant initial temperature} \quad , \tag{23}$$

$$q_c(t)\left[1 - \frac{h_w/RT_o}{H_e/RT_o}\right] = \sigma \epsilon T^4 \text{ at } W_x = 0 \quad , \tag{24}$$

$$\frac{\partial T}{\partial W_x} = 0 \text{ at } W_x = W_{ins} \quad . \tag{25}$$

It is apparent that if the heat conducted into the solid is very small compared to that radiated from the surface, the weight of the system for a given backface temperature depends on the lumped quantity $\rho k/C_p$ rather than on ρk and C_p separately. This assumption was verified by many calculations using transient finite difference solutions of equations (14) to (17) and then analyzing the results to determine if the trends indicated by equations (22) to (25) were applicable.

The surface temperature must not be allowed to exceed the material limitations. Melting, erosion or decomposition temperatures and a relation between the maximum allowable cold wall heat rate and the limiting surface temperature is necessary. This is provided by the above modified boundary condition at the heated surface which relates $q_{c(max)}$, the maximum cold wall heat flux and surface temperature $T(o,t)$ for a parametric value of H_e/RT_o.

It is thus concluded that for a specified vehicle and trajectory, parametric weight studies for radiation shields may be made in the terms of

material properties ϵ, $\rho k / C_p$, and of the design criteria (maximum surface and backface temperatures). Such studies were made and are presented later in this report along with a discussion of their application.

It should be kept in mind that the model used here assumes a homogeneous slab of insulation, without a thin radiating sheet at the hot surface, or a load carrying substructure. The computational methods (Section III-C.1.) show an easy and simple procedure for adjustment of the weight for the presence of structures on either face of the homogeneous slab.

2. Radiation Shield with Backface Cooling

In the model described above the backface was assumed to be insulated and the temperature rise was calculated. However, if very low backface temperatures are required or if a coolant is available to absorb the heat conducted through the shield, then the boundary condition at the cold surface (backface) may be written as

$$\rho k \frac{\partial T}{\partial W_x} = \dot{W}_c H_c \text{ or } \left(\frac{\rho k}{C_p}\right) \frac{\partial T}{\partial W_x} = \dot{W}_c \left(\frac{H_c}{C_p}\right) ,$$

where $\dot{W}_c$ is the mass vaporization rate of coolant, and H_c is the effective heat capacity of the coolant unit behind the insulation shield. All other quantities have been previously defined. The remaining equations are unaltered and the description of the radiation shield supplemented with backface cooling is

$$\frac{\partial T}{\partial \left(\frac{\rho k t}{C_p}\right)} = \frac{\partial^2 T}{\partial W_x^2} \quad ; \quad 0 < W_x < W_{ins}, \; t > 0 \quad . \tag{26}$$

$$T(W_x, 0) = T_i = \text{constant initial temperature} \quad , \tag{27}$$

$$q_c(t) \left[1 - \frac{h_w / RT_o}{H_e / RT_o}\right] = \sigma \epsilon T^4 \text{ at } W_x = 0 \quad , \tag{28}$$

$$\left(\frac{\rho k}{C_p}\right) \frac{\partial T}{\partial W_x} = \dot{W}_c \frac{H_c}{C_p} \text{ at } \dot{W}_x = W_{ins} \quad . \tag{29}$$

Notice that in this model it is assumed that there is no temperature rise at the rear surface while in practice there may be some. This assumption was investigated in the parametric studies (Section IV) over a range of backface temperature rises and was found to be justified for the range of interest.

All other assumptions are the same as those described above for the uncooled radiation shield. Therefore, given a specific vehicle and trajectory parametric weight, studies for radiation shield supplemented by cooling units may be made in terms of insulation and coolant properties, i.e., $\rho k/C_p$, ϵ, H_c/C_p and design criteria (maximum surface and backface temperatures). The total weight may be minimized by selecting the optimum insulation weight W_{ins} and corresponding coolant weight W_c.

The parametric study results may be thus presented in terms of the total weight for fixed values of the material parameters $\rho k/C_p$, ϵ and of the design criteria ($q_{c(max)}$) for maximum surface temperature and given backface temperature rise).

3. Radiation-Ablation Shield

Even though it is known that radiation is the prime mode of energy dissipation for long duration glide vehicle re-entry for any protection system, it is necessary to investigate high-temperature ablative materials to determine the benefits (if any) of supplementing the radiation cooling by an ablation mechanism. Ablation mechanism involving phenomena of a rather complex nature and not always well understood, it was necessary to select the simplified model of surface ablation (Section II) to keep the parametric studies within practical limits and to determine the trends later to be compared with those for other systems. Using a model similar to that described for pure radiation systems except that the surface of the heat shield is assumed to recede at a constant temperature, the equations based on weight rather than thickness are:

$$\frac{\partial T}{\partial\left(\frac{\rho k t}{C_p}\right)} = \frac{\partial^2 T}{\partial W_x^2} \; ; \quad \rho s = W_A < W_x < W_T \quad . \tag{30}$$

At the ablating surface $W_x = W_A$,

$$-k\rho \frac{\partial T}{\partial W_x} = q_c(t)\left[1 - \frac{h_w/RT_o}{H_e/RT_o}\right] - \sigma\epsilon T^4 - \dot{W}_A F \quad , \tag{31}$$

where

$$\rho \dot{s} = \dot{W}_A = 0 \text{ for } T(W_A,t) < T_A = \text{constant} \quad ,$$

$$\rho \dot{s} = \dot{W}_A \geq 0 \text{ for } T(W_A,t) = T_A = \text{constant} \quad .$$

At the cold surface $W_x = W_T$,

$$\frac{\partial T}{\partial W_x} = 0 \text{ (perfectly insulated)} \quad . \tag{32}$$

Again the initial temperature is constant at T_i.

$$T(W_x,0) = T_i \quad . \tag{33}$$

In the above equations $\dot{W}_A$ is the mass ablation rate, and F is the amount of heat absorbed by one pound of the ablating shield. It includes blowing (transpiration) effects, but excludes the sensible heat ($C_p[T_A - T_i]$). All of the radiation shield parameters still appear; however, the ablation temperature and F are added. Graphical correlation of an ablation thermal protection system for a fixed vehicle trajectory based on the above model would involve plotting the effect of ρk, C_p, T_A, and F on both the total required weight and the weight loss due to phase change. It is noted also that the above equations do not maintain a relationship between weight and the lumped properties $\rho k / C_p$. However, as a result of the concurrently developed computational methods (Section III C) a modification of the above model may be made to result in good agreement with total weight as determined using equations (30) to (33). This modification is made to the boundary condition at the heated surface by replacing the conducted heat by its steady state equivalent $\dot{W}_A C_p (T_A - T_i)$, the rate at which sensible heat of the shield is lost by ablation. With this the equations become:

$$\frac{\partial T}{\partial\left(\frac{\rho k t}{C_p}\right)} = \frac{\partial^2 T}{\partial W_x^2} \; ; \quad \rho s = W_A < W_x < W_T, \; t > 0 \quad . \tag{34}$$

At the heated surface $W_x = W_A$,

$$q_c(t)\left[1 - \frac{h_w/RT_o}{H_e/RT_o}\right] - \sigma \epsilon T^4 = \dot{W}_A \left[C_p (T_A - T_i) + F\right] = \dot{W}_A \, q^*_{or} \quad , \tag{35}$$

where

$$\rho \dot{s} = \dot{W}_A = 0 \text{ for } T(W_A,t) < T_A = \text{constant} \quad ,$$

$$\rho \dot{s} = \dot{W}_A \geq 0 \text{ for } T(W_A,t) = T_A = \text{constant} \quad .$$

At the backface $W_x = W_T$,

$$\frac{\partial T}{\partial W_x} = 0 \text{ (perfectly insulated).} \tag{36}$$

The initial temperature is constant, i.e.,

$$T(W_x,0) = T_i = \text{constant} \quad . \tag{37}$$

In the modified model, the ablation rate $\dot{W}_A$ is computed based on instantaneous steady state but the conduction within the heat shield is calculated transiently. Also the parameter $\rho k/C_p$ is preserved as a common element to previously discussed non-ablating systems.

The parametric weight studies may be thus carried out and graphically presented in terms of $\rho k/C_p$, ϵ, T_A, and q^* for a fixed vehicle trajectory and design backface temperature limits, ΔT_R.

The assumptions made in constructing the above model were necessary for practical reasons, as otherwise the parametric study would be near impossible to carry out. To consider variable thermal properties k, ρ, and C_p, even for simple linear variations, would result in data generation for beyond the means of this program and at that it is doubtful that it would serve any valuable purpose. The properties used then are considered to be mean properties for the range of temperature variation expected. The above holds true for the assumption of a constant ablation temperature. Even though numerical computer programs are available (and are recommended for final design) including variable ablation temperature (as well as thermal properties), parametric studies could not be carried out on large scale since computer costs would be excessive. A constant mean ablation temperature was shown to be a fair approximation in reference 10 and in many cases the change during the ablation period is relatively small. It was also found that calculation could be made assuming an average value of q^* to result in total weight predictions agreeing well with calculations using a variable q^*. As explained below in greater detail (see discussion of approximate methods) best agreement was obtained by choosing q^* at the midpoint of the ablation period.

As used in this study of parameter significance, ablation is restricted to mass loss by surface recession, i.e., ablation is assumed to be a surface phenomenon. Some materials presently considered for re-entry heat shields undergo internal chemical reactions when heated (Ref. 53) and the applicability of this study to such materials has to be established by additional comparisons. This parametric study is intended as first approximation (or screening) tool for determination of the most important parameters; the results of the experimental program (below) indicate that it is, although conservative estimates are being obtained.

4. Radiation-Ablation with Backface Cooling

The backface cooling was incorporated into the radiation-ablation shield model in the same manner as in the radiation systems. The equations based on weight follow directly from the preceding discussions and are:

$$\frac{\partial T}{\partial\left(\frac{\rho k t}{C_p}\right)} = \frac{\partial^2 T}{\partial W_x^2} \quad ; \quad \rho s = W_A < W_x < W_T, \; t > 0 \quad . \tag{38}$$

At the ablating surface $W_x = W_A$,

$$q_c(t)\left[1 - \frac{h_w/RT_o}{H_e/RT_o}\right] - \sigma\epsilon T^4 = \dot{W}_A \, q^*_{or} \quad , \tag{39}$$

where

$$\rho\dot{s} = \dot{W}_A = 0 \text{ for } T(W_A,0) < T_A = \text{constant} \quad ,$$

$$\rho\dot{s} = \dot{W}_A \geq 0 \text{ for } T(W_A,0) = T_A = \text{constant} \quad ,$$

and at the cold surface it is assumed the cooling package with an effective heat of vaporization is absorbing the heat conducted through the shield, i.e.,

$$\left(\frac{\rho k}{C_p}\right)\frac{\partial T}{\partial W_x} = \dot{W}_c\left(\frac{H_c}{C_p}\right) . \tag{40}$$

All assumptions made for the previous ablation model hold here except at the backface. As in the other models no external or internal structures are included since the effect of structure may be included by methods applied to the radiation shield. Note should be taken that the backface is assumed to experience no temperature rise while in practice some change

will occur. This assumption was investigated as in the case of the radiation shield and it was found to be justified for the ΔT_R range of interest.

Parametric studies should be thus conducted to give the total weight as a function of $\rho k/C_p$, ϵ, q^*, T_A, and H_c/C_p for fixed vehicle trajectory and design criteria considered.

5. Thermostructural Criteria

The backface temperature T_b was utilized in the above analysis of parametric relations for the four shields since it affects directly their thermal performance and provides a good link for the design and analysis of the overall thermal protection system. The latter design depending on the mechanical performance of the shield and the load carrying member may not necessarily employ an optimized shield design. The overall system thermostructural design requires the definition of problems arising in the design, the basic relations of the parameters for their solution, and the analysis of basic geometrical configurations associated with the systems considered.

a. Definition of Problems

In the course of the analysis, extremely complex problems have to be solved. For the purposes of this report, it would not be possible nor desirable to cover them all in detail. Instead, they will be briefly outlined and illustrated while the significant parameters and design criteria will be brought out. In the analysis, the problem is defined by:

1) Geometrical configuration, i.e., contour and thickness,

2) Environments, such as aerodynamic loads, temperature componentry, loads, and structure,

3) Materials and their application in the structure for carrying or transmitting the loads. For example:

a) Is the heat-shield material isotropic or anisotropic and what is its mechanical and thermal expansion properties in the principal directions at a specified time? What is the strain rate of these materials?

b) A back-up structure, compatible with the heat shield, should be designed to carry whatever load the heat shield cannot. If the axial load is high, then higher longitudinal strength properties would be desired. Similarly, if the

lateral rotational symmetric load is dominating, then it may be desirable to have the mechanical properties higher in the circumferential direction.

4) Allowable stress and strain used to design vehicles. This would depend on the requirements for the performance of that particular portion of the vehicle. Some of the stress allowables would be:

a) The ultimate strength of the material. This could include any elastic, viscoelastic, and inelastic effects.

b) Buckling criterion, i.e., stress which corresponds to the maximum permissible deflection such as those that may occur in buckling deflections due to thermal or load environments.

c) Strain deflection and deformation criteria. This criteria will mean a deflection large enough to change the aerodynamic performance or strain incompatibility between back-up and heat shield.

Usually, based on the environments and material properties, the criteria in (4) define the method of analysis of various portions of the vehicle.

b. Vehicle Configurations

Representative design of three different type vehicles may be categorized for:

1) High heat flux type (ablator type),

2) Low heat flux type (ablator type),

3) Very low heat flux (glider type radiation, heat sink, and ablator combination).

Typical heat shield and back-up structure composition for the latter two will be briefly discussed.

1) Ballistic satellite capsule

An illustration of a ballistic satellite vehicle with low heat flux is given in figure 9. The shape is a multi-layer and multi-regional shell. The illustrated regions being formed are as follows:

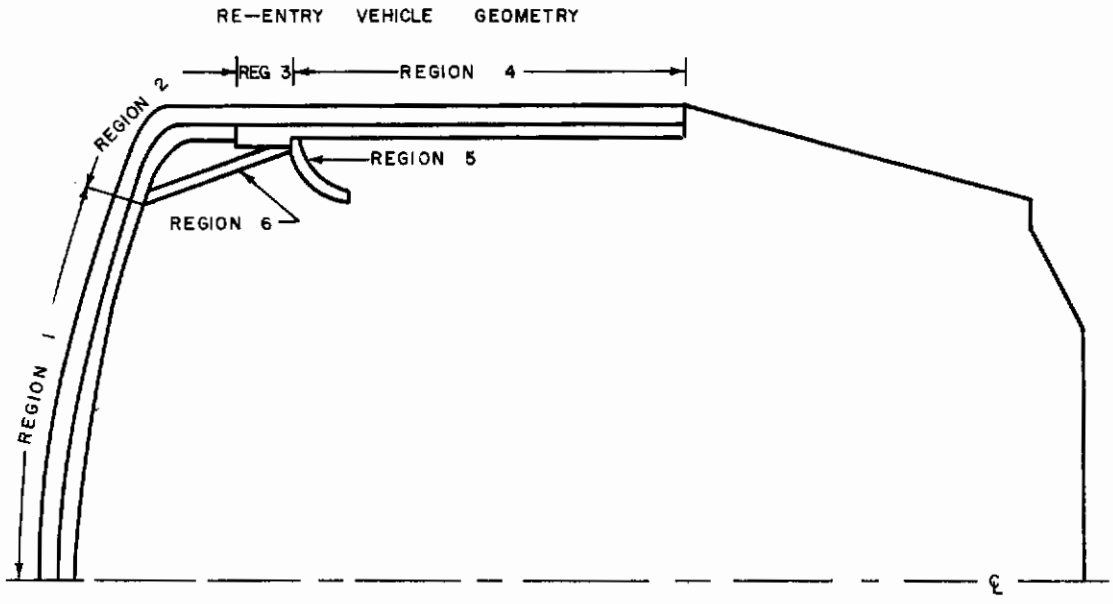

REGION	HEAT SHIELD	STRUCTURE	RADIUS
1	0.47 in.	0.170	81.0
2	1.37 in	0.040	6.00
3	0.42 in.	0.071	35.8
4	0.42 in.	0.071	35.8
5		0.103	
6		0.071	

Figure 9 RE-ENTRY VEHICLE GEOMETRY

a) Region 1, by shallow spherical shell,

b) Region 2, by toroidal shell,

c) Region 3, by short cylinder,

d) Region 4, by long cylinder,

e) Region 5, by ring stiffener, and

f) Region 6, by conical shell.

2) Geometry of vehicle of lift-winged variety

A typical re-entry glider vehicle may be considered as basically a delta-winged style aircraft modified for re-entry trajectories. It consists of a fuselage and full-length wing section that can be idealized into convenient geometries such as spheres, longitudinal sections of cylinders, and flat plate sections for purposes of performing the thermostructural analysis. The fuselage nose section and wing leading edges are the locations of maximum aerodynamic heating during the re-entry glide phase and are the regions of maximum concern for thermal protection. It may be assumed here that these regions are determined by a composite structure of heat shield and back-up structure combination.

The mathematical analysis of the above systems yielded significant material parameters affecting the weight. It permitted their grouping and minimized thus the number of interactions with environmental and design factors to be investigated in the course of the program. It became possible to reduce the radiative system study to manageable size even for a broad range of trajectory and structural conditions. However, it became equally obvious that the scope of studies of systems involving mass transfer could not compare with the former unless either correlation methods were improved, or simplified calculation procedures developed. In the former case, data from other regimes possible could be utilized or general relations established. In the latter, data could be generated more rapidly and economically. Both avenues of approach were explored.

B. CORRELATION METHODS

The need (and desires) for determination of simple relationships between the thermal protection system parameters, parallels those of simple experimental performance criterion. Conversely, the lack of simple correlations due to involved interactions indicates difficulties in the experimental areas.

A correlation method is required to conduct a broad systems performance study and an improvement in the graphic methods commonly used might permit extrapolation of available data from other regimes to those of interest here. The derivation of significant parameters in the preceding section by reduction of the number of potential parametric relations, made the graphic method acceptable. The cost and time element involved in the generation of the data for such correlation, however, is still prohibitive for large scale studies. The general correlation procedure adapted for use in the parametric studies for system evaluation is described below:

1. Performance Correlation

Based on the preceding studies, the relationship between cold wall heating (Q_c) and effective heat capacity (Q^*_{eff}) or weight (W) is established for the significant material parameters, typical environment, and backface condition for a given protection system. As a result, the most important material parameters are selected for further study of environmental and structural effects for each system. Typically best system (and materials associated with them) configurations are then compared for the flight corridor and structural concept selected for the application.

The outline of steps taken in such correlation follows:

1) Selection of vehicle application(s).

2) Selection of typical flight path for each application including typical heating distribution.

3) Selection of thermal protection system(s) for evaluation,

   a) Mode of protection,

   b) Materials (or working media),

      1 Study of effects of material parameter variation, or

      2 Study of typical materials behavior.

4) Study of gross effects of structural design criteria (heat capacity and temperature of the substructure used) including substructure cooling effects.

5) Selection of minimum number of vehicle applications.

6) Selection of typically best thermal protection systems for each application.

7) Selection of structural concept(s).

8) Evaluation of environmental effects on the shield-substructure composite including:

a) Flight regime (performance profile),

b) Body motion and geometry including shape change effects,

c) Cooling function (cabin or structure),

d) Reusability potential.

The specific steps taken for each thermal protection system, the parameters and the environmental and structural effects considered for them are described in the Application Performance Studies.

Two alternatives were considered to supply the information required for the outlined procedure. The first approach was to be based on relations established by dimensional analysis to be verified for other regimes. The second was to be based on data calculated by computer simulation of the application by either new or established methods and presented graphically.

2. Dimensional Analysis

Since the reviewed literature did not reveal any general non-graphic correlation method permitting quick system evaluation, and since the derivation of parameters of significance (proceeding concurrently) indicated that such a method would be needed as one of the alternatives for a systematic study of thermal protection, the dimensional analysis of the problem was attempted. This technique was successfully used in forced and natural convection heat transfer studies for correlation of many parameters and offered a logical avenue of approach. The differential equations describing heat sinks, radiation, and ablation shields were investigated to find the dimensionless groups involving material properties, design criteria, thermal environment, and thickness (or weight). Correlation formulae were then constructed as product solutions of the dimensionless groups to determine the maximum surface and backface temperature rise for a given set of material properties, heat flux, enthalpy, and weight of shield and structure. Solutions for radiative systems were investigated first since this mechanism is predominant in the regime of interest. Data from literature and those generated at Avco were used as inputs to the correlations. A typical correlation tried (see Appendix VIII for derivations) for a radiation shield and structure appears as:

$$\Delta T_r(\max) = \lambda \left[\frac{q_c^{(\max)} L}{k}\right]\left[\frac{\alpha Q_c}{L^2 q_c^{(\max)}}\right]^a \left[\frac{t_f - t_e\ q_c^{(\max)}}{Q_c}\right]^b \left[\bar{H}_e\right]^c \left[\bar{\epsilon}\right]^d \left[\frac{\rho_s C_s}{\rho C_s \ell}\right]^e , \qquad (41)$$

where

$\Delta T_r(\max)$ = the maximum structure (backface) temperature rise, °R,

λ, a, b, c, d, e = unknown constants to be determined,

$q_c(\max)$ = maximum cold wall heat transfer rate, Btu/ft^2-sec,

Q_c = integrated cold wall heat transfer rate, Btu/ft^2,

ρ = density of heat-shield surface material, lb/ft^3,

k = conductivity of heat-shield surface material, Btu/sec-ft-°R,

C_p = specific heat of heat-shield surface material, Btu/lb-°F,

ρ_s = density of substructure, lb/ft^3,

C_s = specific heat of substructure, Btu/lb-°R,

L = thickness of heat-shield surface material, ft,

ℓ = thickness of substructure, ft,

t_e = end of critical heating, sec,

t_f = impact time of the vehicle, sec,

$\bar{\epsilon} = \left(\frac{q_c^{(\max)} L}{k}\right)^3 \left(\frac{\sigma \epsilon L}{k}\right)$ = modified emissivity factor, dimensionless,

$\bar{H}_e = H_e/RT_o$ = dimension stagnation enthalpy,

RT_o = reference enthalphy = 33.86 Btu/lb.

The constants were evaluated and the correlation was tested by predicting temperatures for a broad range of re-entry environments, thermal properties,

and thickness. However, it was found after several attempts that the correlations tried would not predict accurately the system performance for a broad range of conditions. The technique was abandoned as not sufficiently reliable at the time, and not likely to be developed in the near future.

3. Graphic Presentation

Since the dimensional analysis approach did not prove to be fruitful even in the absence of mass transfer, the graphic correlation of performance was adopted. It was thought to be more advantageous as an alternative to the dimensional analysis to concentrate on development of simplified approximate methods for calculating the transient performance of thermal protection systems and using such data for graphic presentation according to the previously described procedure. The approximate calculation procedures (described below) were based to a great extent on the determination of the significant parameters established in the previous section.

C. ANALYTICAL AND COMPUTATIONAL TECHNIQUES

The integrated approach to the design and evaluation of a thermal protection system necessitates consideration of both thermal and structural aspects of the problem. The emphasis in this program is on the development of thermal aspects of the analysis while providing sufficient information on the structural analysis indispensable for efficient system design. Hence, the thermal analysis methods and techniques given in the body of the report account for structural effects on the thermal design, as well as provide thermal effect information necessary for structural analysis. For completeness of the picture the structural analysis methods and techniques required and used in thermal protection design are supplied in Appendixes VII, IX, X.

1. Radiation System

The first procedure described for calculating the total system weight applies to a single material used as a radiation shield. There are two reasons for first describing this system: 1) the assumptions developed for the simple radiation system apply to the other systems, 2) the procedures developed for other systems are based on modification or additions to the procedure used for a simple radiation shield.

The physical model of the thermal system is shown in figure 10. The shield is assumed to be a homogeneous material with constant thermophysical properties. These properties are assumed to be characteristic of a self-insulating radiation shield (i.e., low thermal conductivity and high surface emissivity) so that the primary means of thermal protection is by surface radiation and heating reduction by enthalpy correction due to the wall temperature. This system would also represent an ablation shield if the aerodynamic environment were not sufficiently severe

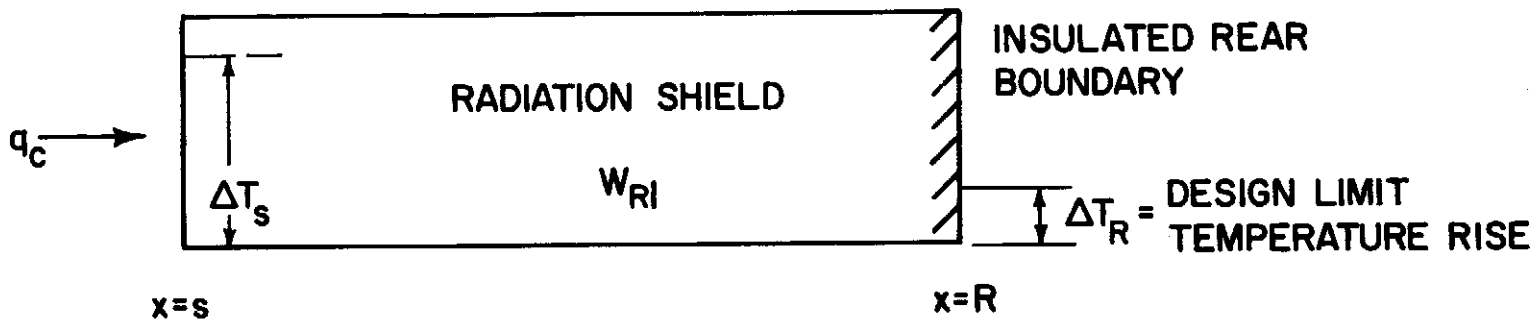

Figure 10 RADIATION SHIELD

for ablation to occur. The sinusoidal profile of aerodynamic heat input and decaying rate of the stagnation enthalpy as shown in figure 11 are representative for vehicles re-entering at circular velocity. It is assumed that a thermal protection system is required from a re-entry altitude of 300,000 feet until the termination of the trajectory.

For this type of re-entry environment, it is the hypothesis that the actual problem, which involves variable surface temperature, may be simulated by an equivalent problem involving a constant surface temperature which produces approximately the same transient history at the backface temperature. The analytical solution of the equivalent problem is known, and may be used to avoid the necessity for machine calculation. In order to use this solution, a series of assumptions is made which relates the conditions of the real environment to those satisfying the equivalent problem.

As shown in figure 10, the surface of the shield is located at $x = s$ and the rear of the shield at $x = R$. The surface $x = s$ is exposed to a transient cold wall heat rate, $q_c(t)$, and the surface $x = R$ is insulated. Let the enthalpy of the air at free stream and wall temperatures be H_g and h_w, respectively. H_g is given as some function of time, and a functional relation between h_w and the surface temperature, T_s, is given. The thermophysical properties k, ρ, C_p, and ϵ are constants, and t_f is the duration of the heat input as measured from 300,000 feet where t is arbitrarily chosen as zero and the temperature of the bar is some uniform value, T_s. It is required to find the total system weight, W^N required in order that the surface $x = R$ just reaches some specified design limits, T_R, occurring at t_R, during the interval $(t_f - t_i)$. Mathematically, the problem is to solve the following equation:

$$\frac{\partial T}{\partial t} = a \frac{\partial^2 T}{\partial x^2} \quad , \tag{42}$$

subject to the following initial and boundary conditions:

at $t = 0$,

$$T(x,o) = T_o \quad ; \tag{43}$$

at $x = s$,

$$q_c \left(1 - \frac{h_w}{H_g}\right) - \epsilon\sigma (T_s + 460)^4 = - \left(k \frac{\partial T}{\partial x}\right)_{x=s} \quad ; \tag{44}$$

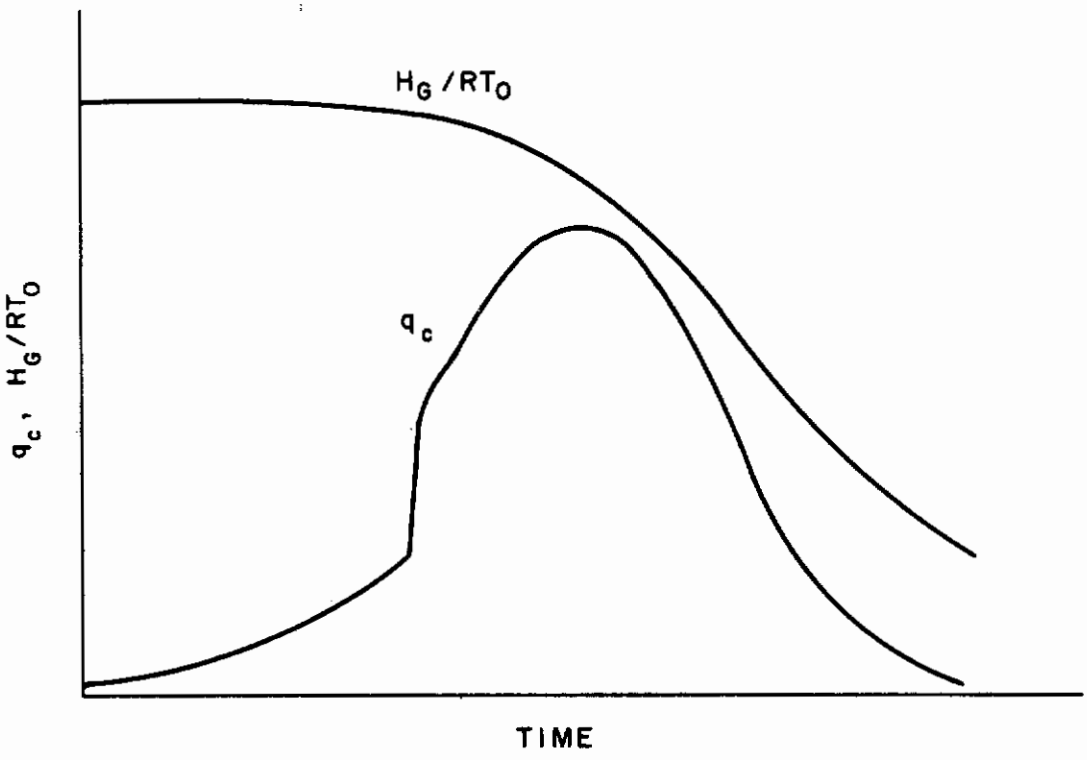

Figure 11 TYPICAL HEATING DATA AT A STATION OF A RE-ENTRY VEHICLE

at $x = R$,

$$\left(\frac{\partial T}{\partial x}\right)_{x=R} = 0 \quad . \tag{45}$$

The nonlinearities arising in the boundary condition will now be removed.

To do this, q_c is replaced by an equivalent heat rate, q_c' , which starts at an initial time, t_i , defined as

$$t_i = t_{q_c(max)} - \frac{2\int_{t_o}^{t_{q_c(max)}} q_c \, dt}{q_{c(max)}} \quad . \tag{46}$$

In equation (46), $q_{c(max)}$ is the maximum value which q_c achieves over the trajectory, and $t_{q_c(max)}$ is the time at which this maximum occurs. One condition placed on the transformation is that the total heat, Q_c , be the same for both pulses.

$$Q_c = \int_{t_i}^{t_f} q_c' \, dt = \int_{o}^{t_f} q_c \, dt \quad . \tag{47}$$

The variable enthalpy, H_g , is replaced by its time average, H_g' .

$$H_g' = \frac{1}{(t_f - t_i)} \int_{t_i}^{t_f} H_g \, dt \quad . \tag{48}$$

The equivalent heat rate q_c' is then chosen such that the rate of heat conduction into the bar is q_k .

$$q_c \left(1 - \frac{h_w'}{H_g'}\right) - \epsilon\sigma (T_s + 460)^4 = q_k \tag{49}$$

where q_k is such that a constant surface temperature results. As a consequence, the hot wall and emissivity corrections are independent of time, and the problem is linearized.

The problem is now one of finding the temperature response in a finite bar, one end of which is held at a constant temperature, the other end of which is insulated. The solution to this problem is given by Carslaw and Jaeger (Ref. 54):

$$\frac{\Delta T(x,t)}{\Delta T_s} = 1 - \frac{4}{\pi} \sum_{n=0}^{\infty} \frac{(-1)^n}{2n+1} \left\{ \exp\left[- \frac{(2n+1)^2 \pi^2 \alpha t}{4(R-s)^2} \right] \right\} \cos \frac{(2n+1)\pi(R-x)}{2(R-s)} \quad . \tag{50}$$

Integrating equation (49) over the time interval from t_i to t_R, where t_R is the time at which the backface reaches its design limit temperature, T_R, the total heat conducted into the material is found to be

$$Q_c \left(1 - \frac{h'_w}{H'_g} \right) - \epsilon\sigma (T_s + 460)^4 (t_R - t_i) = W C_p \Delta T_M \quad . \tag{51}$$

In equation (51), Q_c is given by equation (47) and the corrections $\left(1 - \frac{h'_w}{H'_g} \right)$ and $\epsilon\sigma(T_s + 460)^4$ are constants which are functions of the surface temperature T_s only. On the right-hand side of equation (51), W is the weight of the shield required to limit the backface temperature rise to the specified limit ΔT_R over the time interval $(t_R - t_i)$, and ΔT_M is the average temperature rise in the bar when these conditions are met.

At this instant, some unique value of $\frac{k\rho t}{C_p W^2}$ exists and there is a temperature distribution in the bar given by equation (50) from which ΔT_M could be calculated if t_R and T_s were known.

Consider first the case where the rear face reaches a maximum temperature (just equal to the design limit) at some time $t_R < t_f$ and subsequently falls below this value. In order for this to happen when using equation (50) the entire bar must have equilibrated at a uniform temperature T_R at time t_R. Hence, at this instant $T_s = T_R$. Furthermore, from equation (50), this condition corresponds very nearly to a value of unity for $\frac{k\rho t}{C_p W^2}$. Thus

$$W = \sqrt{\frac{\rho k}{C_p}} \sqrt{t_R - t_i} \tag{52}$$

Substituting equation (52) into equation (51) and solving for $\sqrt{t_R - t_i}$ gives

$$\sqrt{(t_R - t_i)} = \frac{\sqrt{\rho k C_p \Delta T_R^2 + 4\epsilon\sigma (T_R + 460)^4 Q_c (1 - h'_w/H'_g)}}{2\epsilon\sigma (T_R + 460)^4} - \frac{\Delta T_R \sqrt{\rho k C_p}}{2\epsilon\sigma (T_R + 460)^4} \quad (53)$$

Hence the required weight W can be obtained from equations (52) and (53).

Consider next the case where the design limit temperature is reached precisely at the instant t_f, and the bar subsequently reaches a much larger equilibrium value at time $t_R > t_f$. This case is the more probable of two conditions, since the average surface temperature experienced during reentry is much larger than the allowable backface temperature rise, $T_s >> T_R$. To solve for this condition by a hand calculation, an iteration procedure is required, since there are essentially two unknowns in equation (51), namely, T_s and W. Consequently, some choice must be made for a value of T_s to start the iteration. The following procedure involves the selection of different values of T_s until a convergence of equation (51) is obtained.

Since the primary means of protection is through surface radiation, assume for the first approximation, T'_s, that h'_w/H'_g and $WC_p\Delta T_R$ are both zero. Solution of equation (51) for T_s then gives the maximum possible value for T_s:

$$T'_s = 4\sqrt{\frac{Q_c}{\epsilon\sigma(t_f - t_i)}} - 460 \quad . \quad (54)$$

Knowing T'_s and T_R, the ratio $\frac{\Delta T_R}{\Delta T'_s}$ can be formed. To facilitate the iteration procedure, equation (50) was solved for the value of $\frac{\Delta T_R}{\Delta T_s}$; also $\frac{\Delta T_M}{\Delta T_s}$ was obtained by integration of $\frac{1}{\Delta x}\int \frac{\Delta T_x}{\Delta T_s} dx$, where $s \leq x \leq R$. These results are presented as a function of $\frac{k\rho t}{C_p W^2}$ in figure 12. For abbreviation, let

$$\sqrt{\frac{k\rho(t_f - t_i)}{C_p W^2}} = A \quad . \quad (55)$$

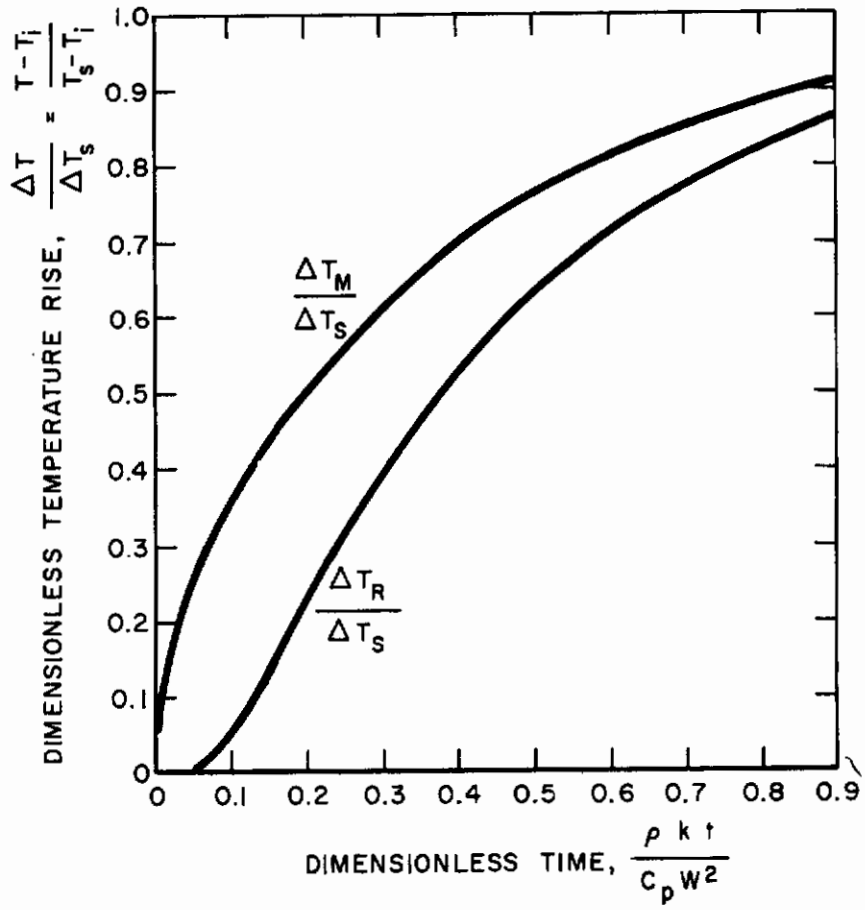

Figure 12 BACKFACE AND MEAN TEMPERATURE RISE IN A FINITE MEDIUM WITH A CONSTANT SURFACE TEMPERATURE (T_s) AND INSULATED REAR BOUNDARY

Then,

$$W' = \sqrt{\frac{k\rho\,(t_f - t_i)}{C_p A'}} \quad . \tag{56}$$

Equation (56) gives the maximum possible value for W. Using T_s' and the functional relation between h_w' and T_s', a hot-wall correction may now be applied to Q_c : $Q_c\left(1-\frac{h_w'}{H_g'}\right)$. This represents the minimum possible hot-wall input. Using this input and the first approximations W' and $\Delta T_M'$, a second approximation for T_s may be found from equation (51):

$$Q_c\left(1-\frac{h_w'}{H_g'}\right) - \epsilon\sigma\,(T_s'' + 460)^4\,(t_f - t_i) = W' C_p\,\Delta T_M' \quad . \tag{57}$$

Solving for T_s'',

$$T_s'' \sqrt[4]{\frac{Q_c\left(1-\frac{h_w'}{H_g'}\right) - W' C_p\,\Delta T_M'}{\epsilon\sigma\,(t_f - t_i)}} - 460 \quad . \tag{58}$$

Equation (58) gives a minimum value for T_s. The procedure is repeated by forming the new ratio $\Delta T_R/\Delta T_s''$ entering figure 12, and finding the new value of $A'' = \frac{k\rho(t_f - t_i)}{W''^2}$ to be solved for W'' and also the new value of $\frac{\Delta T_M''}{\Delta T_s''}$ to be used with A''' in solving for W'''. The process is repeated until a suitable convergence is obtained usually by the third iteration. The final weight found is designated as W^N. For the simple radiation shield, $W_{R1} = W^N$.

a. Composite Systems

This section describes three types of composite radiation systems. The results obtained for the homogeneous system are modified to include the thermal effect of (a) a structure at the rear surface of a radiation shield, (b) a hot radiating structure at the outer surface, and (c) a liquid-cooled shield.

1) Protected structure

The system being considered is shown in figure 13a. The problem is to find the weight W_{R1} of radiative shield required to guard a given structure whose weight W_{st} and properties are known, so that the structure will be limited to a specified temperature rise ΔT_R at the instant of impact, t_f .

Three assumptions are made to perform this calculation:

a) The structure is purely capacitive,

b) The total amount of thermal energy stored in the shield and structure is the same as that stored in a single radiative shield designed for the same backface temperature limit, and

c) The heat per unit mass stored in the radiation shield of the composite system is the same as the heat stored per unit mass in a single radiation shield designed to the same backface temperature limit.

As a consequence of the first assumption, the temperature of the structure is always uniform and the energy stored in the structure at impact is

$$Q_{st} = W_{st} C_{P_{st}} \Delta T_R \quad . \tag{59}$$

As a consequence of the second assumption, the total heat stored in the shield and structure of the composite system is equal to the heat stored in the pure radiation shield:

$$Q_{st} + Q_{R1} = Q^N = W^N C_p \Delta T_M^N \quad . \tag{60}$$

As a consequence of the third assumption, the required weight W_{R1} of the radiation shield portion of the composite system is

$$W_{R1} = W^N \frac{Q_{R1}}{Q^N} \quad . \tag{61}$$

Solving equation (60) for Q_{R1}/Q^N and substituting into (61), the required weight is found to be:

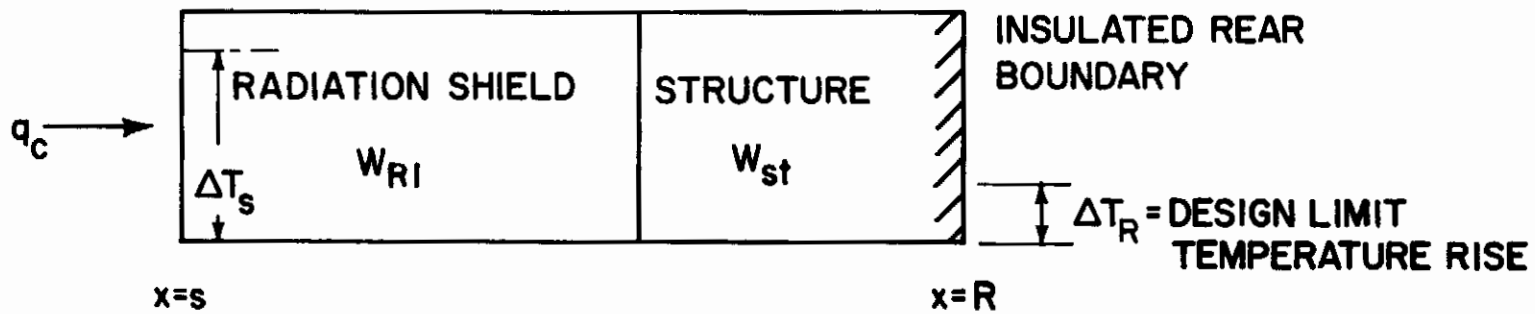

Figure 13a RADIATION SHIELD PLUS STRUCTURE

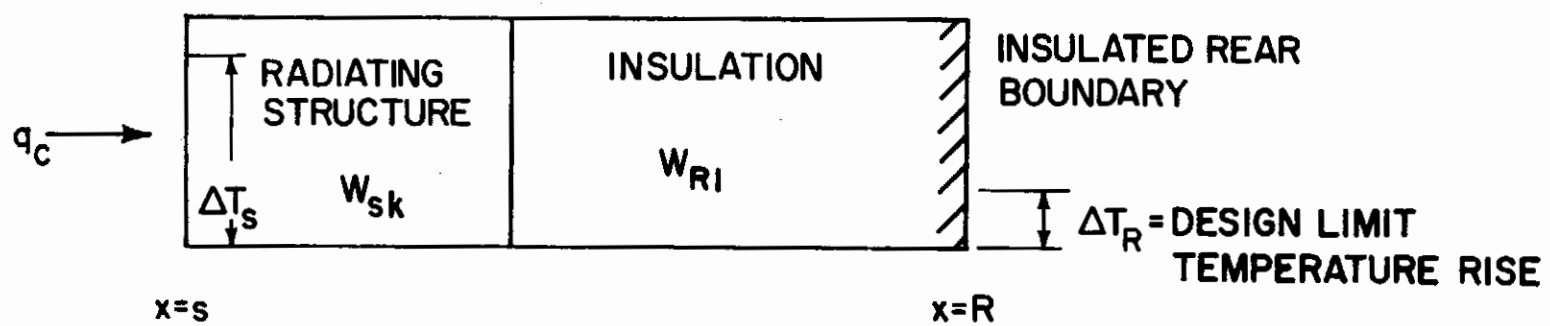

Figure 13b INSULATED HOT STRUCTURE

$$W_{R1} = W^N \left(1 - \frac{W_{st}\, C_{p_{st}}\, \Delta T_R}{W^N\, C_{p_{R1}}\, \Delta T_M^N}\right) . \tag{62}$$

2) Insulated hot structures

The inverse of the previous case is that of a hot structure acting as a radiation shield and backed by insulation, as shown in figure 13. The problem is to find the insulation weight W_{R1} required to limit the backface of the insulation to a maximum temperature rise of ΔT_R. The mass and properties of the structure are given.

If W_{R1} and W_{sk} are the weights of insulation and hot structure required to limit each of their respective backfaces to the same temperature rise ΔT_R for the same ΔT_s and time, then the $\frac{k\rho t}{C_p W^2}$ parameter of each of these materials is the same. Thus, the weight W_{R1} of insulation material equivalent thermally to a given weight of structural material is

$$W'_{R1} = W_{sk} \sqrt{\frac{(k\rho/C_p)_{R1}}{(k\rho/C_p)_{sk}}} . \tag{63}$$

In the problem under consideration, the total weight is the sum of the weight of insulation and hot structure:

$$W_{total} = W_{R1} + W_{sk} . \tag{64}$$

The problem is now converted into an equivalent one in which only the insulation material is used. The total weight of insulation alone required to limit the backface temperature rise to the specified value is W^N. This weight may be calculated by the procedure for simple radiation systems, using the emissivity of the hot structure instead of that of the insulation. The equivalent insulation weight of the hot structure is given by equation (63). Thus, solving equation (64) for W_{R1}, the required insulation weight of the system is found:

$$W_{R1} = W^N - W_{sk} \sqrt{\frac{(\rho k/C_p)_{R1}}{(\rho k/C_p)_{sk}}} . \tag{65}$$

3) Liquid-cooled shield

The thermal system as shown in figure 14 consists of an outer thickness of a high-temperature-resistant material and an inner layer of liquid. The purpose of the liquid is to act as a coolant for the structure by absorbing through vaporization the thermal energy flowing away from the surface of the radiation shield. The liquid coolant is assumed to be in perfect thermal contact with the shield and maintained at a uniform temperature (T_R). The thermal effect of the structure is accounted for by including its heat capacity with the effective heat capacity of the liquid coolant (H_c). This condition of a constant surface temperature along with a constant coolant temperature during the heating period allows the assumption that a portion of this period may be simulated by a steady-state condition. Therefore, the approximate heating is such as to maintain initially the surface of the shield (thermally insulated from coolant) at constant surface temperature until a time t_{ss}; thereafter, the shield and coolant are subject to a constant heating rate.

The time $(t_{ss} - t_i)$ required to reach a steady-state condition is assumed to be equivalent to the time required for the shield under transient conditions to achieve the same mean temperature ΔT_M as exists during steady state. From figure 11,

$$(t_{ss} - t_i) = f\left(\frac{\Delta T_M}{\Delta T_s}\right) = \frac{C_p W^2 A}{k\rho}. \tag{66}$$

During the steady-state period, the following equations and conditions exist:

$$\frac{\partial^2 T}{\partial x^2} = 0 \quad s < x < R \quad , \tag{67}$$

$$T(x,t) = T_s + (T_R - T_s)\,\frac{x-s}{R-s} \quad ; \tag{68}$$

at $x = s$

$$q_c\left(1 - \frac{h_w}{H_g}\right) - \sigma\epsilon\,(T_s + 460)^4 = -\left(k\,\frac{\partial T}{\partial x}\right)_{x=s} \quad , \tag{69}$$

$$q_c = \frac{Q_c}{t_f - t_i} \quad , \tag{70}$$

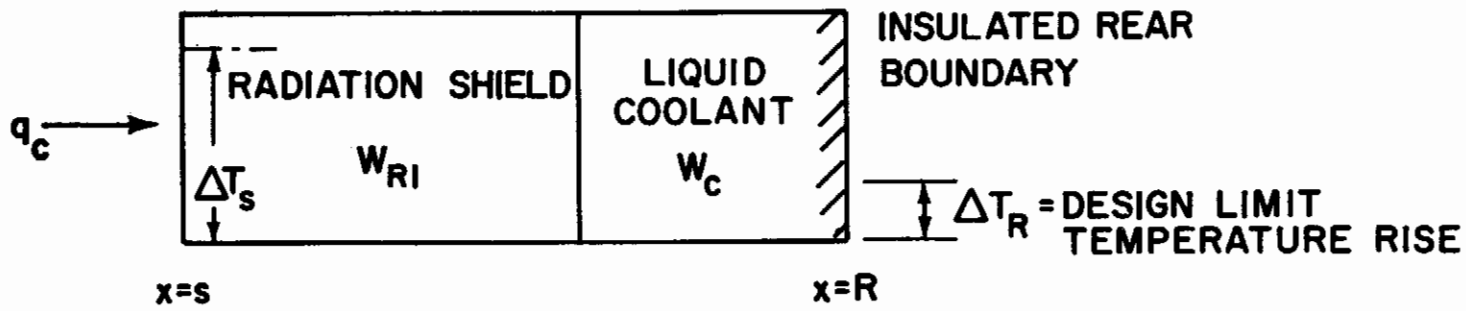

Figure 14 LIQUID-COOLED RADIATION SHIELD

$$-\left(k\,\frac{\partial T}{\partial x}\right)_{x=s} = -k\,\frac{T_s - T_R}{R-s}\,, \tag{71}$$

$$\left(\frac{\partial T}{\partial x}\right)_{x=R} = \left(\frac{\partial T}{\partial x}\right)_{x=s}\,. \tag{72}$$

The total system weight (W_T) required for the above conditions is given by the following equations:

Weight of the shield:

$$W_{R1} = \rho(R-s)\,. \tag{73}$$

Weight of the coolant:

$$W_c = \frac{k(T_s - T_R)}{H_c(R-s)}\left[(t_f - t_i) - \frac{(R-s)^2 A}{a}\right]\,. \tag{74}$$

Total system weight:

$$W_T = W_{R1} + W_c\,. \tag{75}$$

Solving equation (75) for the shield thickness which gives the minimum total weight,

$$\frac{\partial W_T}{\partial x_{R1}} = \rho - \frac{k(T_s - T_R)(t_f - t_i)}{H_c(R-s)^2} - \frac{k(T_s - T_R)A}{H_c a} = 0\,; \tag{76}$$

therefore,

$$R - s = \sqrt{\frac{k(T_s - T_R)(t_f - t_i)}{\rho H_c\left[1 - \dfrac{C_p A (T_s - T_R)}{H_c}\right]}}\,, \tag{77}$$

$$\frac{W_{R1}^2 C_p}{\rho k (t_f - t_i)} = \frac{C_p (T_s - T_R)}{H_c} \frac{1}{\left[1 - \frac{C_p A (T_s - T_R)}{H_c}\right]}, \tag{78a}$$

$$\frac{W_T^2 C_p}{\rho k (t_f - t_i)} = 4 \frac{C_p (T_s - T_R)}{H_c} \left[1 - \frac{C_p A (T_s - T_R)}{H_c}\right] . \tag{78b}$$

Equations (78a) and (78b) are plotted in figure 15 as a function of $\frac{H_c}{C_p (T_s - T_R)}$ and A. Since T_s and A are unknown, an iteration procedure is required for a solution. This procedure involves the selection of different values of the steady-state conduction flux until a convergence is obtained.

Assume, for the first approximation T_s' that the steady-state conduction flux is zero and solve equation (69) for T_s'. Knowing T_s' and T_R, the ratio of $\frac{\Delta T_M}{\Delta T_s'}$ can be formed and the value of the duration term A can be obtained from figure 11. Figure 13 may then be used to find the value of W_{R1}' corresponding to the values of T_s' and A.

Solving for the steady-state flux using T_s' and W', a second approximation for T_s may be found from equation (69). The procedure may be repeated by forming the new ratio $\frac{\Delta T_M}{\Delta T_s''}$ and solving for the corresponding values of A'' and W_{R1}''.

Since T_s' is the maximum possible value and T_s'' the minimum value, a convergence of the solution is assured. To facilitate the solution of the equation for the value of T_s, figure 16 was plotted to yield design charts of T_s as a function of the steady-state heating rate q_c, conduction flux $\rho k \frac{(T_s - T_R)}{W_{R1}}$, and H/RT_o.

As indicated in figure 16, the effect of the conduction flux on the surface temperature is negligible for shield materials with low ρk products, and the first approximation of T_s is sufficient, being within 5 percent of the final value.

2. Ablation System

The system as shown in figure 17 is composed of a single material, satisfying both insulation and ablation requirements. The term "ablation," as

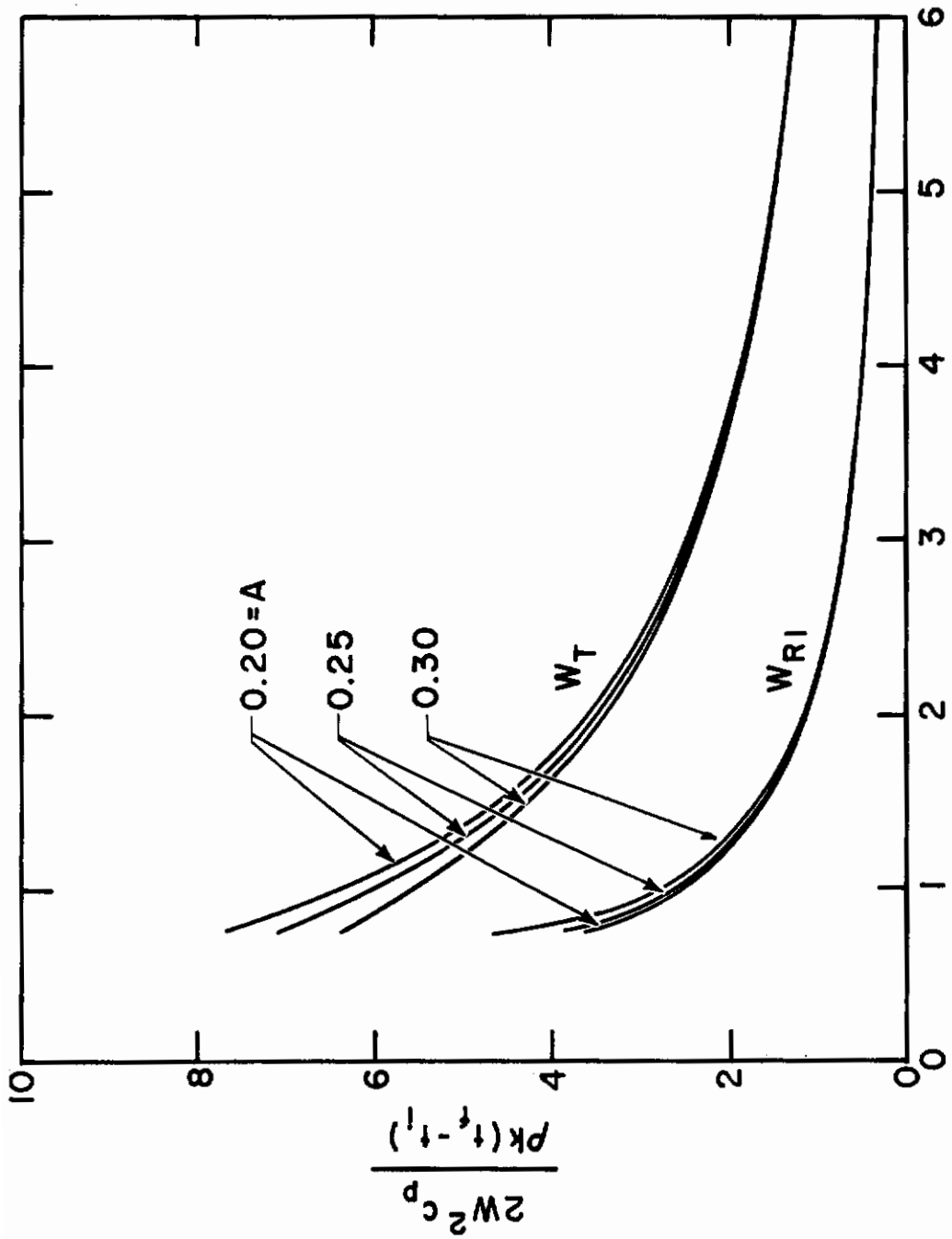

Figure 15 REQUIRED WEIGHT FOR A LIQUID-COOLED RADIATION SHIELD

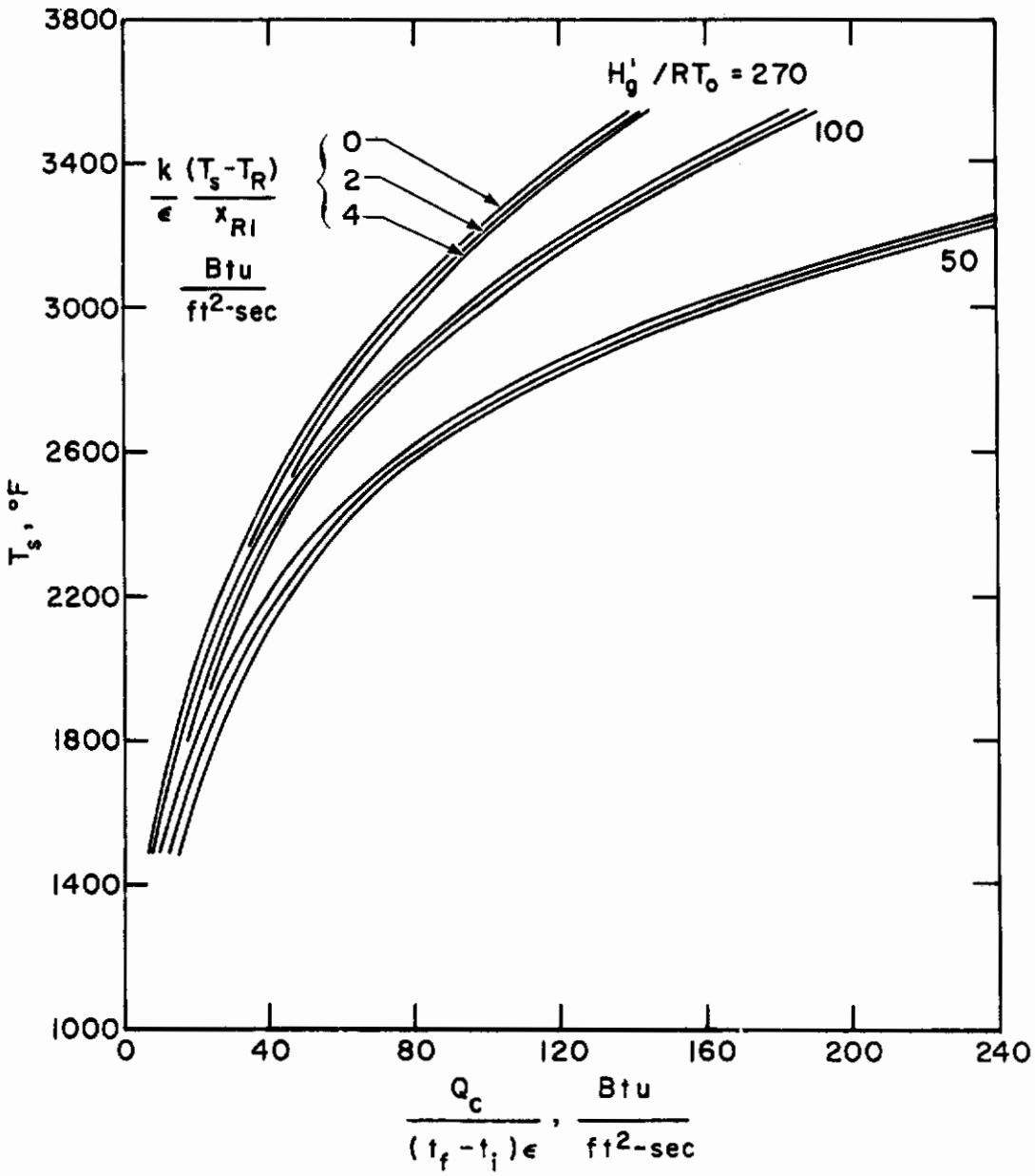

Figure 16 STEADY-STATE ENERGY BALANCE

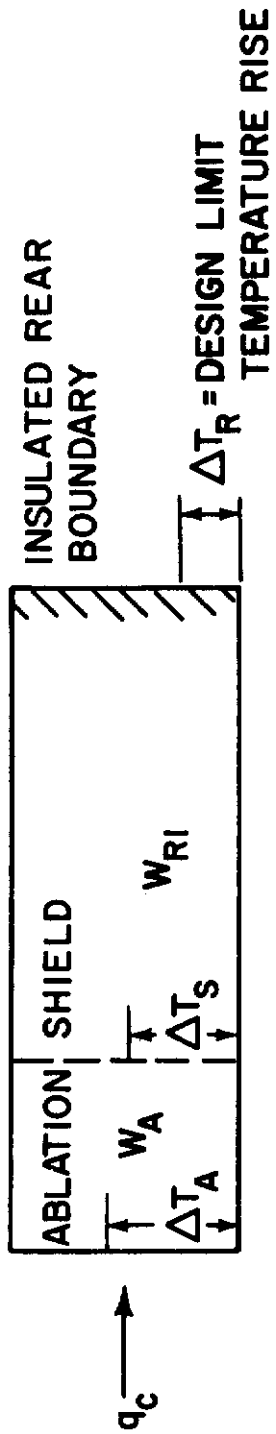

Figure 17 SIMPLE ABLATION SHIELD

used here, may be described as the surface recession of a material due to the absorption of heat through a phase change of degradation reaction.

The approximate computation procedure for an ablation system is divided into two sections: the ablation weight and insulation weight calculations.

a. Ablation Weight

Using the same heat input and air enthalpy as illustrated in figure 10, it is assumed that when the heat rate reaches some value at time t_{ia} the material begins to ablate with a constant surface temperature T_A. An instantaneous heat balance at the surface of the material is then

$$q_c \left(1 - \frac{h_w}{H_g}\right) - \epsilon\sigma (T_A + 460)^4 = - \left(k \frac{\partial T}{\partial x}\right)_{x=s} + \dot{W}_A (q^* - C_p \Delta T_A) \quad . \tag{79}$$

At any instant t_{ia} just prior to the onset of ablation (and just subsequent to its termination t_{fa}), $\dot{W}_A = 0$. An estimate of t_{ia} and t_{fa} can be made by setting $-\left(k \frac{\partial T}{\partial x}\right)_{x=s} = 0$ and picking some reasonable value for H_g; the value chosen is that existing at peak heating. For such conditions, t_{ia} and t_{fa} may be found from the given q_c versus time relation at those points where

$$q_c = \frac{\epsilon\sigma (T_A + 460)^4}{(1 - h_w/H_g)} \quad . \tag{80}$$

As t_{ia} approaches $t_{q_{c(max)}}$ the maximum surface temperature will just reach the ablation temperature and then decrease. Under these conditions equation (80) may be improved by deriving another expression which accounts for the amount of heat conducted into the solid. The expression may then be used to determine the level of cold-wall heat flux needed to cause ablation or the limiting cold-wall heat flux that a radiation shield can withstand without exceeding some prescribed design limiting surface temperature.

For a radiation shield it can be assumed that the effective heat flux and surface temperature reach their maximum values simultaneously with the maximum cold-wall aerodynamic heat rate. At peak heating the instantaneous heat balance at the surface with no ablation is

$$q_{c(max)} = \frac{\left(-k \left.\frac{\partial T}{\partial x}\right|_{x=s} \right)_{max} + \epsilon\sigma (T_A + 460)^4}{1 - h_w/H_g \text{ peak heating}} \quad . \tag{81}$$

The maximum effective heat flux may be approximated by assuming that the shape of the effective heat flux history is sinusoidal of the form

$$-k \left.\frac{\partial T}{\partial x}\right|_{x=s} = q_{eff(max)} \sin^2 \left(\frac{\pi t}{2 \left[t_{q_c(max)} - t_i \right]} \right) , \tag{82}$$

where $t_{q_c(max)}$ and t_i are as defined in equation (46).

Solving the one-dimensional heat conduction equation with equation (82) as a boundary condition and assuming the slab is essentially semi-infinite gives the following relationship between the surface temperature T_s at peak heating and the maximum effective flux (Ref. 55):

$$\left(-k \left.\frac{\partial T}{\partial x}\right|_{x=s} \right)_{max} = 1.82 \sqrt{\frac{k\rho c}{2 \left[t_{q_c(max)} - t_i \right]}} \; \Delta T_s \quad . \tag{83}$$

Putting equation (83) into (81) results in a relationship between the maximum surface temperature and maximum cold-wall heat flux, given as:

$$q_{c(max)} = \frac{1.82 \sqrt{\frac{k\rho c}{2 \left[t_{q_c(max)} - t_i \right]}} \; \Delta T_s + \epsilon\sigma (T_s + 460)^4}{\left(1 - \frac{h_w}{H_g} \right)_{\text{peak heating}}} \quad . \tag{84}$$

As stated above, equation (84) will determine whether ablation will occur for a given value of $q_{c(max)}$. For $t_{ia} < t_{q(max)}$,

$$Q_A = \left(1 - \frac{h_w}{H_g} \right) \int_{t_{ia}}^{t_{fa}} q_c \, dt - \epsilon\sigma (T_A + 460)^4 (t_{fa} - t_{ia}) \quad , \tag{85}$$

where, as before, h_w corresponds to T_A, and H_g is that existing at peak heating. The corresponding ablation weight loss W_A is found by assuming that a steady-state condition exists (Ref. 56):

$$W_A = \frac{Q_A}{q^*} \quad , \tag{86}$$

where the usual definition of q^* is used:

$$q^* = C_p \Delta T_A + f [H_A + \eta (H_g - h_w)] \quad . \tag{87}$$

In this definition, C_p, ΔT_A, f, H_A, and η are given, h_w corresponds to T_A, and best agreement with computer runs was obtained by choosing the H_g at the midpoint, $1/2\ (t_{fa} - t_{ia}\ )$, of the ablation period.

b. Insulation Weight

The heat stored in the material just at the instant the ablation ceases is

$$Q_k = W_{ins} C_p \Delta T_M \quad . \tag{88}$$

In equation (88), W_{ins} is the "insulation weight," i.e., the weight of the required heat shield after the ablation mass loss, and ΔT_M is the mean temperature of this insulation weight.

It is assumed that an exponential temperature distribution corresponding to average steady-state ablation rate exists in W_{ins} at the instant T_{fa}:

$$\Delta T\,(x, t_{fa}) = \Delta T_A\, e^{-\dot{s} x/\alpha} \quad . \tag{89}$$

For this distribution, the following expression can be obtained for Q_k:

$$Q_k = \rho C_p \int_0^\infty \Delta T \, dx = \frac{k \Delta T_s}{\dot{s}} \quad . \tag{90}$$

In this expression $\dot{s}$ is taken to be the average value during the ablation period:

$$\dot{s} = \frac{W_A}{\rho (t_{fa} - t_{ia})} \quad . \tag{91}$$

The mean temperature corresponding to a semi-infinite bar is obtained from the constant wall temperature chart (Fig. 11) for the parameter $\frac{k\rho t}{C_p W^2} = 0.05$. This yields:

$$\Delta T_M = 1/4\, \Delta T_s \quad . \tag{92}$$

Combining equations (88) through (92), the required insulation weight is found to be

$$W_{ins} = \frac{4\,(t_{fa} - t_{ia})}{W_A} \left(\frac{\rho k}{C_p}\right) \quad . \tag{93}$$

The insulation weight given by equation (93) is that corresponding to a barely noticeable backface temperature rise at the instant t_{fa} . The sum $(W_A + W_{ins})$ is not the total weight of shield required, since the heating from the end of ablation to impact has not been accounted for. The problem is to find the amount of insulation required such that the backface temperature rise does not exceed a given design value. During the post-ablation period, the problem is simply that of a radiation shield which starts (at time t_{fa}) with an initial temperature distribution. To use the procedure described for the radiation system, it is necessary to transform the time scale such that the problem "starts" at some "adjusted" time, t_{adj} , and runs thenceforth with some constant surface temperature, such that a temperature distribution corresponding to $\frac{k\rho t}{C_p W^2} = 0.05$ exists at t_{fa} and a backface temperature rise of ΔT_R is achieved. Using a value of $\frac{k\rho t}{C_p W^2} = 0.05$ and solving for t , the time required to establish the distribution corresponding to this value is found to be

$$t = \frac{0.05}{(\rho k/C_p)}\, W_{ins}^2 \quad . \tag{94}$$

Using equation (93) for W_{ins} , the following expression is obtained:

$$t = \frac{4}{5}\left(\frac{\rho k}{C_p}\right)\left(\frac{t_{fa} - t_{ia}}{W_A}\right)^2 \quad . \tag{95}$$

Relating this to the time scale used in the problem, the "adjusted" time t_{adj} is found to be

$$t_{adj} = t_{fa} - \frac{4}{5}\left(\frac{\rho k}{C_p}\right)\left(\frac{t_{fa} - t_{ia}}{W_A}\right)^2 \quad , \tag{96}$$

where $t_{adj} \geq t_i$, and t_i is as defined by equation (46). The total heat Q_c applied to the bar during the adjusted heating period is

$$Q_c' = \int_{t_{adj}}^{t_f} q_c \, dt - Q_A \qquad \text{if } t_{adj} \leq t_{ia} \quad ,$$

$$Q_c' = \int_{t_{adj}}^{t_f} q_c dt - \frac{Q_A (t_{fa} - t_{adj})}{(t_{fa} - t_{ia})} \quad \text{if } t_{adj} \geq t_{ia} \quad . \tag{97}$$

The first part of this expression is the integrated cold-wall heat applied to the bar, and the second term is the heat absorbed by ablation after t_{adj}.

The additional weight of material, W^N, required to achieve the design limit temperature rise ΔT_R at the backface at impact is calculated by the procedure described for radiation, using Q_c' in place of Q_c, and t_{adj} in place of t_i in equations (54) through (58). The total weight of shield required, W_T, is then the sum of W_A and W^N:

$$W_T = W_A + W^N \quad . \tag{98}$$

Thus, the ablation shield computation procedure may readily be extended to a composite structure and liquid cooling.

3. Comparison with Known Solutions

This section is concerned with the validation of the assumptions and approximations described in the preceding discussion. Since each assumption cannot be justified by mathematical rigor, the gross effect of the assumptions will be demonstrated by comparison with known solutions.

a. Analytical Comparison

Exact solutions are not available for either a radiation or ablation shield subject to a transient heat flux such as that experienced during

re-entry. Therefore, only a limited comparison is made, with an analytical solution for a heat sink protective system. The solution is for the transient temperature in finite homogeneous material. The exposed surface is subject to a sinusoidal time-varying heat flux and the thermal effects of the surface enthalpy and radiation are neglected. To make a comparison, equation (51) is modified by eliminating the enthalpy and radiation term. Thus equation (51) reduces to

$$Q_c = \mathbb{W} C_p \Delta T_M = Q_k \quad . \tag{99}$$

If instead of $\mathbb{W}$, the value of ΔT_R is assumed unknown, then from figure 11 the values of T_s and T_R may be obtained, corresponding to the value of ΔT_M from equation (99) and of $(k\rho/C_p)\frac{t}{\mathbb{W}^2}$. Therefore, by using the same total heat input (Q_c) and duration (t) a direct comparison can be made between the backface temperature resulting from a sinusoidal flux and a flux producing a constant surface temperature. The result of such a comparison is presented in figure 18, shown as the percent difference in weight required as a function of the ratio $\frac{k\rho t}{C_p \mathbb{W}^2}$. Although this represents an accurate comparison for a heat sink, it does not indicate the effect on the accuracy of the method if the enthalpy and radiation terms are included. Since these terms tend to reduce the conduction flux, and shift it closer to that of the constant temperature, it is possible that the accuracy of the method will improve when these terms are included.

b. Numerical Comparison

The numerical solution used for making the comparisons solves the actual transient problem by means of difference equations, implicit in time and central in space. A description of this solution and an analysis of its accuracy are reported in references 4, 13, and 14.

Employing the same boundary and initial conditions as described for the approximate method, numerical results were obtained for two types of radiation systems and an ablation system. These systems were exposed to a transient heating environment of a glide re-entry trajectory. Using the numerical results as a reference, the percent difference in weight as calculated by the two solutions was computed as a function of the thermal properties and rear surface temperature rise.

The results of this comparison are shown in figures 19, 20, and 21 for the single material radiation shield, liquid-cooled radiation shield, and

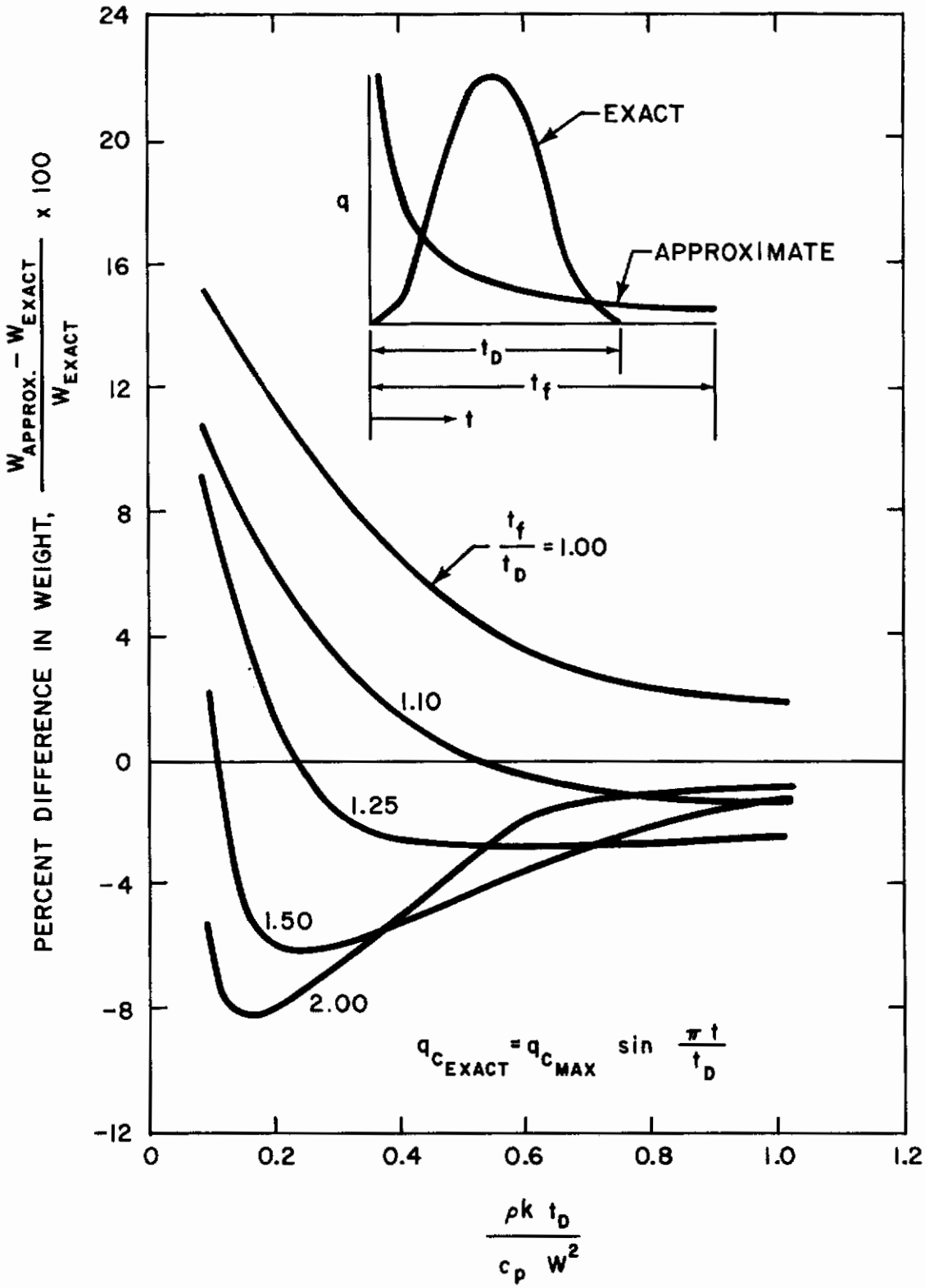

Figure 18 COMPARISON OF HEAT-SINK WEIGHT PREDICTED BY APPROXIMATE AND ANALYTICAL SOLUTION

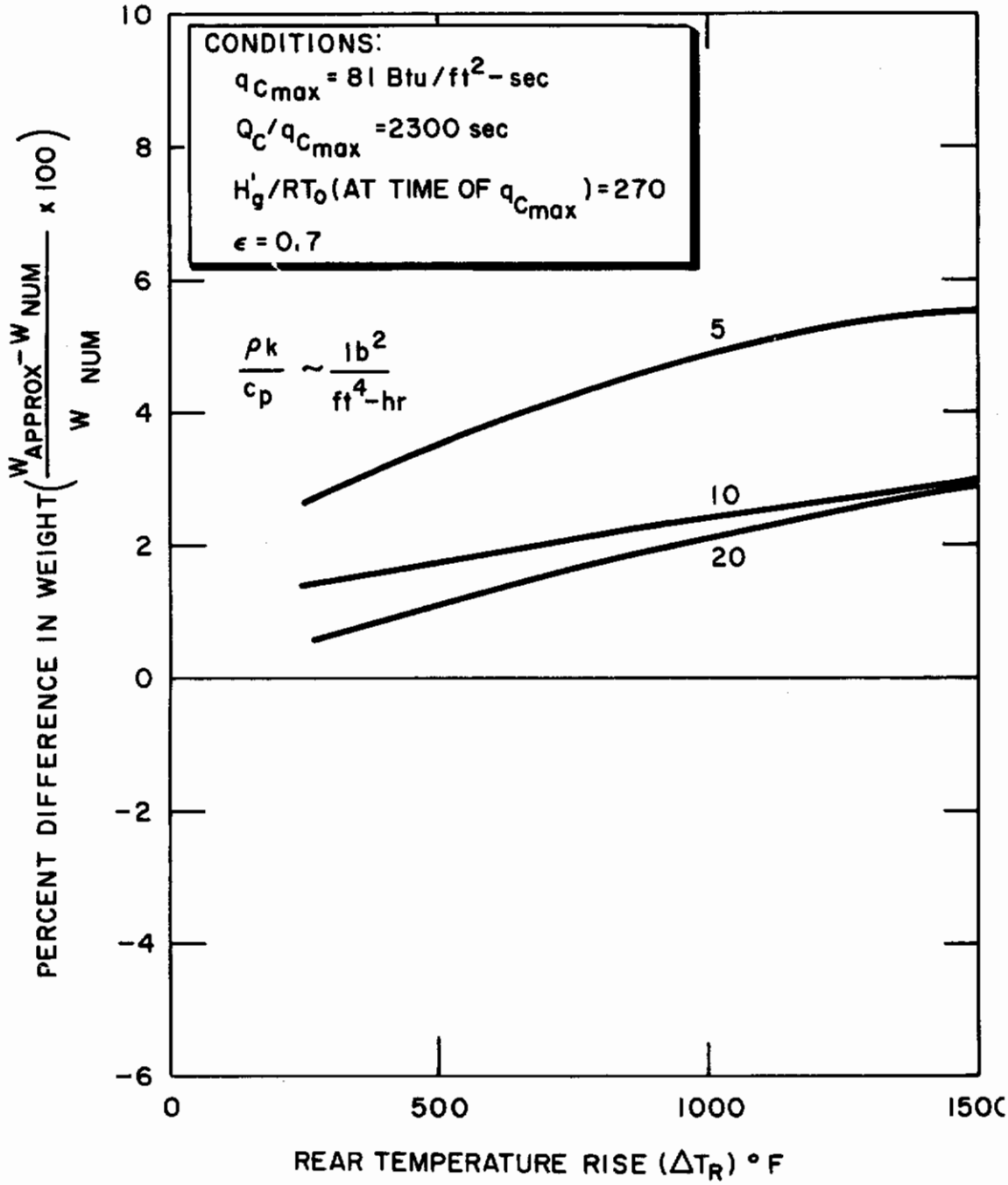

Figure 19 COMPARISON OF RADIATION SHIELD WEIGHTS PREDICTED BY APPROXIMATE AND NUMERICAL SOLUTION

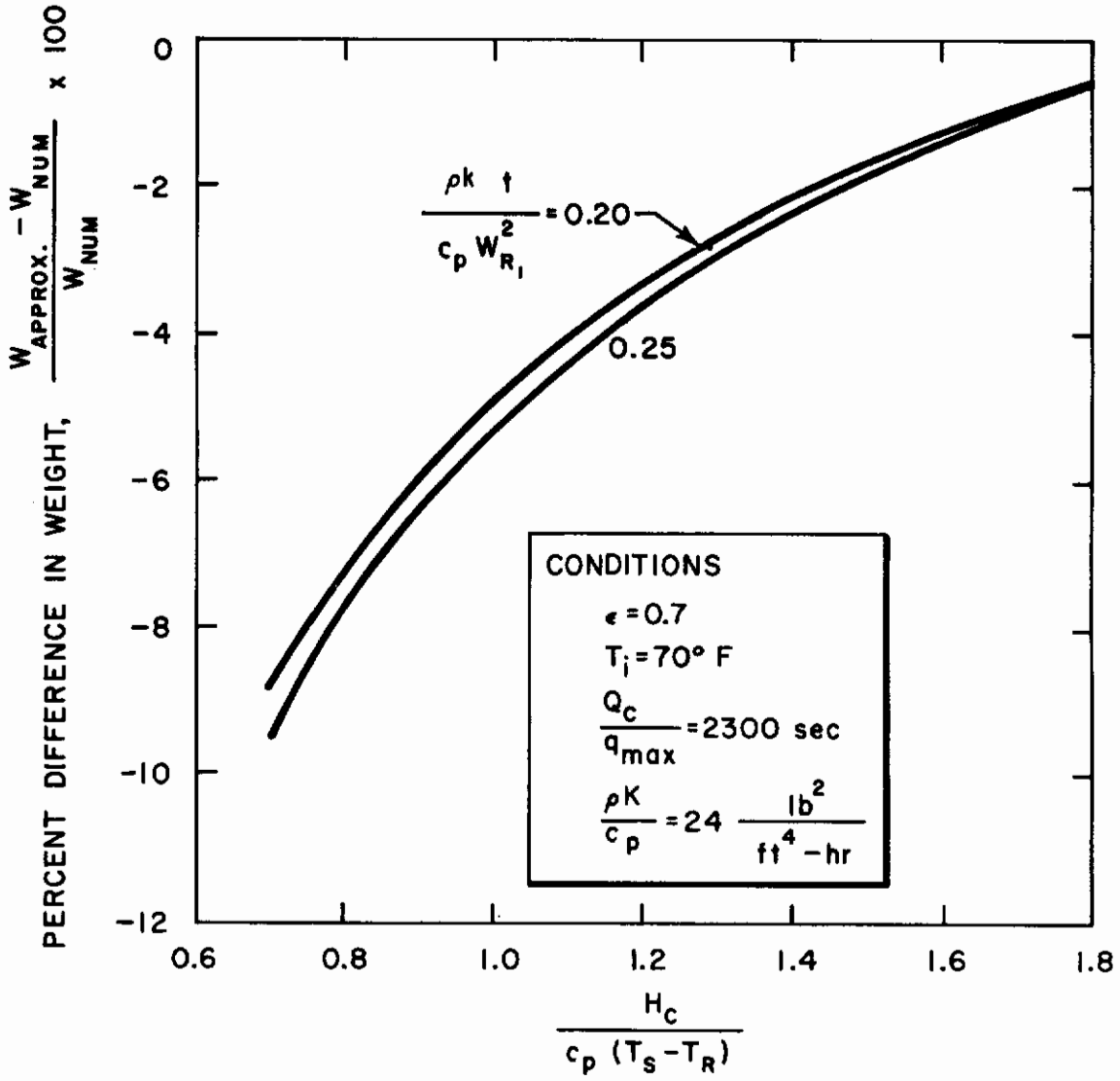

Figure 20 COMPARISON OF LIQUID-COOLED RADIATION SHIELD WEIGHTS PREDICTED BY APPROXIMATE AND NUMERICAL SOLUTION

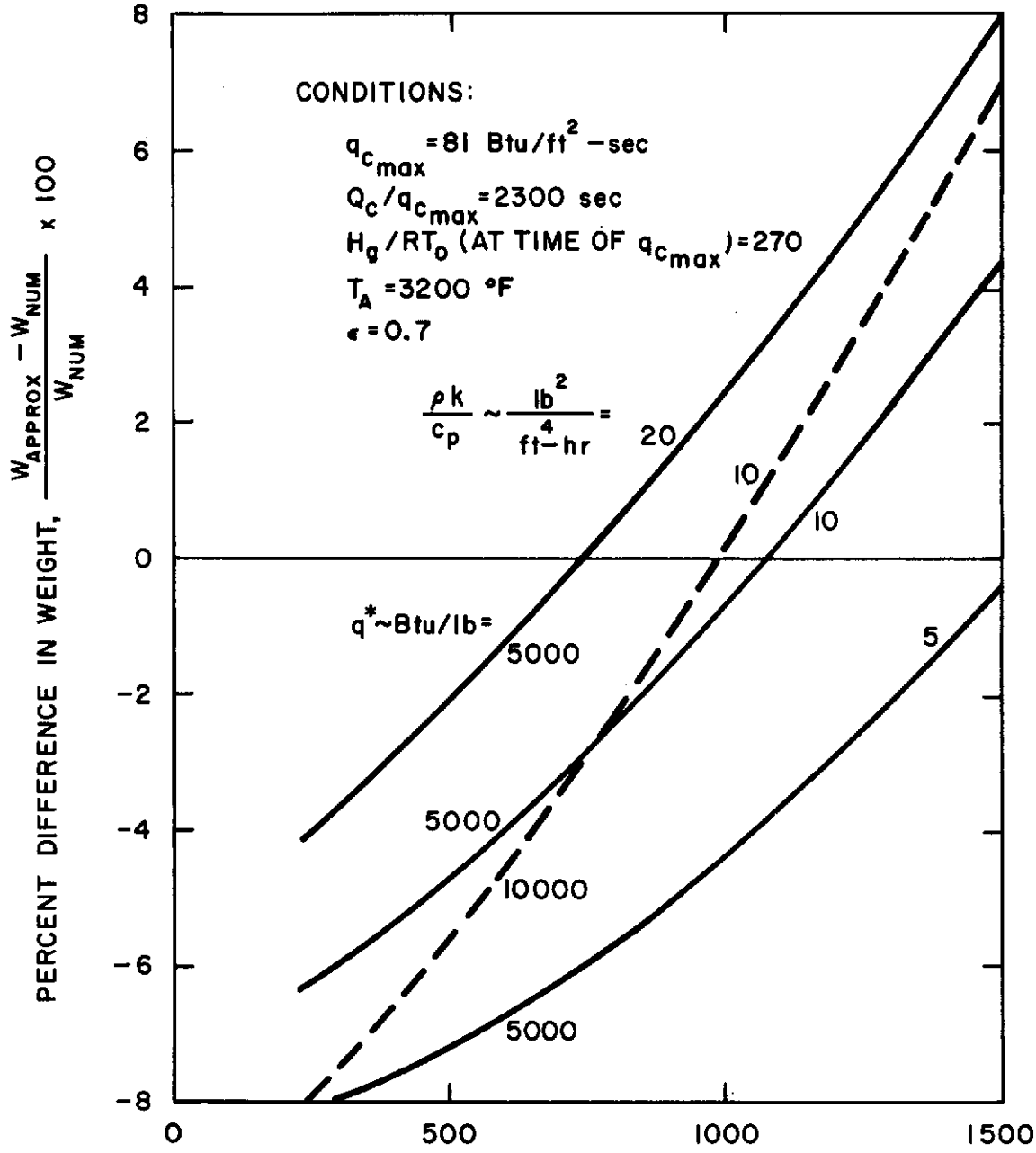

Figure 21 COMPARISON OF ABLATION SHIELD WEIGHTS PREDICTED BY APPROXIMATE AND NUMERICAL SOLUTION

ablation shield, respectively. For the range of parameters investigated for the three systems, the maximum difference in weight as calculated by the two solutions is 9 percent, while the average difference is 4 percent. The accuracy of the approximate method as applied to the three systems is shown to improve as values of the following thermal parameters decrease:

$$T_R/T_s \ , \ \frac{C_p (T_s - T_R)}{H_c} \ , \ \text{and } q^* \ .$$

These comparisons clearly indicate that the various assumptions involved in the approximate method do not significantly affect the required weight of the thermal protection system. Since only a limited comparison is made, no general rule for accuracy can be made concerning other re-entry trajectories and thermal properties. However, for other trajectories for which the method has been applied, the calculated weights were within 9 percent of the values obtained using a numerical solution.

4. Design and Evaluation Methods

The method described above is extremely useful in the system sizing, preliminary selection of materials, and design. Reference 3 provides similar ease in heat sink calculations. The final design requirements, however, often impose very stringent weight limitations and operating temperature limits, and the thermal stress analysis always depends on the calculation of the temperature distribution. It is thus necessary to provide more all-inclusive and exact analytical techniques and calculation methods for the above purpose.

a. One-Dimensional Problems

Methods have been developed and are reported in the literature for one-dimensional calculations of heat flow in composite structures with and without receding surface (see Appendix II). The method used in generating some of the information given in this report was described in references 10 and 14 although improvements in computer programs providing the solution were made since and thermal stress computations were incorporated. Solutions to the thermal problems involved when decomposition in depth occurs are described in Appendix V. The solutions associated with problems of thermal stress, creep, buckling are given in Appendixes VII, IX, X.

b. Two-Dimensional Problems

The solution of two-dimensional problems is more difficult to obtain and considerably less information is available on this topic. Where no

surface recession is involved, relatively simple shapes have been treated numerically (Refs. 57 and 58) with a minimum of simplifying assumptions. Reference 29 treats a simplified case of a receding graphite wing leading edge, and reference 27 shows an example of two-dimensional ablation of a rectangular body. A number of approaches and simplifications of two-dimensional heat flow problems with and without boundary recession is discussed in Appendix XI and calculations for wing leading edge are shown in this report under Design and Development Techniques. Appendix XII deals among others with multi-dimensional structural strength problems.

The methods and techniques discussed in the above sections were applied in the parametric and design studies.

IV. APPLICATION PERFORMANCE STUDIES

The information generated in Section III, together with certain unpublished Avco RAD data were used to study the glide re-entry vehicle as described in Section IV. A below. Application of these data to the ballistic capsule is discussed in Section IV. B and in Appendix IV.

A. GLIDE RE-ENTRY VEHICLE

A survey of the literature published up to the middle of 1961 (Appendix II), disclosed very little information specifically pertinent to applications involving lifting vehicles. Publications and manuscripts in preparation since that time indicate the recent increased interest in these applications. Such data as are published do not permit the generalization required to establish material and design performance trends, since they do not cover a sufficiently broad range of material parameters, vehicle and flight regime conditions, or structural design criteria. The parametric studies performed under this contract attempt to supply such information in a systematic manner. The general outline given in Section III. B. 1 was followed to select a typical application. The aerodynamic configuration was selected as typical of a vehicle with a nose cap and wing leading edge of 7-inch radius, while the rest of the vehicle was simply characterized by an arbitrary environmental heating and load distribution. The reference aerodyramic characteristics were selected for a vehicle with a 45-degree bank angle at (L/D) max and 13-degree angle of attack. The flight regime is illustrated in figure 22 which shows cold wall heating rate and stagnation enthalpy as functions of time during re-entry. Other trajectories in the flight corridor were selected for use in later parametric studies of the interaction of weight and thermal environment. These environments are shown in figures 23 and 24.

1. Systems Evaluation

The mathematical derivation of significant parameters in Section III. A allowed a detailed study of four systems: radiation shield, radiation shield with backface cooling, radiation-ablation shield, and radiation-ablation shield with backface cooling. It should be noted here that a shield using an ablative material may not reach temperatures causing substantial decomposition rates, and thus may be considered as a radiative shield.

Two other systems utilizing mass tranfer principles but without dimensional ablation (recession) were evaluated in less detail: ceramic matrix impregnated with a plastic and a forced transpiration (mass injection) system. The matrix mechanism study is applicable to the case of ablative plastics acting as radiation shields without dimensional ablation. The transpiration system study, because of the state-of-the-art, did not progress much beyond the "tooling-up" phase. The radiation shield studies were carried out to the furthest extent (in generalization) both because of evident

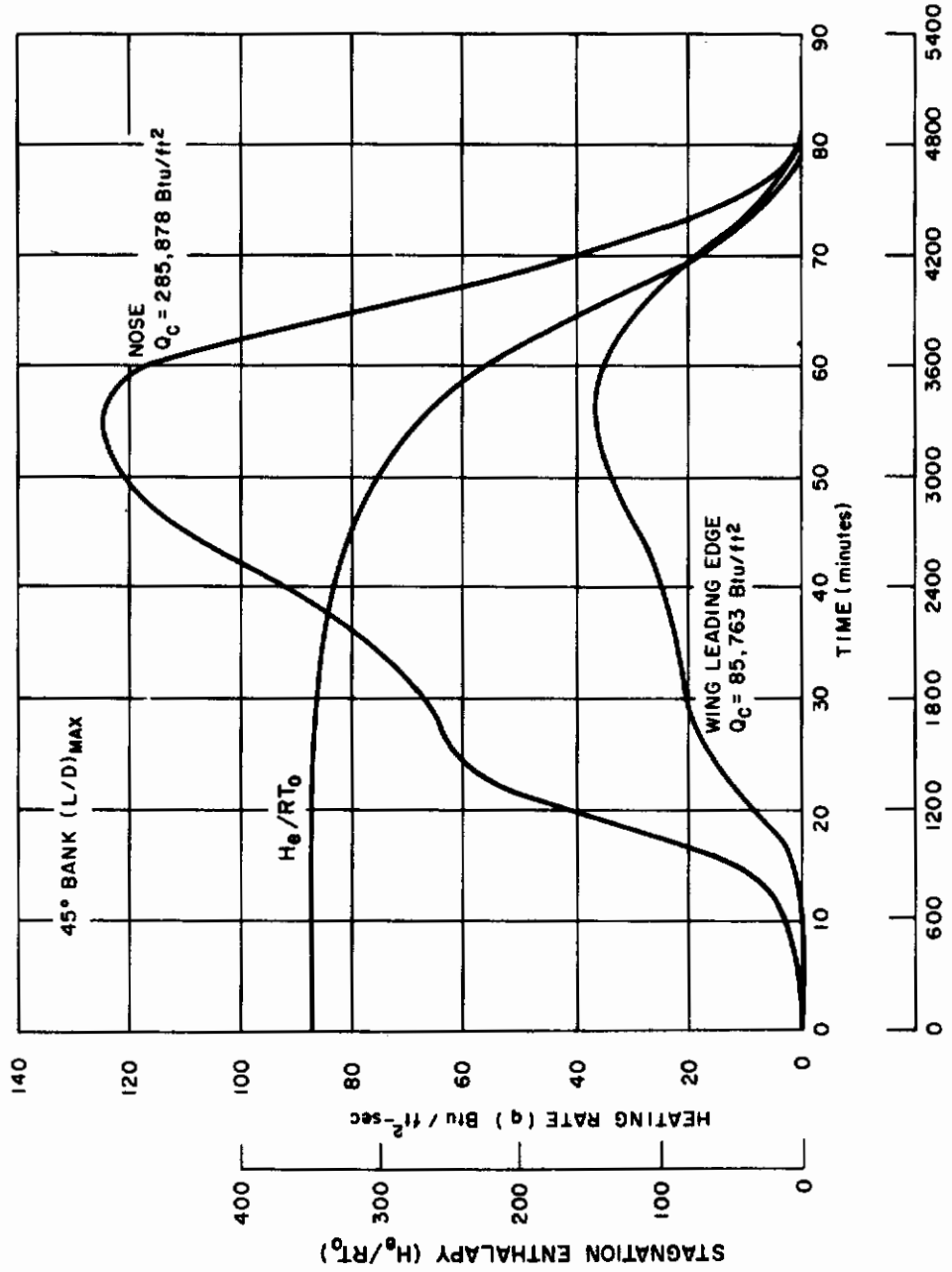

Figure 22 TYPICAL RE-ENTRY GLIDE VEHICLE HEATING RATES AND STAGNATION ENTHALPY, 45° BANK AT (L/D) MAX

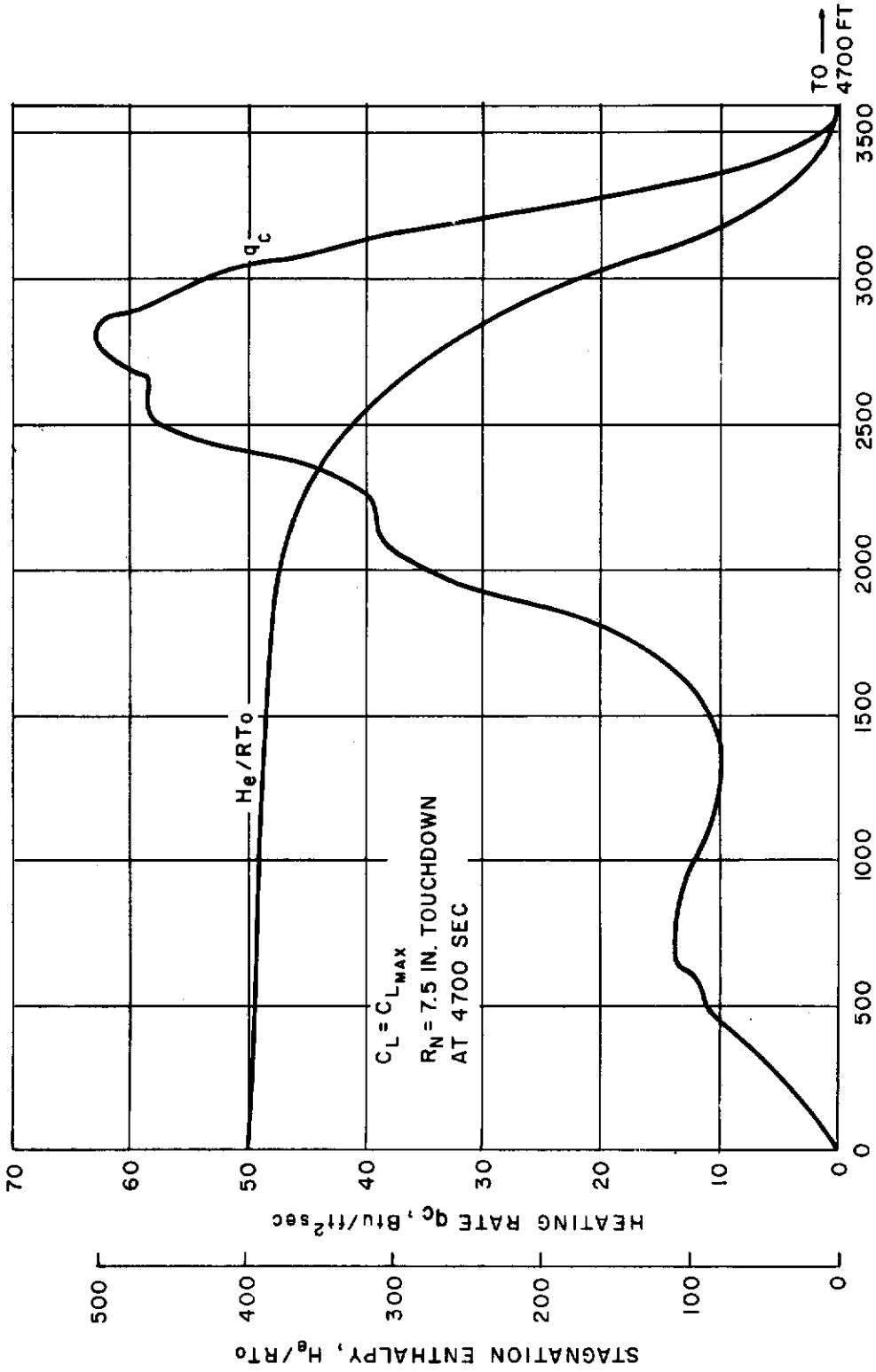

Figure 23 RE-ENTRY GLIDE VEHICLE HEATING RATES AND STAGNATION ENTHALPY $C_L = C_L$ - MAX

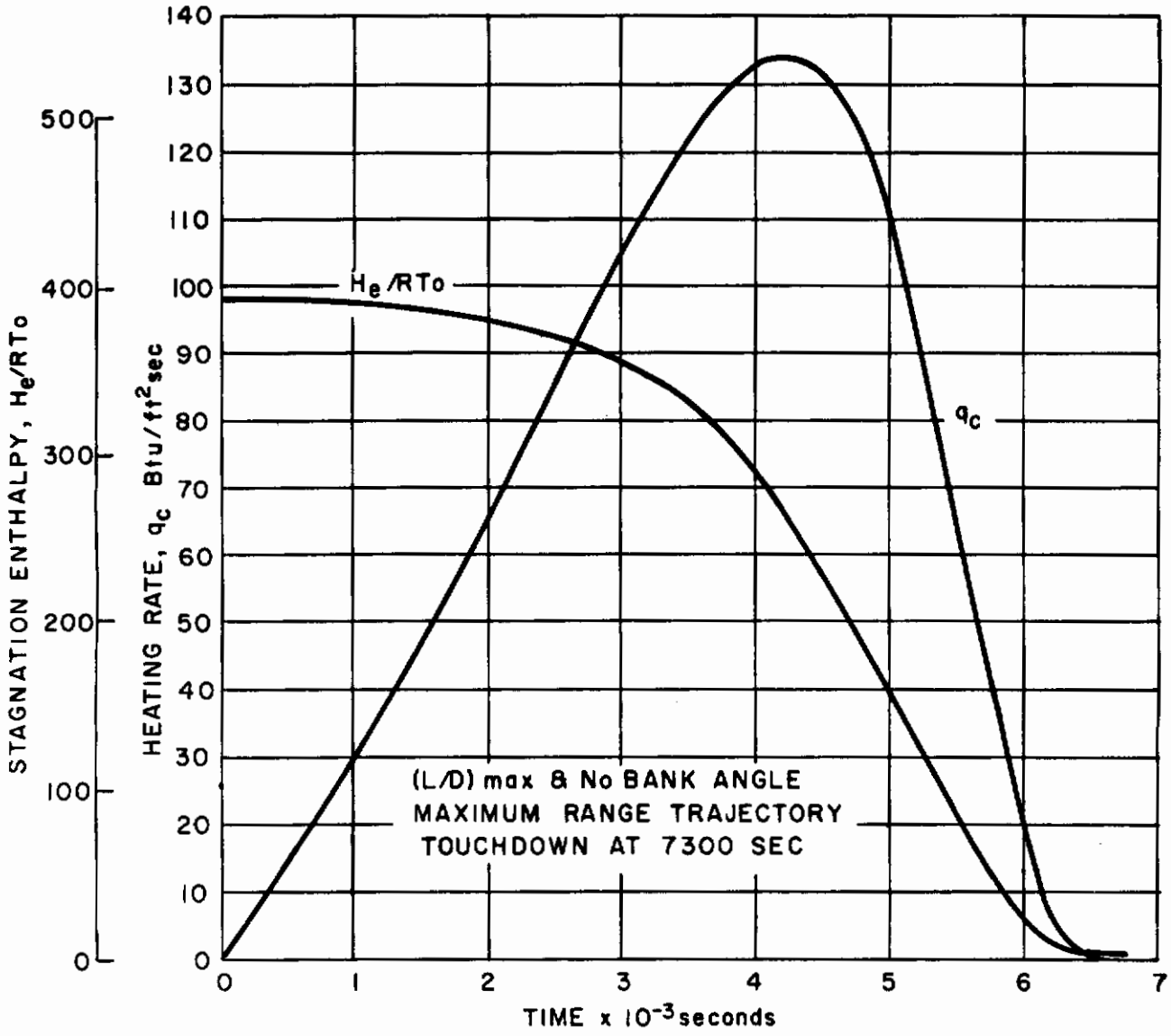

Figure 24 RE-ENTRY GLIDE VEHICLE HEATING RATES AND STAGNATION ENTHALPY 0° BANK AT (L/D) MAX

desirability, and because of lesser complexity. Conversely, the ablation-radiation shield study was less general and limited to one vehicle and specific trajectories, especially since the time and cost of computing would be excessive otherwise. Even limiting ablation to one vehicle and trajectory would result in large time and cost expenditure if standard finite difference solutions were used. Fortunately, the computational techniques reported in Section III. C. were developed under this contract, permitting rapid generation of large numbers of data points by means of desk calculators. Although more exact computer programs were used to generate these data at the beginning, the new method was also used. As the reliability of the method became more evident it was mechanized for computer use and used extensively, thus minimizing the cost and time associated with the conventional computer programs. The basic studies were made without including the additional thermal capacity of a backup structure; however, the application of the newly developed computation techniques allowed for extending the scope of the calculations to include structure; subsequent studies included the effect of other environments on shield and structure performance as well.

The operating principles and mechanism were reviewed in Section II, indicating their general limitations and advantages.

The significance of various parameters and parametric groups was established in Section III. A.

a. Radiation Shield Parametric Study

A parametric study for a radiation thermal protection system was completed for the re-entry environment shown in figure 22. The calculations were made assuming a single material with constant thermal properties k, ρ, C_p, and emissivity, as described by equations (14) to (17). Calculations were then made to determine whether the trends previously discussed under Section III. A. 1 were valid for the selected application. In particular ρk and C_p were treated as separate parameters along with the environmental conditions $q_c(t)$ and H_e/RT_o, emissivity and design backface temperature rise.

The parametric study was performed for values ρk from 3.0 to 18.0 Btu-lb/hr-ft^4-°F and C_p from 0.10 to 1.0 Btu/lb-°F. The effect of variation of these properties on weight is shown in figure 25 for a heating profile characterized by $q_c(\max)$ = 37 Btu/ft^2-sec (Q_c = 85,873 Btu/ft^2) and three discrete values of ρk. Similar calculations were performed for two other heating profiles: $Q_c(\max)$ = 81 Btu/ft^2-sec (Q_{c_2} = 185,820 Btu/ft^2) and $q_c(\max)$ = 124 Btu/ft^2-sec (Q_c = 285,820 Btu/ft^2). Investigation of figure 25 indicates that the weight depends on the reciprocal of the square root of C_p for fixed values of ρk and the remaining parameters. A similar analysis shows that the weight varies as the square

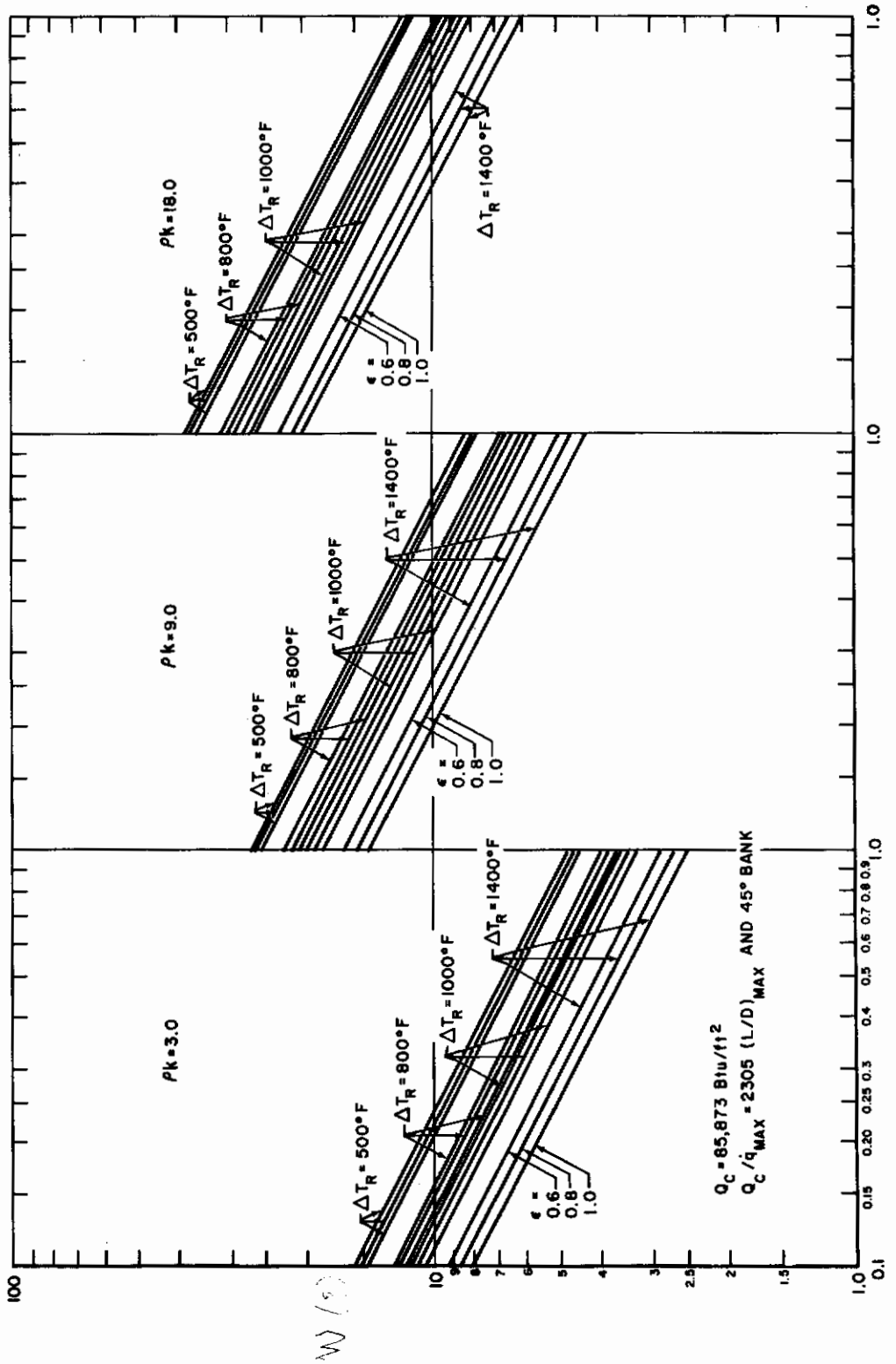

Figure 25 EFFECT OF SPECIFIC HEAT AND DENSITY-CONDUCTIVITY PRODUCT ON THE REQUIRED WEIGHT OF A RADIATION SHIELD

root of the ρk product for fixed C_p and the remaining variables. It is now apparent that the weight depends on the square root of $\rho k / C_p$ and that the number of variables may be reduced, since for the typical environment and range of properties of interest ρk and C_p have been eliminated as separate parameters. The complete parametric study for a single slab radiation shield for this particular environment is given in figures 26, 27, and 28 and the trends of weight with variation of $\rho k / C_p$, ϵ, ΔT_R and q_c (max) are indicated. This trend, $W = \sqrt{\rho k / C_p}$, will remain as long as the heat conducted into the solid is significantly smaller than the total cold wall heat input. Under these conditions ρk will not affect the surface temperature, and the conduction within the solid, which depends on $\rho k / C_p$, will determine the weight. In other words, if the surface temperature is not affected by thermal properties, the temperature distribution is a function of $\rho k t / C_p w^2$ only. For fixed time it is then apparent that weight varies as the square root of $\rho k / C_p$.

Figures 26, 27, and 28 indicate the weight assuming no design limiting surface temperature criteria. However, using equation (84) figure 29 was constructed to yield the values of the maximum allowable heat flux (for a given limiting surface temperature) as a function of material properties. For values of the thermal properties parameter $1/\epsilon \sqrt{\rho k C_p}$ less than a 5.0 Btu/ft^2-°F-hr$^{1/2}$, figure 29 indicates that the maximum allowable heat flux depends primarily on the maximum surface temperature criterion and very little on thermal properties. This is the region of very little conduction into the solid compared to the total cold wall heat input, and the finding is in agreement with the previous conclusions that for a given heat flux the surface temperature does not depend heavily on thermal properties, for $\sqrt{\rho k C_p}/\epsilon$ less than about 5.0 and that the weight varies as the square root of $\rho k / C_p$.

In addition, it was found that the correlation could be further generalized to include heating duration in the significant parametric groups which would extend the correlation to include other thermal environments. This was accomplished by replacing $\rho k / C_p$ by $\rho k / C_p \ (t_f - t_i)$ in the correlation curves of required weight versus $\rho k / C_p$ (figs. 26 to 28). The symbol t_i represents the adjusted time when heating begins and t_f is the final time (see Section III. C. 1). The resulting correlations are presented here in figures 30, 31, and 32.

An additional correlation, figure 33, of maximum allowable heat flux level for a given limiting surface temperature was generalized by replacing $\rho k C_p$ in figure 29 by $\frac{\rho k C_p}{t_f - t_i}$. The new set of generalized

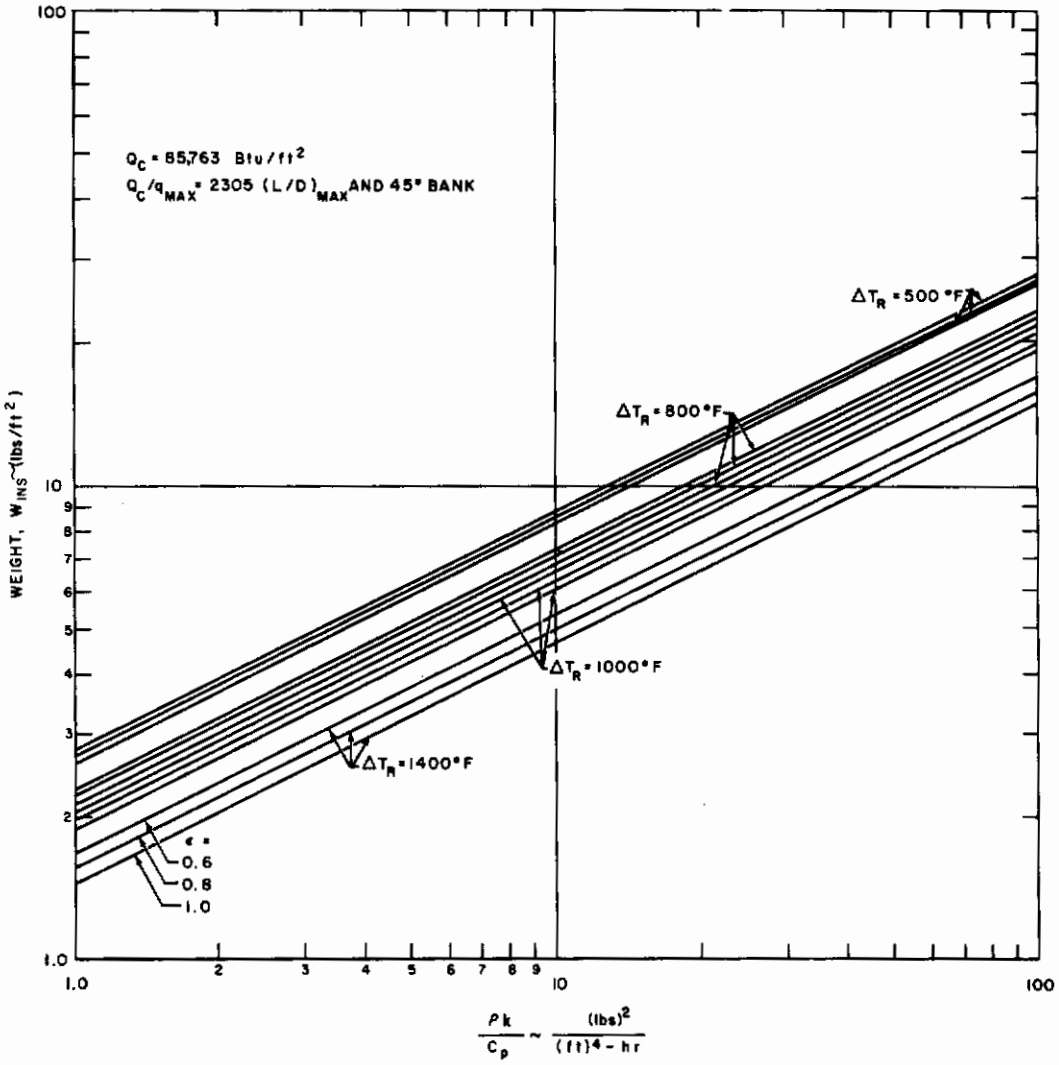

Figure 26 EFFECT OF THERMAL PROPERTIES AND DESIGN CRITERIA ON THE REQUIRED WEIGHT OF A RADIATION SHIELD FOR A TYPICAL RE-ENTRY GLIDE VEHICLE, Q_c = 85,763 BTU/FT^2

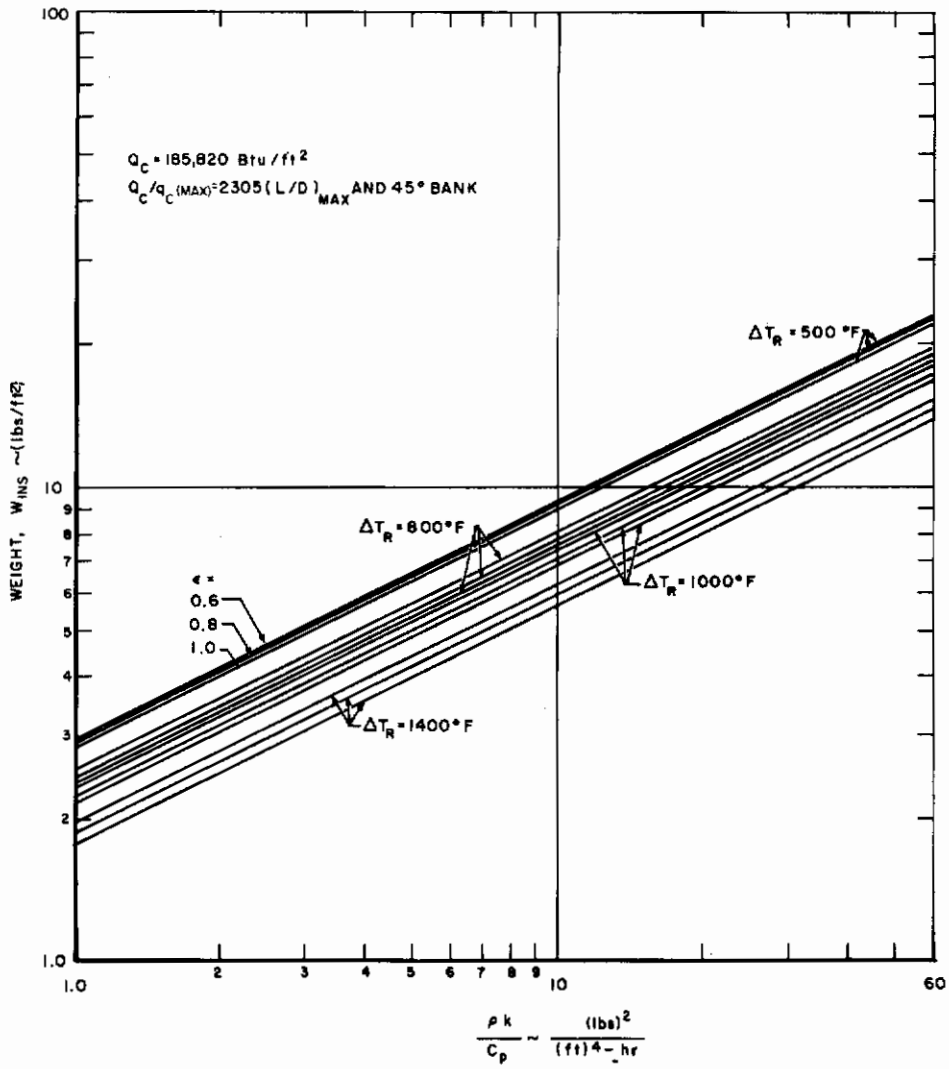

Figure 27 THE EFFECT OF THERMAL PROPERTIES AND DESIGN CRITERIA ON THE REQUIRED WEIGHT OF A RADIATION SHIELD FOR A TYPICAL RE-ENTRY GLIDE VEHICLE, Q_c = 185, 820 BTU/FT^2

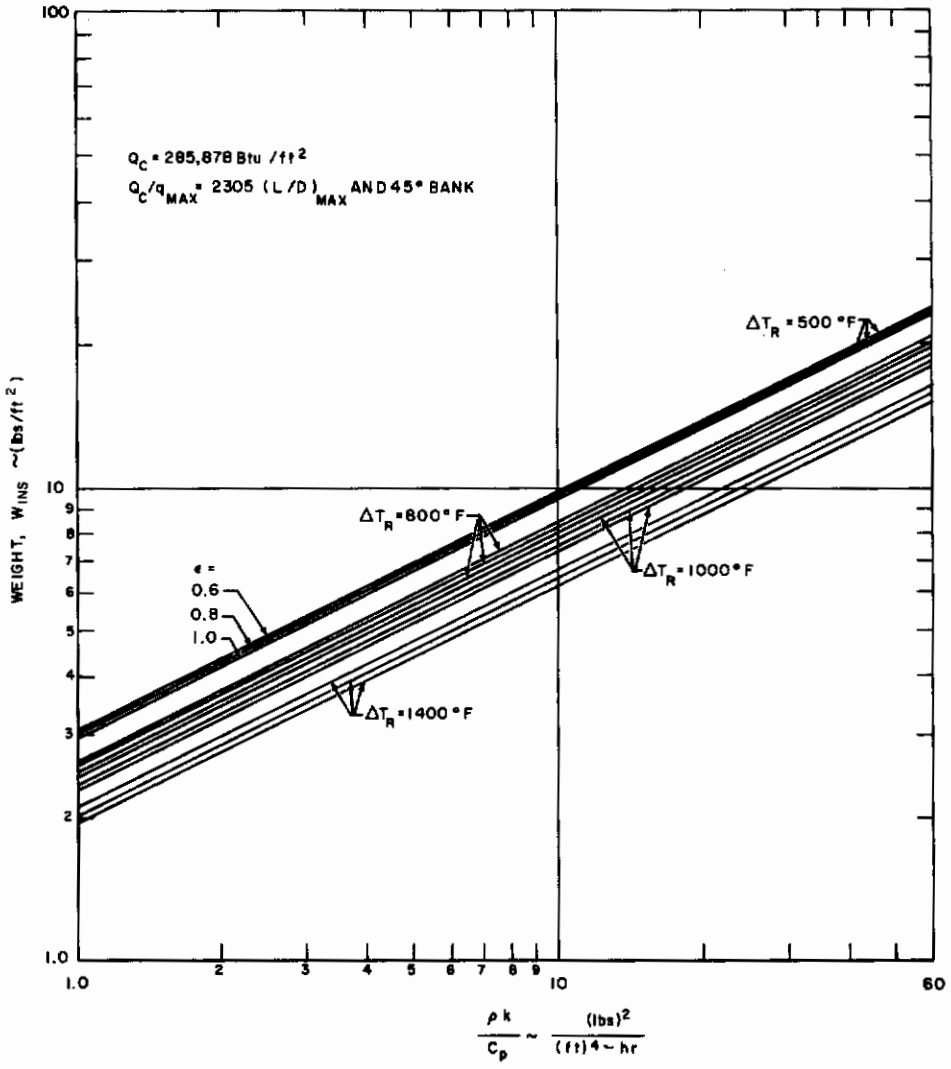

Figure 28 THE EFFECT OF THERMAL PROPERTIES AND DESIGN CRITERIA ON THE REQUIRED WEIGHT OF A RADIATION SHIELD FOR A TYPICAL RE-ENTRY GLIDE VEHICLE, Q_c = 285, 878 BTU/FT²

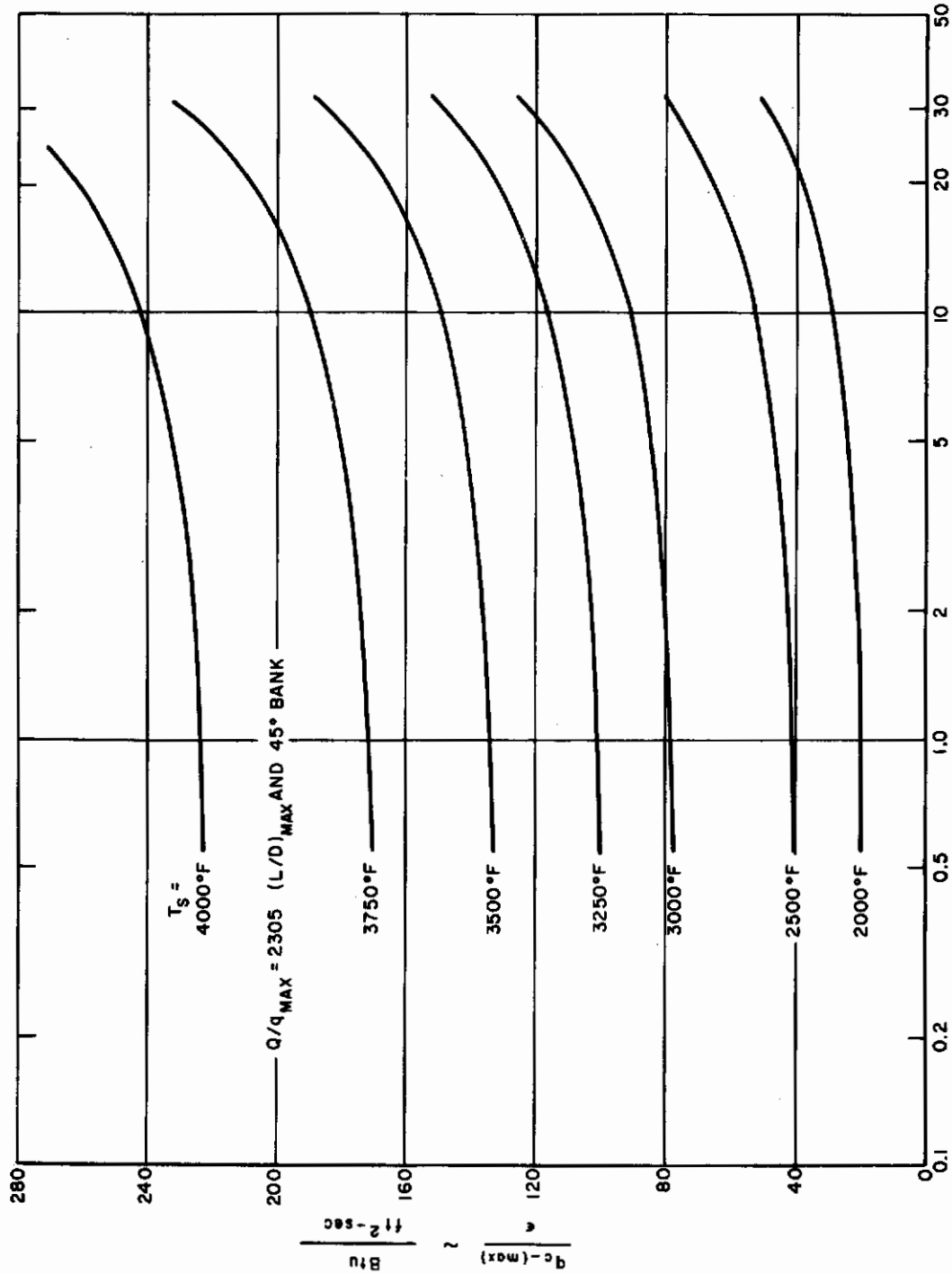

Figure 29 MAXIMUM ALLOWABLE HEAT FLUX AS DICTATED BY THE LIMITING DESIGN SURFACE TEMPERATURE AND THERMO-PHYSICAL PROPERTIES FOR A TYPICAL RE-ENTRY GLIDE VEHICLE RADIATION SHIELD

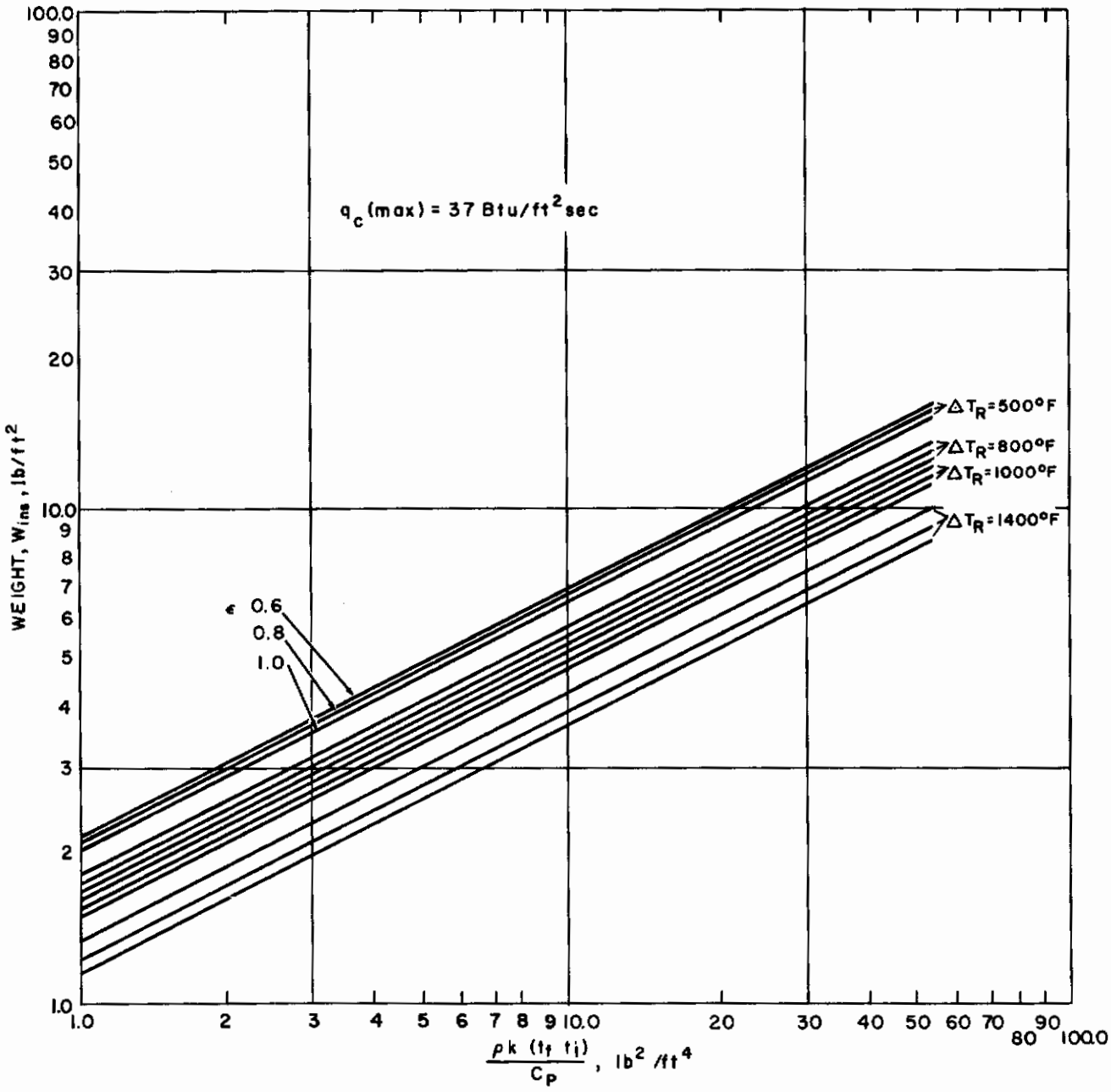

Figure 30 GENERALIZED CHARTS FOR DETERMINING THE EFFECTS OF THERMAL PROPERTIES AND DESIGN CRITERIA ON THE WEIGHT OF A RADIATION SHIELD q_c (MAX) = 37 BTU/FT^2 SEC

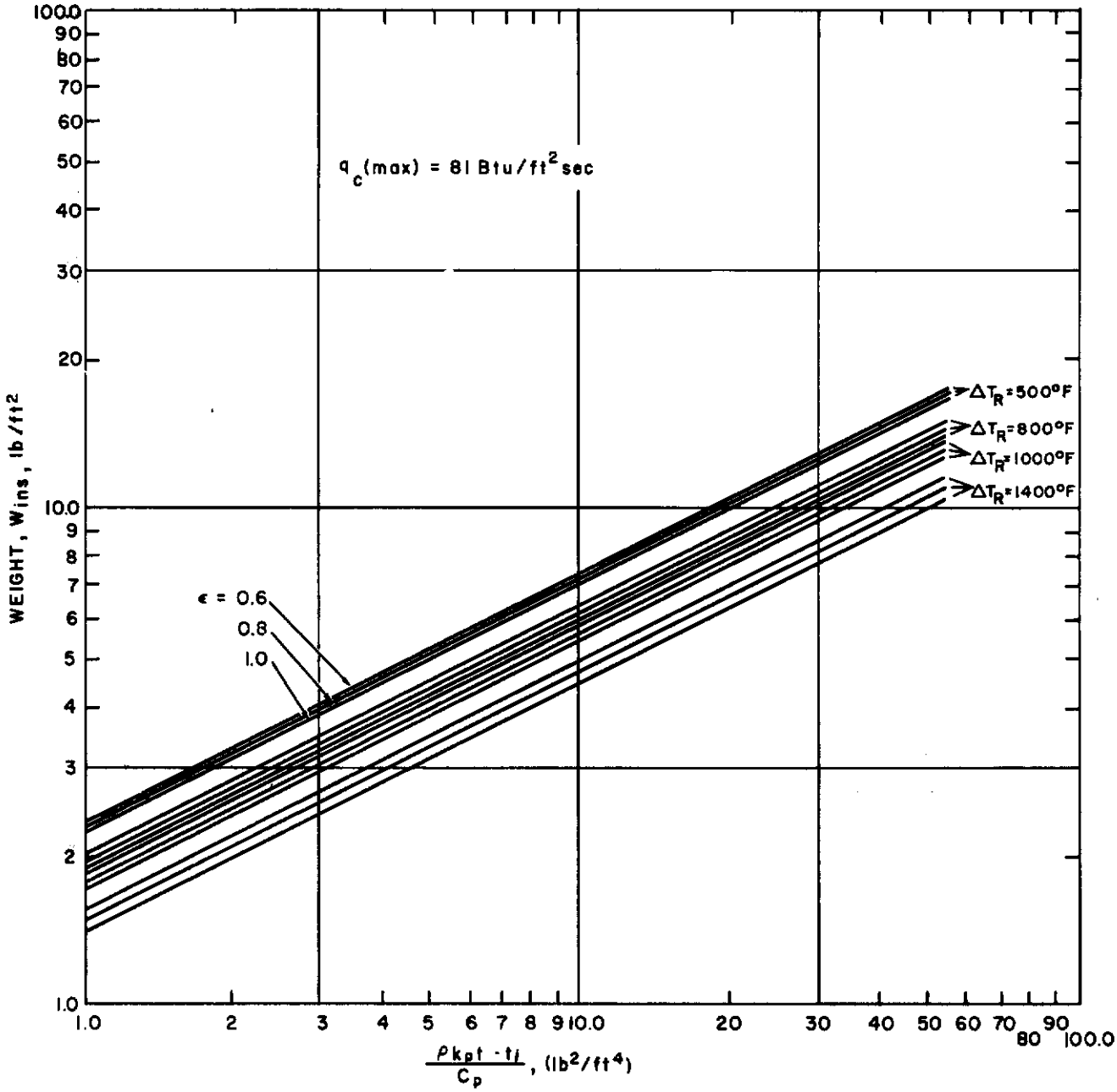

Figure 31 GENERALIZED CHARTS FOR DETERMINING THE EFFECTS OF THERMAL PROPERTIES AND DESIGN CRITERIAL ON THE WEIGHT OF A RADIATION SHIELD q_c (MAX) = 81 BTU/FT^2-SEC

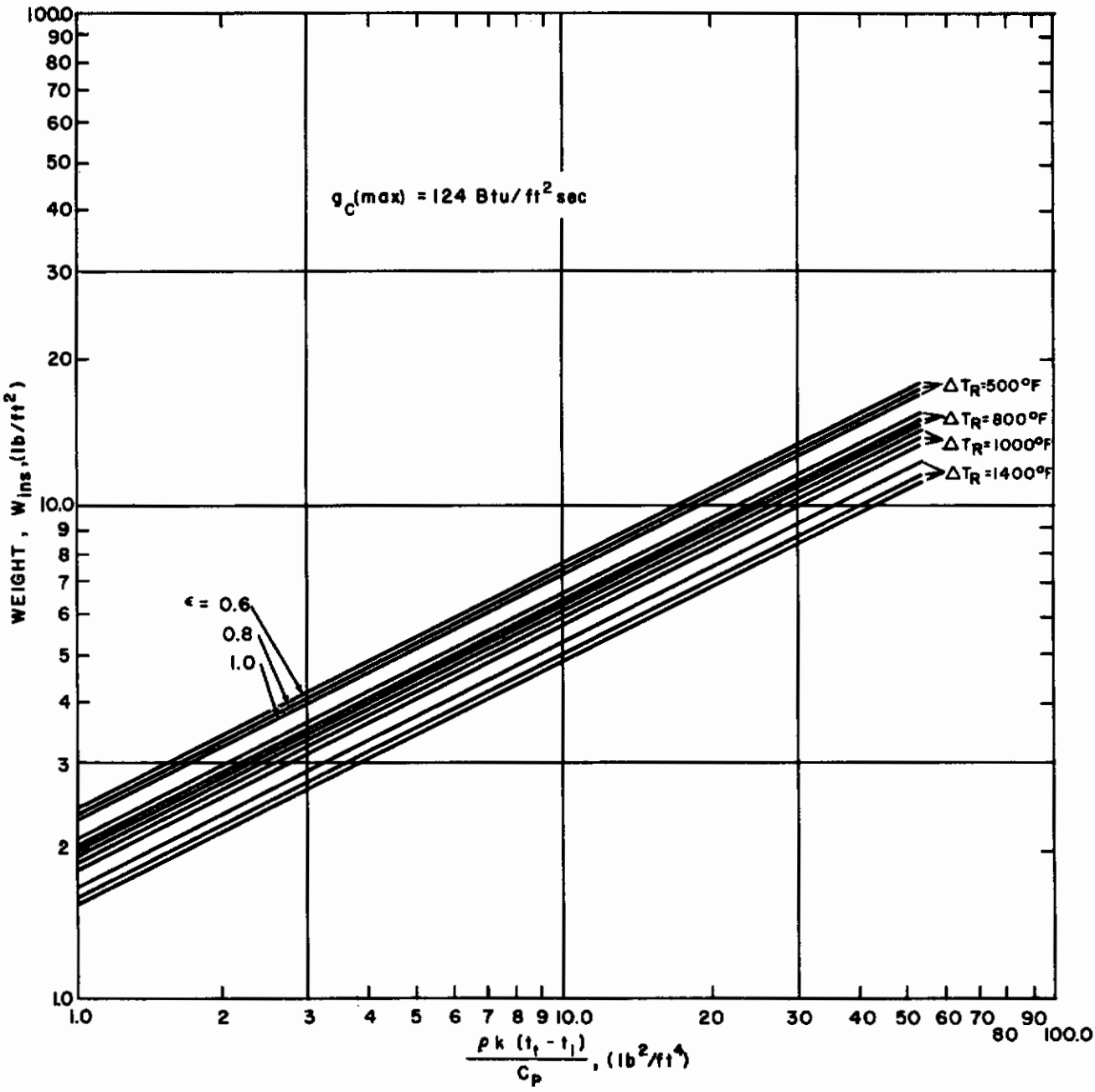

Figure 32 GENERALIZED CHARTS FOR DETERMINING THE EFFECTS OF THERMAL PROPERTIES AND DESIGN CRITERIA ON THE WEIGHT OF A RADIATION SHIELD q_c (MAX) = 124 BTU/FT^2 SEC

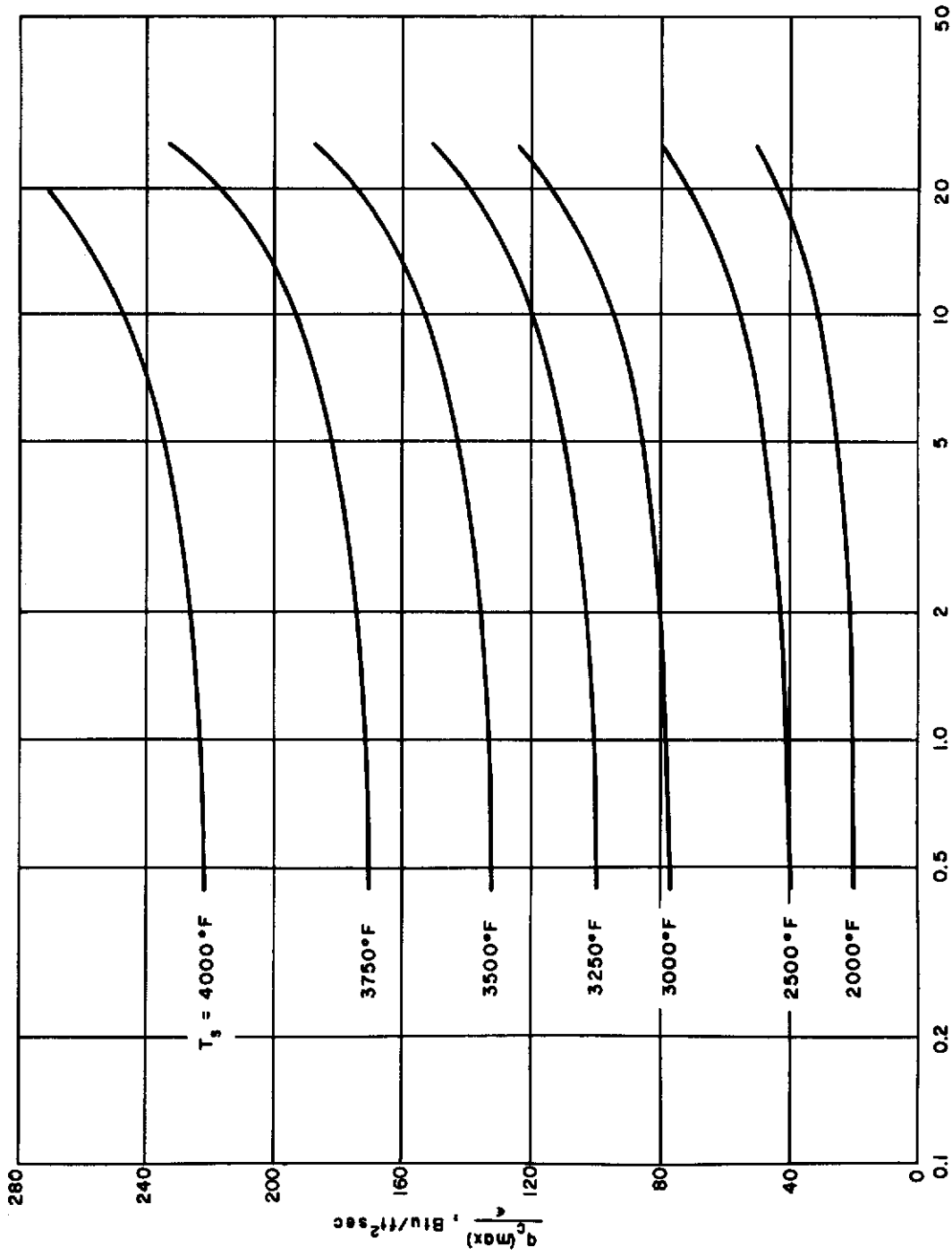

Figure 33 GENERALIZED RELATIONSHIP BETWEEN THE MAXIMUM ALLOWABLE HEAT FLUX, LIMITING SURFACE TEMPERATURE, AND THERMO-PHYSICAL PROPERTIES FOR GLIDE RE-ENTRY VEHICLE RADIATION SHIELDS

graphs presented here (Figs. 30, 31, 32, and 33) have been found valid provided the heat conduction into the shield is significantly less than the heat radiated away from the surface, and the average value of stagnation enthalpy, H_e/RT_o falls in the region $160 < H_e/RT_o < 260$. These generalized curves may be used for a wide range of trajectories to determine system performance.

Since the previous calculations ignore the presence of a substructure, it is advantageous to extend the analysis by performing a limited number of calculations which will include the thermal capacity of the substructure and hence demonstrate several important effects. First, the results are indicative of the reductions in shield weight due to the thermal capacity of the structure, and in addition demonstrate the capability of the techniques developed to evaluate composite systems. The influence of thermal properties of the insulation and the thermal capacity, $W_s C_s$, of the structure on the weight, W_{ins}, are indicated in figure 34 for one body location with q_c (max) = 81 Btu/ft^2-sec. The effect of ΔT_R was shown previously in figures 26, 27, and 28. As an example consider a composite system of a high-temperature plastic and a steel substructure of 2.0 lb/ft^2 which is not to exceed a temperature rise of 1000° F. The thermal capacity of the structure $C_s W_s \approx 0.20$ Btu/ft^2-° F and selecting $\rho k/C_p = 25$ lb^2/ft^4-hr which is representative of experimental materials of the X-5000 series, results in a shield weight $W_{ins} =$ 10.7 lb/ft^2. Adding the weight of substructure gives a total of $W_T =$ 12.7 lb/ft^2 and, therefore, the increase in total weight is 2.0 lb/ft^2 less than if the structure weight, W_s, had been added directly to the homogeneous shield weight assuming no structure. The reductions in shield weight vary with the particular composite under consideration but such design curves are readily constructed and together with structural analysis can be used to evaluate built-up systems. In fact, a rather general set of design curves for composites of shield and substructure can easily be constructed which are valid for a wide range of glide vehicle applications. Using newly developed calculation procedures, charts similar to figure 35 for several other values of emissivity and design backface temperature rise, can be made and the resulting set of generalized design curves can be used for preliminary evaluation of the composites of heat shield and substructure. Using these charts together with equations (63) and (65), which account for the presence of a hot radiating skin at the surface, it is relatively straight forward to evaluate built up configurations (see Section III. C).

In summary, it may be concluded that generalized performance relationships for homogeneous radiation systems have been provided for a broad range of glide type re-entry environments. Data have been supplied for generalized design charts to include substructure interaction

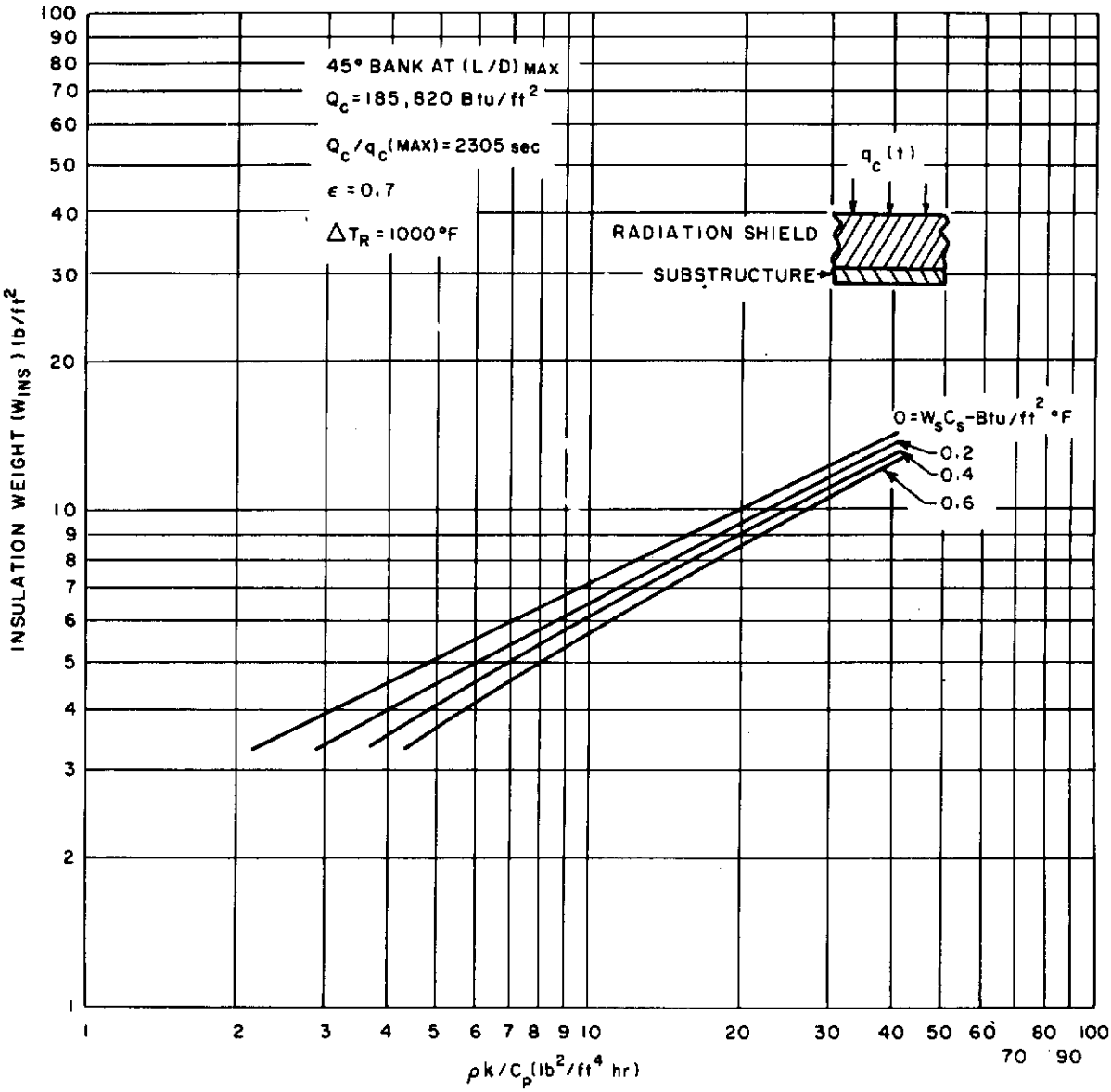

Figure 34 EFFECT OF STRUCTURE AND THERMAL PROPERTIES ON THE SHIELD WEIGHT OF A COMPOSITE RADIATION SHIELD PLUS STRUCTURE 45° BANK AT (L/D) MAX

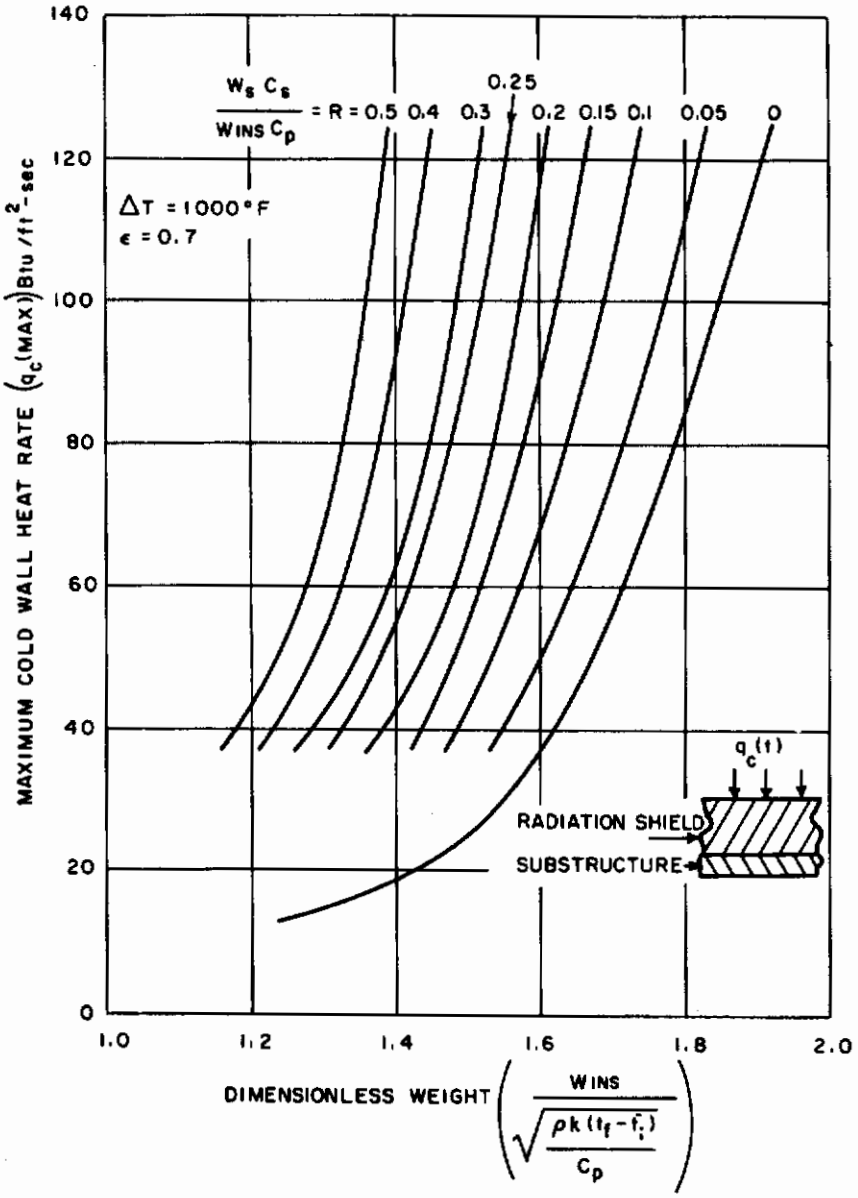

Figure 35 GENERALIZED CORRELATION OF INTERACTION BETWEEN SHIELD WEIGHT SUBSTRUCTURE THERMAL CAPACITY AND THERMAL ENVIRONMENT FOR A RADIATION SHIELD

with heat-shield weight. The remaining data may be generated by hand calculations and the computer program developed under this contract. The data for composites of shield plus substructure can also be used for preliminary evaluation of high temperature plastics or ceramics which experience very little or no surface recession.

b. Radiation Shield With Backface Cooling

Realizing the trends established for self-insulating radiation systems, as described above, a similar generalization was sought for systems supplemented by backface cooling. It was found that the same trend, i.e., weight variation with the square root for $\rho k/C_p$ for a particular trajectory was valid and that generalizations to other trajectories could be accomplished by relating total required weight (of both shield and coolant), to $\rho k Q_c / C_p \; q_c(\max)$. This trend will again continue as long as the energy conducted into the solid is very much less than the energy radiated away from the surface, and provided ablation occurs.

Calculations were made to determine the effect of the maximum heating rate $q_c(\max)$, coolant parameter H_c/C_p, emissivity ϵ, and backface temperature rise ΔT_R on the total weight. The results of these parametric studies are presented in figures 36, 37, and 38 for values of the backface temperature rise from 0° to 500° F. In practice, however, the backface temperature rise will most likely be held to less than 200° F; for these cases ΔT_R does not change the required weight substantially as may be seen from the graphs. Therefore, the assumption of no temperature rise at the backface results in only slight over estimates of required weight. To facilitate the use of data for liquid-cooled radiation shields, figure 39 was constructed which allows for immediate calculation of the required insulation and coolant weight for a given thermal environment $q_c(t)$ and Q_c, coolant parameter H_c/C_p, and material properties $\rho k/C_p$ and ϵ. Since figures 36, 37, 38, and 39 give total weight, the weight of the coolant and insulation separately can be determined from equation (78) of Section III. C. 1. The additional design criteria for determining the maximum allowable cold wall heat flux for a given maximum surface temperature may be satisfied by using figure 33 discussed above for uncooled radiation shields.

For cooled systems operating at low backface temperature ($T_R < 200°$ F), the thermal interactions of load carrying substructure and the shield are insignificant, thus the weight of the substructure may be added directly to the weight of shield and substructure.

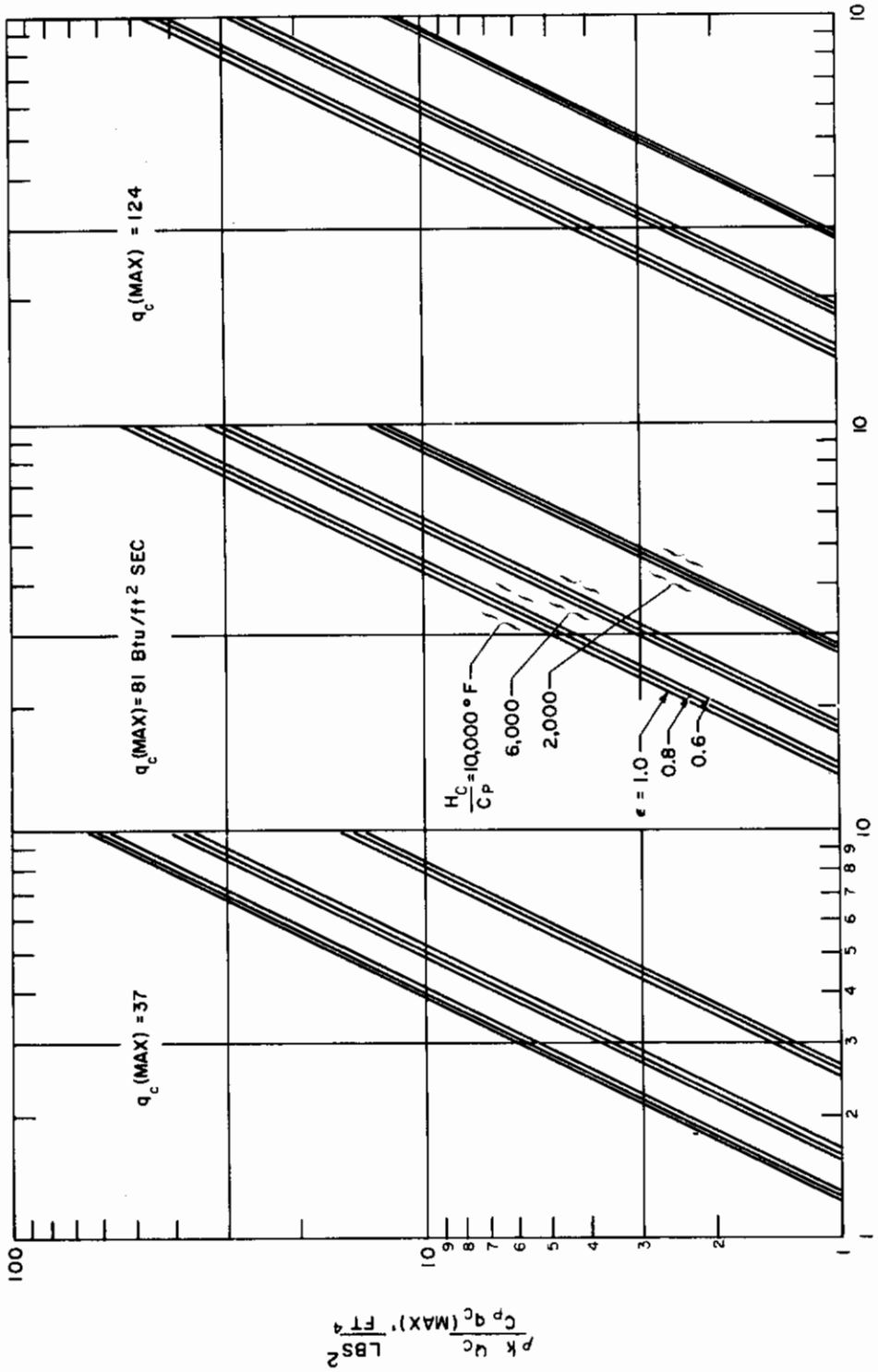

Figure 36 EFFECT OF RE-ENTRY ENVIRONMENT AND THERMAL PROPERTIES ON THE WEIGHT OF A LIQUID-COOLED RADIATION SHIELD - COOLANT TEMPERATURE RISE (ΔT = 0°F)

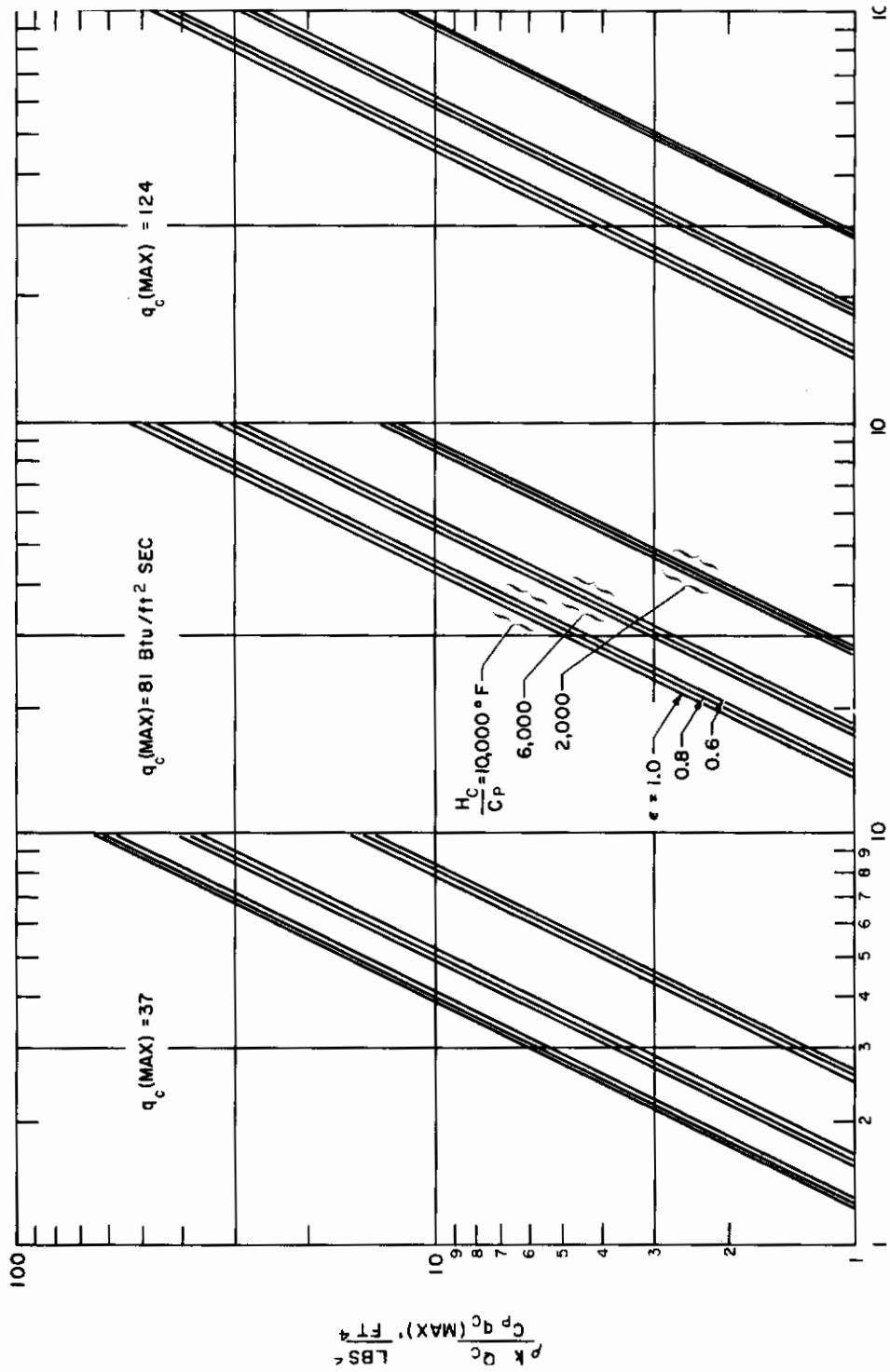

Figure 37 EFFECT OF RE-ENTRY ENVIRONMENT AND THERMAL PROPERTIES ON THE WEIGHT OF A LIQUID-COOLED RADIATION SHIELD - COOLANT TEMPERATURE RISE (ΔT = 142 °F)

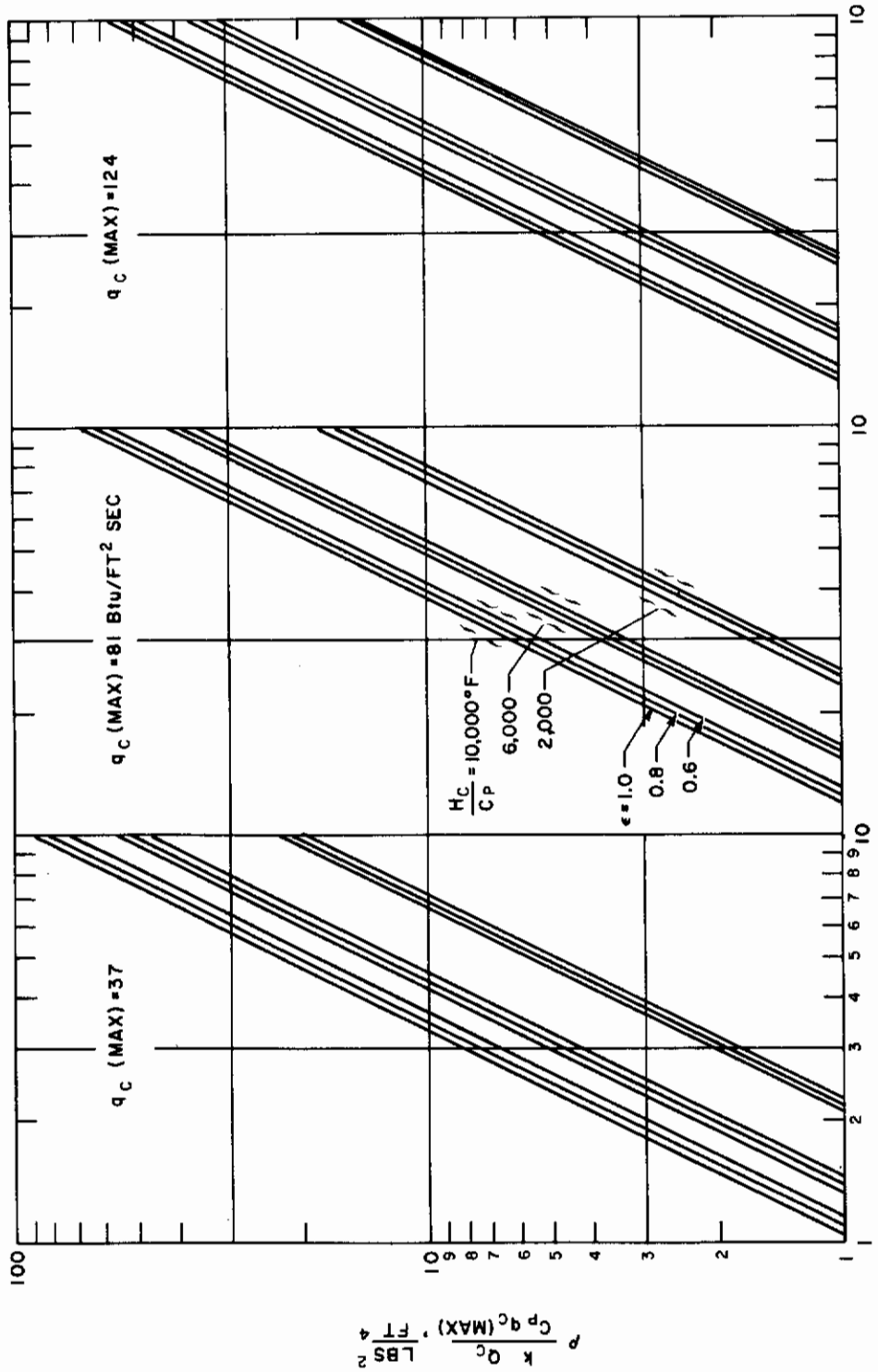

Figure 38 EFFECT OF RE-ENTRY ENVIRONMENT AND THERMAL PROPERTIES ON THE WEIGHT OF A LIQUID-COOLED RADIATION SHIELD - COOLANT TEMPERATURE RISE (ΔT = 500 °F)

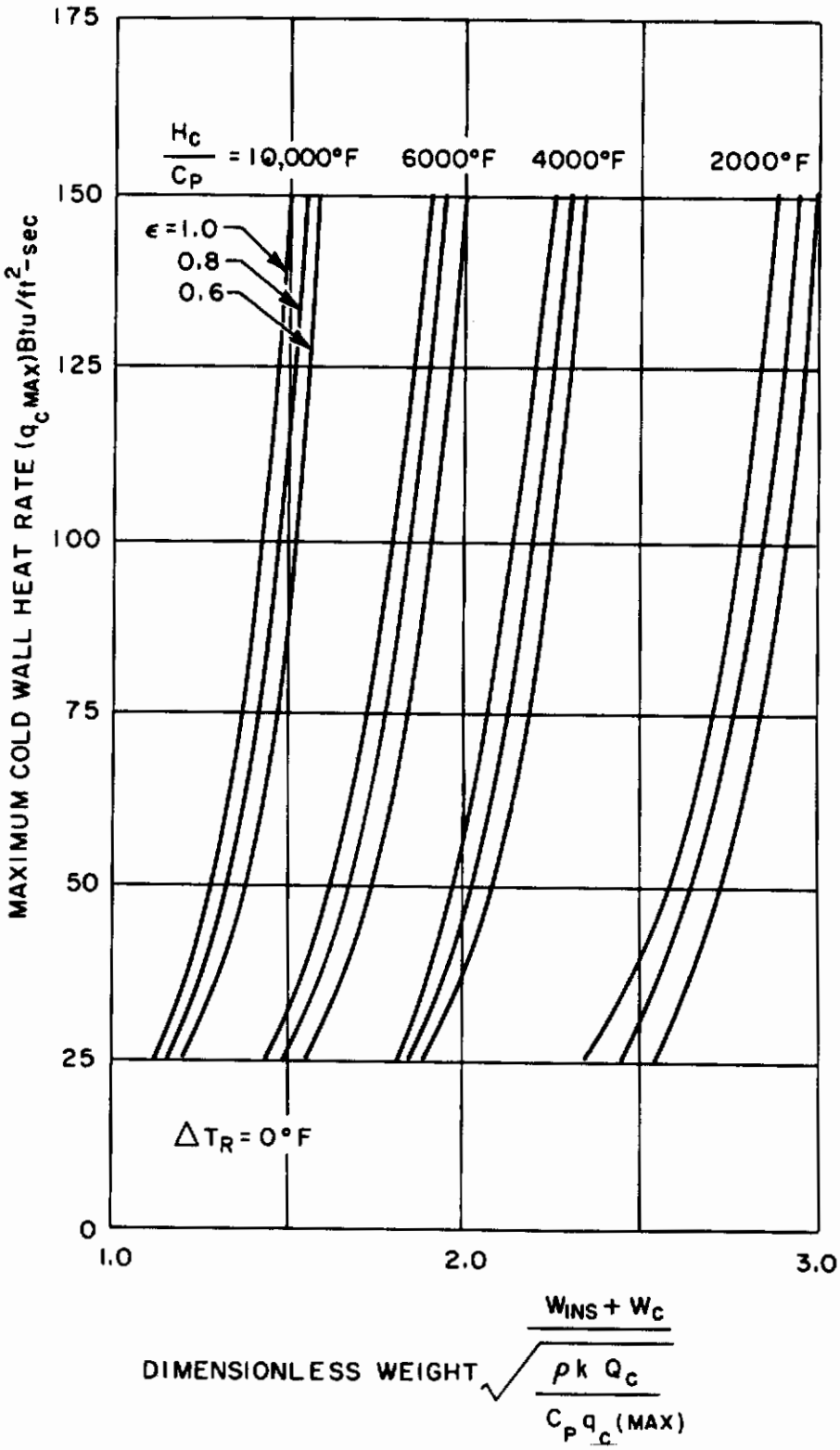

Figure 39 DIMENSIONLESS WEIGHT OF A RADIATION SHIELD (WITH BACKFACE COOLING) FOR A GIVEN THERMAL ENVIRONMENT AND COOLING PARAMETER (ΔT_R = 0°F)

c. Radiation-Ablation Shield

Since the trends associated with ablation are more complicated than those encountered for radiation systems, a qualitative analysis of radiation-ablation shield performance is given first and the trends are indicated by figures 40, 41, and 42. The solid line in figure 40 shows the variation of the weight loss with the effective heat of ablation (q^*). The weight loss approaches infinity as q^* approaches zero, while it decreases hyperbolically to zero when q^* approaches infinity, and no ablation occurs. The dotted line in figure 40 represents ablated weight as function of the changes in thermal properties and backface temperature rise. Decreasing ablation temperature, (T_A), emissivity, ϵ, ρk, and increasing allowable backface temperature T_R result in larger weights ablated.

Figure 41 presents the variation of insulation weight (weight after ablation stops) with q^*. The solid horizontal line represents the weight of the radiation shield for reference purposes. For a given set of properties, its weight depends on the ratio of allowable backface temperature rise to the average radiation surface temperature, T_{rad}, and the duration of flight. For a radiation-ablation shield and a radiation shield with the same thermal properties $\rho k/C_p$, ϵ, and allowable backface temperature limit, ΔT_R, the insulation weight for the ablation shield (solid curve in figure 41) will always be lower than the weight of the radiation shield, remembering $T_A < T_{rad}$. For very high heats of ablation no weight loss occurs and the insulation (total) weight is less than that of the radiation shield. The amount of savings depends only on the ratio (T_A / T_{rad}) since all other properties and the duration of heating experienced by the insulation are the same. As q^* decreases (holding $\rho k/C_p$, ϵ, T_A, and T_R constant) the insulation weight decreases since the adjusted duration of heating which the insulation experiences is getting smaller. The amount of decrease in insulation weight depends on the ratio T_A/T_{rad} and the adjusted times ratio t_{abl}/t_{rad}. The remaining dashed curve in figure 41 shows that the insulation weight will decrease with lower $\rho k/C_p$ and T_A. From the above discussion it is apparent that although low $\rho k/C_p$ and high ϵ reduce the total ablation shield weight, no such statement can be made about ablation temperature since a high value of T_A reduces ablation weight while low-temperature reduces insulation weight. The same is true for q^*, as may be seen from figure 42 which results from combining the curves of figures 40 and 41 (ablation weight plus insulation weight). Here it may be seen that an optimum value of q^* exists which is not necessarily $q^* \to \infty$. This trend is important since it clearly points out the commonly held misconception that higher heat of ablation will always reduce the weight, all properties and conditions remaining fixed. Therefore, both parameters, ablation temperature and heat of ablation possess optimum values with respect to minimum weight, and these minima will change with aerodynamic heating and material properties.

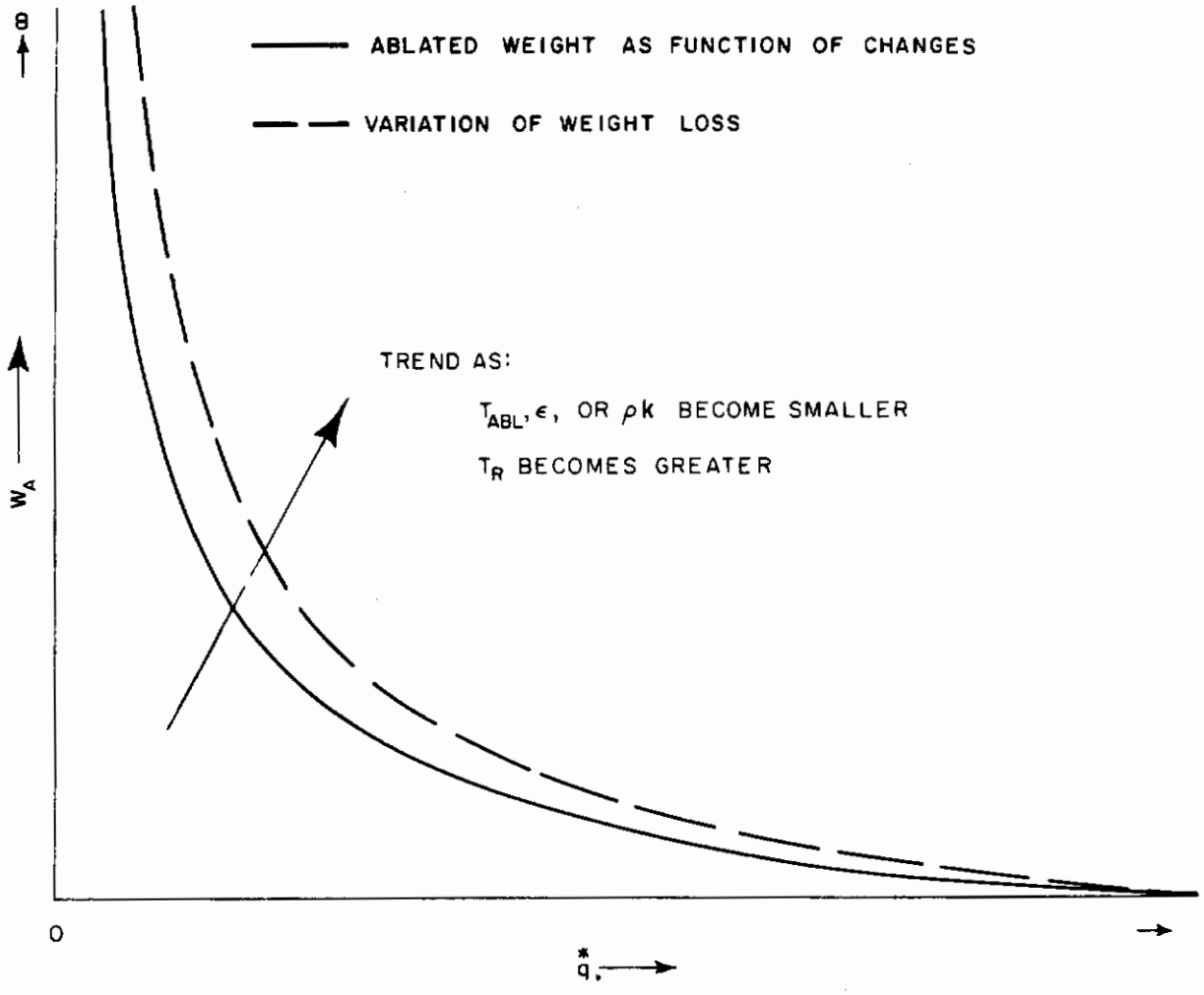

Figure 40 TREND OF ABLATED WEIGHT AS INFLUENCED BY MATERIAL PROPERTIES OR CHARACTERISTICS AND DESIGN CRITERIA

TRENDS:

AS $q^* \longrightarrow 0$, $W_{INS} \longrightarrow C_1$

AS $q^* \longrightarrow \infty$, $W_{INS} \longrightarrow C_2$

AS $T_A \longrightarrow T_{RAD}$, $W_{INS} \longrightarrow W_{INS_{(RAD)}}$

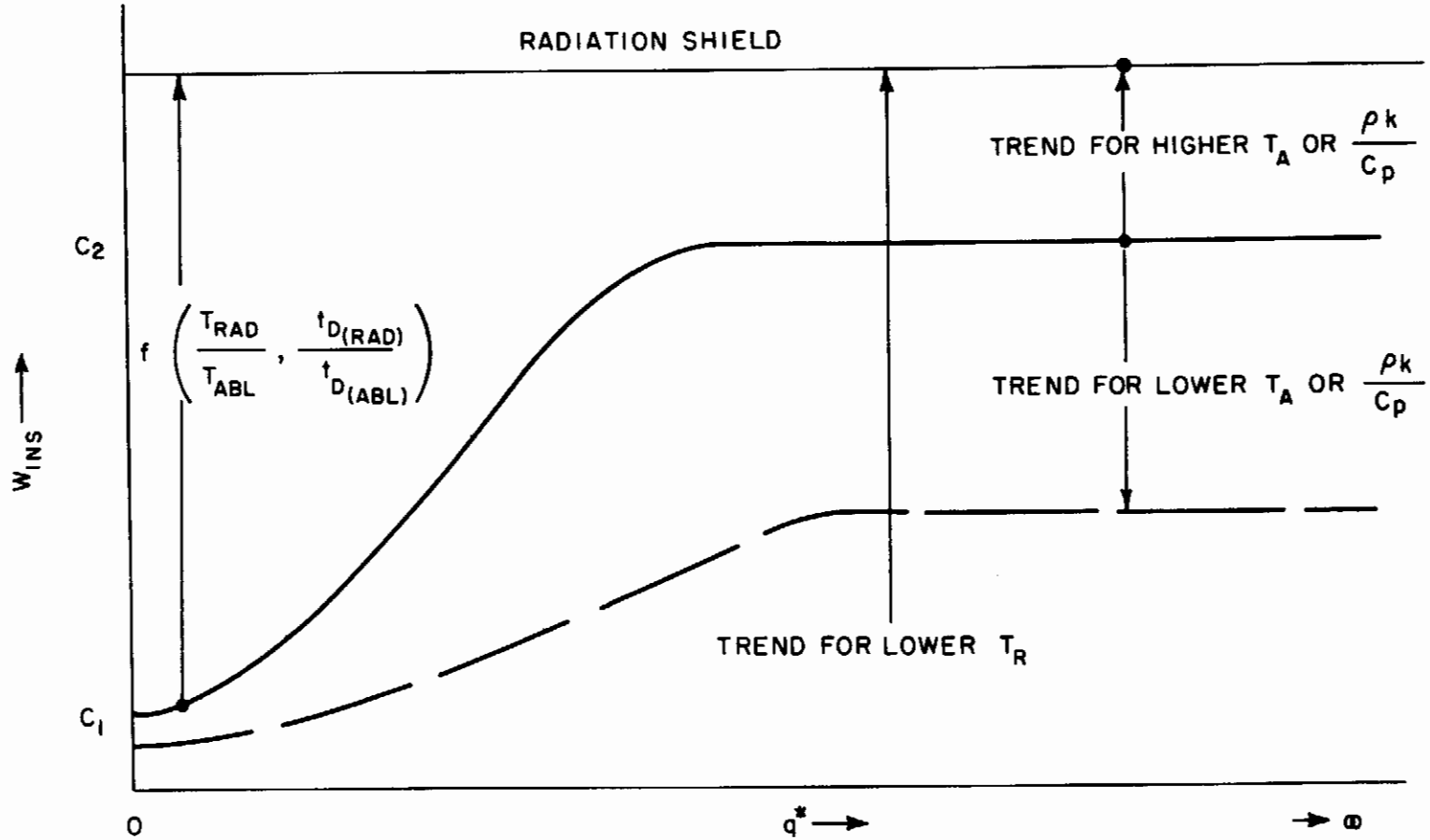

Figure 41 TRENDS OF REQUIRED INSULATION WEIGHT AS INFLUENCED BY MATERIAL PROPERTIES OR CHARACTERISTICS AND DESIGN CRITERIA

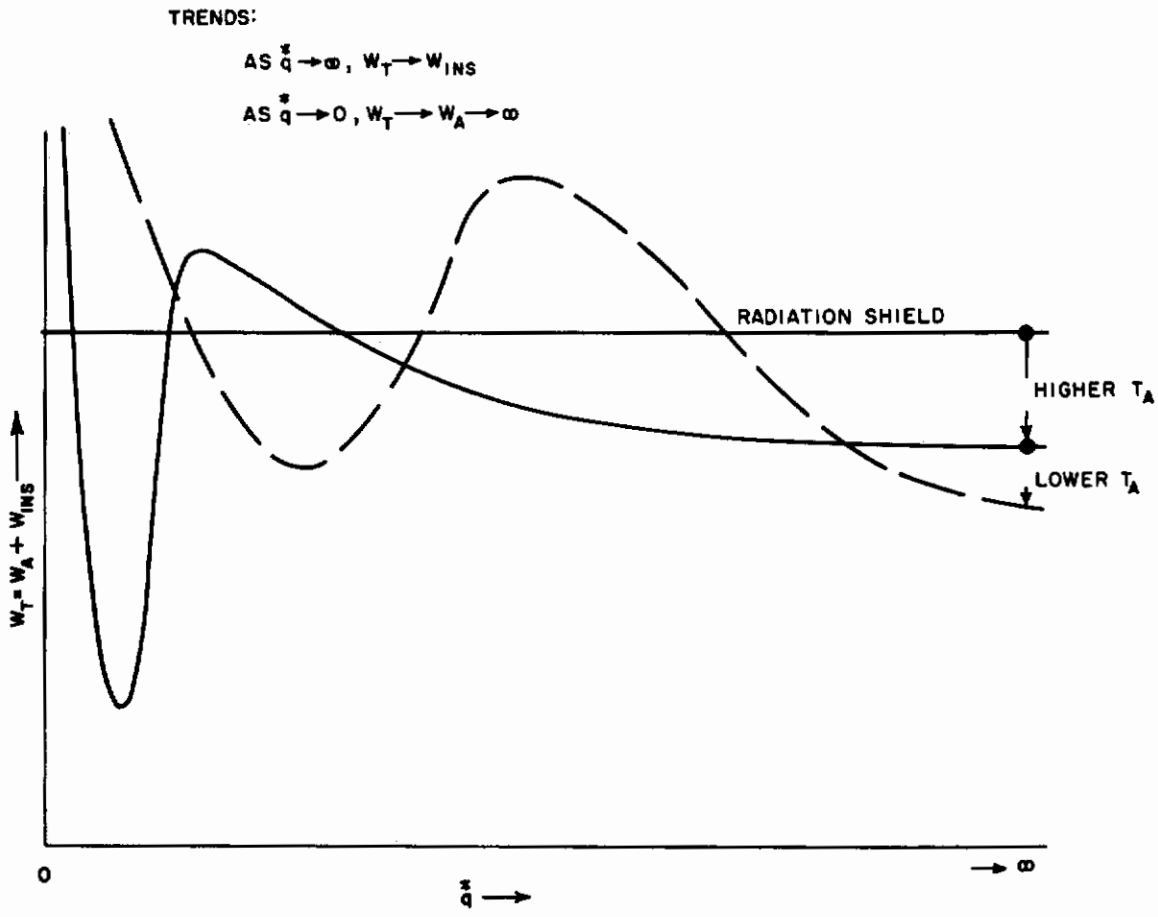

Figure 42 TRENDS OF TOTAL REQUIRED HEAT-SHIELD WEIGHT AS INFLUENCED BY MATERIAL PROPERTIES OR CHARACTERISTICS AND DESIGN CRITERIA

1) Effect of thermal properties and characteristics on weight

The results of the parametric study are presented in figure 43 of the text and figures XII-1 to XII-15 of Appendix XII. This graphical presentation shows the interaction of the ablation temperature with the effective heat of ablation and it compares the calculated weights with those of the radiation shield weight. The aerodynamic environment (fig. 22) is fixed and no structure is assumed present for this phase of the study. However, the environmental and structural effects are included in later studies. This phase of the study serves then to indicate how material properties, characterisitics, and allowable backface temperature affect the heat shield weight. The horizontal lines in figure 43 represent the weight of the comparable radiation shield. The temperatures associated with horizontal lines are maximum attainable surface temperatures and only materials with ablation temperatures below these maxima will ablate. An immediate conclusion from this phase of the parametric study suggests itself by comparison with similar studies for high-performance ballistic missiles (Refs. 17 and 24); for typical glide vehicles the weight requirement is more sensitive to the ablation temperature than to the heat of ablation while for ballistic missiles the reverse trend is true. For the long duration, low-heat flux re-entry studies under this contract, q^* may not be applied as a performance criterion as is often done for the high-heat flux short duration ballistic missile re-entry. Even in ballistic applications depending on conditions it may be misleading. Of more significance, although not a figure of merit, is the choice of materials with an appropriate surface temperature for each application such that the length of the ablation period is controlled. Admittedly, difficulties with "tailoring" of ablation temperatures to the application will arise and the temperatures may have to be measured to greater accuracy than was previously required. Figure 44 (and similar working curves in Appendix XII) gives an indication of the extent to which ablation temperature and the heat flux profile (body location) interact with the required weight. Since a large portion of the shield of a glider requires insulation, the use of high-temperature (2000° F) insulators combined with presently available ablation materials will produce a logical design concept and will help to obtain more reasonable weights. Ablation materials successfully used for ballistic missiles do not have sufficiently low conductivity by themselves to provide the insulation requirements for glide vehicle re-entry. Either materials with lower $\rho k / C_p$ have to be used or back-up insulation provided. These results indicate that ablative materials will be useful, if the mass loss were regulated by proper surface temperature selection as demonstrated by the tests of some experimental ablative plastics (Section VI).

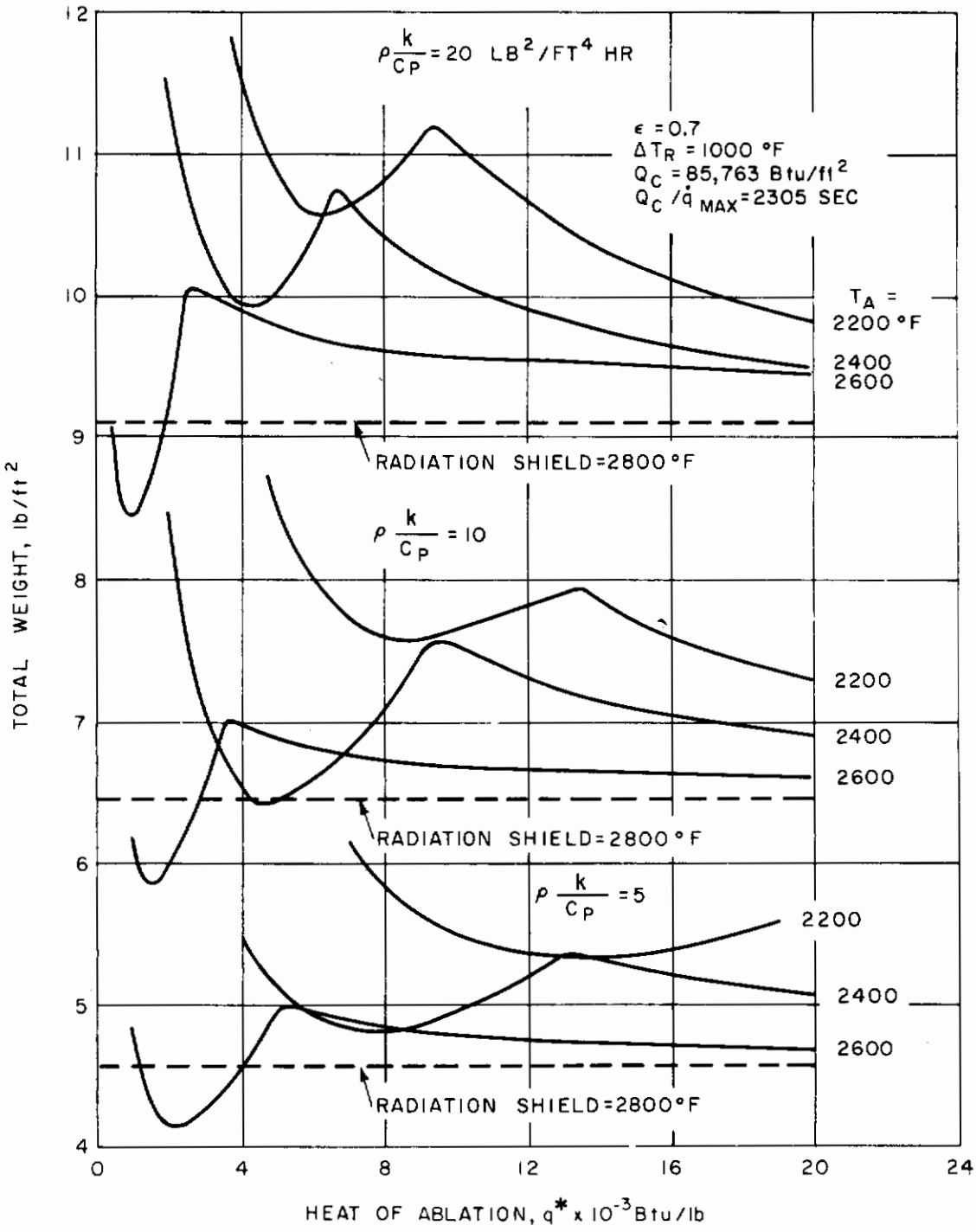

Figure 43 INFLUENCE OF HEAT OF ABLATION ON THE TOTAL SHIELD WEIGHT FOR VARIATION OF THE THERMAL PROPERTIES, Q_c = 85,763 BTU/FT^2, ΔT_R = 1000°F

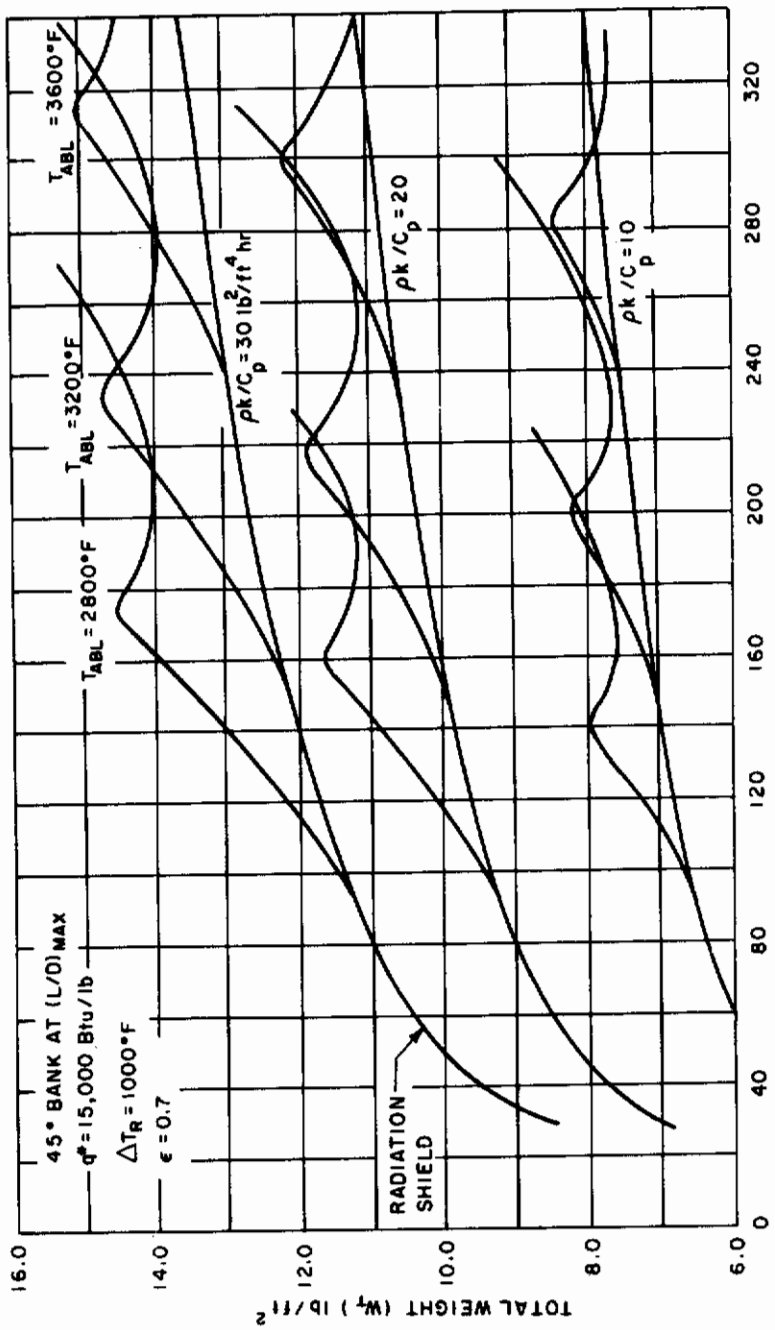

Figure 44 INTERACTION OF ABLATION TEMPERATURE AND HEAT OF ABLATION ON THE TOTAL WEIGHT

The efficiency of a heat shield may be measured by dividing the total cold wall heat input by the required weight, $Q^*_{eff} = Q_c/W_T$ (Btu/lb) and, therefore, calculations of efficiencies are easily obtained from the weight curve. An example of the magnitude of the efficiencies are given in figure 45 for the selected trajectory. Notice that the values are higher than normally encountered in ballistic missile design (Refs. 17, 24) and that $Q^*_{eff} >> q$. This is due to large total heat inputs Q_c, encountered in glide vehicle re-entry which are primarily dissipated by radiation cooling even for ablative plastics.

2) Effect of substructure thermal capacity on weight

Since ablation systems are more complex and environment dependent than radiation shields, no generalizations of the nature demonstrated in figures 30, 31, 32, 33, and 35 for a radiation system could be made in terms of substructure thermal capacities and the mal environment for an ablating system. Therefore, calculations have to be made to determine the interactions for each application encountered. These calculations are, however, easily made using the procedures developed and explained in Section III. C. 1. As an example of the order of magnitude of structure interactions calculations were made for a system analogous to that previously discussed (see Section IV. A. 2.) for radiation systems. Selecting a René substructure of 2.0 lb/ft^2 the thermal capacity $C_s W_s \approx 0.20$ Btu/ft^2-°F. This radiation-ablation shield is also similar to the case discussed above as $\rho k/C_p = 25$ lb^2/ft^4-hr; however, here ablation occurs at about 3000° F and $q^* = 10,000$ Btu/lb which is not near optimum for this application. The body location corresponds to a maximum heating rate of 81 Btu/ft^2-sec and the weight is based on a 1000° F structure temperature rise. Using figure 46 to determine the shield weight, gives $W_{ins} = 13.0$ lb/ft^2 and adding 2.0 lb/ft^2 of substructure gives a total weight of $W_T \approx 15.0$ lb/ft^2. Comparing this with the case of no structure which weighs 14.25 lb/ft^2 it is seen that adding 2.0 lb/ft^2 of René to the homogeneous radiation-ablation shield results in a net increase of only 0.75 lb/ft^2. For system selection several materials (shields and substructures) may have to be evaluated in a similar fashion to determine the most efficient design. Such analyses are presented in more detail in a later section on "Design and Development Techniques."

3) Effect of thermal environment of shield weight

The interaction of trajectory with ablation shield weight again requires that each individual application be evaluated, since no

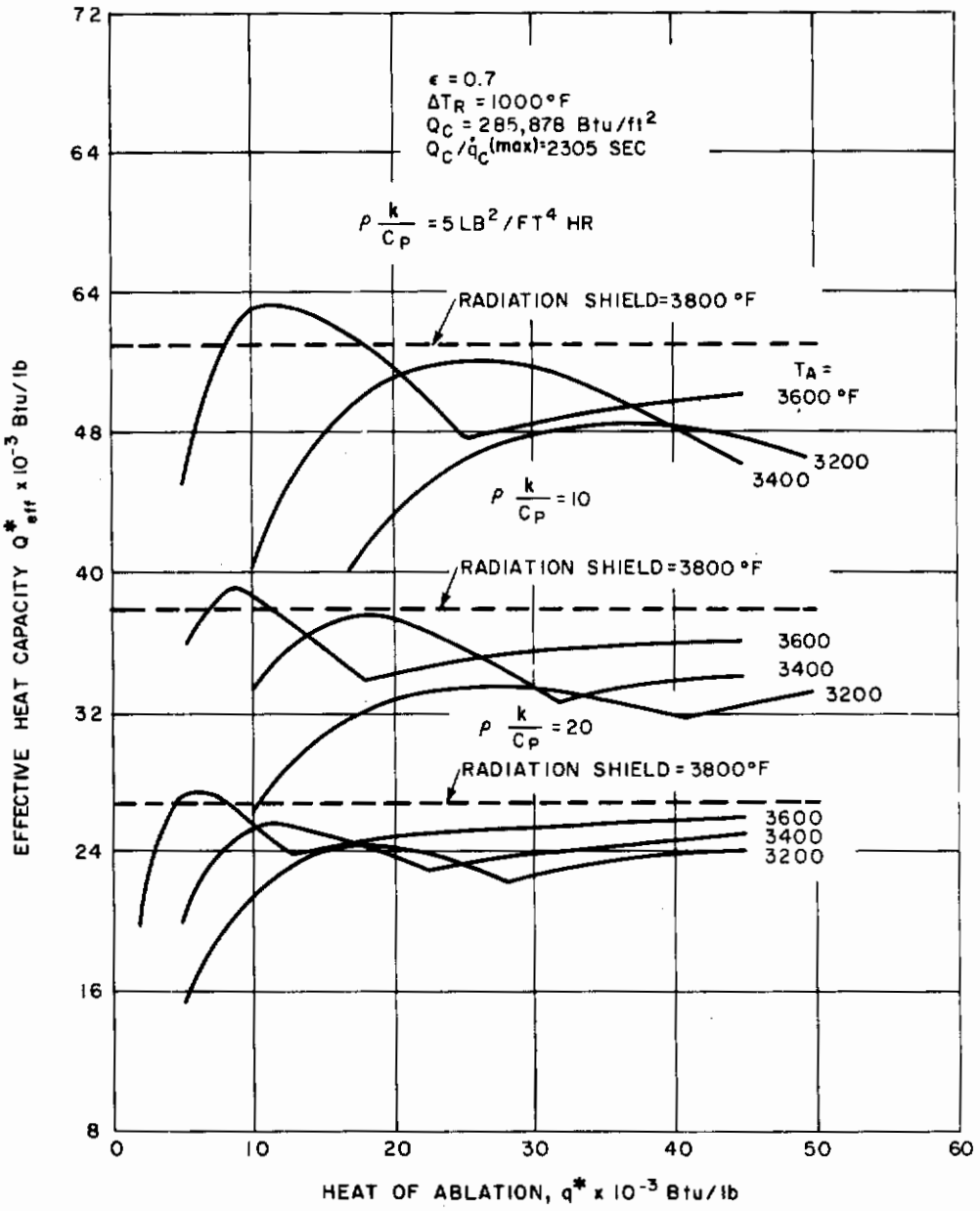

Figure 45 INFLUENCE OF THE HEAT OF ABLATION ON THE EFFECTIVE HEAT CAPACITY FOR VARIATION OF THERMAL PROPERTIES, Q_c = 85,763 BTU/FT^2, ΔT_R = 1000° F

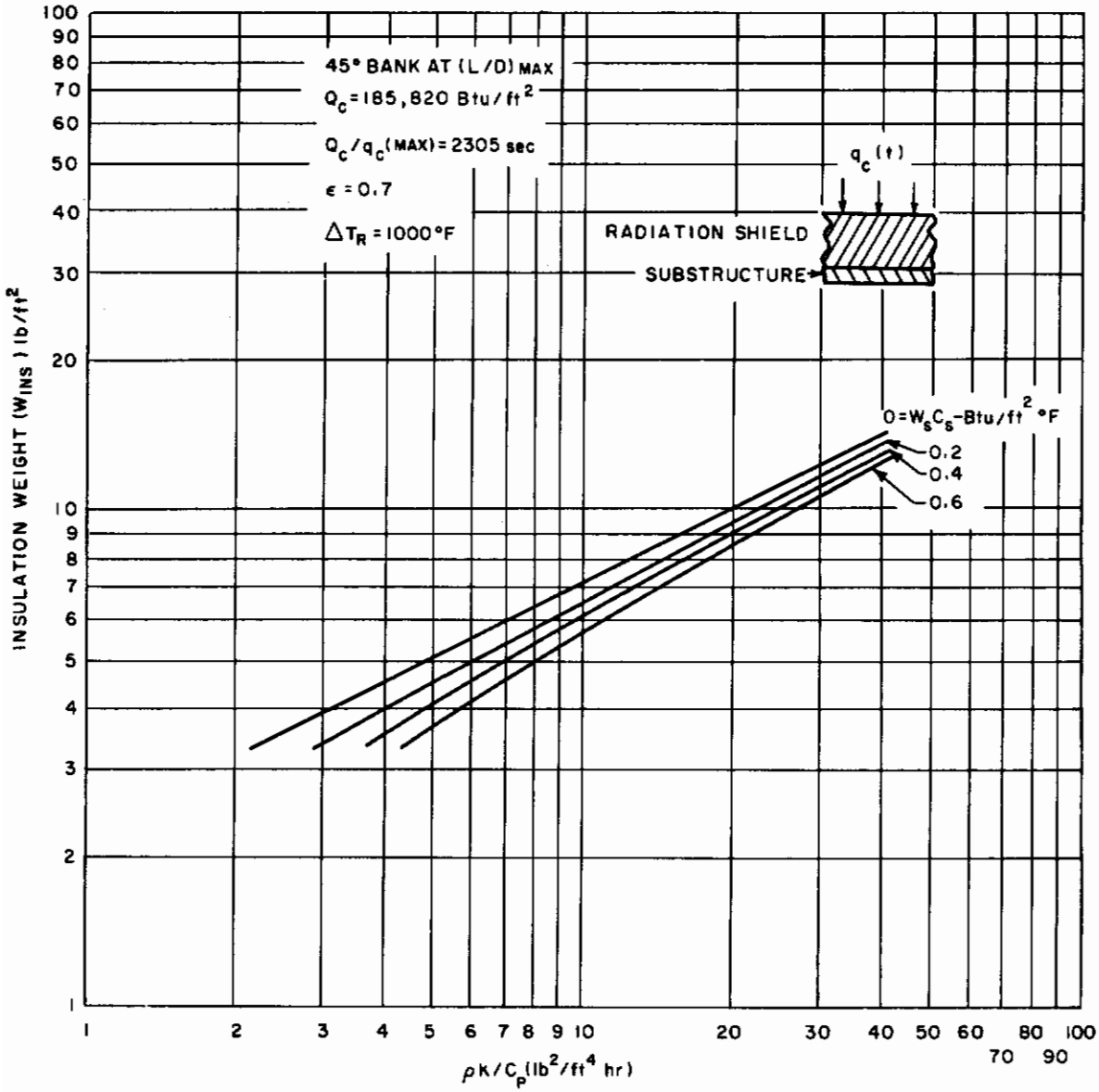

Figure 46 EFFECT OF STRUCTURE AND THERMAL PROPERTIES ON THE SHIELD WEIGHT OF A COMPOSITE (ABLATION SHIELD PLUS STRUCTURE) THERMAL PROTECTION SYSTEM

general design curves covering wide ranges of glide vehicle re-entry is possible. However, useful studies and design charts can be made to cover the re-entry corridor under consideration. Figures 22, 23, and 24 were used as representative of the re-entry thermal environment the vehicle would experience for its flight corridor. The trajectories were defined in terms of critical heating duration, $2\ Q_c/q_{max}$, and their adjusted total duration, $t_f - t_i$. A linear relation was assumed to exist between $Q_c/q_c\ (max)$ and $t_f - t_i$ which is only a slight departure from reality. Thermal evaluations were then made for radiation ablation systems in terms of the maximum heating rate, $q_c(max)$ and duration parameter $Q_c/q_c\ (max)$ for various material properties $\rho k/C_p$, ϵ, T_A, and q^* along with design rear temperature. The underlying assumption was that one heating profile may be used to approximate another for weight calculation purposes by "stretching" or "squeezing" the critical duration, $Q_c/q_c\ (max)$, or total duration $t_f - t_i$ and varying the amplitude of the rates by changing $q_c\ (max)$. It was found by making calculations using the actual heating rates that even for profiles as shown in figures 22, 23, and 24 which have somewhat dissimilar shapes the assumption was valid. This allowed for evaluation of a particular radiation ablation shield (or of several simultaneously) over the re-entry corridor by constructing curves such as figure 47 (see Appendix XII for others). With several curves of this type each for a distinct value of maximum heating rate $q_c(max)$ which corresponds to a particular trajectory, a quick analysis can be made to determine whether a given material (or several materials) would survive over part of or the entire flight corridor. For the trajectories studied no general trend was concluded for ablation systems, however for the selected ablation characteristics T_A and q^* the trend is somewhat similar to that of the radiation shield, i.e., of similar but displaced slope. Such trends can not necessarily be extrapolated to other applications since they can lead to erroneous conclusions. Calculations for evaluating each system and flight corridor need be made to determine the performance trends.

Summarizing, radiation ablation shield parametric studies were made for a selected vehicle and trajectory, in terms of $\rho k/C_p$, ablation temperature, heat of ablation, allowable backface temperature rise and body location ($\dot{q}_c\ (max)$). Interactions of substructure and thermal environment on shield weight were demonstrated for specific cases.

d. Radiation-Ablation Shield with Backface Cooling

Calculations for ablation systems utilizing backface cooling were limited to those cases needed for comparisons with other systems since

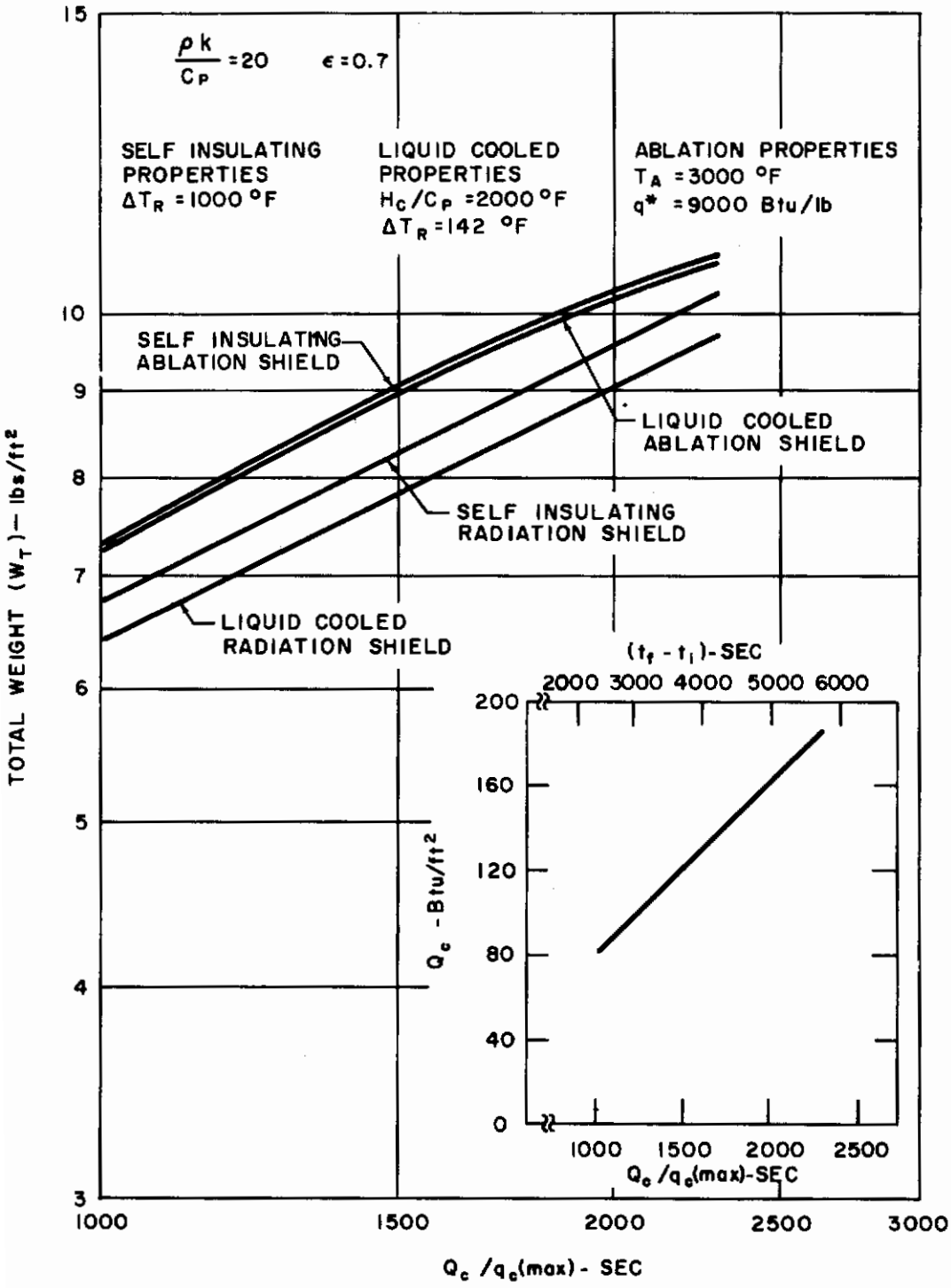

Figure 47 EFFECT OF THERMAL ENVIRONMENT ON THE WEIGHT OF RADIATION - ABLATION SHIELDS AND RADIATION SHIELDS
q_c (MAX) = 81 BTU/FT^2 - sec

the ablation trends have been covered in a rather detailed fashion in the previous discussion. As will be discussed later,(Section IV. A. 2) the weight reductions due to backface cooling are less for ablation systems than for radiation systems.

Generalized design charts are not possible for the same reasons as in uncooled ablation and interaction with environment must be evaluated for each particular system and application. The effect of substructure thermal capacity becomes insignificant for low level (T_R <200° F) backface temperature likely experienced in liquid cooled systems. Load carrying substructure weights can be added directly to the ablation, insulation, and coolant unit weight without considering thermal interactions.

e. Transpiration System

The investigation of a transpirative thermal protection system naturally centers around the mechanism of transpiration. Previous to this study analytical and experimental work had been done which indicated the possible utility of transpiration, but did not clearly define the parameters of interest in the design of a thermal protection system. Therefore, the work reported here is the result of efforts in each of two directions:

1) The utilization of existing techniques of analysis and calculation in the investigation of the parameters of interest in heat transfer, and

2) The derivation of more sophisticated techniques of analysis and calculation.

To minimize later changes, very simple systems were selected for investigation under item one above. Computer programs based on references 59 and 60 were used. These calculations are for air in chemical equilibrium injected into the boundary layer of a hemisphere 0.625-feet in radius. Injection is normal to the sphere surface at each point and thermal equilibrium is assumed. Unless otherwise stated, results are for the case of zero net heat transfer to the wall. That is, the energy equation at the wall is

$$+ k \left(\frac{\partial T}{\partial y}\right)_w = \dot{m} \left(h_w - h_c + h_v\right) + \sigma \epsilon T_w^4 \quad , \quad \text{where}$$

k is thermal conductivity, T is temperature, y is length, $\dot{m}$ is mass flow, h is enthalpy, σ is the radiation constant, ϵ is emissivity,

subscripts w, c, and v refer to wall, coolant, and vaporization, and y is chosen so that $\left(\frac{\partial T}{\partial y}\right)_w > 0$ implies heat transfer to the wall. Also, it should be realized that required mass flows presented for the stagnation point are merely limiting values of the required mass flows in the stagnation region. Total properties at the stagnation point were calculated using references 61 and 62.

The initial coolant temperature is the temperature of the transpiration fluid before it is injected. This temperature is 200°K., unless otherwise stated.

Two modes of thermal protection by transpiration were considered separately. When a fluid is injected through a surface, it affects the aerodynamic and thermodynamic conditions of that surface. This effect may be thought of as local in nature and is the most efficient way to utilize a given mass in transpiration. However, for reasons of a structural nature, it is advisable to consider the thermal protection afforded by the downstream effects of excessive local transpiration. Such a system, which may be thought of as discrete in nature, cannot be used to protect a surface region which at some time includes the stagnation point. Hence, the use of a discrete injection system implies excessive local transpiration in the stagnation region, with additional discrete transpiration at downstream locations, as required.

The spike effect occurs when the injected momentum flux per unit area is too high. In general, the higher the specific heat of a species, the lower is its density. Hence the injected momentum flux increases if a gas with a higher specific heat is used. These effects are shown for a perfect gas in figure 48.

Stagnation point air flows required for local thermal protection of a nonradiating wall at 500°K are presented as a function of free stream velocity and altitude in figure 49. As one would expect, the required mass flow increases with free stream density and free stream velocity. In figure 50, results are presented for a wall radiating with an emissivity of .6 at a temperature of 1500°K. A radiating wall at a temperature of 1000°K is the subject of figure 51.

The effect of a heat of vaporization was obtained by including a heat of vaporization term in the energy equation. The effect of this term is shown in figure 52 in which the required mass flow is plotted versus wall temperature for the injection of air, air and a radiating wall, air with a heat of vaporization, and air with a heat of vaporization and a radiating wall.

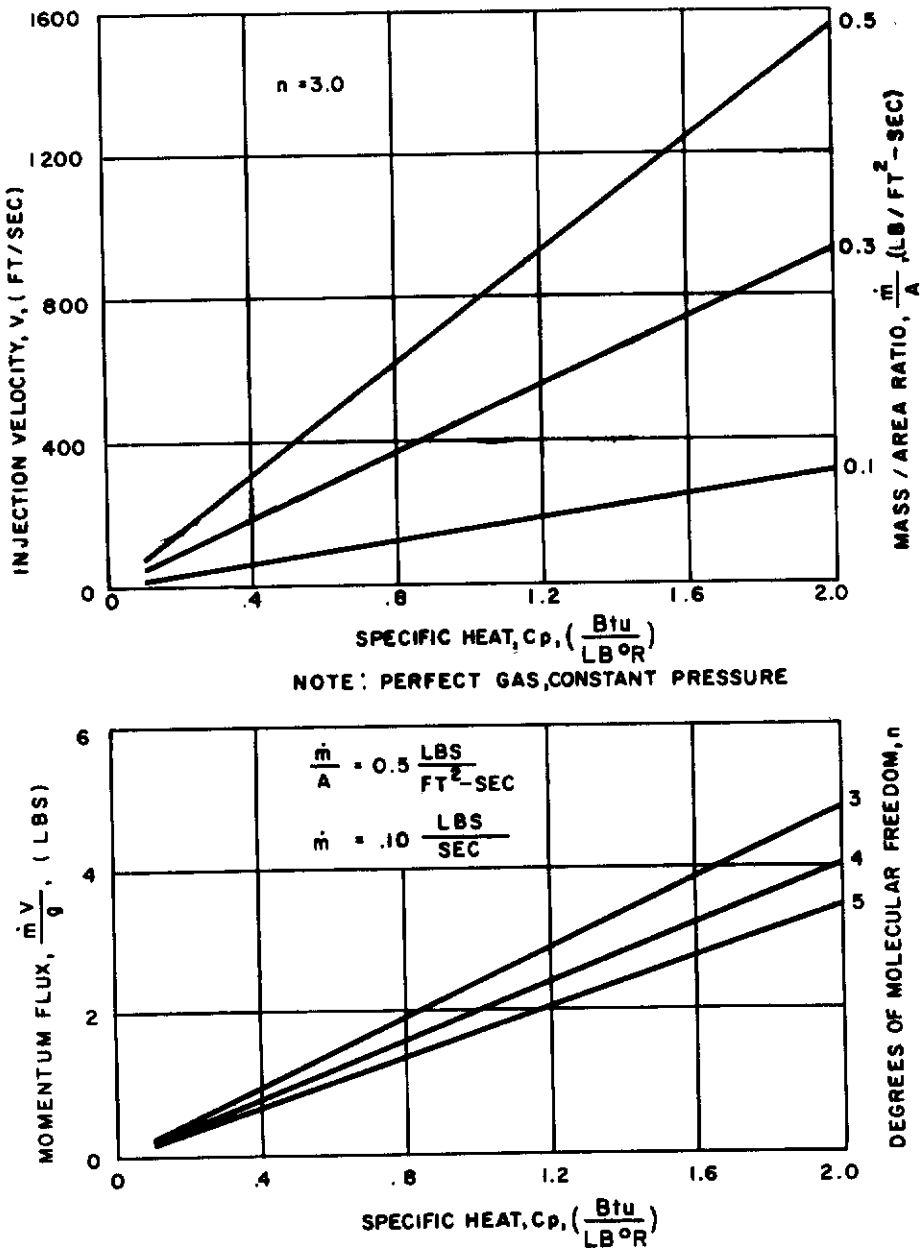

Figure 48 EFFECT OF SPECIFIC HEAT ON THE INJECTION VELOCITY AND INJECTION MOMENTUM FLUX

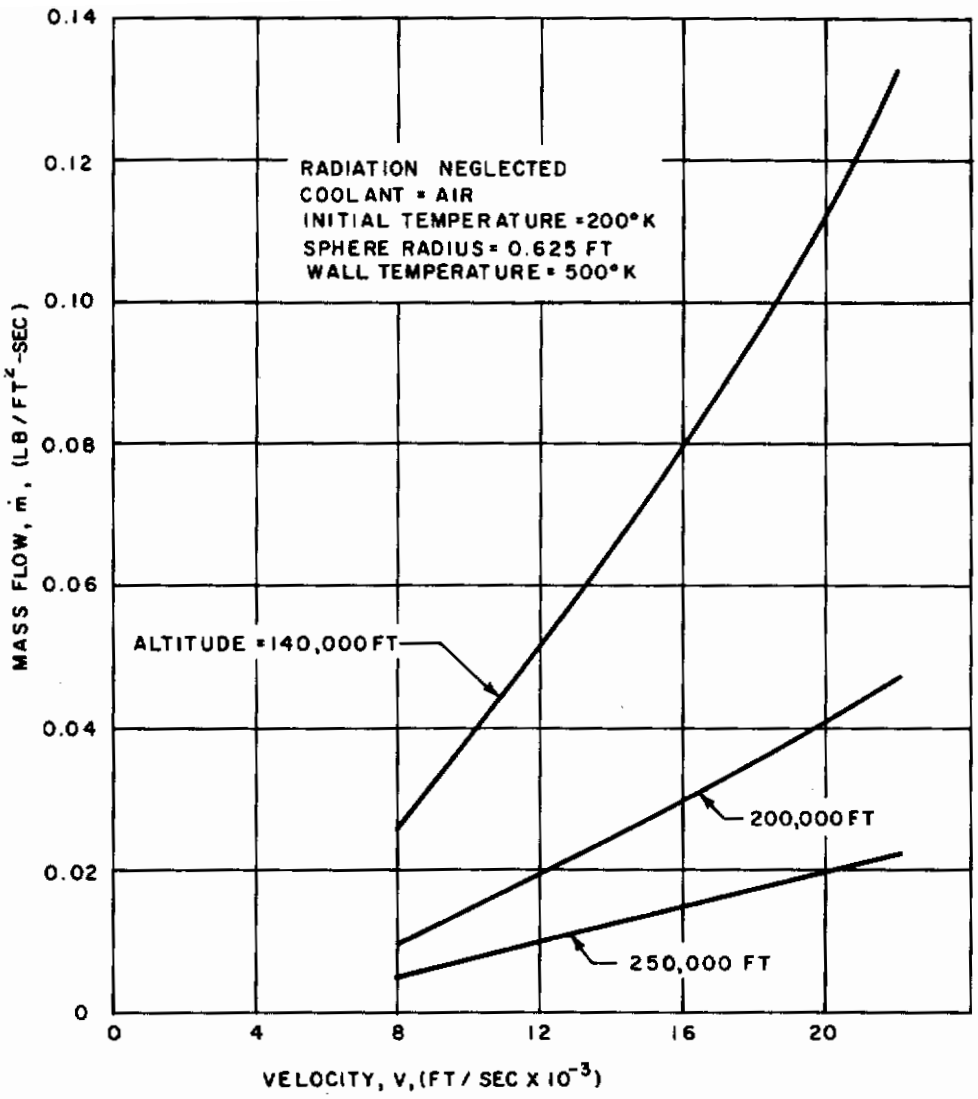

Figure 49 EFFECT OF AMBIENT DENSITY (ALTITUDE) ON TRANSPIRATION RATE

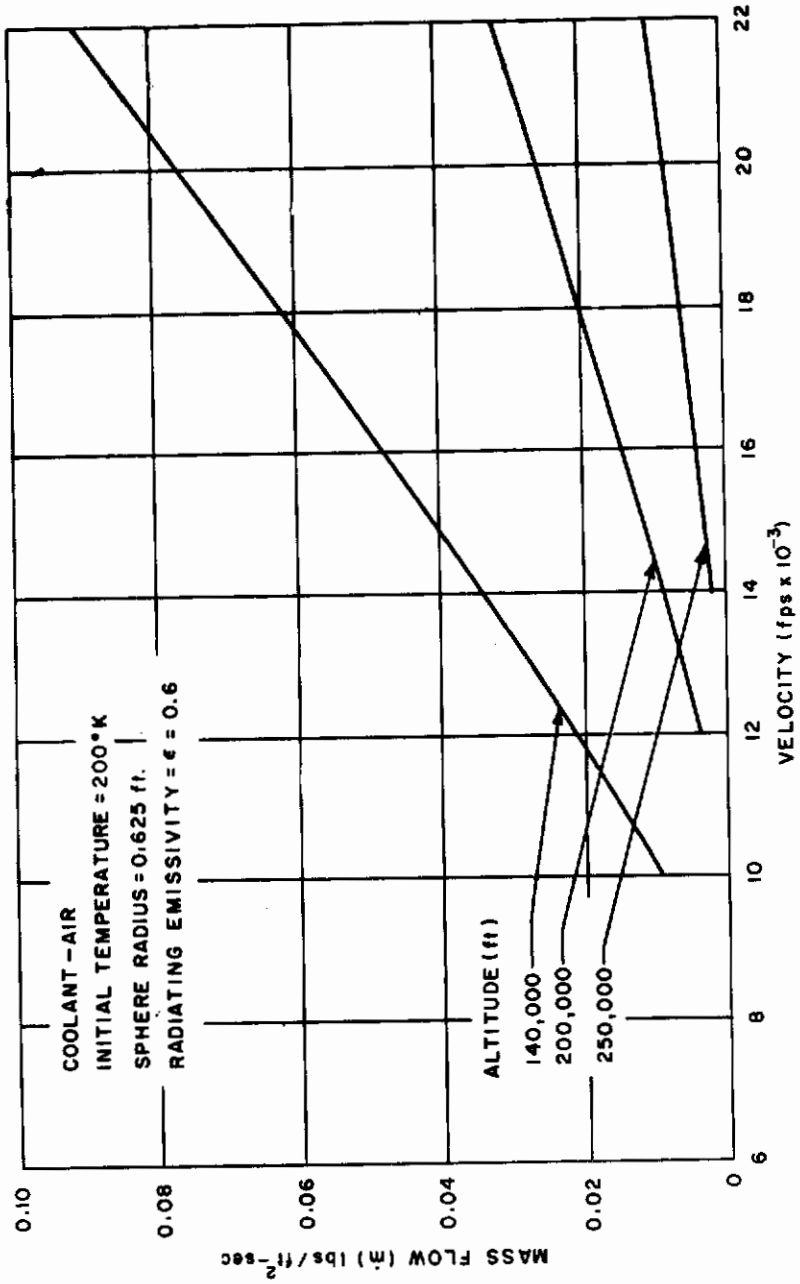

Figure 50 TRANSPIRATION MASS FLOW VERSUS VELOCITY, ALTITUDE A PARAMETER, WALL-TEMPERATURE 1500° K

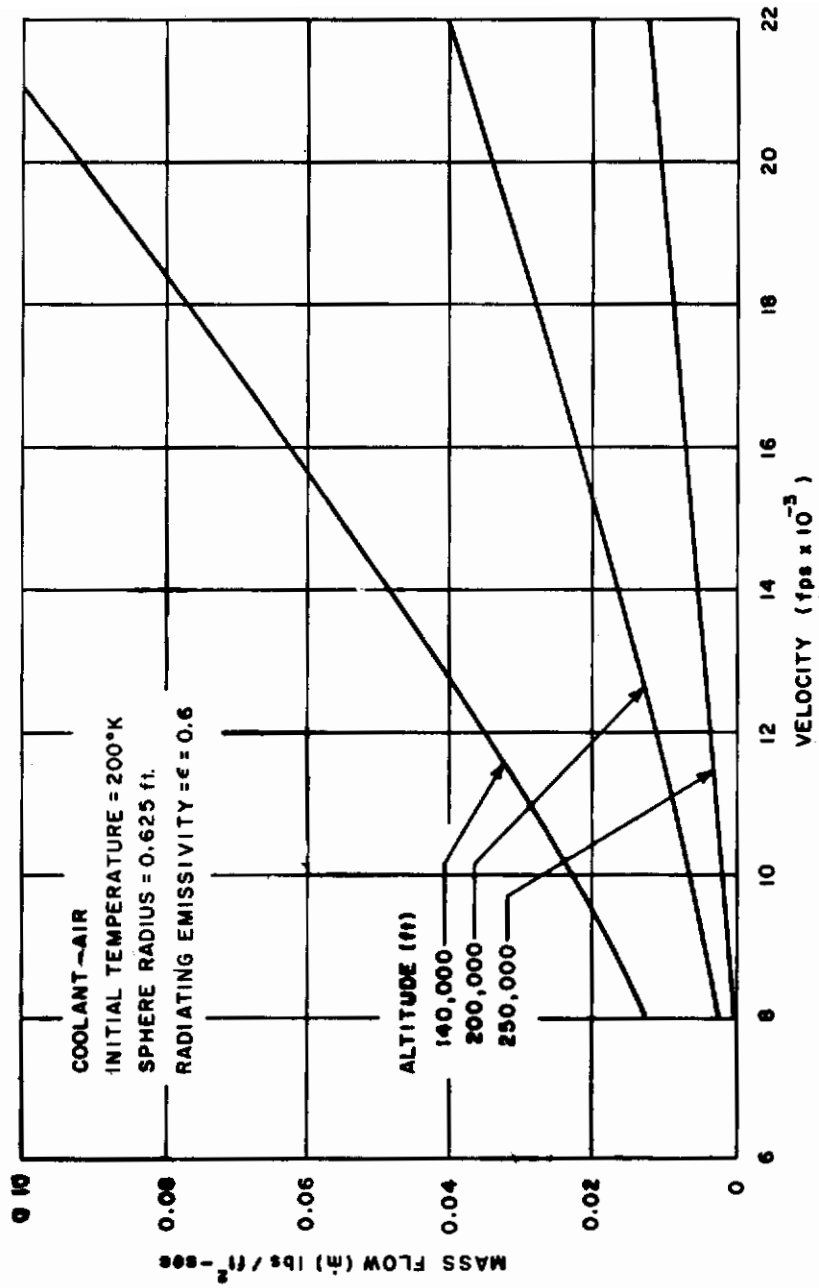

Figure 51 TRANSPIRATION MASS FLOW VERSUS VELOCITY, ALTITUDE A PARAMETER, WALL TEMPERATURE 1000° K

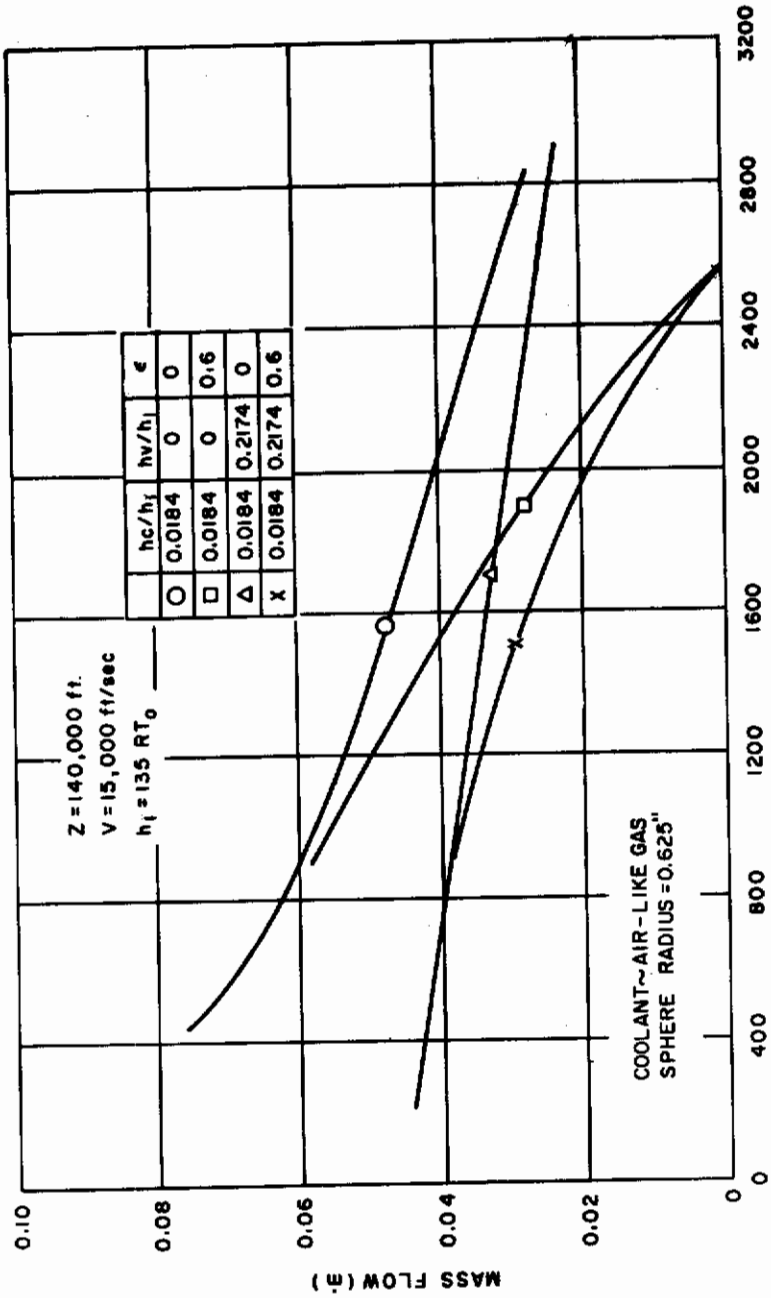

Figure 52 AIR TO AIR TRANSPIRATION AT 140,000 FEET AND 15,000 FEET PER SECOND

From figure 52 it is seen that the equilibrium radiation wall temperature for this condition is 2670°K and that radiation, even with an emissivity of .6 is quite significant. Additionally these curves suggest that a radiative-transpirative system offers distinct possibilities as a means of thermal protection. The major problem of such a system is the high wall temperature and the internal heat transfer it causes. Hence a successful practical transpiration system requires a system having an insulative outer layer. Such a layer will produce the steep thermal gradient necessary for small internal heat transfer and large externally radiated flux.

The figure also shows that radiation is significant at higher temperatures, whereas the heat of vaporization is only significant for the high mass fluxes usually required for low-wall temperatures.

The investigation of the downstream effect of excessive local transpiration in the stagnation region is an appreciably more complicated problem than the foregoing. Therefore, one altitude-velocity point was selected and the effects of the amount of an injected mass were determined for a non-radiating adiabatic wall. The point selected requires the greatest injected mass flow for the preservation of low-wall temperatures of any point in the trajectory presented in figure 53.

In figure 54, the variation of downstream wall enthalpy is shown for transpiration in the stagnation region. It appears that the effects are not long lasting, but it should be noted that the ratio of the total surface area for an angle of .37 radians to the surface area for an angle of .25 radians is over two to one. That is, these results are for a small mass flow (0.0033 lb/sec) followed downstream through an area greater than the injected area. A similar effect is shown in figure 55, essentially for the product of the friction coefficient and the Reynolds number. Here the value without injection is also shown for two different values of beta, where $\beta = \frac{2 \ln V_1}{\ln \xi}$, and V_1, is the velocity at the edge of the boundary layer and ξ is the transformed x coordinate. Again, the persistence of the transpiration effect is shown, making it clear that higher mass flows should be considered.

The air flows required for zero net heat transfer to a non-radiating stagnation point have been correlated (Refs. 63 and 64). This correlation is presented in figure 56. In figure 57, the high mass flow region of the correlation curve is expanded in an effort to show that, although the numerical differences are trivial, the calculations do indicate that an extremely high mass flow would be required to maintain the wall enthalpy precisely at the coolant enthalpy. It is, assumed that this enthalpy is appreciable less than the stream

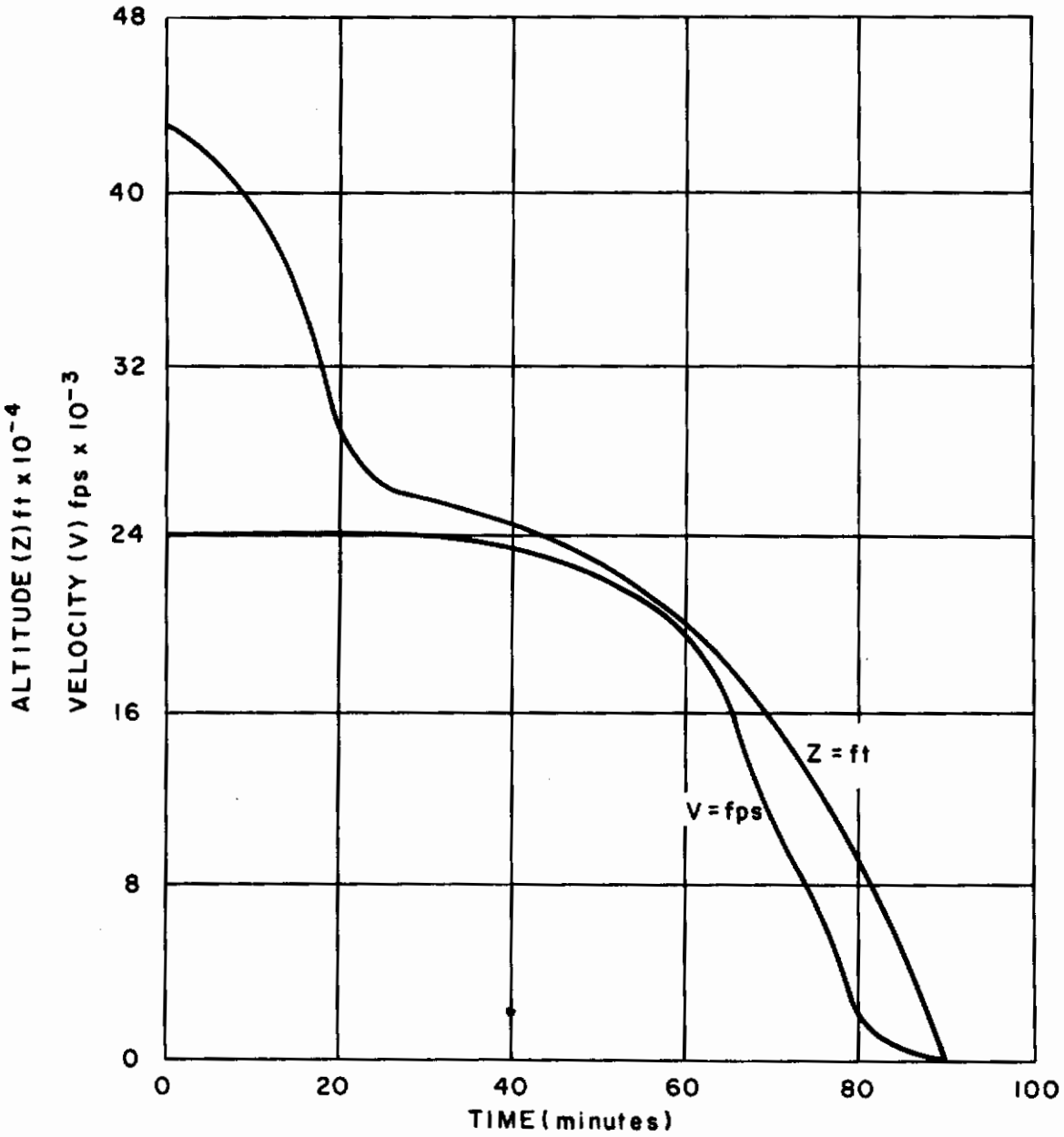

Figure 53 TYPICAL GLIDE VEHICLE TRAJECTORY - VELOCITY AND ALTITUDE

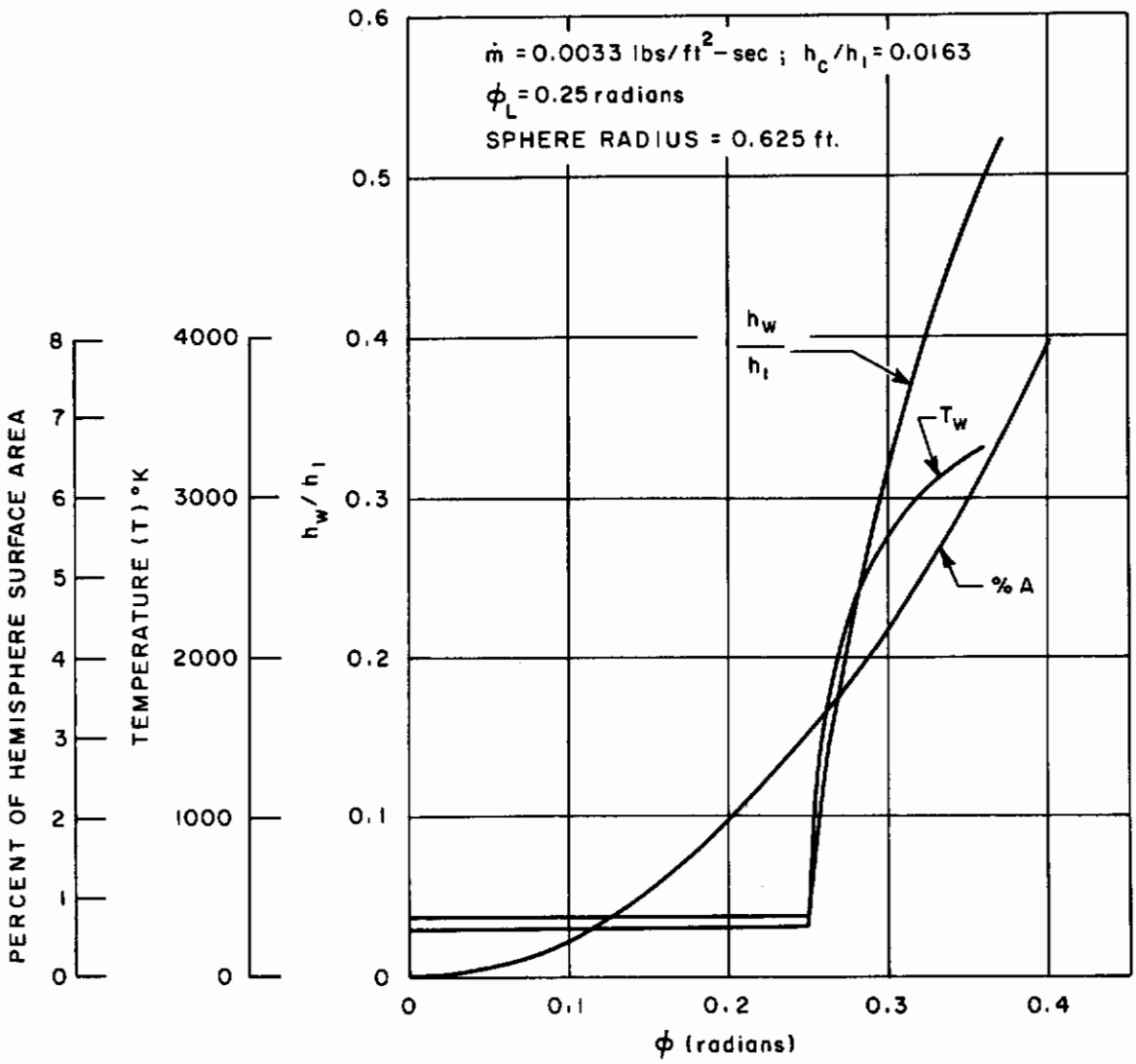

Figure 54 DOWNSTREAM EFFECT OF TRANSPIRATION ON WALL ENTHALPY

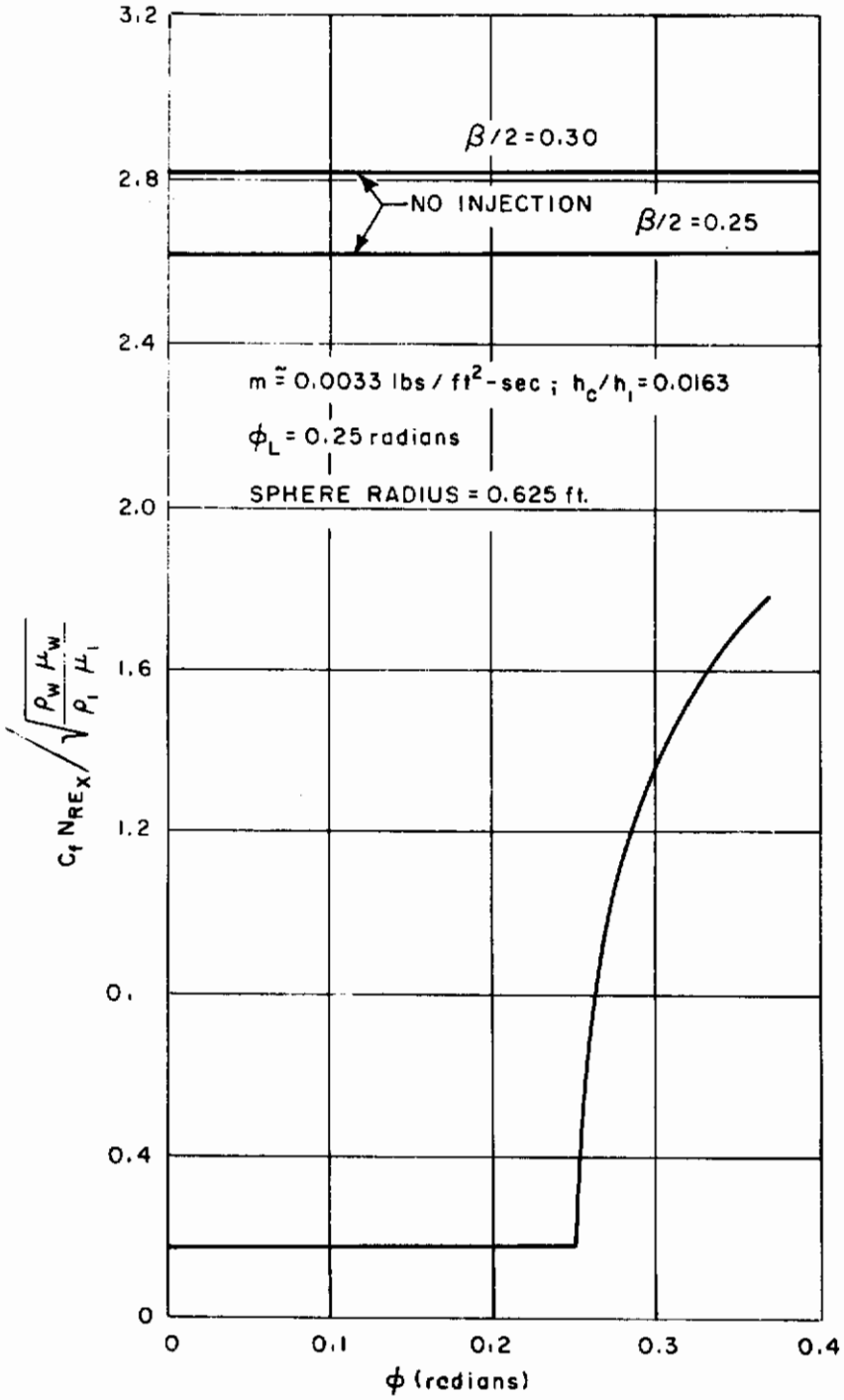

Figure 55 DOWNSTREAM EFFECT OF TRANSPIRATION ON FRICTION COEFFICIENT

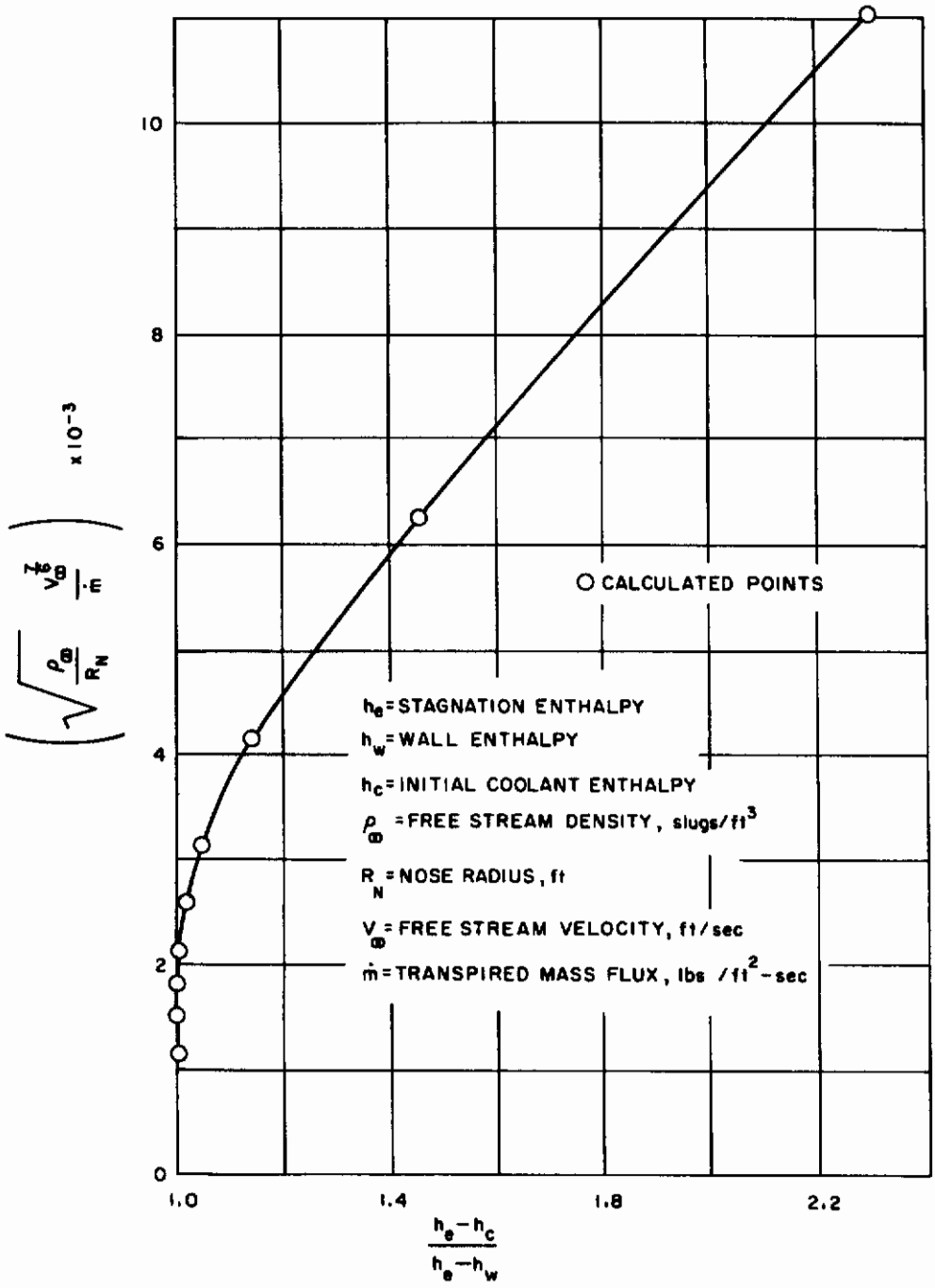

Figure 56 CORRELATION OF AIR TO AIR TRANSPIRATION

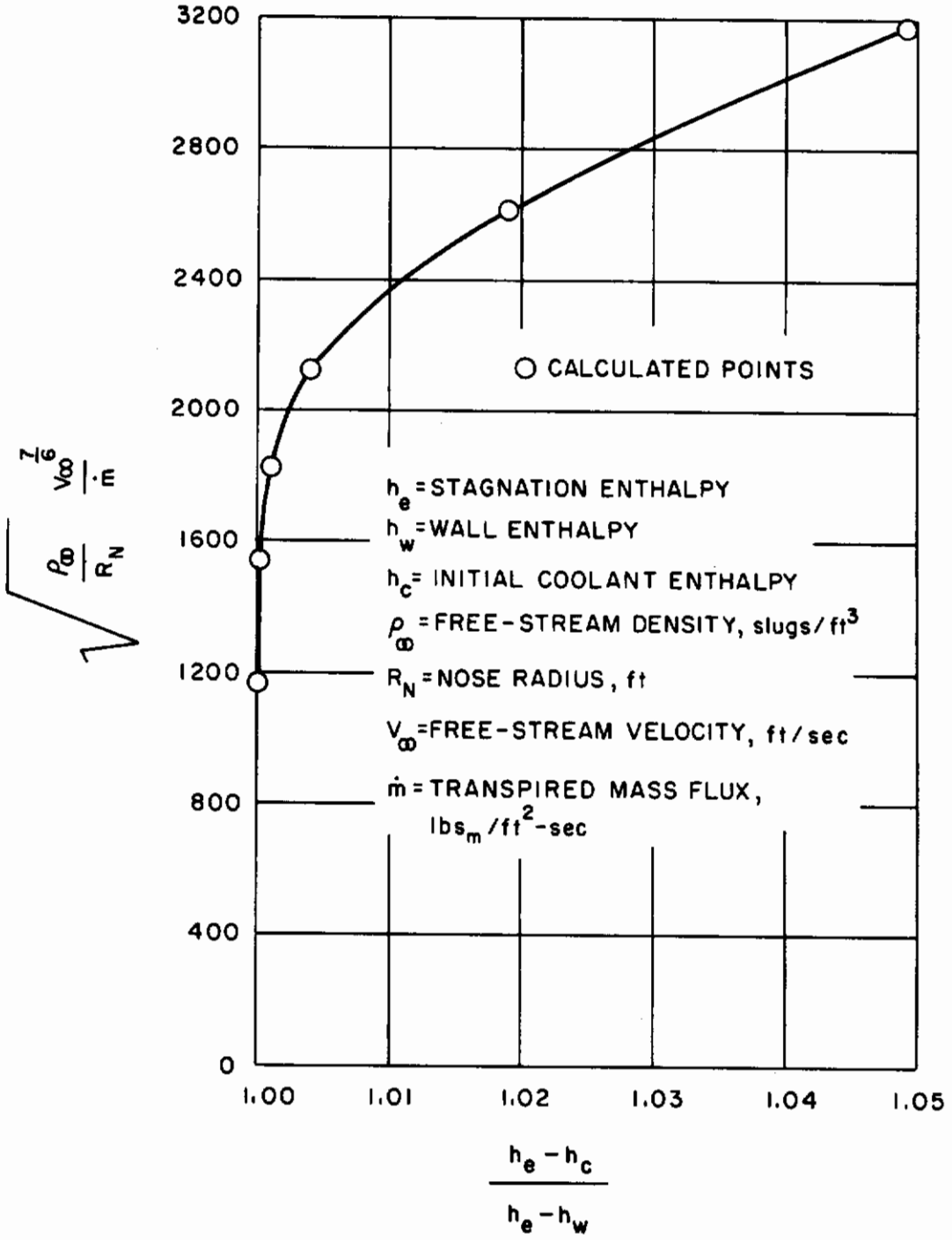

Figure 57 CORRELATION OF AIR TO AIR TRANSPIRATION $\left(\frac{H_e - H_c}{H_e - H_w}\right)$ NEAR ONE

enthalpy.) However, this mass flow is not in general infinite, since the boundary layer will be lifted by some finite flow. For purposes of a first approximation, a value of $\sqrt{\frac{\rho_\infty}{R_w}} \cdot \frac{V^{7/6}}{in} = 2500$ can be integrated over the trajectory time and a total stagnation point mass flow obtained.

To establish a basis for comparison, the typical glide vehicle re-entry trajectory of figure 53 has been selected.

The stagnation point results have been applied to this trajectory in figure 58. Although no definite conclusions can be drawn from this plot, further refinements may be made to obtain an approximate system weight.

If the similarity solution mass flow parameter, $f\{0\}$, is integrated around the reference hemisphere, we obtain a ratio of total mass flow for local transpiration to the stagnation point mass flow equal to 1.865. This procedure results in a conservative estimate of the required mass for the hemisphere, knowing the mass flow required at the stagnation point. From reference 65 one may estimate that the use of helium in place of air would afford a reduction in required mass flow by a factor of at least two-thirds. If, then, the conditions of the lowest curve in figure 58 can be met, about 30 pounds of helium would protect the reference hemisphere through the trajectory of figure 53. If one adds about 20 pounds for such non-structural hardware as a pressure vessel, the system weight ratio would be about 20 pounds/ft^2.

Although the final design of a transpiration system cannot be undertaken on the basis of the work reported here, this study does show that there is indeed some promise in such attempt. The difficult nature of the mechanistic analyses used here has prevented any major investigation of actual design problems and techniques in the allotted time. Of primary importance are the transient analyses of a real system having a finite thermal capacitance, the engineering analysis of the heat transfer within such a system, as well as an experimental evaluation of system effectiveness and various transpiration fluids. Additionally, high-temperature insulating materials which can be manufactured are required.

In essence then, the engineering analysis of systems and materials can only follow the scientific analysis of the phenomena in question. The phenomenological analyses on which this work is based are contained in references 59, 60 and Appendix XIII. The analysis of the stagnation region was extended to include the laminar boundary layer flow of dissociated air in chemical non-equilibrium. This analysis is given in Appendix XIV.

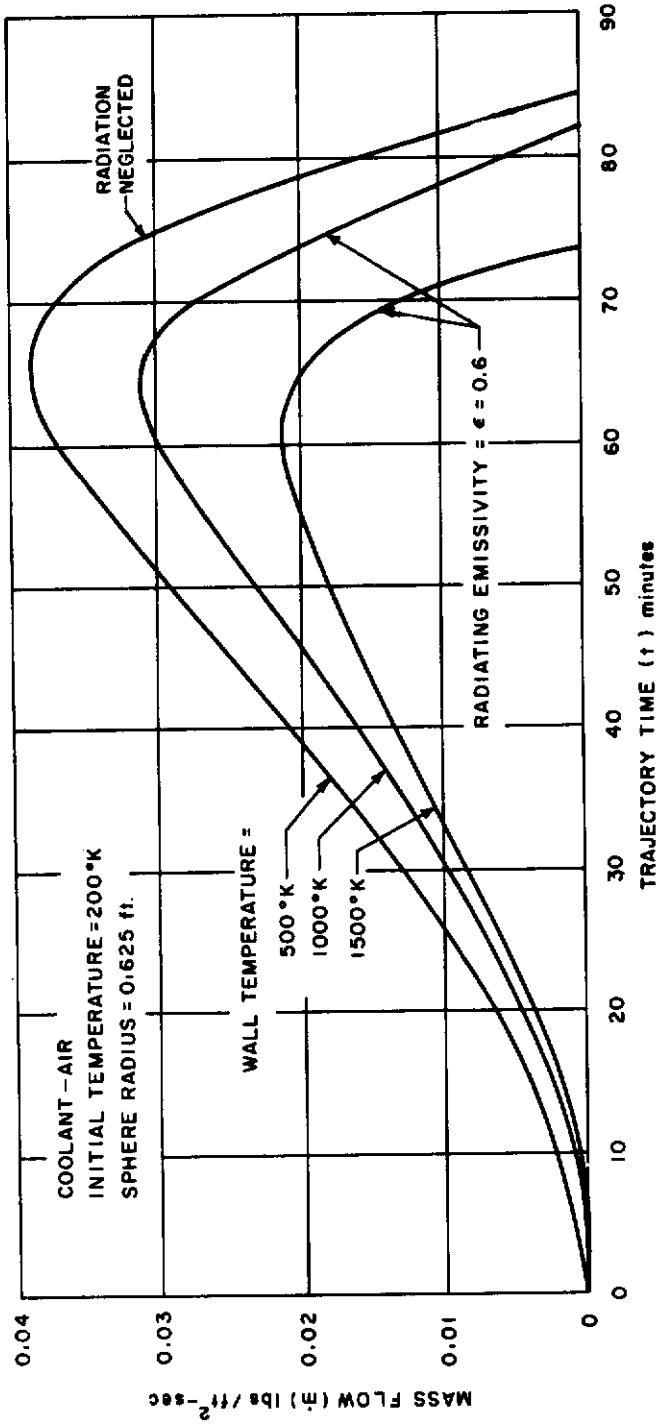

Figure 58 TRANSPIRATION MASS FLOW VERSUS TRAJECTORY TIME

f. Plastic Impregnated Matrixes

A material combining the advantages of self-regulating mass transfer with the dimensional stability of a radiation shield is of interest for certain glide vehicle applications. Such a system might consist of a porous refractory matrix filled with a thermally decomposable polymeric material. The absence of surface recession in such a system, while a desirable feature, precludes the possibility of drawing any conclusions regarding its performance on the basis of steady state considerations. The analysis of this type of system requires a completely transient treatment of a number of phenomena associated with ablation and radiation shields.

As an example of the type of system under consideration, calculations have been made for a zirconia matrix filled with polytetrafluoroethylene. Preliminary considerations indicated such a system might be feasible although attempts at fabrication have not been successful to date. Analysis of this system has been made using the theoretical treatment of Munson and Spindler (Appendix V) by means of analogue simulation. The properties employed are listed in table 4 and have been estimated on the basis of the properties of the pure components. Simulations were carried out for a system weight of 10 lbs/ft^2 over the trajectory of figure 59. Two total heat inputs were assumed corresponding to two vehicle locations. Time-temperature histories of several locations in the material are shown in figures 60 and 61. Corresponding time-density histories are shown in figures 62 and 63.

As can be seen from the figures, the material with properties as assumed in table 4 did not survive the heat input condition without losing all of the polymeric filler. In this case the backface temperature reached a maximum in excess of 2200°F. For the less severe heating condition the polymer at the backface survived the entire heating period and the temperature never exceeded 1000°F.

The calculations indicate that the material as assumed is not particularly promising for glide vehicle application. One of the limiting factors is the high thermal conductivity associated with the basic matrix. Subsequent to these calculations a material consisting of zirconia filled with polymethylmethacrylate has been fabricated and tested. This system appears to show more promise than the assumed system discussed here. The theoretical and experimental results for this second material will be presented in a later section of this report.

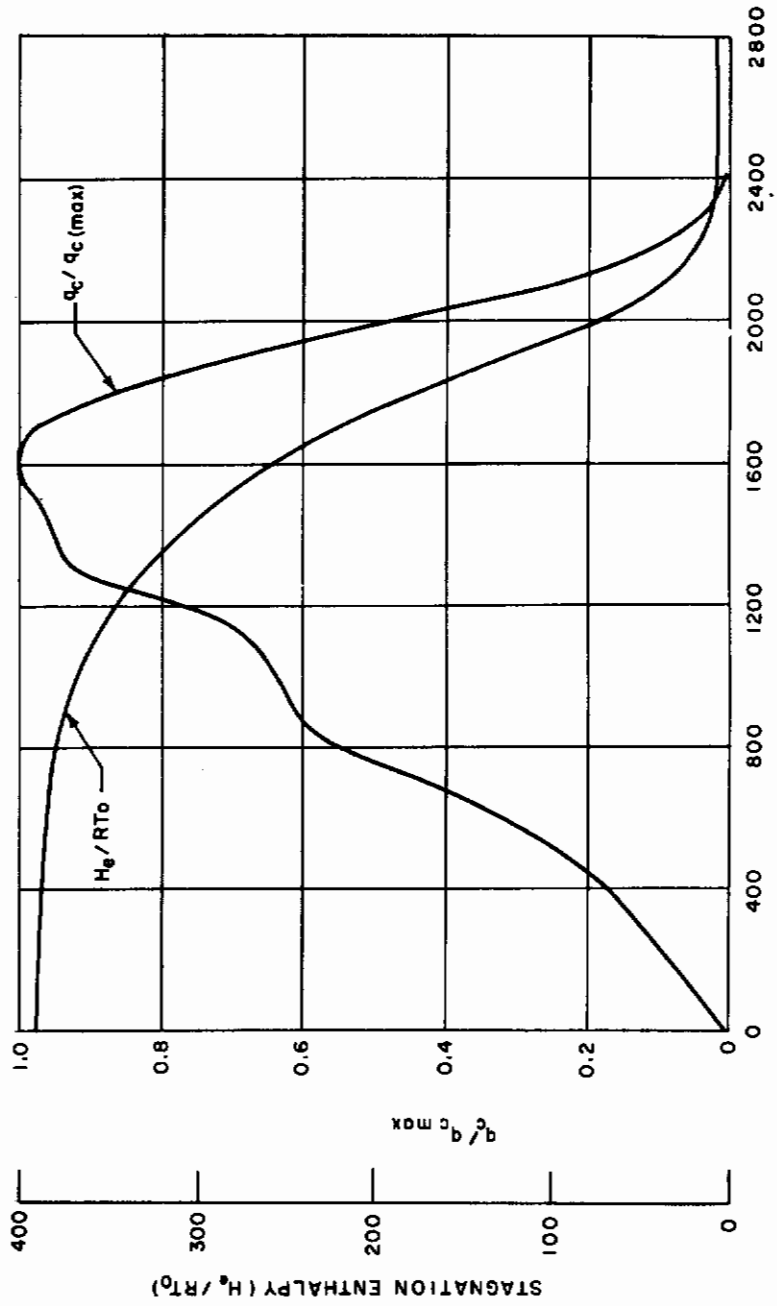

Figure 59 COLD WALL HEATING RATES AND STAGNATION ENTHALPY EMPLOYED FOR ANALYSIS OF IMPREGNATED MATRICES

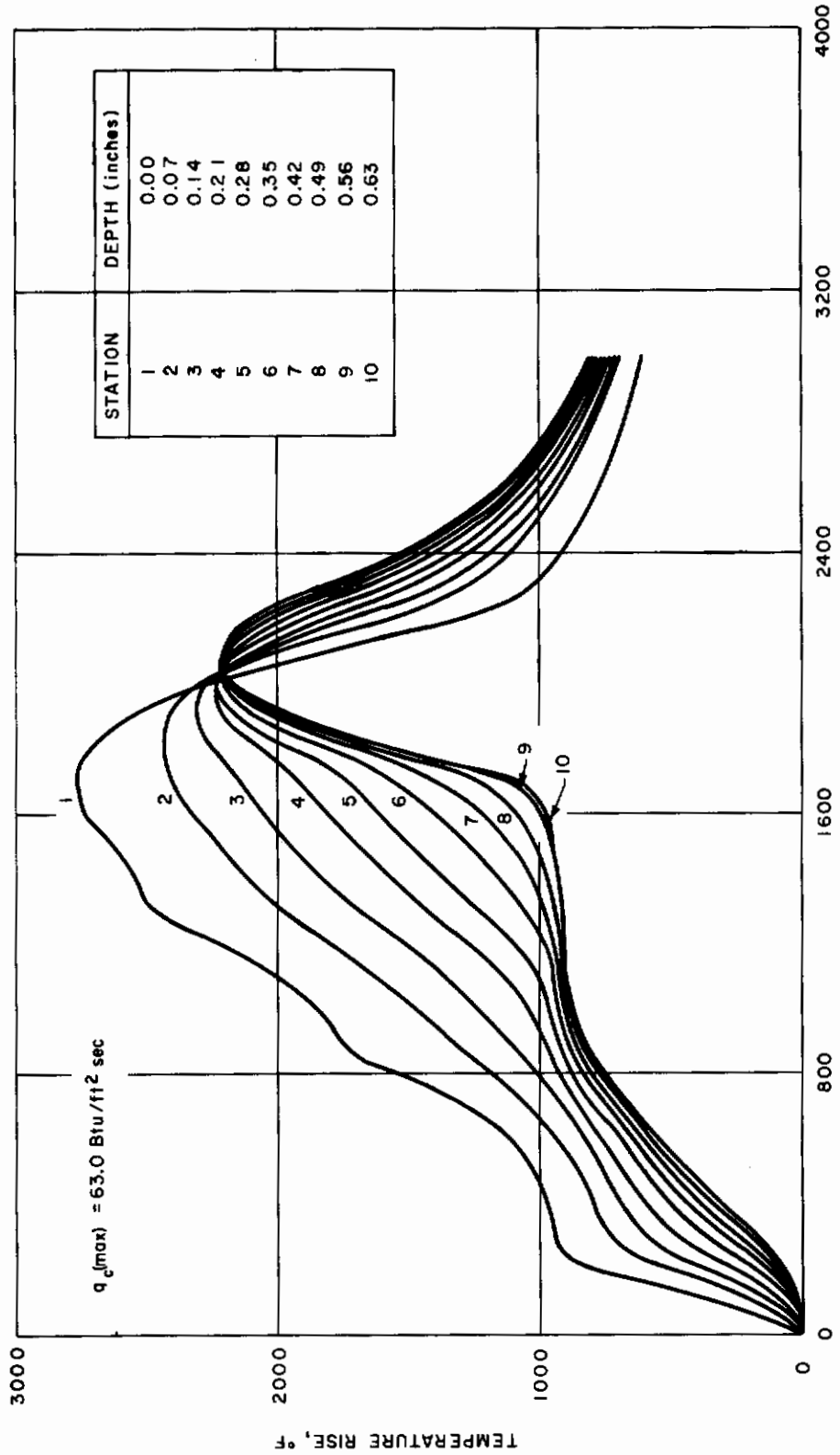

Figure 60 TEMPERATURE HISTORY OF TEFLON FILLED ZIRCONIA -- HIGH HEAT FLUX

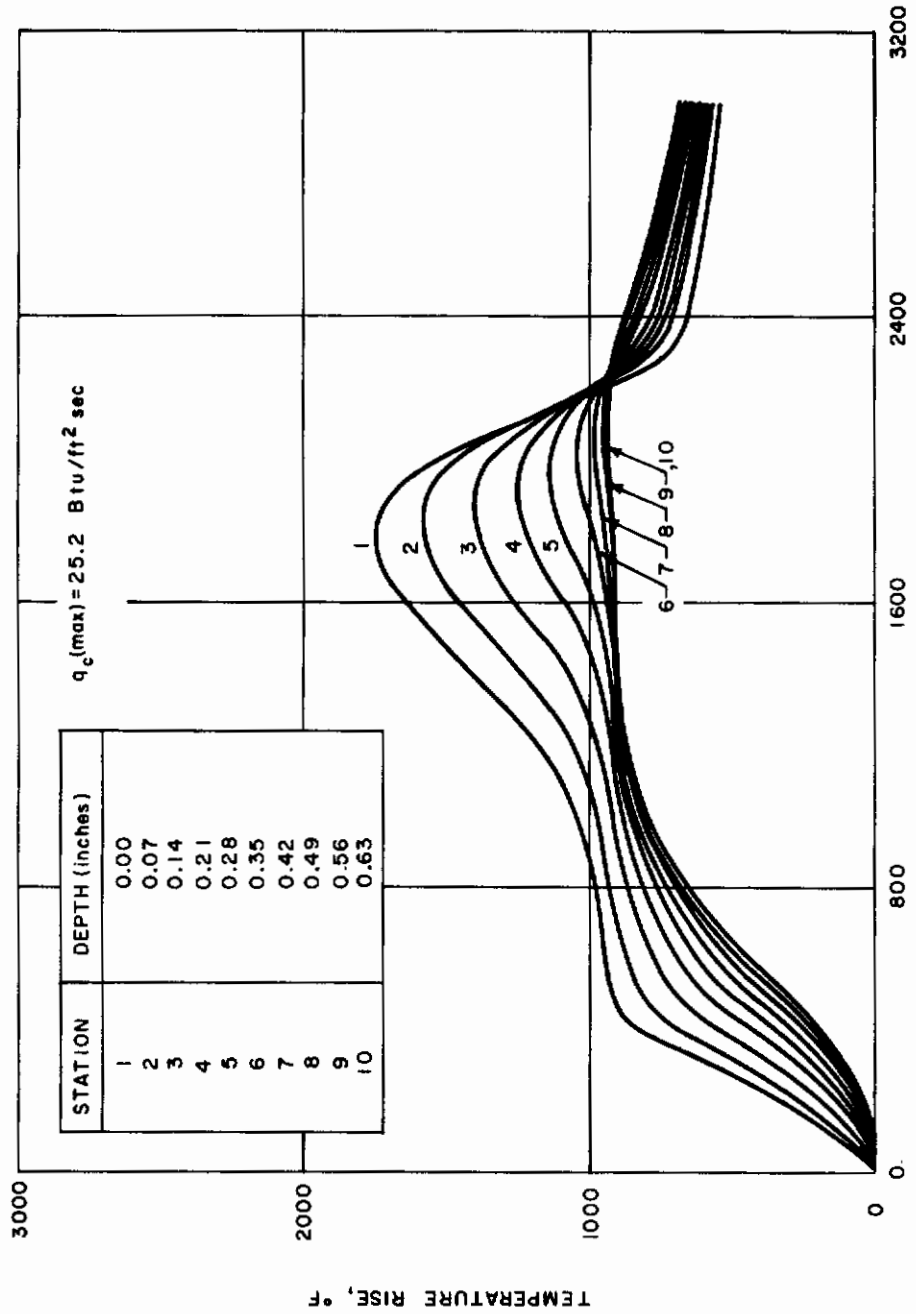

Figure 61 TEMPERATURE HISTORY OF TEFLON FILLED ZIRCONIA -- LOW HEAT FLUX

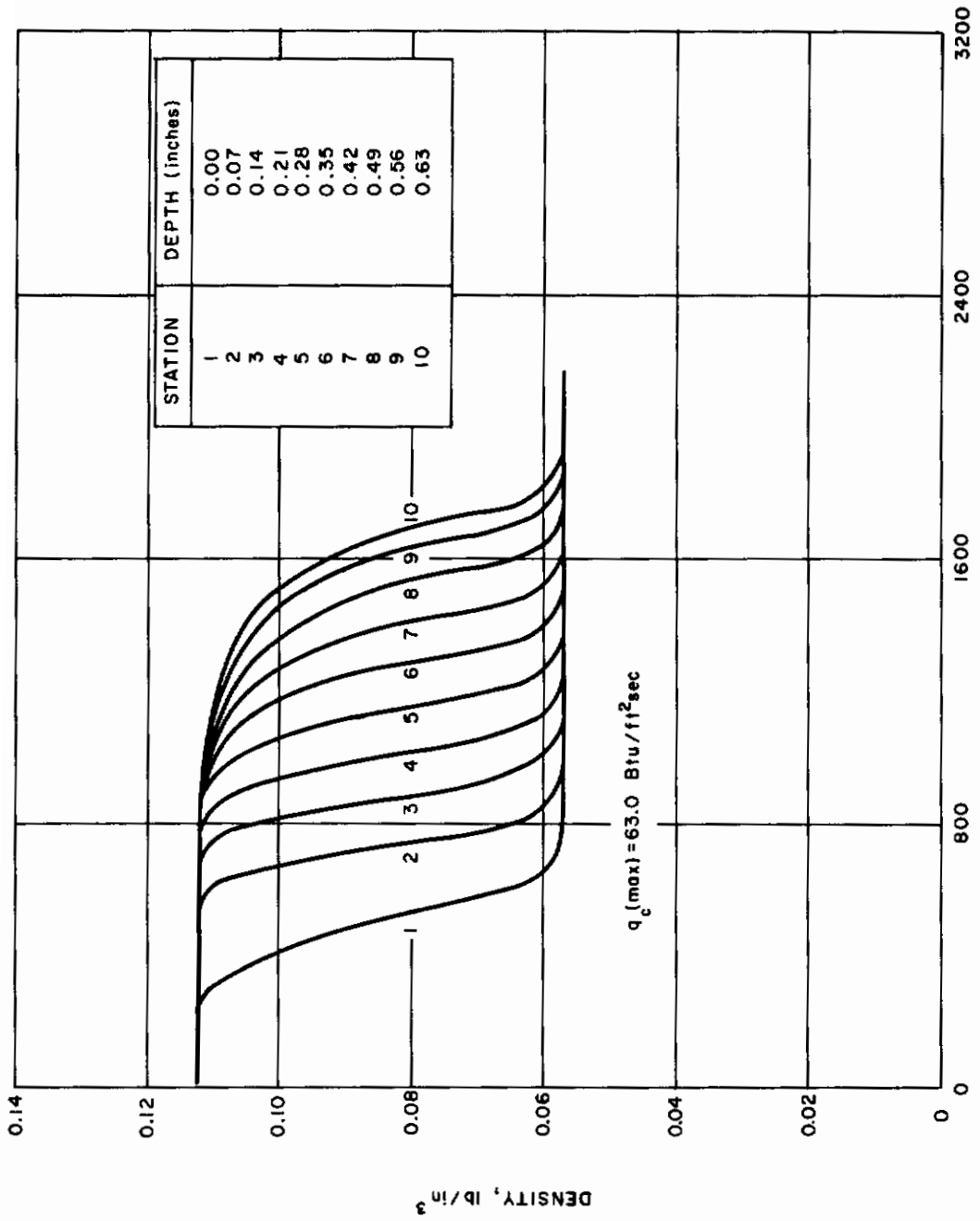

Figure 62 DENSITY HISTORY OF TEFLON FILLED ZIRCONIA -- HIGH HEAT FLUX

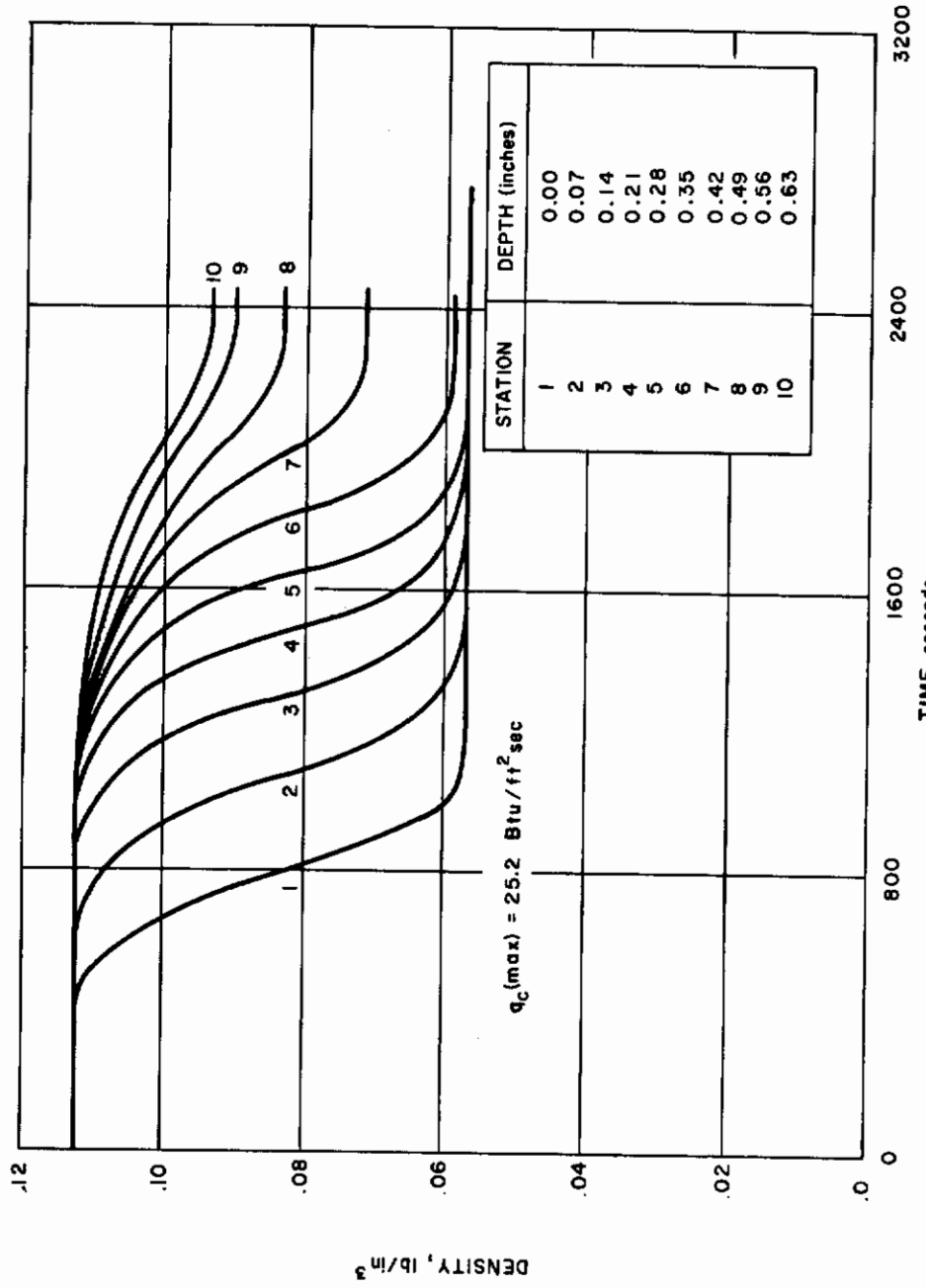

Figure 63 DENSITY HISTORY OF TEFLON FILLED ZIRCONIA -- LOW HEAT FLUX

TABLE 4

THERMAL PROPERTIES OF THE TEFLON IMPREGNATED ZIRCONIA

Property	Filled Matrix	Unfilled Matrix
C_p (Btu/lb-°F)	0.215	0.14
k (Btu/ft-hr-°F)	0.404	0.306
ρ (lb/ft^3)	194	98
C_p (g) (Btu/lb)	0.28	----
ΔH_c (Btu/lb)	680	----
A (sec^{-1})	4.70×10^{18}	----
B (°R)	72,900	----
ϵ_R (emissivity)	0.6	0.6
η Transpiration factor	0.43	----

2. Comparisons of System Performance

Parametric studies, described above were used for comparisons of thermal protection systems performance. These include: first comparisons of the effects of the basic mechanisms on weight to grasp the importance of the various modes of cooling for glide vehicle application, and, secondly, to make preliminary comparisons of weights and determine limitations of some built-up configuration composed of existing materials or those in the development stage. The comparisons are based on thermal considerations deferring detailed structural analysis of the interaction between skins, shields, and substructures to Section VIII for specific cases.

a. Comparisons of Weight Trends for the Simplified Thermal Protection Mechanisms

Using the data generated above for the parametric studies (IV-A), comparisons of the weights required for the four systems can be made and several conclusions concerning the basic thermal protection mechanisms can be drawn. The parametric studies for the radiation-ablation system show that optimum values of T_A and q^* exist for a given body location ($q_{c(max)}$) and that values near these optima are necessary if the

ablation shield were to weigh less than the radiation shield. These requirements can be demonstrated by choosing near optimum values for several levels of heating as shown in figures 64, 65, and 66. The maximum heating rates q_c (max) = 37, 81, and 124 Btu/ft^2 sec are representative of the stagnation points of the wing leading edge, fin leading edge, and nose cap respectively for the given trajectory. Since the amount of heat absorbed by the ablation process depends primarily on the heating rates q_c (max), ablation temperature T_A, q^*, and emissivity, but very little on $\rho k / C_p$ then for a given body location and emissivity, a near optimum set of ablation characteristics (T_A and q^*) may be chosen. It can be seen that the required ablation characteristics change substantially with heating rates and therefore materials which experience the ablation mechanism have to be carefully controlled. However, materials which decompose in depth but experience very little surface recession (Section VI) will perform similarly to the radiation shields and will be very usefull in high heating areas, where metal skin radiation systems are prohibitive.

The reductions in weight resulting from backface cooling of both radiation and radiation ablation systems are also indicated in figures 63, 64 and 65. The value of the coolant parameter H_c / C_p = 2000° F was selected as representative of water cooling packages. It is clearly indicated in all three figures that the weight reduction due to backface cooling is less when ablation occurs. This is to be expected since backface cooling acts to decrease insulation weight as opposed to ablation weight. In fact, the backface cooling reverses the order of system performance since a weight cross-over exists for the uncooled cases while for the cooled systems the radiation shield always weighs less than the ablation shield. Also the magnitude of the weight reductions especially for radiation systems is large enough to make an attractive system particularly in areas where structure temperature must be kept at very low levels.

It should be remembered that factors other than those discussed above also enter the performance picture of a thermal protection system. Allowable maximum surface temperature for radiation shields or reliability of cooling packages for the liquid-cooled systems may be considered as examples of such factors. These, along with structural aspects, must be considered together to make a final selection of a thermal protection system.

b. Comparisons of Specific System Performance for the Selected Trajectory

A preliminary evaluation of several specific thermal protection systems can now be made based on the completed parametric studies and newly developed conputational technicues. The practical concepts of thermal protection systems currently included in glide vehicle applications may be represented by the following configurations:

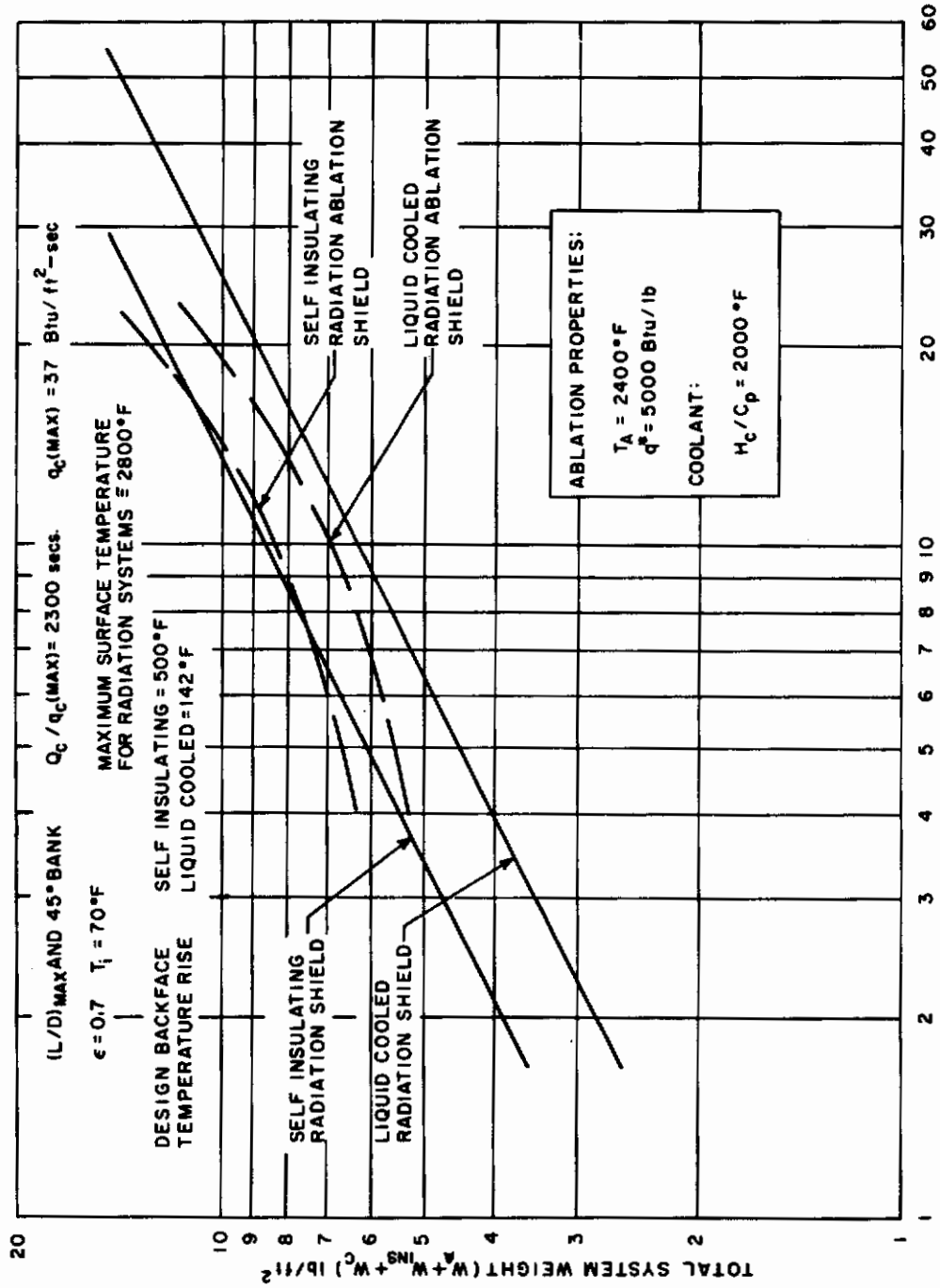

Figure 64 COMPARISONS OF WEIGHT TRENDS FOR SIMPLIFIED THERMAL PROTECTION SYSTEMS q_c (MAX) = 37 BTU/FT^2 - SEC

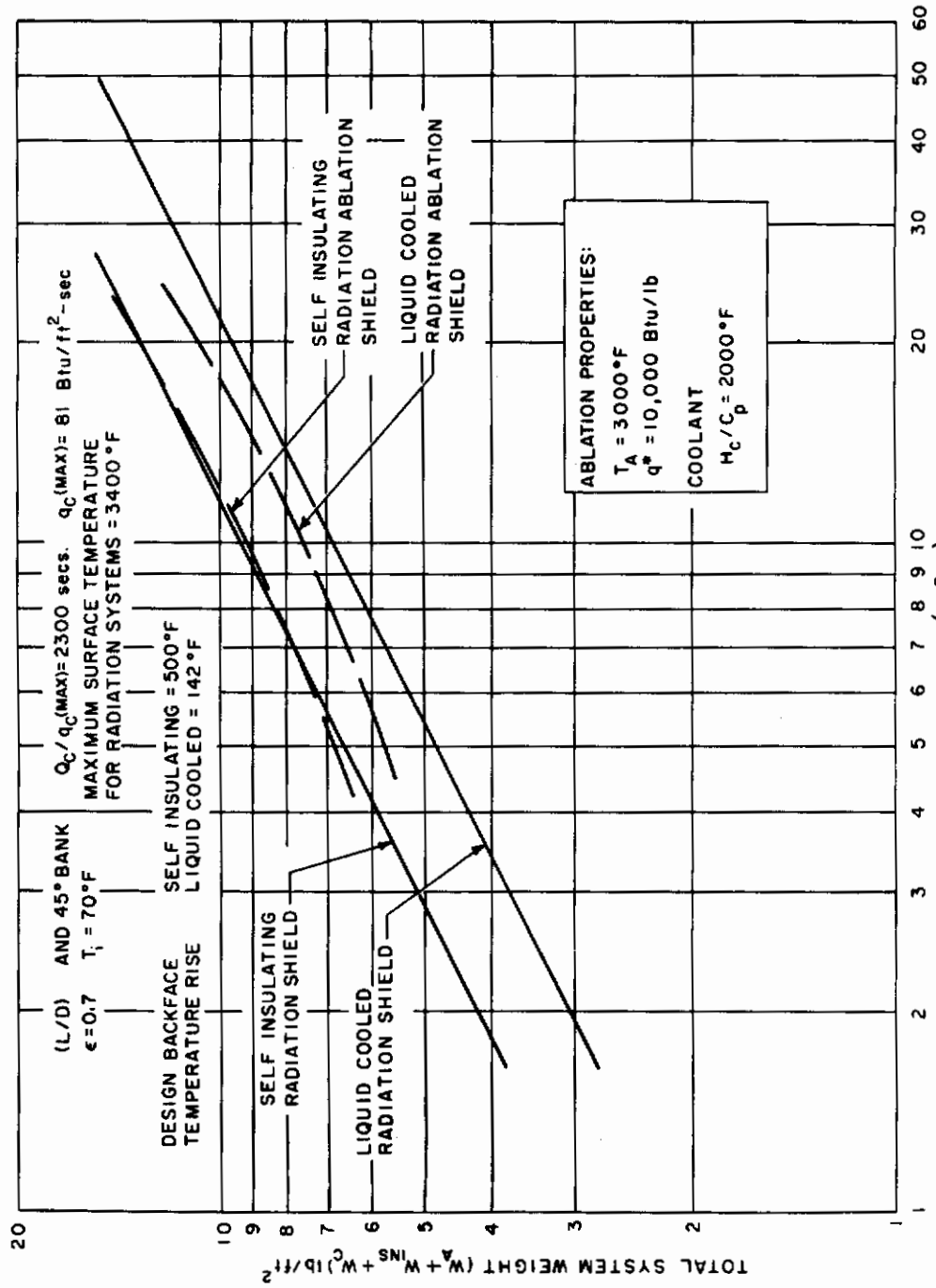

Figure 65 COMPARISONS OF WEIGHT TRENDS FOR SIMPLIFIED THERMAL PROTECTION SYSTEMS q_c (MAX) = 81 BTU/FT^2 - SEC

1) Metallic radiating skin plus lightweight insulation and load carrying substructure.

2) Same as above except substructure is kept at low levels by liquid cooling.

3) Ablating plastics, ceramics, etc., plus a load carrying substructure.

4) High-temperature plastics, ceramics, and graphites (which experience very little or no surface recession) plus a load carrying substructure (with or without an intermediate layer of lightweight insulation).

A typical thermal performance of specific systems of the categories listed above are shown in figure 66. In the lower heat input areas below $q_{c(max)}$ = 40 Btu/ft^2-sec, radiating systems consisting of 0.015-inch of coated molybdenum radiating skins plus MIN-K insulation and a 0.06-inch René load carrying substructure result in lightweight thermal protection systems. For fuselage areas such systems appear most promising. For the wing leading edge, the molybdenum skin is at its maximum surface temperature limit and the system, although lightweight, is subject to possible failure if limits are exceeded. In areas such as the cabin where heating is on the order of $q_{c(max)}$ of 25 Btu/ft^2-sec, a similar system supplemented with cooling of the backface requires even less weight and in addition can keep internal temperature to low levels required for life support. For heating comparable to the wing leading edge or higher, surface temperatures become excessive for molybdenum and either ablation materials or high temperature ceramics, plastics, or graphite which experience very little surface recession look attractive if not mandatory. Heating in excess of $q_{c(max)}$ = 40 Btu/ft^2-sec results in weight requirements of higher order than for low heat input areas. However, these critical areas of the vehicle are usually small compared to the total vehicle area and the overall penalties are not necessarily critical. Materials such as the X3000 that would experience ablation and surface recession as indicated by figure 67 have practical upper limits for their use above which weight losses become unacceptable. On the other hand, high-temperature plastics, ceramics, or graphites which experience negligible surface recession may be used even though weights appear to be large. The performance of the high-temperature materials shown could be substantially improved by designing composite systems which would replace a large portion of the shield weight with insulations of the type used in the molybdenum skin radiation system.

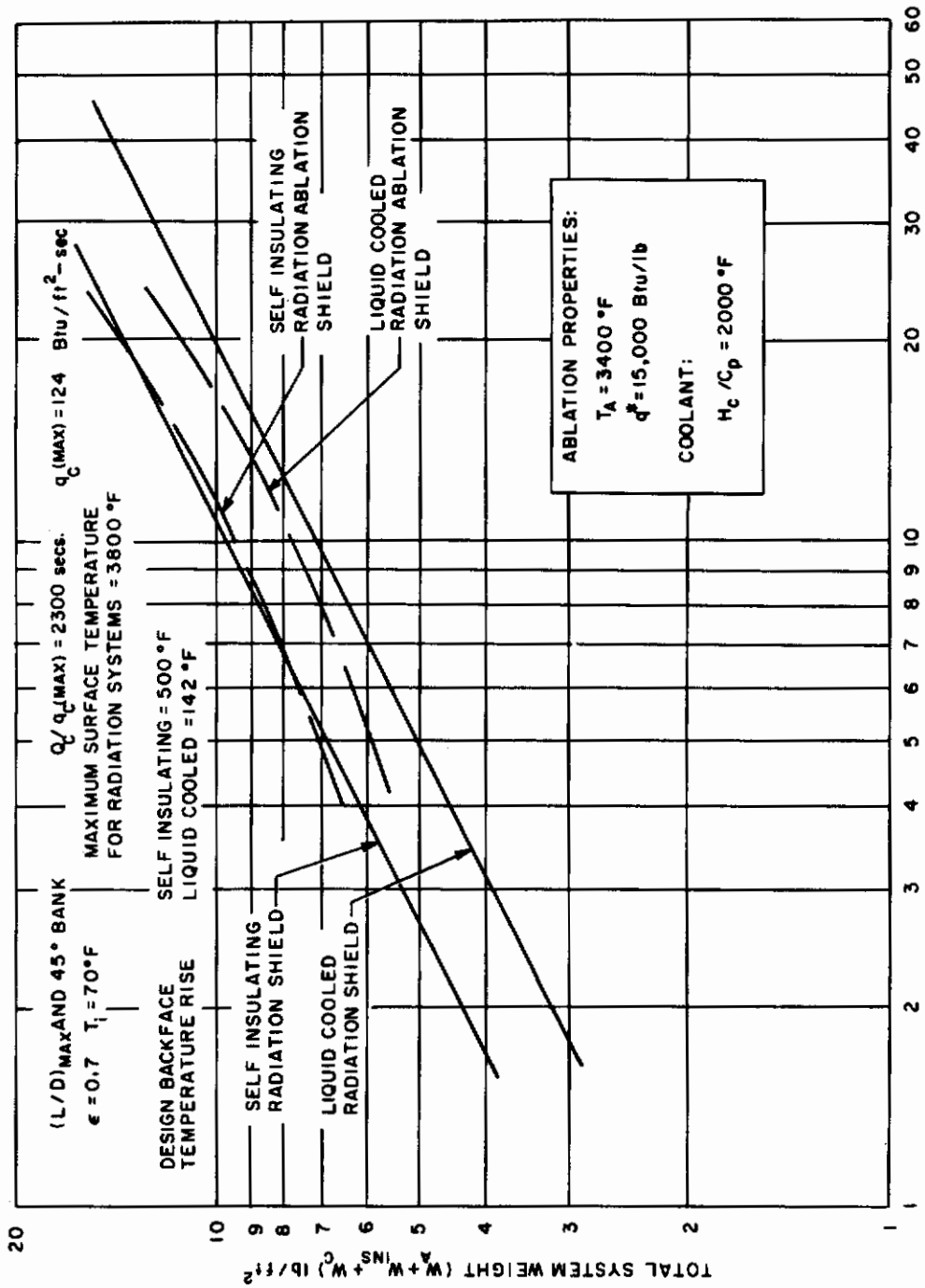

Figure 66 COMPARISONS OF WEIGHT TRENDS FOR SIMPLIFIED THERMAL PROTECTION SYSTEMS q_c (MAX) = 124 BTU/FT^2 - SEC

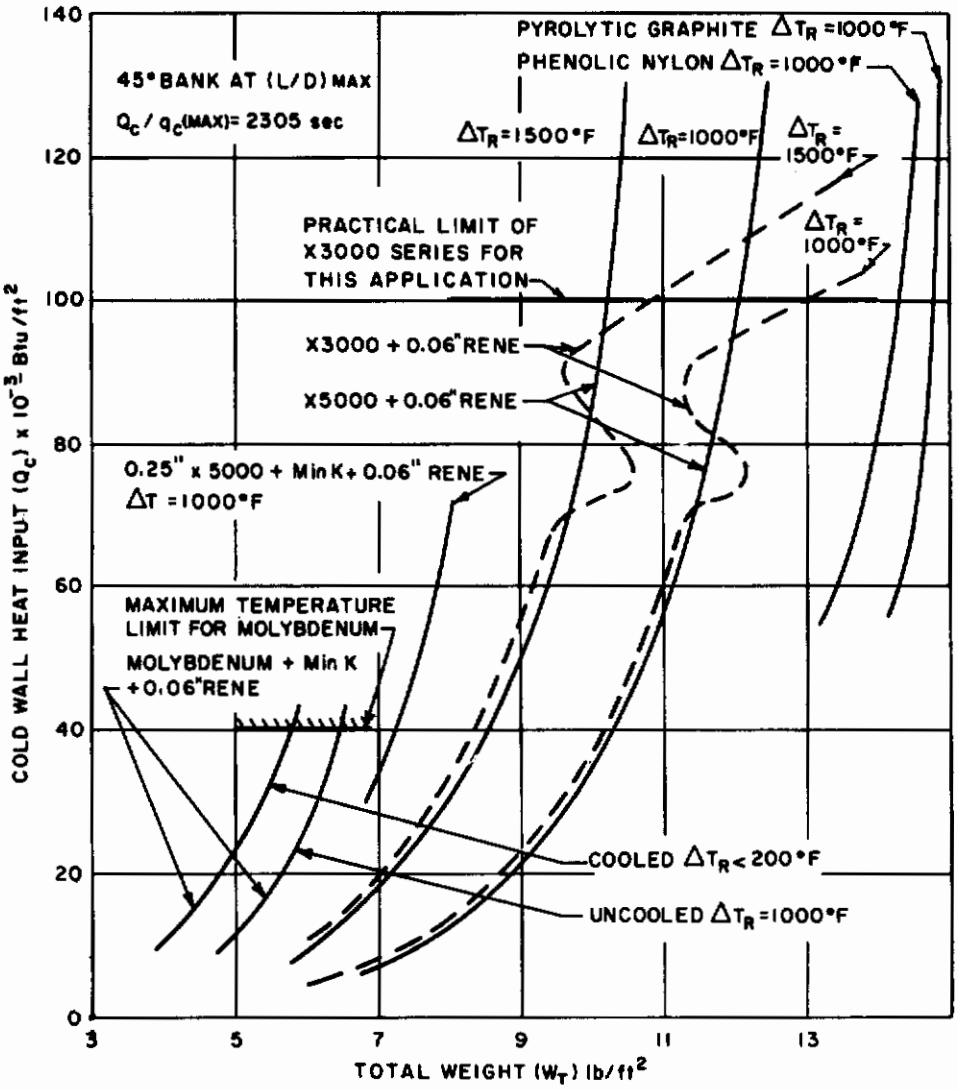

Figure 67 COMPARISONS OF SPECIFIC SYSTEMS PERFORMANCE FOR THE SELECTED TRAJECTORY - 45° BANK AT (L/D) MAX

Such a configuration composed of a layer of high-temperature plastic (X5000 series) plus insulation and 0.06-inch René substructure reduces the weight penalty associated with maximum heating rates $q_c(\text{max})$ of 40 Btu/ft^2-sec. Composites of this nature are in the development stage but they appear promising enough to merit the required investigation. It should be noted in particular that the analytical models used in the parametric studies are conservative thus overestimating the weight requirements. The experimental results when compared with such models show temperature response lower than predicted. The more exact model applied in the previous section to the impregnated matrix or high-temperature plastic (Appendix V) shows on the other hand a much better agreement. As a result relatively lower effective $\rho k/C_p$ values for ablative plastics than those used for a non-decomposing insulation should be used in comparisons.

The plastic impregnated matrix system, or the transpiration system were not investigated sufficiently in detail to obtain meritorious comparisons. The matrix system will not look overly competitive until lower material density and thermal conductivity is obtained.

The investigation described above established fairly clearly the relative merits of various systems, and the prime considerations of importance in the evaluation of systems performance. The radiation shields were found to lend themselves to a generalized treatment, and their performance is less dependent on the environment than that of systems utilizing mass transfer. Thus, it should be possible to obtain an experimentally measurable performance criterion which may be determined in process of ground testing. The interaction of many performance factors for radiation-ablation shield make such determination unlikely unless a complete simulation of the environment is provided. The testing and simulation requirements, as well as the feasibility of a general experimental performance criterions are discussed in detail in the sections to follow.

B. BALLISTIC RE-ENTRY CAPSULE

Considerable more attention in the literature was given to this application compared to the lifting vehicles. This is understandable as the ballistic capsule is a direct extension of the high-performance ballistic missile. Even in this case, however, no direct extrapolation of results from ballistic missile results is feasible due to radical changes in the external environment. No systematic parametric studies concerning materials performance under varying environmental conditions for various structural design criteria were found in the literature, although several classes of materials were evaluated. The search of unpublished information within Avco RAD revealed a set of data falling within the scope of this program (obtained under AF Contract No. AF04(647)-347) which lend itself to such parametric studies with a minimum of effort. The result of the parametric studies were published (Ref. 23) and are shown in Appendix IV. The appendix gives design data for satellite re-entry lasting as long as 8 minutes and subjected to a variable heat pulse which does not exceed 75 Btu/ft^2-sec. The objectives of the report were to:

1. Present design for the heat shield of a typical satellite capsule to survive a broad range of aero-thermodynamic re-entry conditions, and to evaluate material performance under those conditions.

2. Demonstrate and correlate the effect of material, environmental, and design parameters on shield design, especially of the surface temperature.

3. Outline the approach, problems, and steps taken in a typical heat-shield design for satellite re-entry.

It deals principally with thermal protection by ablation, but includes evaluation of simple radiation shields. The regime represents a transition of region between high-performance ballistic re-entry and long duration glider type re-entry. In fact the environment falls within the specified limit of interest (75 Btu/ft^2-sec heating rates for approximately 5 to 10 minute pulse). These data did offer an insight into the problems which were to be encountered in glider type long duration re-entry. The shield efficiency is evaluated for various aerothermodynamic environments, structural design criteria, and material parameters (thermal properties, heat of ablation, and temperature). The desirability of relatively low ablation temperatures and high-structural temperatures is demonstrated, and design safety factors are discussed. The significant parameters are defined and evaluated. The limits of requirements for optimum performance are shown. The limitations of the investigated system may be defined for specific designs depending on overall vehicle specifications.

V. SYSTEM AND MATERIAL SELECTION

The selection of the thermal protection system, material configuration, and component materials is the essential task and responsibility of the designer striving for an efficient high-performance system. Thus, the determination of performance criteria compatible with and of direct use in the design practice is a prerequisite for proper selection process. Furthermore, relationship of these criteria with the significant physical parameters must be established before a meaningful experiment can be devised to determine them. To accomplish these purposes, it is necessary to establish the significance of the parameters for a given process (see Section III. A) and correlate them with the performance criteria sought (Section IV). Based on such studies, meaningful experimental criteria may be chosen to both evaluate the materials and to use in the design practice.

In the design problems where experimental determination of performance under simulated conditions is extremely costly, it is useful to develop a "yardstick" of performance measurable under other than complete simulation of environment.

Thus the desire to establish a universal figure of merit which may be used for comparison of thermal protection systems performance is understandable. Such figure of merit is of great help to the designer in material and system selection for the many applications and vehicles considered in the re-entry field. It is of equal help to the material developer in his quest for the best material. Since in any air or space borne application the importance of maximizing the payload/vehicle weight ratio cannot be overemphasized, such figure of merit of necessity becomes a weight efficiency parameter. Because the re-entry heating is one of the primary factors to be considered in thermal protection system design, it is desirable that such figures of merit also indicate the "per pound" ability of the system to absorb heat.

A. ANALYTICAL APPROACH

Many performance criteria have been proposed in the literature, some of heat capacity nature and others indicating "insulating values." These were shown in table 3. Because of the diversity of approaches, no single best criterion has been agreed upon, and a great deal of confusion exists concerning the role it should play, or the basis it should be founded on.

The difficulties encountered in the attempts to correlate the data, due to both their heterogeneity and limited quantity, are reflected as well in the attempt to compare the criteria and techniques (analytical and experimental). Most of the criteria and parameters, as well as experimental techniques used or proposed (including Q^* concepts), are applicable to quasi-steady-state conditions or constant inputs, and thus, their usefulness will be predicated by the approach of

actual conditions to those states. It is also predicated on the capability of the equipment to simulate numerous environments if no theoretical means are available to predict performance otherwise.

1. System and Design Performance Criteria

The performance criteria proposed in evaluation of protection systems may be divided into the following two categories: (a) those depending on the quasi-steady or constant input data for determination of a criterion i.e., assuming that the transient conditions will not upset the relative ratings independent of external conditions, and (b) those depending on the use of a number of independently determined properties and characteristics used in detailed transient computations of performance for various external conditions (sometimes referred to as "conventional" methods).

Both approaches have deficiencies: the first fails to recognize the significance of insulation requirements and often of the effect of environment for any mode of thermal protection, but it minimizes the number of parameters and computations required; the second requires a larger number of experimental determinations and computations of temperature distributions, but offers a fairly good tool for evaluation, provided that experimental data are available and theoretical model agrees with the experiment.

A generalized performance evaluation has to relate the weight required for successful re-entry with the various factors discussed in Section IV.

2. Figure of Merit

While it may not be too difficult to agree on the form of the figure of merit, essentially an engineering performance criterion, it is difficult indeed to agree on the method of its determination and its "universal" applicability when related to material, system, vehicle, and application.

In the early evaluations and design of ablative thermal protection systems the experimental effective heat of ablation, q^* (determined under nearly simulated re-entry conditions) was used as such criterion together with $\rho L = W$ product computed analytically for a given system, application, and vehicle. The effective heat capacity Q^*_{eff} (computed analytically) eventually was found to provide quick material and system comparison. Hence, the term q^* came of age and became synonymous or identified with the thermal protection system performance and efficiency. Investigations of conditions other than high-speed ballistic re-entry indicated desirability of systems, materials, and composite structures unlike those of ballistic missiles. Study of such systems and refined studies of even the ballistic re-entry indicated that the q^* concept as such was not universal, that it broke down entirely under certain circumstances, and that it could be meaningless if not misleading in

the effort to select best suited materials and systems. Thus, it was found necessary to determine all the pertinent properties and characteristics of a material and to perform design application calculations prior to selection of a material and system. The performance criterion, Q^*_{eff} or similar weight criterion, was computed for the application and only then the system could be qualified. Depending on the design criterion, environment and type of system (heat sink, radiative, or ablative), different material parameters were found to be of primary significance. Surface temperature and emissivity, heat of ablation, thermal conductivity, $k\rho$ product (or insulation value), and thermal diffusivity assumed different roles depending on the above factors and had to be measured experimentally.

The expenditure of time and money associated with the proper determination of all the factors was found at times to be excessive, which together with difficulties in property determination prompted the quest for a quick relatively inexpensive but reliable and universally applicable "one shot" experimental determination of a material and system performance criterion. Such quest was denoted here for simplicity as the "Q* concept validation" effort and its purpose was to:

a. Determine any performance parameter (figure of merit) answering the above description (not necessarily the conventional q^*) for composite materials,

b. Develop (if possible) an experimental technique for such determination,

c. Validate the concept and technique by analytical methods parallel to the effort in (a) and (b).

The "validation" term was taken to mean either to verify or to demonstrate the limitations or incompatibility of the concept with the problem on hand.

To proceed with the "validation" effort, it is necessary to examine the factors affecting performance of a re-entry shield-structure composite under the many and varied re-entry conditions. Even if the primary concern evolves around the thermal performance of the shield, one must consider the effect of the substructure (load carrying member of the composite) and of the environment, in addition to the material performance. Thus, one finds (Section IV) that the ultimate selection of a material depends not only on the material properties and characteristics but also very heavily on the shield-substructure design criteria (e.g. operating temperature, thermal stress, and thermal compatibility of the components), aerothermal environment, geometrical configuration, and location on the vehicle, as well as on the interaction of all these factors. It is then evident that unless exact simulation of re-entry is achieved, no

direct measurement of performance on the ground may be made and directly applied to the design, and that the Q* concept (if verified) may apply only to screening or ranking of systems and materials. The questions remain as to (1) what degree of simulation is required to make relative evaluation of candidate systems and materials, (2) what is the most direct way to do so, and (3) which are the "best" (compatible with design) experimental criteria to be determined. If no single criterion is feasible for all systems, means and ways have to be established to bring the evaluation to a common denominator universally applicable, be it measured directly or computed on the basis of various experiments. It will be noted that certain applications, thermal protection system, and design criteria may be more amenable than others to the determination of their performance criterion. It may be then necessary, when evaluating various cases, to use a mixed model of analytically and experimentally determined values. In this latter case it will be of particular importance to reconcile the theoretical and experimental results. The experimental criterion determined may not necessarily be the same for various systems considered, and their comparison may have to be pursued on an analytical basis.

The essential requirement for positive confirmation of the figure of merit is the agreement of performance rating from the laboratory experiment with trajectory computed rating. This implies agreement of theory used for computation with experimental data under widely varying conditions establishing the validity of the mathematical expression of physical phenomena.

The preceding discussion although quite general in nature brings out the difficulties encountered in generalizing a figure of merit to be determined experimentally and raises serious doubt about its validity, especially concerning the "universality" of an experimentally measured criterion. In addition to technical problems, difficulties arise of semantic (terminology) nature.

a. Terminology

Several definitions of "Q*" exist, and are based on various environmental inputs and states. In addition, many other symbols are used in the literature describing the same "heat of ablation."

In reference 10, a complete set of "Q*" definitions is given together with definitions of aerodynamic inputs associated with "Q*" computation for ablative systems under quasi-steady and transient conditions. This system has been adapted for use in the work performed under this contract. In the same place (Ref. 10), as well as in reference 17, the performance (efficiency) criterion of Q^*_{eff} or effective heat capacity was introduced and discussed. Its bounds for various conditions, associated temperature criteria (T_b), and ablation effectiveness criterion (L_{ab}/L_{ins}) were also defined and will not be repeated at this time.

In reference 1, another systematic but not all-inclusive set of definitions is provided which may be made equivalent to that in reference 13; however, the heat flux associated with the " Q^* " definitions leaves loopholes for interpretation, and Q^* is incorrectly called a material property. Appendix I summarizes the Q^* and heat flux terminology employed in the course of this study, as well as some other definitions used in the report. No attempt will be made to produce equivalents found in the literature. The " Q^* " concept in general is applied in the literature to ablative systems and sometimes it is extended to the heat sinks. The usage of Q^* in reference 1 is geared clearly to ablative processes. On the other hand the effective weights (W_t) as defined, are applicable to any system when properly calculated. The usage (Ref. 1) of the weight criterion is made only on quasi-steady state basis, and produces misleading results in terms of insulation requirements.

b. Technical Merits

Assuming that a uniform terminology is established, the more serious problem of technical validity of " Q^* " concept has to be resolved. The following points have to be established:

1) Applicability to all thermal protection systems,

2) Applicability to transient as well as steady states, and

3) Feasibility of experimental determination for: (a) application directly to material and system selection; and (b) prediction of design performance independently of the application (flight regime).

The positive answer to the questions implied in the above would then validate the concept. Whereas the first two points may be established rather rapidly (Q^*_{eff} in Btu/lb or W_g or W_t of reference 1 criteria satisfy these requirements), the question of how this criterion is determined analytically or experimentally is not straightforward. The interaction of environment and design conditions with material parameters is introduced, and item (3) cannot be established universally.

Moreover, it is clear that since Q^* is not a property, it cannot be considered for an overall protection system independently of flight regime or for non-absorptive systems. Hence, the requirement for simulation of environment arises and it becomes necessary to differentiate between an overall system selection criterion associated with an application, and a material criterion representative of more than one heat (mass) transfer mechanisms affecting the single material performance itself. In this latter case it is possible that if one mechanism (e.g. ablation) for a given application were predominant and another (e.g.

internal conduction) of relatively minor effect $(L_{abl}/L_{ins}) \to \infty$, the q^* figure of merit would have been sufficient for material ranking. The same might have been said about ϵT^4 criterion for a predominantly radiative shield, had the insulation requirement been non-existent. The various parameters, however, considered for use as performance criteria in table 3 suffer shortcomings when either the "universality" test is applied, or the feasibility of experimental determination is considered because in most applications a "mixed" and usually transient transfer regime exists in one or another form.

While extensive use of various "Q^*" concepts is made in the literature, no specific attempts to justify it or evaluate its merits are made except in references 1, 10, 17, and 23.

The discussion (Ref. 1) of Q^* centers on the thermal capacity of the absorption systems. Proper equations are given, and the effect of environmental factors is discussed. It is apparent, however, that reference 1 considers the breakdown of the concept for radiative systems, and simplifies considerably the applicability of the concept for absorptive systems as well. It is postulated here that Q^* (assumed to be equivalent to q^* in terminology used here) cannot be the sole criterion for performance for all environments. The environmental and trajectory parameters may reverse the order of rating of materials resulting from a basically steady-state characteristic. The ΔW (Ref. 1) or the insulation requirements due to thermal conductivity, surface temperature, and pulse duration, together with trajectory effects which will produce instantaneous Q^* values different from those determined in ground testing, may well cause a reversal in material rating. Thus, it is difficult to determine "effective flux" and "effective environment" for selection of the proper "effective Q^*" without actual trajectory analysis. References 10, 17, 23 and 24 show some of these effects, and give a detailed discussion of Q^* applicability for discrete regions of performance. The literature reviewed in the course of this program did not reveal evidence contradictory to their evaluation (Refs. 10, 17, 23, 24). The basic difficulty with a single criterion, Q^* concept usage or experimental determination, is that for most systems such a criterion is not a property but rather it is a characteristic dependent on the environment.

The parametric studies for the glider vehicle conducted during this program for trajectory as well as for test environment showed that for a radiative system it is possible to define a single response criterion to be used as a ranking or selection criterion (T_b) although the "universal" criterion (of Q^*_{eff} or W_t type) for direct design use must be computed. The same studies indicate, however, that if mass transfer is involved no single criterion exists even for ranking purposes, and

the emphasis has to be shifted in the experiment towards understanding of material behavior and property determination. Ironically enough, q^* itself seems to be of less significance than surface temperature, but the temperature is not sufficient to rank the materials without additional property data, or without investigation of the environmental effects on it. The ultimate evaluation of the performance for a system with mass transfer present still calls for calculations. The above procedure has been referred to as "conventional" approach (Ref. 2) and often as such in this report. Exception to such usage really should be taken. The conventional approach in practice has been to select an often arbitrary performance criterion (of q^* type), and select systems on that basis without any valid analytical justification or flight confirmation. The procedure described in "Simulation Requirements" (below) is actually seldom applied; thus, if followed, it is unconventional whether it results in "Q^* concept" verification for some systems, or in an effort requiring determination of a number of characteristics and properties, from a valid mathematical expression of physical phenomena. The extent of performance calculations to follow should be immaterial in establishing the concepts. The simplification of the procedure should be made as circumstances warrant, depending on resolution required, criticalness of weight problems involved, and the controlling design criteria in areas other than the thermal protection system itself.

Thus, it is apparent that unless complete simulation is attained in each case (see "Simulation Requirements") no single "universal" performance criterion would be feasible for direct design application, or for that matter, for ranking purposes either. However, it may be feasible to establish a single-ranking criterion for some systems and some applications, while for others more parameters would be necessary.

The review of methods and criteria used in interpretation and correlation of thermal protection systems performance and comparison of the evaluation techniques indicated that no "best" technique or criterion was available. Such a technique or figure of merit necessarily would have to apply equally to selection of a material within a single protection system, as well as for comparison of different systems which, at the same time, could utilize a single, uniform experimentally determined criterion. Furthermore, an insufficient number of flight applications have been investigated in the literature to prove the validity of the presently used criteria, while present studies indicate (Figs 43 and 44) conditions under which the figure of merit may not be valid. It was indicated thus that a very serious effort had to be made to generate performance data for the regime of interest. The adopted approach since no single criterion is feasible should consist of the following steps.

1) For each of the systems considered, choose if possible an individual criterion (or criteria) based on system parametric study permitting selection of the best material for the system. Develop experimental technique (with proper environment simulation) for such a criterion determination, and compare the rating based on the experiment with that obtained by design calculations.

2) If criterion selection is not feasible proceed with "conventional" material evaluation. Conduct experiments to extend material knowledge.

3) Select the best thermal protection system by actual design (or design parametric study) with the best candidate material (or composite) chosen on the basis of (1) or (2) above, and compare the resulting Q^*_{eff} of each design. The material properties would be determined as necessary in "conventional" methods.

Using the above approach, the number of experiments would be minimized and a still logical selection base would be provided. Were it possible for some applications to determine Q^*_{eff} experimentally, the above steps would automatically reduce to one, satisfying the basic objective of the program.

The essentials of the above approach were adhered to in the development or improvement of experimental techniques for the " Q^* concept" validation studies. The techniques recommended for purely radiative system represent steps 1 and 3, while systems involving mass transfer represent steps 2 and 3. The experimental parameters to be measured were intimately related to those used in the correlation techniques and to the design performance criteria. It was apparent that if such parametric groups were found to correlate the data in a reliable fashion, they could also form the basis of experimental test procedures.

B. EXPERIMENTAL EVALUATION TECHNIQUES

The objective of this phase of the effort was to determine experimentally a response parameter (performance criterion) with a minimum variety of tests, and with a minimum of additional measurements and/or computations to determine a figure of merit for the system.

Parametric studies reported in Section IV furnished the parameters significantly affecting the system performance, and were also used to establish partially the simulation requirements and the observables to be measured.

Materials used for test samples were chosen to allow whenever possible a comparison of theoretical and experimental results. This entailed the selection of materials with relatively well known properties to allow for analytical verification

of "conventional" and "Q* concept" selection techniques to be developed under this contract. The overall aim was to develop techniques and methods for – rather than development, test or selection themselves of new materials for an application. This use of known materials was of additional importance when a single criterion could not be selected and better understanding of the mechanism was required. In such cases experimental data were to be compared with accepted design models and with more exact theories concerning material behavior according to Step 2 in previous section. Otherwise, establishment of additional measurements might have been involved to complete the step even for "known" materials.

The experimental techniques for the systems to be tested will be discussed after discussion of the simulation requirements.

1. Simulation Requirements

The problem of system or material selection may be boiled down in its essence to the requirements of environment simulation. Obviously, if perfect simulation is attained, the selection (and often the design) may proceed on purely experimental basis by testing a response parameter which is at the same time the design criterion. In such case one may dispense with the effort to develop theories explaining the physical behavior or to establish analytical design procedures. However, the many re-entry environments cannot be easily timewise simulated over their complete flight paths and, therefore, it is necessary to determine the degree of simulation required to permit selection. This task requires development of mathematical models describing physical phenomena and methods to obtain solutions. As a result the physical phenomenon is described in terms of certain parameters, the more sensitive of which may in turn be used as selection criteria, while the solution obtained may be used for design purposes as well.

The steps in establishing the simulation requirements and selection of criteria should follow in this order:

a. Verification of theory with experiment for a broad range of environmental variations should be established. This may require independent determination of parameters involved. Their sensitivity may be determined by the parametric model studies. The interpretation should allow for experimental errors associated with both the independent measurements of material parameters (e.g. surface temperature, emissivity, thermal properties) and of the response parameters (e.g. temperature or recession rate) measured in verification tests.

b. Assuming that the verification is achieved, the design requirements are inspected to choose a proper response parameter and measurement to be used as a selection criterion. This may be done by virtue

of design parametric studies (similar to those in Section IV) to establish the sensitivity of selection with respect to the environment or other factors. If the studies indicate insensitivity to some or all environment parameters, the next step (c) may be skipped and the system and material may be ranked on its own parameter merits.

c. Using the now verified analytical techniques, the response parameter (e.g. T_b and/or shield weight or efficiency) is calculated for a representative environment for the system(s), application(s), and materials covering the range of anticipated parameter variation. The ranking for the systems and materials is thus established for the environment(s). (See figures 64 to 67, and also trajectory rating in figures 68 to 72.)

d. Partial experimental simulation of the environment as required is now duplicated by computer (see figures 68 to 72) either by

1) calculating the response to some environmental factors (per step b above), or

2) calculating the response to all environmental factors but on local time point basis or partial time sequence of flight path portion deemed significant.

If the ranking of systems and/or materials in step d agrees with the one computed in step c, the minimum simulation requirements have been established and the experimental technique for measurement of the response may be recommended.

If the analytical exercise indicates that the ranking in step d does not agree with that in step c, either the complete simulation is required or the "conventional" approach (determination of all properties required by the verified theory) must be used. In either case the level of confidence is high since the experiment and theory were reconciled prior to such exercise.

On the other hand, if the experiment and theory were not reconciled, the confidence level decreases, and a dilemma exists. If the theoretical analysis is used for design purposes, the requirement for properties still exists and selection will proceed based on the analytical exercise. Thus the selection of a material based on an experimental criterion (without complete simulation) will not be accepted by the designer without a large safety factor, since his study indicates a possible reversal of ranking. However, if the theory is incorrect, it may well be that the complete simulation is not required and materials will be developed or selected which in actuality are not the best ones for the application.

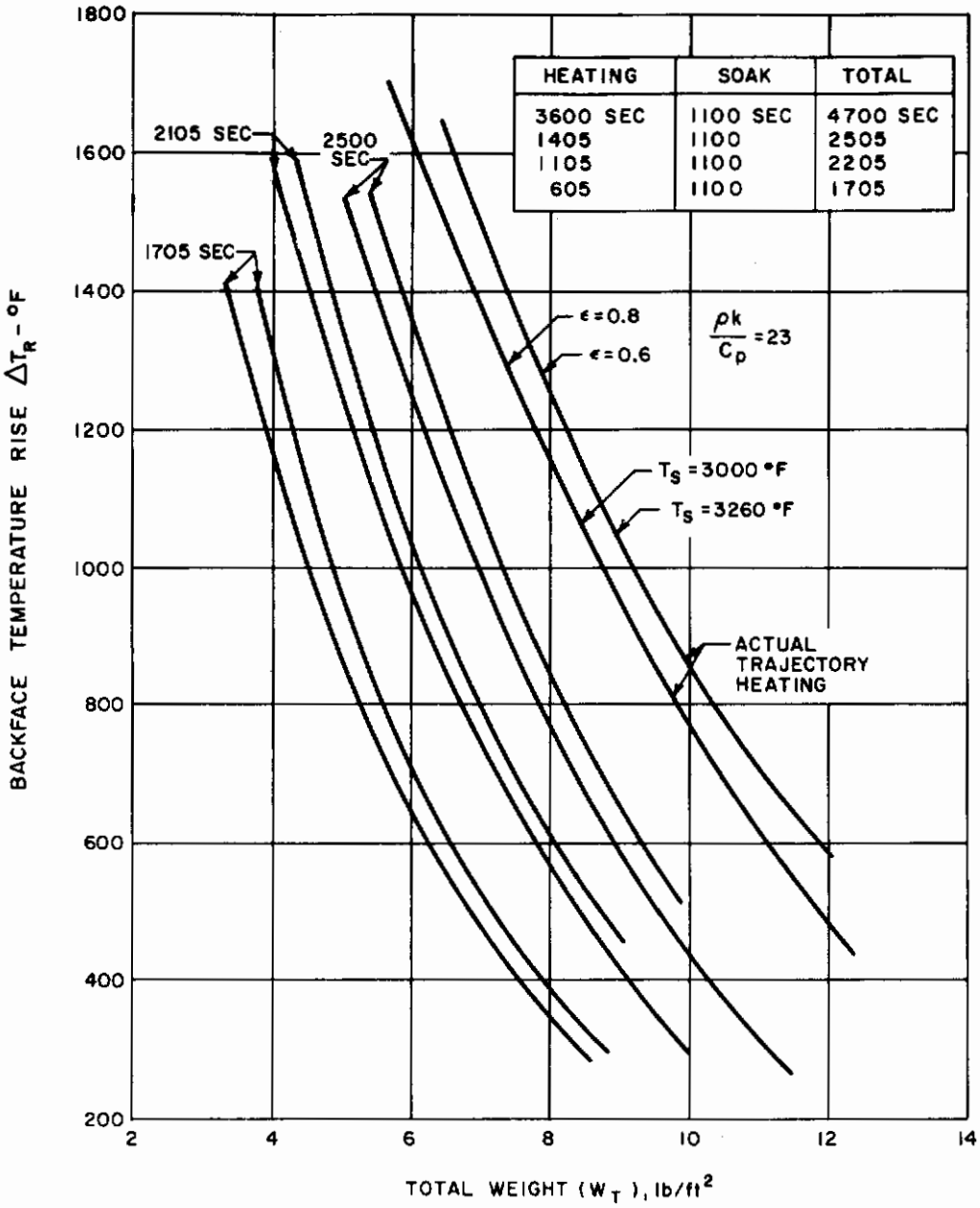

Figure 68 ANALYTICAL SIMULATION OF THE TEMPERATURE RESPONSE FOR ACTUAL TRAJECTORY AND GROUND TEST -- RADIATION SYSTEMS -- CONSTANT $\rho k/C_p$

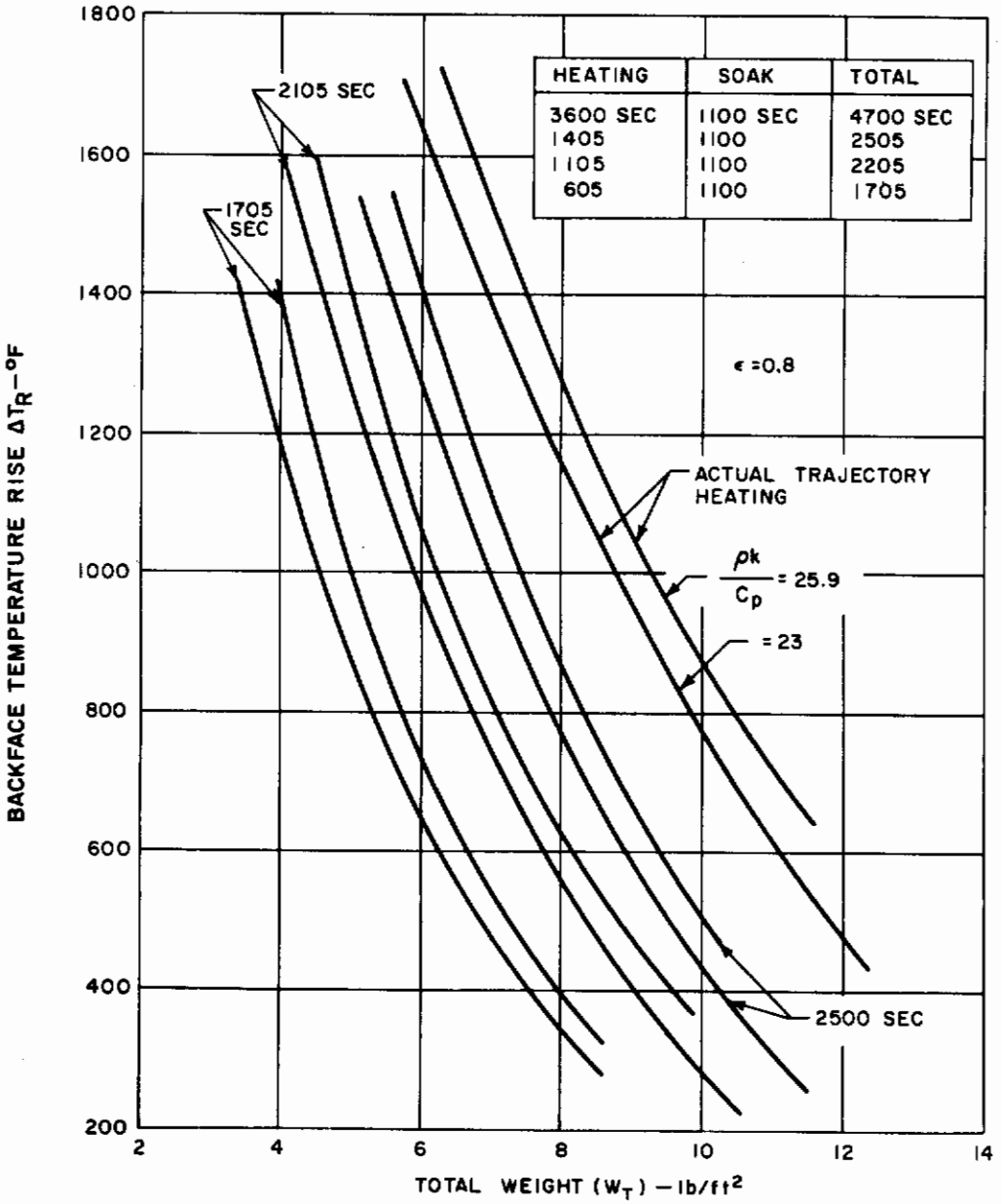

Figure 69 ANALYTICAL SIMULATION OF THE TEMPERATURE RESPONSE FOR ACTUAL TRAJECTORY AND GROUND TEST--RADIATION SYSTEMS--CONSTANT EMISSIVITY

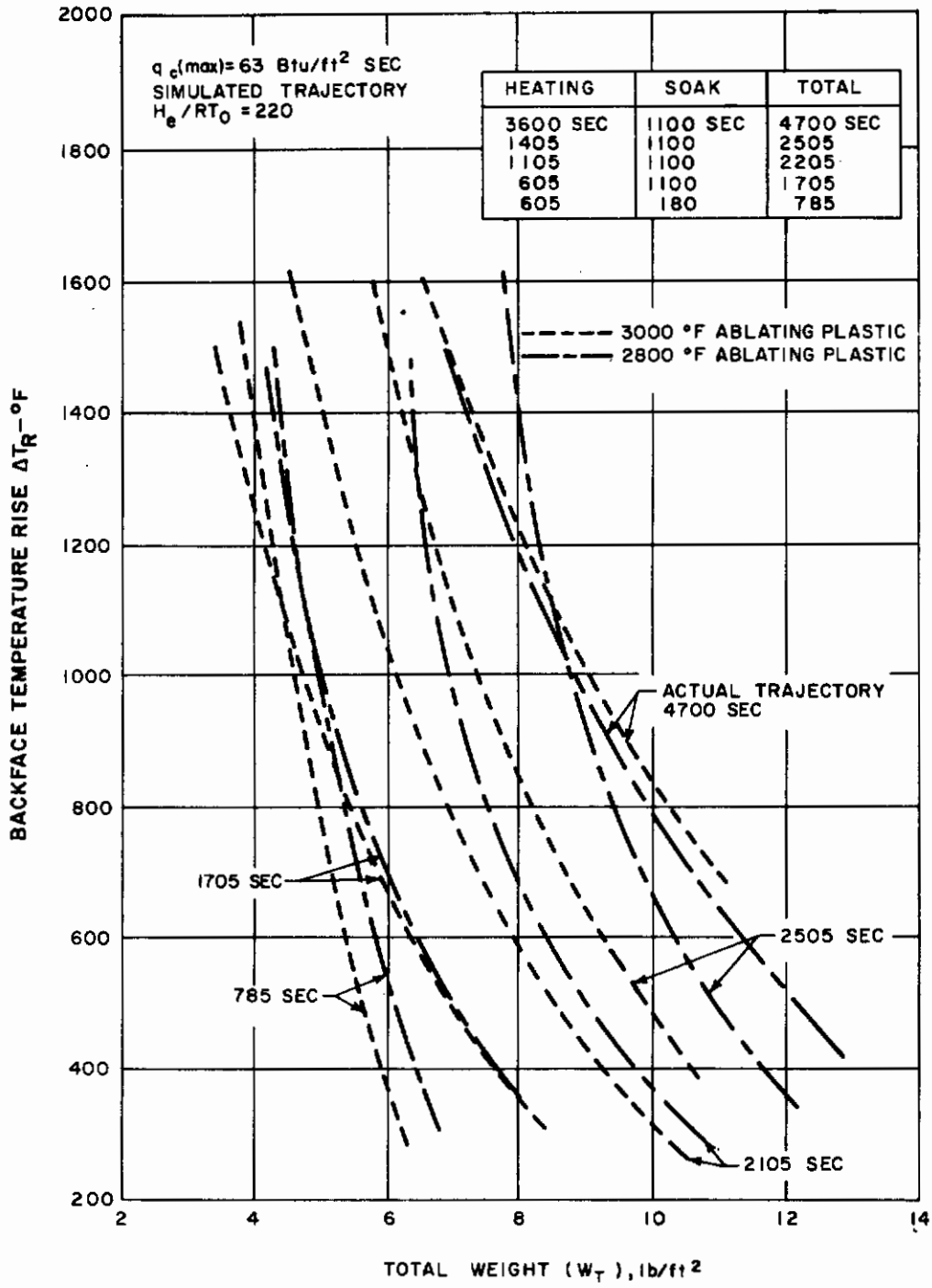

Figure 70 ANALYTICAL SIMULATION OF THE TEMPERATURE RESPONSE FOR ACTUAL TRAJECTORY AND GROUND TEST -- ABLATION SYSTEMS

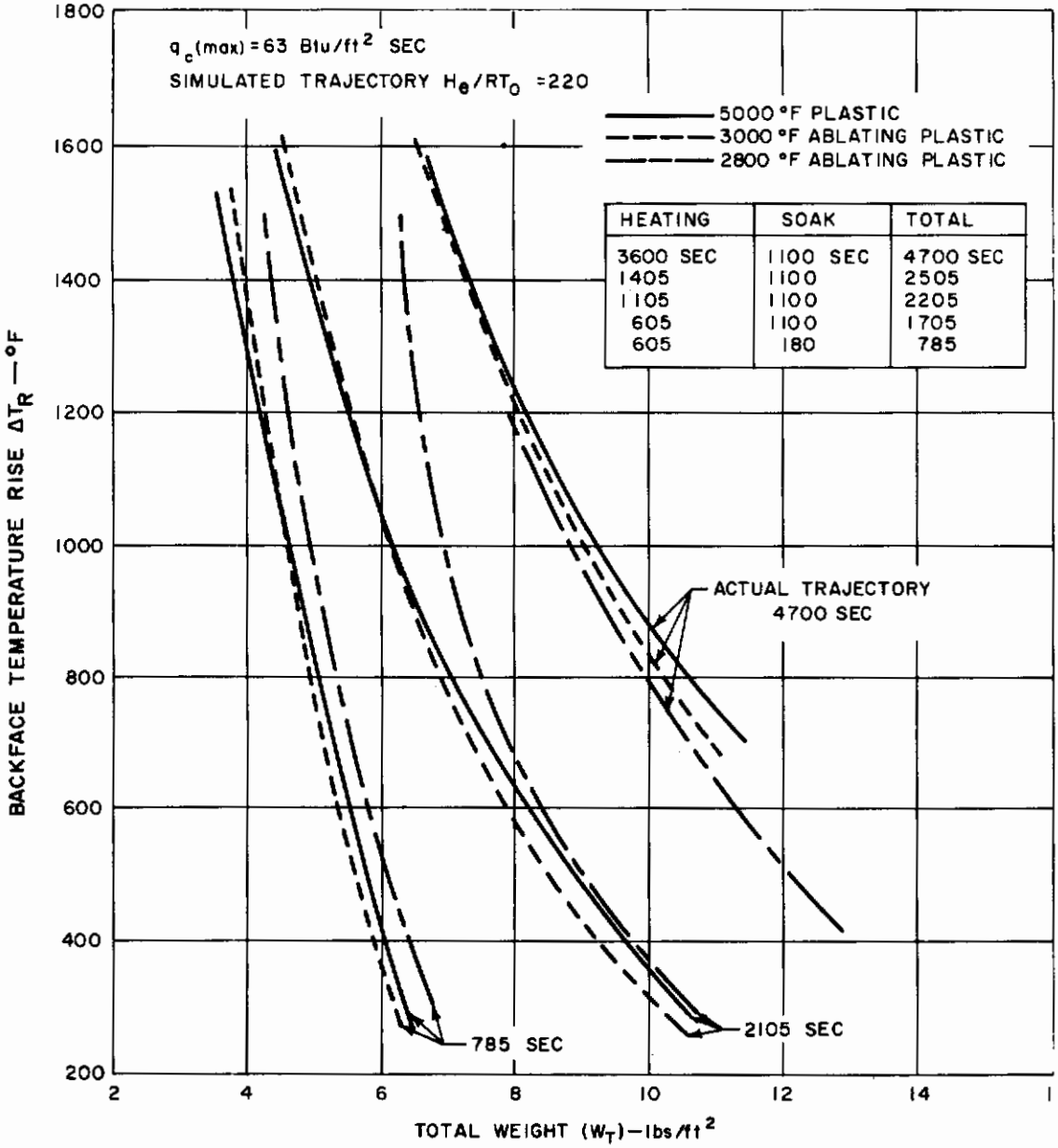

Figure 71 ANALYTICAL SIMULATION OF THE TEMPERATURE RESPONSE FOR ACTUAL TRAJECTORY AND GROUND TEST -- RADIATION AND ABLATION SYSTEMS

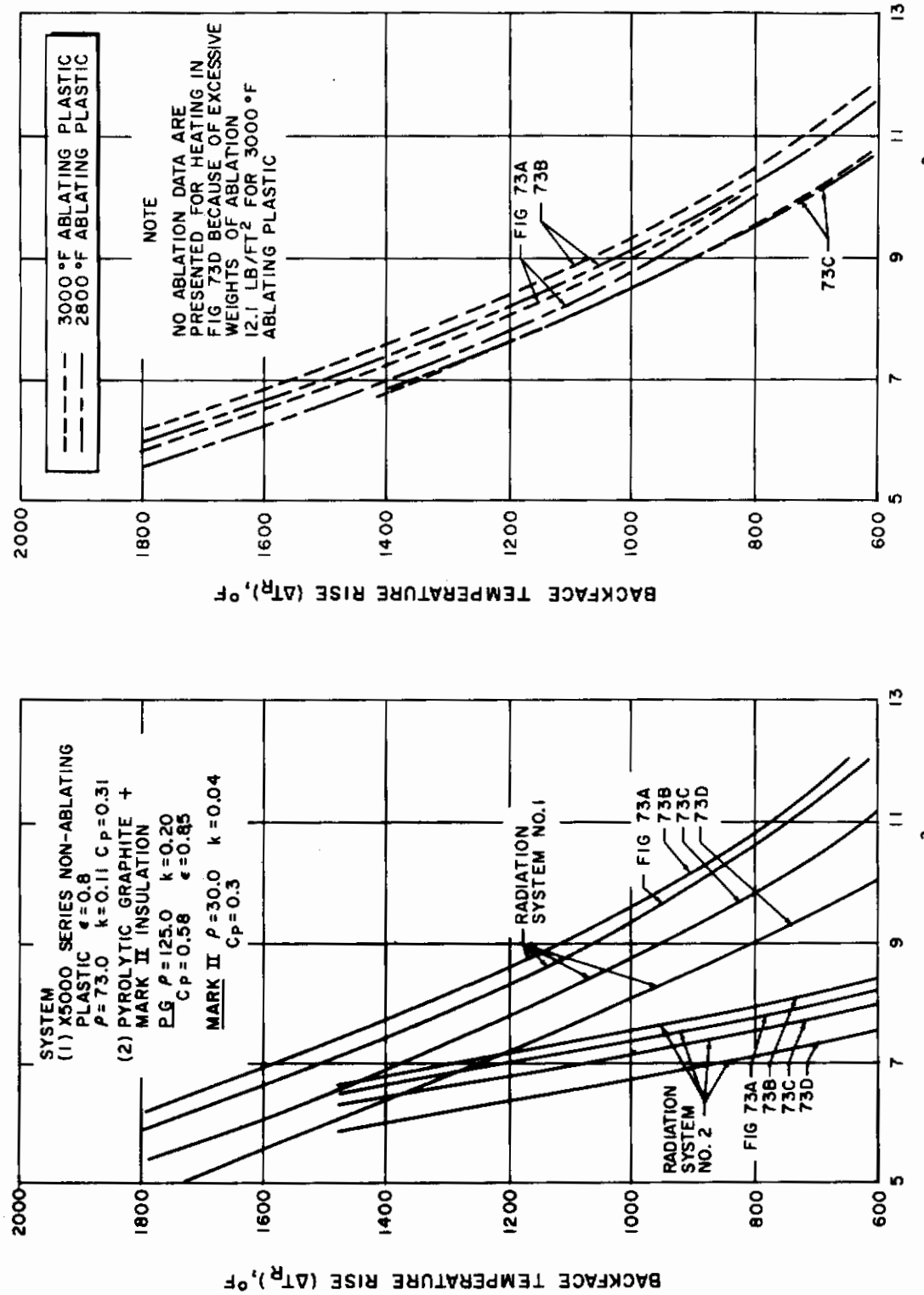

Figure 72 ANALYTICAL SIMULATION OF THE TEMPERATURE RESPONSE FOR ACTUAL TRAJECTORY, GROUND TEST, PREDICT PARTIAL SIMULATION OF TRAJECTORY

Hence, the often stressed necessity for proper verification of theories and experiments is not always feasible at the early stage of system and material selection process. Obviously a compromise has to be achieved and limits of the validity of the analytical solution have to be established to make a decision whether to use the "conventional" approach or the experimental ranking in a test. If the demands on ranking resolution are not too strict, widely differing materials may perhaps be evaluated; for close resolution, however, it will be necessary to reconcile theory and experiment in the course of further action.

If one applies the preceding philosophy in practice, it is obvious that the parametric study very quickly will indicate the path. The radiation shield study for the glider reduced itself to relatively simple relations and thus of simulation requirements. The response parameter can be easily determined (T_b), since rankings in steps c and d agreed readily as evidenced by figures 68, 69 and 72. The subsidiary mass transfer present in the other system did not permit establishment of simple relations for the glider and thus the simulation requirements are much stricter. Reversals of rankings from step c to step d are observed (figs. 70, 71, 72) within the system itself as well as in comparison with the radiation shield. On the other hand it is possible that for another application where mass transfer is the predominant mode, and say 90 percent of the system is removed, a simple criterion like q^* would be sufficient. In a mixed regime (say 50 percent of material removed) q^* criterion would not be sufficient. For the present case, glider q^* is shown to be relatively insignificant compared to T_A (fig. 44) but T_A itself is not always sufficient. Thus "conventional" methods would be called for in the selection process.

To substantiate such recommendations, it is necessary to reconcile the experiment and the theory. In the case of a radiative shield, it is not too difficult of a task (see Section VI), in the ablation case it is difficult since decomposing plastics are involved. The analytical simulation used for the most part assumed surface type (see discussion in reference 27) of ablation while indeed an in-depth process occurs. Therefore, a number of experiments were devoted to compare the two types of calculations to establish if possible the bounds of the solutions. It appears that the approximate solutions represent for the case of the glider an upper bound (See Section VI) and thus the trends discovered using them are valid if not the absolute numbers. Since arbitrary property values were used in the analytical studies, the cross-overs in rankings may be shifted to other T or W values, but still will remain in existence. Thus either "conventional" methods using proper theory have to be recommended or a degree of simulation (if not complete) has to be established closer than it was feasible in the course of this study. In any case the experiments were and still are required to assure an agreement between the test and theory over a wider range of environmental conditions. The performance criterion likely to be used is the

T_b and T_s since q^* is not a sensitive criterion over the range of conditions encountered in the glider re-entry. This is not surprising as relatively small mass loss rate may be allowed, radiation mechanism is predominant, and T_b is one of the significant design criteria. Another reason, in favor of "conventional" methods is the thermostructural requirement calling for the knowledge of temperature distributions within the shield to assure its compatibility with the structure and reliability which cannot be assured without thermal stress calculations. The latter requirement is equally valid for radiative shields without subsidiary mass transfer as for those with it, and necessitates detailed calculations for material systems considered for design.

It may be concluded from the preceding discussion that even in the absence of a facility to obtain the required degree of simulation, the experiments of the type described in this report, if properly designed and interpreted, have the merit of improving the knowledge of material behavior. This is perhaps more important for selection purpose than establishing of "universal" figures of merit which cannot be firmly proved by analysis for all conditions. The acquired knowledge on the other hand will help with evaluation of the multitude of condition which could not be covered by an experiment.

The specific simulation requirements for the purely radiative system and a radiative system with mass transfer are given below with the description of the recommended technique.

The development of the approximate method for calculation of weight and backface temperatures (Section III) was utilized in the analysis of experimental requirements in a twofold manner:

a. To determine the areas of agreement in materials ranking between ground test and trajectory predictions even though simulation is not achieved. This was done for various material properties and for the degree of simulation of the environment (including time element) by presently accepted methods while trajectory was calculated by the simplified procedure. The bound of application thus determined analytically was verified by comparison of analytical prediction with experimental results (see Section VI).

b. To provide alternate simulation requirements parallel to the assumptions made in Section III which would then result in material response in ground test similar to that actually occurring in flight, in the same manner the approximate calculations provide weight and temperature data. This avenue of approach was not successful as the requirement was equally difficult to meet as that of trajectory simulation.

2. Radiative System (No Mass Transfer)

The parametric studies indicated that only partial environment simulation was required, thus the following procedure was established:

Step 1

Select heat flux (q_c) levels and enthalpy (H/RT_o) for arc test such that the surface temperature (T_s) of the test material will reach values expected during flight. The test run duration should be sufficient for significant temperature response (T_b) at the rear boundary. The atmosphere required to observe surface effects should also be provided.

Step 2

Measure T_s and emissivity ϵ if feasible and observe surface behavior. From figure 12 it may be seen that material performance will depend on its properties only, independent of environment effects other than implied in step 1. Thus the ΔT_b observed from tests of various materials (equal weight samples) under the arc test conditions will provide a figure of merit for material ranking. The observation of the surface appearance will provide some information on surface resistance to the environment, and a more complete temperature traverse will be helpful for mechanism evaluation.

Step 3

Select best material on the basis of minimum ΔT_b.

Step 4

To verify the procedure, estimate $\rho k/C_p$ from the test and compare with figure 12 and for a given trajectory, data check the material heat flux tolerance (using graphs similar to figure 8).

Step 5

Use graphs or empirical relationship for a given trajectory of $Q^*_{eff} = f(\epsilon, T_b, \rho k/C_p)$ to calculate the weight requirements for comparison with other systems for design application.

The predicted weight-temperature (ΔT_b) relationships for the trajectory and various duration arc ground tests indicated (Figs. 68, 69 and 72) no reversal in ratings for radiation mechanism. The experimental data for

some radiative shield materials testing (see Experimental Program) agree with the prediction within the experimental error range reasonably expected (two-dimensional effects). It may then be concluded that T_b may be used as a ranking criterion for comparison of radiative shield thus verifying a "Q* concept" for this type of protection.

This result is not too surprising since the analysis indicated a relative independence of the performance criteria, from the environment as long as surface tolerance of the temperatures resulting from the net heat flux (q_{or}) can be demonstrated. The details of experiments are given in the "Experimental Program." Not all measurements called for by the procedure were made due to the limitations of the program, and the sample geometry could be improved to eliminate some of the two-dimensional effects. However, the agreement of trends indicated in the analytical study and of the experiment demonstrated the feasibility of the technique. Arc experiments were chosen because other facilities either provide no sufficient air flow (e.g. quartz lamps) or their atmosphere is not representative of the re-entry. Furthermore, had a criterion been developed for ablative systems (see below), it would have been desirable to conduct tests in the same type facility to eliminate one of the experimental uncertainties.

The parametric studies of this system provided the required significant system and material parameters to be used as test variables and presented the analytical justification of the experimental procedure to verify the " Q* concept" for a broad range of conditions.

It would be of value to conduct a systematic ground test program including a number of radiative shield structures and rank them for future comparison with well instrumented flight test vehicles for the final proof of the method. In the interim, the relatively simple tests shown to be sufficient (by analytical methods compared with experiments) should be extended for additional proof to include partial simulation of the trajectory. This would further demonstrate relative ranking of various radiative shield materials.

3. Radiative System with Mass Transfer (Radiation Ablation Shield)

The use of ablating shields as means of thermal protection of vehicles experiencing a low flux exposure of long duration (over 5 minutes) was thought not practicable until recently (Ref. 1), however it was shown here (as well as by others) applicable to 10 minute flights for a ballistic capsule. Parametric studies conducted under this program have shown that the use of the newer ablating plastics or matrices impregnated with plastics is feasible if not optimal in plain configurations. A combination of a high-temperature ablative plastic backed up by high-temperature (2000°F) insulator appears to be quite competitive with a pure radiation shield, (fig. 67) and, therefore, such systems merit consideration for certain areas of a glider vehicle.

Thus, an effort was devoted to the study of experimental techniques, possibly leading to a figure of merit for such system. Especially so, since the idea of "Q* " figure of merit originated with such system studies for other applications. The listing below of q* equations for various ablative systems indicates immediately that the concept itself is not as simple as originally thought and becomes more complicated as more exact representation of mechanism is achieved. The equation for the heat of ablation of materials forming a liquid layer is similar to that in equation (102) given for surface ablation process.

$$q^* = \bar{C}_p (T_w - T_o) + f[h_v + \eta (H_e - h_w)] \ , \tag{100}$$

where the evaporated fraction $f = \frac{m_v}{m}$.

The evaporated fraction, surface temperatures, etc., are calculated from exact analyses and accounting properly for the aerothermochemistry of the boundary layer gas. For composite materials, this is modified to include the component materials

$$q^* = x(q^*)_1 + (1 - x)(q^*)_2 \ . \tag{101}$$

Where subscripts refer to component materials and x is the mass fraction of the major component; however, the $\dot{s} = f(T_w)$ relationship may be different from that used for pure flowing materials.

The mathematical model employed for materials decomposing in depth results in an expression for the steady state heat of ablation, q^* , as given in equation (102).

$$q^* = \left\{ C_g + \frac{A_2}{\rho_o} \right\} (T_w - T_o) + \frac{\rho_2}{\rho_o} f[h_v + \eta_2 (H_e - h_w)]$$

$$+ \left(\frac{\rho_o - \rho_2}{\rho_o} \right) [\Delta H_c + \eta_1 (H_e - h_w)] + \left(\frac{A_1 - C_g}{\rho_o} \right) \int_{T_o}^{T_w} \rho(T)\, dt \ . \tag{102}$$

The q^* figure of merit is definable in quasi-steady state and at that not for all mechanisms. Its determination is contingent of achievement of that state in the experiment. The calculations shown in Appendix V indicate

that a relatively long time is necessary to achieve an internal quasi-steady state. Reference 15 shows that the steady-state values obtained on the ground do not necessarily correspond to the instantaneous values for the trajectory. Present studies (Figs. 43 and 44) show that for a system considered for glide vehicles q^* is not the most significant measure of performance for reasons already discussed. Thus the original q^* cannot be used in the present quest for a performance criterion. During early stages of this program, a modification of that criterion to a $q^* /(\rho\sqrt{\alpha})$ parameter was suggested. This new criterion was to be determined over a range of environment parameters while simultaneous determinations of T_s, ϵ, etc. would have been made. The findings of the parametric studies have shown meanwhile the surface temperature to be major influence on the material performance, indicating thus that any criterion not including surface temperature would be of little value. The modified criterion would be of value only for materials with similar ablation temperatures and thus not sufficient for the regime of interest. Several other attempts to produce a "one-shot" criterion failed for the reason of inability to account for all major factor interactions. Even for systems where radiation mechanism is by far the predominant transfer mode, the backface temperature - a good measure of performance for radiators (see previous discussion) -, was found insufficient when mass transfer occurs at the surface. This was shown in figures 70, 71, and 72 demonstrating the reversal of rankings with respect to other plastics or radiative shields in absence of sufficient degree of simulation of the flight path. The extension of test time in constant input experiment did not produce improvement in the ranking sequence, nor did the hypothetical improvement of simulation in time wise manner indicate promise at this time. Again because of the limitations of the program it was not feasible to ascertain analytically the exact simulation requirement, and perhaps not desirable in view of the gaps in the information on properties required to analyze some aspects of the ablation process. The reference is made to the necessary comparison of ablation calculations used in parametric studies with the more exact model described in Appendix V. The calculations by approximate methods are shown there to be conservative when compared with the more exact theory for a material for which the necessary property data are available. Similar trends were observed in the experiments conducted here, (see Experimental Program). It may be deduced that while the trends of the parametric studies of the system or those shown in figures 70, 71, 72 are correct, the actual cross-overs might occur at value points other than those indicated. The determination of the simulation requirements would depend on relocation of the curves by calculations according to the more exact methods. The lack of property data and the economics of the computer precluded such parametric calculations. Especially so, that the applicability of the "Q^* concept" for a mass transfer system was shown to depend on a very close, if not complete, simulation of the environment. The attractiveness of the "conventional" approach is thus increased when the requirement for simulation of a multitude of environments is considered for a great number of materials.

The experimental techniques were thus chosen in keeping with the approach outlined in the "Simulation Requirements." i. e., to increase the knowledge of material behavior by reconciling the experiment and theory and to increase the confidence in the "conventional" selection techniques. In this case such methods may be in the long run more economical and less time consuming than an experimental program striving for sufficient degree of simulation.

The response parameter, T_b , was chosen for ease in comparison with radiative shield, and because it represents a design criterion as well as the measure of all transfer processes in the protection system. It is thus a good measure of comparison of the experiment and theory. The experiments leading to material and system selection follow the "conventional" method (unless complete simulation is feasible):

Step 1

Select widely varying environmental conditions bracketing (but not necessarily simulating) the application, for an arc test of sufficient duration to produce significant backface temperature response (ΔT_b).

Step 2

Measure T_b , s, and $T(x)$ (T_s and ϵ , if feasible) during the test. Estimate the density variation in depth [$\rho(x)$] from post-test examinations. Determine by independent experiments all properties required for the model of decomposition (ablation) used in calculations.

Step 3

Calculate the observables, especially T_b by the analytical methods and compare with experiment. If necessary, modify the theory consistent with experimental accuracy to obtain agreement over the range of conditions.

Step 4

Select material based on the basis of minimum ΔT_b for equal weight samples (if degree of simulation is sufficient) or calculate the ΔT_b for a given application.

Step 5

Calculate Q^*_{eff} ($\mathbb{W}_t$) for comparison with other systems for design application.

If the mass transfer phenomena for a given material or application can be represented by the approximate methods used in the parametric studies, the procedure may be applied without much difficulty using the calculation methods shown in Section III. The development of this rapid and inexpensive approximate evaluation method should partially eliminate objections to additional testing of "conventional" properties. Such objections are usually based not so much on the cost and time involved in the additional testing proper (small compared to the basic tests), but on the cost and time involved in the conventional calculation procedures used in evaluation. Where more exact methods are required, the evaluation by "conventional" technique is a necessity whether or not it is found difficult or to one's liking. The primary objective of the test becomes the reconciliation of the experiment and theory, rather than "one-shot" figure of merit determination. The experiments for decomposing plastics considered for radiation shield materials were thus conducted with the former goal in mind. They are described under the "Experimental Program."

The test of build-up components (or cooling devices) behind the primary shields would essentially follow the techniques established for the radiative shield. In the case of the ablative primary, however, it would be necessary to program experimentally the computed shield-component interface time-temperature history by some means (e.g. quartz lamps) and record the backface temperature response.

It should be reiterated here that if a complete simulation of the environment is possible, Q^*_{eff} or W_t may be determined directly. The present ground facilities, however, although quite advanced relative to the state-of-the-art at the beginning of this program, do not as yet simulate all the environmental factors. Without exact knowledge of the mechanisms involved in the transfer process which may be attained by the type of experiments described below, it will not be possible to ascertain the adequacy of present simulation capabilities with a high degree of confidence.

The parametric study results seem adequate for a gross comparison of the systems considered and to indicate fruitful openings in the material development effort. In conjunction with the experiments conducted they are adequate for the regime of interest. For other applications, e.g. super-orbital re-entry, considerably more emphasis on an ablating system will be required. The evaluation of the transpiration (mass injection) system has not reached the stage where specific recommendations for testing can be made other than those for an ablating system. A closer study would undoubtedly result in modifications especially concerning sample size and geometry.

Methods, techniques, and criteria discussed, developed, and recommended in this and previous sections afford systematic means for selection of materials within the two systems selected for study. They should be of help in developing materials with "desirable" characteristics within reasonable bounds as they indicate either their trade-offs, or limits of variation. Means of comparisons with other systems based on Q^*_{eff} are also given.

VI. EXPERIMENTAL PROGRAM

The experimental program was planned to execute experimental techniques devised to examine the "Q* concept" and if possible to estimate "Q*" values without resort to conventional techniques. Because of lead times involved in procurement of representative samples, it was assumed that the concept will be validated for systems considered in the study, and samples were ordered prior to actual verification. Otherwise, the timing of the actual testing was geared to the analytical studies to establish the requirements for:

1. Observables to be measured (parameters of significance),
2. Degree of simulation necessary,
3. Experimental techniques development, and
4. Modification and shake-down of the existing facilities.

As noted in the review of the state-of-the-art, the basic procedures and facilities used in the field for testing were found to be acceptable for the purpose of the program, although the operating conditions were not available in detail. The utilization of such facilities was found to be wanting in the areas of more complete instrumentation, and thus in the interpretation of data shedding light on material behavior. The observables measured, although of intrinsic value were not found to be useful for direct design application or material development, as they are often not proven to be significant from the design point of view. These conclusions led to the timing of the experiment towards the end of analysis. On the other hand they made the selection of experimental techniques and facilities that much easier since the basic procedure with some improvements could be accepted. The simulation requirements were given careful consideration in the selection of the facility. Since the analysis (parametric performance studies, and test condition analysis, figures 68 through 73) of the radiative system indicated that a figure of merit satisfying the "Q*-concept" was feasible for it without complete simulation required, Channel 3 of the Avco 10 MW facility (described below) was selected as reliable and relatively inexpensive tool. Radiation-ablation systems were tested in the same facility for direct comparison purposes. On the other hand since a similar analysis of design performance and of projected test conditions with varying degrees of simulation indicated that the "Q*-concept" was not applicable for the sufficient degree of resolution for systems with surface mass transfer, it was deemed not necessary to institute an all embracing simulation test program. Instead, experiments were devised which, while indicative of material performance, mostly served to increase the knowledge of material behavior by comparisons of theory and experiment. Such experiments substantiate the need for "conventional" technique concerning the primary shield behavior to supply information for both design and

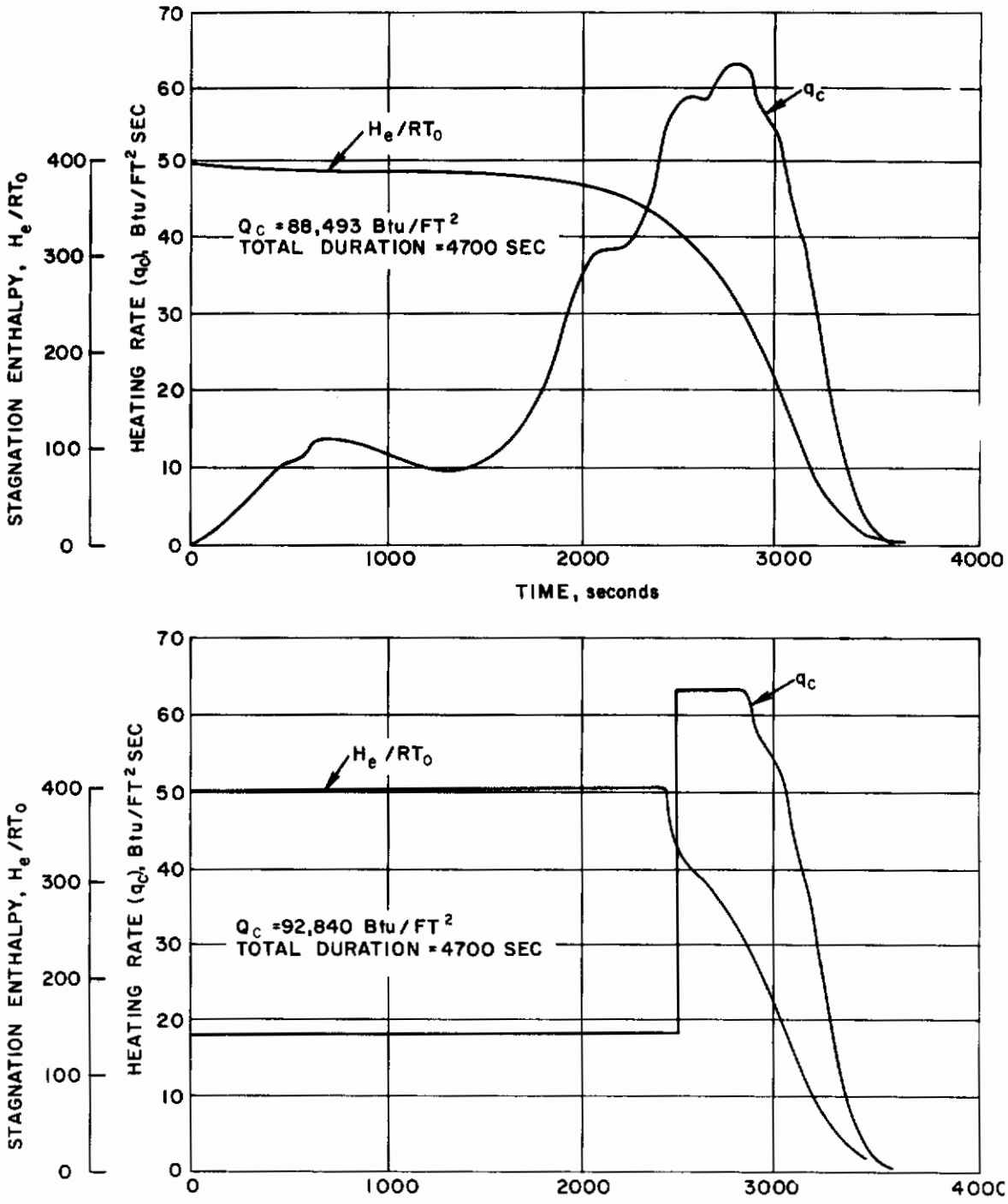

Figure 73 THERMAL ENVIRONMENTS USED FOR ANALYTIC SIMULATION OF TEMPERATURE RESPONSE DURING GROUND TEST (PARTIAL SIMULATION) AND ACTUAL TRAJECTORY

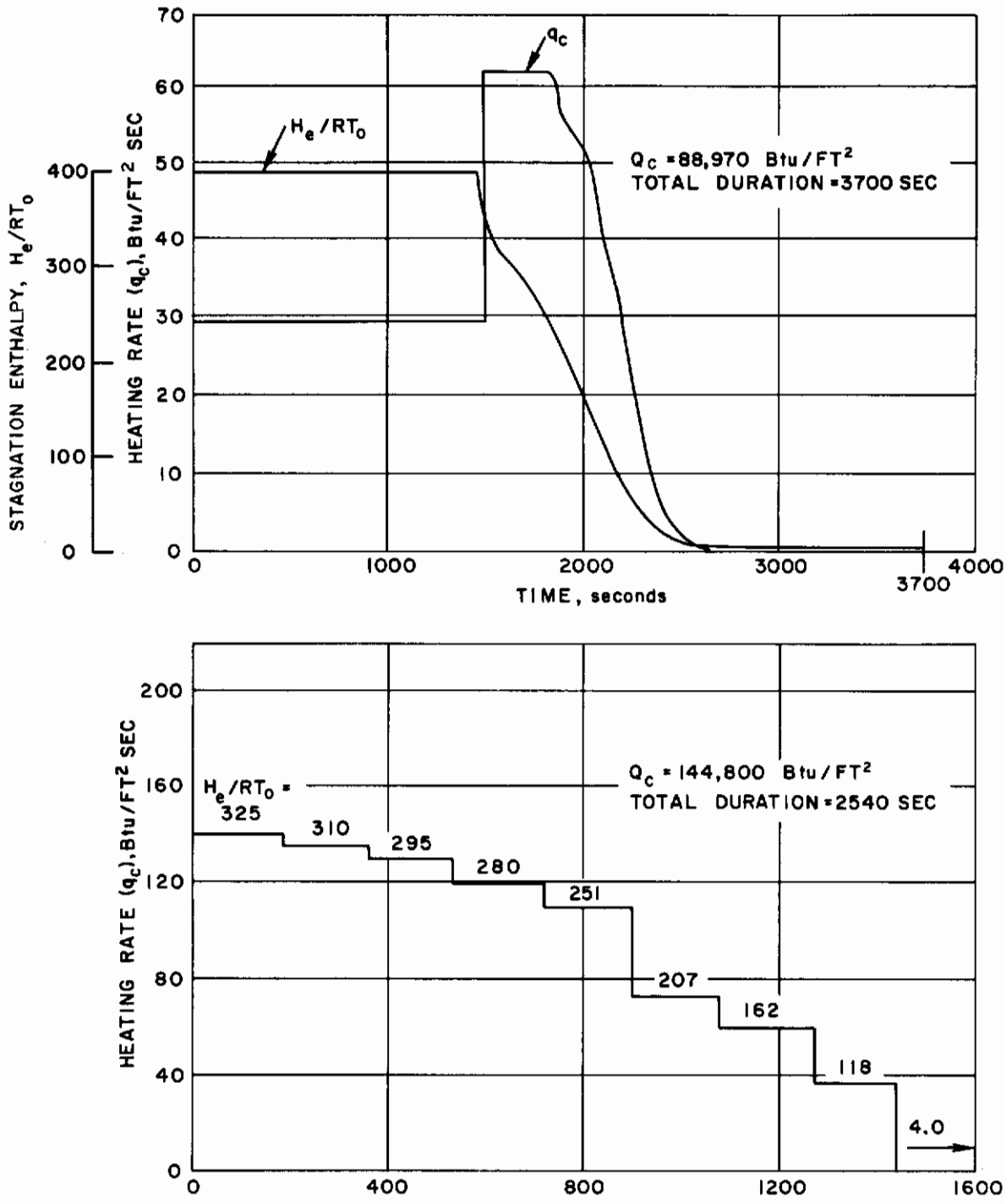

Figure 73 (Cont'd)

material development efforts. They were also needed to establish the bounds of analytical methods used in parametric studies when confronted with the improved knowledge of the material.

To verify the validity of analytical assumptions used in the process of the "Q*-concept" validation, varying environmental conditions were provided utilizing two sets of conditions in the Channel 3 program, and a variable time simulation of part of glide vehicle trajectory on OVERS facility (described below). The latter tests served the purpose of establishing the validity of theory over a broader range of conditions including variable heat flux and enthalpy inputs.

The need of experimental determination of properties needed for conventional techniques was obviated to some extent by the use of typical materials with relatively well-known properties. Such determinations would have been needed otherwise to compare the analytical prediction based on conventional techniques with the new experiments utilizing "Q*-concept" when verified.

Finally, a minimum of built-up components were tested as the analysis of the radiative shield indicated, also, that additional composites behavior did not depend on the environment and thus could be tested by providing a temperature and flux simulation at the interface. This, in the case of radiative shield means a complete configuration single test, and for ablative coating conventional primary shield evaluation, but a test satisfying above requirements without recourse to calculations concerning performance of a given built-up configuration.

In keeping with the overall scope of the program "pure" radiation and radiation shields utilizing ablating plastic (referred to as "radiation-ablation" shields) were tested. The samples tested and conditions used were representative of nose cap and leading edge of a typical glide-re-entry vehicle. The overall simulation requirements were discussed at length in preceding sections.

A. HYPERTHERMAL WIND TUNNEL TESTS--CHANNEL 3 AVCO 10 MEGAWATT FACILITY

This experimental program was intended to demonstrate the technique for the testing of thermal protection systems under simulated glide vehicle re-entry conditions and to provide an experimental basis for comparing the performance of different systems with the predictions of the analytical studies described elsewhere in this report. It is emphasized that it was not the purpose of this test program to compare new materials or to select the optimum materials for a particular application, but rather to test those materials whose properties are sufficiently well known that their performance in particular systems can be compared with analytical predictions, thus affording experimental evaluation of the figure of merit proposed for these systems.

1. Test Environment

a. Test Time

The conditions associated with glide re-entry require that for valid simulation of the aero-thermodynamic parameters significantly affecting the thermal protection system performance, the prevailing low-heat flux at relatively high enthalpies are maintained for long exposure times. Based on this criterion, test times in the order of ten minutes or longer were deemed necessary.

b. Mach Number

For blunt bodies the actual Mach number simulation is not too important. It suffices to test in a high enough supersonic stream that will result in reasonably simulated pressure and velocity gradients on the front face of the test specimen. As a result of this a free stream Mach number from 2 to 3 was considered satisfactory for the purpose of the present investigation.

c. Pressure Level

Though in some heat transfer simulation the pressure level is not as important as the pressure gradients, for ablation study purposes it becomes very desirable to simulate the density altitude. Since a good portion of the heat effects for glide re-entry will occur between 300,000 and 100,000 feet altitude, testing at those very low pressures was required.

2. Test Facility

Considering the simulation requirements described above and in Section V. B. 1, Avco's Channel 3 arc tunnel was found to be well suited for the required tests and it was used almost exclusively for this program.

a. Description

The tests were performed in Channel 3 of the Avco 10 MW facility (Aerodynamics Section, Engineering Department). This test channel is an enclosed free-jet wind tunnel with a single arc air heater. The arc is powered by battery banks which may be arranged to provide the desired voltage and current capabilities. The arc operates with water-cooled copper anode and cathode thus minimizing air flow contamination and allowing long run times. An external electromagnetic field is used for arc stabilization.

Air is injected tangentially into a swirl chamber, subsequently passed through the anode nozzle into a limited plenum chamber and then exhausts into a 20-inch diameter test chamber through a 2-inch exit diameter nozzle. Nozzles for Mach numbers 2 and 3 were used depending on the required test conditions.

The flow in the test chamber is collected by a bellmouth diffuser connected to the main vacuum system. A half spanning model support strut is adjustable along the test section length. For these tests the models were positioned 1-inch from the nozzle exit.

The bellmouth diffuser and the model support strut are internally water-cooled while the test chamber is externally water-cooled.

To maintain the window glass clear the windows are mounted on extended window ports with internally water-cooled coils. Figure 74 is a diagram of this tunnel and a compete view of the test facility is shown in figure 75.

b. Simulation Capabilities

The stagnation simulation capabilities (enthalpy, heat flux, and pressure) of Channel 3 arc driven wind tunnel are shown in figure 76 for a typical 7-inch nose radius model in a Mach number 2 stream. Higher Mach number nozzles render lower stagnation point heat flux.

The present operating regime is bound by a lower stagnation pressure limit of approximately 0.006 atmospheres governed by the existing vacuum system and a maximum gross input power to the arc of 2 megawatts. Higher enthalpies and stagnation pressures than those shown on figure 76 have been attained but such accomplishments are beyond the interest of this program.

c. Extended Capabilities

At present, the available vacuum and cooling water storage capacities limit the run time to 1/5-hour. Additional vacuum and water storage being installed will extend the run time in the facility to over one hour. Imminent installation of power and mass flow controls will enable programming of heat flux and enthalpy along a re-entry trajectory.

3. Experimental Technique

Glide re-entry is characterized by low heat fluxes for long exposure times at enthalpy levels similar to ballistic re-entry. The aero-thermodynamic re-entry environment for a typical glide re-entry vehicle was shown in

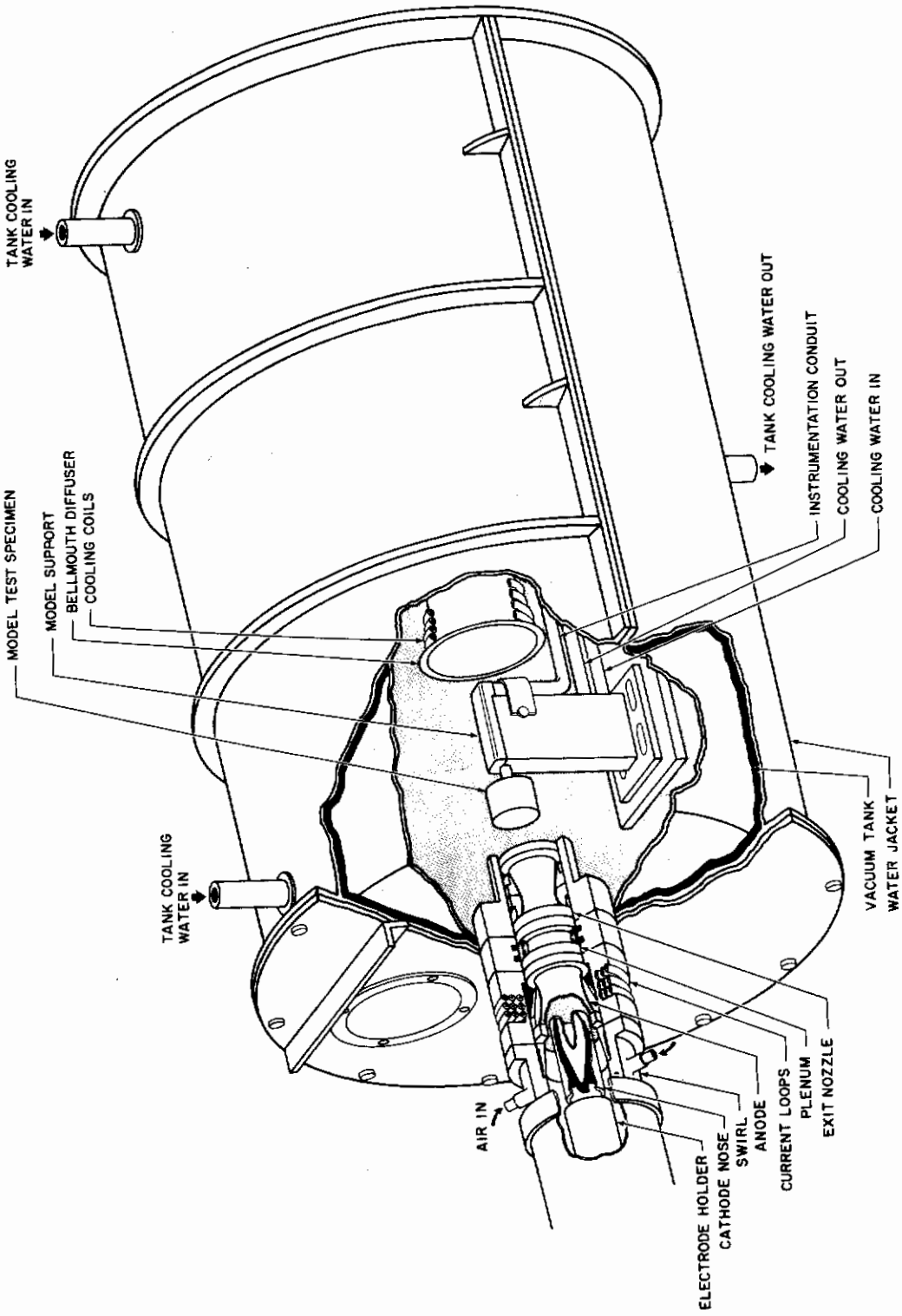

Figure 74 SCHEMATIC OF CHANNEL 3

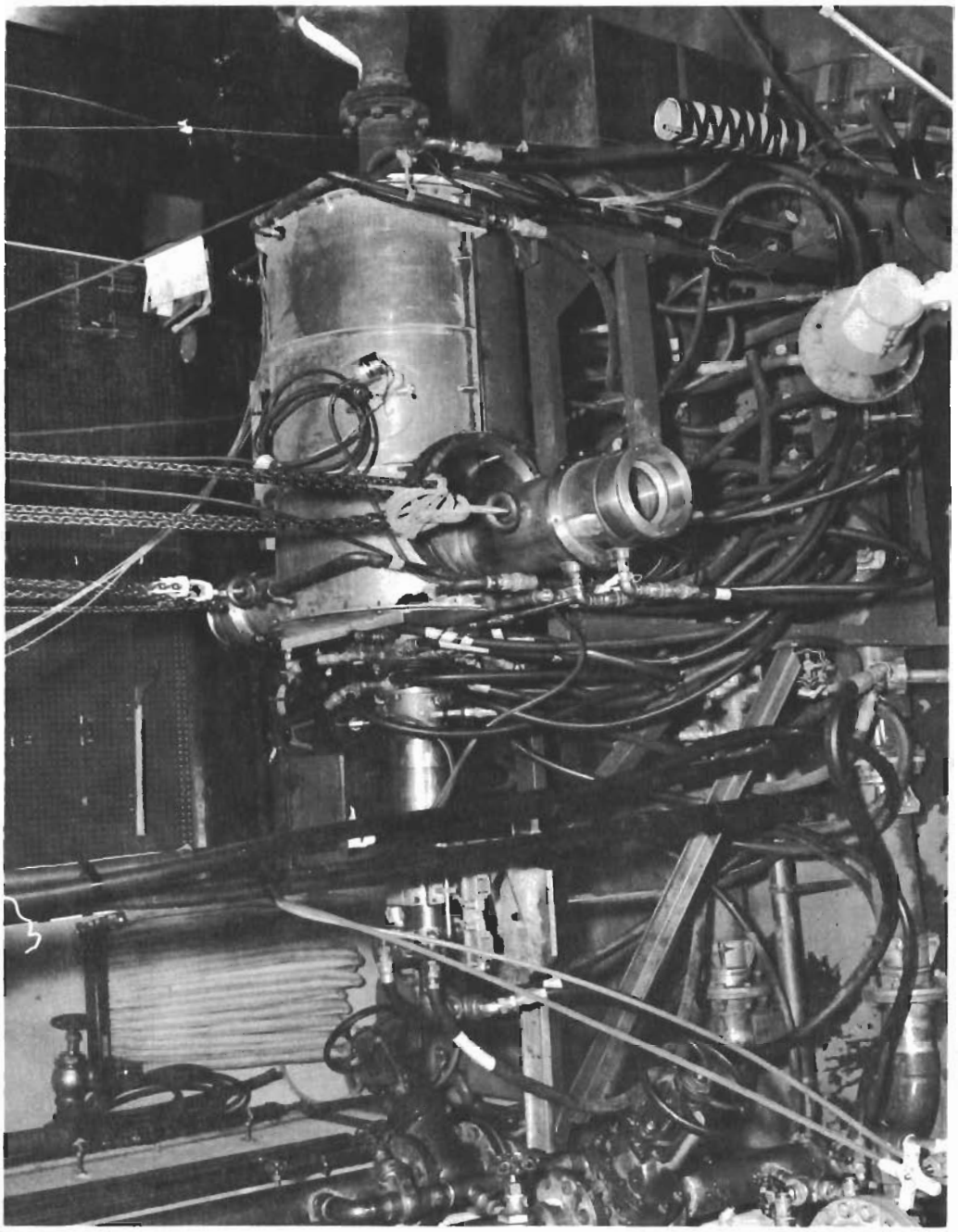

Figure 75 COMPLETE VIEW OF CHANNEL 3

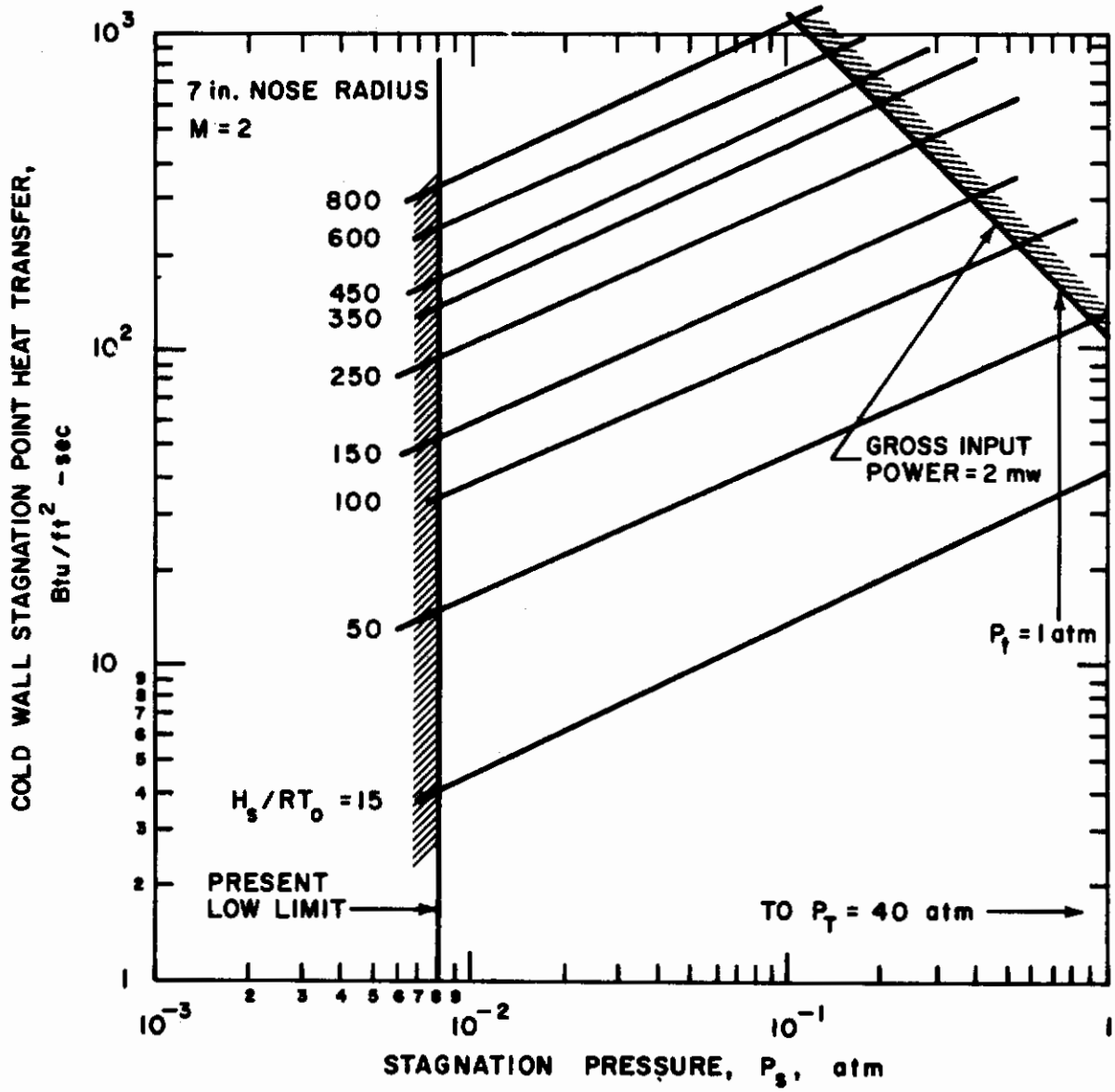

Figure 76 STAGNATION CAPABILITIES OF THE CHANNEL 3 ARC DRIVEN SUPERSONIC WIND TUNNEL

figures 22, 23, and 24. Since the present maximum test time is 1/5-hour for constant flow conditions, a judicious choice of test conditions within the known capability of the test facility was made.

a. Test Procedure

Radiation and radiation-ablation models of selected materials were tested at two different test conditions for 1/5 hour test times. The nominal test conditions chosen were as indicated in Table 5.

TABLE 5

TEST CONDITIONS FOR THE CHANNEL 3 EXPERIMENTAL PROGRAM

Test Conditions	H_e/RT_o	q_c Btu/ft^{2}sec.	P_e atm.
1	205	70	0.0088
2	150	55	0.01105

The test conditions were obtained by adjusting the mass flow, arc current, arc voltage, and Mach number in the test facility.

Backface temperature histories were recorded on a CEC oscillograph. The models were weighed and measured before and after the test. Other effects were recorded with still photographs and motion pictures. Heat flux and enthalpy were computed from calorimeter and pressure model data using established computer programs.

b. Test Samples and Materials

Materials selected for testing were representative of the various categories considered for re-entry heat-shield applications. Thus, molybdenum skin backed by high-temperature insulation and pyrolytic graphite in a similar configuration may be taken as typical radiation shields, although some ablation may be expected in the case of the graphite. Zirconia matrix filled with polymethylmethacrylate represents a case of internal ablation providing external dimensional stability and radiation shield characteristics. The X4000 and X5000 samples of the experimental series of Avco high-temperature plastics under development represent a class of ablative plastics which may or may not ablate dimensionally under glider re-entry application. They differ principally in the maximum surface temperature that may be reached prior to the time when significant recession may take place. Teflon was tested as a typical low-temperature (1000°F) ablating material on the other and of the spectrum of ablators. The known properties of the above materials were shown in Table 2.

1) Calibration models

Pressure and calorimeter models were used to calibrate the flow. Pressure distributions from the graphite pressure model and temperature-time histories from the copper plug calorimeter model are used together to compute the heat flux and boundary layer shear distribution. The pressure and calorimeter models are illustrated in figures 77 and 78 respectively.

2) Radiation models

These were pyrolytic graphite (front face manufactured by General Electric) and molybdenum (all surfaces were coated by the Chromalloy Corporation W-2 diffusion process for oxidation protection) models built with flat faces for ease of manufacture. Both categories were made with a 1-inch thickness of Mark II insulation, 1/4-inch of which constituted a "hot face" layer. The graphite models were constructed with a commercial grade of graphite for the body and pyrolytic graphite for the insert in the face, 0.250-inch thick sunk in a recess to fit flush; no adhesive was used. A sketch of the graphite model is shown in figure 79.

The molybdenum models were treated with a chromium diffusion process to prevent oxidation. Three types of models in this category differed by the distance at which the Mark II insulation was mounted from the front face. Sketches of the molybdenum models are shown in figure 80. These models were also provided with backface thermocouples. The backface in the case of these models was considered to be the aft face of the Mark II insulation slug. Because of the difficulty in attaching thermocouples to the insulator, a phenolic disk was incorporated between the adapter and the insulator to provide a bonding surface for the thermocouple. Once bonded to the phenolic, the junction was passed through holes drilled in this piece to come into contact with the aft face of the Mark II insulation.

3) Radiation-ablation models

These models are 7-inch spherical radius blunt nosed cylinders, 1.75-inch diameter in cross section as shown in figure 81. One center and two outboard thermocouples were located on the backface of the specimen to record backface temperature histories during the test. The distance "ℓ" from the spherical front surface to the backface varied for different models this distance "ℓ" represents the thickness of the heat shield in the prototype vehicle.

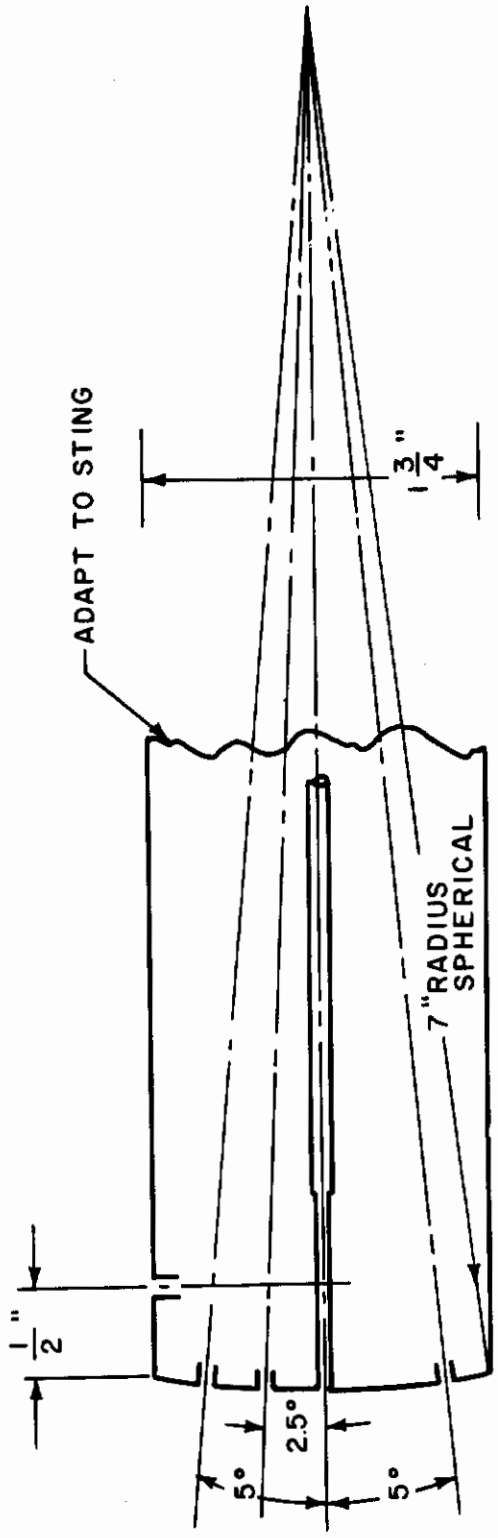

Figure 77 PRESSURE CALIBRATION MODEL FOR CHANNEL 3

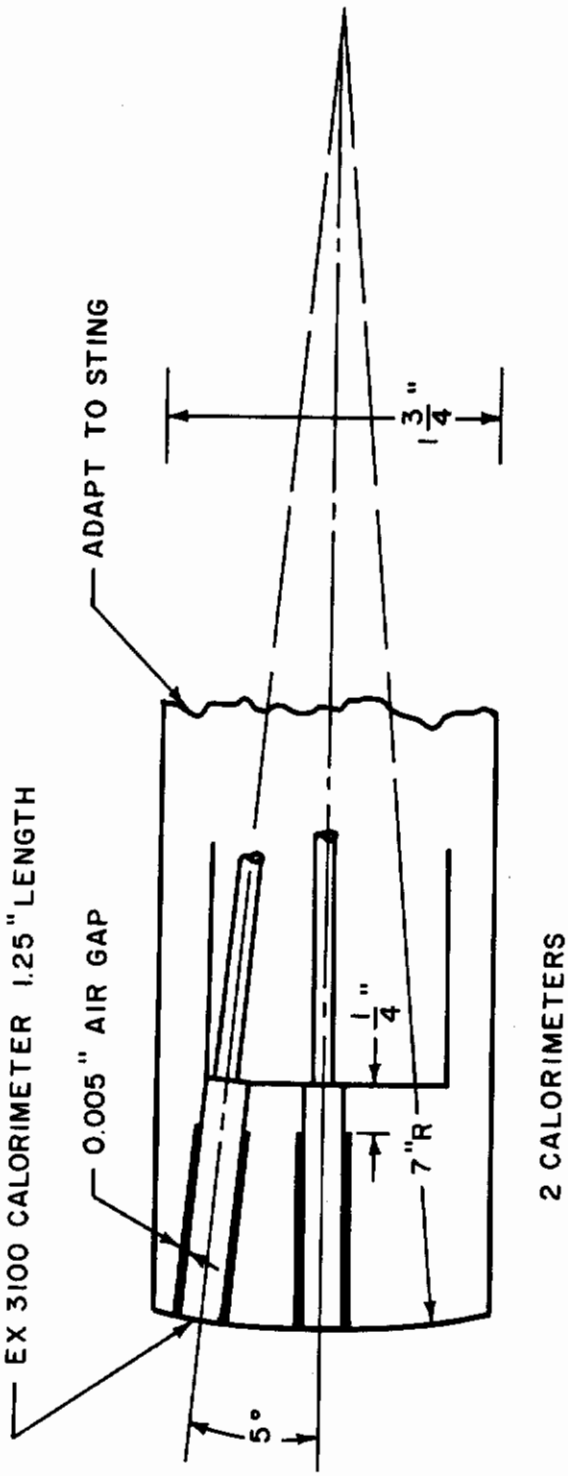

Figure 78 CALORIMETER MODEL FOR CHANNEL 3

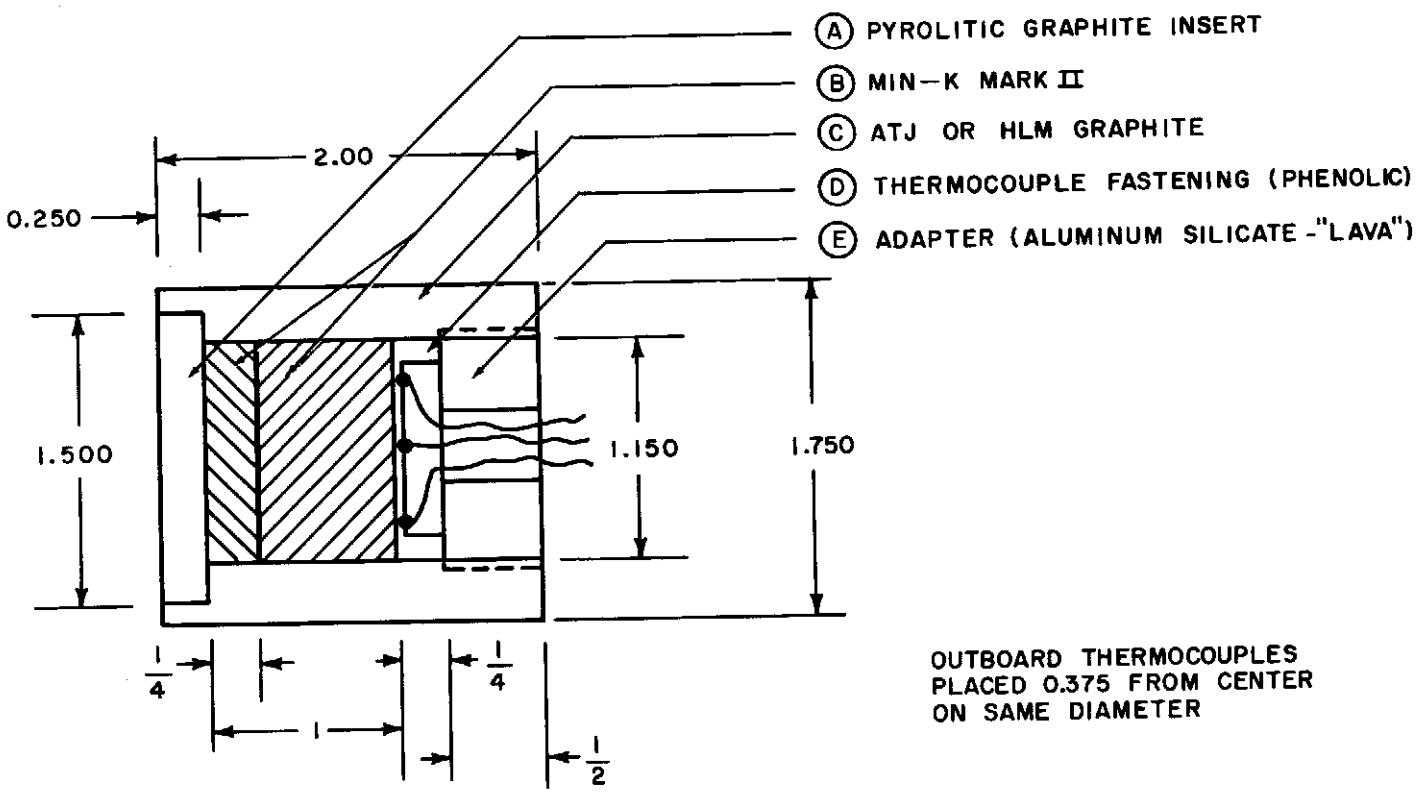

Figure 79 PYROLYTIC GRAPHITE RADIATION SHIELD MODEL ASSEMBLY

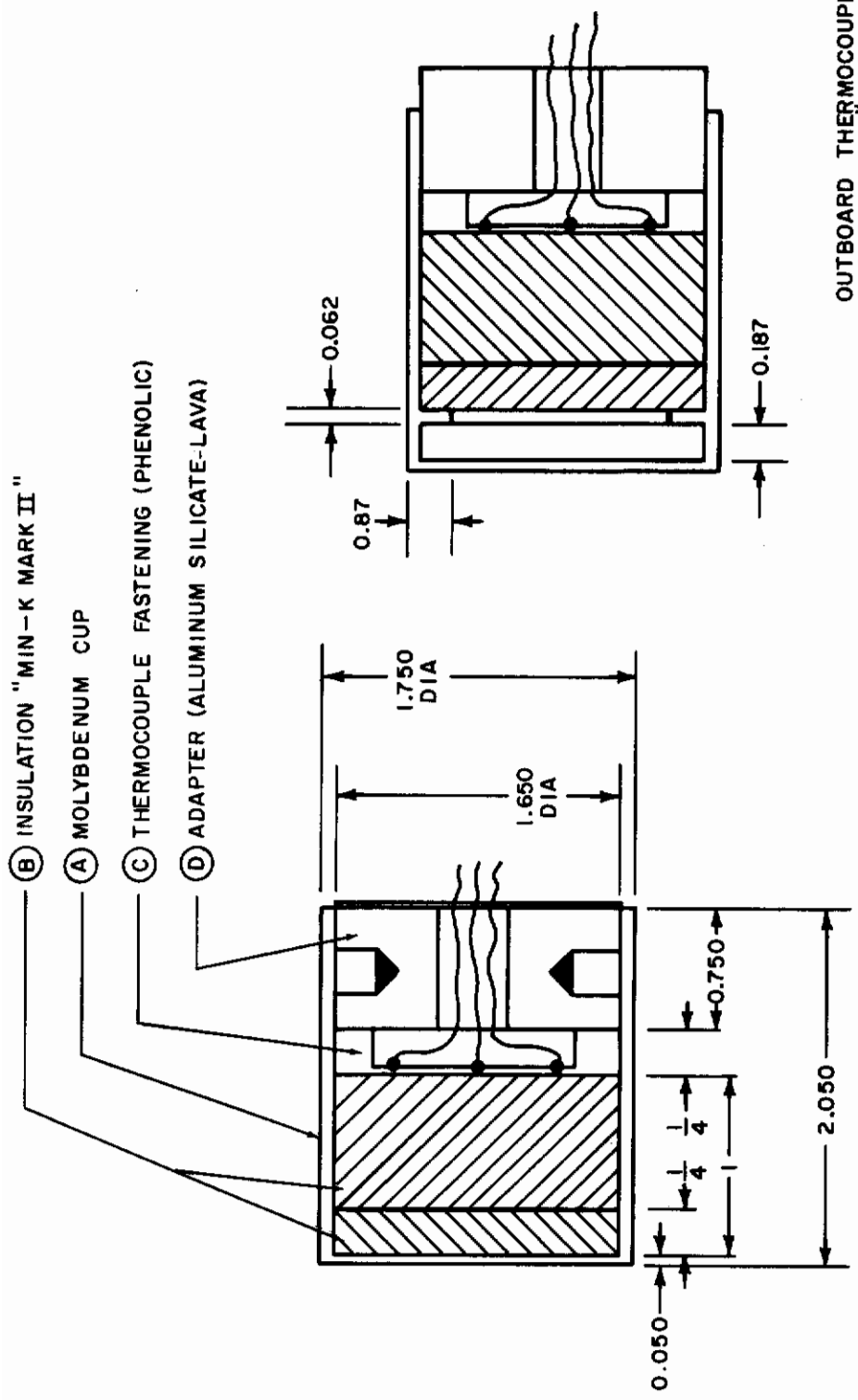

Figure 80 MOLYBDENUM RADIATION SHIELD MODEL ASSEMBLY

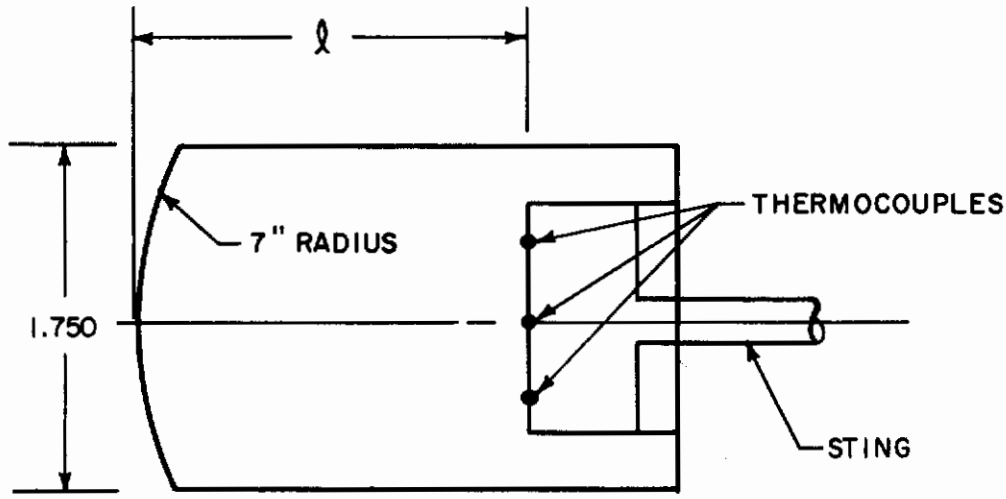

Figure 81 RADIATION-ABLATION MODEL ASSEMBLY

Models of four different materials which would ablate under certain conditions were used; these were X4000, and X5000 series (experimental materials under development as Avco RAD) Teflon, and zirconia matrix filled with polymethylmethacrylate.

4. Data Reduction Procedure

A major portion of the data reduction concerns the thermodynamic calibration of the stream. Of the three test condition variables at the stagnation point, heat flux q_s, pressure p_s, and enthalpy H_e, only the stagnation pressure can be measured directly.

The stagnation heat flux q_s can be determined by calorimetry. A copper model is equipped with two copper plug calorimeters as shown in figure 78. The copper calorimeters are 1/4-inch diameter slugs with chromel-alumel thermocouples buried at the null point just below the surface (see reference 67). Heat flux calibration tests are of very short duration to prevent the model from reaching melting temperature. These very short tests, of a few seconds only, permit the validation of the assumption that the heat flux measured by the calorimeter corresponds to cold wall stagnation flux. Heat fluxes are determined from Avco digital machine solutions of the one-dimensional Fourier heat conduction equation with appropriate boundary conditions and measured temperature versus time values.

In addition to the measurements just described, the gas enthalpy was also determined from power and flow measurements and it was also approximated by exposing a known ablator, Teflon in this case, for which the heat of ablation has been found experimentally. The stagnation enthalpy is then calculated by equating the measured stagnation heat flux to the heat flux in Fay and Riddell theory (see reference 68) at the measured stagnation pressure for a given nose radius. The nose radius here is the effective nose radius. This is the radius of an equivalent hemispherical nose that would produce the same velocity gradient at the stagnation point as the model under investigation (see reference 8).

The heat of ablation for the specimen materials investigated was simply calculated by computing the total heat input on the frontal area divided by the mass loss due to ablation. The total heat input was approximated by assuming a uniform heat flux equal to the stagnation point heat flux. No hot wall correction was made.

5. Results and Discussion

a. Radiation Tests

Several molybdenum and pyrolitic graphite radiation models were tested at test condition 2 (see table 6): an enthalpy of 150 RT_o, heat

flux of 55 Btu/ft^2 sec, and 0.01105 atmospheres stagnation pressure. The test results are presented in table 6 and photographs of the models before and after the test are shown in figures 82, 83, 84, and 85 respectively. Typical backface temperature histories for these models are plotted in figures 86, 87, and 88.

The distance "ℓ" is not defined in these models as in the ablation models: in the present case the thickness of the Mark II internal insulation was 1-inch, 1/4-inch of which constituted a hot surface as described under "models."

The change in dimension "ℓ" on the molybdenum models is irrelevant. More significant is the apparent change in wall thickness but since the exposed surface roughed up, no attempt was made at recording small dimensional changes. The recession in the pyrolitic graphite is simply the change in thickness of the flat slug insert. In model 73 the slug separated temporarily thus exposing the Mark II insulation to the plasma for a portion of the test run; however, the backface temperature history does not show any indication of this happening.

All the radiation models reached relatively high backface temperatures during the test due to two-dimensional heat flow effects. For these tests at a heat flux of 55 Btu/ft^2 sec the maximum temperature at the backface was approximately 900° F. The minor internal design configuration changes (Type 1 and 2 Molybdenum Models) did not result in any noticeable differences in the backface temperature.

b. Radiation-Ablation Tests

A number of ablation materials were tested under different test conditions as listed in table 5. The materials tested were X4000 series, X5000 series, zirconia matrix filled with polymethylmethacrylate, and teflon. Models of each material varied in the "ℓ" dimension, the shield thickness.

The heat flux at the outboard calorimeter is also reported in table 5 as a check against the stagnation flux reading. The minor differences between the two readings are attributed to some extent to non-uniformity in the free stream but mostly to the interpretation of the heat flux histories calculated by the digital computer from the calorimeter and pressure readings. The run time in most cases was in the order of 1/5-hour.

Typical radiation-ablation models before the test are shown in figures 89 and 90. Backface temperature histories for representative ablation models are plotted in figure 91 through 96 and photographs of the models after the test are shown in figures 97 through 100.

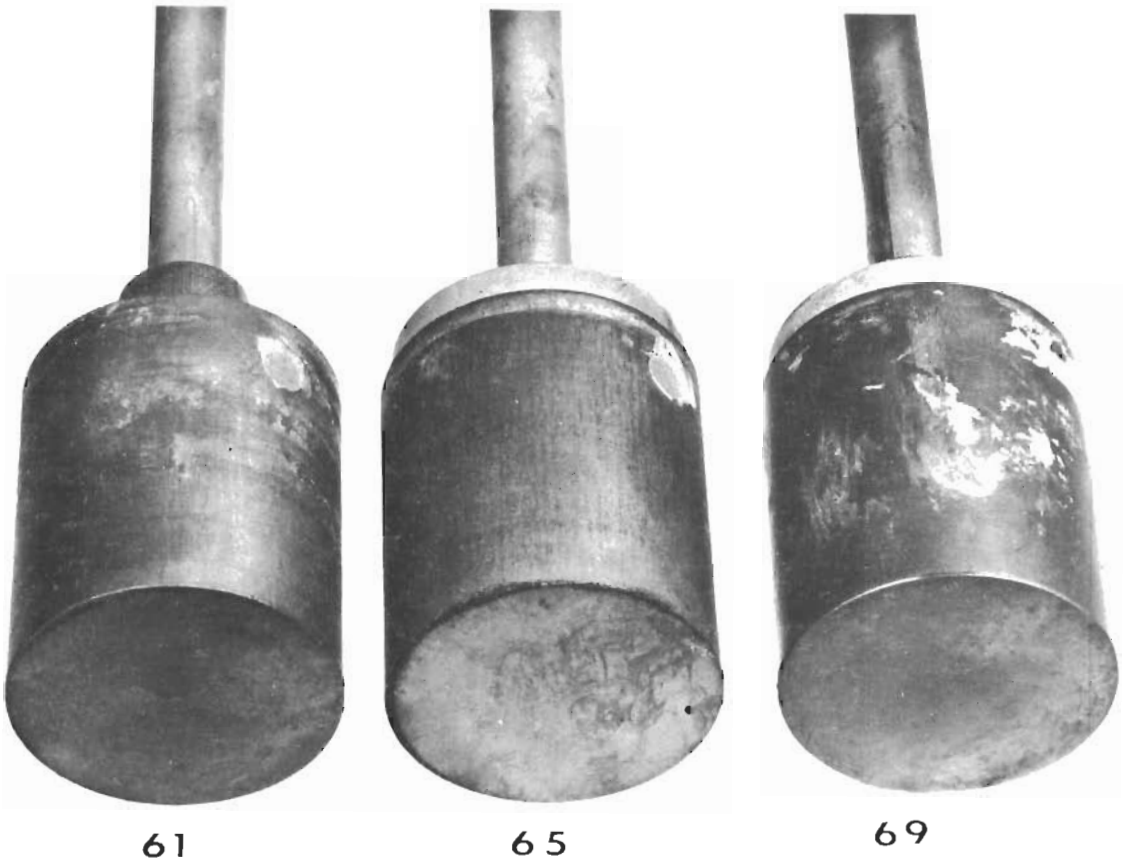

Figure 82. MOLYBDENUM MODELS BEFORE TESTING

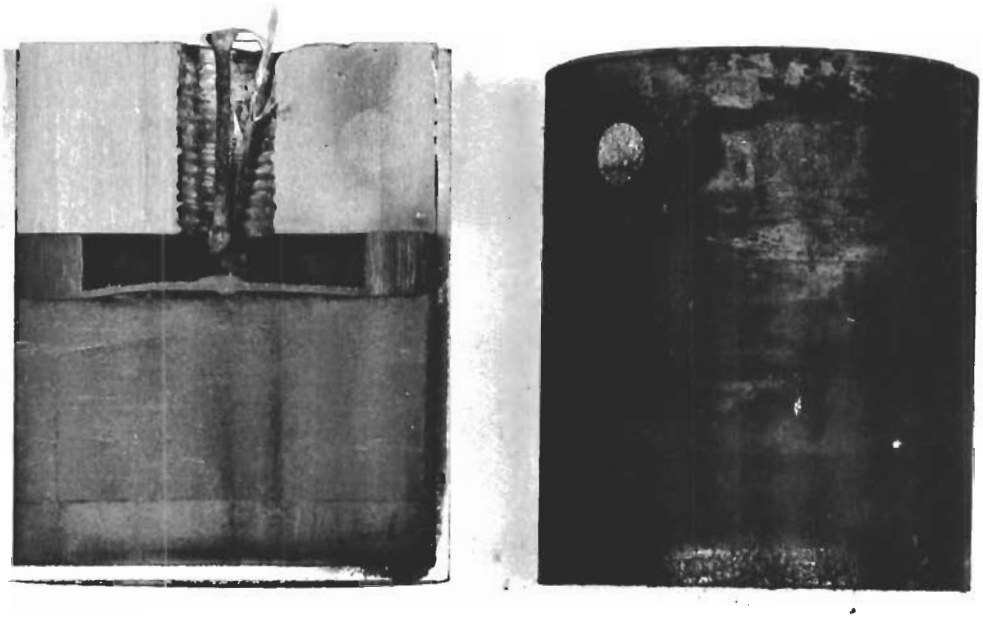

Model 59

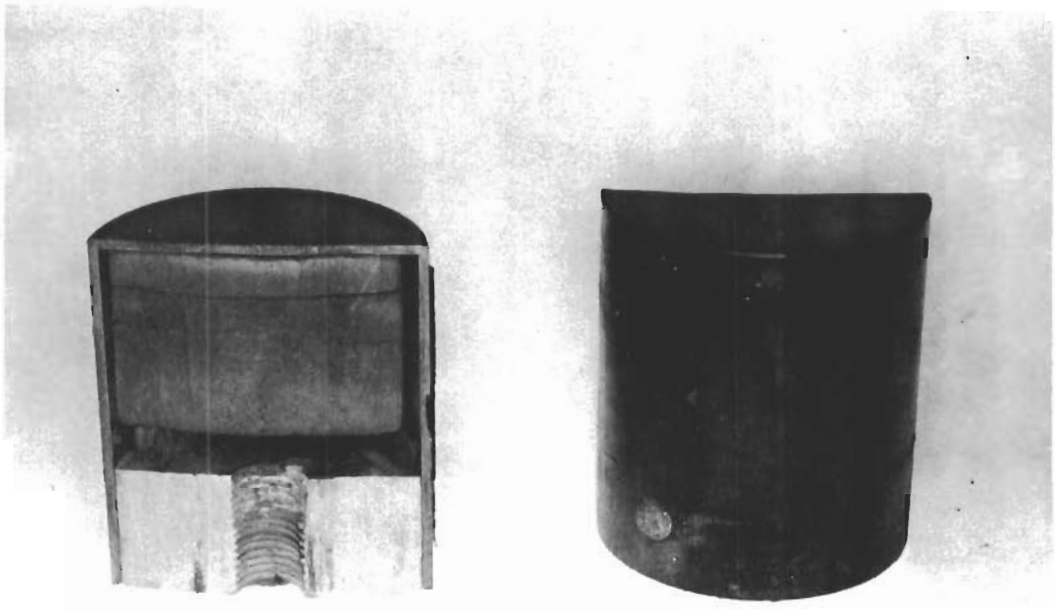

Model 60

Figure 83. Molybdenum Radiation Models (Type 1) After Tests

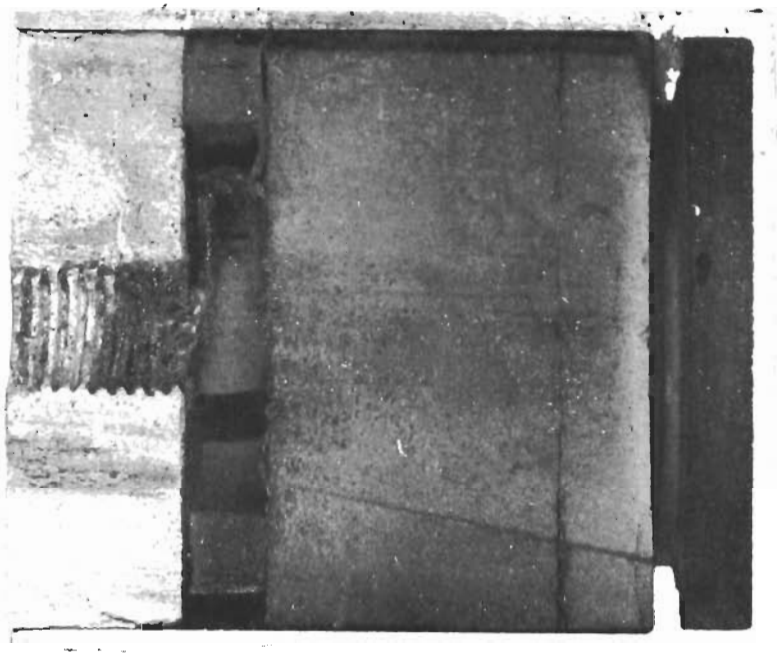

Figure 84 MOLYBDENUM RADIATION MODELS (TYPE 2) AFTER TESTS

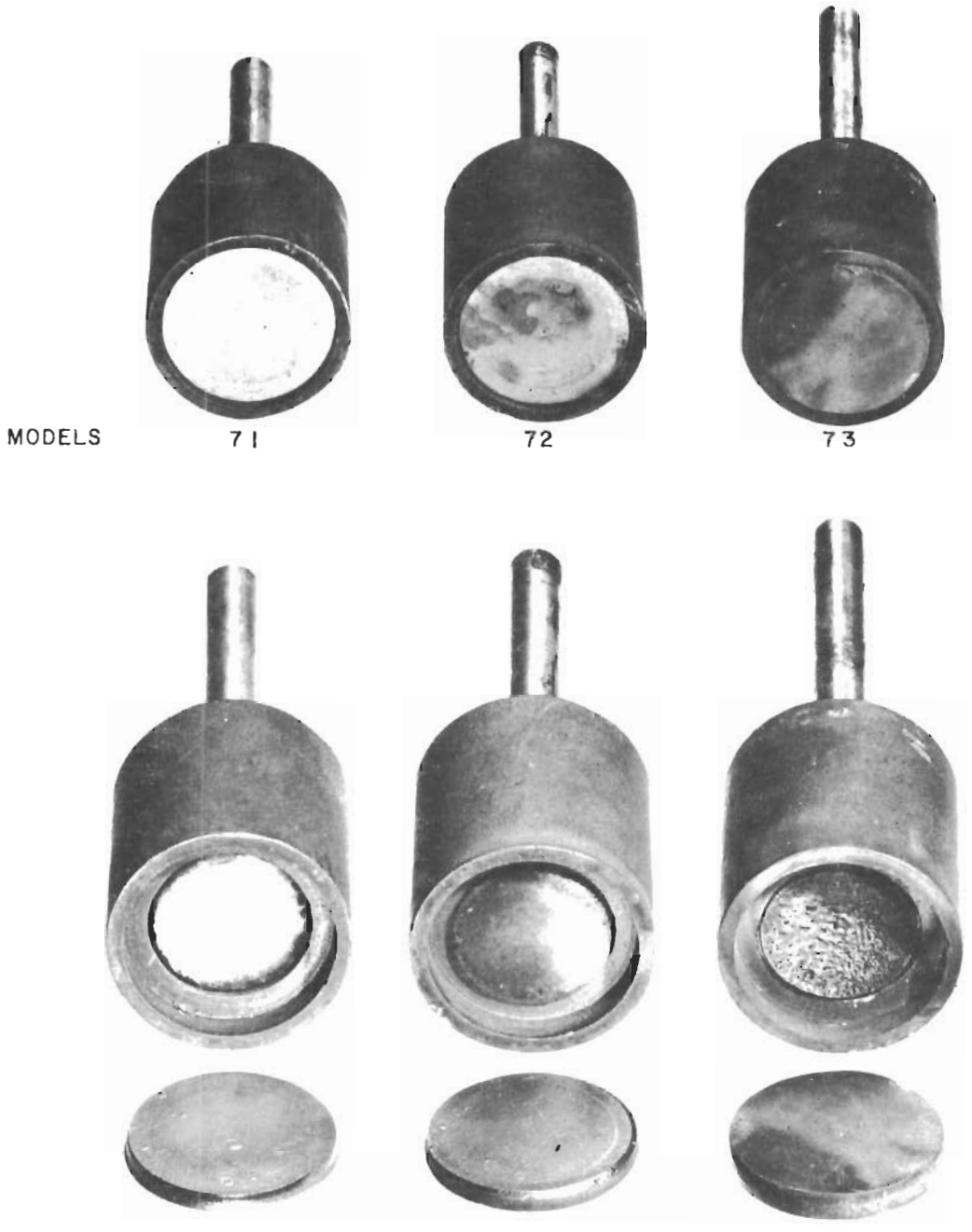

Figure 85 PYROLYTIC GRAPHITE SAMPLES AFTER TESTS

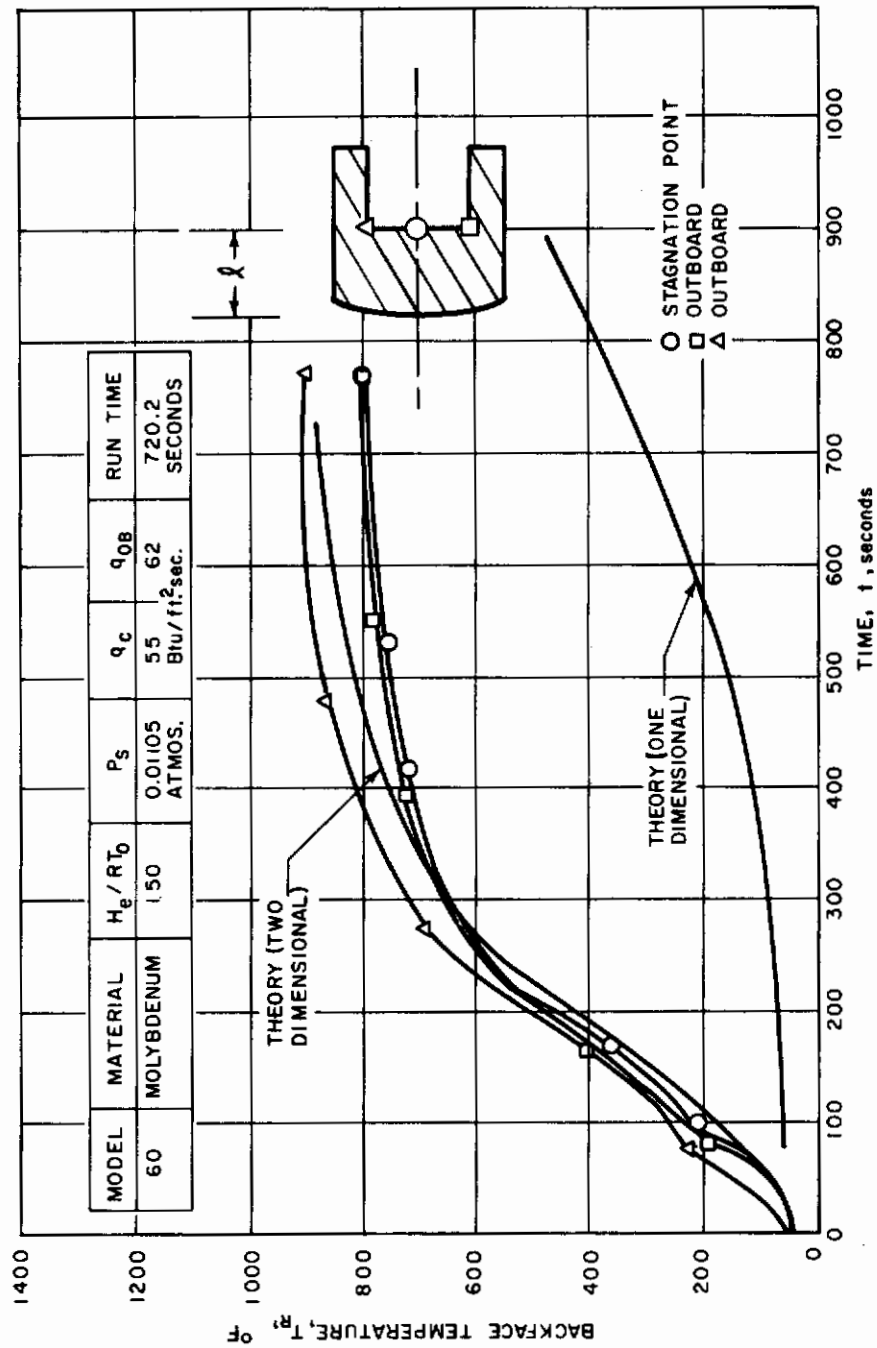

Figure 86 BACKFACE TEMPERATURE HISTORY OF A MOLYBDENUM (TYPE 1) RADIATION SHIELD MODEL

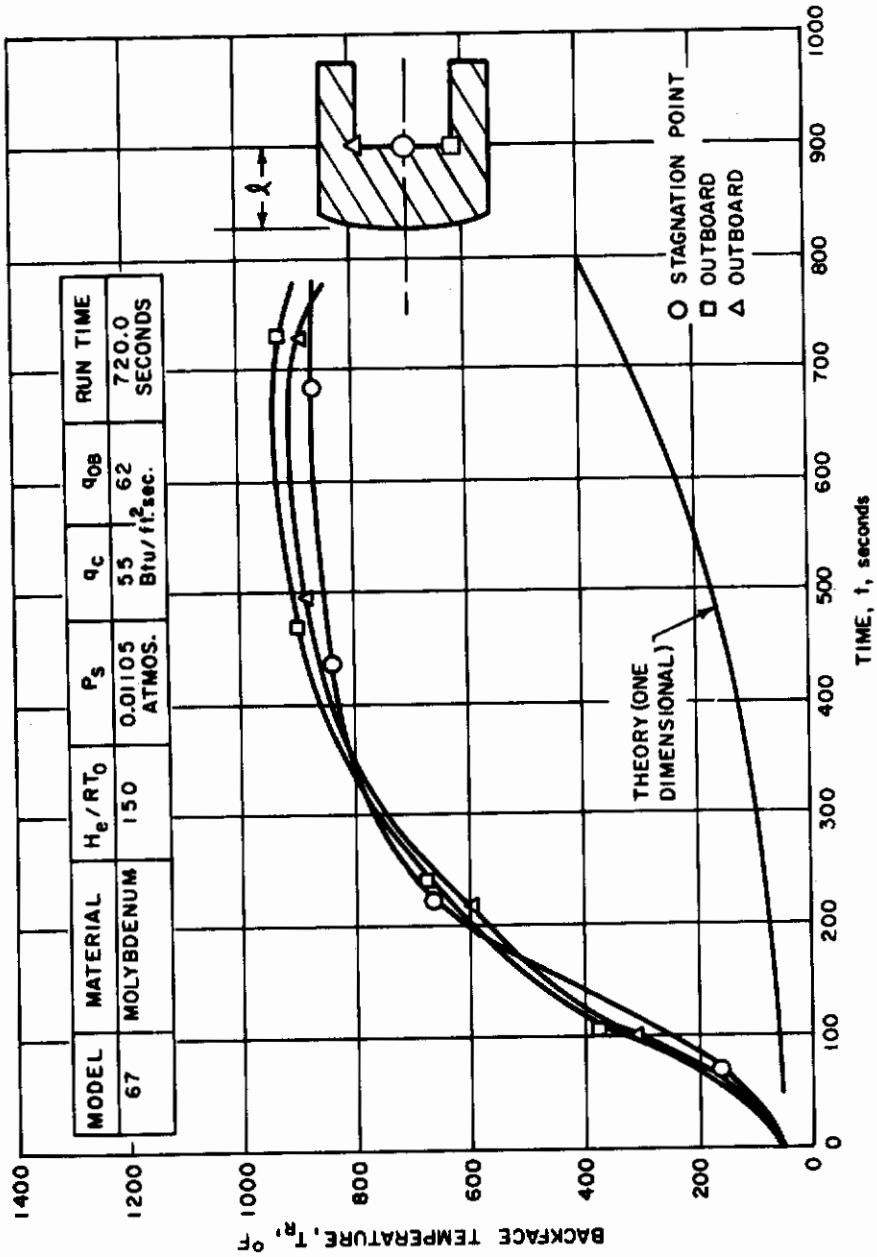

Figure 87 BACKFACE TEMPERATURE HISTORY OF A MOLYBDENUM (TYPE 2) RADIATION SHIELD MODEL

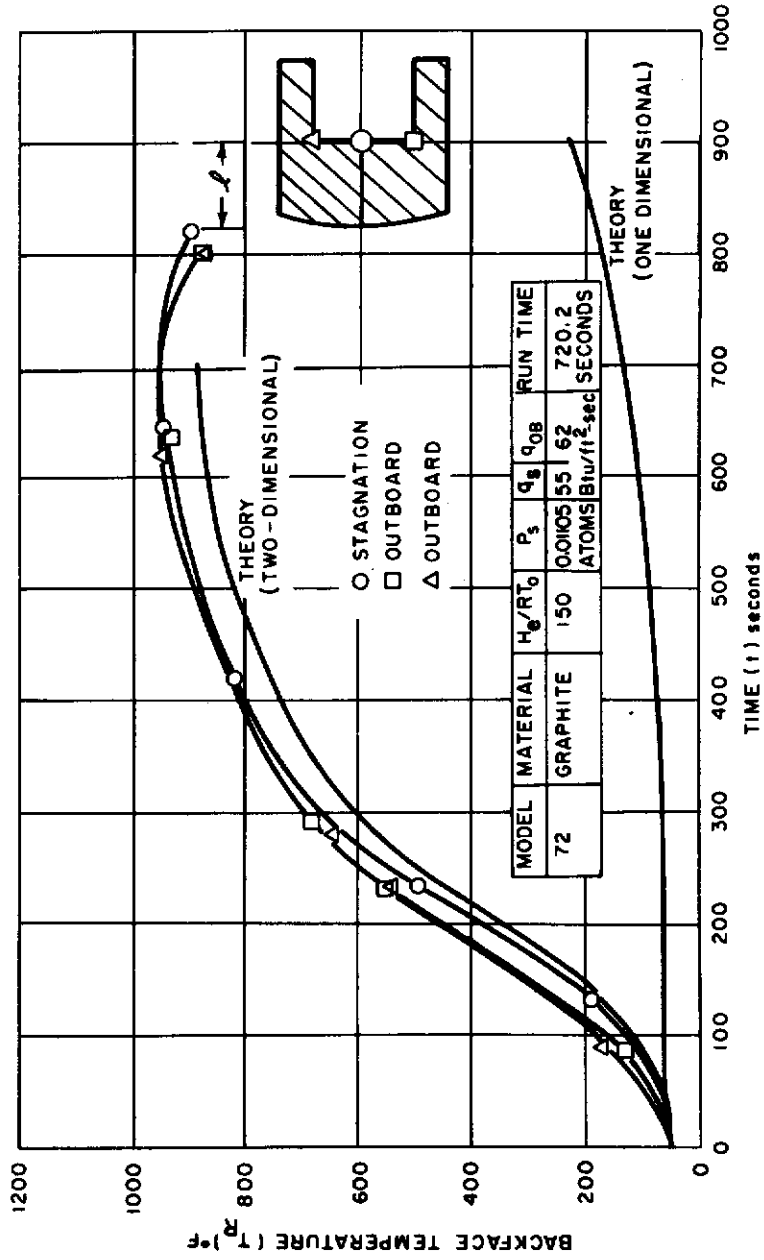

Figure 88 BACKFACE TEMPERATURE HISTORY OF A PYROLYTICGRAPHITE RADIATION SHIELD MODEL

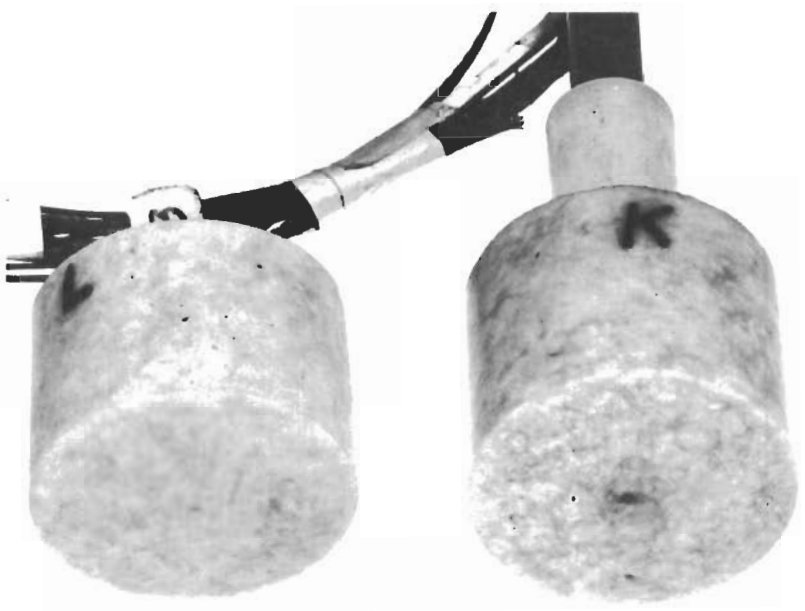

MODEL 2 MODEL 9

X4000 SERIES ABLATION MATERIAL

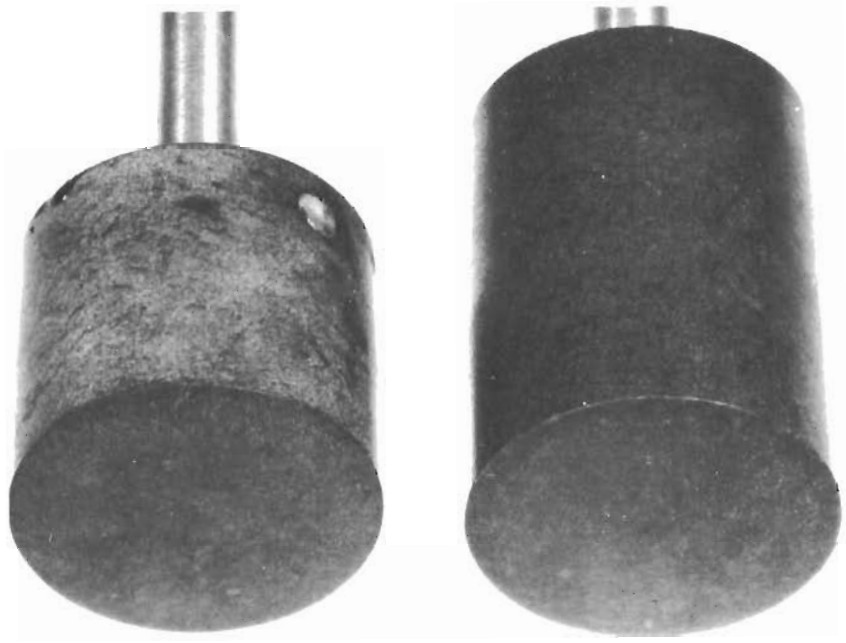

MODEL 12 MODEL 26

X5000 SERIES ABLATION MATERIAL

Figure 89 ABLATION MODELS BEFORE TESTS, AVCO EXPERIMENTAL HIGH-TEMPERATURE PLASTICS X4000 AND X5000 SERIES

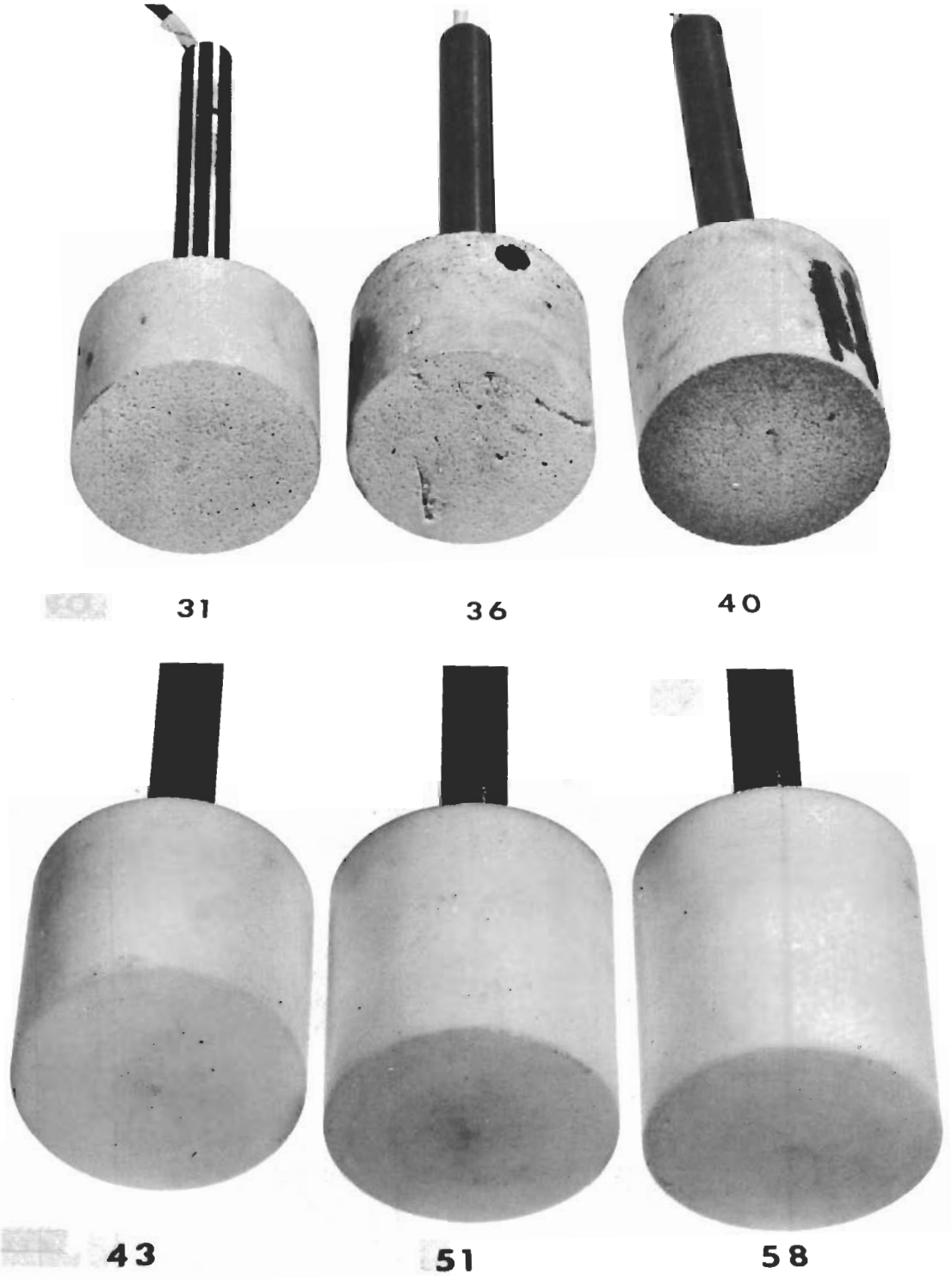

Figure 90 ABLATION MODELS BEFORE TESTS TEFLON AND ZIRCONIA MATRIX IMPREGNATED WITH POLYMETHYLMETHACRYLATE

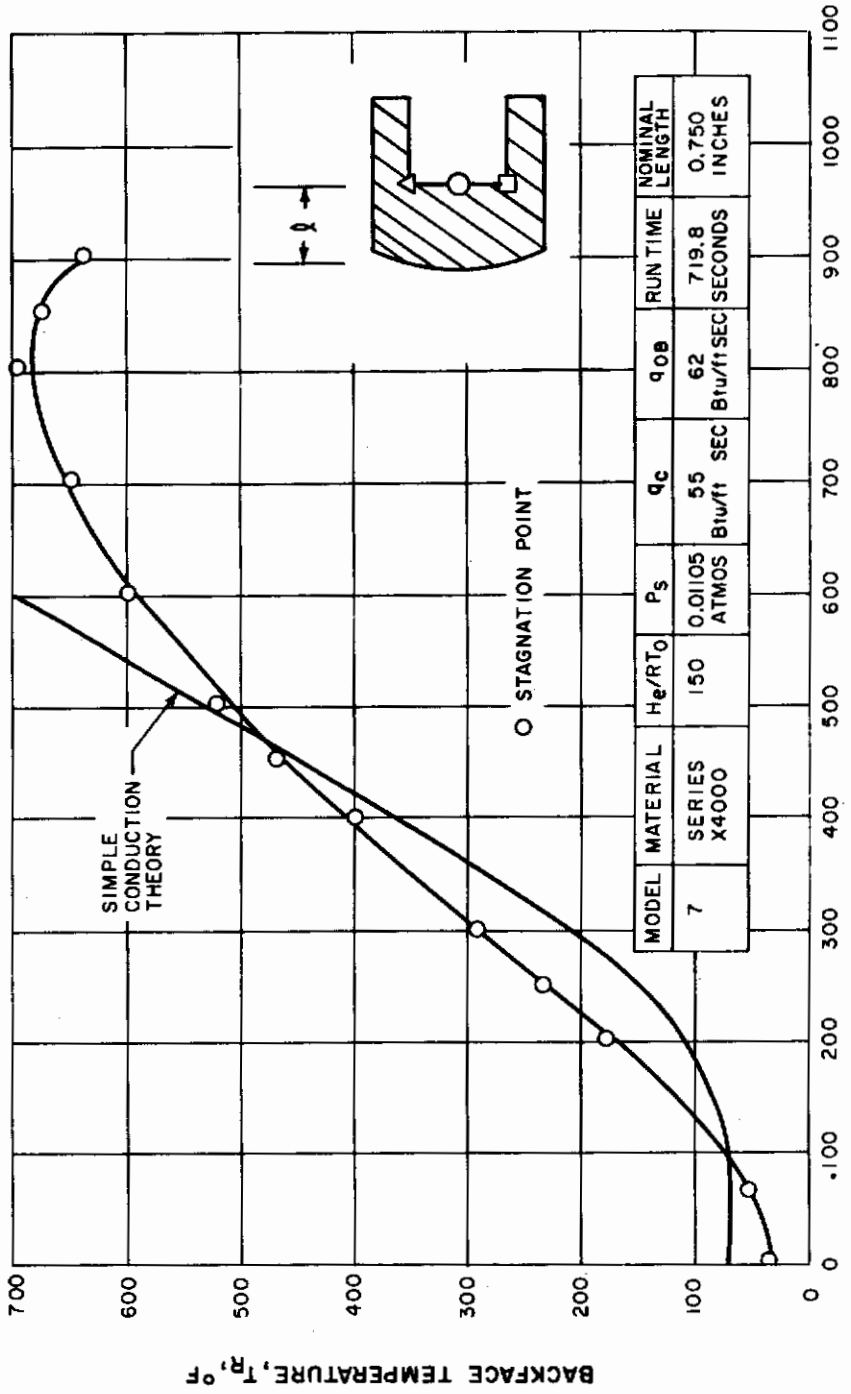

Figure 91 BACKFACE TEMPERATURE HISTORY OF X4000 RADIATION-ABLATION MODEL (CONDITION 2)

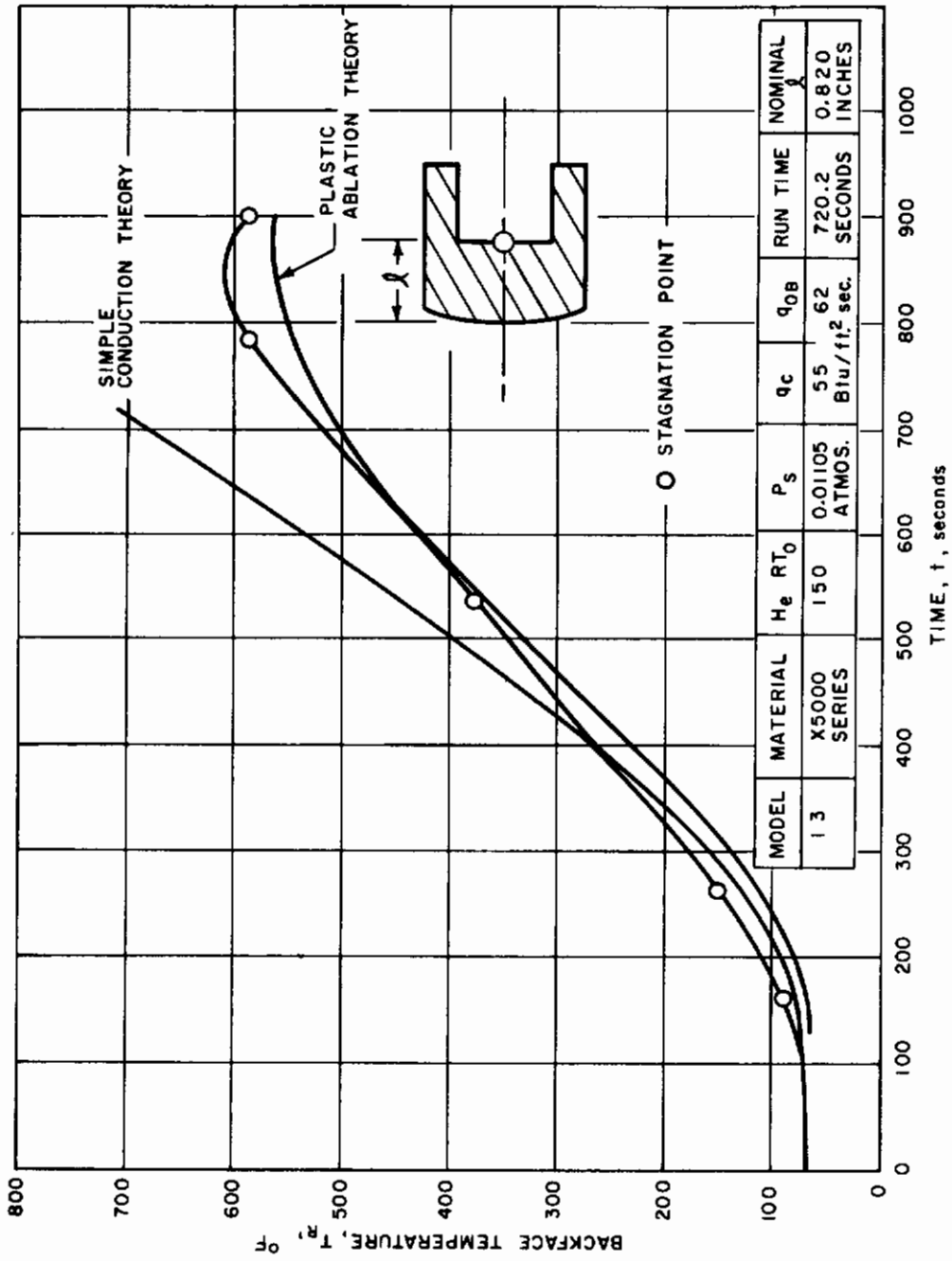

Figure 92 BACKFACE TEMPERATURE HISTORY OF X5000 RADIATION-ABLATION MODEL (CONDITION 2)

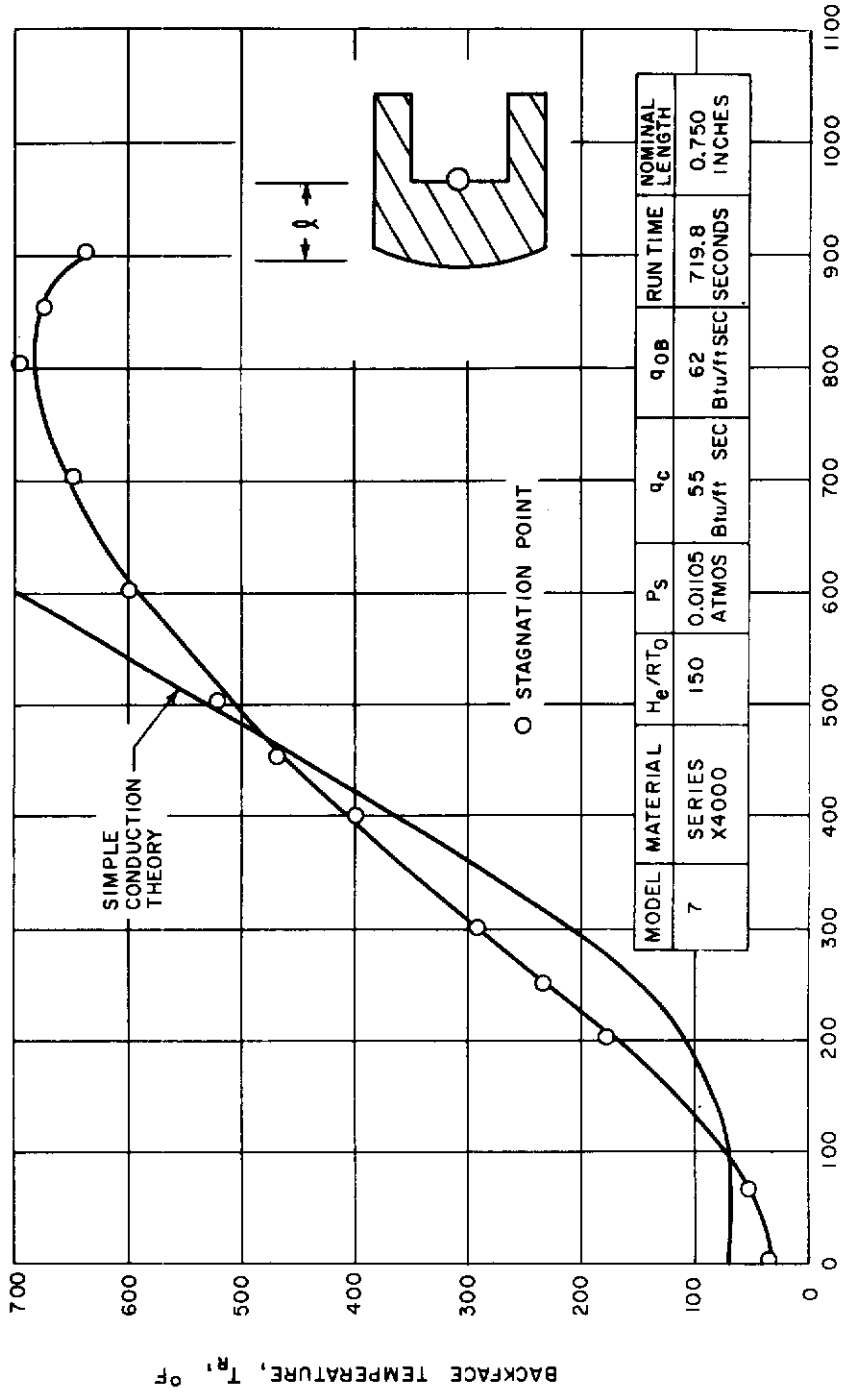

Figure 93 BACKFACE TEMPERATURE HISTORY OF X5000 RADIATION-ABLATION MODEL (CONDITION 1)

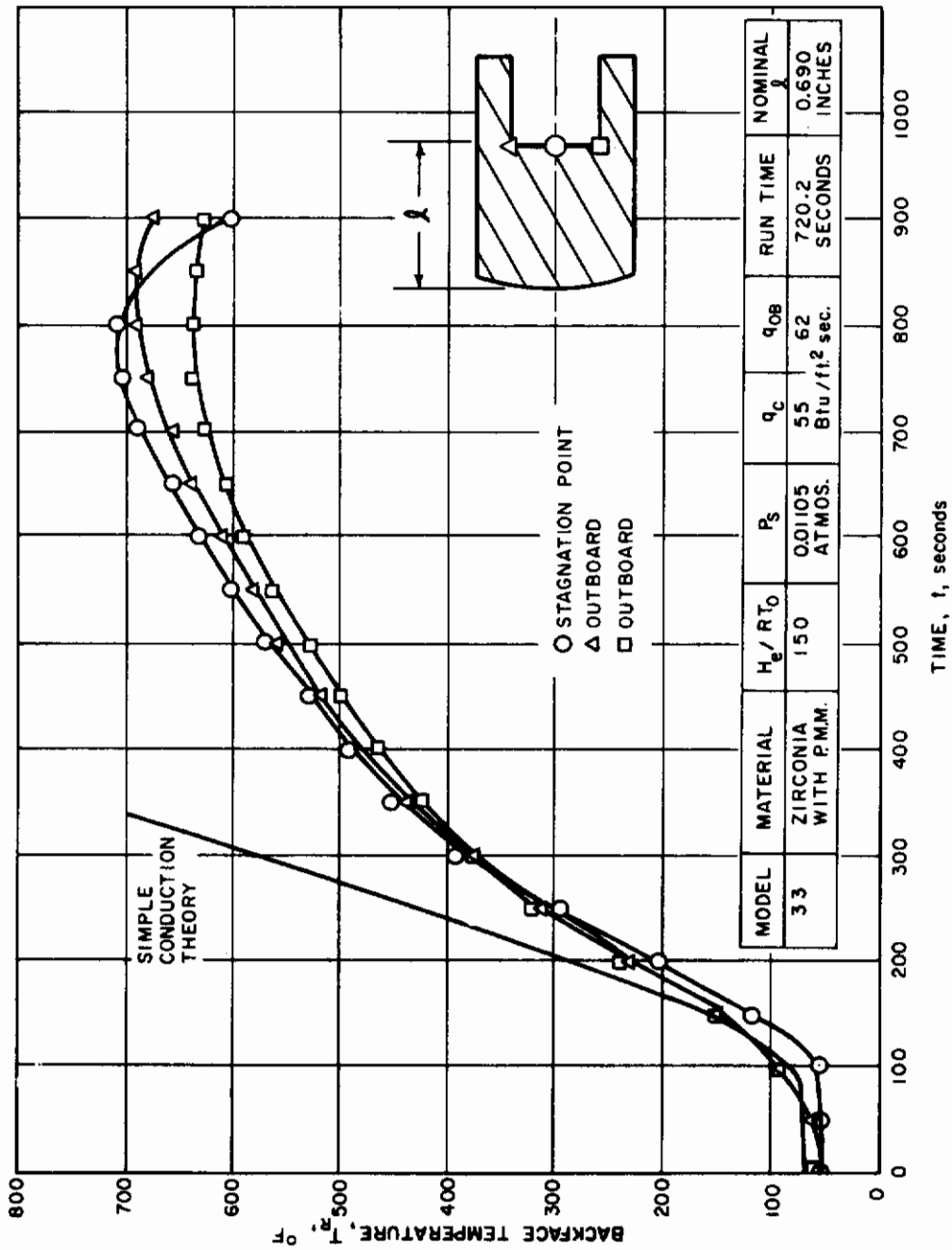

Figure 94 BACKFACE TEMPERATURE HISTORY OF THE ZIRCONIA MATRIX IMPREGNATED WITH POLYMETHYLMETHACRYLATE MODEL (CONDITION 2)

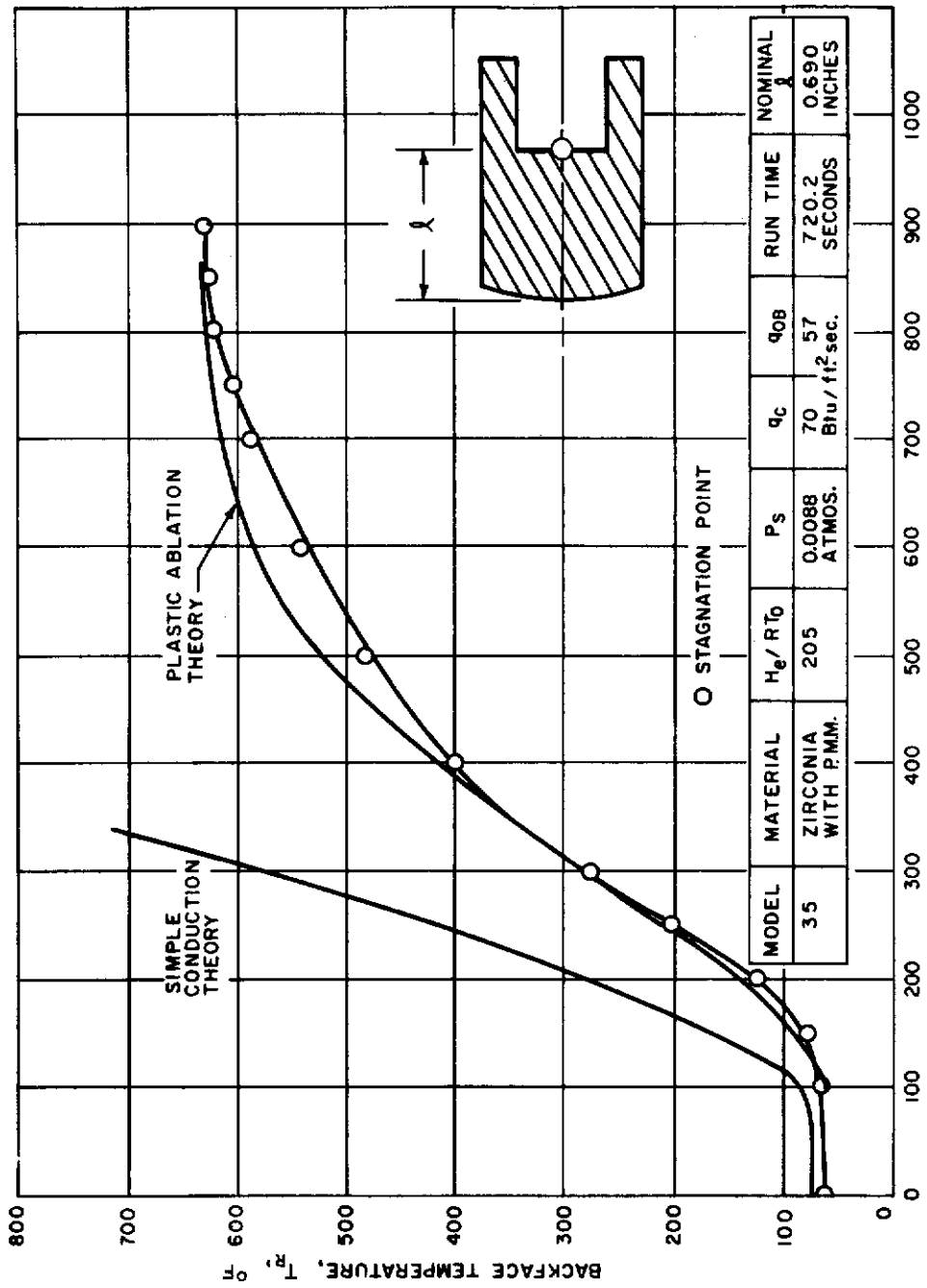

Figure 95 BACKFACE TEMPERATURE HISTORY (CONDITION 1) OF ZIRCONIA RADIATION ABLATION SHIELD

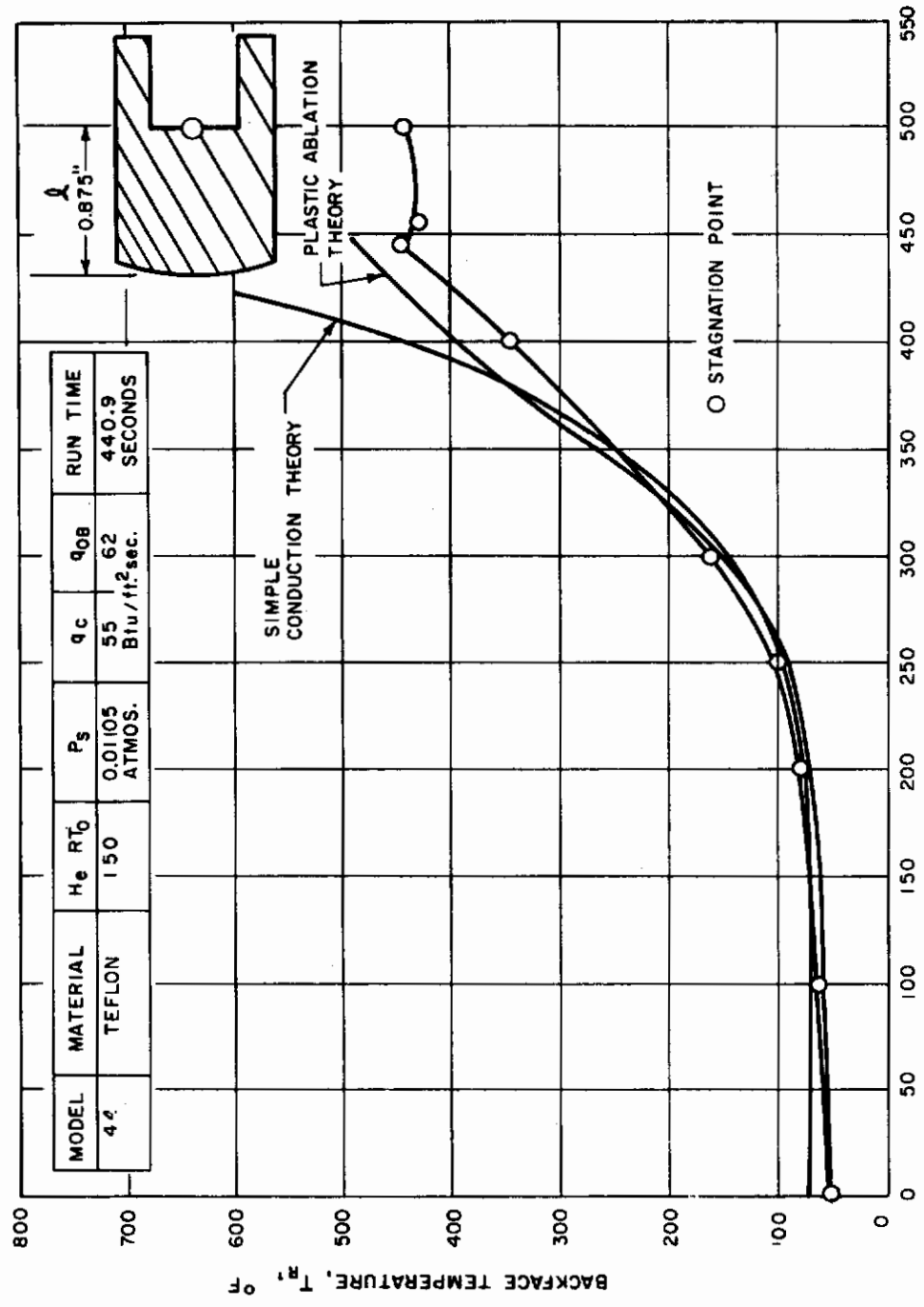

Figure 96 BACKFACE TEMPERATURE HISTORY OF THE TEFLON ABLATION MODEL (CONDITION 2)

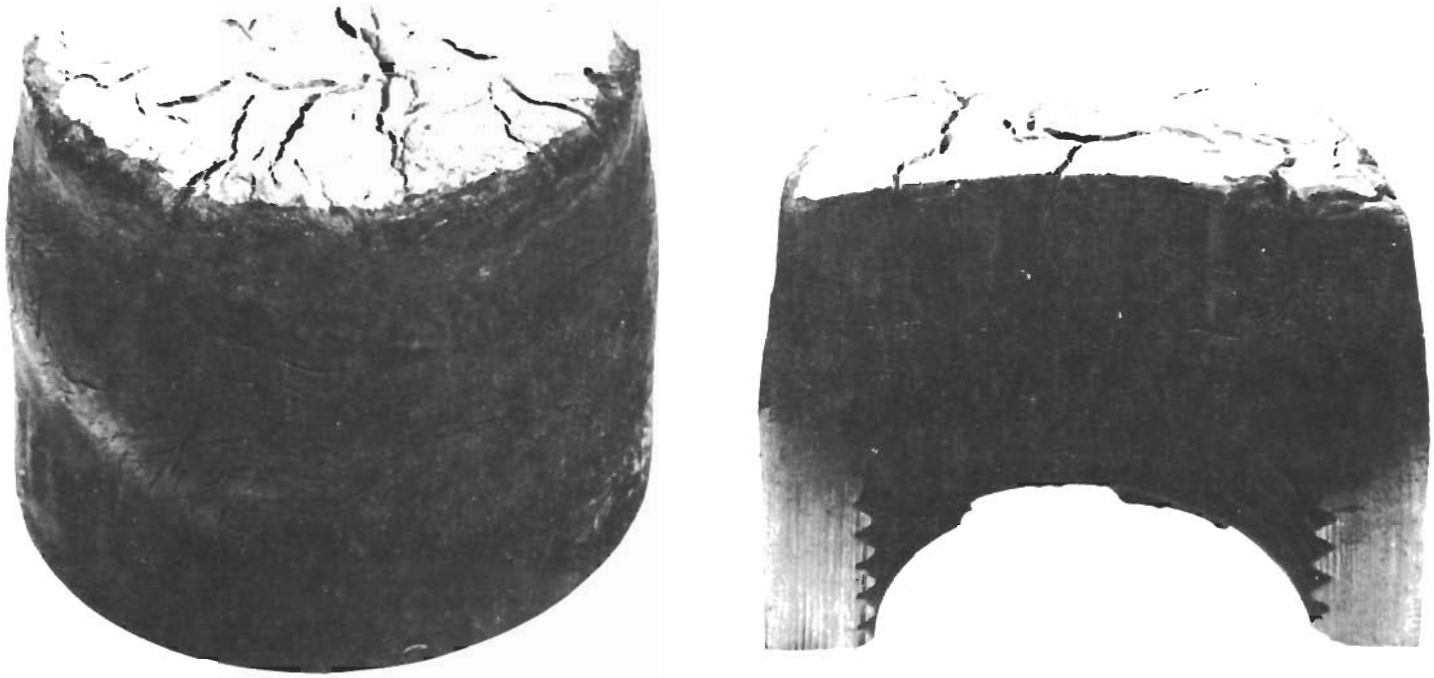

MODEL 1

Figure 97 X4000 RADIATION ABLATION MODEL AFTER TEST

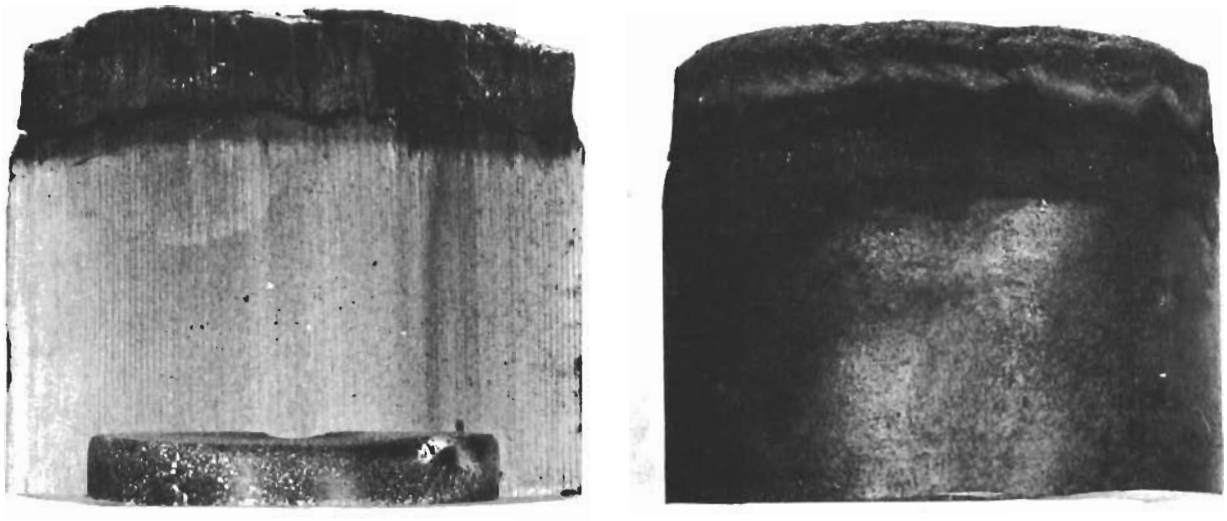

MODEL 19

Figure 98 X5000 RADIATION ABLATION MODEL AFTER TEST

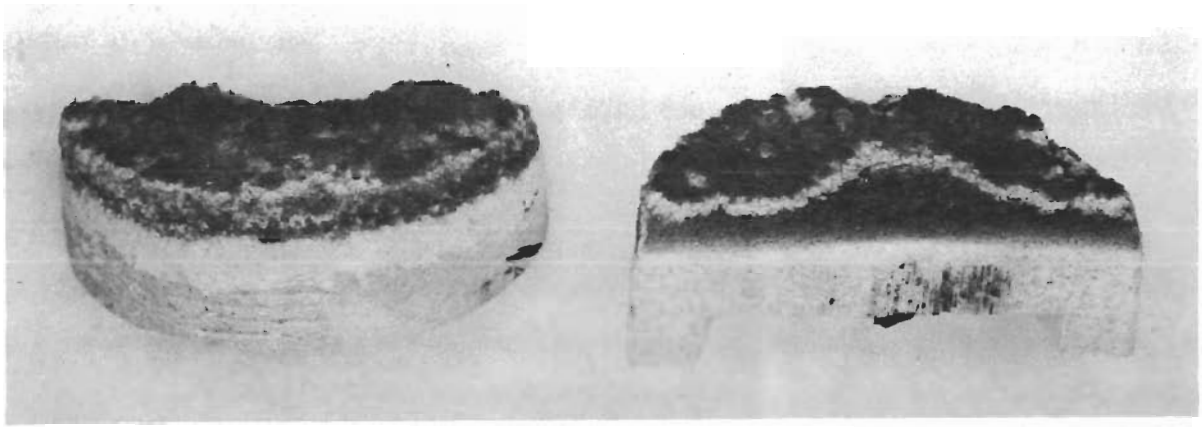

Model 33

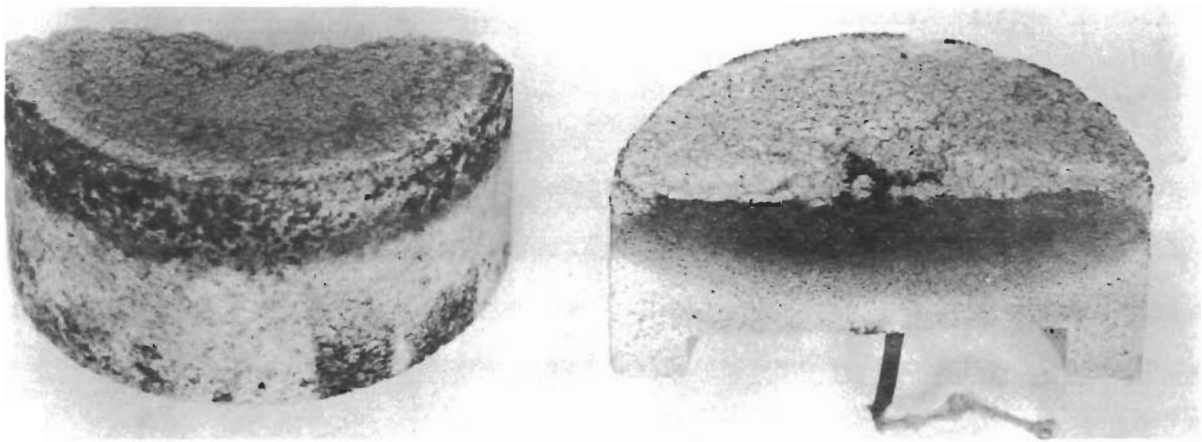

Model 35

FIGURE 99. ZIRCONIA MATRIX IMPREGNATED WITH POLYMETHYLMETHACRYLATE AFTER TEST

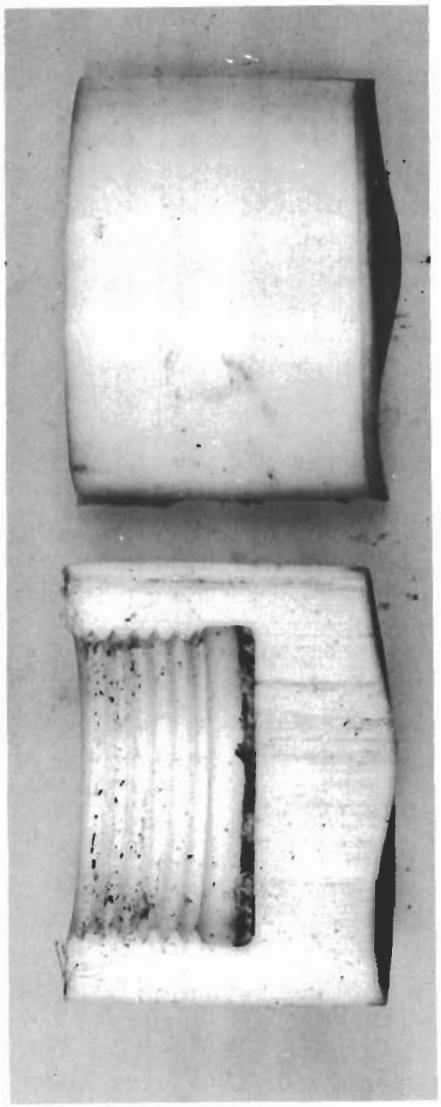

Figure 100 TEFLON MODEL AFTER TEST

Dimensional examination of the charring material models indicates an increase in the "ℓ" dimension due probably to thermal expansion with the exception of models 28 and 37. These two exceptions could be attributed to possible spalling. The Teflon models, displayed considerable surface recession in all cases.

A review of the temperature data reveals consistent trends and repeatability. In some cases a thermocouple read somewhat different from the other two. As the heat input is quite symmetric and uniform across the front surface these temperature variations at such close locations are most likely due to defective thermocouple bond or to material behavior. The uniform discoloration seen on the cross sectional surfaces are indicative of uniform heat flux distribution on the exposed surface.

The appearance of the experimental ablative plastics is typical of the non-reinforced class observed in short duration tests for ballistic reentry conditions.

The "char layer" in the zirconia filled with polymethymethacrylate models is thinner than for the X4000 and X5000 series materials. However, the backface temperatures on the zirconia matrix models are more consistent but higher, than in the cases of the X4000 and X5000 series materials.

The various ablation patterns on the Teflon models are a direct result of its rapid recession rate. The initial recession rate distribution modifies the original contour which, in turn, varies the heat flux distribution in self search for a stable condition.

c. Photomicrographs

Typical models were bisected and high magnification photographs taken of the cross-sectional surface. The surfaces to be photographed were first impregnated with epoxy and polished. Thus the voids show in light color and only those areas of the material which are dark in pigment show dark in the photographs.

The molybdenum model collected a foreign layer along the border as if pushed there by the air stream. This foreign substance is probably a combination of stream contaminants and a residue of chromium coating. The middle layer is an oxidized layer. Figure 101 shows these layers and the location in the model where the photomicrograph was taken. The pyrolitic graphite did not show any visible change in structure and hence no photographs were taken.

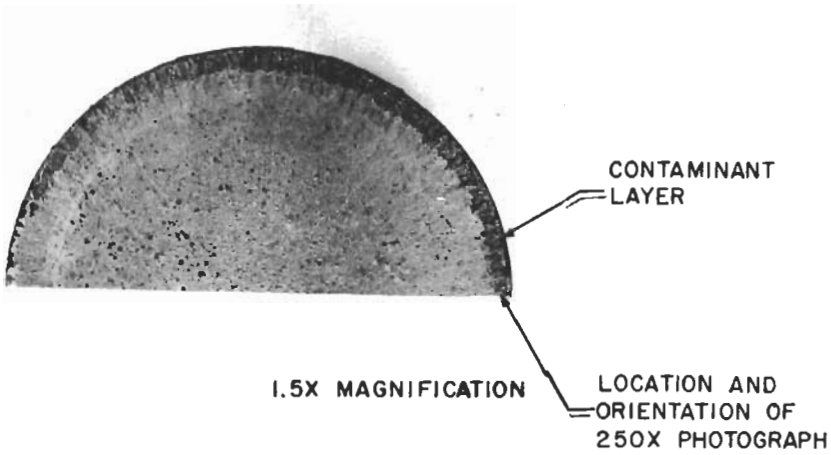

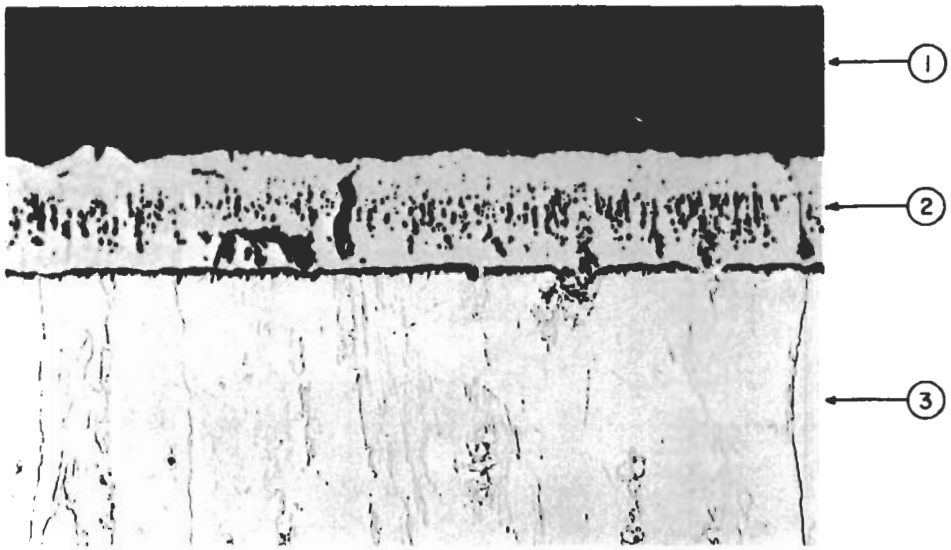

Figure 101 PHOTOMICROGRAPH OF MOLYBDENUM SURFACE AFTER TEST

The zirconia matrix material filled with polymethylmethacrylate presents the char layer with a light and a dark zone, the former nearer the front surface of the models, a zone of incipient deterioration follows the dark zone. Photographs of these light and dark zones are shown in figure 102.

The X4000 and X5000 series materials ablated in a similar manner to each other showing a distinct char layer followed by virgin material. A view of the more deteriorated region near the model front surface on an X4000 series material model is shown in figure 103. The interior of the char layer in X4000 and X5000 series material models are shown in figures 103 and 104. The appearance of the char layer interior from these two materials is almost identical.

The Teflon did not show any structure at high magnification and thus was not photographed.

d. Motion Pictures

Regular color motion pictures were taken of representative tests. The movies taken are listed under remarks in Table 6 and are available in the 10 MW Arc Facility Film Library under the following serial numbers:

Material	Run No.	Wind Tunnel Film Library Serial No.
X4060	215	2-0215-3
Zirconia +	214	2-0214-3
X5026	219	2-0219-3
Moly	223	2-0223-3
Graphite	226	2-0226-3
Teflon	234	2-0234-3

B. ORBITAL VEHICLE RE-ENTRY SIMULATOR

This facility was also used in the course of the program as a tool for the simulation of re-entry. The simulator consists of an electric-arc gas heater and exit nozzle, 500 kilowatt rectifier power supply, and a 12,000 cubic feet per minute two-stage vacuum pumping system.

The electric-arc heater consists of a thoriated-tungsten cathode, and a copper water-cooled anode, and exit nozzle. The design of the unit is based on a constricted arc configuration and can be operated with nitrogen or air as a working fluid. Provision is made for oxygen injection into the arc plenum chamber. This feature made it possible to systematically change the chemical composition of the exhaust impinging on the test specimen.

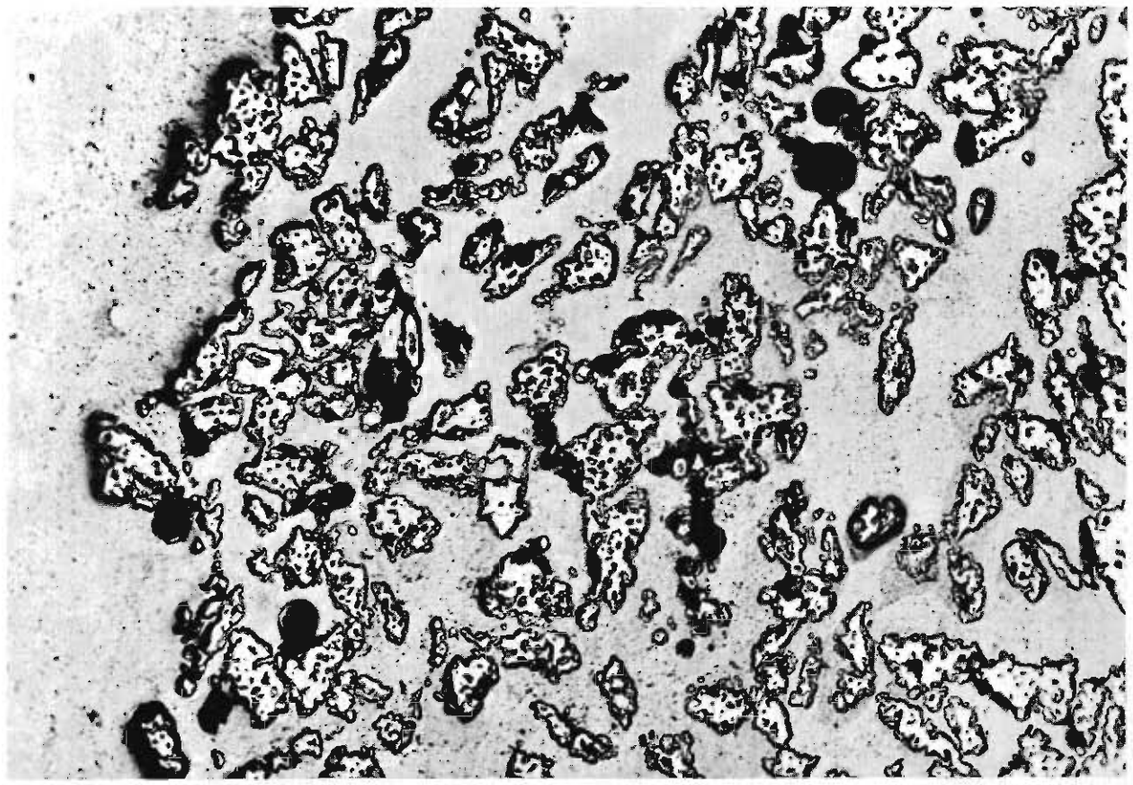

AFT (dark) ZONE

100X MAGNIFICATION

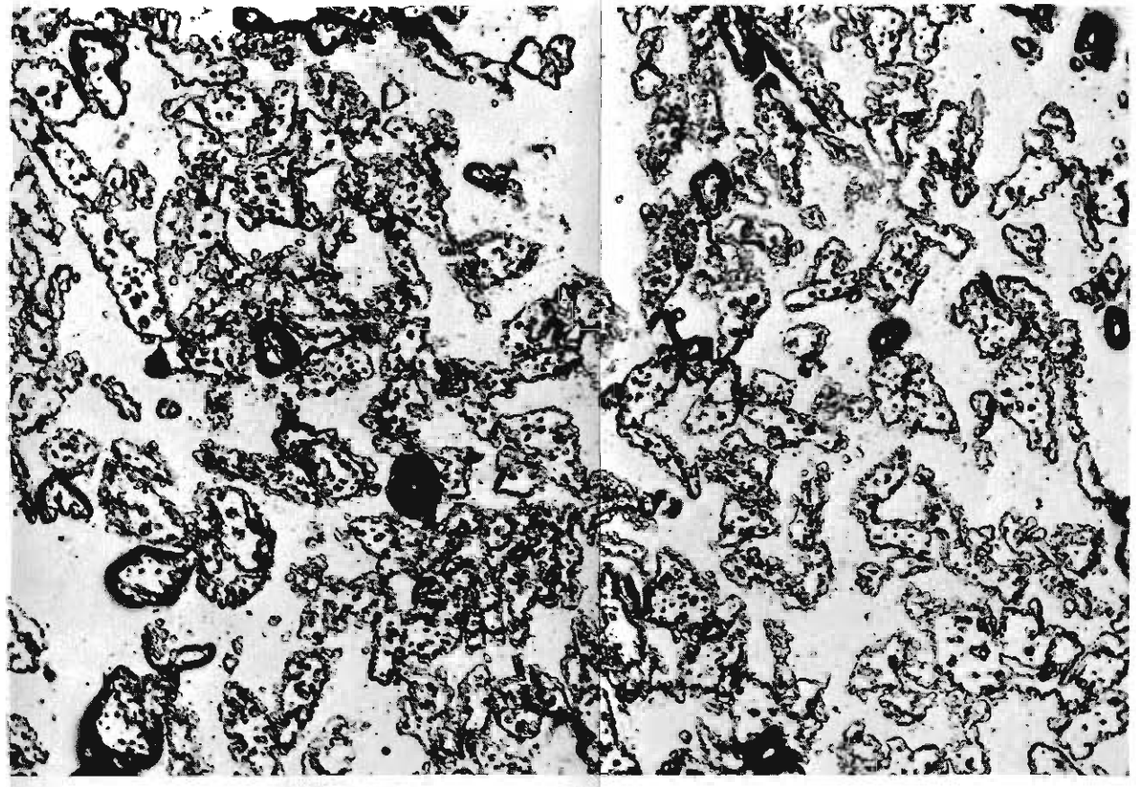

FORWARD (light) ZONE

100X MAGNIFICATION

MODEL 37

Figure 102 PHOTOMICROGRAPHS OF ZIRCONIA MATRIX FILLED WITH POLYMETHYLMETHACRYLATE AFTER TEST

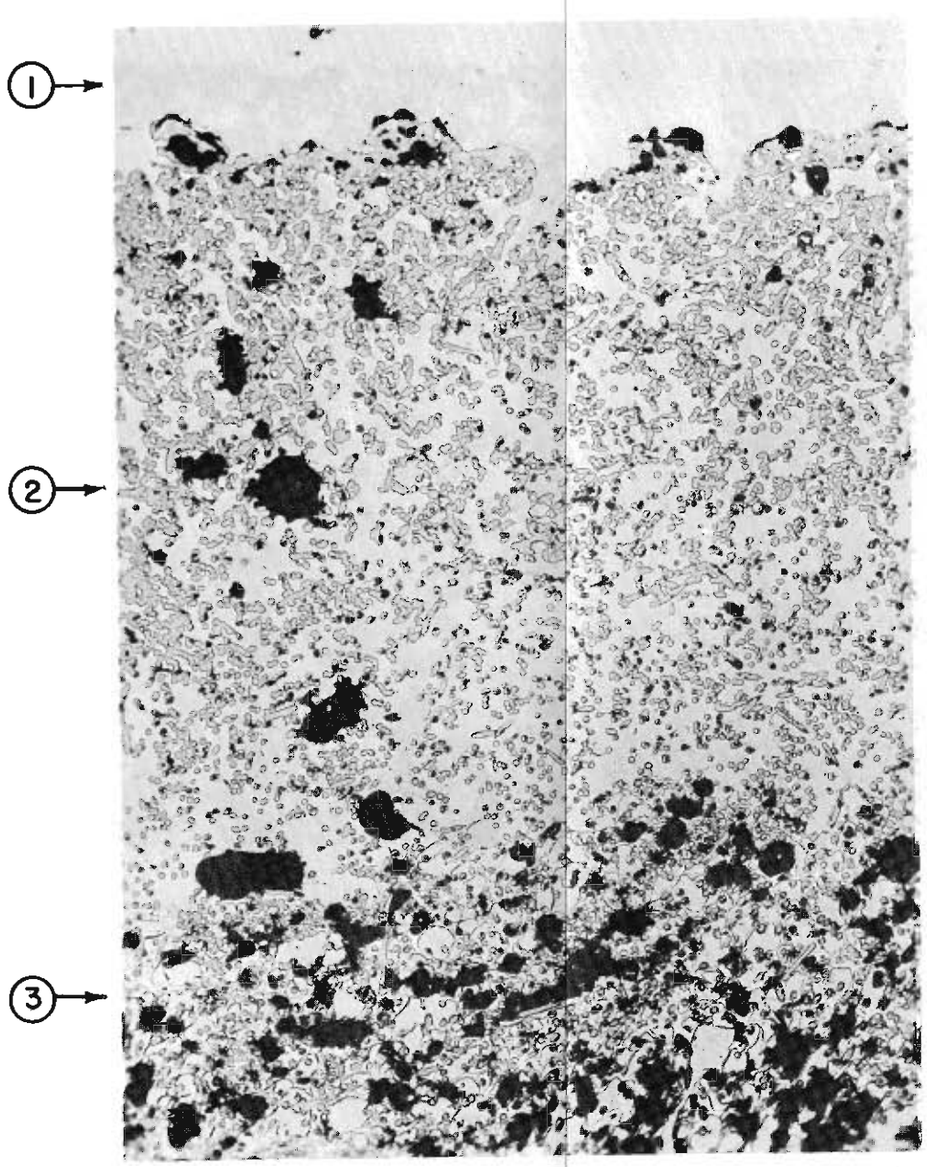

NEAR THE SURFACE REGION

100X MAGNIFICATION

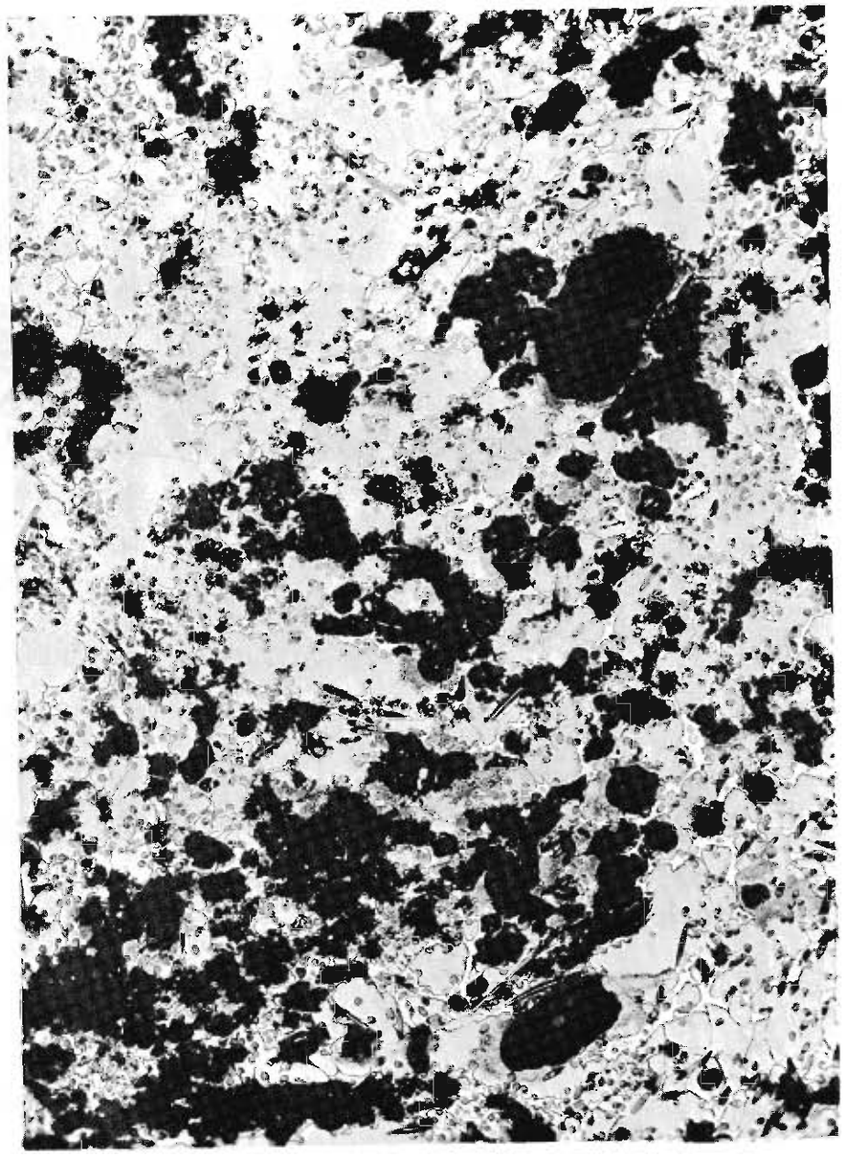

INTERIOR REGION

100X MAGNIFICATION

(1) EXTERIOR

(2) NEAR THE SURFACE LAYER

(3) START OF INTERIOR REGION

Figure 103 PHOTOMICROGRAPH OF X4000 MODEL AFTER TEST

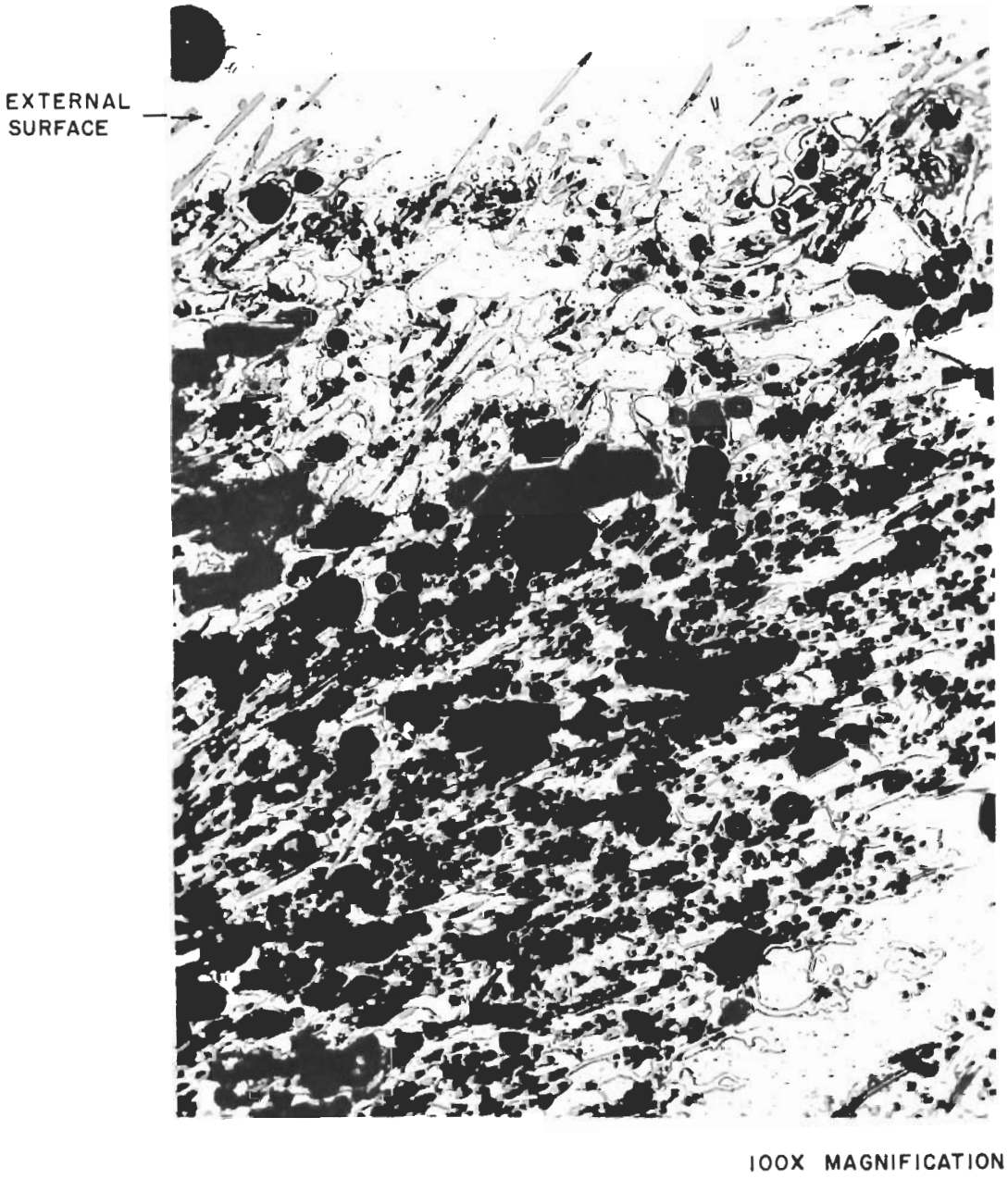

Figure 104 PHOTOMICROGRAPH OF X5000 MODEL AFTER TEST

TABLE 6

RESULTS OF CHANNEL THREE EXPERIMENTAL PROGRAM

Run Number	Model Number	Material	Length (inches)	Weight (lb/ft^2)	Enthalpy (H_e/RT_o)	Stagnation Pressure P_s (atms.)	Cold Wall Heat Flux (Btu/ft^2 sec.) Stag Point	Outboard Point	Run Time (sec)	Weight Loss (Grams)	Model Recession $\Delta\ell$ (inch)	Backface (Centerline) Temperature at End of Heating (°F)	Overall Heat of Ablation q^* (Btu/lb)	Remarks
217	1	X4000 Series	0.500	3.00	150	0.01105	55	62	720.1	18.0	+0.071	1250	16,440	
256	2		0.500	3.00	150	0.01105	55	62	720.1	18.7	+0.096	1275		Photomicrograph
215	7		0.750	4.50	150	0.01105	55	62	719.8	22.5	+0.054	660	13,110	Photomicrograph and Motion Pictures, 24 Frames/sec.
255	9		0.750	4.50	150	0.01105	55	62	720.1	20.7	+0.077	720		
175	11	X5000 Series	0.820	4.50	208	0.0088	70	57	700.0	14.7	+0.056	412	25,000	
241	12		0.820	4.50	150	0.01105	55	62	720.1	19.0	0	645	15,500	
219	13		0.820	4.50	150	0.01105	55	62	720.2	18.9	+0.078	630	15,600	Motion Pictures, 24 Frames/sec.
174	18		1.230	6.77	205	0.0088	70	57	720.4	14.6	+0.065	200	25,809	
181	20		1.230	6.77	205	0.0088	70	57	720.2	17.2	+0.053	248	21,840	Photomicrograph
222	22		1.640	9.0	150	0.01105	55	62	720.4	17.6	+0.079	188	16,810	
218	23		1.640	9.0	150	0.01105	55	62	719.9	16.7	+0.122	185	17,700	
176	24		1.640	9.0	205	0.0088	70	57	671.1	14.4	+0.145	136	24,380	Photomicrograph
187	27	Zirconia Matrix...	0.510	7.5	205	0.0088	70	57	720.2	7.5	0		50,100	
212	33	Zirconia Matrix...	0.690	10.0	150	0.01105	55	62	720.2	8.1	+0.015	895	36,500	
196	35	Filled with Polymethylmethalcrylate	0.690	10.0	205	0.0088	70	57	720.2	8.2	+0.006	600	45,800	
253	37		0.690	10.0	205	0.0088	70	57	720.0	8.9	-0.107	650		Photomicrograph
210	39		0.860	12.5	150	0.01105	55	62	720.1	7.6	+0.020	460	38,860	
234	44	Teflon	0.875	10.0	150	0.01105	55	62	440.9	57.8	-0.560		3,070	Motion Pictures, 24 Frames/sec.
236	45		0.875	10.0	150	0.01105	55	62	480.2	69.4	-0.684	420	2,840	
239	48		1.100	12.55	150	0.01105	55	62				115	3,020	
246	49		1.100	12.55	150	0.01105	55	62	480.2	73.5	-0.872	190	2,650	
216	50		1.100	12.55	150	0.01105	55	62	450.0	71.5	-0.917	295	2,530	
220	53		1.100	12.55	150	0.01105	55	62	609.6	85.5	-1.108	660	2,820	
245	54		1.310	15.00	150	0.01105	55	62	480.1	67.9	-0.717	110	2,910	
244	55		1.310	15.00	150	0.01105	55	62	480.1	69.4	-0.750	120	2,840	
223	60	Molybdenum Type 1			150	0.01105	55	62	720.2	2.3	0	800	128,600	Motion Pictures, 24 Frames/sec.
242	61				150	0.01105	55	62	720.2	3.6	0	750	82,100	
224	63	Molybdenum Type 2			150	0.01105	55	62	720.3	3.2	0	700	92,500	
238	64				150	0.01105	55	62	719.9	3.4	0	780	87,000	
225	71	Pyrolytic-graphite			150	0.01105	55	62	720.1	7.5	-0.095	890	39,400	
226	72				150	0.01105	55	62	720.2	7.5	-0.090	950	39,400	Motion Pictures, 8 Frames/sec.
257	73				150	0.01105	55	62	720.2	3.3	-0.028	860	89,500	

A summary of the operating characteristics are given below and more details are presented in Appendix III.

Gas Enthalpy, 2500 to 20,000 Btu/lb,

Arc Chamber Pressure, 0.05 to 1.0 atmospheres,

Model Surface Pressure, 0.01 to 0.20 atmospheres,

Mach Number, approximately 3,

Nozzle Throat Diameter, 1 inch,

Nozzle Exit Diameter, 3 inch.

In the design and construction of the simulator, particular attention has been focused on the problems of arc jet calibration. A series of "local" heat transfer, enthalpy, mass flux, and stagnation pressure probes have been designed, constructed, and developed suitable for operation in a high-temperature gas stream. To make optimum use of the probes the test chamber has been equipped with three pneumatically operated probe (or sample) holders. During the course of a single run it is thus possible to establish the thermodynamic and fluid mechanic aspects of the exit jet both before and after the insertion of a specimen.

The 500 kilowatt rectifier power supply for the simulator has been specially designed to permit a wide variation (factor of 10) in the electric power input to the arc during a run. This feature makes it possible to program the simulated flight velocity and attitude as a function of time. For example, during a single run the simulated flight velocity can be varied by a factor of nearly ten and the simulated attitude by as much as one hundred thousand feet. During the variation of the arc power level and gas flow, provision is made for keeping the exit jet perfectly expanded to avoid shock wave--sample interaction. The test was conducted to provide an environmental variation differing from channel 3 conditions, and to test the design calculation model under time variable heat flux and enthalpy and to extend the running time. Time did not permit the more exact analysis (Appendix V). This type of test to be conducted on either of the two facilities employed are required to test the theories under a broad range of operating conditions.

The test was performed on an X-5000 similar model and test conditions were varied throughout the test and are presented in table 7. The heat fluxes were not measured but can be determined for the given data from standard stagnation point heat flux theory. Figure 3 presents the recorded temperature rises of the thermocouples (located on the backface of sample). One of the thermocouples was open prior to testing and could not be used. The test was terminated after the sample had ablated back to the sample holder (approximately

1/4-inch of material ablated). The two thermocouples that were used, agreed quite well with each other up to a time of approximately 14 minutes after which they deviated, possibly due to side heating or cooling (holder water-cooled). Calculations were performed using methods described above in Section III. C. and are shown in comparison with experimental results in figure 105. The reasonable agreement between analysis and experiment is indicative of the validity of the analytical procedures used for the parametric studies and recommended for use in design and development techniques (Section VII). The actual agreement of the approximate design calculation with the experiment during heating may not be as good for later times and, therefore, more exact calculations are required. This necessity was illustrated for channel 3 runs.

TABLE 7

TEST CONDITIONS FOR THE OVERS EXPERIMENTAL PROGRAM

Time Interval (Minutes)	Enthalpy (Btu/lb)	Cold Wall Heat Flux (Btu/ft^2-sec)	Stagnation Pressure	
			mmHg	atm
0 to 3	11000	142	6.8	0.0089
3 to 6	10500	118	7.6	0.0099
6 to 9	10000	156	9.6	0.0126
9 to 12	9500	137	9.3	0.0121
12 to 15	8500	128	9.1	0.0119
15 to 18	7000	89	7.3	0.0096
18 to 21	5500	72	6.6	0.0086
21 to 24	4000	48	6.2	0.0081

Note: 1. Enthalpy was calculated from a heat balance.
2. Pressure was measured by a probe.
3. 5 to 10 seconds time interval elapsed in making change from one test condition to another.

C. INTERPRETATION

The experimental techniques suggested in Section V. B were partially implemented in the pilot experiments performed for radiation and radiation-ablation

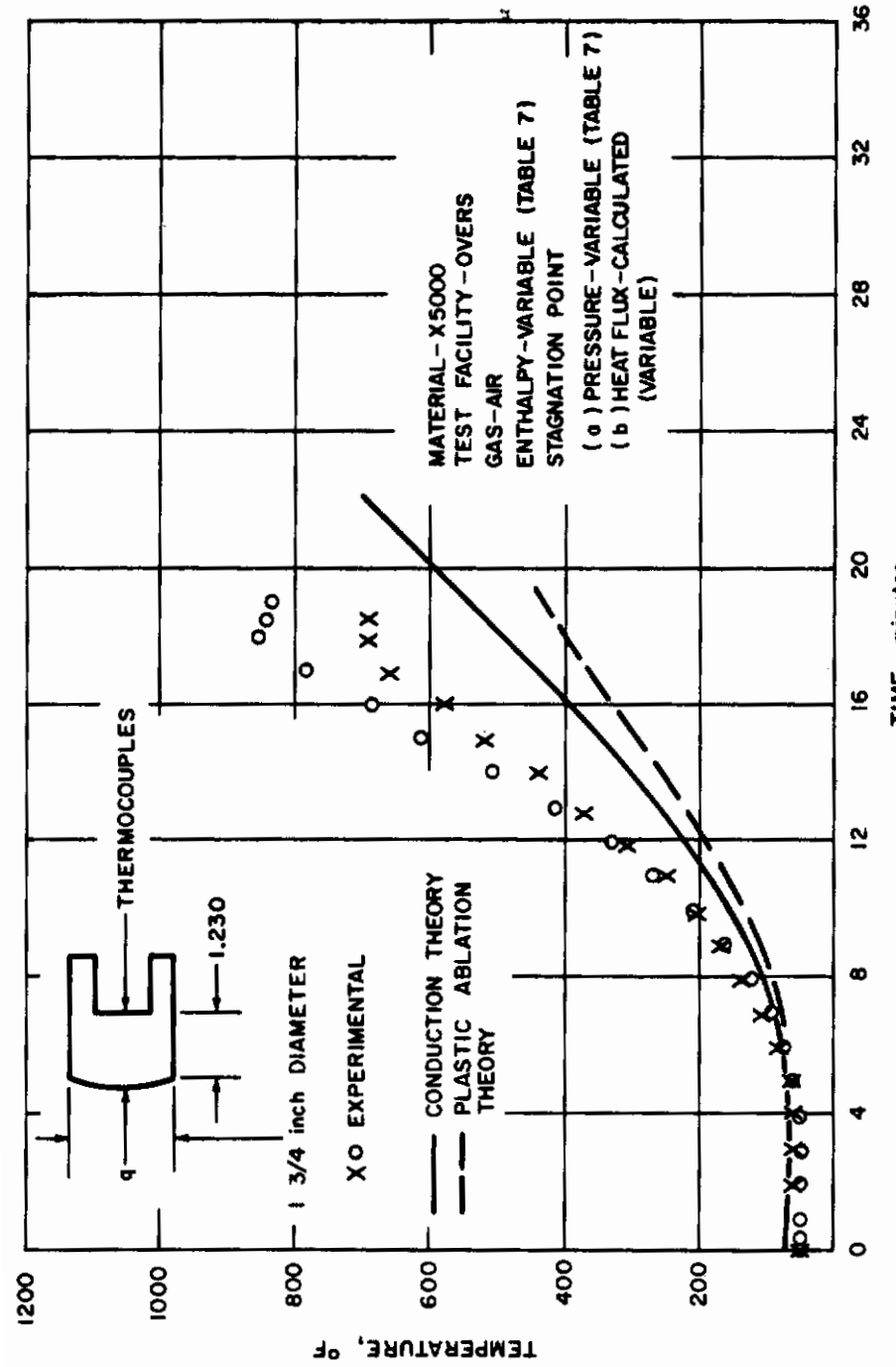

Figure 105 BACKFACE TEMPERATURE HISTORY OF X5000 RADIATION ABLATION MODEL DURING OVERS TEST

tests. It is a common practice to report the temperature response (if measured) in the sample, its mass loss and surface recession (if any), and external appearance. The interpretation, however, is usually limited to calculation of heats of ablation and ranking of the material according to this and T_b response criteria and/or to some discussion of stream conditions. Comparisons with the theory are usually limited to prediction concerning surface characteristics, i.e., equilibrium temperature and recession. Since the tests and their results reported above are not considered by any means final, an attempt was made here to extend the interpretation towards the understanding of material behavior in depth be it due to configuration (as in the case of radiation shields), or to internal mechanism (as in the case of radiation-ablation samples). Such interpretation is useful and necessary for both improvement of the testing techniques (sample configuration and shielding from side effects) and the comparison of theory and experiment.

1. Radiation System

The molybdenum and pyrolytic graphite samples (figs. 79 and 80) displayed backface temperature responses (figs. 87 and 88) which due to geometric non-uniformities could not be matched by a one-dimensional analysis. It was, therfore, necessary to perform two-dimensional thermal analyses to obtain reasonable agreement with experiment. It was then concluded that one-dimensional calculations would also give good agreement with experiment if a "one-dimensional" model could be made as is essentially the case for ablation material models. These results indicate the validity of the analytical methods (Section III, C) of prediction and of the conclusions from the parametric studies based on them. The testing techniques for final evaluation of these type of shields should be, however, further refined. Surface temperatures, and internal temperatures in addition to the backface should be measured, and the sample configuration and fabrication method should be improved. Either an actual shield configuration should be fabricated, or two-dimensional effects should be minimized for simplicity of evaluation. The calibration of the testing facilities to obtain better accuracy in heat flux (presently estimated at ± 10 to 15 percent) pressure, etc. measurements is always desirable.

2. Radiation-Ablation System

Teflon, zirconia matrix impregnated with polymethylmethacrylate and a high-temperature ablative plastic (X-5000 series) were selected for comparisons with theoretical predictions as representative of three classes of materials. Since the conclusions based on analytical studies pointed to the break-down of the "Q^*-concept" for such classes of materials, emphasis was put on the verifications of theoretical analysis by experiment to justify such conclusions. The experimental results (Figs. 91 to 96) were compared with predictions based on the method discussed in Section III. C and on the more

exact analysis described in Appendix V. Although materials were selected with the availability of the properties data in mind, still some of the properties needed for exact (Appendix V) analysis were not completely available for high-temperature plastics. Thus it may be seen that the agreement between the experiment and the more exact theory grows progressively with the knowledge of properties. The Teflon results (Figures IV-2 and 96 in Appendix V) show excellent agreement, as well as those for the zirconia matrix (fig. 95) because the basic information on the properties is available. For the zirconia matrix, density changes within the model were predicted and are shown in figure 106. The density profile at 880 seconds is representative of the final state of the model since the temperature distribution at this time is essentially uniform (see figure 107). Visual inspection of the zirconia matrix photograph (fig. 99) indicates that analytical predictions of decomposition are in agreement with the test results. The agreement for the high-temperature ablative plastic tested here is not quite as good, because some of the property data are not available. On the other hand, the experiment described in Appendix V for another high-temperature silica-epoxy plastic for which the necessary properties were determined independently shows excellent agreement of experiment and theory in terms of the response parameters. Considering the experimental uncertainties involved, it may be said that a preliminary reconcilliation of theory and experiment has been achieved.

The comparison in the same figures 91 to 96 of the approximate analysis (Section III. C. 2) with the experiment shows a varying degree of agreement, with the analysis being conservative and generally predicting higher temperature response than actually observed. The degree of conservatism cannot be directly translated into actual performance profiles because of the dependency on the environment.

As a result of this limited test program, it may be said that the trends determined by the analysis are valid as basic agreement between experiments and predictions was achieved. As noted in Section V. B. 1 (simulation requirements) more extensive tests covering a broader range of environmental conditions are required for complete evaluation of the theory compared to experiment. The comments made under "Radiation Systems" above concerning improvement of testing techniques are, equally valid here.

3. Determination of Relative Material Performance

Having established the degree of reliability of analytical methods for predicting material responses it now remains to determine the relative ranking of the materials tested based on the results in table 6. It has been a practice in the past to use a heat of ablation, q^*, approach to obtain a measure of the thermal performance of materials subjected to simulated

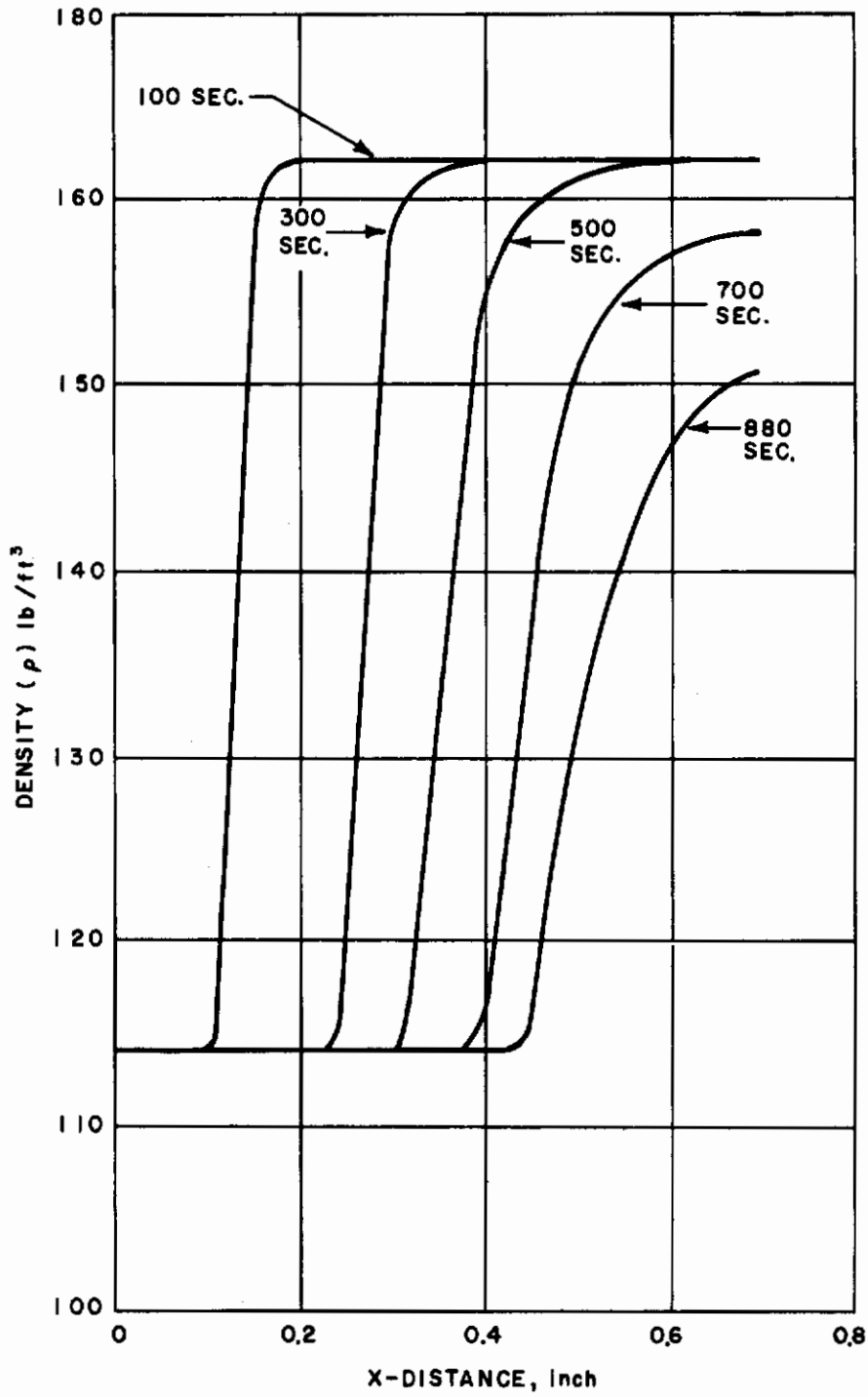

Figure 106 PREDICTED DENSITY CHANGES FOR A ZIRCONIA MATRIX FILLED WITH POLYMETHYLMETHACRYLATE

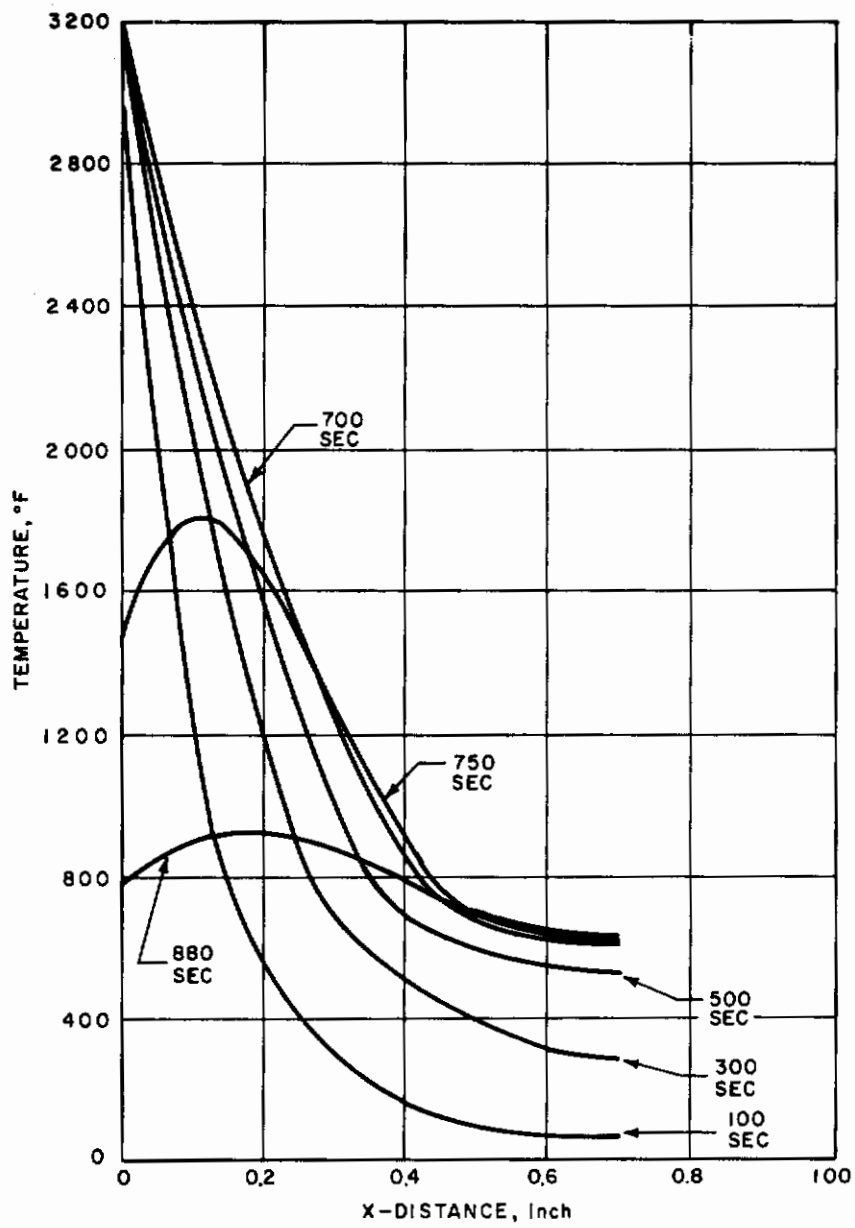

Figure 107 PREDICTED TEMPERATURE DISTRIBUTIONS FOR A ZIRCONIA MATRIX FILLED WITH POLYMETHYLMETHACRYLATE

re-entry conditions corresponding to a point on the flight path. This type of ranking could be made using the average cold-wall heat of ablation for 720 second runs for condition 2 reported in table 6 and the ranking of the samples tested would be:

a. Molybdenum - Mark II,

b. Pyrolytic graphite - Mark II,

c. Zirconia matrix filled with polymethylmethacrylate,

d. X5000 and X4000 series,

e. Teflon.

Another ranking could be based on the backface temperature response for equal weight samples. Using data from table 6 and plotting backface temperatures at the end of heating for various weight samples (see figure 108), a relative ranking of the tested samples is determined. All samples except the molybdenum and graphite models were tested at three different weights (thicknesses). However, some tests did not run full length due to arc operating difficulties and, therefore, only two weights of zirconia filled with polymethylmethacrylate are available. Still, the spread between the different samples is large enough to establish a ranking at least for the backface temperature range of 400° to 900° F. Such ranking would be:

a. X5000 and X4000,

b. Molybdenum - Mark II,

c. Pyrolytic graphite - Mark II,

d. Zirconia matrix filled with polymethylmethacrylate,

e. Teflon.

As already discussed above in (1) the molybdenum and pyrolytic graphite samples experience large two-dimensional conduction effects and the ranking would change if the effects are eliminated as indicated by figure 108. Hence, backface temperatures as recorded from test give misleading rankings unless supplemented with analysis. Neither q_c^* or backface temperature necessarily gives the correct rating of material performance even for constant heat flux environments and experimental measurements combined with analytical methods are needed to determine the proper order of material performance.

VII. DESIGN AND DEVELOPMENT TECHNIQUES

The analytical and experimental studies in the previous sections of the report brought out the interdependence of environmental, material, and design factors bearing on the performance of the thermal protection system. Methods and techniques useful in material evaluation, selection, and in the development effort were established. On the other hand new analytical methods were developed and existing methods were recommended in the text and Appendixes V and VII for application in system design, evaluation, and selection. The groundwork necessary for design and development of a vehicle was thus established and it is possible to proceed with the required iterative study necessary for an integrated design. While no attempt will be made here to actually design a vehicle, illustrative analyses will be made representative of the typical design cycle charted below.

1. Aerodynamic studies to select a number of aerodynamic shapes compatible with body motion requirements (stability, c.g., c.e.p., etc.) assuming a vehicle weight distribution.

2. Determination of aerodynamic heating and flow conditions for a number of flight paths giving the velocity, enthalpy, pressure shear, loads, etc.

3. Determination of structural concepts and associated structure material and thickness.

4. Selection of mode(s) of heat absorption required to accommodate heating (heat sink, mass transfer, radiative, or internal cooling).

5. Determination of design, material performance, and structural limiting criteria (flight path, system effective heat capacity, structural temperature limits, etc.).

6. Preliminary iteration of aerodynamic, thermodynamic, and structural effects to reduce the number of shapes, flight paths, structural and heat absorption concepts using more realistic geometry and weight figures.

7. Preliminary determination of aerodynamic shape, thermal protection system (including its weight), and structure.

In the continuing design studies many modifications and changes are introduced, but the basic flow chart above is followed.

Within the scope of this study the analysis associated with determination of the aerodynamic characteristic was not called for; however, their effects are

accounted for in the thermostructural and materials aspects. Thus, only items 3, 4, 5, 6, and partially 7 were of major interest. Particular emphasis is given in the analysis below to the implications for materials development and selection, design techniques, vehicle sizing procedures, and the illustration by sample calculation of the typical design stemming from the studies conducted under this contract.

A. IMPLICATIONS FOR MATERIAL DEVELOPMENT AND TESTING

The performance comparison of thermal protection systems considered for glide re-entry application shown in Section III indicates a general perference for radiative system design. Such self insulating systems which, in addition to the predominately radiative mode of heat rejection, may use mass transfer for cooling effect, also appear competitive.

Protection systems utilizing ablative plastics for a subsidiary mode of cooling by mass transfer (in addition to the predominant radiative rejection and conduction restriction with insulation) also appear attractive weightwise. A composite of ablative coating, high-temperature insulator, and load carrying structure may indeed be competitive with "pure" radiative shields in certain areas of the vehicle and for certain flight regimes.

Thus the effort in the material development for gliders presently directed to inorganic materials for outer coatings and insulators perhaps should be reoriented to investigate also the merits of some organic materials up to now considered undesirable. This would be of interest as the use of ablating plastic would afford more flexibility in the flight corridors of gliders and perhaps allow consideration of super-orbital as well as orbital re-entry.

Table 8 was compiled to indicate, for the evaluated systems, values of significant materials parameters necessary to achieve "reasonable" unit weights. These values are compared with typical material properties of existing compounds, or which may be achieved within the next few years.

For the selected thermal environment which serves as a basis for table 8, practical upper limits can be established for the thermal conduction parameter $\rho k/C_p$. As indicated, the heating rates in the nose region are too high to allow for the use of hot radiating thin skins with an insulated load carrying substructure. Temperature limits of both the radiating skin and insulation are exceeded for presently available materials. For the relatively low heating rates experienced during glide vehicle re-entry, the thermal efficiencies of pyrolytic graphite cannot be realized since $\rho k/C_p$ values are too high, i. e., $\rho k/C_p > 40$ lb^2/ft^4-hr. Hence, plastics and ceramics capable of withstanding the heating are most promising for nose cap application. Even though the required values of $\rho k/C_p$ depend heavily on the backface temperature (and somewhat less on substructure thermal capacity), it is apparent that values in excess of 30 lb^2/ft^4-hr would impose large

TABLE 8

VALUES OF SIGNIFICANT THERMAL PARAMETERS
NECESSARY TO ACHIEVE A GIVEN UNIT WEIGHT

TOTAL WEIGHT (W_S) LB/FT^2	BODY LOCATION AND HEATING LEVEL	RADIATION SHIELD (HOT SKIN)	RADIATION SHIELD (HIGH TEMPERATURE PLASTIC) X5000	RADIATION-ABLATION SHIELD (HIGH TEMPERATURE PLASTIC) X3000	RADIATION SHIELD (HIGH TEMPERATURE PLASTIC) NO RECESSION	ACTIVE COOLED RADIATION SHIELD (HOT SKIN)
		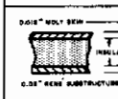	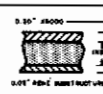	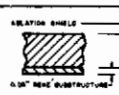	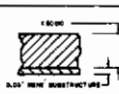	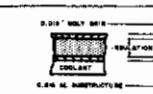
8	Nose Cap			$X3000\frac{\rho k}{C_p}$ = 12.3 ϵ = 0.7 T_A = 3400°F q^* = 10,000 Btu/lb ΔT_R = 1500°F	$X5000\frac{\rho k}{C_p}$ = 14.0 ϵ = 0.7 ΔT_R = 1500°F	
10	(Stagnation Point)			$X3000\frac{\rho k}{C_p}$ = 19.2 ϵ = 0.7 T_A = 3400°F q^* = 10,000 Btu/lb ΔT_R = 1500°F	$X5000\frac{\rho k}{C_p}$ = 22.0 ϵ = 0.7 ΔT_R = 1500°F	
12	q_c (max) = 124 $\frac{Btu}{ft^2 \cdot sec}$			$X3000\frac{\rho k}{C_p}$ = 27.6 ϵ = 0.7 T_A = 3400°F q^* = 10,000 Btu/lb ΔT_R = 1500°F	$X5000\frac{\rho k}{C_p}$ = 32.0 ϵ = 0.7 ΔT_R = 1500°F	
6	Wing Leading Edge	Moly Skin ϵ = 0.8 Insulation $\frac{\rho k}{C_p}$ = 4.6 ΔT_R = 1000°F	$X5000\frac{\rho k}{C_p}$ = 23 ϵ = 0.7 Insulation $\frac{\rho k}{C_p}$ = 2.0 ΔT_R = 1000°F	$X3000\frac{\rho k}{C_p}$ = 7.4 ϵ = 0.7 T_A = 3200°F q^* = 5000 Btu/lb ΔT_R = 1000°F	$X5000\frac{\rho k}{C_p}$ = 8.8 ϵ = 0.7 ΔT_R = 1000°F	
8	(Stagnation Point)	Moly Skin ϵ = 0.8 Insulation $\frac{\rho k}{C_p}$ = 8.2 ΔT_R = 1000°F	$X5000\frac{\rho k}{C_p}$ = 23 ϵ = 0.7 Insulation $\frac{\rho k}{C_p}$ = 3.6 ΔT_R = 1000°F	$X3000\frac{\rho k}{C_p}$ = 12.8 ϵ = 0.7 T_A = 3200°F q^* = 5000 Btu/lb ΔT_R = 1000°F	$X5000\frac{\rho k}{C_p}$ = 15.6 ϵ = 0.7 ΔT_R = 1000°F	
10	q_c (max) = 17 $\frac{Btu}{ft^2 \cdot sec}$	Moly Skin ϵ = 0.8 Insulation $\frac{\rho k}{C_p}$ = 12.8 ΔT_R = 1000°F	$X5000\frac{\rho k}{C_p}$ = 23 ϵ = 0.7 Insulation $\frac{\rho k}{C_p}$ = 5.6 ΔT_R = 1000°F	$X3000\frac{\rho k}{C_p}$ = 19.3 ϵ = 0.7 T_A = 3200°F q^* = 5000 Btu/lb ΔT_R = 1000°F	$X5000\frac{\rho k}{C_p}$ = 24.4 ϵ = 0.7 ΔT_R = 1000°F	
4	Fuselage	Moly Skin ϵ = 0.8 Insulation $\frac{\rho k}{C_p}$ = 2.3 ΔT_R = 1000°F	$X5000\frac{\rho k}{C_p}$ = 23 ϵ = 0.7 Insulation $\frac{\rho k}{C_p}$ = 0.6 ΔT_R = 1000°F		$X5000\frac{\rho k}{C_p}$ = 4.9 ϵ = 0.7 ΔT_R = 1000°F	Moly Skin ϵ = 0.8 Insulation $\frac{\rho k}{C_p}$ = 2.5 Coolant $\frac{H_c}{C_p}$ = 2000°F ΔT_R < 200°F
6	q_c (max) = 75 $\frac{Btu}{ft^2 \cdot sec}$	Moly Skin ϵ = 0.8 Insulation $\frac{\rho k}{C_p}$ = 5.2 ΔT_R = 1000°F	$X5000\frac{\rho k}{C_p}$ = 23 ϵ = 0.7 Insulation $\frac{\rho k}{C_p}$ = 2.1 ΔT_R = 1000°F		$X5000\frac{\rho k}{C_p}$ = 11.0 ϵ = 0.7 ΔT_R = 1000°F	Moly Skin ϵ = 0.8 Insulation $\frac{\rho k}{C_p}$ = 5.6 Coolant $\frac{H_c}{C_p}$ = 2000°F ΔT_R < 200°F
8		Moly Skin ϵ = 0.8 Insulation $\frac{\rho k}{C_p}$ = 9.2 ΔT_R = 1000°F	$X5000\frac{\rho k}{C_p}$ = 23 ϵ = 0.7 Insulation $\frac{\rho k}{C_p}$ = 3.6 ΔT_R = 1000°F		$X5000\frac{\rho k}{C_p}$ = 19.8 ϵ = 0.7 ΔT_R = 1000°F	Moly Skin ϵ = 0.8 Insulation $\frac{\rho k}{C_p}$ = 10.0 Coolant $\frac{H_c}{C_p}$ = 2000°F ΔT_R < 200°F
4	Cabin	Moly Skin ϵ = 0.8 Insulation $\frac{\rho k}{C_p}$ = 2.6 ΔT_R = 1000°F	$X5000\frac{\rho k}{C_p}$ = 23 ϵ = 0.7 Insulation $\frac{\rho k}{C_p}$ = 1.1 ΔT_R = 1000°F		$X5000\frac{\rho k}{C_p}$ = 5.8 ϵ = 0.7 ΔT_R = 1000°F	Moly Skin ϵ = 0.8 Insulation $\frac{\rho k}{C_p}$ = 2.7 Coolant $\frac{H_c}{C_p}$ = 2000°F ΔT_R < 200°F
6	q_c (max) = 15 $\frac{Btu}{ft^2 - sec}$	Moly Skin ϵ = 0.8 Insulation $\frac{\rho k}{C_p}$ = 6.0 ΔT_R = 1000°F	$X5000\frac{\rho k}{C_p}$ = 23 ϵ = 0.7 Insulation $\frac{\rho k}{C_p}$ = 2.4 ΔT_R = 1000°F		$X5000\frac{\rho k}{C_p}$ = 13.2 ϵ = 0.7 ΔT_R = 1000°F	Moly Skin ϵ = 0.8 Insulation $\frac{\rho k}{C_p}$ = 6.1 Coolant $\frac{H_c}{C_p}$ = 2000°F ΔT_R < 200°F
8		Moly Skin ϵ = 0.8 Insulation $\frac{\rho k}{C_p}$ = 10.6 ΔT_R = 1000°F	$X5000\frac{\rho k}{C_p}$ = 23 ϵ = 0.7 Insulation $\frac{\rho k}{C_p}$ = 4.4 ΔT_R = 1000°F		$X5000\frac{\rho k}{C_p}$ = 23.4 ϵ = 0.7 ΔT_R = 1000°F	Moly Skin ϵ = 0.8 Insulation $\frac{\rho k}{C_p}$ = 10.7 Coolant $\frac{H_c}{C_p}$ = 2000°F ΔT_R < 200°F

weight penalties. High-temperature plastics which retain their dimensional stability and have values of $\rho k/C_p$ between 20 to 25 lb^2/ft^4-hr are in the development stage and such materials offer means to efficient thermal protection. No theoretically lower limits will exist on $\rho k/C_p$ since minimum values are desired. For practical purposes, limit values may be reached from manufacturing considerations or tolerances on very small thicknesses. The requirements indicated by table 8 for wing leading edge application shows that in addition to the above mentioned systems the hot-radiating thin-skin with an insulated substructure is also competitive. Coated molybdenum skins having emissivities of about 0.80 may be combined with lightweight insulations to keep the substructure temperature within allowable limits. Insulations having $\rho k/C_p$ < 8 lb^2/ft^4-hr are available but few (if any) will currently withstand the temperature levels (over 2300°F) existing at the molybdenum insulation interface. Also the required allowable surface temperatures of the radiating skins are approaching upper limits for heating rates greater than 40 Btu/ft^2-sec. Hence the case for pure radiating skins is marginal for the wing leading edge application. Alternately, the radiating skins could be replaced by a layer of dimensional stable plastic to alleviate the problem of limiting design temperatures. Such materials when combined with a sublayer of insulation will survive high heating rates (and surface temperatures) and could also reduce the interface temperatures to the low values required by the lightweight insulation.

For the lower heating regions, as on the fuselage, all indicated systems are applicable thermally and the choice is heavily influenced by other factors such as simplicity, reusability, etc. In particular, the pure radiation shield supplemented with backface cooling may be necessary for life support in cabin areas where internal temperature levels must be held low. Insulation parameters of $\rho k/C_p$ less than 5.0 lb^2/ft^4-hr and coolant unit parameters H_c/C_p = 2000°F are required but when combined with radiating skins the resulting thermal protection systems are efficient for this application.

For all glide vehicle applications, emissivities should be maximized since the primary mode of cooling is radiation. An acceptable lower limit is difficult to generalize and need be determined from parametric studies and design charts for a given environment.

The charts generated from the parametric studies given in Appendix XII served as a source for this sample table, and should be used for similar evaluations for other flight paths of the corridor investigated, range of weights desired or for other areas of the vehicle as described by representative heat inputs.

Proper usage of the chart will permit quick evaluation of new candidate materials and indicate charactertistics to be strived for in development of new material systems to fit application requirements. This may be done whether insulation materials, radiation shields, or ablative plastics are considered.

The implications for material testing are of relatively simple nature. Radiative shields may be tested directly in an arc-jet facility of similar type to OVERS or Channel 3; however, when ablative materials are concerned, experiments along the "conventional" lines are recommended as long as complete ground simulation of flight is not accomplished. Careful consideration should be given to testing under various conditions bracketing the application, and a proper theoretical model should be used to provide an analytical tool for design when verified by experiment. Usage of unproven figures of merit should be discouraged as it may be misleading in the direction of material development effort and for the designer. This was illustrated in the previous discussion of intepretation of experimental results where it was pointed out that the ranking of materials based on q_w^* or measured backface temperatures may result in erroneous material selection.

B. DESIGN PROBLEMS AND TECHNIQUES

The thermal design and materials problems and the techniques to solve them considering the significant design criteria were discussed in detail throughout this report. Preferred procedures will be shown below. The application of the methods in the actual vehicle design and development cycle will be shown in the next section as related to sizing of the vehicle and by sample design cases. Since less specific attention was given to the aerostructural and thermostructural interface occurring in the design, the treatment of such problems will be described in this section in more detail because of its importance for an integrated design picture. For structural analysis purposes a loads program was available and used for digital computers to compute the forces (shear, moment, axial) acting upon a re-entry vehicle due to symmetric or assymetric pressure distributions. Pressures, axial force, shear, and moment are calculated for selected stations chosen from a non-dimensional pressure distribution obtained from aerodynamic considerations.

It is beyond the scope of the present discussion to give a complete thermal environment, for it would involve ground handling, powered flight, out of atmosphere flight, as well as the re-entry flight thermodynamics. For structural analysis it is assumed that the temperature distribution, material properties, and loads at a particular time t are given as well as the pressure and heat-flux distribution for a typical vehicle as a function of time of re-entry.

Failure criteria of the heat-shield material for ascent heating (including acoustics) in orbital flight and re-entry are mandatory, and rigidity properties are needed. These criteria are design inputs and will be discussed for the particular problem of a lifting winged re-entry vehicle.

1. Thermal Design

For preliminary design, analysis, or evaluation, the method developed in this program (Section III. C.) is recommended as it will permit a gross selection of the mode of protection and of the desirable materials. Appendix

XV gives a complete set of sample calculations. Since no temperature gradient information is acquired, only gross thermostructural optimization may be performed, but is usually sufficient for the first approximation.

More exact numerical machine solutions are required to provide temperature distributions needed in the thermostructural design. These may be obtained for system optimization by methods described in reference 14 and sometimes only approximating the solution if either decomposition in depth (Appendix V) occurs or large ablation surface temperature change occurs in time (Ref. 10 and 15). For semi-transparent heat-shield materials the internal radiation transport may alter the temperature distributions significantly and analysis similar to reference 69 must be used for final evaluation of thermal designs.

The final design evaluation should proceed depending on the mechanism involved either by reference 14, Appendix V, or references 10, 11, 15. Two-dimensional analysis similar to that shown in Appendix XI should be performed as required.

The selection of materials for the systems considered may proceed by ground testing of candidate materials for pure radiative shields, and by "conventional" methods where mass transfer is involved.

For overall system comparison including a complete build-up configuration either Q^*_{eff} or W_T criterion should be used.

2. Combined Thermostructural Optimization

The most unique design problem for a re-entry vehicle is associated with the structural integrity of the heat shield-substructure composite. In a re-entry vehicle, it is the purpose of the heat shield to keep the load carrying structure at a temperature consistent with its load carrying ability. On the other hand, the strain in the substructure must be compatible with the allowable strains in the heat shield to insure that no heat-shield failures can be induced. Further, since the heat shield and the substructure are subject to large temperature changes during re-entry, thermally induced strain can cause heat-shield failure or even structural failures without consideration of the load induced strains.

In many heat shield-substructure designs it has been customary to bond the heat shield to the substructure with a high-temperature rigid type of adhesive. For a heat-shield design of this type, it is necessary to consider the following possible failure modes:

a. Failure during early re-entry due to temperature gradients in the heat shield.

b. Failure in the heat shield due to thermal incompatibilities between the structure and heat shield as the structure heats up.

c. Failures of the heat shield due to high strains and/or deflections in the substructure due to concentrated loads.

d. Bond failures between the structure and heat shield due to thermal incompatibilities between the structure and heat shield.

e. Heat shield or structural failures due to combined thermal induced loading and applied loading.

The severity of the heat-shield structural design problem is controlled largely by a large number of heat-shield properties such as modulus of elasticity versus temperature, thermal expansion versus temperature, strength versus temperature, strain to failure in the operating temperature range, and the thermal performance of the heat shield as an ablator and as an insulator. Perhaps the most severe controlling factor is the degree of matching between the thermal expansion of the heat shield with that of the substructure versus temperature if a rigid type bond is used between the heat shield and substructure. If a flexible bond is used, the problem with substructure heat shield strain compatibility is much reduced so matching of thermal expansions between the heat shield and structure are much less stringent. It should be noted that if there is a good match between the thermal expansion behavior of the heat shield and the substructure from a thermally induced stress point of view the rigid bond design and the flexible bond design become nearly the same with the exception that for the gradient stress situation the rigid bond design will show more margin.

The problems associated with actual design of a heat shield depend in large measure on the design criteria used as well as on the properties of the materials which make up the heat shield, bond, and substructure. The actual strength requirements and design problems associated with the design of a heat shield-structure composite depends in large part on the design criteria set up for the design and the materials selected for the composite.

a. Procedure of Analysis

The steps which are usually followed in the design of a heat shield-substructure composite regardless of the criteria used is generally as follows:

1) Using the predicted flight envelope, calculate the heat transfer from the boundary layer to the vehicle.

2) Using several structural temperatures and substructure thicknesses at each re-entry vehicle position in the trajectory with the criteria selected, calculate the temperatures and temperature gradients in the heat shields under consideration for the flight corridor (see Section III).

3) Check the heat shield for structural margin using the substructure thicknesses and substructure temperatures selected using a one-dimensional analysis for the worse trajectory in the flight corridor. This will allow selection of the possible thermally induced failure modes and a preliminary assessment margin situation. The substructure thicknesses are selected so the thickness is adequate at the temperature selected to carry the load.

4) After Item 3 is complete, the thickness distribution of the heat shield can be selected. This study will establish the combination of heat-shield thickness and substructure thickness which will result in adequate margins and a minimum weight for the heat shield-substructure composite.

5) The heat shield and substructure is then analyzed for combined thermal induced loadings and applied loads and the margins determined throughout the re-entry vehicle. This analysis includes flexural and extensional stresses and will bring in the actual details of the structure.

6) Analyze the complete heat shield-substructure composite for the other loading conditions associated with re-entry and launch which could result in strains which could induce heat-shield failures.

In the preceding discussion, emphasis was placed on a particular thermostructural design problem for re-entry vehicles. There are many more thermostructural design problems other than the one described which confront the designer. Some of these are:

1) Cold cycling the re-entry vehicle during shipping, handling, and storage. This design condition may be in some cases worse than re-entry heating for the heat shield.

2) Thermal compatibility between the re-entry vehicle structure and the payload under temperature gradients associated with re-entry and cold cycling.

3) Interface between the re-entry vehicle and spacer since the re-entry vehicle is protected by a heavy heat shield while the spacer is subject to greater temperature fluctuations.

In every case the steps taken for a thermal-structural analysis are the same, i.e., the temperatures and temperature gradients must be known, the variation of material properties must be known, and a mathematical model for the structure must be available.

3. Structural Dynamics Problems in Re-entry Vehicle Design

A re-entry vehicle is subjected to a number of loadings which are dynamic in nature (including thermally induced dynamic response). By dynamic in nature it is meant that as a consequence of the time dependency of the loads, the flexibility of the vehicle and its distributed inertia play a part in the loads in members for which the vehicle must be designed. For example, for any re-entry situation the applied aerodynamic loads are reacted by inertia loads to keep the vehicle in balance and for any launch loading situation, inertia loadings as well as aerodynamic loads and thrust loads must be included in determining the loads in members. For cases where dynamic response is important, the rate of load onset if sufficiently great and of sufficient duration that initially the inertia loads are reacting to the applied loads and when deflections in the structure reach a sufficient magnitude to balance the applied loads, the local inertia of the vehicle has sufficient kinetic energy to cause the structural deflections to exceed the static values.

A number of problems exist in the structural design of the vehicles which require consideration of the dynamic response loads. Unfortunately structural response analysis requires a knowledge of a structure and its flexibilities, its inertia distribution, and the character of the load inputs. Usually during initial design, none of this information is available for the initial sizing of the vehicle. (An exception is the situation where the acoustic environment or the vibration are specified for design and hence these inputs fall in the criteria category.) To circumvent the need for lengthy iterations in initial design study, it is usually necessary for the structural designer to resort to his experience in sizing a structure for those cases where dynamic loads may be important. For cases where the loading is impulsive, a response factor of 2.0 is often used. For cases where the inputs are oscillatory, a response factor is estimated which is constant with past experience on similar vehicles.

The final dynamic analysis of the vehicle is then accomplished by dividing the vehicle into a number of shells (or rings) and then consider the system as a spring-mass-system. The influence coefficients between the rings are determined from the thin shell program outlined in Appendix VII.

As in the static design situation, the structural designer must, when designing a structure for a dynamic loading situation, first define his criteria, his input, and then perform his analysis. The quality of the job will depend largely on the experience and ability of the investigator and the time he can spend to reach its solution.

C. SYSTEM SIZING

1. Preliminary Thermal Analysis and System Selection

The thermostructural sizing of the vehicle must be preceded by the selection of the protection mode and of the associated material system. This is typically accomplished by performing system parametric studies (Section IV) utilizing concepts in Section V and ground testing (Section VI), and ideally obtaining materials based on their desirability according to Section VII, A implications. In practice, however, materials actually available (table 2) are sized against the requirements shown previously in table 8. A typical procedure is followed below.

Having determined material requirements necessary for efficient thermal protection systems (table 8) and selecting materials which are available or in the development stage (table 2) the evaluation of several built-up configurations was performed and individual component and total weights were determined and are given in table 9. The system performances are compared at three body locations: nose, wing leading edge, and fuselage cabin area. Two basic substructures were selected based on preliminary analysis. They are Rene'41 capable of maintaining structural integrity to about 1600 °F and PH-15-7 molybdenum steel capable of withstanding 1100 °F.

The materials for pure radiation shields are 0.012-inch molybdenum skins and insulation. The choice of insulation depends on the trade-off between the maximum allowable temperatures, i.e., higher service temperatures are accompanied by higher $\rho k/C_p$. For areas where fuselage heating rates are under $q_{c(max)} = 15$ Btu/ft^2-sec insulation service temperatures on the order of 1800 °to 2000 °F are necessary. Both rigid and foam insulations are available for this application, e.g. pyroceram foam, Min-K, and Mark II, as indicated by table 2. The systems evaluated for the fuselage, (1 and 2 of table 9) are based on Mark II insulations. The choice of substructure based on thermal analysis would be Rene'41 since its higher allowable temperatures result in total weights less than systems using PH-15-7 molybdenum substructures although the weight spread between the two systems is less than 0.20 lb/ft^2.

Where very low-temperature levels are required in the above the systems, supplemented with suitable coolant units, have been investigated (see reference 70) and no additional weight penalties are associated with these systems due to tradeoffs between insulation and coolant weight.

For the higher heat input area of the wing leading edge, $q_{c(max)} = 37$ Btu/ft^2-sec, the pure radiation shields are operated at upper limits. The coated molybdenum skins are required to operate at temperatures over 2700 °F along with the necessary insulations. Such systems are marginal for this

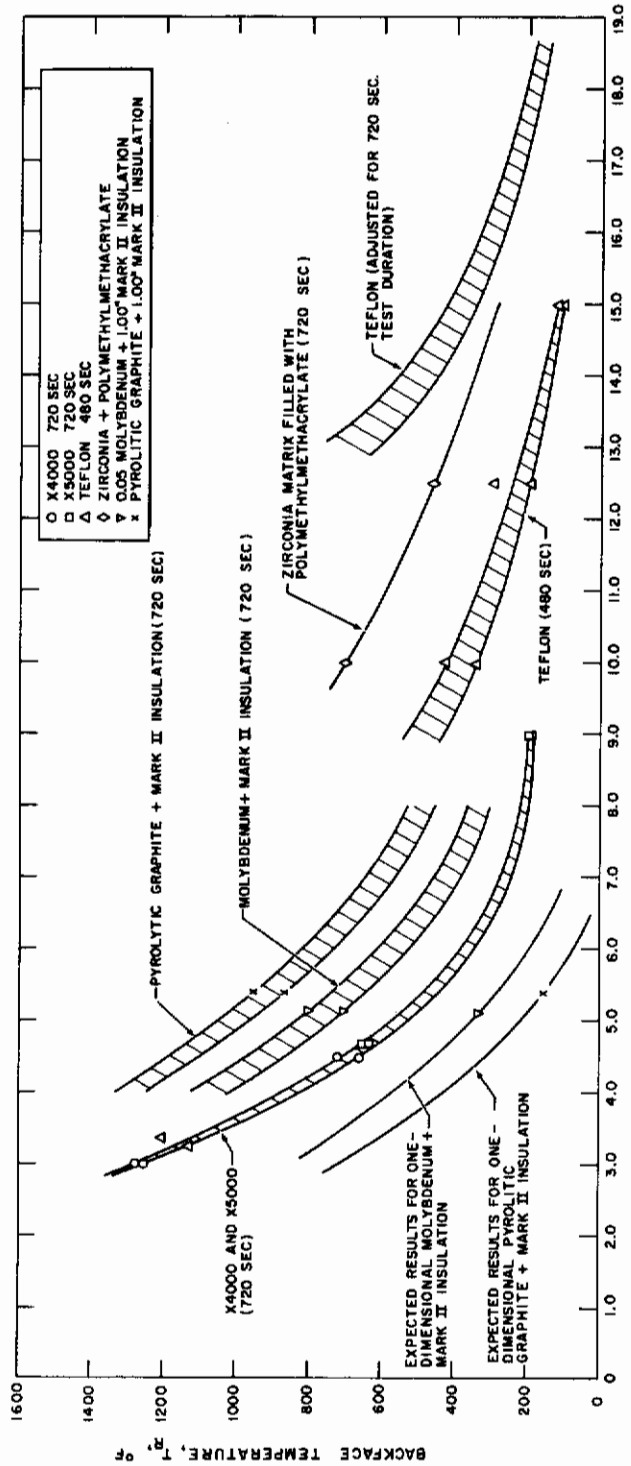

Figure 108 EXPERIMENTAL RANKING OF MATERIAL PERFORMANCE BASED ON MEASURED BACKFACE TEMPERATURES

application using these materials. To circumvent this difficulty, a high-temperature plastic (of the Avco X-5000 series) was evaluated to determine the magnitude of associated weight penalties again (using a Rene'41 substructure). Hence comparing systems 1 and 4 (table 9) indicates about a 4.3 lb/ft^2 weight penalty associated with a composite of X5000 and a Rene'41 structure. This increase is due to the fact that $\rho k/C_p$ for the X5000 plastic is much higher than the Min-K insulation employed in the pure radiation system. The weight can be reduced by combining the high-surface temperatures of the X5000 with the low $\rho k/C_p$ of Mark II insulation as indicated by system (7) of table 9. The total weights are comparable to the pure radiation shield and temperature limits of the shield (3000°F) insulation (2300°F), and substructure (1500°F) are maintained. A similar composite system for the nose cap again results in a efficient thermal protection system of 8.0 lb/ft^2. Of course problems other than thermal must be considered before a choice of the system is made. Even without the use of insulators a system such as (4) composed of X5000 and Rene'41 substructure results in a total weight of about 10 lb/ft^2 which is still competitive for this portion of the vehicle.

Based on preliminary thermal analyses, pure radiation shields are recommended for the low-heat input fuselage area. In particular, systems (1) and (3) would be selected for more detailed thermostructural analysis. For the wing and nose, systems (4) and (7) utilized high-temperature plastics, Min-K and Rene'41 are recommended for more detailed analysis and integrated design. A typical procedure will be shown in Section VII. D.

2. Two-dimensional Thermal Effects

Inspection of a typical wing leading edge geometry and boundary inputs suggests a problem area where two-dimensional effects should be accounted for to narrow down both the shield proper design as well as the structural analysis.

To determine the magnitude of the two-dimensional effects a transient analysis of a wing leading edge was performed. The geometry under consideration (see figure 109) is composed of a high-temperature ablating plastic of X3000 series and a load carrying substructure. The geometry indicates that several problems, due to the two-dimensional effects, should be considered. There are the longitudinal gradients in the shield and substructure, locally high-temperature at the interface between the plastic heat shield and molybdenum skin along the wing, and the effects of ablation on the two-dimensional temperature distribution.

The formulation of the two-dimensional problem is given in Appendix XI. The properties used in the calculation are shown in table 10 and the thermal environment, $q_c(t)$, H_e/RT_o, and flux distribution along the surface are

TABLE 9

PRELIMINARY UNIT WEIGHTS OF THERMAL PROTECTION SYSTEMS FOR THE NOSE, WING LEADING EDGE, AND FUSELAGE OF A GLIDE VEHICLE

Thermal Protection System		Vehicle Location					
		Nose $q_c(max) = 124$ Btu/ft^{2}sec		Wing Leading Edge $q_c(max) = 37$ Btu/ft^{2}sec		Cabin $q_c(max) = 15$ Btu/ft^{2}sec	
		Thickness	Weight	Thickness	Weight	Thickness	Weight
1 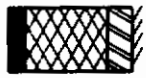 $\Delta T_R = 1500°F$	Moly	Not Applicable (Surface temperature would exceed allowable limit)		0.012	0.63	0.012	0.63
	Mark II			0.53	0.89	0.51	0.85
	Rene'			0.060	2.58	0.060	2.58
	Total			0.60	4.10	0.58	4.06
2  $\Delta T_R = 1000°F$	Moly			0.012	0.63	0.012	0.63
	Mark II			0.96	1.60	0.71	1.18
	Mo Steel			0.060	2.40	0.060	2.40
	Total			1.03	4.63	0.78	4.21
3 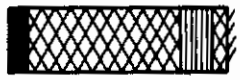 $\Delta T_R = 0°F$	Moly			0.012	0.63	0.012	0.63
	Mark II			1.02	1.69	0.79	1.31
	Coolant			0.13	0.65	0.18	0.91
	Aluminum			0.015	0.21	0.015	0.21
	Total			1.17	3.18	1.00	3.06
4 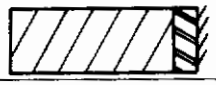 $\Delta T_R = 1500°F$	X5000	1.58	8.70	1.06	5.83		
	Rene'	0.030	1.29	0.060	2.58		
	Total	1.61	9.99	1.12	8.41		
5 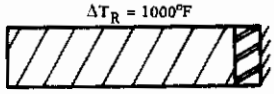 $\Delta T_R = 1000°F$	X5000	1.98	10.91	1.56	8.60		
	Mo Steel	0.030	1.20	0.060	2.40		
	Total	2.01	12.11	1.62	11.00		
6  $\Delta T_R = 0°F$	X5000			1.14	6.29		
	Coolant			0.71	3.68		
	Aluminum			0.015	0.21		
	Total			1.87	10.18		
7  $\Delta T_R = 1500°F$ $\Delta T_{INF} = 2500°F$	X5000	1.04	5.72	0.02	0.11		
	Mark II	0.45	0.75	0.53	0.89		
	Rene'	0.03	1.29	0.06	2.58		
	Total	1.52	7.76	0.61	3.58		

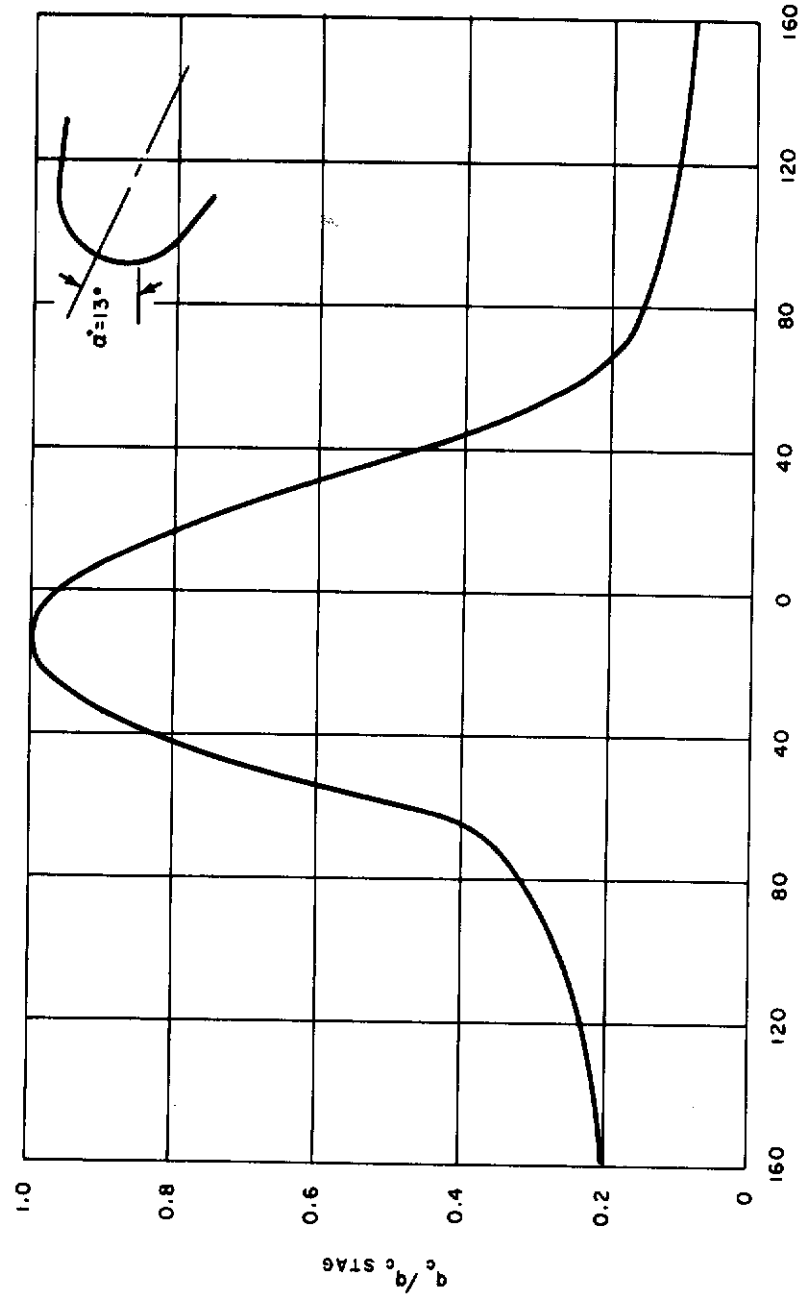

Figure 109 HEATING DISTRIBUTION OVER THE SURFACE OF A WING LEADING EDGE FOR A GLIDE VEHICLE

TABLE 10

PROPERTIES OF MATERIALS USED IN TWO-DIMENSIONAL THERMAL ANALYSIS OF A WING LEADING EDGE

Heat Shield (X3000 Plastic)

k = 0.10 Btu/hr-ft-°F
ρ = 72 lb/ft^3
C_p = 0.30 Btu/lb°F
ϵ = 0.7
T_A = 2500°F
q^* = 5000 Btu/lb

Insulation (Mark II)

ρ = 30 lb/ft^3
C_p = 0.3 Btu/lb°F
k = 0.04 Btu/hr-ft-°F

Structure

ρ = 515 lb/ft^3
C_p = 0.16 Btu/lb-°F
k_r = 10 Btu/hr-ft-°F
k_θ = 1 Btu/hr-ft-°F

Molybdenum

ρ = 634.0 lb/ft^3
C_p = 0.065 Btu/lb°F
k = 80.0 Btu/hr-ft-°F
ϵ = 0.2 and 0.7

shown in figures 23 and 109. One-dimensional calculations were also made and compared with two-dimensional results.

In the region of the interface between the plastic heat shield and the molybdenum skin, large transitions are indicated by one-dimensional analysis due to the mismatch of the emissivities (see figure 110). However, even for the extreme case of uncoated molybdenum ($\epsilon \approx 0.2$) the two-dimensional calculations show a significant smoothing of the temperature in that region. For coated molybdenum ($\epsilon \approx 0.70$) the local hot spots and critical gradients at the interface are almost non-existent.

The total amount of ablation is virtually unaffected by two-dimensional flow for the plastic shield considered. It is pointed out, however, in Appendix XI that the two-dimensional analysis must be available as in other cases which cannot be determined a prioi, such effects may be significant. For the case under consideration here, the amount ablated is small and does not change the contour of the heating edge enough to significantly alter the aerothermodynamic environment. The region of ablation and the two-dimensional temperature distributions are indicated by the isothermal diagrams presented in figures 111 and 112. Figure 111 represents the temperature distribution at a time near peak heating conditions and only small two-dimensional disturbances are indicated. At a later time, after ablation has ceased, the surface contour and temperature distribution are as indicated by figure 112 and show greater two-dimensional conduction.

It may be thus seen that in the load carrying member (substructure) the temperature gradients normal to the surface are not excessive (either for one-or two-dimensional analysis). The longitudinal gradients are also decreased and are less severe for this particular case than if one-dimensional analysis only was performed. This type of analysis as well as the one-dimensional calculations for other build-up configurations (below) indicated that the thermal effect of the substructure for a glider vehicle may be treated in terms of its temperature limit and heat capacity as was done in the parametric studies. On the other hand the thermal compatibility of the component lamina and thermal stress in the shield itself must be evaluated carefully.

3. Mechanical Vibration and Acoustical Noise

All evidence to date indicates that during the powered subsonic portion of a vehicle flight, the sound field of the rocket or jet engine is the most important source of vibration in the vehicle. The acoustical excitations due to powerplant operation are expected to be greatest on the ground due to reflection of acoustic energy from the physical surroundings. At higher altitudes the reflection conditions can be neglected. The near noise field of these engines may have an overall spectrum level of 170 db's which peaks around the third octave band (150 to 300 cps).

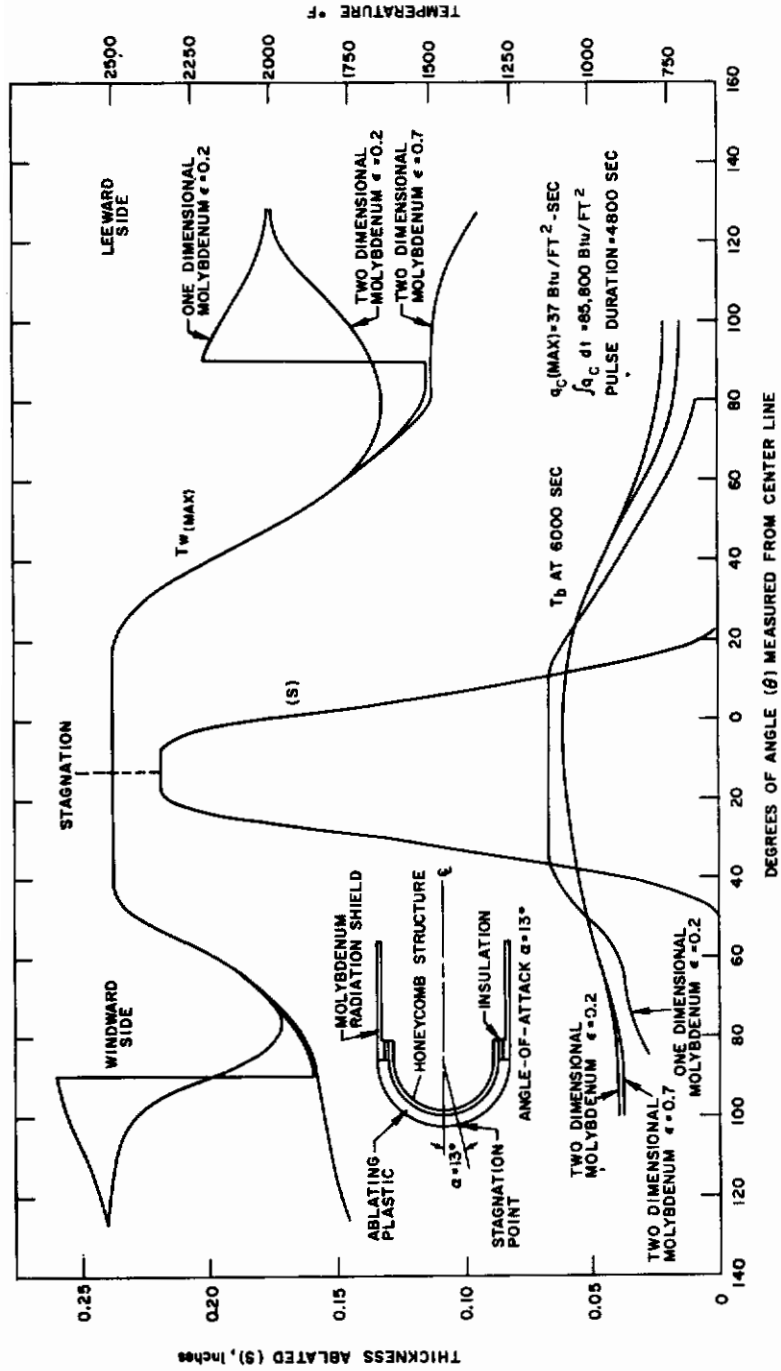

Figure 110 COMPARISON OF ONE-AND TWO-DIMENSIONAL ANALYSIS OF TEMPERATURE AND ABLATION PROFILES OVER A WING LEADING EDGE

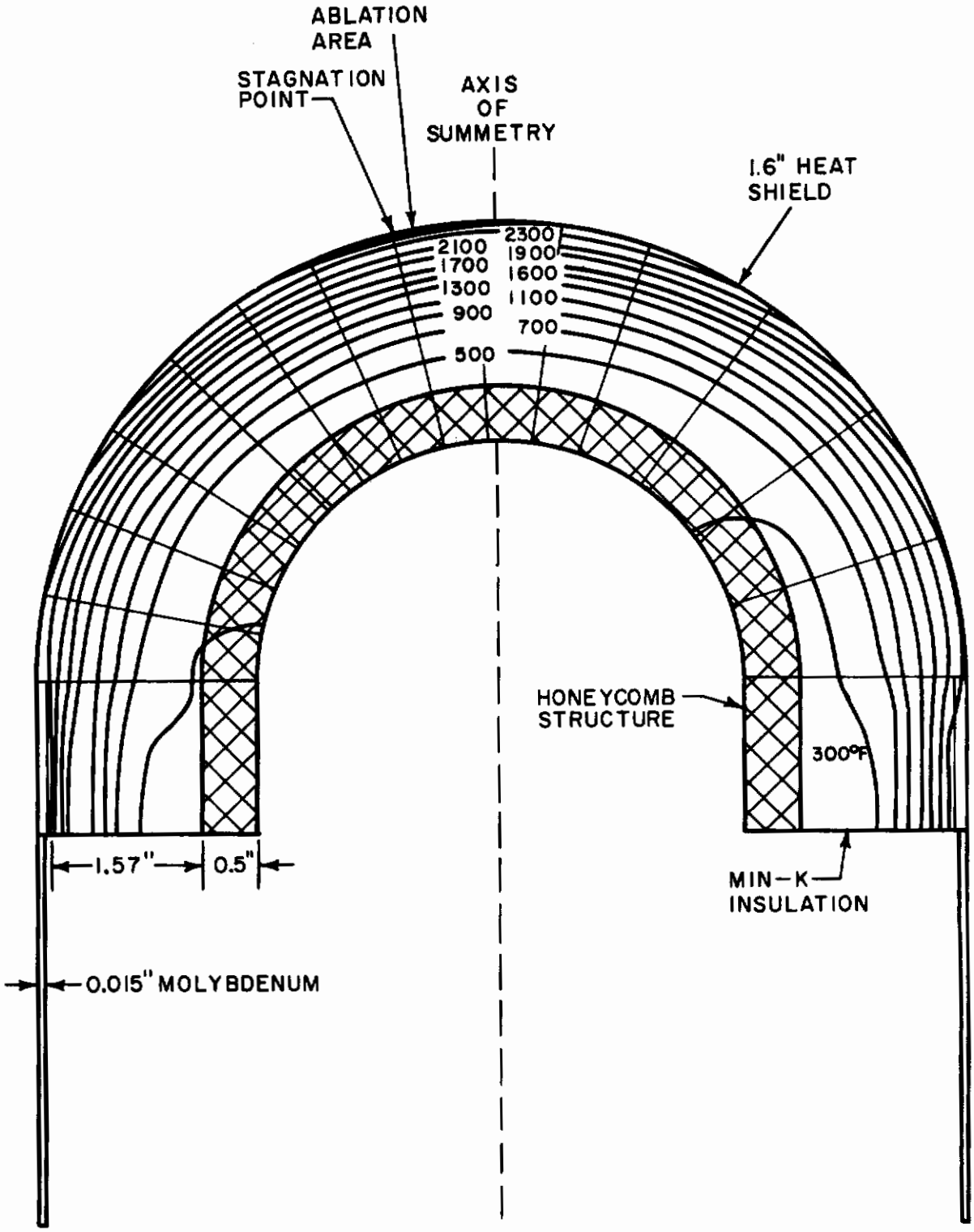

Figure 111 ISOTHERMS IN A WING LEADING EDGE DURING RE-ENTRY
t = 3000 SECONDS

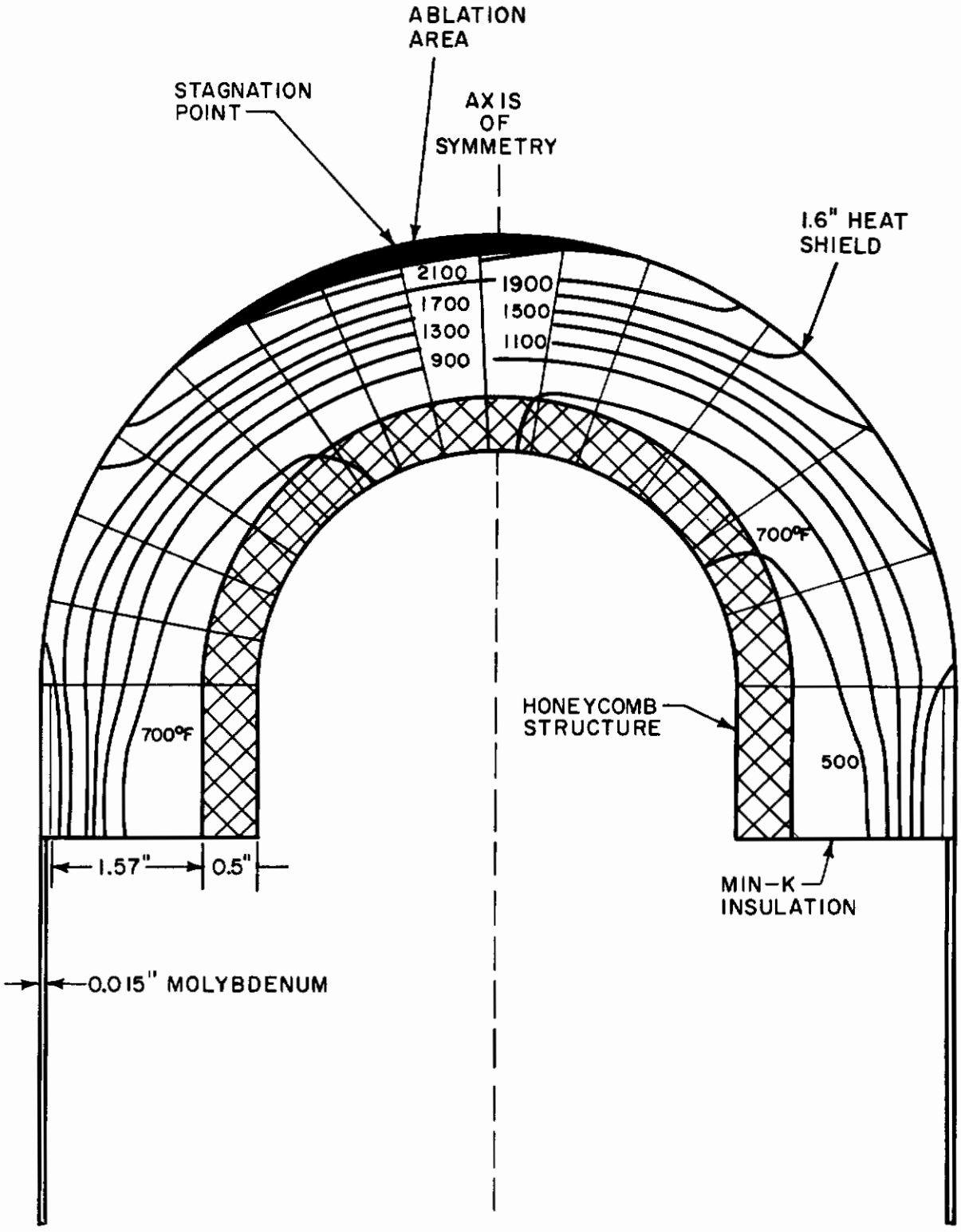

Figure 112 ISOTHERMS IN A WING LEADING EDGE DURING RE-ENTRY
t = 4000 SECONDS

As the speed of the vehicle increases aerodynamic effects such as flutter, divergence, and boundary layer noise will increase in importance. However, the chances of flutter and divergence occurring will be lessened by adequate preliminary design analysis. Boundary layer noise, on the other hand, will increase in direct proportion to the local dynamic pressure conditions. This noise is produced by the pressure fluctuations at the surface of the relief caused by the turbulent flow conditions. Recent investigations indicate that the overall spectrum peaks starting at the sixth octave band (1200 to 2400 cps).

The total noise field generated by a super-position of powerplant and boundary layer noise during the boost phase may reach a first maximum near the end of the first stage burnout. As the vehicle increases to higher altitudes where the density of the air is very low, the boundary layer noise decreases to a minimum. Although the acoustic power of the second or third stage boosters will not change, corresponding sound pressure levels may decrease due to the decreasing characteristic impedance of air.

While the vehicle is in low-density flight conditions, boundary layer noise is at a minimum and consequently the only vibrations which may exist are those which are produced by external reaction controls or by internally mounted equipment.

Upon re-entry of the vehicle into a higher density atmosphere, the boundary layer noise, again generated by the increase of the local dynamic, will reach its second maximum.

The acoustical energy generated by these phenomena is propagated by the air to the surface of the vehicle. This progressive wave system impinges on the structure of the vehicle at different incident angles where, at certain frequencies, different kinds and modes of vibration of the structure can be excited. If such a structure contains a thermal protection system, it will be necessary for this system to show both functional and structural adequacy after exposure to this type of environment. In demonstrating its adequacy, the material of the thermal protection system must show no deterioration, and the method of heat-shield attachment to the substructure must not fail.

D. THERMOSTRUCTURAL ANALYSIS AND DESIGN EXAMPLES

The thermal and material configuration concepts proposed on a preliminary basis must now be investigated from the structural point of view to establish: (a) structural concepts compatible with the aerodynamic and thermal loads, and (b) analysis requirements.

1. Re-entry Glide Vehicle

The purpose in this phase of the study is to demonstrate the procedure involved in sizing of the material compatibility of the leading edge and nose cap of a glider type vehicle. Following this, an example is given of the

type of analysis following Section VII. B. 2 that one should use to determine the elastic stresses in a ballistic type satellite capsule for final study of material compatibility. The analysis for both cases with a computer program description is given in Appendix VII. For a complete analysis of the re-entry problem one would follow the iteration mentioned in VII B. 2.

a. Sizing of a Leading Edge

1) Analysis

The procedure of analysis is given in Section VII. B. 2. and the methods of analysis are given in Appendix VII.

Performance of the analysis through this phase approximates the thermal stresses in the major portion of the critical areas and permits parametric studies to be made. Detailed design problems, such as thermal stresses at attachments and discontinuities, are not considered. In addition, maneuvering and other dynamic loads are left for a more detailed design.

The type of nose and leading edge construction consideration consists of a metal sheet substructure supporting the heat-shield material. Several different thicknesses of heat shield and structure are treated in the analysis. Figures 113a and 113b show the size and geometry of the nose and leading edge.

2) Materials for glider type vehicles

The heat-shield material selected as a reference for the nose and leading edge analyses of a glider is a high-temperature plastic charring material. The Avco X5000 series, being a non-metallic compound, exhibits material property behavior which is very strongly dependent on temperature. For this particular material, the most predominant effects are the modulus of elasticity and ultimate strength. As noted in Section IID, the information presently available on materials of this nature is incomplete and the analyses are performed on the basis of best information available. Figures 114 and 115 show the order of magnitude of the material properties that are considered.

The structural support of the heat shield is provided by a sheet metal substructure adequately reinforced by bracing and framing. This type of substructure was selected since the analysis of the dynamic environment indicated load levels not warranting the use of double-wall construction. Under different condition other types of load carrying members would have to be considered.

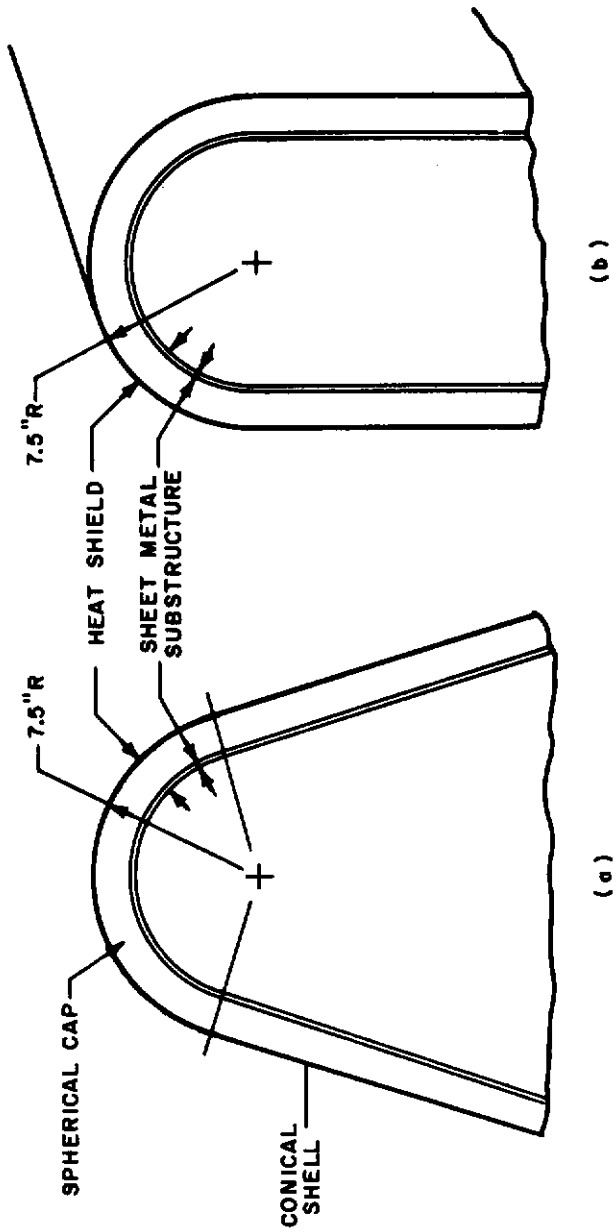

Figure 113 FUSELAGE NOSE AND WING LEADING EDGE GEOMETRY

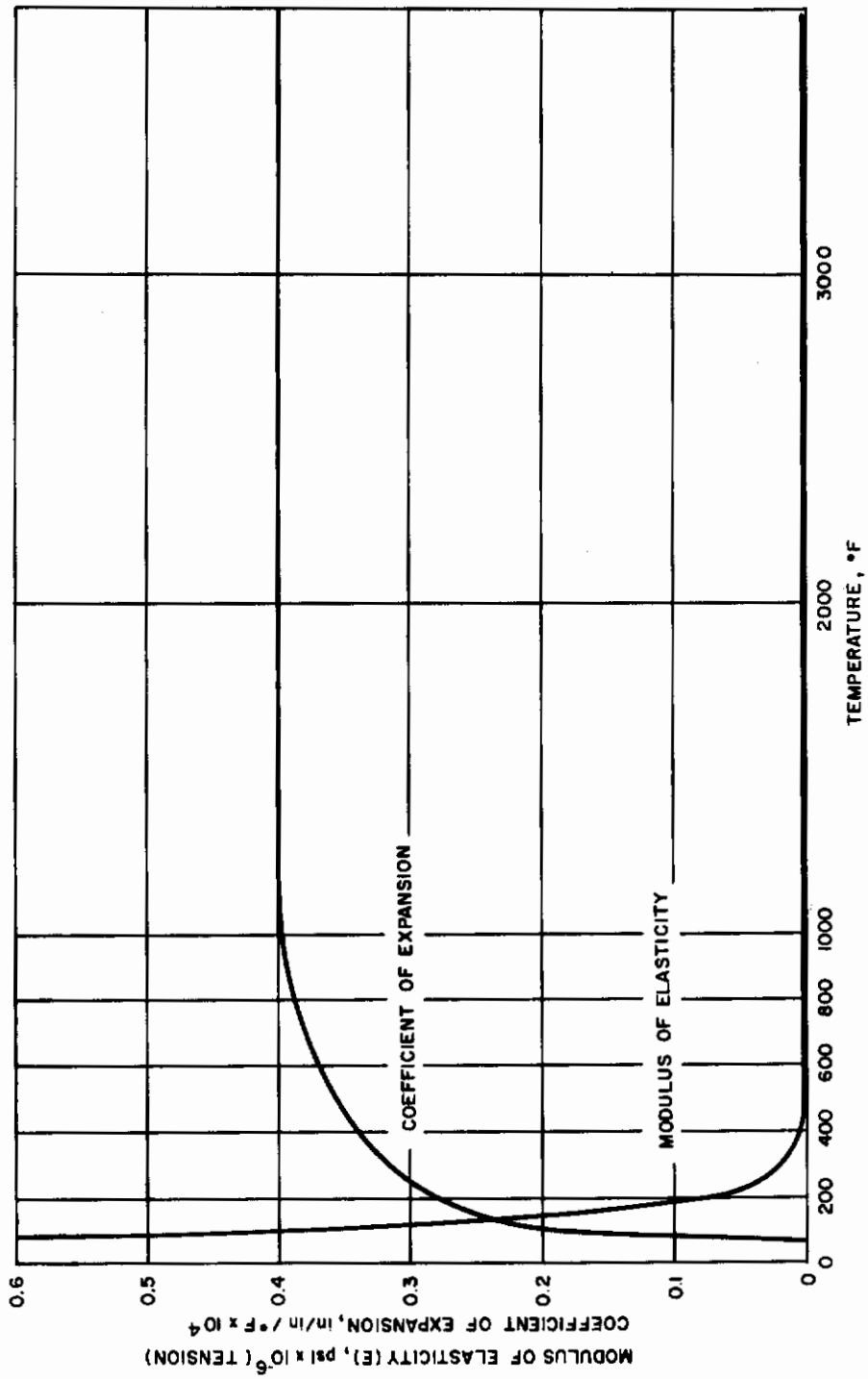

Figure 114 COEFFICIENT OF EXPANSION AND MODULUS OF ELASTICITY OF X5000 SERIES MATERIAL

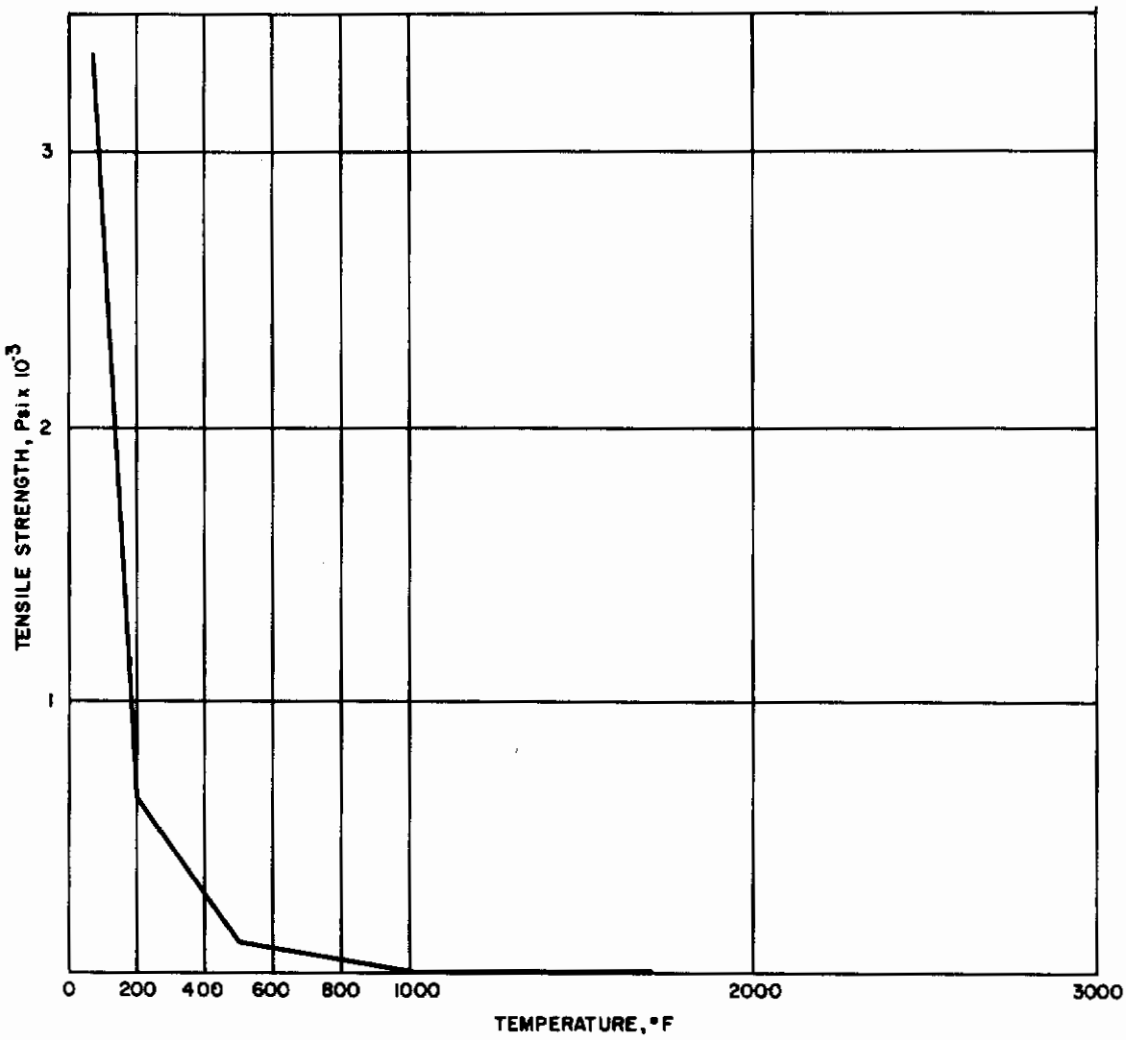

Figure 115 ULTIMATE TENSILE STRENGTH OF X5000 SERIES MATERIAL

The materials considered for the substructure are 7075 aluminum, PH-15-7 Mo steel, and Rene' 41. Properties for these materials may be found in many standard references. The thickness of the heat shield is established on the basis of the limiting temperature of the structure. For purposes of this study, the limiting temperatures are established as follows:

a) Rene' 41 = 1500° to 1600°F,

b) PH-15-7 Mo Steel = 1000° to 1100°F,

c) 7075 Aluminum = 600° to 650°F.

The corresponding thickness of heat shield for both the nose and leading edge are tabulated below:

Structure Temperature (°F)	Heat-Shield Thickness	
	Nose Section	Leading Edge
	(inch)	(inch)
1500 to 1600	1.640	1.100
1000 to 1100	1.940	1.600
600 to 650	2.400	2.100

The use of pyrolytic graphite as a heat-shield material was considered, but it was determined that the analytical techniques presently available are not adequate to realistically evaluate its structural behavior. This is due to the anisotropy of the material. In particular, the coefficient of thermal expansion varies by a factor of approximately 16 between expansion along the grain and across the grain. This wide variation of material properties precludes its being analyzed by conventional elasticity formulation.

3) Discussion of Results

The results of the analyses performed are presented in figures 115 through 121. Figures 115 through 118 show the stress distribution for the nose section as a function of time and figures 119 through 121 show the same information for the leading edge. The time scale of 6000 seconds represents the total time elapsed from

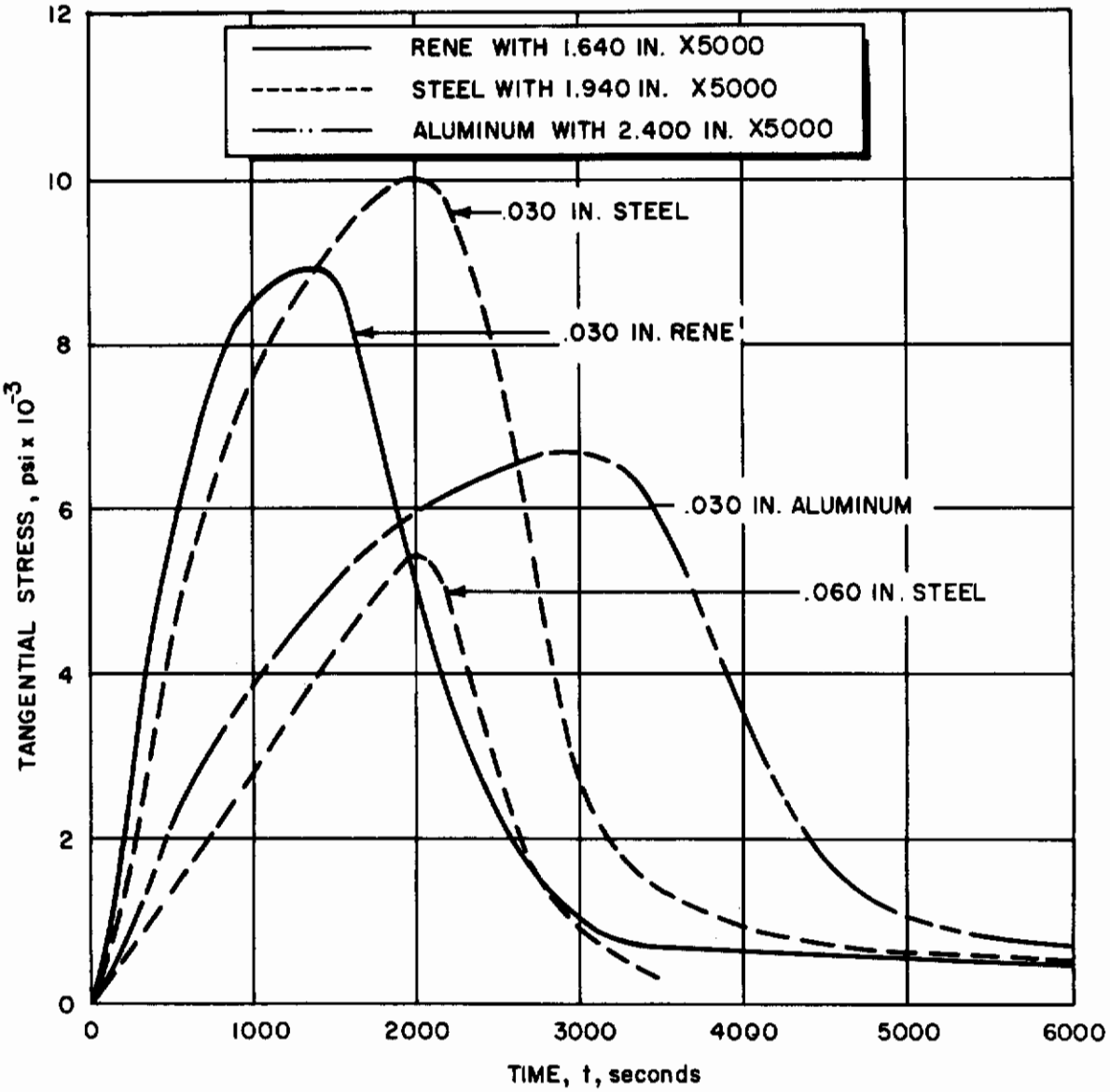

Figure 116 TANGENTIAL STRESSES VERSUS TIME FOR THE NOSE SECTION SUBSTRUCTURE

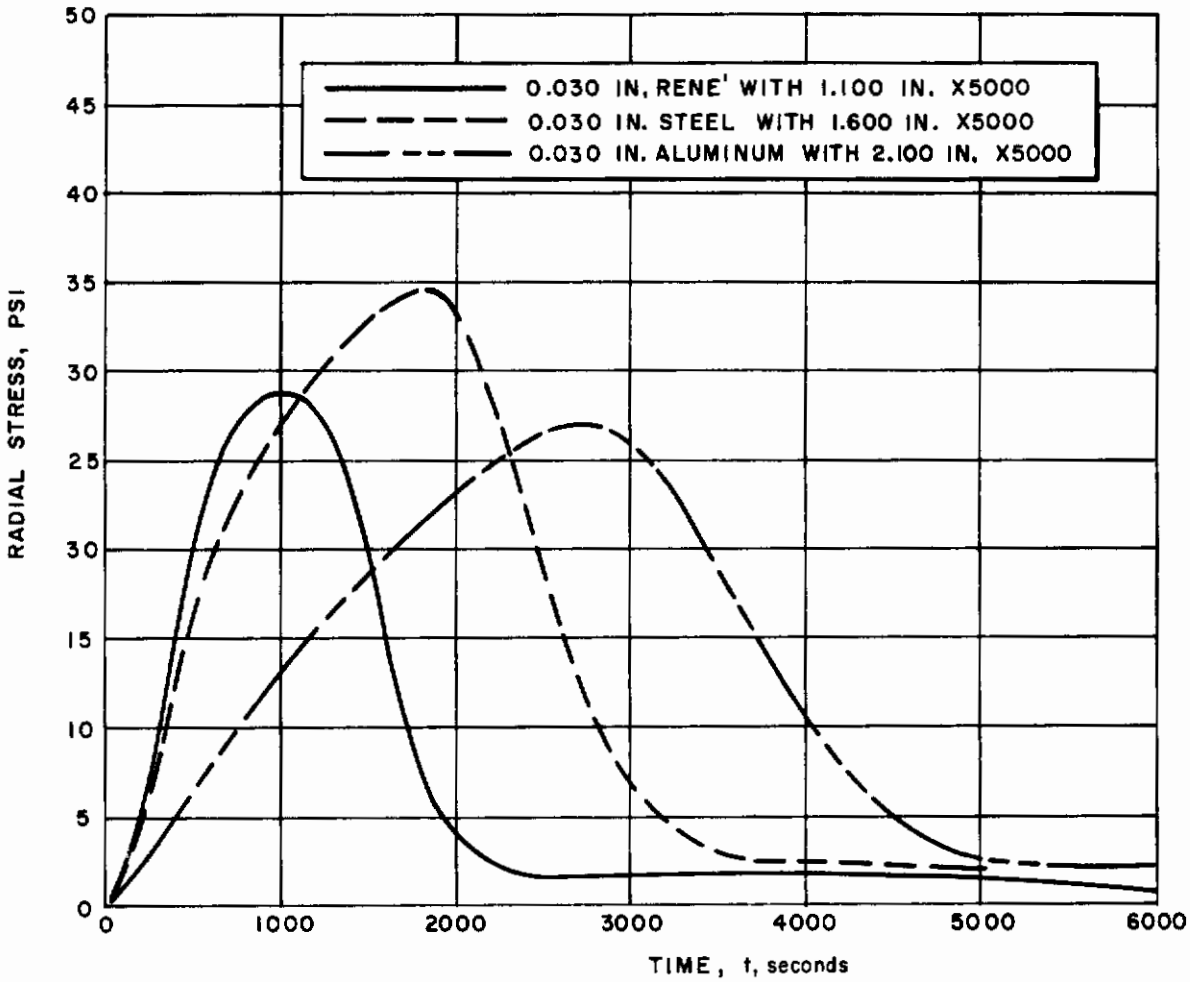

Figure 117 RADIAL STRESSES VERSUS TIME - INTERFACE BETWEEN NOSE SECTION HEAT SHIELD AND SUBSTRUCTURE

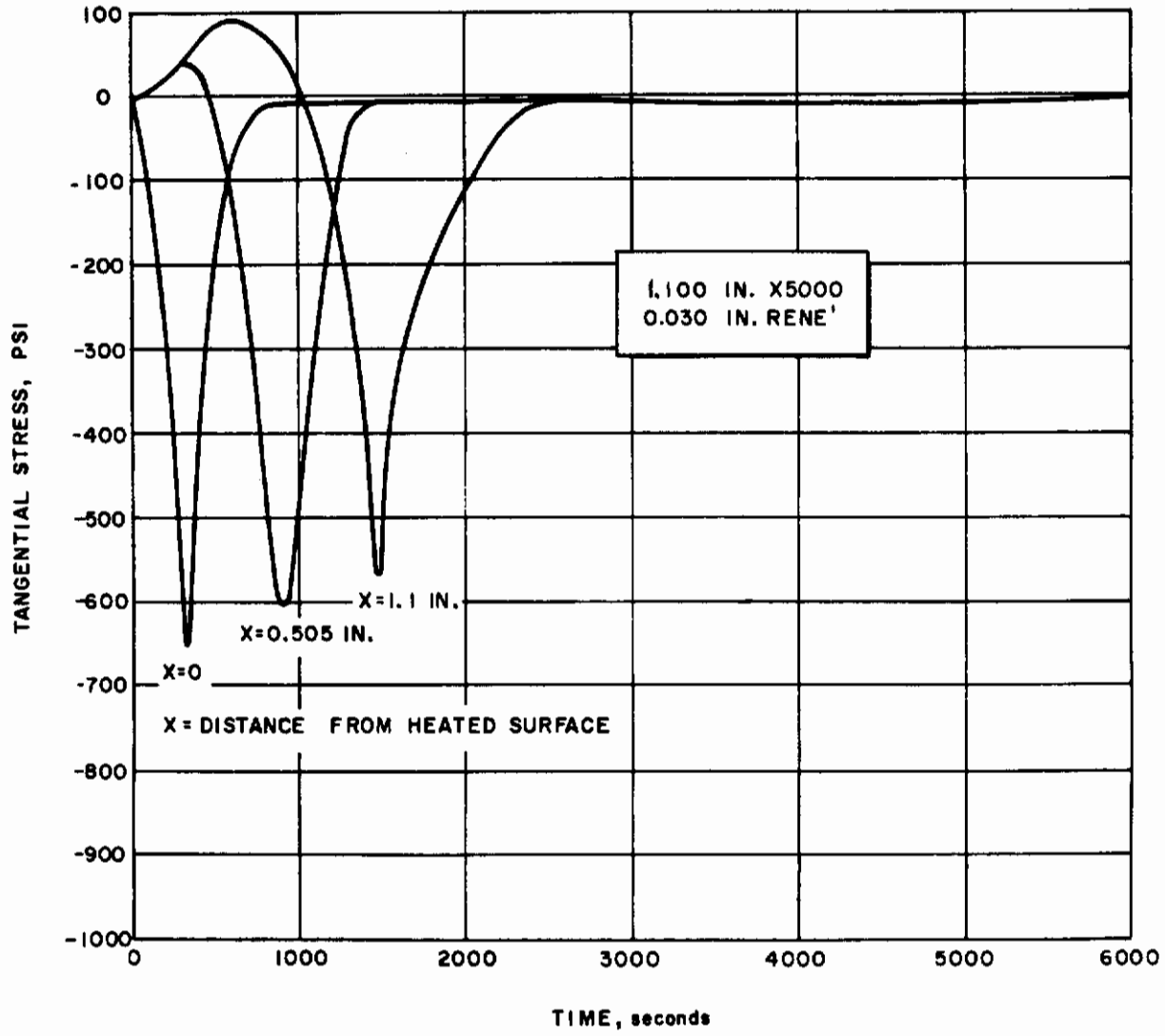

Figure 118 TANGENTIAL STRESSES VERSUS TIME FOR THE NOSE SECTION HEAT SHIELD

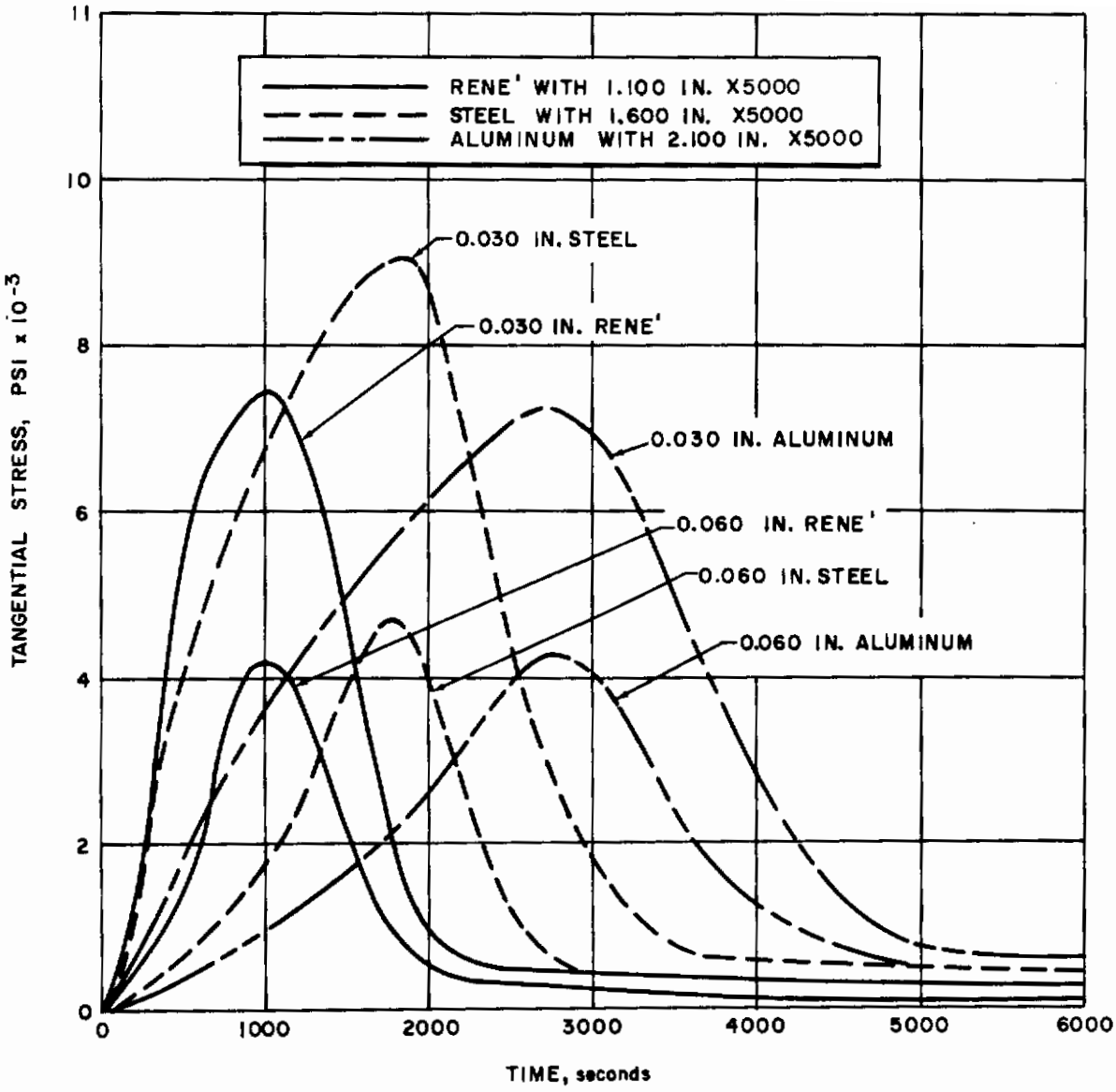

Figure 119 TANGENTIAL STRESS VERSUS TIME FOR THE LEADING EDGE SUBSTRUCTURE

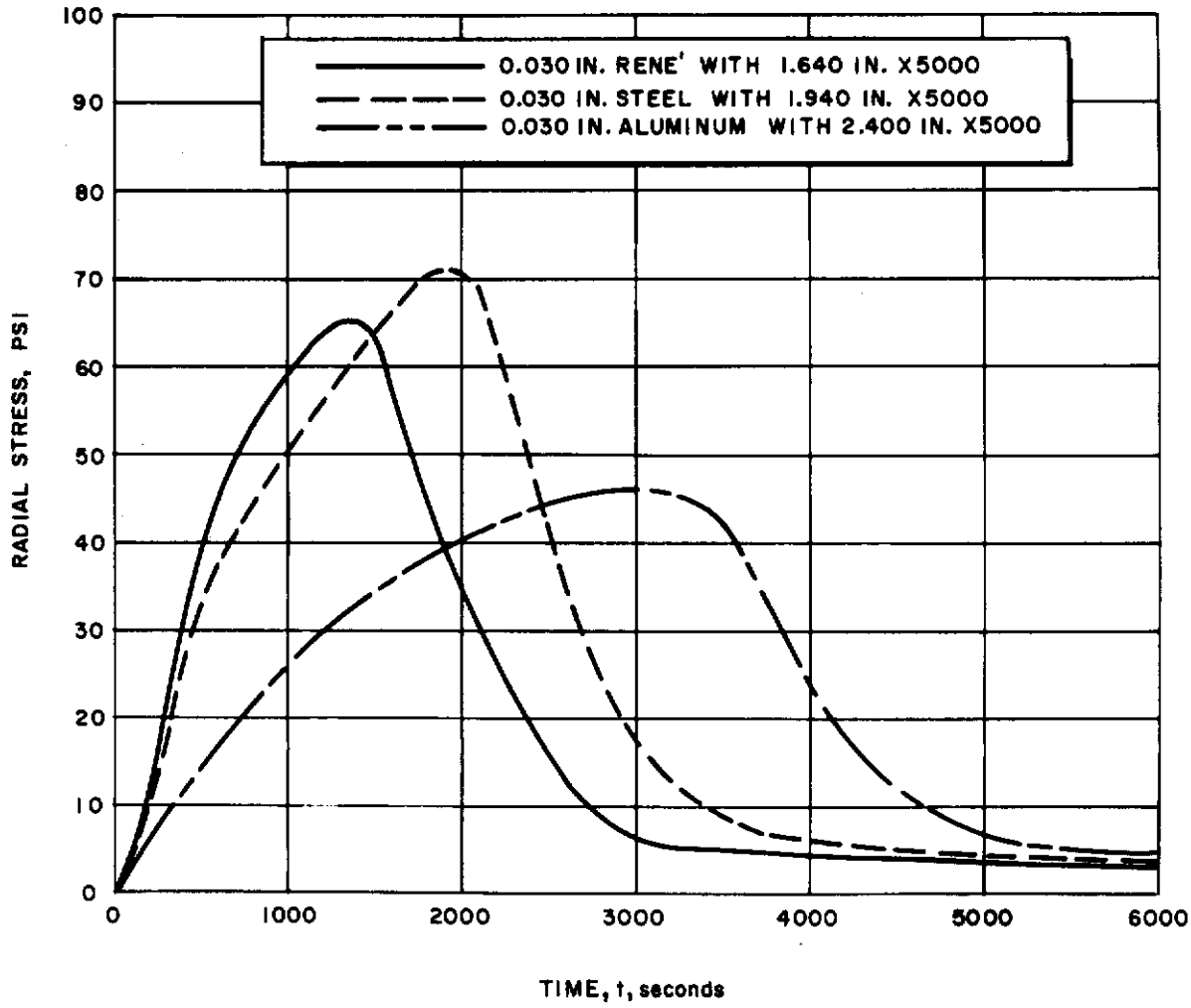

Figure 120 RADIAL STRESSES VERSUS TIME FOR THE LEADING EDGE SUBSTRUCTURE

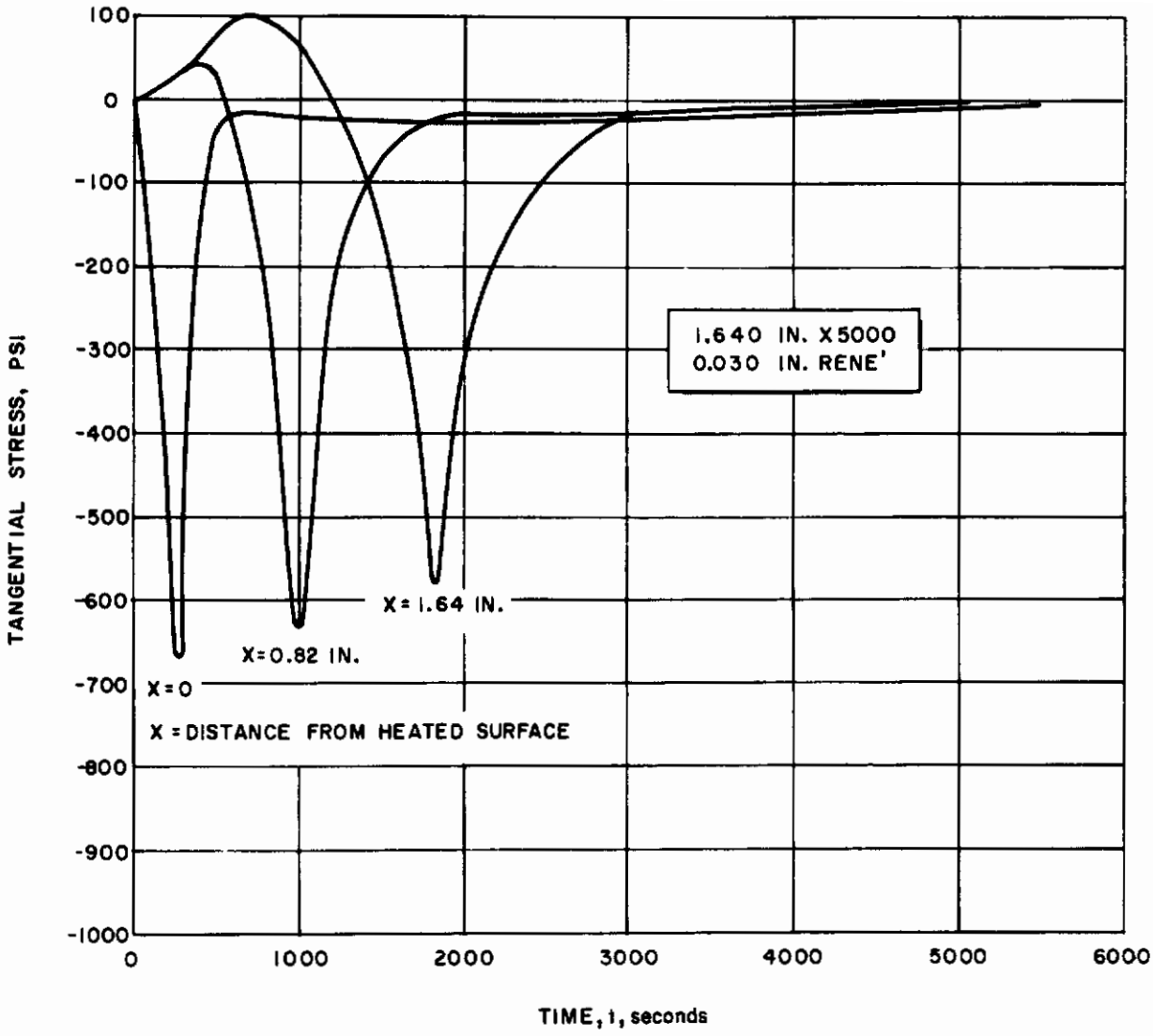

Figure 121 TANGENTIAL STRESS VERSUS TIME FOR THE WING LEADING EDGE HEAT SHIELD

start of the re-entry glide path to time maneuvering commences. These results were obtained from the thin shell thermal stress program and are applicable to the stagnation point where the maximum heating occurs.

There are certain observations that should be made with respect to these curves. The tangential stress in the heat shield reaches a maximum of 650 psi in compression for the cases considered. In addition, at any time of the cycle the maximum stress in the heat shield occurs at the point where the temperature is approximately 150°F. At temperatures above this range the tangential stress is markedly reduced. Similarly, the radial stress at the interface and the tangential stress in the substructure reach their maximum values in the early stages of the cycle when the temperature at these locations is below 200°F. At the latter stages of the cycle, as the substructure reaches its limiting temperature, the stresses are again reduced markedly.

Investigation of the effect of changing substructure thickness shows that the interface radial stress is increased and the structure tangential stress is reduced with increasing thickness. It is also determined that within the range of thicknesses considered there is negligible effect on the heat-shield tangential stresses.

The effect of the meridional gradient was found to result in slight increase in stress in the heat shield. At locations other than the stagnation point it is found that the peak stress location shifts through the thickness in the heat shield. The stress in the structure peaks at the vicinity of geometric discontinuities but is still within acceptable limits.

4) Conclusions

In general, the analysis shows that the maximum stress in the heat shield is not appreciably affected by the thickness of the heat shield or the rigidity of the substructure within the limits considered. The radial stress at the interface of the heat shield and substructure and tangential stress in the substructure are dependent on structure rigidity.

The maximum stress conditions for aerodynamic heating are found to occur during the early stages of the trajectory prior to the application of maneuvering loads. At the time when maneuvering loads would be applied, the stresses are reduced to almost negligible values enabling the two design conditions to be treated independently in most cases. The stress conditions that exist at local discontinuities arising from non-uniform heating of structural attachments would have to be designed to meet both conditions simultaneously.

The stress levels determined by the analyses provide considerable margin to prevent any short-time creep effects and to allow considerable latitude in designing for the dynamic load conditions.

2. Ballistic Satellite Re-entry Capsule

As an illustration of the analysis, the vehicle with low-heat flux is analyzed, the configuration is given in figure 9. The shape is a multi-layer and multi-regional shell. The illustrated regions being formed as follows:

a. Region 1, by shallow spherical shell,

b. Region 2, by toroidal shell,

c. Region 3, by short cylinder,

d. Region 4, by long cylinder,

e. Region 5, by ring stiffener, and

f. Region 6, by conical shell.

The purpose of the conical shell is to help to support the launch loads. The pressure distributions and heat input are given in figure 122. The temperature dependence of modulus with specimen in tension was given in figure 8. To accomodate the temperature variation and material property each layer was subdivided to give a total of ten layers.

Using the digital computer and the program for the stress distribution in the shell the stresses along the outer and inner surface of heat shield are determined and given in figures 123 and 124. The stresses along the inner surface of the back-up structure are given in figure 125. The radial displacement of reference surface shell is given in figure 126. The stress distribution through the thickness at the apex of region 1 is given in figure 127. It is interesting to notice that the back-up structure is in tension over most of the structure, while the heat shield is in compression.

Using the determined stress distribution, one can probably determine whether any structural instability or plastic deformation might occur.

The thermal analysis input was given in Appendix XI.

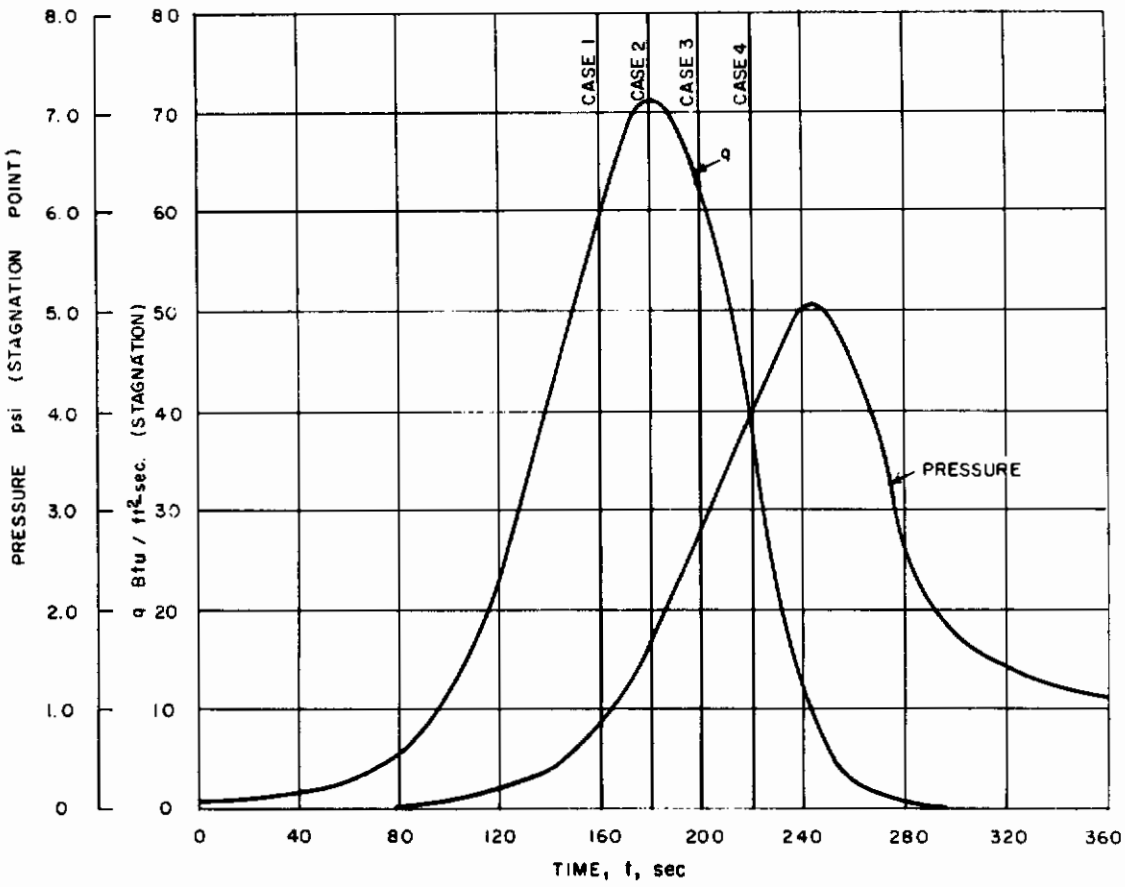

Figure 122 STAGNATION PRESSURE AND HEAT FLUX DISTRIBUTION

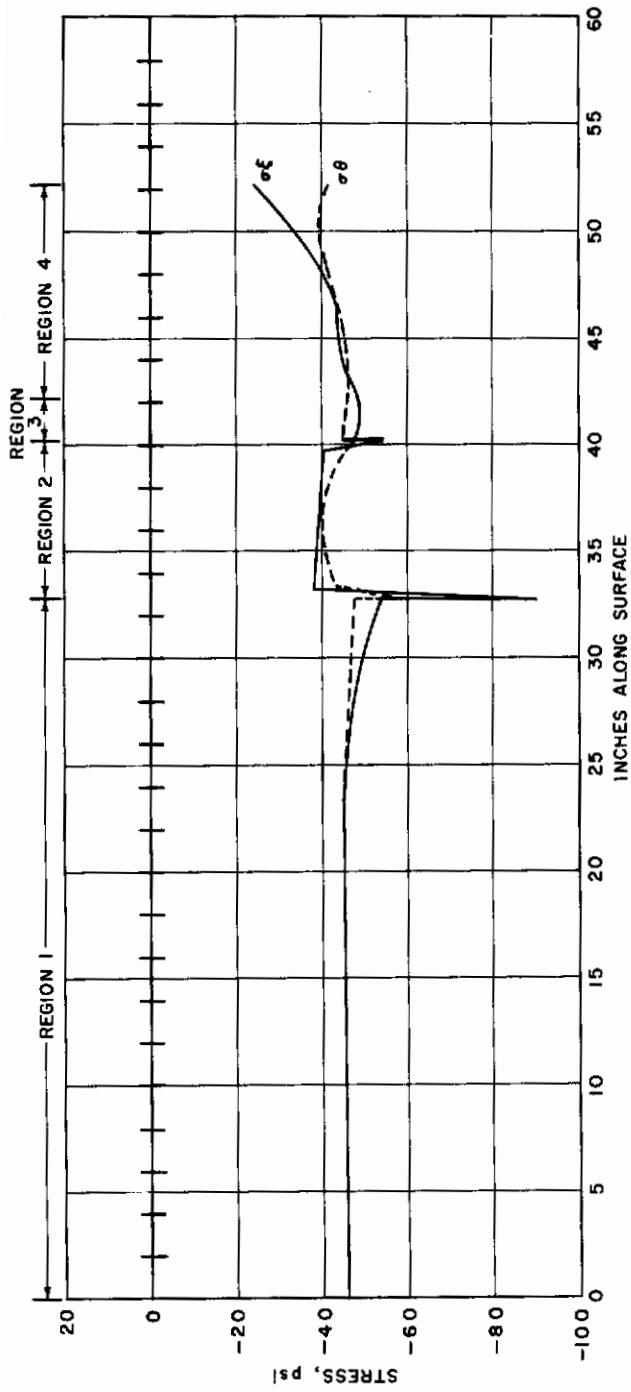

Figure 123 STRESS ON OUTER SURFACE OF THE HEAT SHIELD AS A FUNCTION OF DISTANCE ALONG THE SURFACE

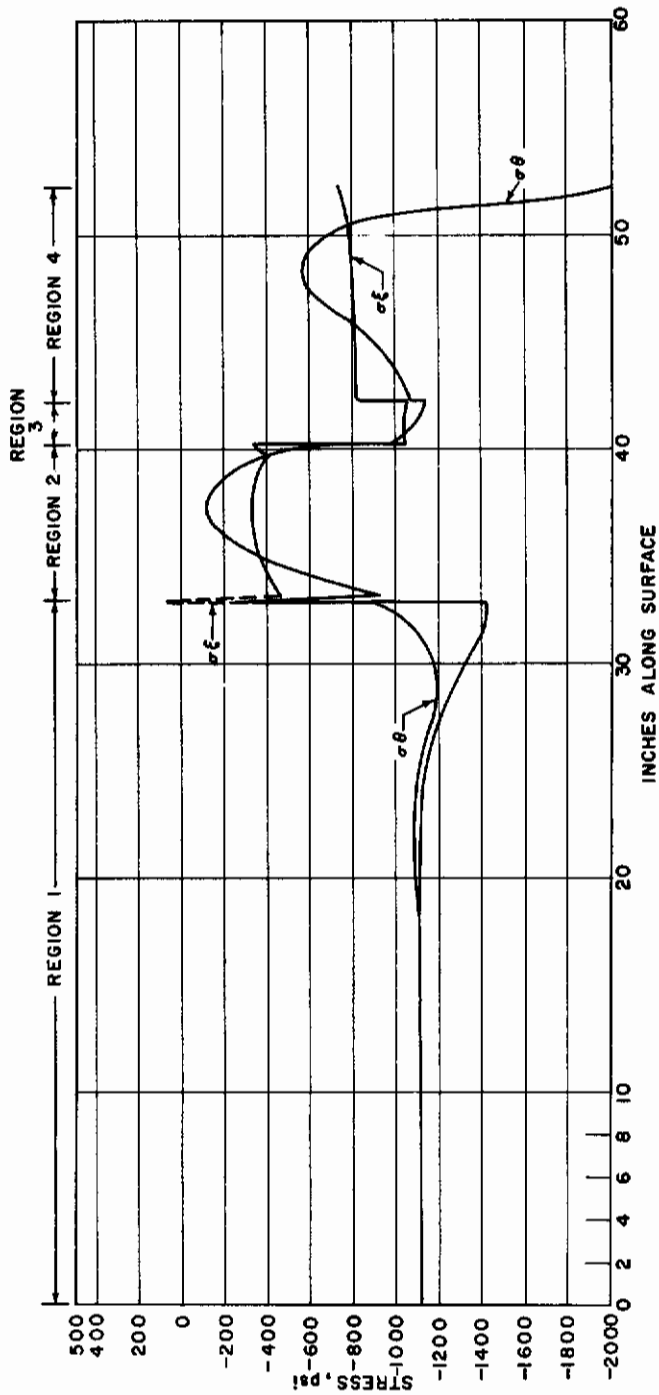

Figure 124 STRESS ON INNER SURFACE OF FUNCTION OF DISTANCE ALONG THE SURFACE

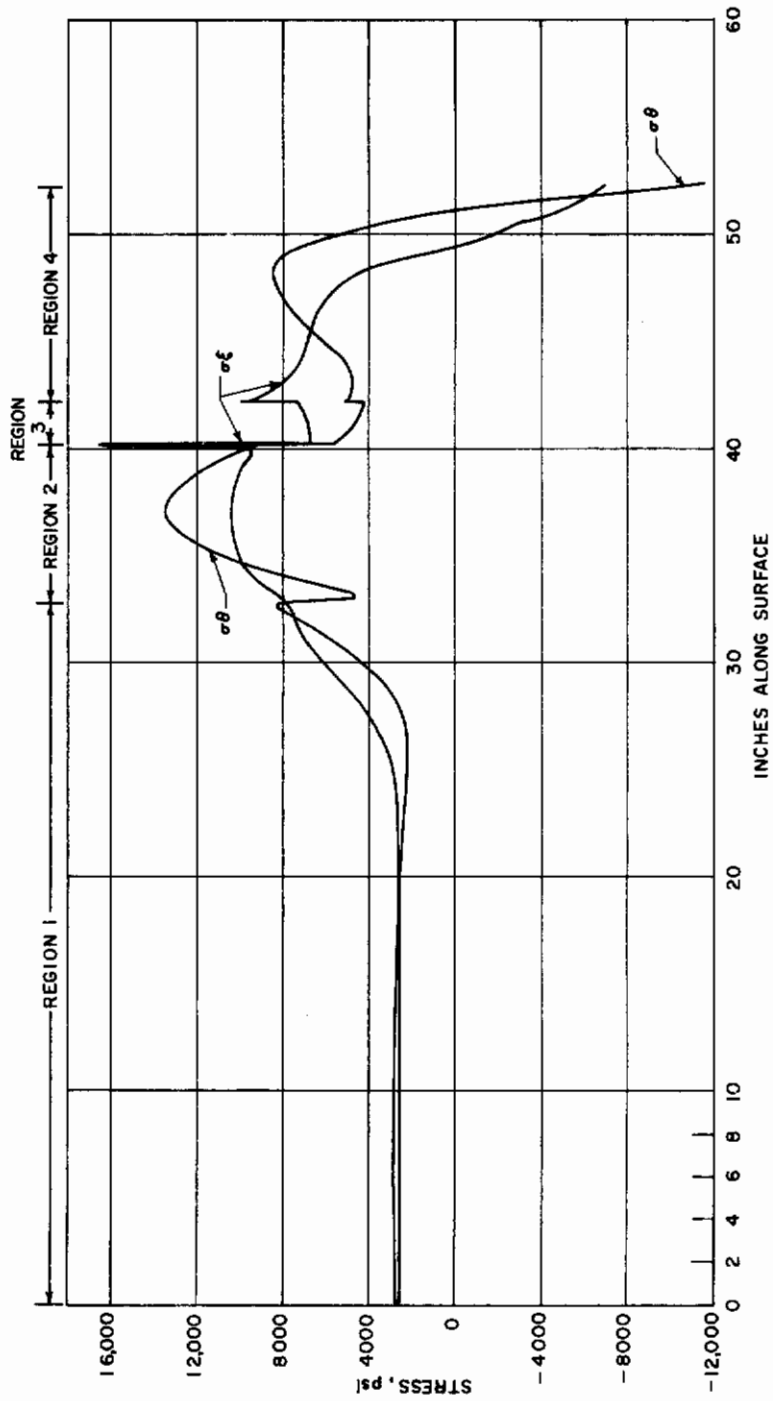

Figure 125 STRESS ON THE INNER SURFACE OF THE SUBSTRUCTURE AS A FUNCTION OF DISTANCE ALONG THE SURFACE

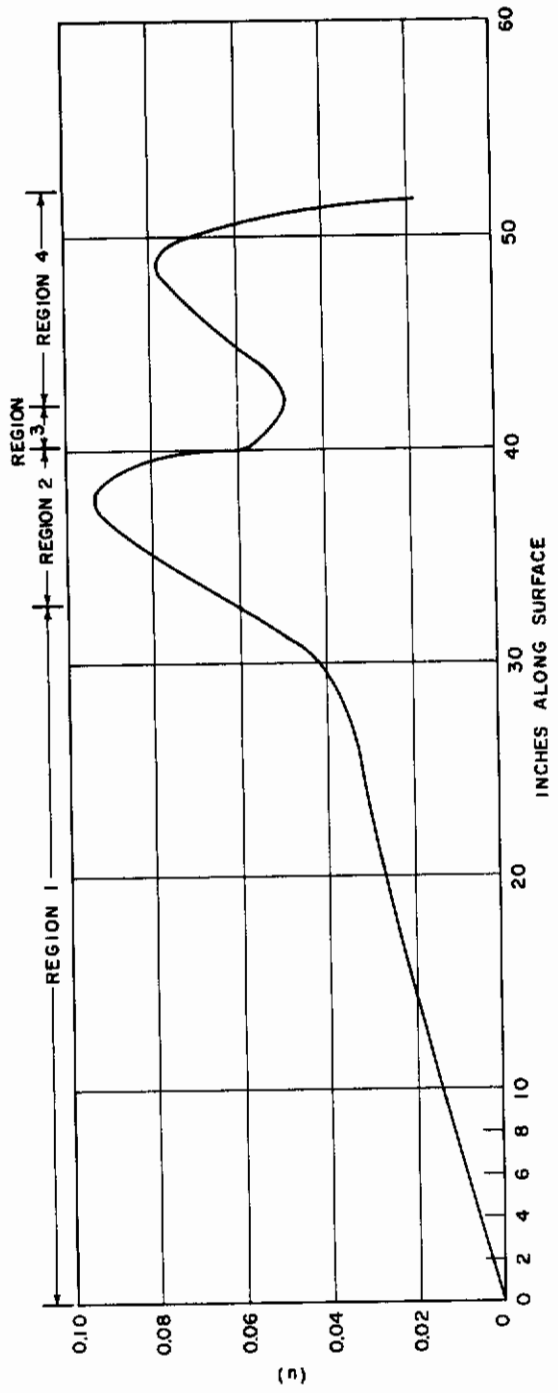

Figure 126 RADIAL DISPLACEMENT AS A FUNCTION OF DISTANCE ALONG THE SURFACE

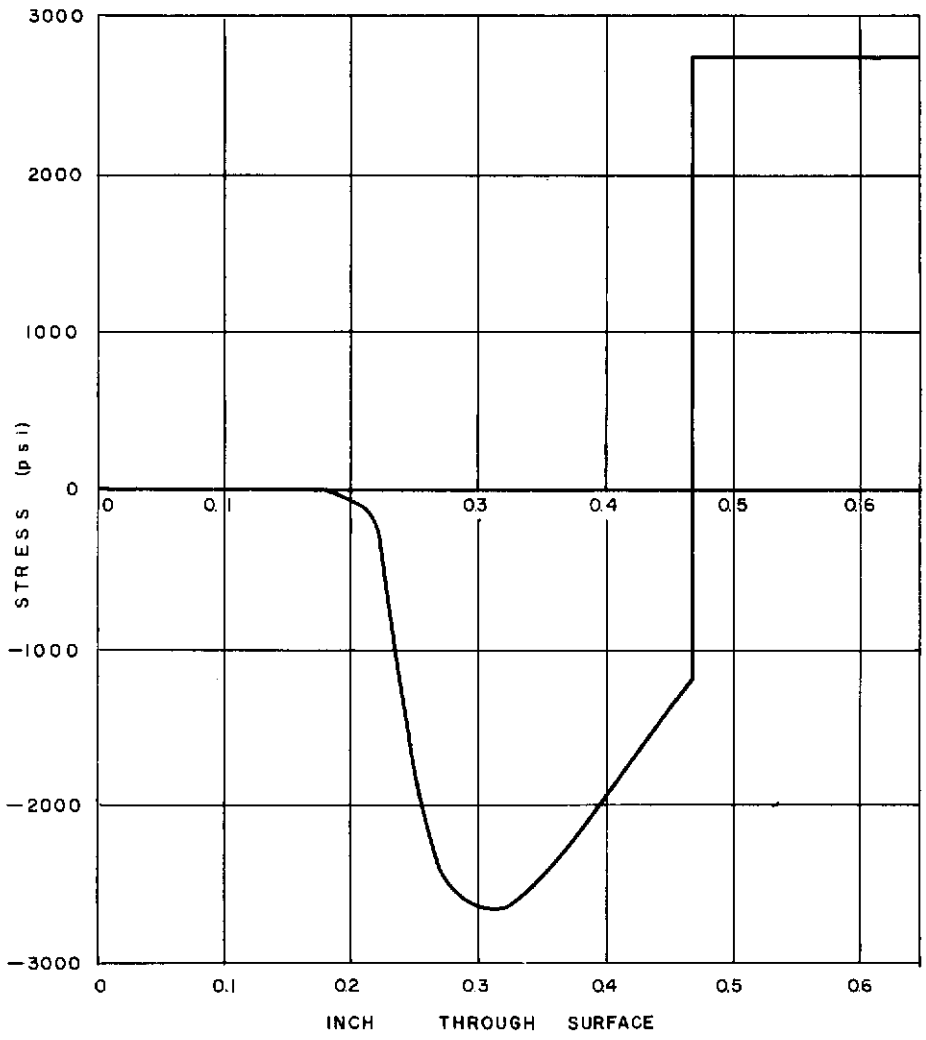

Figure 127 STRESS THROUGH HEAT SHIELD AND BACKUP STRUCTURE AT THE APEX OF THE SPHERE

VIII. SUMMARY AND CONCLUSIONS

A study has been conducted, under the terms of Air Force Contract AF-33(616)-7483, of material and system concepts applied to thermal protection systems designed for hyperthermal environments. In this study, the pertinent factors affecting the function of such systems were ascertained for a number of different systems and re-entry applications. The study included a review of the unclassified literature, a survey of the environmental simulation capability of existing test facilities, and technical contributions extending knowledge of the relationships between factors influencing the performance of thermal protection systems.

The study was centered about the tasks of collecting, generating, and correlating information in four broad areas. The first of these was an investigation concerned with the criteria used for performance evaluations of materials in particular system designs. The second concerned the methods and techniques used for experimental and theoretical acquisition of the necessary system parameters. The third concerned data correlation techniques used for system design and materials selection and development efforts. The fourth area of investigation was concerned with design and development techniques for vehicle sizing, using built-up shield-structure components. Along with these, studies were conducted of the basic mechanisms of heat and mass transfer associated with particular modes of energy dissipation and of the load carrying and transmission capacity of the system.

The scope of the study was limited to applications involving environmental regimes typical of glide re-entry vehicles; however, the methods, techniques, and criteria developed are useful for other applications.

As the survey of literature and facilities progressed, it became evident that many gaps existed in the available information and that it would be necessary to generate much new information in order to offer a coherent representation of the relationships involved. Accordingly, the data generation effort conducted under phase two of the contract, was initiated to run concurrent with the phase one literature and facilities review. The experience of Avco RAD personnel was freely used in the investigations of the mechanism of decomposition of plastic materials, combustion phenomena and structural analyses; as a result, much previously unpublished information on these subjects was included. Thus, information not available elsewhere was provided during the phase two studies, on physical phenomena and system parameters of importance in various re-entry applications. Selection of significant parameters for materials and overall thermal protection systems was made and parametric studies were conducted to provide information for the designer and to aid in materials development. These studies were conducted for systems of primary interest for glide re-entry. At the same time correlation methods and new computational techniques were developed for use in phase three for structural design studies, as well as for

the parametric studies conducted in phase two. A considerable effort was devoted to examination of the "Q* - concept." Use of a modified form of this concept as a figure of merit for rating system performance was found to be justified in the case of radiative systems, but not applicable to mass transfer segments of the system highly dependent on the environment when such environment cannot be simulated. Experimental techniques and facilities were improved and modified to permit meaningful determination of performance criteria needed for materials ranking and to extend the knowledge of material behavior.

A rapid, inexpensive, and accurate thermal design method was developed for the sizing studies conducted under phase three. The method was also used to extend the range of the parametric studies conducted under phase two. The environmental factors and structural effects in the aero-thermostructural interface were studied, design and development techniques for initial sizing of the vehicle were established or clarified, and methods provided for final design. The dependence of the thermal protection system on aerodynamic environment was shown for a particular glide re-entry flight corridor and a range of load carrying substructures. Desirable material characteristics to strive for in the materials development effort may be deduced from the parametric studies, which cover an extensive range of conditions. Systematic means for material and system selection were provided for radiative systems, radiative systems with subsidiary mass transfer (ablation), and for combinations of these systems with forced backface cooling. In addition, strides were made toward application of forced transpiration (mass injection) systems for re-entry use.

The studies conducted under this contract have been performed with the aim of: 1) providing an insight into the factors governing the application of materials properties and structural concepts to thermal protection systems designed for hyperthermal environments, and 2) devising methods and techniques useful in material development, system design, and evaluation. Particular emphasis has been placed upon the orbital glide re-entry application and its transient aspects. It has been demonstrated that, at the present time, radiative systems are superior for this application. It has also been shown that the performance of radiative systems is materially enhanced by backface cooling depending on the efficiency of the latter mechanism.

It has been demonstrated that ablative plastics may be used to advantage in this application. It has been shown that the weight penalty associated with the use of these materials is very small, even when evaluated by conservative methods.

The studies also indicate that combined radiation-ablation systems have considerable merit for the orbital glider re-entry application. The principal advantage of such systems is their low cost and increased versatility, since they are readily adaptable to other applications (such as super-orbital re-entry). In operational situations, provisions for replacing the ablated portions of the system could be made to insure re-usability.

Critical examination of the "Q*-concept" for ranking materials failed to reveal a single universal figure-of-merit which can be used for all systems and all environments. For radiative systems and for the non-ablative portions of ablative systems, it appears that such a figure-of-merit exists, although it is of a form different from the conventional Q*. For other systems "conventional" analysis must be applied.

Correlations were obtained for material parameters as related to performance rating in different systems. These correlations are indicative of the trends and may be used as a guide for materials development efforts as well as for system design and selection.

The short-cut methods developed during these studies were found of great value because of cost and time savings and may be used for vehicle sizing and preliminary design. More exact methods should be used for final designs.

IX. RECOMMENDATIONS

As a result of these studies, areas for further investigations have been singled out. In particular, the following items appear to be in most urgent need of further work.

The feasibility of extending the operational corridor of re-entry gliders should be investigated. This study should consider super-orbital applications as well as increased performance capability of sub-orbital vehicles. For this purpose, the methods, techniques, and criteria developed in the course of the present study should be used to obtain the trade-offs associated with the full utilization of various materials, systems, and structural concepts.

A materials development effort should be directed toward systems allowing maximum flexibility in extension of the operational capabilities. This effort should include consideration of high-temperature organic compounds, with and without structural reinforcement.

Future materials testing programs should be directed towards better quantitative understanding of material behavior. The interpretation of the experiments should aim at providing the designer with information on significant performance parameters rather than attempting to obtain some lumped figure-of-merit.

Additional effort should be expended in analytical and experimental studies of simulation and instrumentation requirements, as well as testing facilities operation.

Work towards correlation of theory and experiment should be continued for the decomposing plastic class of materials. A successful correlation appears well within the capabilities of existing technology, and will permit full evaluation of the usefulness of these materials for orbital and super-orbital re-entry applications. Present indications are that for the orbital applications, use of these materials should result in an increased system efficiency, while an increase in system reliability appears likely for the super-orbital case.

X. REFERENCES

1. National Academy of Science, Materials Advisory Board, Report on Thermal Protection Systems, by Panel on Thermal Protection Systems (1 June 1959).

2. RAD, A Proposal for the Study of Thermal Protection Systems, Avco RAD-MS-60-3 (25 January 1960).

3. Mascola, R. E., Temperature Response in Slabs Subject to a Sinusoidal Heat Pulse, Avco RAD-9(7)-TM-60-72 (December 1960).

4. Hurwicz, H. and M. Klamkin, Conductive Heat Transfer in a Re-entry Body, Analysis of Computational Methods and Their Reliability, ASME Paper No. 59-HT-23 (1959).

5. Hearne, L. F., Heat-Sink Materials for Re-entry Heat Shield, Lockheed Missiles and Space Division, LMSD-450966 (August 1959). Confidential

6. NASA, Joint Conference of Lifting Manned Hypervelocity and Re-entry Vehicles, A Compilation of the Papers Presented, Part II (13-14 April 1960). Secret (Title Unclassified)

7. NASA, Thermal Protection Systems, National Academy of Science, MAB-151-M (6 January 1959). Confidential (Title Unclassified)

8. Adams, M. C., Recent Advances in Ablation, ARS J., 29, (9), (1959) pp. 625-632.

9. Schwartz, H. S., Conference on Behavior of Plastics in Advanced Flight Vehicle Environments, WADD Technical Report 60-101 (September 1960).

10. Fleddermann, R. G. and H. Hurwicz, Analysis of Transient Ablation and Heat Conduction Phenomena at a Vaporizing Surface, Chemical Engineering Symposium Series, 57, (32) 24 (1960), also Avco RAD-TR-9(7)-60-9 (April 1960).

11. Zlotnick, M. and B. Nordquist, Calculations of Transient Ablation, Presented at International Heat Transfer Conference, September 1961, Boulder, Colorado, also Avco RAD-9-TM-60-83 (January 1961).

12. Adams, E. W., Analysis of Quartz and Teflon Shields for a Particular Re-entry Mission, Proc. of 1961 Heat Transfer and Fluid Mech. Inst., Pasadena, California (June 1961) p. 222.

13. Lotkin, M., The Calculation of Heat Flow in Melting Solids, Quarterly of Applied Mathematics, 18, No. 1 (1960).

14. Brown, J. and R. E. Mascola, Numerical Solution of the Heat Conduction Equation for a Composite Solid with a Receding (Decomposing) Surface, Avco RAD-2-TM-58-101 (September 1958).

15. Hurwicz, H. and R. G. Fleddermann, Computer Simulation of Transient Ablation and Heat Conduction Phenomena at a Vaporizing Surface, Presented at the ARS Space Flight Report to the Nation, New York, October 1961, Paper No. 2209-61, also Avco RAD-TR-9(7)-60-9 (April 1960).

16. Steg, L., Materials for Re-entry Heat Protection of Satellites, ARS J., 30 (September 1960) p. 815.

17. Hurwicz, H. and J. D. Brown, Critical Aero-Thermodynamic Parameters in Thermal Protection Design of Space Re-entry Bodies, Part II: Trajectory and Structural Design Criteria Considerations, Avco RAD-TR-61-18 (28 December 1961).

18. Roberts, L., An Analysis of Ablation-Shield Requirements for Manned Re-entry Vehicles, (1960), NASA-TR-R-62.

19. Collins, J. A., C. Toscano, D. Moodie, and W. Wolz, Transient Behavior of Composite Thermal Protection Systems, Paper No. 1695-61, Presented at ARS Conference, Palm Springs, Cal. (April 1961).

20. Wood, R. M. and R. J. Tagliani, Heat Protection by Ablation, Douglas Aircraft Company, Engineering Paper No. 923, presented at IAS National Meeting, New York (January 1960).

21. Swann, R. T., An Engineering Analysis of the Weights Ablating System for Manned Re-entry Vehicles, Fifth Symposium on Ballistic Missile and Space Technology, Los Angeles (August 1960).

22. Roberts, L., Radiation and Ablation Cooling for Manned Re-entry Vehicles, Presented at the 2nd International Congress of the Institute of the Aeronautical Sciences (September 1960).

23. Hurwicz, H. and R. Mascola, Thermal Protection of Satellites with Cold Wall Ablation, Presented at ARS Space Flight Report to the Nation, October 1961, New York, Paper No. 2152-61, also Avco RAD-TR-23-60-34 (December 1960).

24. Hurwicz, H. and J. D. Brown, Critical Aero-Thermodynamic Parameters in Thermal Protection Design of High-Performance Re-entry Bodies, Presented at ARS Space Flight Report to the Nation, New York, October 1961, Paper No. 2151-61, also Avco RAD-TR-61-18 (June 1961).

25. Baer, D. and A. Ambrosio, Heat Conduction in a Semi-Infinite Slab with Sublimation at the Surface, Space Technology Laboratories, Inc., Paper No. TR-59-0000-00610 (February 1959).

26. Sanders, R. W., Transient Heat Conduction in a Melting Finite Slab: An Exact Solution, ARS, 30, No. 11 (November 1960).

27. Hurwicz, H., Aerothermochemistry Studies In Ablation, to be presented at Fifth AGARD Combustion and Propulsion Colloquium (9-13 April 1962) in Braunschweig, Germany.

28. Bartlett, E. P., A Systematic Method for Determination of Ablation Rates in a Corrosive Environment, Sixth Symposium on Ballistic Missile and Space Technology (28-30 August 1961) Los Angeles.

29. Nolan, E. J. and S. M. Scala, The Aerothermodynamic Behavior of Pyrolytic Graphite During Sustained Hypersonic Flight, ARS Conference on Lifting Re-entry Vehicles, No. 1696-61, Palm Springs, California, (April 1961).

30. Moore, J. A. and M. Zlotnick, Combustion of Carbon in an Air Stream, ARS Journal, 31, (October 1961) pp. 1388-1397.

31. Lees, L., Convective Heat Transfer with Mass Addition and Chemical Reactions, Combustion and Propulsion Third AGARD Colloquium, Palermo (1958) Pergamon Press, New York, pp. 451-498.

32. Cohen, C. B., R. Bromberg, and R. P. Lipkis, Boundary Layers with Chemical Reactions Due to Mass Addition, Jet Propulsion, 28, (October 1958) pp. 659-668.

33. Hartnett, J. P. and E. R. G. Eckert, Mass Transfer Cooling with Combustion in a Laminar Boundary Layer, Proceedings of the Heat Transfer and Fluid Mechanics Institute, Stanford Univ. Press (June 1958) pp. 659-668.

34. Bromberg, R. and R. P. Lipkis, Heat Transfer in Boundary Layers with Chemical Reactions Due to Mass Addition, Jet Propulsion, 28, (October 1958) pp. 668-674.

35. Denison, M. B. and D. A. Dooley, Combustion in the Laminar Boundary Layer of Chemically Active Sublimating Surfaces, J. Aero. Sci., 25, (April 1958) pp. 271-272.

36. Scala, S., Surface Combustion in Dissociated Air, Jet Propulsion, 28, (May 1958) pp. 340-341.

37. Emmons, H. W., The Burning of Carbon, Ramo-Wooldridge Corporation, Internal Memo (August 1954).

38. Kaufman, W. F., W. H. Armour, and L. Green, Jr., Thermal Protection Methods for Fluorine-Hydrogen Rockets, Sixth Symposium on Ballistic Missile and Aerospace Technology (28-30 August 1961) Los Angeles, California.

39. Bartlett, E. P. and M. R. Denison, Experimental Ablation Rates in a Turbulent Boundary Layer, Presented at Annual ASME Meeting, Paper No. 60-WA-208 (December 1960).

40. Denison, M. R., Combustion in the Turbulent Boundary Layer of Chemically Active Sublimators, Technical Report U-166, Aeronutronic, Newport Beach, Calif. (10 March 1958) To be published in Journal of the Aero Space Sciences.

41. John, R. and H. Schick, Testing of Reinforced Plastics Under Simulated Re-entry Conditions, Part II: Experimental Determination of the Steady-State Heat of Ablation, presented at Third Pacific Area Meeting of ASTM, (October 1959, also Avco RAD-TR-9(7)-60-11 (June 1960).

42. Bell Aerosystems Company, AMC Interim Report 7-799 (I), Manufacturing Methods for Insulated and Cooled Double-Wall Structures (May 1960).

43. Bell Aerosystems Company, AMC Interim Report 7-799 (II), Manufacturing Methods for Insulated and Cooled Double-Wall Structures (October 1960).

44. Roberts, L., Mass Transfer Cooling Near the Stagnation Point, NASA TR-R-8 (1959).

45. Eckert, E.R.G. and J.N.B. Livingood, Comparison of Effectiveness of Convection-Transpiration and Film Cooling Methods with Air as Coolant, NASA Report 1182 (1954).

46. Warren, C.H.E., An Experimental Investigation of the Effect of Injecting a Coolant Gas at the Nose of a Blunt Body, Guggenheim Aeronautical Laboratory, California Institute of Technology, Hypersonic Research Project Memo No. 47 (15 December 1958).

47. Huang, P. C. and C. J. Van der Maas, Combined Effects of Axial Load, Thermal Stress, and Creep in Flat Plates, WADC Technical Report 57-442 (March 1958).

48. Patel, S. A., K.A.V. Pandalai, and B. Venkatraman, Creep-Stress Analysis of Some Structures, AFOSR TN 59-665 (July 1959).

49. Patel, S. A. and B. Venkatraman, On the Creep-Stress Analysis of Some Structures, AFOSR TN 60-836 (June 1960).

50. Kaeger, E. M, W. R. Warren, C. J. Hains, and R. E. Geiger, The Capabilities of the Shock Tunnel in the Study of the Aerodynamics of Atmospheric Entry, ARS Preprint 1554-60 (8 December 1960).

51. NASA, The Ames Atmosphere Entry Simulator and its Application to the Determination of Ablative Properties of Materials for Ballistic Missiles (October 1960).

52. Weatherston, R. C., W. E. Smith, A. L. Russo, and R. V. Marrone, Gasdynamics of a Wave Superheater Facility for Hypersonic Research and Development, CAL Report AD-1118-A1, AD 210223 (February 1959).

53. Munson, T. R. and R. J. Spindler, Transient Thermal Behavior of Decomposing Plastics, Part 1: General Theory and Application to Convective Heating, Presented at the 30th IAS Annual Meeting (January 1962) New York.

54. Carslaw, H. S. and J. C. Jaeger, Conduction of Heat in Solids, 2nd ed., Oxford Press, London (1959) p. 282.

55. Mascola, R. E., Temperature Response in Slabs Subject to a Sinusoidal Heat Pulse, Avco RAD-9-(7)-TM-60-72 (December 1960).

56. Landau, H. G., Heat Conduction in a Melting Solid, Quart. Appl. Math., 8, 81 (1950).

57. Hurwicz, H. and J. A. Collins, Thermal Analysis of the Shape 52 ICBM Re-entry Vehicle, Avco RAD TR-9-59-10 (30 March 1959).

58. Wolf, H., Program Analysis for Two-Dimensional Heat Flow, Avco RAD-9-TM-59-1 (17 February 1959).

59. Van Tassell, W. and A. Pallone, Similar Solutions of the Compressible Laminar Boundary Layer Equations for Air in Equilibrium Dissociation and Ionization with and without Air Injection in the Stagnation Region, Avco RAD-TM-61-22 (28 June 1961).

60. Pallone, A., Non-Similar Solutions of the Compressible Laminar Boundary Layer Equations with Applications to the Upstream Transpiration Cooling Problem, Avco RAD-TR-9-60-8 (10 May 1960).

61. Minzner, R., K. Champion, and H. Pond, The ARDC Model Atmosphere, (August 1959).

62. Feldman, S. F., Hypersonic Gas Dynamic Charts for Equilibrium Air, Avco Everett Research Report 40 (January 1957).

63. Levin, L., Internal Communication to H. G. Elrod, Avco RAD, Wilmington, Massachusetts (5 October 1961).

64. Elrod, H. G., Internal Communication to L. Levin, Avco RAD, Wilmington, Massachusetts (8 November 1961).

65. Roberts, L., Mass Transfer Cooling Near the Stagnation Point, NASA TR-R-8 (1959).

66. Eckert, E.R.G. and J.N.B. Livingood, Comparison of the Effectiveness of Convection-Transpiration and Film Cooling Methods with Air as Coolant, NASA Report 1182 (1954).

67. Beck, J. and H. Hurwicz, Effect of Thermocouple Cavity on Heat Sink Temperature, Journal of Heat Transfer, 82, Series C, No. 1, (February 1960).

68. Fay, J. A. and F. R. Riddell, Theory of Stagnation Point Heat Transfer in Dissociated Air, AERL Research Report 1, Rev (April 1957).

69. Boehringer, J. C. and R. J. Spindler, Radiant Heating of Semi-Transparent Materials, Avco RAD-TR-61-8 (April 1961).

70. Alvis, J. F. and G. B. Whisenhunt, A Thermal Protection System for Lifting Re-entry Vehicles: Structures, Materials, and Design Conference, Palm Springs Paper No. 1698-61 (6 April 1961).

APPENDIX I

THERMAL PROTECTION SYSTEM, "Q*", TERMINOLOGY AND DEFINITIONS

The widely varying usage of definitions and terminology associated with thermal protection systems and especially "Q* concepts" demands their clarification. The situation is further complicated by the cross-pollination of terms used in the disciplines concerned with the problem (aerodynamics, applied mechanics, heat transfer, materials, and thermodynamics) and the relatively recent emergence of the application.

It was deemed advisable under the circumstances to elaborate on the terms and definitions used in the body of the report.

1. Effective Heat of Ablation

A figure of merit may be defined for a steady-state ablating material as

$$q^* \equiv \frac{q_o - \epsilon\sigma T_w^4}{m} = \frac{q_o - q_r}{m} \quad , \tag{I-1}$$

that represents heat absorbed per unit mass of ablated material (effective heat of ablation). For a subliming material,[I-1] ($m = m_v$).

$$q^* = \eta(H_e - H_w) + H_v + \bar{C}(T_w - T_i) = \mathcal{F} + \bar{C}(T_w - T_i) \, . \tag{I-2}$$

and

$$q^* = [\eta(H_e - H_w) + H_v]\frac{m_v}{m} + E\bar{C}(T_w - T_i) = F + E\bar{C}(T_w - T_i) \, , \tag{I-3}$$

for a vaporizing, glassy material where F is the heat of ablation. Equation (I-3) has physical significance only in the vicinity of the stagnation point.

The q* of a material is certainly not decisive in choosing an ablating material as other parameters, such as conductivity, must be considered in designing an ablative system for transient operation. However, it is valuable in culling out some undesirable materials and in finding some of the properties of an ablating material by experimental methods. A detailed discussion of various effective heats of ablation is given below:

[I-1] Fleddermann, R.G. and H. Hurwicz, Transient Ablation and Heat Conduction Phenomena at a Vaporizing Surface, Avco RAD, submitted for presentation at the AICHE Symposium (June 1960).

Experimental q* determination is wrought with inherent difficulties of surface temperature and radiation measurement. Somewhat easier measurable quantities (although less meaningful) would be for steady-state ablation:

$$q_c^* = \frac{q_c}{m} \quad , \text{ and} \tag{I-4a}$$

$$q_o^* = \frac{q_o}{m} \quad . \tag{I-4b}$$

The physical significance of q* -- a steady-state figure of merit -- is lost when transient heating conditions are encountered, and as noted above, it cannot be decisive in selection of ablating material for a specific application. Such selection is based on the η and H_v values used in a transient ablation analysis [I-1] together with aerodynamic inputs and material properties. However, equivalent values of effective heats of ablation for the transient cases may be of value in comparing the merits of various materials under similar conditions.

If one were to evaluate ficticious mass ablation rates based on instantaneous conditions, the following figures of merit may be defined:

$$Q_c^* = \frac{Q_c}{M} \text{ where } Q_c = \int_o^{t_f} q_c \, dt \quad , \tag{I-4}$$

$$Q_o^* = \frac{Q_o}{M} \qquad Q_o = \int_o^{t_f} q_o \, dt \quad , \tag{I-5}$$

$$Q_{or}^* = \frac{Q_{or}}{M} \qquad Q_{or} = \int_o^{t_f} (q_o - q_r) \, dt \quad , \tag{I-5}$$

where t_f is the characteristic cycle time, e.g. duration of an experimental run or duration of ablation.

$$Q_{ct}^* = \frac{Q_c}{M_t} \quad , \tag{I-6}$$

$$Q^*_{ot} = \frac{Q_o}{M_t} \quad , \tag{I-6}$$

$$Q^*_{ort} = \frac{Q_{or}}{M_t} \quad , \tag{I-6}$$

$$Q^*_t = \frac{Q_{or} - \int_{-s}^{-L} \rho c T \, dy}{M_t} = q^*_{t_{mean}} \tag{I-6}$$

and

$$F_t = \frac{Q_{or} - Q_w}{M_t} \quad . \tag{I-6}$$

Q^*_t would give a measure of the heat absorbed in the transient ablation process and would represent the equivalent of a mean q^* value during the experiment, while the q^*_t values would represent the true transient instantaneous effective heats of ablation:

$$q^*_t = F_t + E\,\bar{c}\,(T_w - T_i) \quad . \tag{I-7}$$

2. Effective Heat Capacity

The above definitions although useful for comparing ablation efficiencies do not offer a good criterion for comparison of the overall performance of materials where the backface temperatures (T_b) are important. In most of the engineering applications, the rear boundary condition is significant, and it may be accounted for only if the thermal conductivity effect in the unablated portion of the material $(L-S)_f$ is evaluated. The figure of merit Q^*_{eff} accounting for both ablation and conduction mechanism may be regarded as effective heat capacity of the material, and is defined below as:

$$Q^*_{eff} = \frac{Q_c}{M_t + \rho(L-S)_f} = \frac{Q_c}{\rho(S_f) + \rho(L-S)_f} = \frac{Q_c}{\rho L} \quad . \tag{I-8}$$

It is readily seen that Q^*_{eff} and $(L-S)_f$ are functions of both T_b and of the conditions of the run. Cold-wall heating is used as reference since it is a function of aerodynamic environment only, independent of material properties and geometry. For high heat inputs and/or low material conductivities, the energy stored is negligible and $\lim (L-S)_f = 0$, thus,

$$\lim Q^*_{eff} = \frac{Q_{or}}{M_t}\left(\frac{Q_c}{Q_{or}}\right) = Q^*_t\left(\frac{Q_c}{Q_{or}}\right) \quad , \tag{I-9}$$

which is the limit of a pure ablator.

For low inputs and/or high material conductivities, $\lim M_t = 0$ and $\lim y = 0$ thus,

$$\lim Q^*_{eff} = \frac{Q_{or}}{d}\left(\frac{Q_c}{Q_{or}}\right) = \bar{C}\,(T_w - T_i)\left(\frac{Q_c}{Q_{or}}\right) \quad , \tag{I-10}$$

which is the limiting heat capacity of a nonablation heat sink. It reflects thus, the relative importance of ablation (mass loss) and conduction ("insulation" requirement) phenomena by the degree it approaches either of the above limits. It is also obvious that to obtain valid Q^*_{eff}, one has to carry out the transient conduction calculations with great accuracy since relatively small error in the temperature distribution (the energy stored in the body) at the backface may change the $(L-S)_f$ requirement considerably. This will be especially noticeable for t_f shortly after ablation ends.

3. Miscellaneous Definitions

Material -	Individual component of a multi-layer composite.
Material System - (or Structure)	Geometric concept. A composite of materials participating directly or indirectly in the heat exchange process. Includes primary (external) heat-shield material insulation, bonds, and load carrying substructure.
Thermal Protection System (TPS) -	A built-up material system utilizing a particular mode of heat or mass transfer, or active cooling technique for protection of payload.
Flight Regime - (Performance Profile)	Aerothermodynamic and loading environment created by vehicle re-entry and expressed in terms of trajectory characteristic performance (e.g. velocity, heating, enthalpy, pressure).
Vehicle -	Aerodynamic and structural geometric configuration, weight, aerodynamic characteristics (W/C_DA, $L/_D$).
Application -	Vehicle and flight regime.

4. List of Symbols

$\bar{C}$ Average specific heat,

k Thermal conductivity,

L Material thickness,

F Heat of ablation,

$\mathcal{F}$ Effective heat of vaporization,

H Stagnation enthalpy $(h + u^2/2)$,

H_w Specific enthalpy of air at T_w,

m Mass rate of ablation of material per unit surface area,

m_v Mass rate of vaporization of surface per unit surface area,

q Heat transfer rate per unit surface area,

Q Total heat transfer per unit surface area, $\int_0^{t_f} q\, dt$,

q_o Heat transfer rate to non-transpiring wall of temperature T_w,

q_r Rate of energy radiation per unit surface area,

q^* Effective heat of ablation, figure of merit,

Q^*_{eff} Effective heat capacity,

S Position of ablating surface at time t,

t Time,

T Temperature,

ϵ Surface emissivity,

η Transpiration (blowing) coefficient,

H_v Specific latent heat of vaporization,

ρ Density,

σ Stefan-Boltzmann constant,

Subscripts

b or r Backface of ablating material,

c Cold wall,

i Initial Value

f Terminal value,

w Wall,

e Stagnation,

t Transient,

APPENDIX II

BIBLIOGRAPHY OF THERMAL PROTECTION SYSTEMS FOR RE-ENTRY VEHICLES

I. HEAT AND MASS TRANSFER MECHANISMS

A. RADIATION

Boehringer, J. C. and R. J. Spindler, On the Determination of Optical Properties for Calculation of Radiant Heating of Semi-Transparent Materials, presented at the Fourth Sixth Annual Meeting of the Optical Society of America, Paper TE-17, also Avco RAD-TM-61-36 (October 1961).

Chandrasekhar, S., Radiative Transfer, Oxford University Press, London (1950).

Mazur, P., Radiant Interchange Between a Gas-Particle Mixture and a Rocket Nozzle Wall, Avco RAD-TR-7-60-24 (October 1960).

Lee, D. H. K. and J. A. Vaughan, Studies on Thermal Effects of Solar Radiation in Transportable Solar Chamber ASME Paper 60-WA-251 (1960).

Roberts, L., Radiation and Ablation Cooling for Manned Re-entry Vehicles, Presented at the 2nd International Congress of the Institute of the Aeronautical Sciences (September 1960).

Viskanta, R., Heat Transfer in Thermal Radiation Absorbing and Scattering Media, Ph. D. Thesis, Purdue University (1960) also University Microfilms, Inc., Ann Arbor, London.

Boehringer, J. C. and R. J. Spindler, Radiant Heating of Semi-Transparent Materials, Avco RAD-TR-61-8 (April 1961).

Collins, J. O. and S. Speil, Ablation, Heat Sink and Radiation: The Materials That Make Them Work, Materials in Design Engineering, 53, No. 3, (March 1961).

Kivel, B., Radiation From Hot Air and Stagnation Heating, Avco Everett Research Laboratory Research Report 79 (October 1959).

Anderson, M. S., D. H. Trussell and C. W. Strovo, Research on Radiation Heat Shields for Bodies and Leading Edges, USAF-NASA Joint Conference on Lifting Manned Hypervelocity and Re-entry Vehicles, Part I (11-12 April 1960) Confidential.

Seymour Lieblin, U.S., Analysis of Temperature Distribution and Radiant Heat Transfer Along a Rectangular Fin of Constant Thickness, NASA TN D-196 (November 1959).

Howe, J.T., Radiation Shielding of the Stagnation Region by Transpiration of an Opaque Gas, NASA TN D-329 (September 1960).

Kircher, H.P., F.A. Vassallo, and J.G. Carnitz, Study of Thermal Radiation within Solids and Internally Ablating Composite, AD-237 839 (15 June 1960)

Sparrow, E.M., Application of Variational Methods to Radiation Heat-Transfer Calculations, ASME Paper 59-A-120 (1959).

Tatom, J.W., Shell Radiation, ASME Paper 60-WA-234 (1960).

Callinan, J.P. and W.P. Berggan, Some Radiator Design Criteria for Space Vehicles, Transactions of the ASME Journal of Heat Transfer, 81, Series C, No. 3 (August 1959) pp. 237.

Collins, J.A., Radiant Heat Loss From a Ceramic Coated Protective Cover During Ascent and Outer-Space Flight, Avco RAD-2-TM-57-14 (17 October 1957)

Robbins, W.H., An Analysis of Thermal Radiation Heat Transfer in a Nuclear Rocket Nozzle, NASA TN D-586 (January 1961).

Anderson, R.A. and W.A. Brooks, Jr., Effectiveness of Radiation as a Structural Cooling Technique for Hypersonic Vehicles, Journal of the Aerospace Sciences, 27, (January 1960) No. 1, pp. 41.

Kadnanoff, L.P., Radiative Transport Within an Ablating Body, Avco Everett Research Laboratory, Research Report No. 61, (July 1959) (AFBMD TN-59-12).

B. MASS TRANSFER

1. Ablation

Adams, E., Calculation Method for the Transient Melting Process of a Glassy Heat Protection Shield in the Vicinity of the Stagnation Point of a Re-entry Vehicle, ABMA, AD 236 482 (17 May 1960).

Bartlett, E.P. and M.R. Denison, Experimental Ablation Rates in a Turbulent Boundary Layer, ASME Paper 60-WA-208 (1960).

Chicago Midway Lab., Determination of Factors Governing Selection and Application of Materials for Ablation Cooling of Hypervelocity Vehicles, Qtrly. Prog. Rept. CML-TN-M131-11 (June-September 1958).

Eckert, E.R.G. and J.P. Hartnett, The Effect of Combustion on Heat Transfer to the Skin of a vehicle Re-entering the Atmosphere, Paper Presented at Symposium on Mass Transfer Cooling, Rand Corp. (June 1957).

Fleddermann, R. G. and H. Hurwicz, Transient Ablation and Heat Conduction Phenomena at a Vaporizing Surface, Avco RAD-TR-9(7)-60-9 (28 April 1960).

Malott, J. S., The Ablation Heat Shield, S. P. F. Journal, 17, No. 5 (May 1961).

Beecher, N. and R. E. Rosensweig, Ablation Mechanisms in Plastics With Inorganic Reinforcement, ARS Journal, 31, No. 4 (April 1961).

Schmidt, D. L., Behavior of Plastics in Re-entry Environments Part 2, Modern Plastics, 38, No. 4 (December 1960).

Adams, Mac C., Recent Advances in Ablation, ARS Journal, 29, No. 9 (September 1959) pp. 625-632.

Barriault, R. J., One-Dimensional Theory for a Model of Ablation for Plastics that Form a Charred Surface Layer, Avco RAD-2-TM-58-130 (November 1958).

Berninger, C. F., W. Zeh and W. R. Dickson, A Survey of the Design and Analysis Problems of Ablating Re-entry Vehicles (U), presented at the Fourth Symposium on Ballistic Missiles and Space Technology, Los Angeles (1959) Secret.

Bethe, H. A. and M. C. Adams, A Theory for the Ablation of Glassy Materials, Avco Research Laboratory, Research Report No. 38 (November 1958).

Carrier, G., Aerodynamic Heat Transfer to a Melting Body, Space Technology Laboratories, Report No. GM-TM-0165-00268 (8 August 1958).

Citron, Heat Conduction in a Melting Slab Journal of Aero Space Science, (March 1960) also presented IAS 27th Annual Meeting, N. Y. IAS Report No. 59-68 (January 1959).

Bonin, J. H., C. F., Price and D. E. Taylor, Determination of Factors Governing Selection and Application of Materials for Ablation Cooling of Hypervelocity Vehicles, Chicago Midway Labs., U. of Chicago, Ill, WADC Technical Report No. 59-87, pt. 1 (July 1959).

Bonin, J. H., C. F., and D. E. Taylor, Determination of Factors Governing Selection and Application of Materials for Ablation Cooling of Hypervelocity Vehicles, Chicago Midway Labs., U. of Chicago, Ill, WADC Technical Report No. 59-87, pt. 2 (July 1959).

Bonin, J. H., Determination of Factors Governing Selection and Application of Materials for Hypervelocity Vehicles, 1 December 1957 - 1 March 1958, Chicago Midway Labs., U. of Chicago, Ill. Report No. CML-TN-M131-3 (1958).

Bonin, J. H. , Determination of Factors Governing Selection and Application of Materials for Ablation Cooling of Hypervelocity Vehicles, 1 March - 1 June 1958, Report No. CML-TN-M131-6, Chicago Midway Labs., U. of Chicago, Ill. (1958)

O'Neil, R. R., Observations on Ablation and Metallurgical Effects Produced by Surface Heating of the Algoma Meteorite, Astrophysical Observatory, Smithsonian Institution, Cambridge, Massachusetts, Technical Report No. 1; AFOSR TN-57-541 (24 September 1957).

Scala, S. M. and G. W. Sutton, The Temperature and Concentration Profiles in a Hypersonic Boundary Layer with Combustion, Blowing or Sublimation at the Wall, General Electric Co., Philadelphia, Pa., TIS Report No. 57SD406 (4 February 1957).

Carlson, W. O., A Stagnation-Point Solution for a Vaporization and Sublimation in a Laminar, Dissociated-Air Boundary Layer, Aerosciences Lab., General Electric Company, Philadelphia, Pa., Aerophysics Operation Research Memo No. 33; Technical Information Series No. R59SD379, (23 March 1959).

Goodman, T. R., Aerodynamic Ablation of Melting Bodies, Allied Research Associated, Inc., Boston, Mass., WADC Technical Report No. 57-284, (October 1957).

Scala, S. M., Sublimation in a Hypersonic Environment, General Electric Co., Philadelphia, Pa., Report No. R58SD289; Aerophysics Research Memo No. 20 (9 November 1958).

Levy, A. V., H. Leggett, S. R. Locke, Composite Ceramic-Metal Systems For 3000° - 6000°F Service, presented at ARS 15th Annual Meeting, Washington, D. C. (December 1960).

Scala, S. M., The Thermal Degradation of Reinforced Plastics During Hypersonic Re-entry, Aerosciences Lab., General Electric Co., Philadelphia, Pa., Report No. R59SD401 (22 July 1959).

Lew, H. G. and J. B. Fanucci, A Study of Melting Surfaces, Aerophysics Research Memo No. 38; Report R59SD381), Aerosciences Lab., General Electric Co., Philadelphia, Pa. (April 1959).

Hurwicz, H. and T. Brady, On Two- and Three-Dimensional Ablation Simulation, Avco RAD-Technical Report to be published.

Wood, R. M. and R. J. Tagliani, Heat Protection by Ablation, Douglas Aircraft Company, Engineering Paper No. 923, presented at IAS National Meeting (January 1960) New York; and J. Aerospace Engineering (July 1960).

Adams, M. C., W. E. Powers and S. Georgiev, An Experimental and Theoretical Study of Quartz Ablation at the Stagnation Point, Avco Research Lab., Report No. 57 (June 1959).

Goodman, T. R., The Ablation of Melting Bodies with Heat Penetration into the Solid, Allied Research Associates, Inc., Boston, Mass., Report No. AFOSR TN-58-789 (1 August 1958).

Cheng, S. I., On the Mechanisms of Meteoric Ablation, James Forrestal Research Center, Princeton, N. J., Report No. 427, AFOSR TN-58-649 (11 April 1958).

Kadanoff, L. P., Radiative Transport Within an Ablating Body, Avco Research Lab., Report No. 37 (October 1958), also Research Report No. 61 AFBMD TN-59-12.

Bond, A. C., B. Rashis, and L. R. Levin, Experimental Ablation Cooling, National Aeronautics and Space Administration (U), Washington, D. C., NASA RM L58E15A (15 July 1958) Confidential.

Roberts, L., A Theoretical Study of Stagnation-Point Ablation, National Advisory Committe for Aeronautics, Washington, D. C., Technical Note TN 4392 (September 1958), also 31 March to 14 April 1960, NASA TR-R9.

Goodman, T. R. and J. J. Shea, The Melting of Finite Slabs, Report No. AFOSR TN-58-824, Allied Research Associates, Inc., Boston, Mass. (15 August 1958).

Roberts, L., Stagnation-Point Shielding by Melting and Vaporization, NASA TR-R-10, National Aeronautics and Space Administration, Washington, D. C. (April 1959).

Simcoe, C. R. and G. K. Manning, Aerodynamic Heating of Iron Meteorites During Re-entry into the Atmosphere (30 June 1957) Battelle Memorial Inst., Columbus, Ohio.

Hansen, C. F., The Erosion of Meteors and High-Speed Vehicles in the Upper Atmosphere, Technical Note No. TN 3962, National Advisory Committee for Aeronautics (March 1957).

Denison, M. R., Combustion in the Turbulent Boundary Layer of Chemically Active Sublimators, Technical Report U-166, Aeronutronic, Newport Beach, Calif. (10 March 1958). To be published in Journal of the Aerospace Sciences.

Fleddermann, R. G., Steady State Ablation of an Axisymmetric Glasslike Body, Avco RAD-TR-2-58-11 (July 1959).

Denison, M. R., Estimating Transient Temperature Distributions During Ablation, ARS Journal (June 1960).

Feldman, S., On the Instability Theory of the Soft or Melted Surface of an Ablating Body when Entering the Atmosphere, Avco Research Laboratory, Research Report No. 34 (August 1958).

Goodman, The Heat Balance Integral and its Applications to Problems Involving a Change of Phase, Trans. of ASME (February 1958).

Foreht, B. A. and M. J. Rudick, Reinforced Carbonaeous Materials, Astronautics, 6, No. 4 (April 1961).

Hanawalt, A. J., A. H. Blessing and C. M. Schmidt, Thermal Analysis of Stagnation Regions with Emphasis on Heat-Sustaining Nose Shapes at Hypersonic Speeds, Journal of Aero/Space Sci. (May 1959).

Kinard, W. H., Feasibility of Nose Cone Cooling by the Upstream Ejection of Solid Coolants at the Stagnation Point, NACA RM L57K22 (1958) Confidential.

Landau, H. G., Heat Conduction in a Melting Solid, Quart. Appl. Math., 8, No. 1 (1950)pp. 81-94.

Lees, L., Similarity Parameters for Surface Melting of Blunt Nosed Body in a High Velocity Gas Stream, ARS Journal (May 1959).

Otis, D. R., Solution to the Heat Conduction Equation with Variable Thermal Properties and Melting at the Surface, TM-25-7-009, Convair.

Roberts, L., An Approximate Analysis of Unsteady Vaporization Near the Stagnation Point of Blunt Bodies, NASA TN D41.

Roberts, L., On the Melting of a Semi-Infinite Body of Ice Placed in a Hot Stream, Department of Mathematics, MIT, ONR Contract No. NONR-1841 (12) (June 1957).

Swann, R. T., J. South, A Theoretical Analysis of Effects of Ablation on Heat Transfer to an Aribitrary Axisymmetric Body, NACA TN-D-741 (April 1960).

Kinney, M., The Literature and Theory of Ablation: An Annolated Bibliography, North American Aviation, Inc., Autonetic Div, Downey, Calif. EM-6646(May 1961).

Sutton, G.W., On an Approximate Solution to the Problem of Aerodynamic Surface Melting of a Material of Large Prandtl Number, General Electric Company, Aerophysics Operation Research Memorandum No. 17 (8 August 1958).

Denison, M.B. and D.A. Dooley, Combustion in the Laminar Boundary Layer of Chemically Active Sublimating Surfaces, J. Aero. Sci., 25, (April 1958) pp. 271-272.

Scala, S., Surface Combustion in Dissociated Air, Jet Propulsion, 28 (May 1958) pp. 340-341.

Sutton G., The Hydrodynamics and Heat Conduction of a Melting Surface, J. Aeron. Sci., 25, No. 1 (January 1958) pp. 29-32, 36.

Gibson, R.E., A One-Dimensional Consolidation Problem with a Moving Boundary, Quart. of App. Math., XVII (July 1960) No. 2, pp. 123.

Murray, W.D., and F. Landis, Numerical and Machine Solutions of Transient Heat Conduction Problems Involving Melting or Freezing, Part I, Transactions of ASME, 81, No. 2 (May 1959).

Fleddermann, R.G., Heat Transfer to a Vaporizing Ablating Surface, J. Aero/Space Sci., 26, 604 (1959).

Georgiev, S., H. Hidalgo, and M.C. Adams, On Ablation for the Recovery of Satellites, Avco-Everett Research Lab., Research Rept. 47 (March 1959).

Ross, J.H., The Space Age and The Use of Metallic Fibers, Metals Review, 34, No. 5 (May 1961).

Hurwicz, H. and R.J. Spindler, Transient Heat Flow in Translucent Non-Gray Ablating Materials, Avco TR-9(7)-59-27 (10 November 1959).

Kubota, T., Study of Ablation with Ice Model at M-58, Cal. Tech. ARS (1959).

Levy, A.V., S.R. Locke, H. Leggett, Composite Ceramic Systems, Astronautics, 6, No. 4 (April 1961).

Miller, M.L., Transient One-dimensional Heat Conduction Analysis for Heterogeneous Structures Including an Ablating Surface, ASME Paper 59-HT-22 (1959), ASME-AICAE Heat Transfer Conf., Storrs, Conn. (8-12 August 1959).

Otis, D.R., Solving the Melting Problem Using the Electric Analogy to Heat conduction, Trans, ASME, 79, 759 (1959).

Sanders, R.W., Heat Conduction in a Melting Slab: an Exact Solution, Lockheed Rept. LMSD-288274 (July 1960).

Scala, S.M. and G.W. Sutton, The Two-Phase Hypersonic Laminar Boundary Layer--A Study of Surface Melting, Heat Transfer and Fluid Mech., Univ. of Calif. (June 1958).

Scala, S.M., A Study of Hypersonic Ablation, 10th Int. Astronaut. Cong., London (September 1959).

Sunderland, J.E. and R.J. Grosh, Transient Temperature in a Melting Solid, ASME Paper 60-WA-277 (1960).

Ungar, E.W., Final Report on Investigation of High-Speed Particle Erosion of Melting Aerodynamic Surfaces, Battelle Memorial Inst. to the Army Ballistic Missile Agency (15 September 1959).

Ungar, E.W., Particle Impacts on the Melt Layer of an Ablating Body, Battelle Memorial Instutute, ARS J., 30 (9) (September 1960).

Roberts, L., An Analysis of Nose Ablation for Ballistic Vehicles, NASA TN D-254 (28 April to 12 May 1960).

Swann, R.T., An Engineering Analysis of the Weights of Ablating Systems for Manned Re-entry Vehicles, National Aeronautics and Space Administration, Langley Research Center, Langley Field, Virginia, Fifth AFBMD-STL Symposium.

Warren, W.R. and N.S. Diaconis, The Performance of Ablation Material as Heat Protection for Re-entry Satellites, IAS Paper 60-49 (1960).

Chen, Shih-Yuan, and S.J. Allen, Similarity Analysis for Transient Melting and Vaporizing Ablation on Blunt-Nosed Bodies, Presented at ARS Space Flight Report to the Nation, New York (October 1961). Paper No. 2098-61.

McFarland, B.L., Heat Transfer Through a Melting Layer with External Gas Flow, Proc. of 1961 Heat Transfer and Fluid Mech. Inst., Pasadena, Calif. (June 1961). p. 208.

Conference on Behavior of Plastics in Advanced Flight Vehicle Environments compiled by H.S. Schwartz, WADD Technical Report 60-101 (September 1960).

Barriault, R.J. and J. Yos, Analysis of the Ablation of Plastic Heat Shields that Form a Charred Surface Layer, ARS J., 30, (September 1960). p. 823.

Hurwicz, H. and R. Mascola, Thermal Protection of Satellites with Cold Wall Ablation, Presented at ARS Space Flight Report to the Nation, (October 1961) New York Paper No. 2152-61, also Avco RAD-TR-23-60-34 (December 1960).

Hurwicz, H. and J.D. Brown, Interaction of Ablation, Material and Certain Trajectory Parameters in the Thermal Protection Design of Space Re-entry Vehicles (U), Avco RAD-TR-9(7)-59-28 (19 November 1959). Confidential

Diaconis, N.S., J.B. Fanucci and G.W. Sutton, The Heat Protection Potential of Several Ablation Materials for Satellite and Ballistic Re-entry into Earth's Atmosphere, 4th Ballistic Missile Symposium, Los Angeles (August 1959).

Collins, J.O. and S. Speil, Ablation, Heat Sink and Radiation: The Materials That Make Them Work, Materials in Design Engineering, 53, No. 3 (March 1961).

Roberts, L., Radiation and Ablation Cooling for Manned Re-entry Vehicles, Presented at the 2nd International Congress of the Institute of the Aeronautical Sciences (September 1960).

Lotkin, M., The Calculation of Heat Flow in Melting Solid, Quarterly of Applied Mathematics, 18, No. 1 (1960).

Offenhartz, E. and P.H. Rose, Ablation Measurements in Turbulent Flow, Presented at the ARS Space Flight Report to the Nation, New York (October 1961), Paper No. 2099-61.

Zlotnick, M. and B. Nordquist, Calculation of Transient Ablation, Presented at International Heat Transfer Conference (September 1961) Boulder, Colorado, also Avco RAD-9-TM-60-83 (January 1961).

Hidalgo, H., Ablation of Glassy Material Around Blunt Bodies of Revolution, ARS J., 30 (September 1961) p. 806.

Munson, T.R. and R.J. Spindler, Transient Thermal Behavior of Decomposing Materials, Part 1: General Theory and Application to Convective Heating, Presented at the 30th IAS Annual Meeting (January 1962) New York, and Avco RAD-TR-61-10 (3 May 1961).

Bartlett, E.P., A Systematic Method for Determination of Ablation Rates in a Corrosive Environment, Sixth Symposium on Ballistic Missile and Aerospace Technology (August 1961) Los Angeles, California.

Brown, J. and R.E. Mascola, Numerical Solution of the Heat Conduction Equation for a Composite Solid with a Receding (Decomposing) Surface, Avco RAD-2-TM-58-101(September 1958).

Bond, C.E., The Experimental Determination of Turbulent Ablation Phenomena by Use of the Pipe-Test Apparatus, Avco RAD Aerodynamic Section Memo No. 239 (20 October 1961).

Brelant, S., et al, Research on Criteria for Plastic Ablation Materials as Functions of Environmental Parameters, Quarterly Report No: 0401-01-1, Aerojet General Corp. Contract No. AF33(616)-7401 (31 October 1960).

Brelant, S., et al, Research on Criteria for Plastic Ablation Materials as Functions of Environmental Parameters, Quarterly Report No. 0401-01-3, Aerojet General Corp. Contract No. AF33(616)-7401 (1 March 1961).

Lapple, C.E., A.P. Brady, and D.L. Chamberlain, Research on the Mechanism of Ablation of Polymeric Materials, ASD Technical Report 61-204 (June 1961).

Rashis, B. and R.N. Hopko, An Analytical Investigation of Ablation, NASA TM X-300 (July 1960).

Rashis, B. and T.E. Walton, An Experimental Investigation of Ablation Materials, at Low and High Enthalpy Potentials, NASA TM X-263 (1960). Confidential.

Paul, Hans. G., Nose Cone Re-entry Heating for Different Heat Protection Materials, ARMY Ballistic Missile Agency, ASTIA AD No. 149437 (November 1957).

Kalvinskas, Lauanne, Theoretical Studies and Experimental Techniques Used in Ablative Heat Transfer Literature Search No. 102,Jet Propulsion Laboratory (29 May 1959) Confidential.

The Decomposition of Organic Resins at High Temperature in a Vacuum Environment, J.J. Mattice (Wright Air Development Division, Materials Central, Wright-Patterson AFB, Ohio) "Coatings for the Aerospace Environment, Proceedings of Meeting, Wright Air Development Division, (9-10 November 1960) p. 45, Wright Air Development Division, Wright-Patterson AFB, Ohio, WADD TR 60-773.

Ceramic Materials for High Temperature Aerospace Applications, Presented at the ARS Lifting Re-entry Vehicles: Structures, Materials and Design Conference, Palm Springs, Calif., (4-6 April 1961), W.E. Blodgett, R.B. Grekila, H.D. Root (Westinghouse Electric Corp., Research Labs., Pittsburgh, Pa.) American Rocket Society, Inc., New York, N.Y. (1686-61).

Spalding, D.B., Heat and Mass Transfer in Aeronautical Engineering, Aeronautical Quarterly (1960). p. 105.

2. Transpiration

Beckwith, I.E., Similar Solutions for the Compressible Boundary Layer on a Yawed Cylinder with Transpiration Cooling - Vary Cooling, Npr. NACA TN 4345 (1958).

Brunk, W.E., Experimental Investigation of Transpiration Cooling for a Turbulent Boundary Layer in Subsonic Flow Using Air as a Coolant, NACA TN 4091 (October 1957).

Dorrance, W.H. and F.J. Dore, The Effect of Mass Transfer on the Compressible Turbulent Boundary Layer Skin Friction and Heat Transfer, J. Aeron. Sci., 21 (1954) pp. 404.

Eckert, E.R.G., P.J. Schneider, A.A. Hayday, and R.M. Larson, Mass Transfer Cooling of a Laminar Boundary Layer by Injection of a Light-Weight Foreign Gas, Jet Propulsion, 28, (January 1958) pp. 34-39.

Green, L. and K.L. Nall, Experiments on Porous Wall Cooling and Flow Separation Control in a Supersonic Nozzle, IAS annual meeting (January 1959).

Howe, J.T. and W.A. Mersman, Solutions of the Laminar Compressible Boundary Layer Equations with Transpiration Which are Applicable to the Stagnation Regions of Axisymetric Blunt Bodies (1958).

Koffel, W.K., Preliminary Experimental Investigation of Transpiration Cooling for an Afterburner with a Sintered Porous Stainless Steel Combustion Chamber Wall, NACA RM E53D08 (June 1953).

Lees, L., Convective Heat Transfer with Mass Addition and Chemical Reactions, paper presented at third AGARD Combustion and Propulsion Panel Colloquim, Palermo, Italy (17-21 March 1958).

Swenson, B.L., An Approximate Analysis of Film Cooling on Blunt Bodies by Gas Injection Near the Stagnation Point (September 1961) National Aeronautics and Space Administration, Washington, D.C., TN D-861.

Low, G.M., The Compressible Laminar Boundary with Fluid Injection, NACA TN 3404 (March 1955).

Mickley, H.S., R.C. Ross, A.L. Squyres, and W.E. Stewart, Heat, Mass and Momentum Transfer to Flow Over a Flat Plate with Blowing or Suction, NACA TN 3208 (July 1954).

Papell, S.S. and A.M. Trout, Experimental Investigation of Air Film Cooling Applied to an Adiabatic Wall by Means of an Axially Discharging Slot, NASA TN D9 (1958).

Roberts, L. Mass Transfer Cooling Near the Stagnation Point, NASA TR R-8, (1959) Supercedes NACA TN 4391.

Rubesin, M.W. and M. Inouye, A Theoretical Study of the Effect of Upstream Transpiration Cooling on the Heat Transfer and Skin Friction Characteristics of a Compressible Laminar Boundary Layer, NACA TN 3969 (May 1957).

Baer, D. and A. Ambrosio, Heat Conduction in a Semi-Infinite Slab with Sublimation at the Surface, TR-59-0000-00610, STL (24 February 1959).

Bernicker, R.P., An Investigation of Porous Wall Cooling, ASME Paper 50-WA-233 (1960).

Cohen, C.B., R. Bromberg and R.P. Lipkis, Boundary Layers With Chemical Reactions Due to Mass Addition, Jet Propulsion, 28, (10), 659 (October 1958).

Cornish, J.J., A Universal Description of Turbulent Boundary Layer Profiles With or Without Transpiration, Miss. State U., AD 238 068 (20 June 1960).

Chung, P.M. Shielding Stagnation Surfaces of Finite Catalytic Activity by Air Injection in Hypersonic Flight, NASA TN D-27 (August 1959).

Dooley, D. and R. Dennison, Combustion in the Laminar Boundary Layer of Chemically Active Sublimators, Aeronutronics, Systems Pub. U-110 (23 September 1957).

Fanucci, J.B. and H.G. Lew, Effect of Mass Transfer and Body Forces on Two Phase Boundary Layers, Aerophysics Research Memo 35, GE Rept. R59SD 380 (April 1959).

Giedt, W.H., L.L. Cobb, Jr. and E.J. Russ, Effect of Hydrogen Recombination on Turbulent Flow Heat Transfer, ASME Paper 60-WA-256 (1960).

Gross, J.J., D.J. Masson and C. Gazley, Jr., General Characteristics of Binary Boundary Layers with Applications to Sublimation Cooling, Rept. P1371 (8 May 1958).

Hartnett, J.P., D.J. Masson, J.F. Gross, and C. Gazley, Jr., Mass Transfer Cooling in a Turbulent Boundary Layer, IAS Paper 60-66 (28 June to 1 July 1960).

Hartnett, J.P. and E.R.G. Eckert, Mass Transfer Cooling with Combustion in a Laminar Boundary Layer, 1958 Heat Transfer and Fluid Mech. Inst. (June 1958), p. 54-68.

Rubesin, M.W., The Influence of Surface Injection on Heat Transfer and Skin Friction Associated with the High Speed Turbulent Boundary Layer, NACA Research Memorandum No. A55L13 (20 February 1956).

Rubesin, M.W., C.C. Pappas and A.F. Okuno, The Effect of Fluid Injection on the Compressible Turbulent Boundary Layer--Preliminary Tests on Transpiration Cooling of a Flat Plate at m = 2.7 with Air as the Injected Gas, NACA Research Memorandum No. A55L19 (21 December 1955).

Rubesin, M.W., An Analytical Estimation of the Effect of Transpiration Cooling on the Heat Transfer and Skin Friction Characteristics of a Compressible Turbulent Boundary Layer, NACA TN 3341 (December 1954).

Rubesin, M.W. and C.C. Pappas, An Analysis of the Turbulent Boundary Layer Characteristics on a Flat Plate with Distributed Light Gas Injection, NACA TN 4149 (February 1958).

Steinberger, R.L. and R.E. Treybal, Mass Transfer from a Solid Soluble Sphere to a Flowing Liquid Stream, AICHE Journal (June 1960).

Knuth, E.L., Compressible Couette Flow with Diffusion of a Reactive Gas from a Decomposing Wall, 1958 Heat Transfer and Fluid Mech. Inst. (June 1958), p. 104-113.

Leadon, B.M. and C.J. Scott, Mass Transfer Cooling at Mach Number 4.8, J. Aeronautical Sci., 25, 67 (January 1958).

Leadon, B.M. and C.J. Scott, Measurement of Recovery Factors and Heat Transfer Coefficients with Transpiration Cooling in a Turbulent Boundary Layer at M = 3.0 Using Air and Helium as Coolants, Research Rept. 126, Inst. of Tech., Univ. of Minn. (February 1956).

Pappas, C.C., Effect on Injection of Foreign Gases on the Skin Friction and Heat Transfer of the Turbulent Boundary Layer, IAS Rept. 59-78 (January 1959).

Sherwood, T.K. and O. Trass, Sublimation Mass Transfer through Compressible Boundary Layers on a Flat Plate, ASME 59-A-137 (1959).

Short, W.W., Heat Transfer and Sublimation at a Stagnation Point in Potential Flow, ASME Paper 60-WA-20 (1960).

Sogin, H.H. and V.S. Subramanian, Local Mass Transfer From Circular Cylinders in Cross Flow, ASME Paper y0-WA-193 (1960).

Stewart, J.D., Transpiration Cooling: An Engineering Approach, G.E. Rept. MSVD-TIS-R59SD338 (1 May 1959).

Turcotte, D.L., On the Turbulent Boundary Layer with Fluid Injection, Cornell Univ. AD 236 963 (1 August 1960).

Howe, J.T., Shielding of Partially Reflecting Stagnation Surfaces Against Radiation by Transpiration of an Absorbing Gas, National Aeronautics and Space Administration, Washington, D.C., TR R-59 (1961).

Pallone, A., Non-Similar Solutions of the Compressible Laminar Boundary Layer Equations with Applications to the Upstream Transpiration Cooling Problem, Avco RAD-TR-9-60-8 (10 March 1960).

Pallone, A. and W. Van Tassel, Similar Solutions of the Compressible Laminar Boundary-Layer Equations for Air in Equilibrium with and without Air Injection at the Stagnation Region, Avco RAD-TM-61-22 (June 1961).

Chung, P.M., A Simplified Study on the Nonequilibrium Couette and Boundary-Layer Flows with Air Injection, NASA Technical Note D-306, (February 1960).

Bromberg, R. and R.P. Lipkis, Heat Transfer in Boundary Layers with Chemical Reactions Due to Mass Addition, Jet Propulsion, 28, (October 1958) pp. 668-674.

Seban, R.A., Heat Transfer and Effectiveness for a Turbulent Boundary Layer with Tangential Fluid Injection, ASME Paper 59-A-177 (1959).

C. HEAT SINKS

Pohle, F.V. and J.L. Boccio, Transient Temperature Distributions in a Sphere Due to Aerodynamic Heating, Polytechnic Inst. of Brooklyn, N.Y., PIBAL Rept. No. 553 (23 September 1959).

Broglio, L., Heat Conduction in Solids at Hypersonic Speed, SIARgraph No. 45; Technical Note No. 5 (October 1958).

Schlenker, G., An Approximate Solution to Transient Heat Transfer in Compound Thin Shells and Slabs as Applied to the Little John Temperature Conditioning Problem, Rock Island Arsenal, Ill., Technical Rept. No. 58-146 (1 February 1958).

Stalder, J.R., The Useful Heat Capacity of Several Materials for Ballistic Nose-Cone Construction, National Advisory Committee for Aeronautics, Washington, D.C., Technical Note TN-4141 (November 1957).

Hill, P.R., A Method of Computing the Transient Temperature of Thick Walls from Arbitrary Variation of Adiabatic-Wall Temperature and Heat-Transfer Coefficient, National Advisory Committee for Aeronautics, Technical Note TN 4105 (October 1957).

Nonweiler, T., Skin Temperatures and Heat Transfer Over Wedge at Extreme Speeds, College of Aeronautics, Cranfield (Gt. Brit.) Rept. No. 105 (August 1956).

Masson, D.J., Skin Temperature Variation During Re-entry of Scientific Satellite, Rand Corp., Santa Monica, Calif. Research Memo. No. RM-1693 (30 March 1956).

Masson, D.J. and C. Gazley, Jr., Surface-Protection and Cooling Systems for High-Speed Flight, Rand Corp., Santa Monica, Calif., Rept. No. RM-1735 (23 March 1956).

Gazley, C., J.H. Huth, and M.C. Horn, Transient Heat Conduction in Composite Slabs for a Heat Flux Varying Exponentially with Time, Rand Corp., Santa Monica, Calif., Research Memo No. RM-1524 (22 July 1955).

Trimpi, R.L. and R.A. Jones, Transient Temperature Distribution in a Two-Component Semi-Infinite Composite Slab of Arbitrary Materials Subjected to Aerodynamic Heating with a Discontinuous Change in Equilibrium Temperature of Heat-Transfer Coefficient, National Advisory Committee for Aeronautics, Washington, D.C., Technical Note TN 4308 (September 1958).

Gavril, B.D. and F. Lane, Finite Difference Equations and Their Solution for the Transient Temperature Distribution in Composite, Anisotropic, Generalized Bodies of Revolution, General Applied Science Laboratories, Inc., TR 230 26 May 1961.

Collins, J.O. and S. Speil, Ablation, Heat Sink and Radiation: The Materials That Make Them Work, Materials in Design Engineering, 53, No. 3 (March 1961).

Enig, J.W., A Method for the Rapid Numerical Solution of the Heat Conduction Equation for Composite Slabs, Project NOL 321 NAVO Report 6666, Naval Ordnance Laboratory, White Oak, Md. (20 August 1959).

Poritsky, H. and R.A. Powell, Certain Solutions of the Heat Conduction Equations, Quarterly of Applied Mathematics, XVIII, No. 2 (July 1960).

Strinner, G.T., Analog Network to Convert Surface Temperature to Heat Flux, ARS Journal (June 1960) p. 569.

Forster, C.A., Finite Difference Approach to Some Heat Conduction Problems Involving Changes of State, AD 39 378.

Goodman, T.R., The Heating of Slabs with Arbitrary Heat Inputs, Journal of Aero/Space Sci. (March 1959).

Libby, P.A., Preliminary Analysis of the Capabilities of a Composite Slab for an Advanced Heat Sink Design, WADD Tech. Note 59-424, Part II (1959).

Lieblin, S., Analysis of the Temperature Distribution and Radiant Heat Transfer Along a Rectangular Fin of Constant Thickness, NASA TN D-196.

Otis, D.R., A Solution to the Heat Conduction Problems with Variable Thermal Properties and Melting At the Surface, 2J-7-009-TN Convair, (25 August, 1955).

Sutton, G.W., One Dimensional Heat Conduction with an Arbitrary Heating Rate, Journal of Aero/Space Sci. (November 1957).

Beck, J.V. and H. Hurwicz, Study of Thermal Discontinuities and Associated Temperature Disturbances in a Solid Subject to a Surface Heat Flux, Part II, RAD-TR (In publication).

Beck, J.V. and H. Hurwicz, Study of Thermal Discontinuities and Associated Temperature Disturbances in a Solid Subject to a Surface Heat Flux, Part I, Avco RAD-TR-2-59-5 (23 December 1958).

Beck, J.V. and H. Hurwicz, Study of Thermal Discontinuities and Associated Temperature Disturbances in a Solid Subject to a Surface Heat Flux, Part I, Effect of Thermocouple Cavity Near Heat Sink Surface on a Sink Temperature Distribution and its Measurement, Avco RAD-TR-9-59-5 (20 February 1959).

Beck, J.V., Simplified Analytical Method to Determine Surface Temperature in a Solid Heat Sink, Avco RAD-2-TM-58-131(December 1958).

Hurwicz, H. and M.S. Klamkin, Reliability of Re-entry Vehicle Heat Sink Temperature and Thickness Calculations, Avco RAD-TR-2-58-3, Rev. 1 (27 March 1959).

Hervay, G., Temperature Distribution in a Slab Moving from a Chamber at One Temperature to a Chamber at Another Temperature, ASME Paper 60-WA-197 (1960).

Mascola, R., Temperature Response in Slabs Subject to a Sinusoidal Heat Pulse, Avco RAD-9(7)-TM-60-72 (15 December 1960).

Beck, J.V., A Thermal Study of Composite Heat Sinks, ASME 60-SA-22 (1960).

Chu, W., and H.N. Abramson, Transient Heat Conduction in a Rod of Finite Length with Variable Thermal Properties, ASME Paper 60-WA-25 (1960).

Goodman, T.R., The Heat-Balance Integral -- Further Considerations and Refinements, ASME Paper 60-SA-9 (1960).

Brown J. and H. Hurwicz, Thermal Study of a Minimum Weight Copper-Stainless Composite for the Heat Sink of the ICBM Re-entry Vehicle, Avco RAD-2-TM-57-53 (11 September 1957) Confidential.

Gavril, B.D. and F. Lane, Finite Difference Equations and Their Solution for the Transient Temperature Distribution in Composite, Anisotropic, Generalized Bodies of Revolution, General Applied Science Laboratories, Inc., Westbury, N.Y., TR 230 (26 May 1961).

Carslaw and Jaeger, Conduction of Heat in Solids, 2nd Ed., Oxford Univ. Press (1960).

Hickel, R.O., R.P. Cochran, C.R. Morse and R.P. Dengler, Experimental Investigation of Lithium Hydride and Water Absorbers as Possible Heat Sink Materials for Hypersonic and Re-entry Vehicles (To be published).

LoPilato, S.A., C.H. Hastings, Electromagnetic Determination of Nickel Thickness for Re-entry Vehicle Heat Sinks, Materials Research and Standards, 1, No. 3 (March 1961).

II. THERMAL PROTECTION SYSTEMS FOR SPECIFIC REGIMES

A. APPLICATIONS OF BASIC HEAT AND MASS TRANSFER MECHANISMS

Brown, J.D. and H. Hurwicz, Evaluation of Heat Transfer in Heat Shields of RVX1 (Able) Re-entry Vehicles, Part I, Solid Segmented Quartz Heat Shield, Avco RAD-9-TM-59-3 (11 February 1959) Secret.

Collins, J.A. and J.D. Brown, Effects of Flight Envelope Parameters on the Thermal Performance of the Titan Re-entry Vehicle (U), Avco RAD-7-TM-60-61, (7 September 1960) Confidential.

Collins, J.A., Protecting the Minuteman Nose Cone Against Ascent Heating, Avco RAD-7-TM-60-60 (7 September 1960) Secret.

Collins, J.A. and H. Hurwicz, Thermal Study of the Shape 52 Bi-metallic and Magnesium Back-up Heat Sinks, Avco RAD-2-TM-57-55 (27 August 1957) Confidential.

DiPietro, A.L., Evaluation of Heat Transfer in Heat Shields of RVX 3 Re-entry Vehicles, (Quartz and Fiberquartz Materials), Avco RAD-9-TM-59-16 (1959) Secret.

Hurwicz, H., Thermal Analysis of Effects of Voids and Imperfections in the Copper Heat Sink of Shape 13 (U), Avco RAD-2-TM-57-36 (1 August 1957) Secret.

Hurwicz, H., R. Mascola, and J. Brown, Thermal Analysis of Shape 52 Afterbody (Temperature Distribution and Thickness Determination in One-Dimensional Flow), Avco RAD-2-TM-58-18, Rev. 1 (8 April 1958) Secret.

Hurwicz, H., Glass Laminated Plastic Aftershell of Shape 13 Afterbody, Avco RAD-2-TM-57-14 (9 May 1957) Secret.

Hurwicz, H., Stainless Cladding of Shape 550, Avco RAD 04102 (3 August 1956).

Hurwicz, H., Thermal Analysis of Shape 13 Heat Sink, Avco RAD-2-TM-57-40 (30 July 1957) Secret.

Hurwicz, H. and J. Graham, Evaluation of Calculation Procedures Used in Determination of Heat Transfer Rates from 'X-17' Flight Test Data (U), Avco RAD-2-TM-57-24 (22 May 1957) Secret.

Hurwicz, H. and J. Brown, Thermal Analysis of RVX 1 (1, 2, 3, 5, and 6) (Temperature, ablation, and thickness distribution) (16 February 1959).

Hurwicz, H., Thermal Behavior of the Separation Connector on the Afterbody of Shape 13 (U), Avco RAD-2-TM-57-6 (12 April 1957) Confidential.

Graham, J. and H. Hurwicz, Preliminary Thermal Analysis of a Minimum Weight Nickel-Copper-Stainless Composite for the Heat Sink of Shape 52, Avco RAD-2-TM-58-32 (19 March 1958) Secret.

Heller, G., Thermal Control of the Explorer Satellites, ARS Journal, 30, No. 4, (April 1960). pp. 344

Saviano, R.F., Summary of Temperature and Safety Factors for the Shape 52 Re-entry Vehicle Design (U), Avco RAD-2-TM-58-80 (3 July 1958) Secret.

Fleming, W.J., Jr. and F.L. Hines, Development and Evaluation of Re-entry Heating Prediction Methods in the Polaris Fleet Ballistic Missile Program, Fifth AFBMD-STL Symposium, Lockheed Aircraft Corporation, Missiles and Space Division, Sunnyvale, California (1961).

Ishimoto, T. and B.W. Randolph, Prediction of Transient Thermal Environment in Space Vehicles, Electrical Engineering, 79, No. 12 (December 1960).

Chapman, D.R., An Approximate Analytical Method for Studying the Entry into Planetary Atmosphere, NASA TR R-11.

Cheatham, D.C., A Concept of a Manned Satellite Re-entry Which is Completed with a Glide Landing (U), NASA TM X-226, Confidential.

Edgar, J.B., R.D. Hickel, F.S. Stepka, Preliminary Survey of Possible Cooling Methods for Hypersonic Aircraft (U), NACA RM E57L19 (1958) Confidential.

Eggers, A Discussion of Methods for Reducing Aerodynamic Heating in Supersonic Flight, NASA RM A 55F1 (September 1955).

Egger, J. B., and H. J. Allen, A Study of the Motions and Aerodynamic Heating of Missiles Entering the Earth's Atmosphere at High Supersonic Speeds, TN 4047 (1958).

Eggers, A.J., H.J. Allen and S.E. Neice, A Comparative Analysis of the Performance of Long-Range Hypervelocity Vehicles, NACA TN 4046 (1958).

Goodman, G.P. and J. Betts, Exploratory Environmental Tests of Several Heat Shields, National Aeronautics and Space Administration, Washington, D.C., TN D-897 (September 1961).

Henze, W., Jr., The Re-entry Problem, Drexel Inst. ARS (1959).

Hill, J.A., Satellite Re-entry with Lightly Loaded Lifting Vehicles, MIT Naval Supersonic Lab TR 429 (December 1959).

Hurwicz, H. and J.D. Brown, Interaction of Ablation, Material, and Certain Trajectory Parameters in the Thermal Protection Design of Space Re-entry Vehicles (U), Avco RAD-TR-9(7)-59-28 (19 November 1959) Confidential.

Lee, D.H.K. and J.A. Vaughan, Studies on Thermal Effects of Solar Radiation in Transportable Solar Chamber, ASME Paper 60-WA-251 (1960).

Miele, A., Optimum Burning Program As Related to Aerodynamic Heating for a Missile Traversing the Earth's Atmosphere, Dept. Aeronaut Eng, Purdue University, Lafayette, Ind., ARS (1957).

Roth, C.E., Jr., P.E. Prout, and J.T. Mosich, Design Criteria for Upper Atmpshere Sounding Vehicles, Aerojet-General, ARS 813-59 (1959).

Stalder, J.R., A Survey of Heat Transfer Problems Encountered by Hypersonic Aircraft, NACA, Ames Aeronaut, Moffett Field, Calif., ARS (1957).

Steg, L., Materials for Re-entry Heat Protection of Satellite, ARS Preprint 836-59, Semi-Annual Meeting, San Diego (June 1959).

Vandrey, F., Upper Bounds and Conservative Estimates for Aerodynamic Heating at Great Altitudes, Martin, Baltimore, ARS (1956).

Warren, W.R. and N.S. Diaconis, The Performance of Ablation Material As Heat Protection for Re-entry Satellites, IAS Paper 60-49 (1960).

Wong, T.J., G. Goodwin and R.E. Slye, Motion and Heating during Atmosphere Re-entry of Space Vehicles, NASA TN D-334 (September 1960).

Hurwicz, H. and J.D. Brown, Critical Aero-Thermodynamic Parameters in Thermal Protection Design of High-Performance Re-entry Bodies, Presented at ARS Space Flight Report to the Nation, New York (October 1961) Paper No. 2151-61, also Avco RAD-TR-61-18 (June 1961).

Roberts, L., An Analysis of Ablation-Shield Requirements for Manned Re-entry Vehicles, NASA-TR-R-62 (1960).

Swann, R.T., Composite Thermal Protection Systems for Manned Re-entry Vehicles, Presented at the ARS 15th Annual Meeting, Washington, D.C. (5-8 December 1960). National Aeronautics and Space Administration, Langley Research Center, Langley Field, Va. , American Rocket Society, Inc., New York, N.Y., (1569-60).

Collins, J.A., D. Moodie, Thermal Insulation for Lifting Re-entry Vehicles, Presented at the ARS Lifting Re-entry Vehicles: Structures, Materials and Design Conference, Palm Springs, Calif., (4-6 April 1961), (Avco Corp., Research and Advanced Development Division, Wilmington, Mass.) American Rocket Society, Inc., New York, N.Y., (1684-61).

Sutton, W.H., Development of Composite Structural Materials for Space Vehicle Applications, Presented at the ARS Lifting Re-entry Vehicles: Structures, Materials and Design Conference, Palm Springs, Calif. (4-6 April 1961), (General Electric Co., Missile and Space Vehicle Dept., Philadelphia, Pa.), American Rocket Society, Inc., New York, N.Y. (1685-61).

Fried, E., The Interface Thermal Contact Resistance Problem in Space Vehicles, Presented at the ARS Lifting Re-entry Vehicles: Structures, Materials and Design Conference, Palm Springs, Calif. (4-6 April 1961) (General Electric Co., Schenectady, N.Y.), F.A. Costello (General Electric Co., Missile and Space Vehicle Dept., Philadelphia, Pa.), American Rocket Society, Inc., New York, N.Y. (1690-61).

Murphy, A.J., Materials for Astronautic Vehicles, Presented at the AGARD Symposium on Astronautics, Univ. of Rome, Italy (May 1959), Great Britian, College of Aeronautics, Cranfield, CoA Report 139.

Collins, J.A., C. Toscano, D. Moodie, and W. Wolz, Transient Behavior of Composite Thermal Protection Systems, Presented at the ARS Lifting Re-entry Vehicles: Structures, Materials and Design Conference, Palm Springs, Calif. (4-6 April 1961) (Avco Corp., Research and Advanced Development Div., Wilmington, Mass.) American Rocket Society, Inc., New York, N.Y. (1695-61).

Alvis, J.F. and G.B. Whisenhunt, A Thermal Protection System for Lifting Re-entry Vehicles, Presented at the ARS Lifting Re-entry Vehicles: Structures, Materials and Design Conference, Palm Springs, Calif. (4-6 April 1961) (Chance Vought Corp., Astronautics Div., Dallas, Texas) American Rocket Society, Inc., N.Y., (1698-61).

Kaufman, W.F., W.H. Armour, and L. Green, Jr., Thermal Protection Methods for Fluorine-Hydrogen Rockets, Sixth Symposium on Ballistic Missile and Aerospace Technology (August 1961) Los Angeles, California.

Kemp, H.H., and R.F. Riddell, Re-entry Heat Transfer to Satellite Vehicles, Jet Propulsion, 27 (February 1957) pp. 132-137, 147.

Rumsey, C.B. and D.B. Lee, Heat-Transfer Measurements on a Blunt Spherical-Segment Nose to a Mach Number of 15.1 and Flight Performance of the Rocket-Propelled Model to a Mach Number of 17.8(U), NASA TM X-77 (November 1959) Confidential.

USAF-NASA Joint Conference on Lifting Manned Hypervelocity and Re-entry Vehicles (U) (11-14 April 1960) Part I: Confidential, Part II: Secret:

Vitale, A.J. and J.B. Arnaiz, Flight Performance and Aerodynamic Data from Full Scale Flight Tests of Advanced Ballistic Re-entry Vehicles, G.E. Company, Missile and Space Vehicle Department, Philadelphia 4, Pennsylvania, Fifth AFBMD-STL Symposium (1961).

Collins, J.A., Thermal Evaluation of Various Insulators for Heat Shields of ICBM Re-entry Vehicles (Avco TR to be published).

Wood, R.M., R.E. Lowe, H.T. Ponsford, and J.F. Modewell, Thermostructural Design Entry Vehicles for Mars and Venus, Presented at ARS Structural Design of Space Vehicle Conference, Engineering Paper No. 976 (6-8 April 1960).

Moody, D.M. and J.A. Collins, Development of Advanced Insulations for Ballistic Re-entry Vehicles, Avco RAD-TM-61-29 (7 September 1961).

Brown, J.D. and F.A. Shukis, An Approximate Method for Design of Thermal Protection Systems, to be presented at IAS 30th Annual Meeting (January 1962) New York.

Adams, E.W., Analysis of Quartz and Teflon Shields for a Particular Re-entry Mission, Proc. of 1961 Heat Transfer and Fluid Mech. Inst., Pasadena, California (June 1961) p. 222.

Nolan, E.J. and S.M. Scala, The Aerothermodynamic Behavior of Pyrolytic Graphite During Sustained Hypersonic Flight, ARS Conference on Lifting Re-entry Vehicles, Palm Springs, California, Paper No. 1696-61 (April 1961).

Georgiev , S., H. Hidalogo, and M. Adams, On Ablation for the Recovery of Satellites, Avco Research Laboratory Report 47 (6 March 1959).

Glazer, P.E., Thermal Protection of Space Vehicles, Astronautics (April 1960).

Kelley, O.A., Jr., Parametric Weight Study of a Manned Space Entry Vehicle, LAS Paper No. 60-56 (1956).

Lees, L., Laminar Heat Transfer over Blunt-Nosed Bodies at Hypersonic Flight Speeds, Jet Propulsion, 26, No. 4 (April 1956) pp. 259-269.

Report on Thermal Protection System, National Academy of Sciences, Report No. MAB 151-M (June 1959) Confidential.

Roberts, L., An Analysis of Nose Ablation for Ballistic Vehicles, NASA TN D-254 (28 April to 12 May 1960).

Salmassy, O.K., Thermal Protection Systems for Aerodynamic Heating. Part I: Simplified Definitions for Aerodynamic Heating, Avco RAD (June 1959).

Servoss, W.C., and R.A. Foust, Midwest Research Institute Kansas City, Mo. (1960). Development of a system to protect aircraft personnel and equipment from intense thermal radiation (atom bomb thermal protection) primarily search for material which would exhibit reversible color change.

Spindler, R.J., and T.R. Munson, Thermal Response of Missiles which Traverse Nuclear Fireballs, Avco Research and Advanced Development Division, Wilmington, Massachusetts, Fifth AFBMD-STL Symposium (1961).

Swann, R.T., An Engineering Analysis of the Weights of Ablating Systems for Manned Re-entry Vehicles, National Aeronautics and Space Administration, Langley Research Center, Langely Field, Virginia, Fifth AFBMD-STL Symposium (1961).

Wing, D.D., Evaluation of Thermal Problems at Relatively Low Orbital Altitudes, Aero/Space Engineering (March 1960).

Allen, H.J., and A.J. Eggers, Jr., A Study of the Motion and Aerodynamic Heating of Missiles Entering the Earth's Atmosphere at High Supersonic Speeds, NACA TN 4047 and NACA 1381 (1958).

Chrysler, Advanced Techniques in the Design and Testing of the Redstone Re-entry Body, Part II, AD134 318 (1956).

Sutton, G.W., S.M. Scala, L. Gilbert, and S. Blecher, SARV Trajectory Re-entry Ablation, GE MSVD Aerophysics PIR 58 (December 1958).

Detra, R.W., F.R. Riddell and P.H. Rose, Controlled Recovery of Non-Lifting Satellites, Avco Everett Research Laboratory, ARS 784-59 (1959).

Cresci, R.J., D.A. MacKenzie, and P.A. Libby, An Investigation of Laminar, Transitional, and Turbulent Heat Transfer on Blunt-Nosed Bodies in Hypersonic Flow, J. Aero/Space Sci., 27, (6), 401 (June 1960).

Diaconia, N.S., J.B. Fanucci, and G.W. Sutton, The Heat Protection Potential of Several Ablation Materials for Satellite and Ballistic Re-entry into Earth's Atmosphere, 4th Ballistic Missile Symposium, Los Angeles (August 1959).

Eggers, A.J., Jr., T.J. Wong, and R.E. Slye, Some General Considerations of the Heating of Satellites, J. Heat Transfer, ASME Trans Ser C., 81, (4), 308 (November 1959).

Ehricke, K., Re-entry of Spherical Bodies into the Atmosphere at Very High Speeds, Convair-Astronautics, San Diego, ARS (1957).

Fiathers, A.E., Some Aerothermodynamic Considerations of Hypervelocity Vehicles, GE ARS (1959).

Hass, J., and L. F. Drummeter, Jr., Temperature Stabilization of High Reflecting Spherical Satellites, J. Opt. Soc. AM., 49 (9), 918 (1959).

Hurwicz, H., Practical Aspects of Re-entry Vehicle Design, III. Heat Protection Concepts, Lecture given at MIT, Cambridge, Mass. (17 April 1961).

Dukes, W., C. Gosden, G. Kappelt and A. Mirti, Manufacturing Methods for Insulated and Cooled Double Wall Structures, Vol. I,Bell Aerosystems Company. Contract: AF33(600)40100 ASD Project 7-999 Final Tech. Engineering Report (17 December 1959 to 10 March 1961).

Schmitt, A., W. H. Dukes, Development of Double Wall Cooling, Bell Aircraft Corp., Special Weapons Division. Presented at the Institute of Aeronautical Sciences National Midwestern Meeting on Guided Missiles at St. Louis, Missouri (12-14 May 1958).

Weatherston, R.C. and W.E. Smith, A New Type of Thermal Radiator For Space Vehicles, Aero/Space Engineering, 20, No. 1 (January 1961).

Scala, E., Composite Material for Thermal Protection, Metals Review, 33 No. 11 (November 1960).

Gruntfest, I.J., and L.H. Shenker, Thermal Protection for Re-entry, Rocket and Missile Technology, Chemical Engineering Progress Symposium Series No. 33, 57 (1961).

Lux, J.H., Insulation Materials in Missile Applications,Rocket and Missile Technology, Chemical Engineering Progress Symposium Series No. 33, 57 (1961).

B. THERMOSTRUCTURAL PROBLEMS

Anderson, R.A. and R.T. Swann, Structures for Re-entry Heating, USAS-NASA Joint Conference on Lifting Manned Hypervelocity and Re-entry Vehicles (U), Part I (11-12 April 1960). Confidential.

Braun, M.T. and Czarnecki, Structural Aspects of Earth Glide Re-entry Vehicles, American Astronautical Society, Preprint, No. 58-9 (1958).

Budiansky, B. and J. Mayers, Influence of Aerodynamic Heating on the Effective Torsional Stiffness of Thin Wings, IAS Preprint No. 579.

Coppa, A.P., Structural Considerations of Manned Space Vehicles, ARS Journal (January 1960), Note: Radiation Shield Application.

Cord, J.M. and A.B. Burns, Some Aspects of Designing Aluminum Structures for Thermal Environments, IAS Paper No. 60-7 (1960).

Czarnecki, E.C. and G.N. Davison, Dyna-Soar-Glider Flight-Envelope Structural Parameters, USAF-NASA Joint Conference on Lifting Manned Hypervelocity and Re-entry Vehicles (U), Part II (13-14 April 1960). Secret.

Davidson, J.R., Optimum Design of Insulated Tension Members Subjected to Aerodynamic Heating, NASA TN D-117.

Dow, Morris F., A Re-evaluation of Some Airframe Thermal Problems, IAS Preprint No. 639.

Duberg, J.E., Aircraft Structures Research at Elevated Temperatures, Presented to Structures and Materials Advisory Group for Aeronautical Research and Development (NATO) London, England (September 1955).

Goldberg, M.A., Investigation of the Temperature Distribution and Thermal Stress in a Hypersonic Wing Structure, IAS Preprint No. 577.

Heldenfields, R.R., Some Elevated Temperature Structural Problems of High-Speed Aircraft, SAE Preprint No. 599.

Hepler, A.K., B.E. Landry and M.A. Nelson, Development of Truss-Type Dyna-Soar Glider Structures, USAF-NASA Joint Conference on Lifting Manned Hypervelocity and Re-entry Vehicles (U), Part II (13-14 April 1960) Secret.

Gilbey, D.M., An Estimation of the Thermal Stresses During Re-entry in Graphite Heat Shields for Blue Streak Black Knight and Leopard, Royal Aircraft Establishment Tech. Note No. Met. 306 (December 1958).

Mar, J.W. and L.H. Schmit, Some Structural Penalties Associated with Thermal Flight, ASME Preprint No. 56-AV-9 (1956).

Martin, J.E., M.L. Richards, W.W. Kitts and W.W. Hoy, Aircraft Load and Temperature Design Criteria Through Simulation and Random Processes, IAS Paper No. 59-86 (1959).

Morgan, A.J.A. and C. Christensen, Thermal Stresses in Missile Nose Cones, IAS Paper No. FF-24.

Parkes, E.W., Wings Under Thermal Stresses, Aircraft Engineering (December 1954).

Fruendenthal, A.M., On Inelastic Thermal Stresses in Flight Structures, IAS Preprint No. 429.

Pridies, R.A., R.M. Royster, and B.F. Helms, Experimental Study of a Hot Structure for a Re-entry Vehicle, USAF-NASA Joint Conference on Lifting Manned Hypervelocity and Re-entry Vehicles (U), Part I (11-12 April 1960) Confidential.

Rubesin, M.W., The Influence of Aerodynamic Heating on the Structural Design of Aircraft, Report 207, NATO Advisory Group for Aeronautical Research and Development (October 1958).

Schmitt, A., M.A. Brull, and H.S. Wolko, Optimum Stresses of Structural Elements at Elevated Temperatures, ASME Preprint No. 56-AV-11 (1956).

Steinbacher, F.R. and L. Young, Problems in the Design of Aircraft Subjected to High Temperatures, Trans. of the ASME, 77, No. 5 (July 1955).

WADC, Insulation Study for Airframe Structures, WADC TR 58-131, AD 151108 (1958).

Ingram, J.C., Jr., Current Status of Refractory Metals for Structural Applications, USAF-NASA Joint Conference on Lifting Manned Hypervelocity and Re-entry Vehicles (U), Part II (13-14 April 1960) Secret.

Hurwicz, H. and J.D. Brown, Critical Aero-Thermodynamic Parameters in Thermal Protection Design of Space Re-entry Bodies, Part II: Trajectory and Structural Design Criteria Considerations, Avco RAD-TR- (to be published).

Chicago Midway Lab., Thermal Protection of Structural Propulsion, and Temperature Sensitive Materials for Hypersonic and Space Flight, CML-DR-M152-2 (October 1958).

Coppa, A.P., Structural Considerations of Manned Space Vehicles, Missile and Ordnance Systems Dep. GE, Philadelphia, ARS J., 28, 732 (1958).

Gerard, Some Structural Aspects of Orbital Flight, Coll. Eng. ARS J., Vol. 28, 769 (1958).

Hoff, N.J., High Temperature Structures, AD 238 415 (27 June 1960).

Mueller, R.S. and G.D. Cremer, Brazed Sandwich Structures for Missiles and Vehicles, Solar Aircraft, San Diego, ARS, J., 28, 730 (1958).

Sandorff, P.E., Structures for Space Craft, MIT, 28, 733 (1958).

Wood, R.M. and H.T. Ponsford, Thermo-Structural Design for High Temperature Flight, U. Douglas, Eng. Paper 664 (1958). Secret

Hoff, N.J., The Thermal Barrier-Structures, Trans. of the ASME, 77, No. 5 (July 1955).

Hepler, A.K., W.E. Backus, and G.B. Smith, Dyna-Soar Skin Panel Development, USAF-NASA Joint Conference on Lifting Manned Hypervelocity and Re-entry Vehicles (U), Part II (13-14 April 1960) Secret.

Davis, J.E., J.E. Fischler, J.W. Lobbett, Investigation into More Complete Use of Structural Materials Through a Study of the Stress-Temperature- Time Conditions of a Re-entry Vehicle, WADD TR 60-363 (1960).

Walton, J.D., Present and Future Problem Areas for High Temperature Inorganic Coatings, Amer. Ceramic Society Bulletin, 40, No. 3 (March 1961).

Ponsford, H.T., R.M. Wood and R.E. Lowe, Thermostructural Design-Entry Vehicles for Mars and Venus, ARS Journal 31, No. 4, (April 1961).

Van Der Maas, C.J., The Airframe Exposure at High Supersonic Speeds, Proceedings of the Florida Conference on High-Speed Aerodynamics and Structures, II. Confidential.

Davidson, J.R., Optimum Design of Insulated Tension Members Subjected to Aerodynamic Heating, NASA TM D-118 (December 1959).

Hurton, W.H., The Influence of Kinetic Heating on the Design and Testing of Aircraft Structures, Centennial Celebrations Symposium, PIB (1955).

Hoff, N.J., The Effects of Temperature and Time on Aircraft and Missile Structures, Stanford University, Stanford, Calif., SUDAER 99, AFOSR-TN-61-646 (January 1961).

Rosen, B.W., Stresses in Char Layer, Avco RAD-TRR-T300-AM-60-15, (December 1960).

Ponsford, H.T., R.M. Wood, R.E. Lowe, and J.F. Madewell, Thermo-structural Design - Entry Vehicles for Mars and Venus, ARS J., 31, p. 474 (April 1961).

Becker, H., Simplified Thermal Stress Analysis of Re-entry Structures, Presented at the ARS Lifting Re-entry Vehicles: Structures, Materials and Design Conference, Palm Springs, Calif. (4-6 April 1961), New York University, New York, N.Y., American Rocket Society, Inc., New York, N.Y. (1692-61).

Batdorf, S.P., Structural Problems of Hypersonic Flight, Lockheed Missile Systems Div., Sunnyvale, Calif., ARS (1957).

Buell, D.N., Re-entry Structures, Thermal Stresses and Limit Designs, Chrysler, Detroit, ARS J., 28,606 (1958).

III. MATERIAL PROPERTIES DATA AND SYSTEM PERFORMANCE DATA

A. THERMAL AND OPTICAL PROPERTIES AND ABLATION CHARACTERISTICS

Adams, M.C., W.E. Powers, and S. Georgiev, An Experimental and Theoretical Study of Quartz Ablation at the Stagnation Point, AERL Research Rept. 57 (June 1959).

Bethe, H.A. and M.C. Adams, A Theory for the Ablation of Glassy Materials, J. Aero/Space Sci., 26, (6) 321 (September 1959).

Bromberg, R., Transport Property Requirements in Hypersonic Aerodynamics, Ramo-Wooldridge, Los Angeles, ARS J. (1957).

Grunfest, I.J. and L.H. Shenker, Behavior of Reinforced Plastics at Very High Temperatures, Modern Plastics (June 1958).

Grunfest, I.J., L.H. Shenker, and V.N. Saffire, Behavior of Reinforced Plastics at Very High Temperatures--Part II, Modern Plastics (April 1959).

Hidalgo, H., A Theory of Ablation of Glassy Materials for Laminar and Turbulent Heating, AERL Research Note 146 (June 1959).

Keyes, F.G., Summary of Measured Thermal Conductivities and Values of Viscosities, MIT, ARS J. (1957).

Reynolds, W.C., An Investigation of the Ignition Temperature of Solid Metals, AD 138 740 (June 1957).

Scala, S.M., Vaporization of a Refractory Oxide During Hypersonic Flight, 1959 Heat Transfer and Fluid Mech. Inst. (June 1959) p. 181-192.

Scala, S.M. and N.S. Diaconis, The Stagnation Point of Teflon During Hypersonic Flight, GE MSD Aerophysics and Advanced Aerodynamic PIR 86 (August 1959).

Spriggs, R.M. and C.N. Williams, Research on Elevated Temperature Resistant Structural Adhesives, AD 138 073 (June 1957).

Steg, L., Materials for Re-entry Heat Protection of Satellites, Paper Presented at ARS Semi-Annual Meeting, San Diego (June 1959).

Steg, L., Materials for Re-entry Heat Protection Systems, GE MSVD, ARS J. (1959).

Dukes, H.W., F.M. Anthony and H.A. Pearl, Investigation of Feasibility of Utilizing Available Heat Resistant Materials for Hypersonic Leading Edge Applications, Bell Aircraft Report 7008-0252-003.

Anthony, F.M. and H.A. Pearl, Selection of Materials for Hypersonic Leading Edge Applications, IAS Paper No. 59-111 (1959).

Eubanks, A. and D. Moore, Investigation of Aluminum Phosphate Coatings for Thermal Insulation of Air Frames, NASA TN D-106.

Friedman, H.L., The Pyrolsis of Plastics in a High Vacuum Arc Image Furnace, General Electric Company, Missile and Space Vehicle Department, Philadelphia 4, Pennsylvania, Fifth AFBMD-STL Symposium (1961).

Hanst, P.L. and A.C. Walker, Jr., The Infrared Emission Spectra of Plastics Ablating in a Low Enthalpy Air Stream: Measurements of Surface Temperatures and Temperature Profiles Behind the Surface, Avco RAD, Wilmington, Massachusetts, Fifth AFBMD-STL Symposium (1961).

Jennings, R.L. and C.R. Easton, Surface Temperature of Ablating Teflon, Report No. SM-35759, Douglas Aircraft Company (22 May 1959).

Madorsky, S.L., et al, Thermal Degradation of Tetrafluoroethylene and Hydrofluoroethylene Polymers in a Vacuum, Journal of Research, N.B.S., 51, 327 (1953).

Mathauser, E.E., Materials for Application to Manned Re-entry Vehicles, USAF-NASA Joint Conference on Lifting Manned Hypervelocity and Re-entry Vehicles (U), Part I (11-12 April 1960) Confidential.

Mertz, W. and T.E. Shaw, Ablation Characteristics of Phenolic Nylon in Re-entry Vehicle Tests, Fifth AFBMD-STL Symposium, General Electric Company, Missile and Space Vehicle Department, Philadelphia 4, Pennsylvania (1961).

Rashis, B., W.G. Witte, and R.N. Hopko, Qualitative Measurements of the Effective Heat of Ablation of Several Materials in Supersonic Air Jets at Stagnation Temperatures up to 11,000°F (U) (L58E22) (1958) Confidential.

Hansen, C.F., Approximations for the Thermodynamic and Transport Properties of High Temperature Air, NACA TN-4150 (March 1958).

Wilke, C.R., A Viscosity Equation for Gas Mixtures, The Journal of Chemical Physics, 18, No. 4 (April 1959) p. 517-519.

Mason, E.A. and S.C. Saxena, Approximate Formula for the Thermal Conductivity of Gas Mixtures, Physics of Fluids, 1, No. 5 (September-October 1958) p. 361-369.

Maloof, S.R., Tungsten Base Composite, Astronautics (April 1961).

Vogan, J.W., Thermal Protective Surfaces for Structural Plastics, WADD Technical Report 60-110, Part II (October 1960).

Rasor, N.S. and S.D. McCelland, Thermal Property Measurements at Very High Temperatures, The Review of Scientific Instruments, 31, No. 1 (June 1960) p. 595.

Welker, J.E., Comparison of Theoretical and Experimental Values for the Effective Heat of Ablation of Ammonium Chloride, NACA TN-D-553 (November 1960).

Touloukian, Y.S., Collecting, Correlating and Clearing Facilities for Data and Information on Thermophysical Properties, Purdue Univ. Lafayette, Ind. ARS J. (1957).

Walton, J.D., Fused Silica - A Material for Thermal Protection Systems, Georgia Tech., ARS J. (1959).

Zaleski, F.V. and L.F. Salzberg, The Role of Emissivity in the Design of Space Vehicles, WADC, ARS (1959).

Heat Transfer Characteristics of Beryllium as a Solid Heat Sink Material, Unpublished Thermodynamics Section Memo.

Sibulkein, M., Heat Transfer to an Incompressible Turbulent Boundary Layer and Estimation of Heat-Transfer Coefficients at Supersonic Nozzle Throat, J. Aeronaut Sci (February 1956).

UTC, Results of a Measurement of the Emissivity and Temperature of the Combustion Products in the Throat of a TM-3 End Burning Motor, United Technology Corp., Sunnyvale Calif., TM-33-61-U1 (21 June 1961).

Boehringer, J.C. and R.J. Spindler, On the Determination of Optical Properties for Calculations of Radiant Heating of Semi-Transparent Materials, presented at the Forty-Sixth Annual Meeting of the Optical Society of America, Paper TE-17, also Avco RAD-TM-61-36 (October 1961).

Savin, R.C., Ablative Properties of Plastics Under Simulated Re-entry Conditions, National Aeronautics and Space Administration, Ames Research Center, Moffett Field, California, Fifth AFBMD-STL Symposium (1961).

Scala, S.M. and E.J. Nolan, (GE) Aerothermodynamic Feasibility of Graphite for Hypersonic Glide Vehicles, Fifth AFBMD-STL Symposium (1961).

Siegle, J.L. and L.T. Muus, Pyrolysis of Polytetrafluoroethylene, Presented at the 130th National Meeting, American Chemical Society, Atlantic City, New Jersey (September 1956).

Sutton, G.W., Ablation of Reinforced Plastics in Supersonic Flow, Journal of the Aero/Space Sciences, 27, No. 5 (May 1960).

Swan, R.T., Calculated Effective Thermal Conductivity of Honeycomb Sandwich Panels, NASA TN D-171.

Adams, M.C., W.E. Power and S. Georgiev, An Experimental and Theoretical Study of Quartz Ablation at the Stagnation Point, J. of Aero/Space Sciences, 7 (July 1960) p. 535.

Bowman, G.H. and R.C. Savin, An Experimental Investigation in an Atmosphere Entry Simulator of Nylon as an Ablative Material for Ballistic Missiles, NASA TM X-114 (December 1959) Confidential.

Collins, J.A. and H. Hurwicz, Thermal Properties of Certain Materials, Avco RAD-TM-Thermo-2-57-2 (25 February 1957).

Collins, J.A., Preliminary Evaluation of Molybdenum as a Heat Sink Material (U), Avco RAD-2-TM-57-43 (16 August 1957) Confidential.

Collins, J.A., Thermo-Physical Properties of Pure Metals, Alloys, Non-Metals, and Plastics, Avco RAD-2-TR-58-20 (15 December 1958).

Collins, J.A., Preliminary Experimental Evaluation of Various Insulating Materials (U), Avco RAD-2-TM-58-35 (28 March 1958) Confidential.

Collins, J.A., Experimental Evaluation of Rigid and Porous Insulating Materials for Heat Shields of ICBM Re-entry Vehicles, Trans. of the 3rd Technical Symposium on Ballistic Missiles (Sponsored by the U.S. Air Force), Los Angeles, California (14-15 July 1958) Confidential.

Saffes, R.I. and D.S. Mayruth, Refractory Materials: Part II - High Temperature Behavior, Aero/Space Engineering (June 1960).

Serebryakova, T.I., B. Paderno and G.V. Samsonov, Emission Coefficients of Some Powdered High-Melting Compounds, Optics and Spectroscopy (March 1960) p. 212.

B. MECHANICAL PROPERTIES

Carnevale, E.H., W.L. McKay and J.A. Hull, Hypervelocity Impact Effects of Ablative Nose Cone Materials, Avco RAD Wilmington, Massachusetts, Fifth AFBMD-STL Symposium (1961).

Kattus, J.R., Structural Materials for Missile Applications at Very High Temperature, Southern Research Inst., Birmingham, ARS (1956).

C. SYSTEMS EFFICIENCIES

Heimerl, G.J. and P.J. Huges, Structural Efficiencies of Various Aluminum, Titanium, and Steel Alloys, at Elevated Temperature, NACA TN 2975.

Anderson, R.A., Weight Efficiency Analysis of This Wing Construction, Conference of the Aviation Division of ASME, Los Angeles, California (March 1956).

Harris, W.F. and W.S. Pellini, Implications of Thermal Protection System to Materials Development, NAS, ARS J. (1959).

Chicago Midway Labs, Determination of Factors Governing Selection and Application of Materials for Hypervelocity Vehicles, Quarterly Progress Report CML-TN-M131-6 (March-June 1958).

APPENDIX III

EXPERIMENTAL FACILITIES IN OPERATION FOR SIMULATION OF RE-ENTRY THERMAL ENVIRONMENT

A. HOT SHOT, SHOCK AND ARC TUNNELS

FACILITY	DATE STARTED OPERATING OR EXPECTED TO START	MACH NO. RANGE	TUNNEL SIZE	P_T RANGE (PSIA)	T_T RANGE (°K)	R. N. RANGE PER FOOT x 10^{-6}	LENGTH OF TEST RUN
Arnold Engineering Development Center HS-1	Operational	10 to 20	16-Inch Diameter	15,000 to 18,000	4,000 to 8,000	.02 to .268	20 Milliseconds
Arnold Engineering Development Center HS-2	Operational	10 to 20	50-Inch Diameter	15,000 to 18,000	4,000 to 8,000	.02 to .268	20 Milliseconds
Boeing 8-Inch Hot Shot Tunnel	August 1958	10 to 20	8-Inch Diameter	to 15,000	to 8,000	to 4.0	30 - 40 Milliseconds
Boeing 44-Inch Hot Shot Tunnel	Mid 1960	10 to 25	44-Inch Diameter	to 30,000	to 8,000	to 1.0	50 - 150 Milliseconds
Chance Vought 12-Inch Hypervelocity Wind Tunnel	March 1959	14 to 22	12-Inch Diameter	to 20,000	to 4,000	.07 to .5	35 Milliseconds
Convair Shock-Driven Wind Tunnel	Under Construction	6 to 24	10-Foot Diameter	to 100,000		.001 to 50	
Cornell Aeronautical Laboratory 24-Inch Hypersonic Shock Tunnel	September 1959	6 to 17	24-Inch Diameter or 18 x 24-Inch	150 to 6,000	835 to 3,660	.01 to 80	6 - 16 Milliseconds
General Electric Shock Tunnel	1956	5 to 22	30-Inch Diameter	to 5,000	700 to 11,000	.0003 to 120	2 - 8 Milliseconds
Grumman Hypersonic Shock Tunnel	April 1959	6 to 20+	18-Inch Diameter	600 to 20,000	2,000 to 15,000	.001 to 1,000	2 - 4 Milliseconds
Lockheed 3-Inch Shock Tube and Shock Tunnel	September 1957	6 to 9	5-Inch Diameter	100 to 500	2,220 to 8,340	.00015 to .003	500 Microseconds
Lockheed Spark Heated ("Hot Shot") Tunnel	October 1960	11 to 23	24-Inch Diameter	7,500 to 37,500	2,000 to 10,000	.05 to .8	25 Milliseconds

A. (Cont'd.)

FACILITY	DATE STARTED OPERATING OR EXPECTED TO START	MACH NO. RANGE	TUNNEL SIZE	P_T RANGE (PSIA)	T_T RANGE (°K)	R. N. RANGE PER FOOT x 10^{-6}	LENGTH OF TEST RUN
McDonnell Hypervelocity Impulse Wind Tunnel (HIWT)	May 1960	10 to 25	30-Inch Diameter and 50-Inch Diameter	10,000 to 60,000	2,000 to 8,000	.001 to .89	25 - 100 Milliseconds
Naval Ordnance Laboratory 1.5-Inch Hypersonic Shock Tunnel No. 1	September 1957	6 to 12	2 to 6-Inch Diameter Test Core	50 to 1,000	2,000 to 6,000	2 to 100	300 Microseconds to 1 Millisecond
Naval Ordnance Laboratory 1.5-Inch Hypersonic Shock Tunnel No. 2	October 1959	8		50 to 500	2,000 to 6,000	30 to 83	300 Microseconds to 1 Millisecond
Naval Ordnance Laboratory 4-Inch Hypersonic Shock Tunnel No. 3	September 1958	8 to 15	8-Inch Diameter	10 to 200	2,000 to 4,500	5 to 70	3 Milliseconds
North American Aviation Electrodynamic Facility	June 1960	10 to 20	12-Inch Diameter	9,500 to 21,500	3,800 to 8,600	.006 to .78	30 - 50 Milliseconds
North American Aviation Hot-Shot Tunnel	May 1960	10 to 20	12-Inch Diameter	13,000 to 18,000	4,150 to 8,000	.013 to .23	60 Milliseconds
University of Michigan Hot Shot Tunnel	Under Design	12 to 24	24 x 24-Inch		5,000 to 10,000	.002 to 1.0	20 Milliseconds

B. INTERMITTENT AND CONTINUOUS HYPERSONIC WIND TUNNEL

FACILITY	DATE STARTED OPERATING OR EXPECTED TO START	MACH NO. RANGE	TUNNEL SIZE	P_T RANGE (PSIA)	T_T RANGE (°F)	R. N. RANGE PER FOOT x 10^{-6}	LENGTH OF TEST RUN
Arnold Engineering Development Center Tunnel B	Operational	8	50-Inch Diameter	60 to 600	to 900	.25 to 2.5	Continuous
Arnold Engineering Development Center Tunnel B-2	Operational	5 to 7	12 x 12-Inch	40 to 930	115 to 660	1.2 to 20.4	5 Minutes
Ballistics Research Laboratory Aberdeen Proving Grounds Tunnel No. 4	End of 1960	5 to 10	13 to 16-Inch Diameter Test Core	to 2250	to 1500	1.2 to 12.6	Continuous
Boeing 12-Inch Hypersonic Wind Tunnel	1958	5 to 7	12-Inch Diameter	to 1800	to 750	3.5 to 30.5	110 Seconds
California Institute of Technology Jet Propulsion Laboratory 21-Inch Hypersonic Wind Tunnel	August 1959	5 to 9.5	20 x 21-Inch	33 to 640	to 1200	.24 to 3.8	Continuous
David Taylor Model Basin	March 1960	5 to 10	13.5-Inch Diameter	15 to 600	90 to 2540	.15 to 4.0	2 Minutes
Douglas Aerophysics Laboratory 27-Inch Hypersonic Tunnel	Summer 1960	6 to 10	24-Inch Diameter 27-Inch Diameter	50 to 2250	200 to 2000	.8 to 8.0	3.6 Minutes
Fluidyne Hypersonic Flight Simulation Laboratory	Summer 1960	Subsonic to 20	4 to 15-Inch Diameter Test Core	to 2000	to 3500	.001 to 5	To 6 Minutes
Lockheed Hot Flow Test Stand	April 1960	to 10	8-Inch Diameter	to 3,500	50 to 4,500	.25 to 10	Continuous
Massachusetts Institute of Technology Supersonic Laboratory	(M=7.6) January 1960	Subsonic to 7.6	(M=7.6) 10-Inch Diameter	(M=7.6) 40 to 100	(M=7.6) 600 to 1000	(M=7.6) .2 to .8	Continuous
NASA Ames 42-Inch Hypersonic Wind Tunnel	Under Construction	5 to 15	42-Inch Diameter	to 1830	to 4040		Intermittent

B. (Cont'd.)

FACILITY	DATE STARTED OPERATING OR EXPECTED TO START	MACH NO. RANGE	TUNNEL SIZE	P_T RANGE (PSIA)	T_T RANGE (°F)	R. N. RANGE PER FOOT x 10^{-6}	LENGTH OF TEST RUN
NASA Langley 20 x 20-Inch Mach 6 Wind Tunnel	Operational	6	20 x 20-Inch	to 450	to 640		30 Minutes
NASA Langley 24 x 24-Inch Hypersonic Wind Tunnel	Operational	6	24 x 24-Inch	to 15	to 140		Continuous
NASA Langley 96-Inch Hypersonic Wind Tunnel	Under Construction	6 to 7.5	96-Inch Diameter	to 4050	to 4040		
NASA Langley 18-Inch Hypersonic Wind Tunnel	Under Construction	8	18-Inch Diameter	to 2550	to 1040		Continuous
NASA Langley 24-Inch Hypersonic Wind Tunnel	Under Construction	8.5	24-Inch Diameter	to 3000	to 1440		> 30 Minutes
NASA Langley Hypersonic Flow Apparatus	Operational	10	15-Inch Diameter	500 to 1500	1380 to 1500	.7 to 2.0	1 Minute
NASA Langley 31 x 31-Inch Continuous Hypersonic Wind Tunnel	January 1961	10 to 12	31 x 31-Inch	450 to 4500	to 2540	.35 to 3.7	Continuous
NASA Langley 27-Inch Hypersonic Wind Tunnel	Under Construction	13	27-Inch Diameter	to 1200	to 4040		> 60 Seconds
NASA Langley 24-Inch Helium Hypersonic Wind Tunnel	Operational	15	24-Inch Diameter	to 1200	Room		20 Seconds
NASA Langley 20-Inch Hypersonic Wind Tunnel	Under Construction	5 to 20	20-Inch Diameter	> 1200	to 5040		
NASA Langley 11-Inch Hypersonic Wind Tunnel	1947	6 to 10 (Air) 10 and 18 (Helium)	11 x 11-Inch	60 to 700 (Air) 200 to 1500 (Helium)	to 1200 (Air) Ambient(Helium)	.4 to 1.2 (Air) 1.2 to 8.6 (Helium)	8 to 90 Seconds

B. (Cont'd.)

FACILITY	DATE STARTED OPERATING OR EXPECTED TO START	MACH NO. RANGE	TUNNEL SIZE	P_T RANGE (PSIA)	T_T RANGE (°F)	R. N. RANGE PER FOOT x 10^{-6}	LENGTH OF TEST RUn
NASA Langley 22-Inch Helium Hypersonic Wind Tunnel	Under Construction	10 to > 30	22-Inch Diameter	to 4500	to 540		20 to 40 Second
NASA Lewis 24-Inch Hypersonic Wind Tunnel	Operational	7	24-Inch Diameter	to 470	to 800		Continuous
Naval Ordnance Laboratory Hypersonic Tunnel No. 4	1950	6.8 to 10	10 x 10-Inch	75 to 750	470 to 1500	14 to 0.3	Continuous
Naval Ordnance Laboratory Hypersonic Tunnel No. 8	July 1959	5 to 10	M=8 18.5 x 18.5-Inch M=10 24.5-Inch Diameter	75 to 2250	250 to 1500	1.2 to 50	1 Minute to Several Hours
Ohio State University Aerodynamics Laboratory 12-Inch Hypersonic Wind Tunnel	1956	6 to 12.5	12-Inch Diameter	40 to 1500	40 to 2300	.3 to 3.0	30 to 120 Minutes
Polytechnic Institute of Brooklyn Aerodynamics Laboratory	1955	4.3 to 8	M=8 24-Inch Diameter M=6 12-Inch Diameter	100 to 600	140 to 2540	.24 to 8.4	15 to 60 Seconds
Princeton University Helium Hypersonic Wind Tunnel	1950	10 to 20	3-Inch Diameter	400 to 2000	70 to 200	3.6 to 18	Up to 10 Minutes
Rosemont Aeronautical Laboratory Hypersonic Facility, Tunnel No. 4	February 1958	7.0	12 x 12-Inch	50 to 165	50 to 2540	.1 to 1.6	30 to 120 Seconds
Rosemont Aeronautical Laboratory Hypersonic Facility, Tunnel No. 2	(M=7) August 1959	1.5 to 7	12 x 12-Inch	to 500	to 940	(M=7) .2o to 3.6	(M=7) 30 Seconds
Sandia Corporation Pilot Hypersonic Tunnel (SCARF V)	January 1960	4 to 9	.5-Inch Diameter	20 to 275	80 to 2540	.075 to 9.5	60 to 90 Seconds
Sandia Corporation 18-Inch Hypersonic Tunnel (SCARF VI)	January 1961	4 to 11	18-Inch Diameter	20 to 275	80 to 2540	.06 to 12.2	38 to 60 Seconds

B. (Cont'd.)

FACILITY	DATE STARTED OPERATING OR EXPECTED TO START	MACH NO. RANGE	TUNNEL SIZE	P_T RANGE (PSIA)	T_T RANGE (°F)	R. N. RANGE PER FOOT $x10^{-6}$	LENGTH OF TEST RUN
United Aircraft Corporation Research Laboratory 6 x 6-Inch Hypersonic Wind Tunnel	1956	4.25 to 10	6 x 6-Inch	to 850	to 1,400	1 to 23	To 130 Seconds
University of Southern California Low Density Wind Tunnel	November 1958 M=11+ May 1960	2 to 12	40-Inch Diameter	.015 to 150	to 980	.0000003 and Up	Continuous
Wright Air Development Center High Temperature Gas Dynamics Facility	Available for Testing Fall 1960	4	5-Inch Diameter	100 to 580	to 4,000	.28 to 39	20 to 60 Seconds
Wright Air Development Center 2 Foot Supersonic Gas Dynamic Facility	February 1960	1.5 to 5	24 x 24-Inch	.25 to 35	50 to 150	.1 to 7.5	Continuous
Wright Air Development Center Low Density Hypersonic Gasdynamics Facility	Under Construction	5 to 10	24 x 24-Inch	.0135 to 7.3	to 1,500	.001 to 1	18 to 80 Seconds

C. MISCELLANEOUS MATERIALS TESTING INCLUDING PLASMA ARCS

Facility	Gas Composition	Dia. Exit Stream, in.	P_T PSIA	Stream Temp. Range, °K	Stag Enthalpy Range, BTU/lb	Calorimeter Flux, BTU/ft^2-sec	Duration
Chicago Midway Lab							
1.1MW Plasmajet	Air,Co,C	1.25	16	to 14,000	to 10,000	2,000	2.5 min.
2.4MW Plasmajet	H_2O_2,H_2O,Co,C						
80KW Plasmajet	Air, Co, C	0.25	16				
Avco							
500KW Plasmajet	Air,Cu,W	0.5-0.75	16		5000-10,000	1300-1500	20 min.
					4000-8000	800-1000	
					800-3000	125-200	
30KW Plasmajet	N_2+O_2	1-1.5	0.25		3000-7000	35	Cont.
7MW Plasmajet Tunnel	Air, Co, C	0.4-1.2	15-370		450-10,000	to 2500	1 min.
H_2O_2 Rocket Motor	H_2O-H_2	1.5	225		5000	800	1-20 min.
			15			80	1-20 min.
ABMA							
Rocket Motor	Combustion Products		74		T_{Stag}-2940°K	1500	30 sec.
Rocket Motor	"	164 in^2	300		T_{Stag}-2500°K	700	30 sec
Kerosene-H_2O_2 or LOX		3.5 in^2	300		T_{Stag}-2500°K	700	30 sec
Jupiter C Exhaust					T_{Stag}-2500°K	1400	60 sec
Hermes Motor					T_{Stag}-2800°K		10-15 sec
Princeton University							
Helium Wind Tunnel	Helium		0.1-0.2		2500-3000	30	15 sec
Boeing							
"Small" Plasma Jet	Air	1/4					
Rocket Motor	Combustion Products			2800			
RFNA-UDMH							
Rocket Motor	"	2.5		3300			
Oxygen-Gasoline							
Burner	"	2.5		4800			
Oxygen-Cyanogen							
Ram Jet Exhaust	"	18		2100			

C. (Cont'd.)

Facility	Gas Composition	Dia. Exit Stream, in.	P_T PSIA	Stream Temp. Range, ^oK	Stag Enthalpy Range, BTU/lb	Calorimeter Flux, BTU/ft^2-sec	Duration
NASA-Langley							
Ceramic Heated AirJet	Air, 0.5-1%, Zr		95		1300		30-60 sec.
700KW Plasmajet	Air, Co		16	4500	7000	2200	
2MW Plasmajet	Air	6"	1.5	2250	10,000	40	2 min.
2MW Plasmajet	Air	0.75		3800	4000	3400	2 min.
NASA-Wallops Island							
Turbojet	O_2,CO_2,H_2O,N_2	15	115		T_{Stag}-1900^oK		
Rocket Motor	N_2,H_2,H_2O		300		T_{Stag}-2500^oK		
	N_2,H_2,H_2O		300		T_{Stag}-2200^oK		
	O_2,N_2,H_2O		300		T_{Stag}-1900^oK		
Chance Vought							
Materials Test Facility							
Brooklyn Polytechnic Inst.							
Intermittent Tunnel	Air		4.4		1800	100	15 sec.
WADD							
Plasmajet	Air						
ARDC							
Electric Wind Tunnel	Air, Co, C		370		12,000	300	0.01 sec.
Battelle Memorial Inst.							
Rocket Motor							20-40 min.
Cincinnati Testing Labs							
Pebble Bud Heater	Air			2600			30 sec.
Stanford Research Inst.							
R-F Discharge	N_2-O_2		1.3×10^{-4}				0.5-2 hrs.
Arc Image	Air,Argon					500	1-40 sec.
80KW Plasmajet (Water Stabilized)			15		4450	170-750	5-30 sec.

C. (Cont'd.)

Facility	Gas Composition	Dia. Exit Stream, in.	P_T PSIA	Stream Temp. Range, °K	Stag Enthalpy Range, BTU/lb	Calorimeter Flux, BTU/ft^2-sec	Duration
Temple University							
14KW Plasmajet	Argon	0.25		6400	1400	1600	30 sec
Carbon Heater	Argon			3600	800		Cont.
Moly Heater	H_2						
Oxy-Cyanogen Burner	Co, N_2	0.5			T_{Stag}-4800°K	160	Cont.
Oxy-Cyanogen Burner	Co, N_2	2.0	200-300			1000	30 sec
Rocket Motor	Combustion Products				T_{Stag}-3250°K	850	30 sec
Cornell Aero Labs							
Carbon Heater	Nitrogen	0.5	15	2500°K	1270	700	
G.E., M & OSD							
500KW Plasmajet	Air		0.15		10,000		7-10 min.
Water Stabilized Plasmajet	H, O, C		15			4000	30 sec
1000KW Plasmajet	Air, Co, C		150		7000		
Rocket Motor Alcohol-LOX	Combustion		16		T_{Stag}-2100°K	800-1700	

D. ARC TUNNELS, RAMJETS, ROCKET MOTORS

NAME OF FACILITY		CHANCE VOUGHT	PLASMADYNE	GENERAL ELECTRIC	AVCO	AVCO	CORNELL AERONAUTICAL LABORATORY	CHICAGO MIDWAY LABORATORY	STANFORD RESEARCH INSTITUTE	WRIGHT AIR DEVELOPMENT DIVISION	THERMODYNAMICS LABORATORY	AEROJET GENERAL CORPORATION	LANGLEY RESEARCH CENTER	AMES RESEARCH CENTER	AVCO	AVCO CHANNEL 3
LOCATION OF FACILITY		DALLAS, TEXAS	SANTA ANA, CALIFORNIA	PHILADELPHIA, PENN.	WILMINGTON, MASS	WILMINGTON, MASS.	CORNELL UNIVERSITY NEW YORK	UNIVERSITY OF CHICAGO	STANFORD UNIVERSITY	DAYTON, OHIO	CONVAIR SAN DIEGO, CALIFORNIA	AZUSA, CALIFORNIA	LANGLEY FIELD, VIRGINIA	MOFFETT FIELD, CALIFORNIA	WILMINGTON, MASS.	WILMINGTON, MASS.
TEST APPARATUS		RAMJET HEATER	AIR PLASMA ARC WATER COOLED ELECTRODES	ARC HEATING SUPERSONIC WIND TUNNEL	10 MEGAWATT ARC (1) SHROUD (2) WIND TUNNEL (3) PIPE (4) SPLASH	OVERS H ARC	HIGH TEMPERATURE RESISTANCE HEATER H_2	PLASMA AIR ARC	(1) ARC IMAGE AIR AND ARGON (2) ARGON PLASMA ARC	(1) PLASMA ARC, AIR OR ARGON (2) SUPERSONIC ROCKET	HYDROGEN ROCKET MOTOR	ROCKET MOTOR	ARC IMAGE FURNACE	WIND TUNNEL AND SHOCK COMP. HELIUM GUN	MODEL 500 ARC	AIR ARC
SOURCE OF INFORMATION		PRIVATE COMMUNICATION WITH CHANCE VOUGHT TO AVCO	ESTIMATED	MATERIAL FOR RE-ENTRY HEAT PROTECTION OF SATELLITES	INTERNAL COMPANY COMMUNICATIONS	INTERNAL COMPANY COMMUNICATIONS	WADC TR-368 PART II STUDY OF ABLATION OF STRUCTURAL PLASTIC MATERIALS	WADC TR-59-87 DETERMINATION OF FACTORS GOVERNING SELECTION AND APPLICATION OF MATERIALS	WADC TR-59-685 PART II STUDY OF THE MECHANISM OF ABLATION OF REINFORCED PLASTIC	WADD STUDIES ON PLASTIC EXPOSED TO HIGH MASS FLOW THERMAL ENVIRONMENTS	WADD EFFECTS OF HIGH TEMPERATURE, HIGH VELOCITY BASES ON PLASTIC MATERIALS	WADD TR-60-193 THERMAL EROSION OF ABLATIVE MATERIALS	ESTIMATED	THE AMES ATMOSPHERE ENTRY SIMULATOR..... ABLATIVE PROPERTIES OF THERMOPLASTICS...	INTERNAL COMPANY COMMUNICATIONS	PRIVATE COMMUNICATION J. CORDERO
OPERATING CONDITIONS	RUN DURATION	UP TO 20 MINUTES	UP TO 1 HOUR	2 MINUTES	100 SECONDS**	UP TO 60 MINUTES	UP TO 60 SECONDS	60 SECONDS	(1) 40 SECONDS (2)	(1) 30 SECONDS (2) 5 SECONDS	12 SECONDS	20 SECONDS	UP TO 10 MINUTES	LESS THAN 1 SECOND	5 MINUTES	UP TO 15 MINUTES
	POWER SUPPLY	RAMJET BURNING JP-4 FUEL AT COMBUSTION PRESSURE 50 PSI	100 TO 1000 KW USING RECTIFIERS		6 MEGAWATTS	100 TO 1000 KW	1400 KW	1000 KW		(1) (2) 41 KW			300 KW DC MOTOR GENERATOR		35 – 150 KW	2.5 MEGAWATTS
	POWER OUTPUT		50 TO 300 KW TO GAS		3.5 MEGAWATTS TO GAS	50 TO 300 KW	65 KW								8 – 85 KW	UP TO 1.8 MEGAWATTS
	HEAT FLUX	127 BTU/FT²-SEC TO COLD WALL AT FULL POWER 80 INCHES FROM EXHAUST PLANE TO A COLD WATER CALORIMETER	2000 BTU/FT²-SEC TO A 5/8" DIAMETER CALORIMETER	65 BTU/FT²-SEC	(1) UP TO 2400 BTU/FT²-SEC (2) UP TO 480 BTU/FT²-SEC (3) UP TO 1200 BTU/FT²-SEC (4) UP TO 1500 BTU/FT²-SEC	0.1 – 3 KW/CM²	700 BTU/FT²-SEC (MAX.)	2000 BTU/FT²-SEC COLD WALL	(1) 300 BTU/FT²-SEC (2) 750 BTU/FT²-SEC	(1) (2) 1300 BTU/FT²-SEC	3550 BTU/FT²-SEC	1150 BTU/FT²-SEC	1440 BTU/FT²-SEC (MAX.)		20 – 250 BTU/FT²-SEC	5 TO 800 BTU/FT²-SEC
	FLOW RATE	MAX. 20 LB/SEC WITH 1.4 LB/SEC FUEL FLOW RATE. MIN. 8 LB/SEC	MAX. 0.10 LB/SEC M – 2 TO 3 MIN. 0.01 LB/SEC	M – 4.8	(1) 0.10 TO 5 (2) 0.60 TO 4 (3) 0.60 TO 3 (4) 0.10 TO 3 LB/SEC	0.003 – 0.1 LB/SEC	40 LB/FT²-SEC (MAX.)	0.25 LB/SEC		(1) (2) 0.031 LB/SEC	MACH NO. – 1.82 (MAS.)				5 – 40 FT³/MIN.	0.001 TO 0.80 LB/SEC
	ENTHALPY	CALCULATED TO BE* 18,000 BTU/LB NOT YET VERIFIED EXPERIMENTALLY	2000 TO 25,000 BTU/LB	5100 BTU/LB	200 TO 12,000 BTU/LB	2000 TO 25,000 BTU/LB				(1) 3300 BTU/LB (2) 2400 BTU/LB	3600 BTU/LB				10 – 100 BTU/LB	10 TO 800 h/RT_0
	GAS TEMPERATURE	UP TO 4000°F AT STAGNATION THEORETICAL VALUE	3000°K TO 8500°K			1000 TO 10,000 °K	4000°K	4000 °F (STAG.)		(1) 6300°R (2) 3140°R	6320 °F	5000 °F				
	PRESSURE IN CHAMBER	UP TO 50 PSI IN STAGNATION CHAMBER	0.10 TO 1.0 ATMOSPHERES IN ARC CHAMBER		(1) 2.5 TO 26 (2) 0.5 TO 26 (3) 0.5 TO 20 (4) 2.0 TO 26 ATMOSPHERES	0.03 – 5 ATMOSPHERES									0 – 14.7 PSIG.	NOT MEASURED ESTIMATED 0.02 TO 2.0 ATMOSPHERES
	STAGNATION PRESSURE				(1) 2.5 TO 26 (2) 0.02 TO 1.5 (3) (4) 1.0 TO 13 ATMOSPHERES	0.005 – 5 ATMOSPHERES						500 PSIA			1 – 2 ATMOSPHERES	0.015 TO 0.5 ATMOSPHERES
INSTRUMENTATION		THERMOCOUPLES PRESSURE GAGES FLOW CALIBRATION	FLOW CALIBRATION CALORIMETER PRESSURE PROBES ENTHALPY PROBES VELOCITY DEVICES	THERMOCOUPLES CALORIMETER	THERMOCOUPLES CALORIMETER		WATER COOLED CALORIMETER RADIATION PYROMETER THERMOCOUPLES	COPPER CALORIMETER FUSIBLE CALORIMETER SPECTROSCOPE COLOR MOTION PICTURES				(1) CONTINUOUS CHAMBER PRESSURE RECORDING	CALORIMETERS		(1) WATER COOLED COPPER CALORIMETER (2) THERMOCOUPLE IN SAMPLE (3) PYROMETER SURFACE TEMPERATURE (4) THERMOPILE TOTAL RADIATION (5) CAMERA FRONT SURFACE AND SIDE	PRESSURE MEASURING DEVICES AND COPPER CALORIMETERS
SAMPLE GEOMETRY		1-1/2" TO 15" DIAMETER HEMISPHERES AT VARIOUS DISTANCE FROM EXHAUST PLANE	CONES, CYLINDERS HEMISPHERES	BLUNT NOSE CYLINDER	(1) 6" DIAMETER (MAX) (2) 2.5" DIAMETER (3) 1.5" DIAMETER (4) 3.0" DIAMETER	6" DIAMETER STANDARD 3" TO 8" NOZZLE EXITS AVAILABLE	CYLINDER	SPHERES CONES	HEMISPHERES CONES		CYLINDRICAL CONE	NOZZLE INSERTS	CYLINDER		CYLINDERS SPHERES	PRESENTLY USING HEMISPHERE – CYLINDERS UP TO 2.0" DIAMETER INSTRUMENTED WITH THERMOCOUPLES
DEFINITION OF TERMS	HEAT FLUX DENSITY				(A) $q_s = 0.763\,Pr^{-0.6}(\rho_e\mu_e\frac{\beta}{s})^{0.1}(\rho_e\mu_e)^{0.4}\left[1-(L_e^{0.52}-1)\frac{h_D}{h_e}\right](h_e-h_w)$ q_s – STAGNATION POINT HEAT FLUX; Pr – PRANDTL NO. ($C_p\mu/K$); L_e – LEWIS NO. ($D\rho C_p/K$); ρ – DENSITY OF AIR; μ – VISCOSITY OF AIR; h_s – SPECIFIC STAGNATION ENTHALPY OF AIR; h_D – DISSOCIATION ENTHALPY OF AIR PER UNIT MASS; β – STAGNATION POINT VELOCITY GRADIENT		$q_s = \frac{W\,\Delta T}{A}$ W – WATER FLOW RATE; ΔT – TEMPERATURE RISE OF WATER; A – AREA OF CALORIMETER; Q_s – HEAT FLUX DENSITY	$q^* = \rho C_p \frac{dT}{dx}$ q^* – HEAT FLUX; x – LENGTH OF BODY; ρ – DENSITY OF MATERIAL; C_p – SPECIFIC HEAT; $\frac{dT}{dx}$ – RATE OF TEMPERATURE CHANGE WITHIN BODY			$q = St\,\rho v C_p(T_R - T_w)$ q – HEAT FLUX AT STAGNATION POINT; v – VELOCITY; C_p – SPECIFIC HEAT; T_R – ADIABATIC WALL RECOVERY TEMPERATURE	$q_c = h(T_R - T_w)$ q_c – CONVECTIVE HEAT TRANSFER RATE; T_R – RECOVERY WALL TEMPERATURE; T_w – SURFACE TEMPERATURE; h – FILM COEFFICIENT				
	EFFECTIVE HEAT OF ABLATION				(B) $q^* = q_s\left[\frac{H_s - h_w}{H_s}\right]\frac{1}{\rho^*} = \frac{q_s}{\rho^* v}$ q^* – STEADY STATE THERMOCHEMICAL HEAT OF ABLATION; q_s – COLD WALL HEAT INPUT; H_s – TOTAL FREE STREAM GAS ENTHALPY; h_w – TOTAL WALL GAS ENTHALPY; ρ – MATERIAL DENSITY; v – STEADY STATE ABLATION VELOCITY; q_r – NET RADIATION FROM ABLATING SURFACE		$H_{eff} = \frac{q}{V\rho_s}$ q – HEAT FLUX DENSITY OF ABLATING HODEL; V – ABLATION RATE; ρ_s – DENSITY OF MATERIAL BEFORE EXPOSURE	$H_{eff} = \frac{q}{m}$ H_{eff} – EFFECTIVE HEAT CAPACITY OF MATERIAL; q – HEAT FLUX TO A NON-ABLATING BODY WITH SAME SURFACE TEMPERATURE; m – INITIAL MASS ABLATION RATE PER UNIT AREA		$H^* = \frac{q_c}{m_a}$ H^* – EFFECTIVE HEAT OF ABLATION; q_c – HEAT FLUX TO A NON-ABLATING BODY; m – MASS ABLATION RATE				$H_{eff} = \frac{q_c}{m}$ q_c – CONVECTIVE HEAT FLUX TO A NON-ABLATING SURFACE; m – ABLATION RATE EFFECTIVE HEAT OF ABLATION; $H_{eff} = H_A + \phi(H_s - H_w)$; H_A – SENSIBLE HEAT RISE PLUS LATENT HEAT; $H_s - H_w$ – ENTHALPY POTENTIAL ACROSS BOUNDARY; ϕ – TRANSPIRATION FACTOR; $\phi = 1/8\,p^{1/3}$ M > 1; $\phi = 3/5\,p^{3/5}$ M < 1 (TURBULENT FLOW) MOLECULAR WEIGHT OF AIR / MOLECULAR WEIGHT OF INJECTED VAPOR		

*INCORRECT
**BEING EXTENDED
***DATA TAKEN FROM REPORTS GIVES FACILITY CHARACTERISTICS FOR THE PARTICULAR TEST REPORTED AND NOT NECESSARILY THE ENTIRE OPERATING RANGE.
A ALL AVCO HEAT FLUX DENSITY DEFINITIONS ARE THE SAME
B ALL AVCO HEAT OF ABLATION DEFINITIONS ARE THE SAME

APPENDIX IV

THERMAL PROTECTION OF SATELLITES WITH COLD WALL ABLATION*

A. INTRODUCTION

The re-entry bodies of interest in space programs cover a broad range of applications. Satellite capsules designed for recovery after manned or unmanned flight and re-entry merit a special consideration. The problems encountered in capsule heat-shield design discussed in this report will be of interest to those concerned with shield designs for various satellite applications, as the purpose is to:

1. Demonstrate the effect of material, environmental, and design parameters on shield design, with particular emphasis on the surface temperature effects;

2. Present the approach to the design problems for the heat shield of the satellite capsule to survive a broad range of aero-thermodynamic re-entry conditions.

The thermal design of heat shields for re-entry bodies involve three basic steps: selection of the thermal protection system, material evaluation and selection, and the determination of the thickness of the shield-structure composite. In the process of design, whether the re-entry vehicle is a high performance ballistic missile or a low performance satellite capsule, consideration has to be given to the material thermal properties (k, ρ, C_p), ablation and surface characteristics (q^*, T_w, ϵ), aerodynamic performance ($Q_c, V_e, \gamma_e, \alpha, W/C_DA$) and structural criteria (T_s, safety factors, etc.). All of the above inputs bear equal importance in the design of an optimum (minimum weight maximum payload) vehicle. A previous study by Hurwicz and Brown (Ref. IV-1) treated in detail the interdependence of the various re-entry parameters listed above. The trends and correlations established there for high-performance re-entry (with extensions toward the regime of re-entry satellites) were utilized in this study.

Since the re-entry environment of a satellite capsule differs greatly from that of a high-performance re-entry body only basic conclusions drawn from reference IV-1 could be dependent upon and additional parametric studies were required.

*The raw data used in this study were obtained during work on Contract AF04(647)-347 and were correlated and interpreted for application to the present problems under Contract AF33(616)-7483.

The results of reference IV-1 made it possible to limit the number of parameters investigated only to those clearly significant and to concentrate on materials with desirable properties. Furthermore, this being a design rather than a generalized study, attempt was made to limit the parametric variation to that likely to arise with materials suitable for the application.

The necessary design calculations were performed on a high speed digital computer utilizing programs developed for re-entry problems (Refs. IV-1, IV-2) at Avco for transient heat conduction and ablation phenomena. The raw data used in this study were obtained during work on Contract AF04(647)-347 and were correlated and interpreted for application to the present problems under Contract AF33(616)7483.

B. DISCUSSION

The problem of selection of thermal protection system for a specific application has been treated by numerous authors (Refs. IV-1, 4, 5, 6, 7). A particular consideration was given to the various factors affecting the choice of a heat sink, ablation or radiation shield in reference IV-1. The approach outlined in reference IV-1 was followed in the design described in this appendix, which in a sense extends and complements that study.

The feasibility of ablation shields for satellite re-entry has been established in the literature (e.g. references IV-4 to IV-7) even though some resistance to the concept was noted in the early designs. Thus the selection of the mode of protection for a satellite capsule will be performed on the basis of relative efficiency of the thermal protection systems considered, tempered by other environmental effects (angle of attack) and manufacturing considerations. The selection of the class of materials to be used will be dictated by the same considerations. The Q^*_{eff} (references IV-1, IV-8) concept will be used as a criterion of selection as it gives a good measure of effective heat capacity of the shield.*

Preliminary studies of various heat sink, radiation, and ablation shield materials indicated that for the stagnation region of the body (Fig. IV-1) an ablating shield would be most efficient, while the remaining portion would be best protected by either an ablation or radiation shield, depending on the structural temperature requirements. The relative merits based on Q^*_{eff} of the various systems are shown in figure IV-2 for a typical re-entry condition. Approximate as the comparison in figure IV-2 is, it eliminates the heat sink

---

* $Q^*_{eff} = \dfrac{Q_c}{\rho(L_a + L_{ins})}$ for a given T_s .

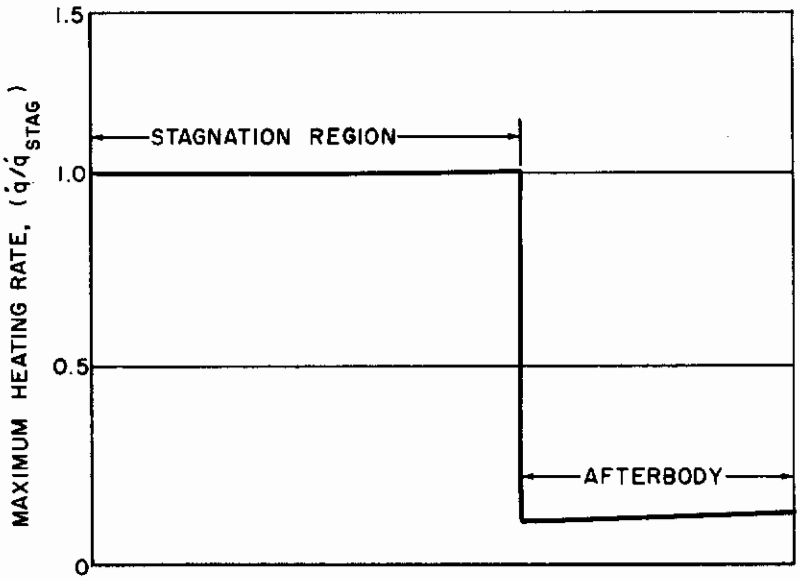

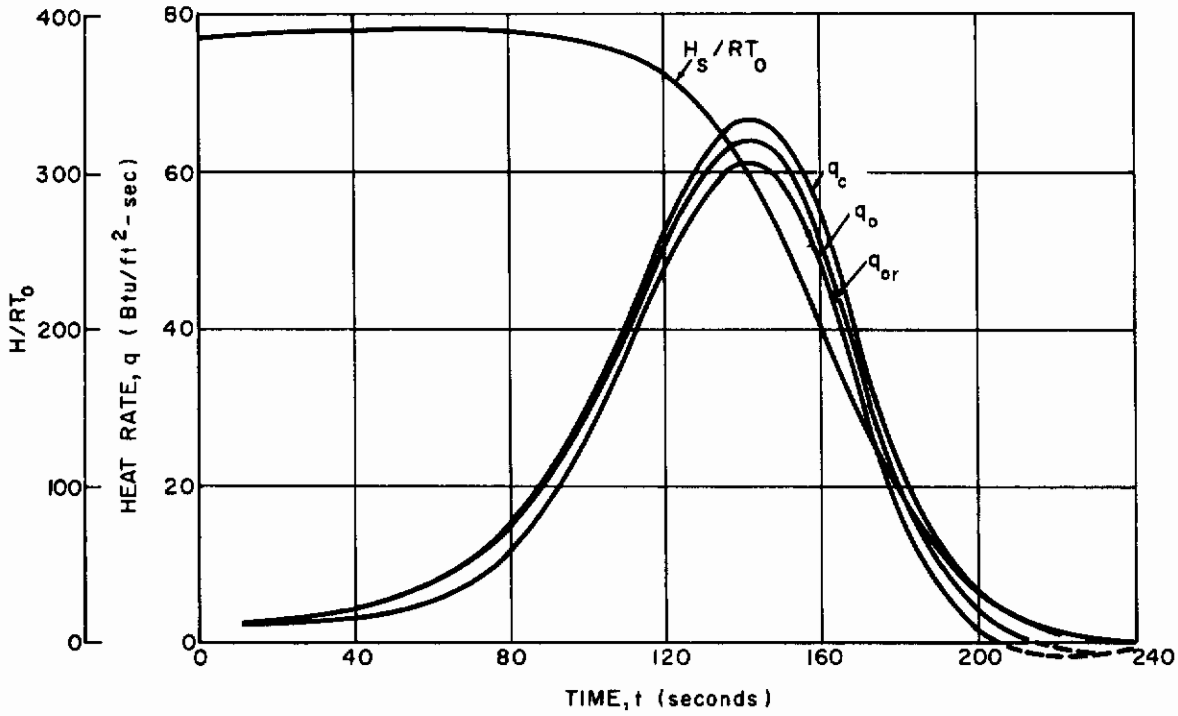

Figure IV-1 AEROTHERMODYNAMIC RE-ENTRY ENVIRONMENT
(FROM REF. IV-14)
$\gamma_e = -3°$, $V_e = 26,000$, $W/C_DA = 33$

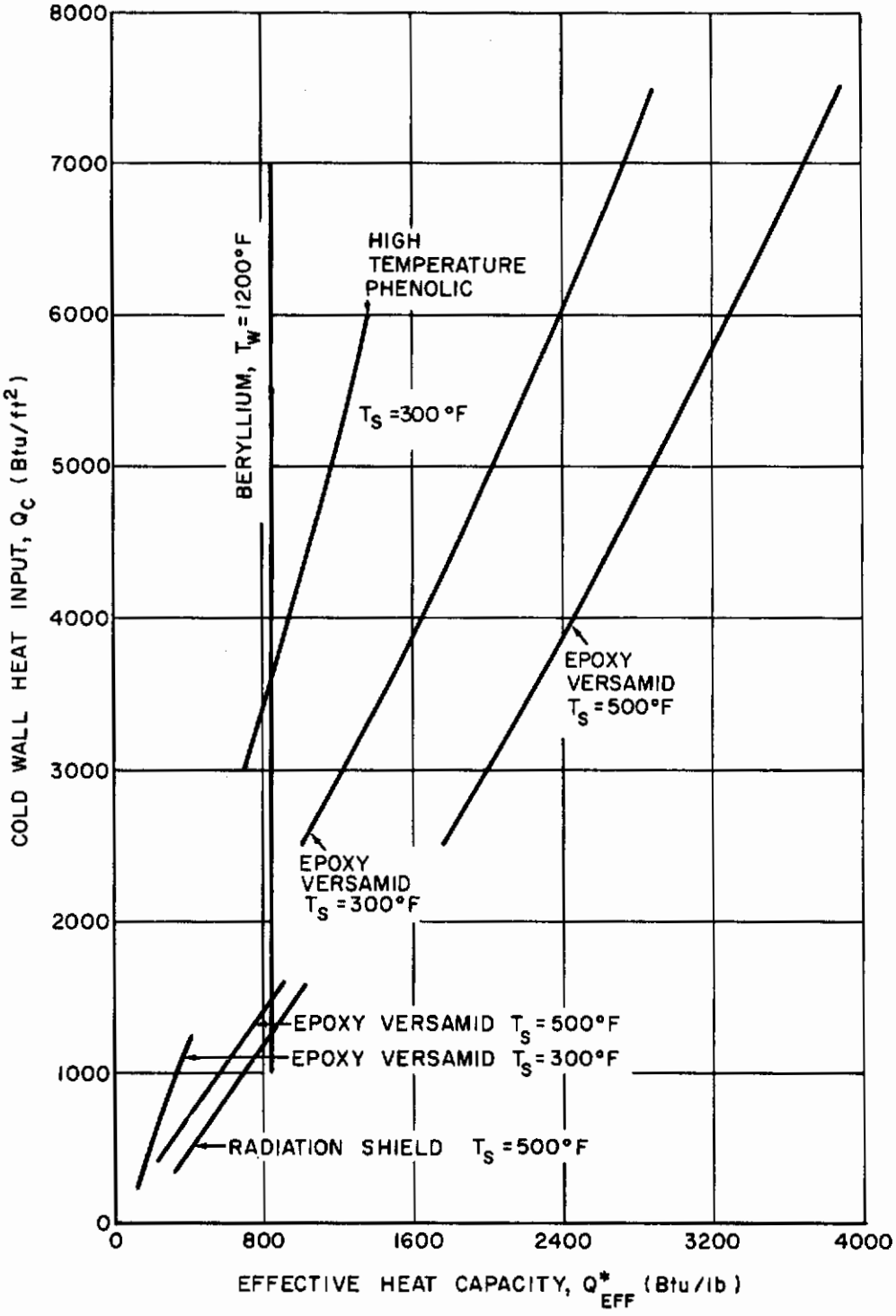

Figure IV-2 EFFICIENCY OF THERMAL PROTECTION SYSTEMS AND HEAT-SHIELD MATERIALS
$\gamma_e = -3°$, $V_e = 26,000$, $W/C_DA = 33$

concept; it corroborates the data in reference IV-1, since one of the best available heat sinks (Be) is less effective than low-temperature ablators at the nose cap.

The trends described in reference IV-1 indicated that the material for re-entry design should have minimum thermal conductivity (< 0.15 Btu/ft-hr-°F), relatively high q* (Btu/lb), and should depend on "low-temperature" ablation for maximum efficiency. High specific heat and low density would be desirable. The search for materials was directed accordingly.

In reference IV-1 Q_c, Q_c/q_{max}, and heating pulse duration were identified as the significant aerodynamic and trajectory parameters together with structural design temperature and safety factors on k, q*, and Q_c as design criteria for heat-shield evaluation under transient conditions.

As a result of the above preliminary evaluation of the design problems, the parameters of significance were defined and both ablation and radiation systems were established for the reference design purposes depending on the heating distribution (including angle-of-attack effect) around the body.

Since the aerodynamic parameter variation, as well as that of structural design criteria is usually defined by the capsule specification, the emphasis was directed to the effects of material parameters, the material selection being left to the designer. The range of surface temperatures (T_w), q*, and thermal conductivity (k) was established to a great extent by the properties materials presently known to have sufficient structural integrity. The variation in conductivity from 0.01 to 0.15 Btu/ft^2-hr-°F was considered to be more than representative of the state of art, and q* values from 2500 to 7200 Btu/lb were investigated. Surface temperatures from 500° to 5000°F were studied. Main effort was directed in the range up to 2000°F since most plastics fall in this range and since materials with higher temperatures did not look too promising (reference IV-1 and figure IV-2). The design conditions used for reference study purposes (Fig. IV-1) are listed below:

V_e = 26,000 ft/sec $\quad \gamma_e = -3° \quad \alpha = 0°$

W/C_DA = 33 lb/ft^2 $\quad Q_c$ = 300 to 8000 Btu/ft^2,

with hypothetical material properties shown in Table IV-1.

The range of aerodynamic parameters studied was selected for a flight envelope:

TABLE IV-1

THERMAL PROPERTIES AND ABLATION CHARACTERISTICS
OF VARIOUS HEAT-SHIELD MATERIALS

MATERIAL	k	ρ	C_p	T_w	H_v	η	ϵ
Epoxy Experimental Data	0.10-0.12* 0.075**	67.4	0.34	1033 to 1250	350	0.55	0.7***
Reference Material	0.10	67.4	0.30	1250	500	0.5	0.7
Polymethylmethacrylate	0.145	72.5	0.35	980	315	0.5	-
Polyethylene	0.19	58.0	0.53	850	435	0.66	-
Porous Teflon	0.14	75.0	0.22	1350	280	0.36	-

* - Steady state 0 to 300° F
** - Arc test effective measurement
*** - Estimated

Re-entry* Velocity - V_e = 26,000 ft/sec,

Re-entry Angle - γ_e = -2 to -5 degrees,

Ballistic Coefficient - $W/C_D A$ = 38 lb/ft^2,

or the corresponding range of

$Q_c/q_{c_{max}}$ = 55 to 130;

Peak heating rate to impact time = 50 to 500 seconds;

The integrated heating (Q_c) = 300 to 10,000 depending on the position on the body;

The angle-of-attack α = 0 to 20 degrees.

The effect of structural temperatures from 200°to 800°F was investigated together with changes in structure heat capacity (ρ, C_p, L_s) from 0.14 to 0.42 Btu/ft^2-°F. The above reference values represent in no sense, optimum conditions, but are used to demonstrate the effects of various parameters referred to a common point of departure.

1. Material Evaluation

The evaluation of materials was conducted for the typical re-entry conditions chosen (Fig. IV-1) and checked at the completion of the design evaluation for extremes to be encountered in the flight envelope and for the design criteria. Thus a limited evaluation of the interdependence of the various material parameters may be afforded prior to the final design.

Following the indications of the preliminary analysis, only the most significant (and most likely to vary) parameters in the material selection (T_w, k and q^*) were investigated over the range of cold wall aerodynamic heat inputs (Q_c). Particular attention was given to the effective heat capacity of the material Q^*_{eff} as reflecting both the ablation loss and insulation requirements. The ratio of L_a/L_{ins} was also determined as a measure of ablation material effectiveness.

a. Surface (Ablation) Temperature

A cursory examination of the problem and intuitive thinking indicate the following effects of surface temperature on the shield design. As the surface temperature increases:

1) The "hot wall" enthalpy correction increases, reducing the effective flux to the heat shield.

*At 400,000 feet altitude.

2) The heat radiated from the heat shield to the outside gas increases and tends to decrease the effective flux.

3) The heat of ablation increases.

4) The shield reaches the ablation temperature at a later time and stops ablating sooner thus tending to decrease the efficiency and effectiveness of the ablation shield.

5) The insulation (thickness remaining after ablation) increases also, thus tending to decrease the material effectiveness.

The first two are very strong advantages of using high ablation temperature while the third effect is very weak for the materials considered here. The last two are strong disadvantages of high ablation temperature. The effective thermal capacity Q^*_{eff} and L_a/L_{ins} is therefore a very strong function of the surface temperature.

The effects reasoned above do not give, of course, the magnitude or the direction of the trend. However, previous studies of higher performance re-entry bodies (figures -1 and -8 in reference IV-1) showed that for heat inputs $Q_c < 10,000$ Btu/ft^2 and for long heat soaking times, the surface temperatures required for efficient shield design decrease with the heat input. Since design data should not be based on extrapolation of trends in reference IV-1 to satellite conditions, a specific design study was necessary.

For the satellite re-entry it would appear thus desirable to use "cold wall" ablation type materials. The actual effect of the surface temperature on the shield thickness has to be determined for two reasons in addition to the above: a) to select the optimum material from those available (desirability of development of low temperature ablators), and b) to allow for the uncertainty in the surface temperature determination and its variation with re-entry environment (heat input and enthalpy). Since no studies were made in the literature for actual satellite re-entry environment, except extrapolated values from reference IV-1, a parametric study was conducted to permit the design evaluation. The effects determined from this study were then utilized for design safety factor criteria, and used as a guide in requirements for experimental accuracy in surface temperature measurements. Hanst (Ref. IV-9) and Jennings and Easton (Ref. IV-10) among others reported measurements of brightness surface temperatures of several plastics and resins ranging upwards to 1800°F. Recesso and Hanst (Ref. IV-11) confirmed some of these measurements by means of internal thermocouples (Fig. IV-9). On the other hand, early temperature measurements for low enthalpy streams as

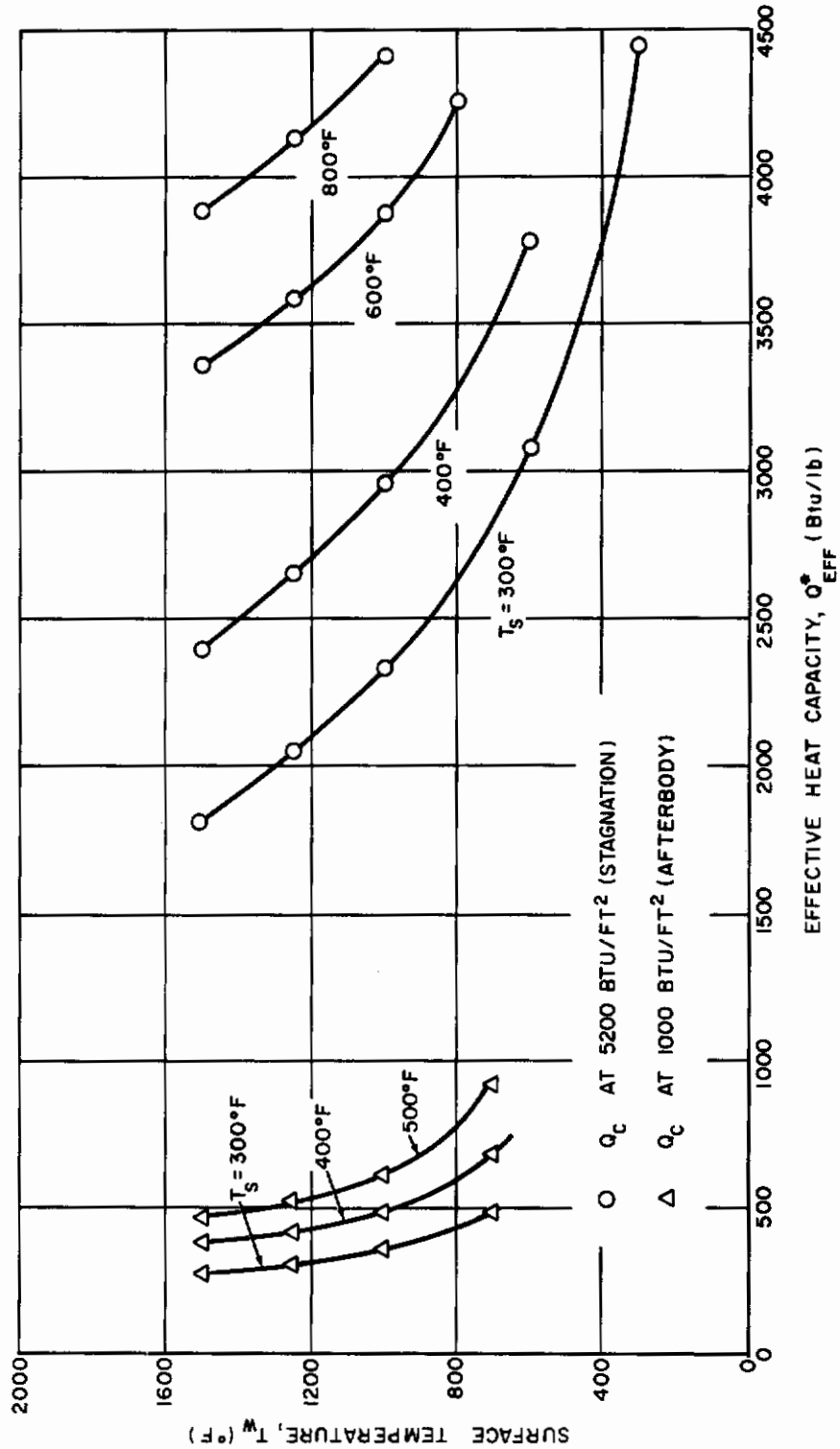

Figure IV-3 SURFACE (ABLATION) TEMPERATURE EFFECT ON REFERENCE DESIGN EFFICIENCY
$\gamma_e = -3°$, $V_e = 26,000$, $T_{initial} = 70°F$

well as for some other materials indicated lower temperature ranges of the order of 400°F. This range (300° to 1500°F) was thus selected for investigation using thermal conductivity, k = 0.10 as representative (Ref. IV-12) of this class of materials. The study was further subdivided into two regions: stagnation (relatively high Q_c) and afterbody (low Q_c) because of the different structure heat capacities due to structural requirements and anticipated heat input levels in these areas.

The relation between surface temperature and Q^*_{eff} is shown in figure IV-3 for heat inputs (Q_c) representative of the above regions. The reference structural temperature was maintained at T_s = 300°F. It may be seen that for a given heat input Q^*_{eff} decreases for higher surface temperatures. For low heat inputs and for T_w = 1500°F the effect of flux reduction due to hot wall enthalpy and radiation loss is overcome by the inefficient (for this case) ablation process. The L_a/L_{ins} ratios are very small, as the insulation requirements increase simultaneously with decrease in ablation (Fig. IV-3). For higher heat inputs the adverse effects of higher T_w tend to be attenuated as the energy conducted into the body decreases. Surface temperature of 300°F produces opposite effects as ablation is the most significant process. For $T_w \approx$ 1000°F and T_s = 300°F an apparent cross-over is reached in the stagnation as the increase in Q^*_{eff} is directly proportional to increase in Q_c for the range of inputs considered and the thickness requirement becomes insensitive to heat input (Fig. IV-10). Similar trends are observed for lower heat inputs except that the curves are shifted towards larger thickness and the insensitive portion would tend towards lower temperatures and heat inputs. It may be noted here that depending on the surface temperatures, the lower than predicted heat inputs (if ablation occurs) may be critical in design and will not afford a safety factor. The study indicates that where T_w may be sufficiently low for stagnation design, materials with lower surface temperatures are desirable for the aft portion. A much lower k is the alternative. Otherwise no advantage associated with mass transfer is realized.

No specific study of the interdependence of T_w and k was made since most of the plastics display conductivity in the range of 0.10 to 0.15 Btu/ft-hr-°F, and it is obvious from previous studies that k should be minimized. The effect of k variation for a given T_w has been, however, made in the following section to account for uncertainty in measurements. Comparison of the level of heat inputs, Q^*_{eff}, conductivities, surface temperatures and pulse duration for high performance (Ref. IV-1), and satellite re-entry, together with the desirability of lower surface temperatures, indicate validity of scaling down the reference figure and of accepting the general

relationships for satellite re-entry application. Further studies should be made to determine these effects as the state of art in material development progresses.

The effect of surface temperature will depend on the allowable structure temperatures. In figure IV-4 the interaction of these parameters is shown for various heat inputs and desired Q^*_{eff}. The increase in T_s attenuates the detrimental effects of high T_w and will accordingly change relationships shown above in figure IV-3. The effect of T_s and structure heat capacity will be discussed in more detail under Aerodynamic and Structural Criteria.

It should be stressed that the evaluation of the T_w effects was conducted on the assumption that the temperature distribution in the body is governed by the ablation and conduction process ignoring the chemical reactions in the surface layer of material. This is a conservative design assumption tantamount to a safety factor. Experimental evidence (Ref. IV-11) indicates that the temperature drop in the surface layer is larger than predicted by the above assumption (Fig. IV-8). The simulation procedure of this phenomenon is briefly treated below, however, it should be noted that if the internal temperature distribution is independent of the surface temperature due to a more or less fixed decomposition temperature below the surface, the conclusions may be altered. The general problem area is beyond the scope of this report. Design calculations based on the $T_w = 1250°F$ as determined in figure IV-9 (relatively independent of heat flux and enthalpy for the trajectory under consideration) would result in heat-shield thickness of reasonable magnitude and would indicate that the class of materials with properties shown in Table IV-1 would be satisfactory for re-entry satellite applications from thermodynamics point of view.

b. Heat of Ablation (q^*, H_v, η)

The materials considered in this study displayed relatively small variations in the heat of ablation values (q^*) (Table IV-1). Defining:

$$q^* = C_p \Delta T_w + f[H_v + \eta (H_s - H_w)] \quad ,$$

and assuming that for the environment investigated the materials will not flow or build-up unstable heavy charred layer, $f = 1$ and the significant components of q^* become H_v and η in addition to the T_w previously discussed.

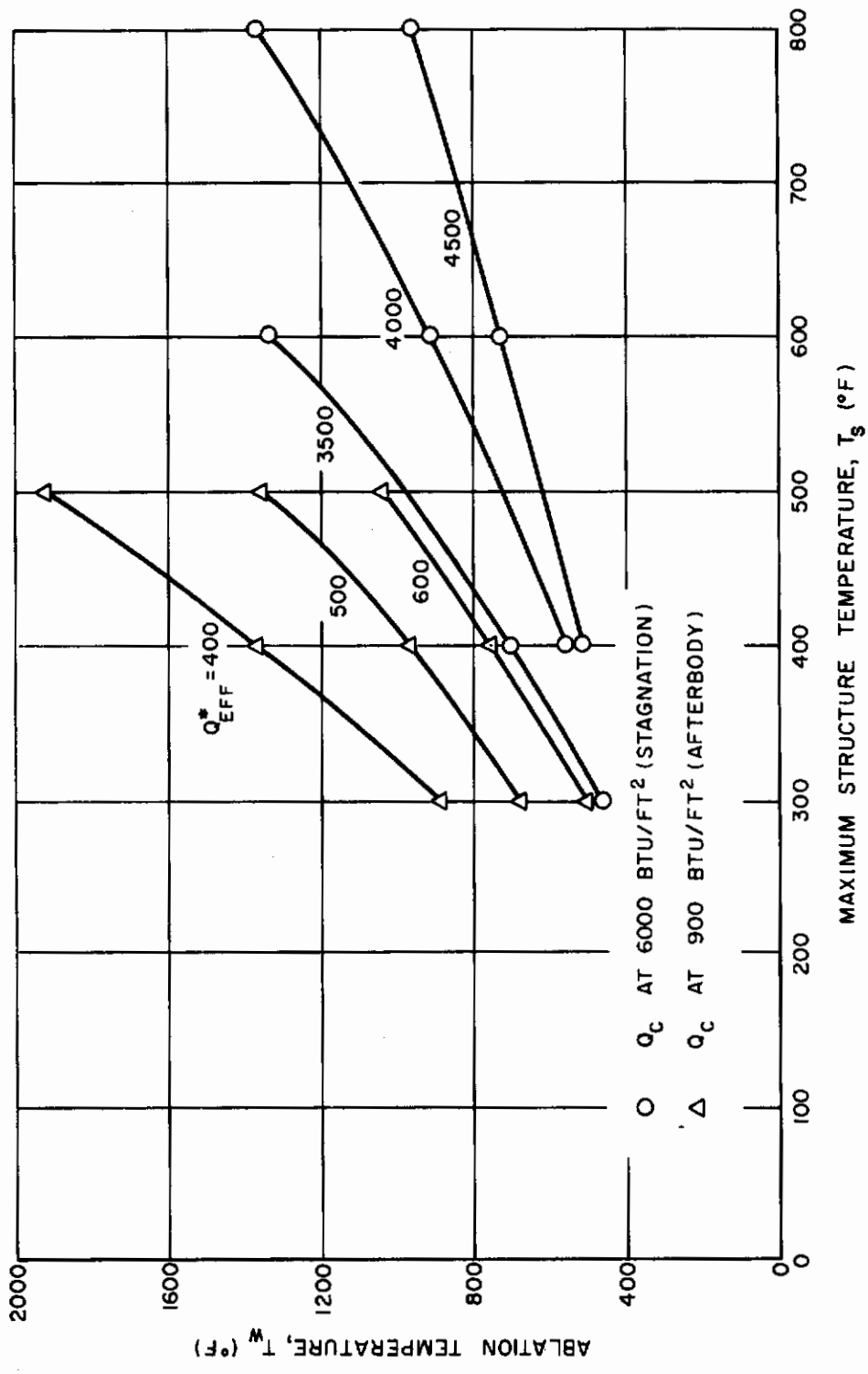

Figure IV-4 INTERACTION OF SURFACE AND STRUCTURE TEMPERATURES FOR VARIOUS AERODYNAMIC HEAT INPUTS
$\gamma_e = -3°$, $V_e = 26,000$, $T_{initial} = 70°F$

For laminar flow the variation of H_v was observed (Ref. IV-11) from 0 to 500 and η from 0.35 to 0.66. The effect of these two ablation parameters on the heat-shield design was determined. Figure IV-5 shows that the thickness requirement does not change significantly with H_v variation considered. For low heat inputs the effect would be even smaller as L_a/L_{ins} is smaller, and since little or no ablation occurs.

On the other hand, the effect of η variation on the Q^*_{eff} is much larger (Fig. IV-6). Within the range of variation, Q^*_{eff} may change by as much as 25 percent depending on the total heat input Q_c. The blowing factor η thus will be an important consideration in material selection and the accuracy in its determination is more significant than of H_v. High blowing factors are desirable.

Because of the small variation in the heat of ablation and conductivity of materials available, no attempt was made to evaluate the relation of q^* and k. The general trends observed in reference IV-1 and figure IV-6 would hold here considering the scaling down of the basic ICBM inputs to the satellite conditions level in conductivity and q^*. It may be concluded that the transpiration is the significant contribution to the heat of ablation rather than the latent or thermochemical heats. This would be equally true for materials with unstable charred layers, except that effective η values would have to be used, H_v not being significant.

c. Thermal Properties (k, C_p)

The uncertainty in the determination of thermal properties especially at elevated temperatures, and the importance of k in heat-shield design (Ref. IV-1) prompted the study of k and C_p effects. The results of the study were used in the design safety factor determination.

The effect of k and C_p on Q^*_{eff} for several heat inputs Q_c is shown in figures IV-7a and IV-7b. The curves bear out the fact that low k and high C_p is desirable and that within the ± 10 percent experimental accuracy the shield thickness may vary as much as 10 percent. It is noted here that for the conditions considered ($k = 0.05$ for the stagnation region and $k = 0.025$ for the low heat input region) offers no additional advantage, as almost all energy is consumed in ablation.

Since in the design procedure the chemical reactions occurring in the surface layer were neglected (see above T_w discussion), an effectively higher k and/or lower C_p was used in the calculations. Effectively larger temperature penetrations than observed (Fig. IV-8) were thus predicted. A simple simulation of the chemical reaction by lowering

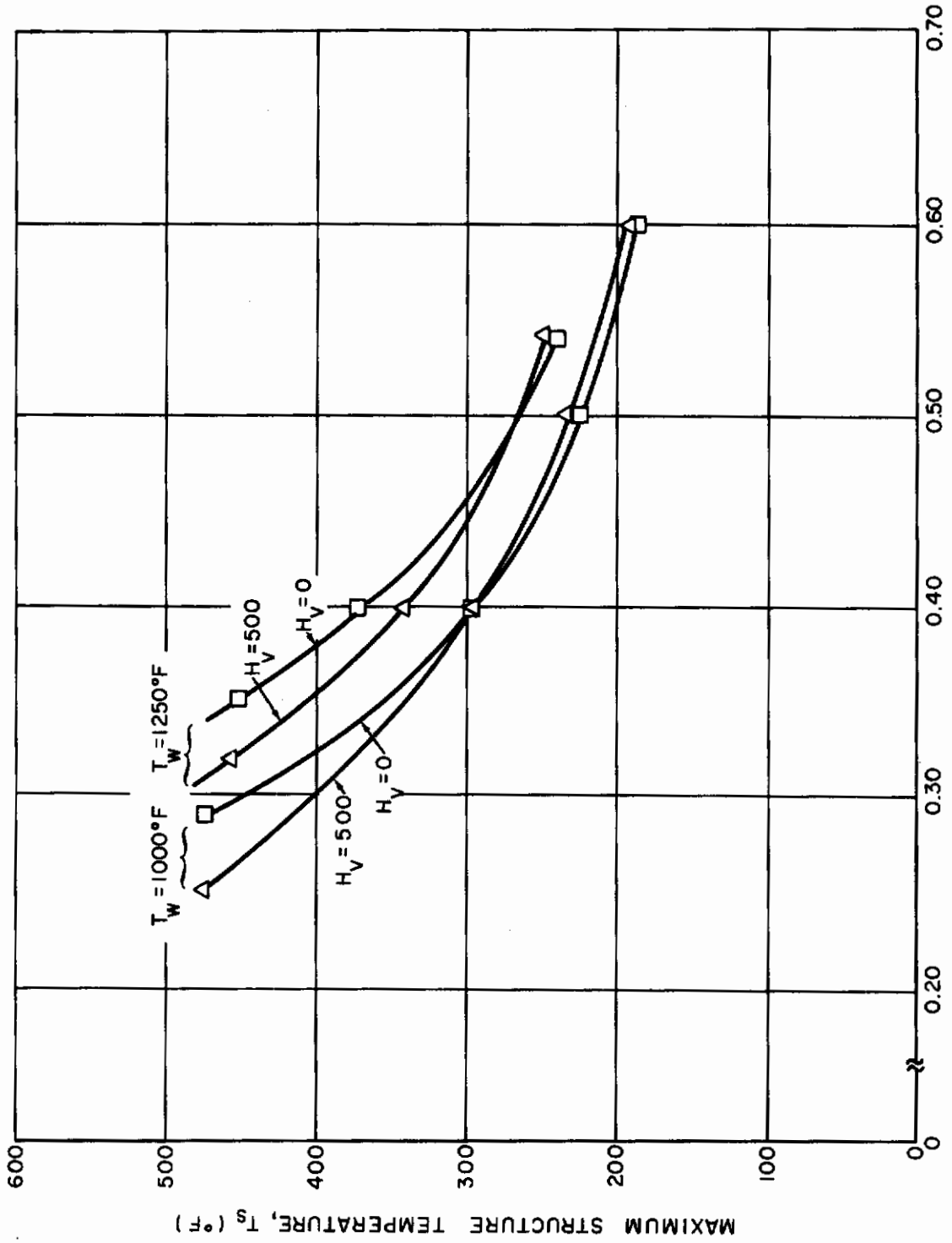

Figure IV-5 LATENT HEAT OF VAPORIZATION (AND CHEMICAL REACTION) EFFECTS ON MATERIAL EFFICIENCY

$\gamma_e = -3°$, $V_e = 26,000$, $W/C_DA = 33$, $Q_c = 5200$ Btu/ft^2

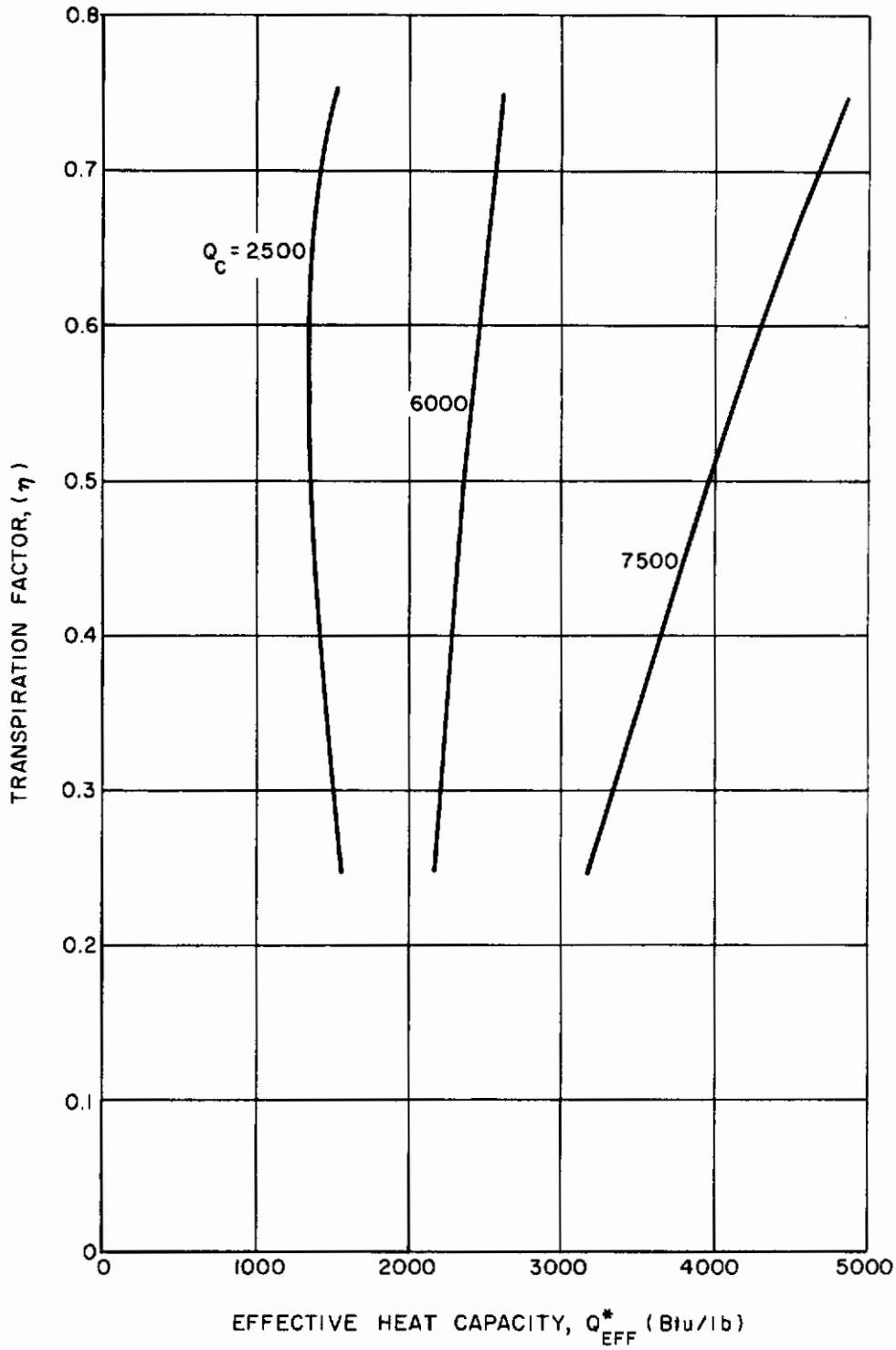

Figure IV-6 TRANSPIRATION EFFECT ON MATERIAL EFFICIENCY
$\gamma_e = -3°$, $V_e = 26,000$, $T_w = 1250°F$, $T_s = 400°F$

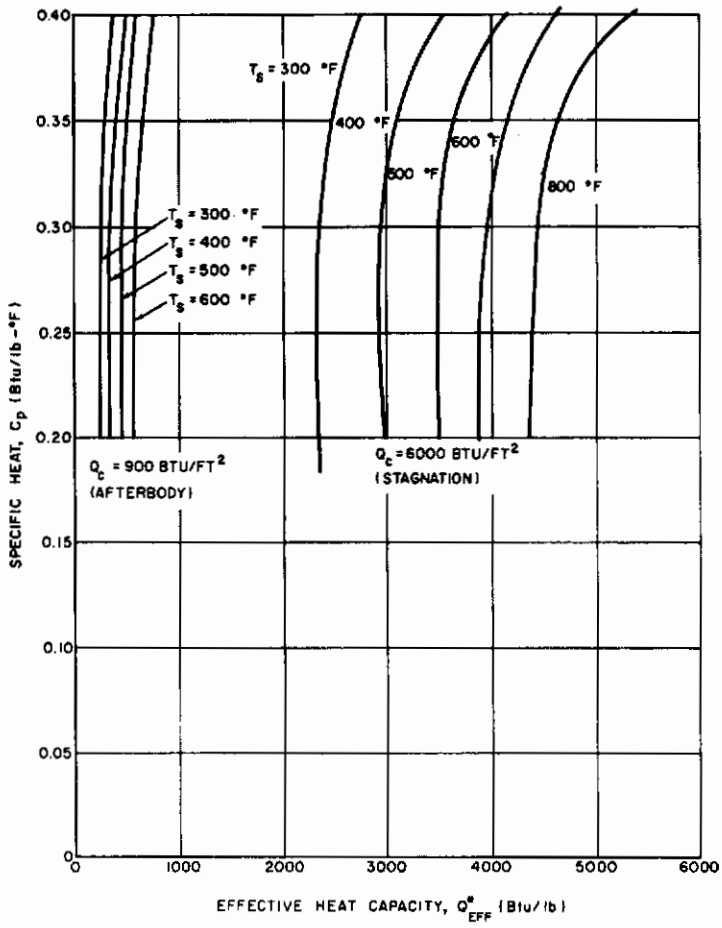

Figure IV-7a THERMAL PROPERTIES EFFECT ON MATERIAL EFFICIENCY
γ_e = -3°, V_e = 26,000, W/C_DA = 33, T_w = 1250°F

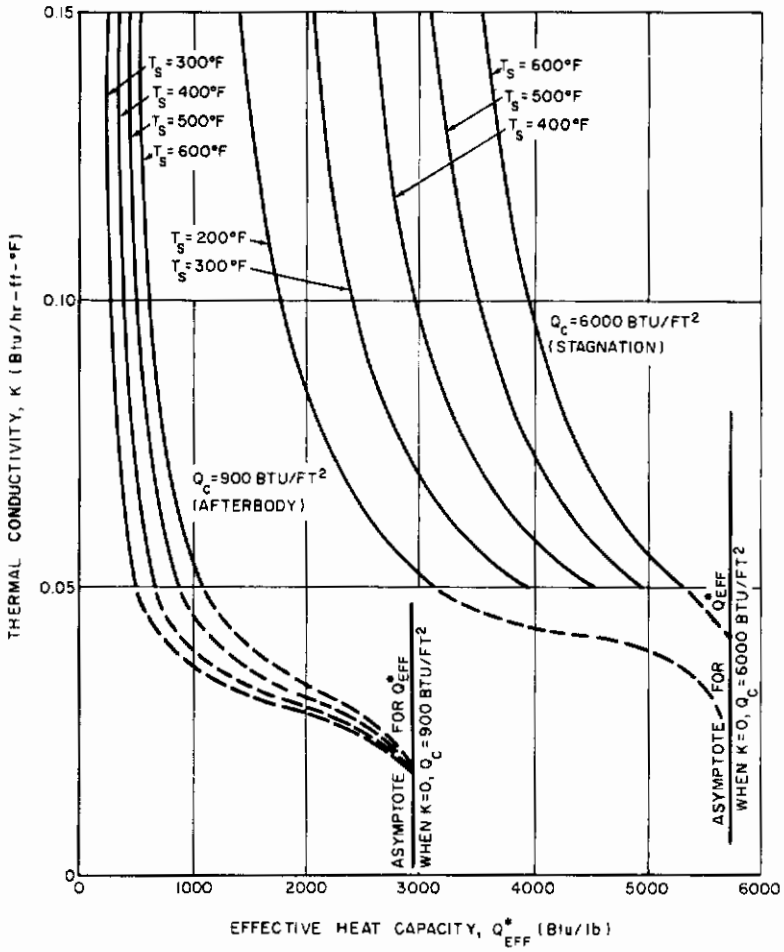

Figure IV-7b THERMAL PROPERTIES EFFECT ON MATERIAL EFFICIENCY
$\gamma_e = -3°$, $V_e = 26,000$, $W/C_DA = 33$, $T_w = 1250°F$

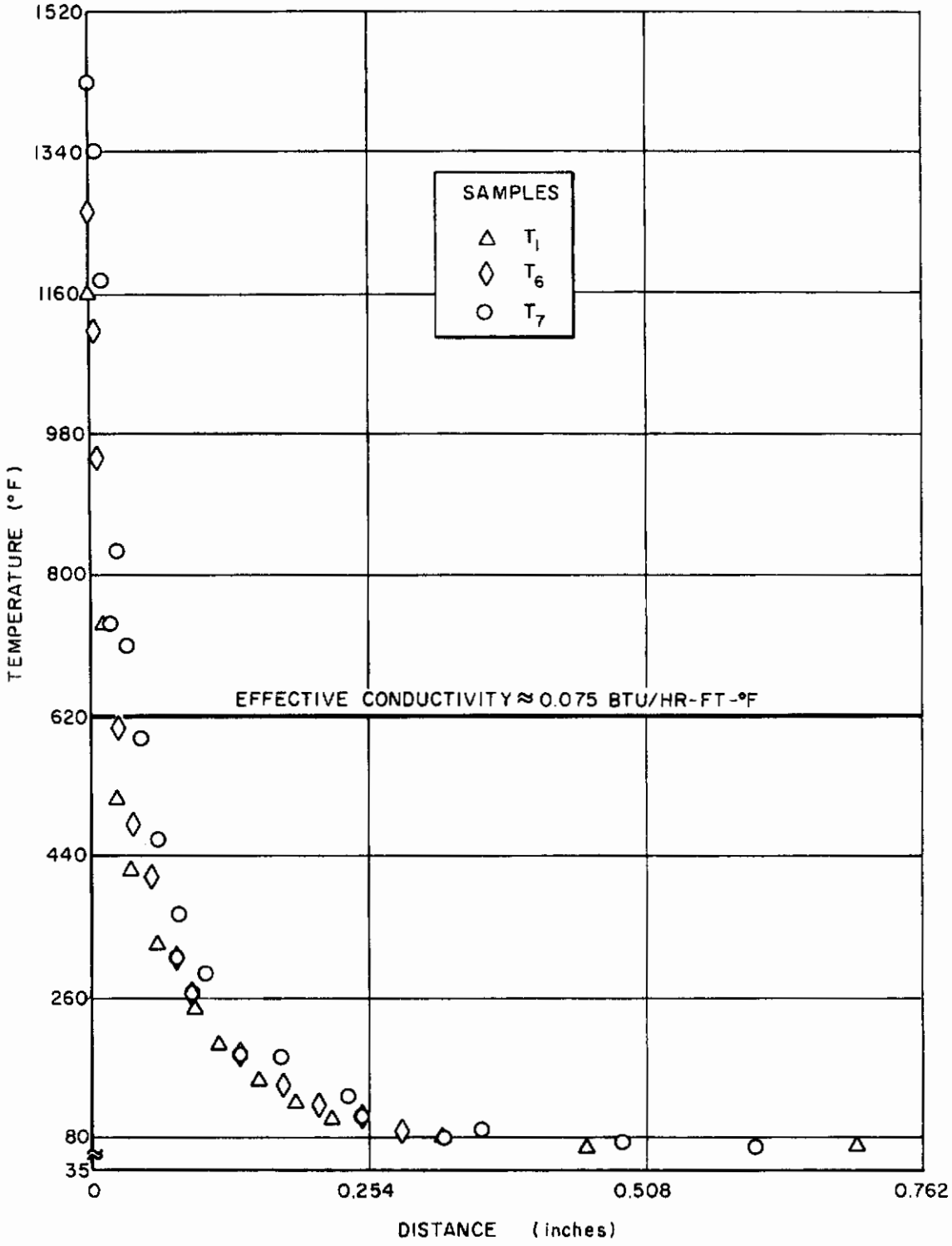

Figure IV-8 TEMPERATURE GRADIENT AND EFFECTIVE THERMAL CONDUCTIVITY IN ARC TEST

high-temperature conductivity was made to agree with the experimental results. The "effective" conductivity was found to be 0.075 which is 35 percent lower than measured values in reference IV-12 and 25 percent lower than k = 0.10 used for reference design purposes. Thus a relative measure of the safety factor may be obtained, and from figure IV-7 indicates a 1.2 safety factor on weight. Also C_p value used for reference design is 15 percent lower than the measured values (Table IV-1 and Ref. IV-12).

It is noted from figure IV-7 that as expected the conductivity plays a more important role in the region of the low heat inputs than for higher inputs. The decrease in conductivity accelerates the onset of ablation and thus increases the efficiency of the material. The interaction of k and T_w will be much more significant in this region from both the conduction as well as ablation point of view. Just as important as the development of lower temperature ablator for this region, is the decrease of the material conductivity to k = 0.025 Btu/ft-hr-°F.

The above evaluation of the principal material parameters affecting the heat-shield design leads to the conclusion that "low temperature" ablators should be used in the satellite re-entry design, and that their thermal conductivities and heats of ablation should be respectively minimized and maximized. The average stagnation Q^*_{eff} falls in the 2500 to 3500 Btu/lb range. Minimizing T_w and k, and maximizing q^* (H_v and η) will increase their efficiency and designing for higher structure temperatures will be helpful.

The low heat input area presents more problems as the Q^*_{eff} does not exceed 1500 Btu/lb. Radiation shield appears competitive, since little advantage of ablation is realized. Lower surface temperatures ($T_w < 700°F$) are needed, or extremely good insulators are required.

2. Heat-Shield Design and Material Selection

The evaluation of materials in the preceding section (for standard re-entry conditions) will be used as a criterion for material selection. In addition to the thermodynamic criteria, the fabrication problems and mechanical strength will have to be considered in the final choice.

a. Material Selection

Figure IV-2 shows a basic comparison of modes of heat absorbtion by heat sink, ablation, and radiation shields. For the stagnation region of the body, the heat sink and radiation modes are definitely less efficient than ablation shield, especially considering that one of

the better heat sink material (Be) is shown in the comparison for most favorable structural allowable temperatures. Even assuming no need for structural member behind Be sink, and light insulation requirements, the ablation shields are still superior. In the cylindrical portion with the materials considered here, the balance is not in favor of ablators, since they mainly behave as heat sinks; however, consideration of angle of attack (see discussion below) will favor the ablation principle.

The advantage of lower surface temperatures were amply discussed above, and thus the selection field has been narrowed to "cold wall" ablators.

Table IV-1 shows the materials considered in this class. As noted previously the thermodynamic characteristics (T_w, k , q^*) of the majority do not vary greatly.

An epoxy plastic has been selected for the reference study purposes is typical of this class of materials. The q^* versus H_e/RT_o curve for the reference is shown in figure IV-9, together with its thermal properties and surface temperatures. T_w = 1250°F was used for reference design purposes. Other values used for reference study purposes are shown in Table IV-1. The re-entry conditions used in this section are standard (Fig. IV-1), and the structural criteria are T_s = 300°F with reference structure heat capacities ($\rho_s C_s L_s$ = 0.43 Btu/ft^2-°F for stagnation and $\rho_s C_s L_s$ = 0.14 Btu/ft^2-°F for the low heat input region) unless otherwise noted.

b. Heat-Shield Design

The design study calculations were made for the reference material, while the parametric study conducted under "Material Evaluation" permits (if necessary) a rapid conversion for other materials. The studies shown in the subsequent section will permit a rapid evaluation of the shield performance under "non-reference" conditions.

1) Ablation shield

The digital programs and calculations procedures used in design computations were the same as in references IV-1 and IV-3 for the transient regime.

The experimentally determined properties are substituted into the following mathematical model which is solved by numerical integration. Assume a one-dimensional heat conduction model with one boundary arbitrarily heated so that ablation (no liquid layer) occurs and dissipates a large amount of re-entry heating.

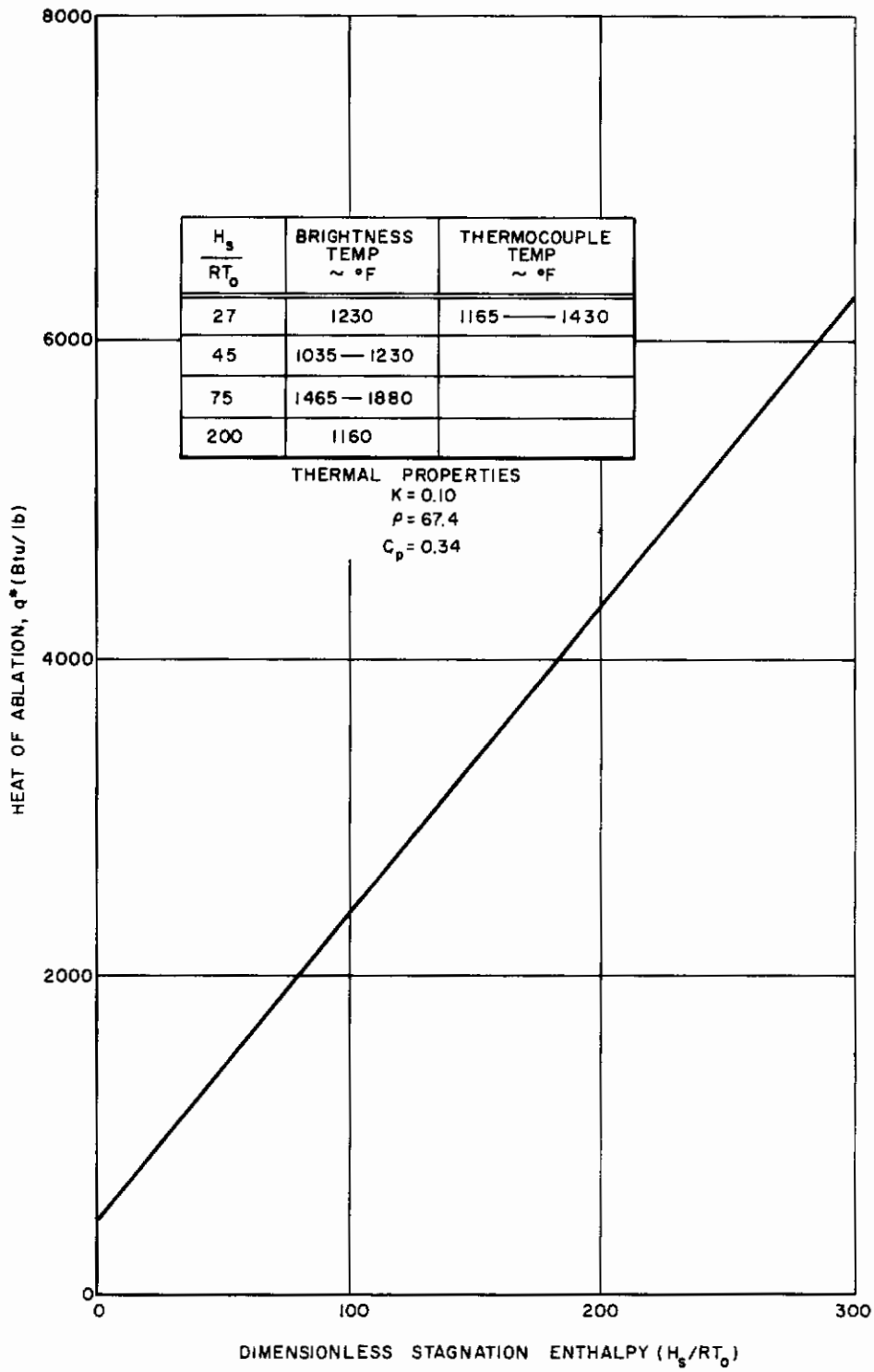

Figure IV-9 EXPERIMENTAL DETERMINATION OF HEAT AND TEMPERATURE OF ABLATION

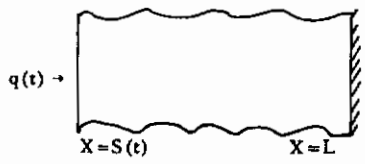

The mathematical statement of the problem is:

$$\rho c \frac{\partial T}{\partial t} = \frac{\partial}{\partial X}\left(k \frac{\partial T}{\partial X}\right) \quad S(t) \leq X \leq L$$

$$\left[-k \frac{\partial T}{\partial X}\right]_{X=S} = q_o(t) - \sigma \epsilon T^4 - \rho \dot{s} [H_v + \eta(H_e - H_w)]$$

$$\left[\frac{\partial T}{\partial X}\right]_{X=L} = 0 .$$

The resulting basic design curves which may be used to obtain the design thickness for a given aerodynamic shape are shown in figure IV-10.

Figure IV-10 may be used to derive heat-shield thickness for structure temperatures other than 300°F and allow for other surface temperatures.

Figure IV-11 shows typical temperature distribution histories and ablation rates, and illustrates the relative importance of the ablation and conduction processes on the thickness determination.

2) Radiation shield

Because of the low heating in the aft region, the radiation shield design was carried for comparison purposes. The design of a radiation shield demands that the maximum surface temperature not exceed a prescribed limit and a second boundary condition limits the structure temperature. The shields considered here consist of a thin layer of stainless steel backed up by Min-K insulation. The metal sheets emit much of the energy and reach a radiation equilibrium (maximum surface) temperature. This type of design is very sensitive to heat flux and safety factors must be very carefully determined.

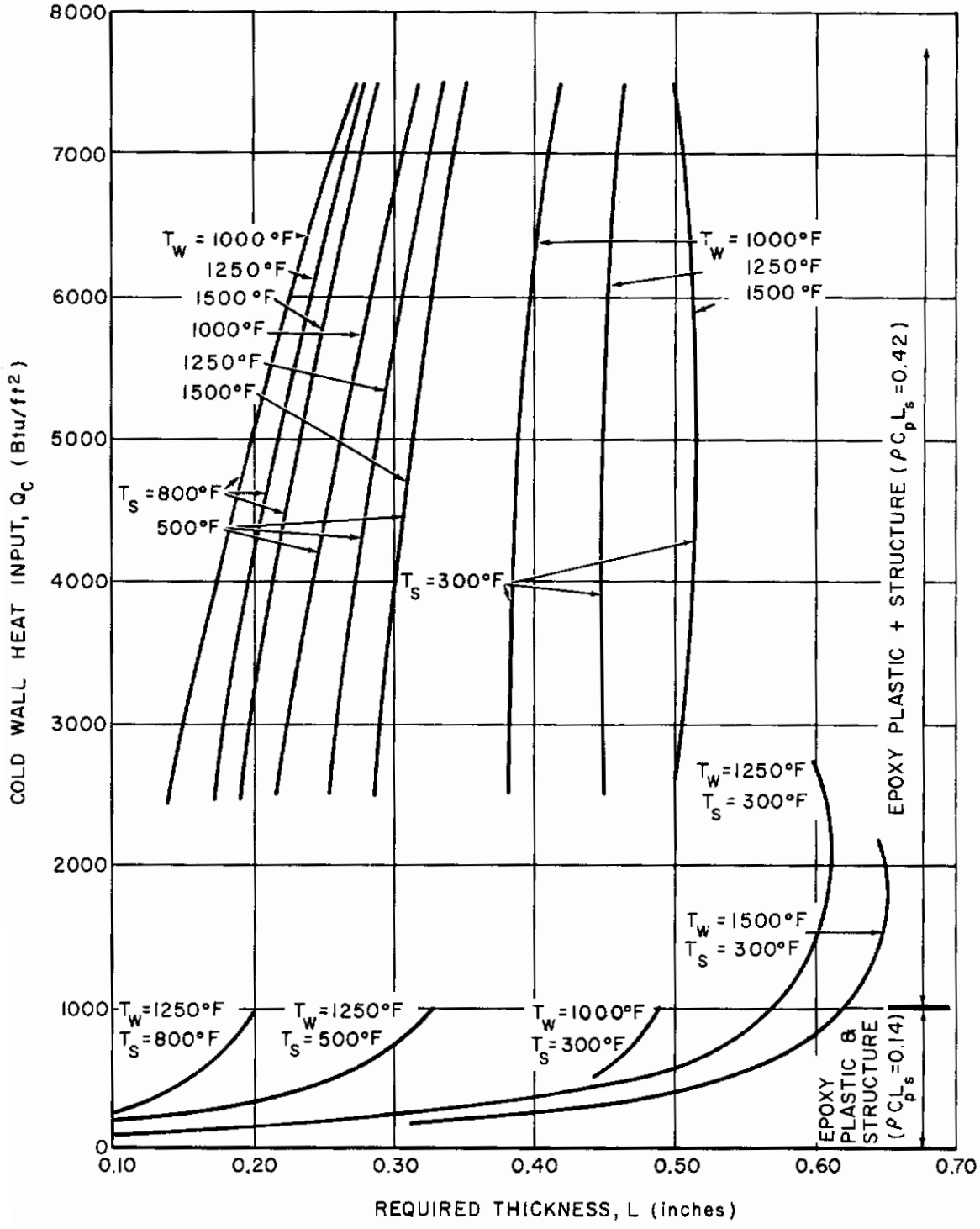

Figure IV-10 RELATIONSHIP OF HEAT-SHIELD DESIGN PARAMETER VARIATION
γ_e = -3°, V_e = 26,000, $W/C_D A$ = 33

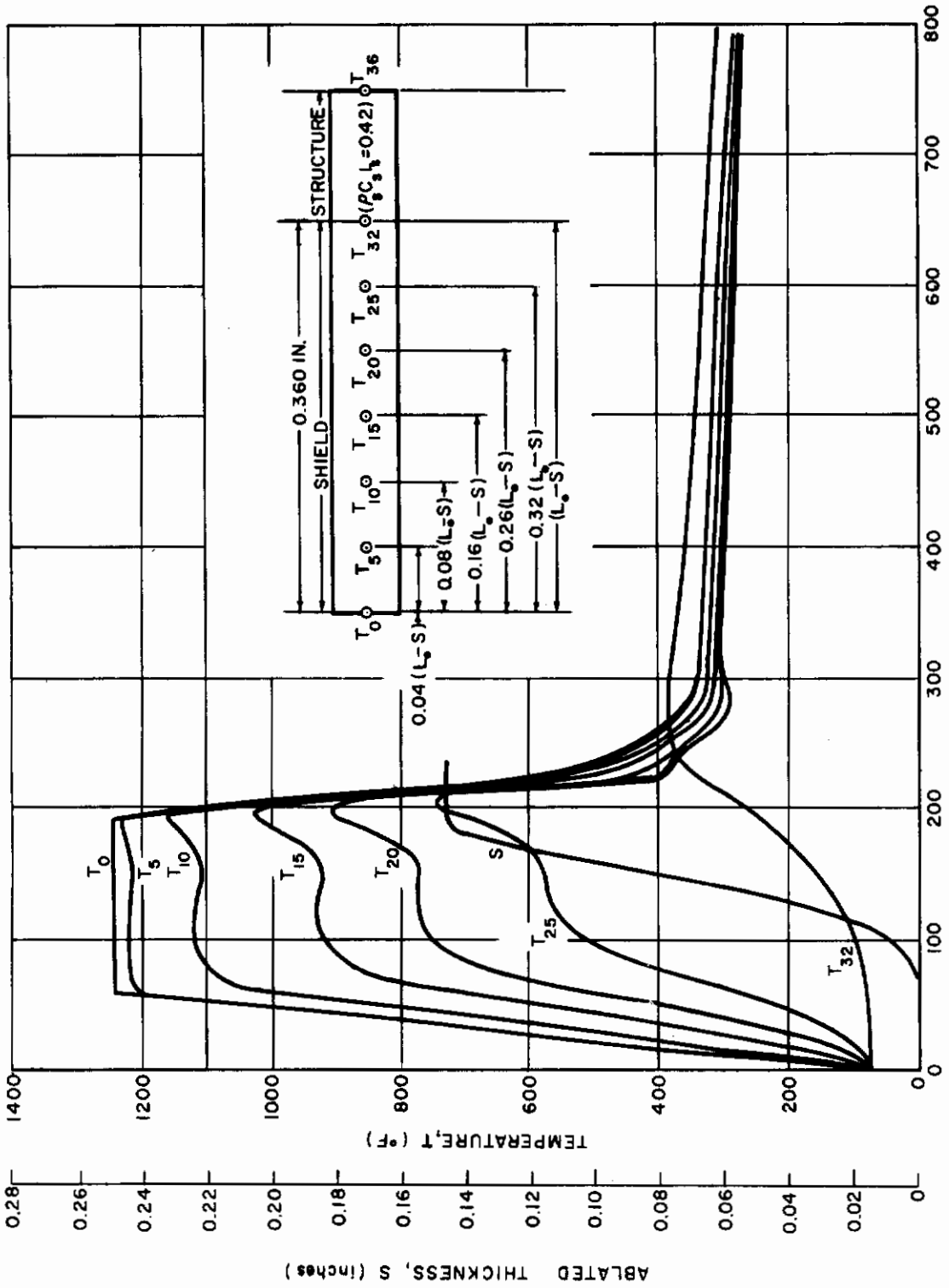

Figure IV-11a TIME-TEMPERATURE HISTORY-STAGNATION REGION;
MATERIAL: 0.360-INCH SHIELD + $\rho_s C_s L_s = .42$
$\gamma_e = -3°$, $V_e = 26,000$, $W/C_DA = 33$, $Q_c = 5000$ Btu/ft^2,
$T_w = 1250°F$, $T_{initial} = 70°F$

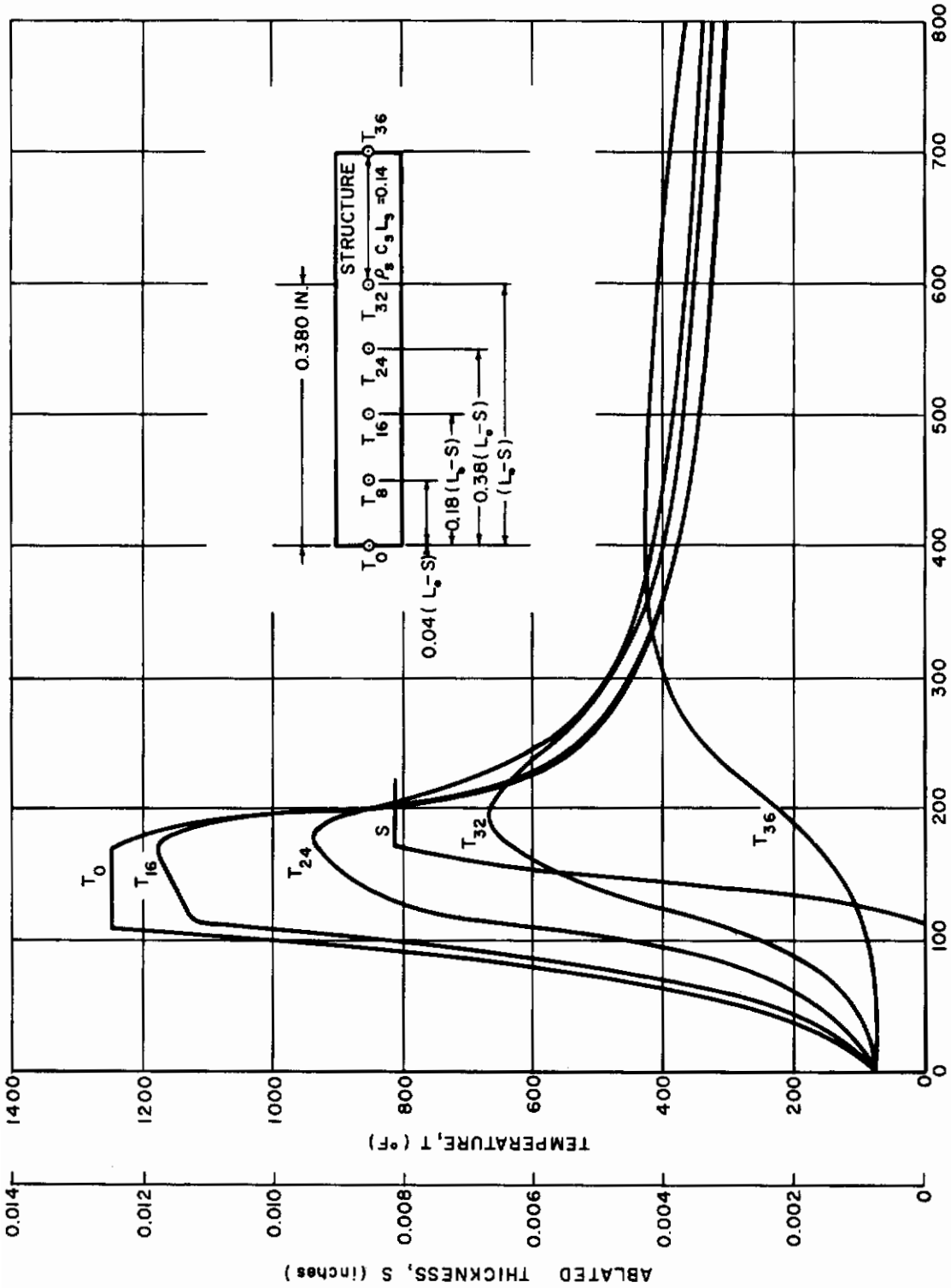

Figure IV-11b TIME-TEMPERATURE HISTORY - CYLINDER REGION;
MATERIAL: 0.380-INCH SHIELD + $\rho_s C_s L_s = .14$
$\gamma_e = -3°$, $V_e = 26,000$, $W/C_D A = 33$, $Q_c = 900$ Btu/ft^2,
$T_w = 1250°F$, $T_{initial} = 70°F$

The mathematical formulation given below is solved numerically with the experimentally obtained thermal properties. Using a one-dimensional model with one boundary heated arbitrarily, a thin metallic shield is placed in front of (and in contact with) a layer of insulation.

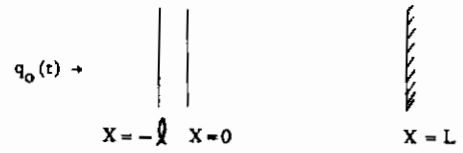

The mathematical statement is:

$$\rho_1 c_1 \frac{\partial T}{\partial t} = \frac{\partial}{\partial X}\left(k_1 \frac{\partial T}{\partial X}\right) \qquad 0 \leq X \leq L ,$$

$$-k_1 \left.\frac{\partial T}{\partial X}\right|_{X=0} = q_o - \rho_0 c_0 \ell \frac{\partial T}{\partial t} - \sigma \epsilon T^4 ,$$

$$\left.\frac{\partial T}{\partial X}\right|_{X=L} = 0 ,$$

where

subscript 0 refers to the metallic shield,

subscript 1 refers to the insulation shield.

Since weight must be limited for efficient design, then $\rho_0 \ell$ must be made small and $\frac{\partial T}{\partial t}$ will also be small since the heat pulse is low and long and changes slowly, i.e., $\frac{\partial q}{\partial t}$ is small. It remains that the heat radiated away from the shield, $\sigma \epsilon T^4$ must be made larger. The radiation shield itself is metallic primarily because emissivity is high (>0.85) and the temperatures may go as high as 2500°F for some well-known feasible materials. The insulator must have a melting temperature at least as high as the "radiation equilibrium" temperature of the shield.

A feasible radiation shield design would have structural support. The angle-of-attack effect on heating may preclude the use of such design as the heating rates may exceed the maximum fluxes (q =40 Btu/ft^2-sec) which a radiation shield may tolerate.

3. Aerodynamic Effects and Structural Design Criteria

It was shown above that a re-entry satellite capsule may be designed to survive the re-entry. The reference material was used for a typical trajectory and rather stringent structural temperature requirements. It will be shown below that the capsule will survive the re-entry for a broad flight envelope (V_e - γ_e) either with minor modifications in shield thickness or relaxation of the low-structural temperature requirements. The evaluation will be limited to the reference material in Table IV-1.

a. Vehicle Aerodynamics Effect

The heat-shield design will be affected by the trajectory traversed by the vehicle and its motions in the flight. The resulting aerodynamic heating (and its variation) Q_c and its distribution will serve as the final input to the shield design. The parameters of concern are the re-entry velocity (V_e) and angle (γ_e), ballistic coefficient (W/C_DA) which will create a thermal environment in terms of Q_c and q_{max} and the significant heating time the shield is exposed to it. As in reference IV-1 the evaluation may be reduced to Q_c/q_{max}, τ_i (pulse duration) and Q_c investigation, the effects of the latter one being shown in preceding sections. In the satellite problem on hand, the most significant variations in the flight envelope are due to γ_e variation which will be shown below. The angle of attack, α , is also of concern and would affect especially low heat input area away from stagnation.

1) Re-entry angle

The re-entry angle affects significantly both Q_c/q_{max} and τ_i , and as it decreases, the critical design points are reached, the pulse shape becomes flat and the duration is extended creating serious insulation problems as the L_a/L_{ins} decreased. The effect on Q_c is somewhat smaller. Velocity will affect primarily Q_c, and thus its effect is similar to the latter. W/C_DA affects primarily pulse duration.

The flight envelope considered here extends from -2 to -5 degrees, with essentially constant (high) re-entry velocities and constant (low) W/C_DA. The heat inputs are of low order of magnitude <7700 Btu/ft^2 and thus the relative effects cannot be readily compared with the high-performance flight envelope. The Q_c/q_{max} are of

order of magnitude different, and variation due to relatively small change in γ_e is much larger. Q_c/q_{max} (seconds) for high-performance re-entry is 8 to 15; while for satellites it is 50 to 150. Since material thermal conductivities are not decreased proportional, not only peak to impact time has to be considered but perhaps the whole pulse duration. Thus the effect of Q_c/q_{max} will be here relatively more important than for ICBM conditions, while pulse duration may be of lesser importance as thermal equilibrium conditions may be approached.

Figure IV-12 shows the relation between γ_e and Q^*_{eff}, for the stagnation region for various allowable structural temperatures. The change in total heating Q_c is from 5100 to 7700 for γ_e's, 2° and 5°, respectively. It is clear that the effectiveness (L_a/L_{ins}) and efficiency (Q^*_{eff}) both decrease as the re-entry angle decreases in magnitude and that lower allowable structure temperatures enhance this trend.

The local weight in the stagnation region increases 100 percent and in the low heating region 150 percent as γ_e varies from 5 to 2 degrees. It may be noted that the change is much more significant for the low angle (2 to 3 degrees) than for larger angles. Curves showing parametric variation of Q^*_{eff} for fixed Q_c and varying Q_c/q_{max}, r_i and γ_e would indicate their relative importance and would be of interest as they might permit evaluation of the effect of velocity and ballistic coefficient changes, should such be considered. In a sense, they would proportion the relative effects of pulse shape and duration contribution to the γ_e effects.

2) Angle of attack

The possible variation in angle of attack (α) would affect primarily the aft portions of the body as the heating may increase by a large factor. The thickness requirements for various heat inputs were illustrated in figure IV-10. Thus it appears that to account for possible variation in the angle of attack, the maximum thickness indicated in figure IV-10 should be used, however the resulting increase in local weight still would not be excessive for an ablator. With the heat inputs obtained from α variation, the advisability of use of a radiation shield or heat sink on the other hand becomes questionable (Fig. IV-2).

The effect of the total heat input for the case considered is of low order as the increasing material efficiency compensates for larger requirements for heat capacity (Figs. IV-2 and IV-10). As noted before, the change in structure temperature allowed will alter the picture.

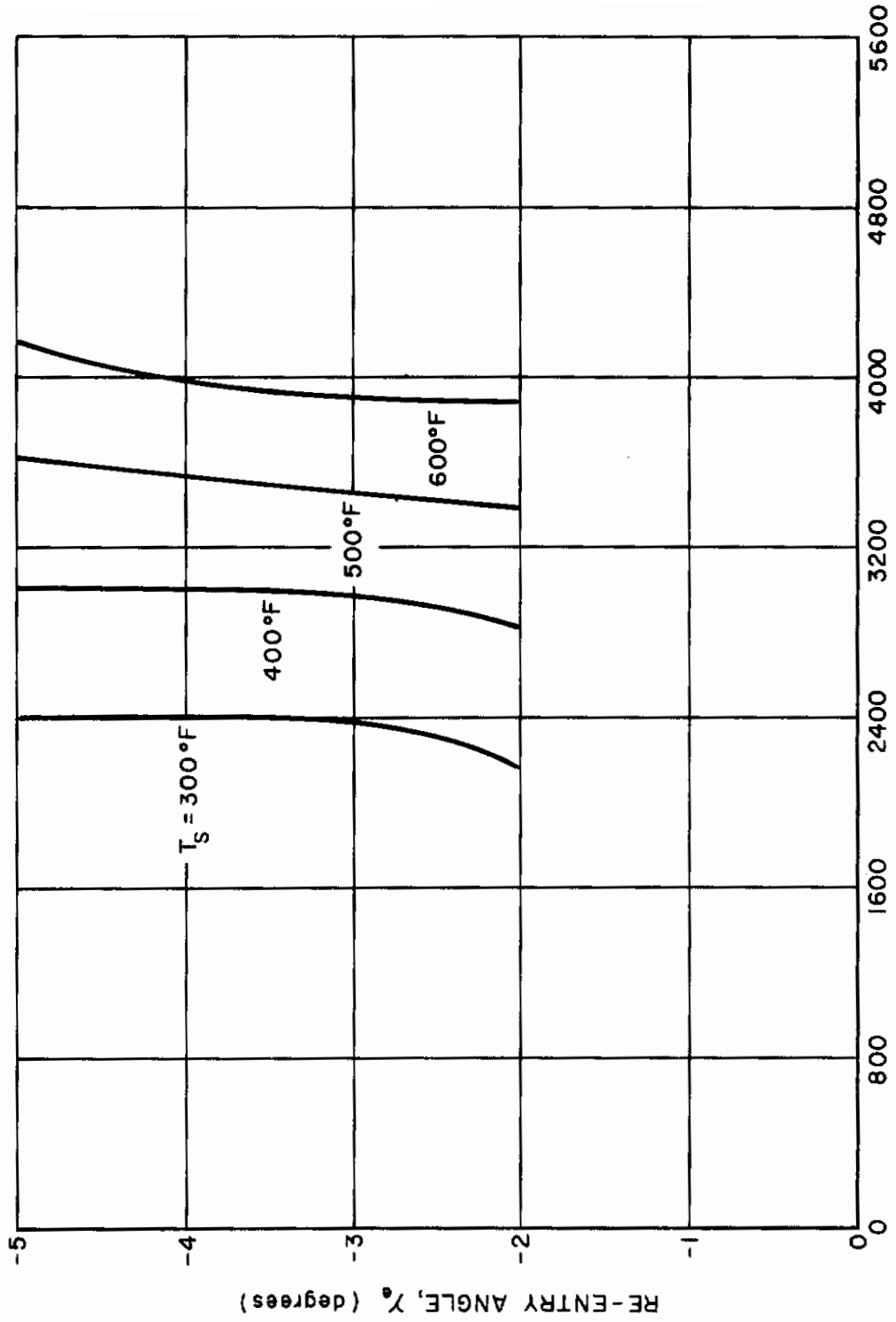

Figure IV-12 RE-ENTRY ANGLE EFFECT ON HEAT-SHIELD EFFICIENCY;
MATERIAL: SHIELD + $\rho_s C_s L_s$ = .42
V_e = 26,000, T_w = 1250°F, $T_{initial}$ = 70°F

b. Structure Temperature and Thickness Effect

These two effects are related to each other as both effectively allow for a higher heat capacity of the structure. T_s changes, in addition, affect the allowable temperature gradient in the shield. It is possible to optimize the heat-shield structure composite by taking advantage of combined thermo-structural analysis, accounting simultaneously for structure strength, temperature, and heat capacity (Ref IV-14). However, such study is beyond the scope of this paper, which merely points out the effect of the latter two variables.

The effect of T_s was shown in combination with other parameters in the preceding figures IV-4, IV-5, IV-10. Figure IV-13 illustrates the increase in Q^*_{eff} with increase in T_s allowable for various design conditions. As with the γ_e effects, the weight savings diminish as the T_s are increased, and between 600° to 800°F would be much smaller than for 300° to 600°F range. It is definitely advantageous to increase structural temperatures from 300° to 500°F as the weight saving will exceed 30 percent in the nose cap, and 45 percent in the cylinder portion. The difference in weight saving for both regions is explained by the heat input levels and structure heat capacity. The effective savings for low heat input areas are much larger, as the insulation requirement is controlling.

The effect of the heat capacity, $\rho_s C_{p_s} L_s$, is shown in figure IV-14 for representative heat inputs and it is clear that increased structure heat capacities are beneficial. This was expected as the shield and structure approach equilibrium before termination of the flight.

4. Design Safety Factors

The safety factor necessary in the shield design for a given re-entry condition simply reflects the uncertainty in either the properties of materials or behavior of the body under conditions which cannot be simultaneously simulated on the ground. Reasonable bounds of uncertainty in knowledge may be, however, attached to the significant parameters and thus the safety factors may be evaluated. Q_c, q^*, T_w, and k are the significant inputs in this case.

Thickness of the shield for the design conditions used here is a weak function of Q_c in the stagnation area (Fig. IV-10). Twenty-five percent uncertainty in Q_c will not affect the thickness. In the lower heat input region, thickness will change with the heat input and a safety factor should be attached to Q_c. The structure temperature will affect the choice as well as the surface temperature, even in the stagnation portion and a "safe value" of heating will have to be assumed.

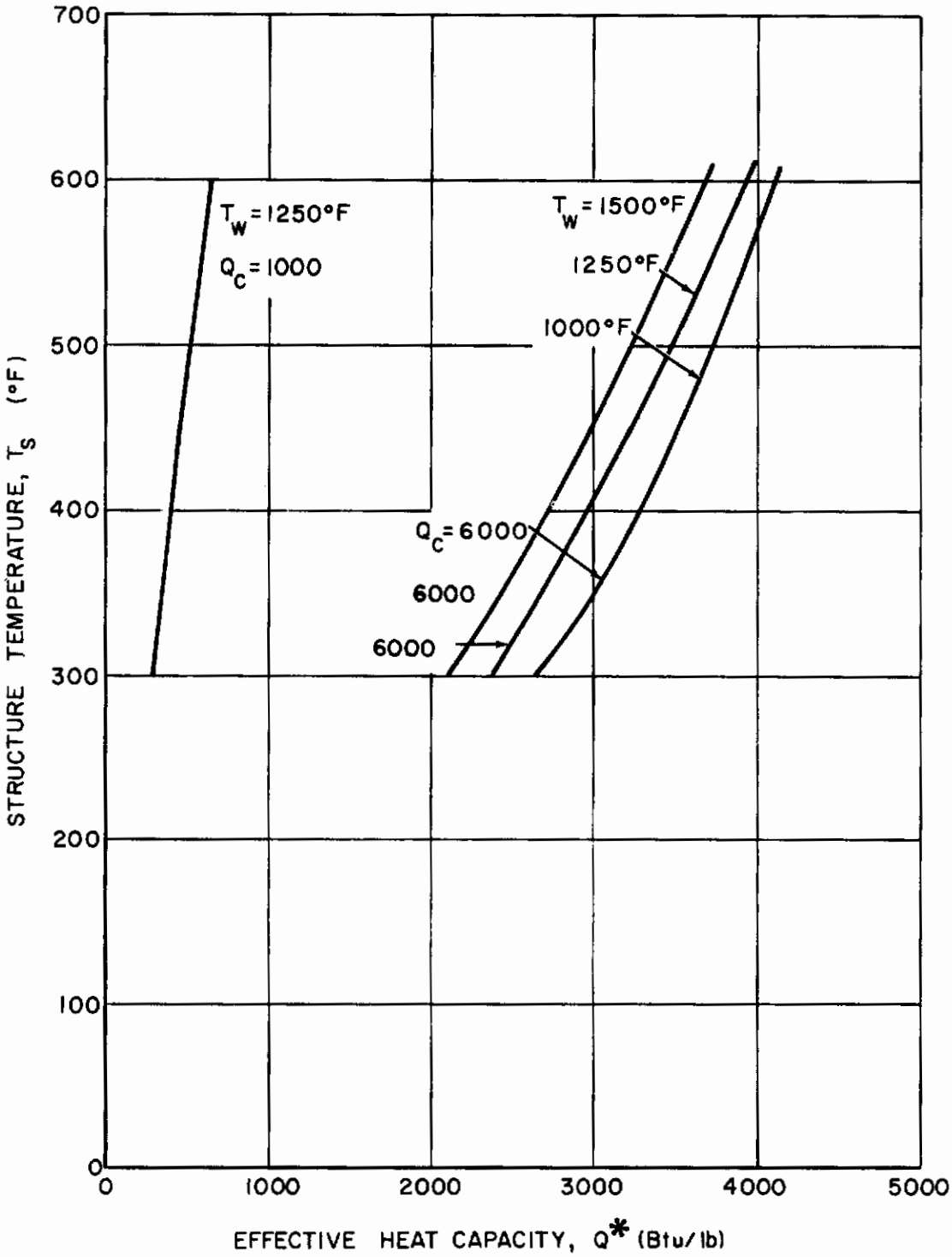

Figure IV-13 STRUCTURE TEMPERATURE EFFECT ON MATERIAL EFFICIENCY

$\gamma_e = -3°$, $V_e = 26,000$, $T_{initial} = 70°F$

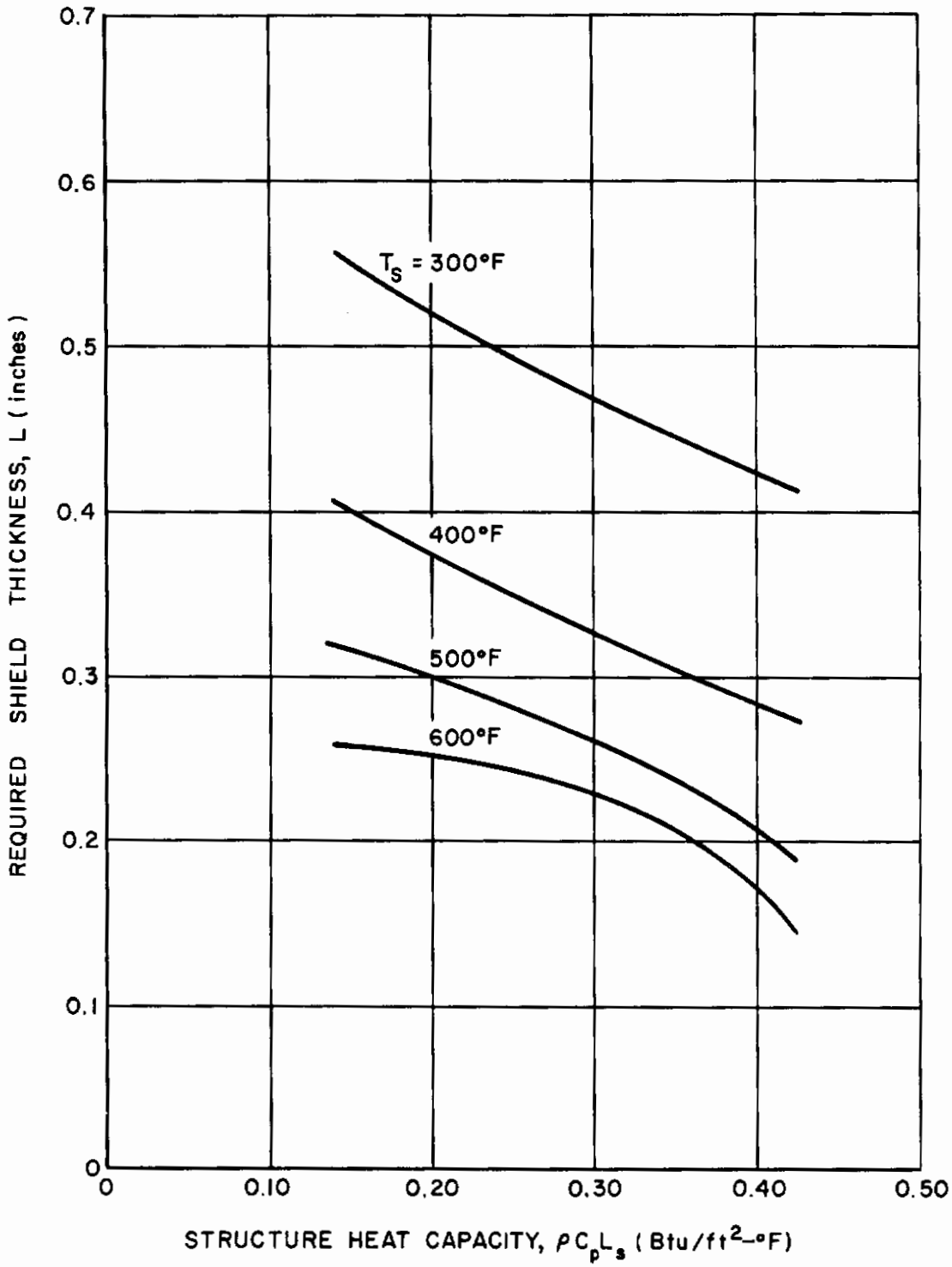

Figure IV-14 STRUCTURE HEAT CAPACITY EFFECT ON MATERIAL EFFICIENCY

γ_e = -3°, V_e = 26,000, $T_{initial}$ = 70°F, T_w = 1250°F, Q_c = 900 Btu/ft^2

The surface temperature produces a significant effect on the shield thickness (Figs. IV-3 and IV-4) and the likely uncertainty should be used as a safety factor. In this case a 10 percent factor appears to be sufficient. The same reasoning applies to the effect of conductivity (Fig. IV-7) and especially so for low heat inputs. Note should be made here that neglecting the chemical reaction in the sub-surface layer provides a safety factor for both T_w and k, under the assumptions of this study. The safety factor on heat of ablation is not significant for low heat inputs as little or no ablation occurs, but it will be important on the stagnation region as shown in figure IV-6. A safety factor on η of the order of 10 percent will be sufficient and H_v effect was shown to be negligible (Fig. IV-5).

In all safety factor evaluations the effect of T_s has to be considered as it strongly affects Q^*_{eff}. The regions of L insensitivity to Q_c or q^*, as the case may be, will vary.

Some of the more important "trade-offs" in shield design, in terms of percent local weight change with change in the more important parameters discussed above, as shown in figure IV-15 illustrating the safety factor requirements.

In conclusion, depending on the structural and trajectory criteria, a careful analysis of safety factor requirements should be made for each design, and no lumped safety factors should be used. As a rule, the uncertainty in the knowledge of the individual parameters should be considered and dictates the safety factor selection. Depending on the weight limitations imposed by the specifications, a "design point" will be selected reflecting a compromise between those and the anticipated combination of uncertainties resulting in the largest weight penalty.

The selection of the "design point" is not a safety precaution, but reflects a desire for a flight envelope flexibility. Usually a thermo-structural analysis will define this point as maximum heating trajectory, i.e., $V_{e_{max}}$ and $\gamma_{e_{minimum}}$. In addition the angle-of-attack effects resulting from attitude control philosophy have to be taken into account for successful design of a re-entry vehicle.

C. SUMMARY AND CONCLUSIONS

Previous studies (Ref. IV-1) of heat shield designs for re-entering space vehicles were extended and applied to a satellite re-entry capsule. The feasibility of low-temperature ablation design was demonstrated with stagnation Q^*_{eff} ranging from 2500 to 4000 Btu/lb. A design study of a heat shield to survive a broad range of the aero-thermodynamic environmental conditions on the $V_e - \gamma_e$ was

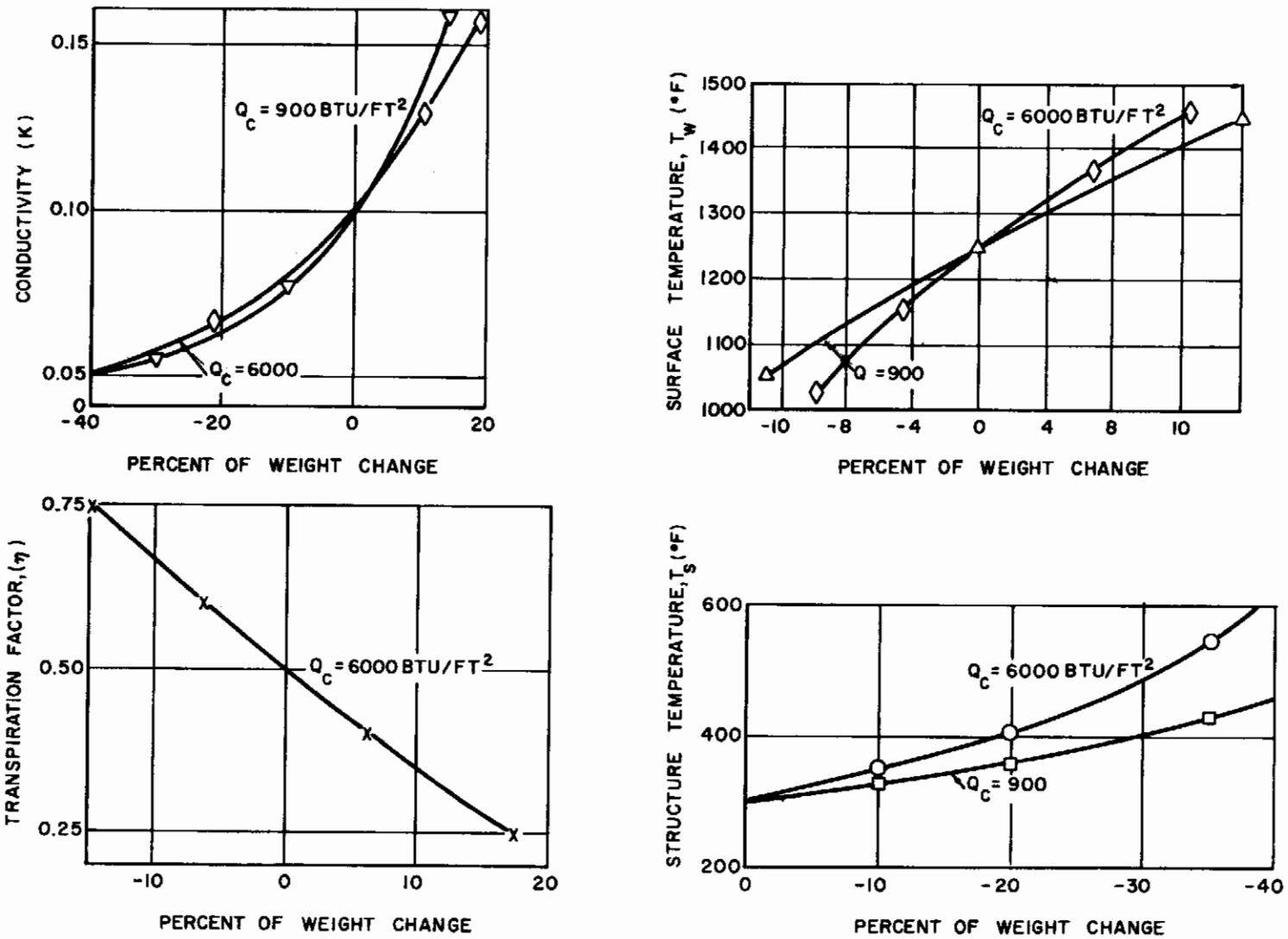

Figure IV-15 TRADE-OFF IN HEAT-SHIELD DESIGN

presented, and its performance evaluated. The approach to heat-shield design problems was described with emphasis on material evaluation and selection importance, and design procedures were outlined. Material, trajectory, vehicle motion, and structural design criteria were discussed, and the most significant re-entry design parameters were determined to be T_w, k, η, T_s, γ_e and α. The mutual dependence of the various factors in the heat shield design was studied and their relationships shown in graphical form. A brief discussion of the safety factors required for design was included. Throughout the study both the stagnation region and aft portions of the capsule were investigated since the heat input levels differ greatly. As the result of the study it was concluded that:

1. Design of satellite re-entry bodies utilizing low-temperature ablation materials presently available ($T_w \leq 1500°F$) is feasible, and preferable to an all heat sink and/or all radiation design.

2. The most significant parameters in the satellite capsule heat shield design are:

   a. Materials - surface (ablation) temperature, thermal conductivity, and blowing (transpiration) factor.

   b. Structural design - structural temperature allowable.

   c. Aerodynamic - re-entry angle, and angle of attack.

3. For the reference design conditions, little weight savings (<7%) in the stagnation region will be realized by increasing structure temperature (T_s) above 600°F, and/or by decreasing conductivity (k) below 0.05 Btu/ft-hr-°F and surface temperature (T_w) below 800°F. There is no upper limit on desirable increases in heat of ablation. In the afterbody, the limits of the parameters will be extended to, respectively, 400°F, 0.025 Btu/ft-hr-°F, and 500°F.

4. Development of lower temperature (T_w=700°F) ablators, or materials with significantly lower conductivities ($k \sim 0.025$ Btu/hr-ft-°F) is needed.

5. The interaction of all parameters should be considered in the heat shield design.

6. Investigation of the chemical reactions occurring in the surface layer is needed to permit better understanding of plastic material behavior and to relax safety factor requirements.

7. Safety factors should be applied to individual re-entry input parameters reflecting the uncertainty in their knowledge.

D. LIST OF SYMBOLS

C_p = Specific heat

f = Fraction of ablation material that is vaporized

H_v = Heat of vaporization (or thermochemical reactions)

H_e = Enthalpy at edge of the boundary layer

H_w = Enthalpy of gas at the wall temperature

k = Thermal conductivity

L_a = Ablated thickness

L_{ins} = Insulation thickness (left after ablation)

L_T = Total thickness required

L_s = Thickness of metallic structure

q_c = Cold wall aerodynamic heat transfer rate

q_o = Hot wall aerodynamic heat transfer rate

q^* = Effective heat of ablation

Q_c = Total cold wall heat input

Q^*_{eff} = Effective heat capacity

T_w = Ablation temperature

T_s = Structure temperature

t = Time

V_e = Initial re-entry velocity

W/C_DA = Ballistic coefficient

X = Space coordinate

α = Angle of attack

ϵ = Emissivity

σ = Stefan-Boltzmann constant

ρ = Density

γ_e = Initial re-entry angle

τ_i = Pulse duration

E. REFERENCES

IV-1. Hurwicz, H. and J. Brown, Interaction of Ablation Material and Certain Trajectory Parameters in the Thermal Protection Design of Space Re-entry Vehicles, Avco RAD-TR-9(7)-59-28 (19 November 1959).

IV-2. Brown, J. D. and R. E. Mascola, Numerical Solution of the Heat Conduction Equation for a Composite Solid With a Receding (Decomposing) Surface, Avco RAD-2-TM-58-101 (September 1958).

IV-3. Brown, J. D., R. E. Mascola, and J. E. Morriello, Numerical Solution and Thermal Evaluation of the Transient Heat Conduction for a Solid with a Receding (Ablating) Surface, Avco RAD (to be published).

IV-4. Georgiev, S., H. Hidalgo, and Mac C. Adams, On Ablation for the Recovery of Radiation, Avco Research Laboratory, Research Report 47 (March 1959).

IV-5. Warren, W. R. and N. S. Diaconis, The Performance of Ablation Materials as Heat Protection for Re-entering Satellites, IAS Paper No. 60-49, Presented at the IAS 28th Annual Meeting, New York (25-27 January 1960).

IV-6. Roberts, L., An Analysis of Ablation-Shield Requirements for Manned Re-entry Vehicles, Technical Report, NASA R-62 (1960).

IV-7. Wood, Dr. Robert M., and R. J. Tagliani, Heat Protection by Ablation, Douglas Aircraft Company, Inc., Engineering Paper No. 813 (21 August 1959).

IV-8. Fleddermann, R. G. and H. Hurwicz, Transient Ablation and Heat Conduction Phenomena at a Vaporizing Surface, Avco RAD-TR-9(7)-60-9 (April 1960).

IV-9. Hanst, P. L., The Infrared Emission Spectra of Plastics Ablating in a Low Enthalpy Air Stream: Measurements of Surface Temperatures and Temperature Profiles Behind the Surfaces, Avco RAD-7-TM-60-11 (29 February 1960).

IV-10. Jennings, R. L. and C. R. Easton, Surface Temperature of Ablating Teflon, Report No. SM-35759, Douglas Aircraft Company, Inc. (22 May 1959).

IV-11. Recesso, J. and P. Hanst, Unpublished Avco RAD Report.

IV-12. Ihnat, M., Unpublished Avco RAD Report.

IV-13. Ricles, R. E., S. Sokolsky, and J. Carswell, Effect of Re-entry Conditions on Heating and Loads for Shape 52, Avco RAD-2-TM-57-87 (November 1957).

IV-14. Rice, R., Unpublished Avco RAD Report.

IV-15. Berninger, C. F., W. Zeh, and W. Dickson, A Survey of the Structural Design and Analysis Problems of Ablating Re-entry Vehicles, presented at Fourth Symposium on Ballistic Missile and Space Technology (August 1959).

APPENDIX V

TRANSIENT THERMAL BEHAVIOR OF DECOMPOSING MATERIALS* PART I GENERAL THEORY AND APPLICATION TO CONVECTIVE HEATING

by T.R. Munson and R.J. Spindler

A. INTRODUCTION

In the past several years an exuberant literature has developed with regard to self-regulating mass transfer for thermal protection. This phenomenon is generally referred to as ablation and interest in the problem seems to have been spurred primarily by the problems associated with hypersonic flight. The status of our understanding of the ablation phenomenon has been adequately covered by Adams (Ref. V-1) and more recently by Hidalgo (Ref. V-2), Steg (Ref. V-3), Barriault and Yos (Ref. V-4), Scala (Ref.V-5), Scala and Gilbert (Ref. V-6), and by Hurwicz (Ref. V-7).

The major portion of the theoretical work which has appeared dealing with the ablation process has been concerned with the behaviour of glassy materials. Predictions based on these treatments have been adequately confirmed by laboratory and flight test experiments. On the other hand, no generally satisfactory treatment of ablation in materials which undergo thermal decomposition in depth has appeared in the literature. The only transient treatment appears to be that of Barriault and Yos (Ref. V-4) which suffers from severe limitations and no calculations appear to have been made with their model. Other treatments have been restricted to steady state (Refs. V-5, 6, 8, 9), usually requiring very drastic and often incompatible assumptions in order to effect a mathematical solution. As a result the expressions obtained are of questionable value even for steady state application. Hurwicz (Ref. V-7) presents a review of the state of the art with regard to ablation in decomposable materials and the arguments for the desirability of a transient analysis.

In practice the ablation phenomenon is most often applied in situations where the environmental parameters are rapidly varying functions of time. This fact coupled with the necessity for working with heat shields of finite thickness and usually within rather tight limits on allowable structural temperatures makes it necessary to perform transient calculations. The advent of modern high speed computers brings these calculations into the realm of practicality for even quite complex systems. In this paper a mathematical model is presented for the transient behaviour of materials which decompose in depth. Numerical results are presented for several cases involving convective heating and comparison is made with experimental results.

*This work was supported by USAF Contract AF04(647)-305,-258, and -806 and is presented here for information purposes.

B. DISCUSSION

Any attempt at a mathematical description of nature involves a series of compromises. In the model presented here, an attempt has been made to strike a balance between physical rigor on one hand and the practical necessity for obtaining numerical results in terms of physically measurable material properties.

Qualitative description of the ablation process in polymeric materials are available in many sources (Ref. V-7) and will not be detailed here. In brief, however, when subjected to environmental conditions severe enough to cause mass transfer in addition to energy transfer by conduction and radiation, certain materials, such as polytetrafluoroethylene, undergo a thermal degradation which yields only gaseous products. Other materials, such as the silica fiber reinforced plastics yield a set of gaseous products and in addition produce a more or less complex porous condensed phase. In either case the flow of gaseous decomposition products toward the heated surface alters the energy transfer process from one of conduction. In the present model, energy transfer within the decomposable material is considered to occur by conduction, convection, and radiation.

Conceptually the virgin material is considered as a hypothetical mixture consisting of an irreducible "char matrix" (denoted by the subscript 2) and an "active material" (subscript 1) which undergoes thermal decomposition yielding only gaseous products. This decomposition reaction is assumed to follow an "n'th" order rate law with the rate constant being a simple Arrhenius function of temperature. The material is assumed to have continuously variable properties throughout and as a result it is neither necessary nor desirable to define a "charring temperature" as in Barriault and Yos (Ref. V-4) or a "reaction zone thickness" as in Scala and Gilbert (Ref. V-6). This feature of the present model provides definite advantages, both conceptual and computational, over a model requiring charring temperatures as a basic input.

Consider a cross section through a typical heat shield of the ablative type. In general the material affording the thermal protection will be backed up by one or more materials which act as structural members, as bonding materials, etc. Figure V-1 illustrates such a cross section for a shield consisting of the primary material with two back up materials acting as a bonding agent and a structural material, respectively. For the present purposes these secondary materials are considered to be nonporous, non-decomposable, and opaque. The heat transfer process in these materials is by simple conduction.

Consider a control volume within the primary material whose surface is receding at an unsteady rate $\dot{s}(\tau)$. Choosing unit cross sectional area for the bar the volume between the planes x and $(x+dx)$ is then dx. Gaseous decomposition products are produced in unit volume at a rate $(-\dot{\rho}_1)$, this being the rate at which the active component of the primary material undergoes thermal decomposition. It is assumed that the gases produced in the decomposition are

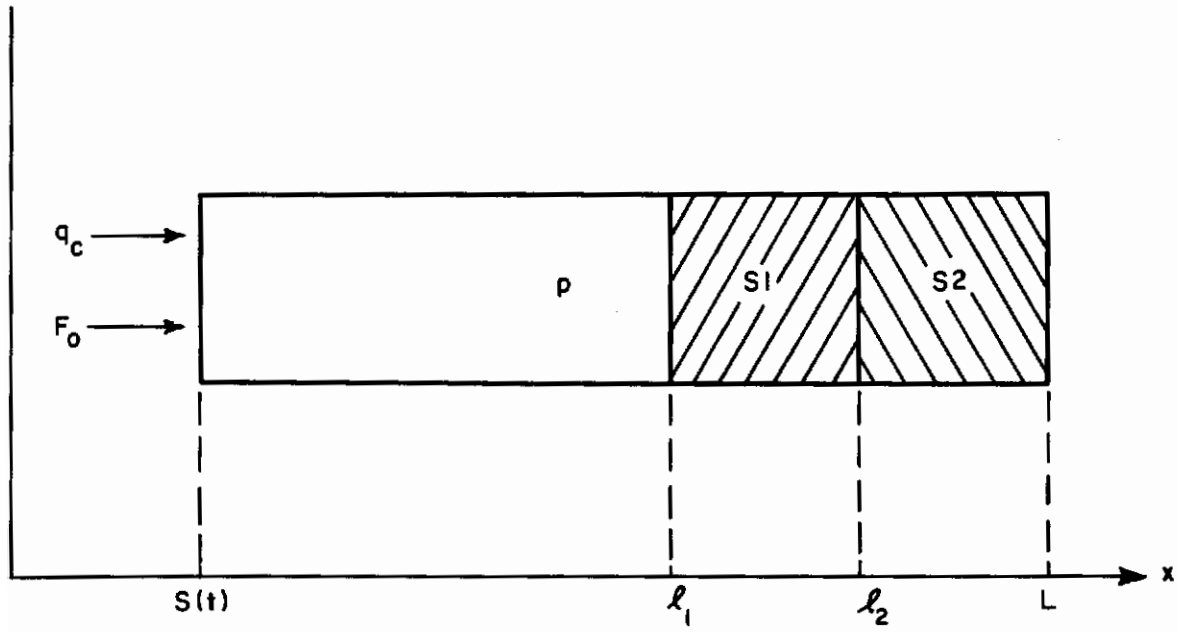

Figure V-1 GEOMETRY AND COORDINATE SYSTEM

free to move in the direction of negative x and that thermal equilibrium exists between the gaseous and condensed phases at all points in the material. Letting w denote the mass of gas flowing across unit cross-sectional area in unit time, continuity requires that equation (V-1) be satisfied;

$$\frac{\partial w}{\partial x} = \dot{\rho} \ . \tag{V-1}$$

In the materials for which the model was developed, there is no evidence that internal pressure forces play any significant role in the ablation process. If this assumption is made, a very considerable mathematical simplification results since there is no need to write a momentum equation for the flow of the decomposition products toward the heated surface.

The total heat, dQ, added to the control volume in time dt is the sum of the contributions due to thermal conduction, dQ_k, by gas flow, dQ_g, by chemical reaction, dQ_c, and by the absorption of radiant energy, dQ_R;

$$dQ = dQ_k + dQ_g + dQ_c + dQ_R \ . \tag{V-2}$$

Considering the one-dimensional case these contributions are given by equations (V-3) through (V-6);

$$dQ_k = \frac{\partial}{\partial x}\left(k \frac{\partial T}{\partial x}\right) dx\, dt \ , \tag{V-3}$$

$$dQ_g = \frac{\partial}{\partial x}(w h_g)\, dx\, dt \ , \tag{V-4}$$

$$dQ_c = \dot{\rho}_1 \Delta H_c\, dx\, dt \ , \tag{V-5}$$

$$dQ_R = -\frac{\partial F}{\partial x}\, dx\, dt \ . \tag{V-6}$$

In these equations k is the thermal conductivity of the bulk material, h_g is the specific enthalpy of the gaseous products, ΔH_c is the heat absorbed per unit mass of gases produced, and F is the radiant flux at any point in the material. Assuming a constant specific heat for the gaseous decomposition products and making use of the thermal equilibrium assumption dQ_g can be written in the form of equation (V-7);

$$dQ_g = C_g \left(w \frac{\partial T}{\partial x} + \dot{\rho}_1 T\right) dx\, dt \ . \tag{V-7}$$

The heat added to the control volume is then given by equation (V-8).

$$dQ = \left[\frac{\partial}{\partial x} \left(k \frac{\partial T}{\partial x} \right) + C_g w \frac{\partial T}{\partial x} + \dot{\rho}_1 (C_g T + \Delta H_c) - \frac{\partial F}{\partial x} \right] dx\, dt . \tag{V-8}$$

The heat equation is found by equating dQ to the change in enthalpy of the control volume and neglecting higher order differential products:

$$\frac{d}{dt} (\rho h) = \frac{\partial}{\partial x} \left(k \frac{\partial T}{\partial x} \right) + C_g w \frac{\partial T}{\partial x} + \dot{\rho}_1 (C_g T + \Delta H_c) - \frac{\partial F}{\partial x} . \tag{V-9}$$

In equation (V-9) ρ and h are the density and specific enthalpy of the control volume. Both the density and enthalpy are considered to be additive functions of the contributions due to the "inactive" and the "active" material present in the control volume. The contributions to average density and specific enthalpy due to the presence of gases have been neglected. Again assuming constant specific heats the density and specific enthalpy may be written in the form of equations (V-10) and (V-11):

$$\rho = \rho_1 + \rho_2 , \tag{V-10}$$

$$h = \left[\left(\frac{\rho_1}{\rho_1 + \rho_2} \right) C_{p1} + \left(\frac{\rho_2}{\rho_1 + \rho_2} \right) C_{p2} \right] T . \tag{V-11}$$

Combining equations (V-10) and (V-11) yields equation (V-12);

$$\rho h = \left[\rho C_{p1} + \rho_2 (C_{p2} - C_{p1}) \right] T , \tag{V-12}$$

or

$$\rho h = A_1 \rho T + A_2 T . \tag{V-13}$$

A similar line of reasoning with regard to the thermal conductivity results in equation (V-14):

$$k = B_1 \rho + B_2 , \tag{V-14}$$

where

$$B_1 = \left(\frac{k_0 - k_2}{\rho_0 - \rho_2} \right) , \tag{V-15}$$

$$B_2 = k_0 - B_1 \rho_0 . \tag{V-16}$$

In these equations the subscript 0 refers to the original undecomposed material. The specific heat and thermal conductivity as defined by equations (V-13) and (V-14) are not temperature dependent in the usual sense but are instead functions of the time-temperature history through their dependence upon the density ρ . The quantity ρ_2 is considered to be a constant and the quantity ρ_1 is assumed to vary in accordance with a "n'th" order decomposition law;

$$\dot{\rho}_1 = -\rho_1^n \, A \exp\{-B/T\} . \qquad \text{(V-17)}$$

Combining equations (V-10) and (V-17) we then obtain equation (V-18).

$$\dot{\rho} = -(\rho-\rho_2)^n \, A \exp\{-B/T\} . \qquad \text{(V-18)}$$

The radiant flux, F , appearing in equation (V-9) is separated into two portions. One portion, F_1 , is due to internal self glowing of the material and the second part, F_2 , is a result of the transport of radiant energy incident on the surface of the material in an environment which includes radiative heating.

The last term in equation (V-9) is then written as the sum of two terms:

$$\frac{\partial F}{\partial x} = \frac{\partial F_1}{\partial x} + \frac{\partial F_2}{\partial x} . \qquad \text{(V-19)}$$

The contribution due to internal self glowing follows the formulation of Kadanoff (Ref. V-10) and Spindler and Hurwicz (Ref. V-11). Details of the formulation can be found in either of these references and will not be repeated here. The applicable relationships are given by the following equations:

$$J_e = 4 m^2 \sigma T^4 , \qquad \text{(V-20)}$$

$$\frac{\partial^2 J}{\partial x^2} = a^2 (J - J_e) , \qquad \text{(V-21)}$$

$$\frac{\partial F_1}{\partial x} = -\frac{a}{a^2} \frac{\partial^2 J}{\partial x^2} , \qquad \text{(V-22)}$$

$$F_1 = -\frac{a}{a^2} \frac{\partial J}{\partial x} . \qquad \text{(V-23)}$$

The formulation of the term in F_2 is straightforward and based on the same exponential absorption law used in formulating F_1. For constant optical properties, an incident flux F_o is attenuated in accordance with equation (V-24) where R_o is the reflectance of the interface $x = s$ and r is the distance traversed by the ray in the primary material;

$$F = F_0 (1 - R_o) \exp [-ar] . \tag{V-24}$$

Designating the reflectance of the interface at $x = \ell$, as R_ℓ and assuming the reflectance of the interface at $x = s$ is the same from either direction, it can easily be shown that consideration of multiple internal reflections results in the following relationships. The apparent reflectivity and apparent transmissivity are given respectively by equations (V-25) and (V-26):

$$R_A = \left\{ R_o + \frac{(1-R_o)^2 R_\ell \exp [-2a(\ell_1 - s)]}{1 - R_o R_\ell \exp [-2a(\ell_1 - s)]} \right\} , \tag{V-25}$$

$$r_A = \left\{ \frac{(1 - R_o)(1 - R_\ell) \exp [-a(\ell_1 - s)]}{1 - R_o R_\ell \exp [-2a(\ell_1 - s)]} \right\} . \tag{V-26}$$

The radiant flux leaving the interface at $x = s$ and travelling in the direction of positive x is then given by equation (V-27):

$$F_2(s) = \left\{ \frac{(1 - R_o)}{1 - R_o R_\ell \exp[-2a(\ell_1 - s)]} \right\} F_o . \tag{V-27}$$

The radiant flux leaving the $x = \ell_1$ interface and travelling in the direction of negative x is given by equation (V-28):

$$F_2(\ell_1) = \left\{ \frac{(1 - R_o) R_\ell \exp [-a(\ell_1 - s)]}{1 - R_o R_\ell \exp[-2a(\ell_1 - s)]} \right\} F_o . \tag{V-28}$$

The total radiant flux at any point x within the primary material is then given by equation (V-29):

$$F_2(x) = (1 - R_o) F_o \left\{ \frac{\exp [-a(x - s)] - R_\ell \exp [-a(2\ell_1 - x - s)]}{1 - R_o R_\ell \exp [-2a(\ell_1 - s)]} \right\} . \tag{V-29}$$

The term in F_2 for inclusion in equation (V-19) is then obtained from equation (V-29) by differentiation:

$$-\frac{\partial F_2}{\partial x} = a(1-R_o)F_o\left\{\frac{\exp[-a(x-s)+R_{\ell}\exp[-a(2\ell_1-x-s)]}{1-R_o R_{\ell}\exp[-2a(\ell_1-s)]}\right\} . \qquad \text{(V-30)}$$

Using the preceding results, equation (V-19) can be written in the form of the following set of equations:

$$-\frac{\partial F}{\partial x} = a(J-J_e)+a(1-R_o)F_o\left\{\frac{\exp[-a(x-s)]+R_{\ell}\exp[-a(2\ell_1-x-s)]}{1-R_o R_{\ell}\exp[-2a(\ell_1-s)]}\right\} . \qquad \text{(V-31a)}$$

$$\frac{\partial^2 J}{\partial x^2} = a^2(J-J_e) , \qquad \text{(V-31b)}$$

$$\frac{\partial J}{\partial x} = -\frac{a^2}{\alpha}F_1 , \qquad \text{(V-31c)}$$

$$J_e = 4m^2\sigma T^4 . \qquad \text{(V-31d)}$$

Equations (V-31) together with the initial and boundary conditions discussed in the next section serve to describe the absorption of radiant energy within the primary material.

Energy transfer within the secondary materials (designated by the subscripts s1 , s2 , etc.) is assumed to be solely by conduction. If it is further assumed that the thermal expansion coefficient of these materials is small, the governing equations including temperature dependent properties are of the form of equation (V-32) where the region of validity is $\ell_i < x < \ell_{(i+1)}$:)

$$(\rho C)_{si}\frac{\partial T}{\partial t} = \frac{\partial}{\partial x}\left(k_{si}\frac{\partial T}{\partial x}\right) . \qquad \text{(V-32)}$$

The complete set of differential and auxiliary equations governing energy and mass transfer within the composite heat shield of figure V-1 is then given by a combination of equations (V-1), (V-9), (V-13), (V-14), (V-18), (V-31), and (V-32). The resulting set of equations are as follows:

$s < x < \ell_1$:

$$(A_1\rho + A_2)\frac{\partial T}{\partial x} = (B_1\rho + B_2)\frac{\partial^2 T}{\partial x^2} + \left\{C_g w + B_1\left(\frac{\partial \rho}{\partial x}\right)\right\}\frac{\partial T}{\partial x} \quad .$$

$$- A(\rho-\rho_2)^n \{(C_g - A_1)T + \Delta H_c\} \exp(-B/T) \, .$$

$$+ aF_o(1-R_o)\left\{\frac{\exp[-a(x-s)] + R_\ell \exp[-a(2\ell_1 - x - s)]}{1 - R_o R_\ell \exp[-2a(\ell_1 - s)]}\right\}$$

$$+ a(J - 4m^2\sigma T^4) \quad , \qquad \text{(V-33)}$$

$$\frac{\partial w}{\partial x} = \frac{\partial \rho}{\partial t} \quad , \qquad \text{(V-34)}$$

$$\frac{\partial \rho}{\partial t} = -A(\rho-\rho_2)^n \exp(-B/T) \quad , \qquad \text{(V-35)}$$

$$\frac{\partial J}{\partial x} = -\frac{a^2}{a} F_1 \quad , \qquad \text{(V-36)}$$

$$\frac{\partial^2 J}{\partial x^2} = a^2(J - 4m^2\sigma T^4) \quad , \qquad \text{(V-37)}$$

$\ell_1 < x < \ell_2$:

$$(\rho C)_{s1}\frac{\partial T}{\partial t} = \frac{\partial}{\partial x}\left(k_{s1}\frac{\partial T}{\partial x}\right), \qquad \text{(V-38)}$$

$\ell_2 < x < L$:

$$(\rho C)_{s2}\frac{\partial T}{\partial x} = \frac{\partial}{\partial x}\left(k_{s2}\frac{\partial T}{\partial x}\right) \quad . \qquad \text{(V-39)}$$

Equations (V-33) through (V-39) together with an appropriate set of initial and boundary conditions completely describe the system.

1. Initial and Boundary Conditions

As initial conditions to the problem, both the temperature and density are specified throughout the primary material and the temperature is specified in the secondary materials. Any arbitrary distributions may be specified but normally the calculations are started for the virgin material at some constant low temperature. The initial conditions are thus given by equations (V-40):

$$T(x,0) = T_o \; (0 \leq x \leq L) \quad , \tag{V-40a}$$

$$\rho(x,0) = \rho_o \; (0 \leq x \leq \ell_1) \; . \tag{V-40b}$$

a. Boundary at x = s

For the cases considered here the surface recedes in a continuous fashion. Discontinuous removal based on a thermal stress criterion can be easily introduced into the computational scheme for those materials which exhibit such phenomena. Based on a continuous material removal process, a heat balance at the receding surface can be written in the form of equation (V-41):

$$q_c \left\{ \frac{H_o - H_s}{H_o} \right\} = - \left\{ (B_1 \rho + B_2) \frac{\partial T_p}{\partial x} \right\}_{x=s} + \rho_2 s f \left\{ h_v + \eta_2 (H_o - H_s) \right\}$$

$$+ (\rho_s - \rho_2) \dot{s} \left\{ \Delta H_c + \eta_1 (H_o - H_s) \right\} + w(s) \eta_1 (H_o - H_s) \; . \tag{V-41}$$

An additional boundary condition associated with the radiant flux F_1, is required. This condition is given by equation (V-42):

$$F_1(s) = - \frac{a}{s} \left\{ \frac{1 - R_o}{1 + R_o} \right\} J(s) \; . \tag{V-42}$$

In addition to these conditions a means of specifying the surface recession rate must be provided. In the present model this is done in two ways depending on the nature of the material being considered. For those materials which form a "char" layer ($\rho_2 \neq 0$) simultaneous measurement of recession rate and surface temperature suggest that $\dot{s}$ is uniquely determined by the surface temperature. Based on this observation,

equation (V-43) is employed to relate these two quantities where the constants are obtained empirically:

$$\dot{s} = \beta_1 T_s^{\beta_2} \exp\{-\beta_3/T_s\} . \qquad (V-43)$$

For materials, such as polytetrafluoroethylene, which form no permanent char ($\rho_2 = 0$) a relation based on the assumption of an instantaneous steady state is employed. This relation is obtained from equation (V-1) following a transformation to a coordinate system based on the surface and results in equation (V-44). Equation (V-44) together with the arbitrary condition given by equation (V-45) then serves to specify the recession rate:

$$\dot{s} = w(s)/(\rho_o - \rho_s) , \qquad (V-44)$$

$$\dot{s} = 0 \text{ for } (\rho_o - \rho_s)/\rho_o < 10^{-4} . \qquad (V-45)$$

b. Boundary at $x = \ell_1$

Three boundary conditions are required at this interface. Again one condition is required for the flux F_1 and is given by equation (V-46):

$$F_1(\ell_1) = \frac{a}{a}\left\{\frac{1-R_\ell}{1+R_\ell}\right\} J(\ell_1) . \qquad (V-46)$$

The second condition is a statement of the energy balance at the interface. Since the secondary materials are assumed to transport energy by conduction only, all energy entering the boundary leaves as a conduction flux:

$$\left(k_{s1}\frac{\partial T_{s1}}{\partial x}\right)_{x=\ell_1} = \left\{(B_1\rho + B_2)\frac{\partial T_p}{\partial x}\right\}_{x=\ell_1} - \frac{a}{a}\left\{\frac{1-R_\ell}{1+R_\ell}\right\} J(\ell_1)$$

$$- (1-R_o)F_o\left\{\frac{(1-R_\ell)\exp[-a(\ell_1-s)]}{1-R_o R_\ell \exp[-2a(\ell_1-s)]}\right\} \qquad (V-47)$$

The third boundary condition at $x = \ell_1$ is required by the continuity equation (V-34). The assumption of non-porous secondary materials then requires that equation (V-48) be satisfied:

$$w(\ell_1) = 0 . \qquad \text{(V-48)}$$

c. Boundary at $x = \ell_2$

The boundary condition at the $x = \ell_2$ interface is obtained simply by equating the conduction flux entering to that leaving the boundary:

$$\left(k_{s1} \frac{\partial T_{s1}}{\partial x}\right)_{x=\ell_2} = \left(k_{s2} \frac{\partial T_{s2}}{\partial x}\right)_{x=\ell_2} . \qquad \text{(V-49)}$$

d. Boundary at $x = L$

A number of boundary conditions may be written at this rear face. These include a constant temperature, radiative cooling, convective cooling, or a condition of insulation. For the present purposes the surface is assumed to be insulated and the applicable condition is given by equation (V-50).

$$\left(k_{s2} \frac{\partial T_{s2}}{\partial x}\right)_{x=L} = 0 . \qquad \text{(V-50)}$$

Equations (V-33) through (V-39) together with the initial and boundary conditions represented by equations (V-40) through (V-50) constitute the mathematical model employed for the transient behavior of decomposable materials. The model as represented by equations (V-33) through (V-50) has been programmed for high speed digital simulation on a Philco S-2000 computer. In addition the model without the radiation terms has been programmed for analogue simulation as reported by Munson and Spindler (Ref. V-12). The digital program has provision for any number of secondary materials ($0 \leq i \leq 10$) all of which are handled in the manner indicated above.

C. APPLICATION TO CONVECTIVE HEATING

In this section the model is applied to several materials subjected to environments which provide heating by convection only. For these cases the temperature levels are so low that internal self glowing is insignificant or, in the case of the silica plastic, the material is so opaque that the radiation may be handled by a surface radiation term in equation (V-41). The theoretical predictions are compared with experimental results and shown to agree within the limitations imposed by a knowledge of material properties and the experimental conditions. A similar comparison between theory and experiment for cases involving external and internal radiation is in preparation (Ref. V-13).

The materials considered in this report are polytetrafluoroethylene (Teflon), a "non-charring" epoxy versamid and a silica fiber reinforced plastic. The properties employed for these materials are listed in Table V-1 and are all either directly or indirectly measured quantities.

1. Teflon

A series of calculations were made using the properties listed in Table V-1 and employing environmental conditions typical of those encountered in the experimental work of John and Recesso (Ref. V-14). These calculations were performed by means of analogue simulation as reported by Munson and Spindler (Ref. V-12). The theoretical results are compared with experiment in figure V-2 where the theoretical results were reduced in accordance with the rules employed in the experiments. Figure V-2 also shows the corresponding theoretical steady state results based on the present theory. Surface temperatures and surface temperature gradients computed from the present model are in good agreement with the experimental work of Hanst (Ref. V-15) and the theoretical work of Jennings and Easton (Ref. V-16).

2. Typical Epoxy Versamid

The data in Table V-1 were employed in the digital simulation of an experiment in which a "non-charring" epoxy versamid plastic was subjected to convective heating by means of an electric arc heated air stream similar to that employed by John and Recesso (Ref. V-14). The sample consisted of 0.1-inch plastic on a 0.06-inch stainless steel sceondary material. Thermocouples were located in the plastic and in the steel. The environmental conditions correspond to a "cold wall" heat flux of 39.7 Btu/ft^2-sec at a stagnation enthalpy of 1140 Btu/lb. The measured and computer thermocouple response is shown in figure V-3. During the experiment the surface position was recorded photographically (Ref. V-14). A comparison of the measured and computed surface position time history is shown in figure V-4.

3. Silica Reinforced Plastic

The data in Table V-1 were used to simulate a test performed in an Avco supersonic tunnel facility designated as Channel 3. The characteristics of this facility are quoted by Hurwicz (Ref. V-7). Figure V-5 shows the schematic cross section of the model and lists the operating conditions employed. The calculations were performed by means of the digital program. The experimental and theoretical thermocouple response is shown in figure V-6. As can be seen from the figure, the agreement is very good even during the period long after the heating period. Calculated temperature profiles at several times during the experiment are given in figure V-7. Based on the computed density profile shown in figure V-8 the weight lost by the model was predicted and found to agree with the experimental weight loss

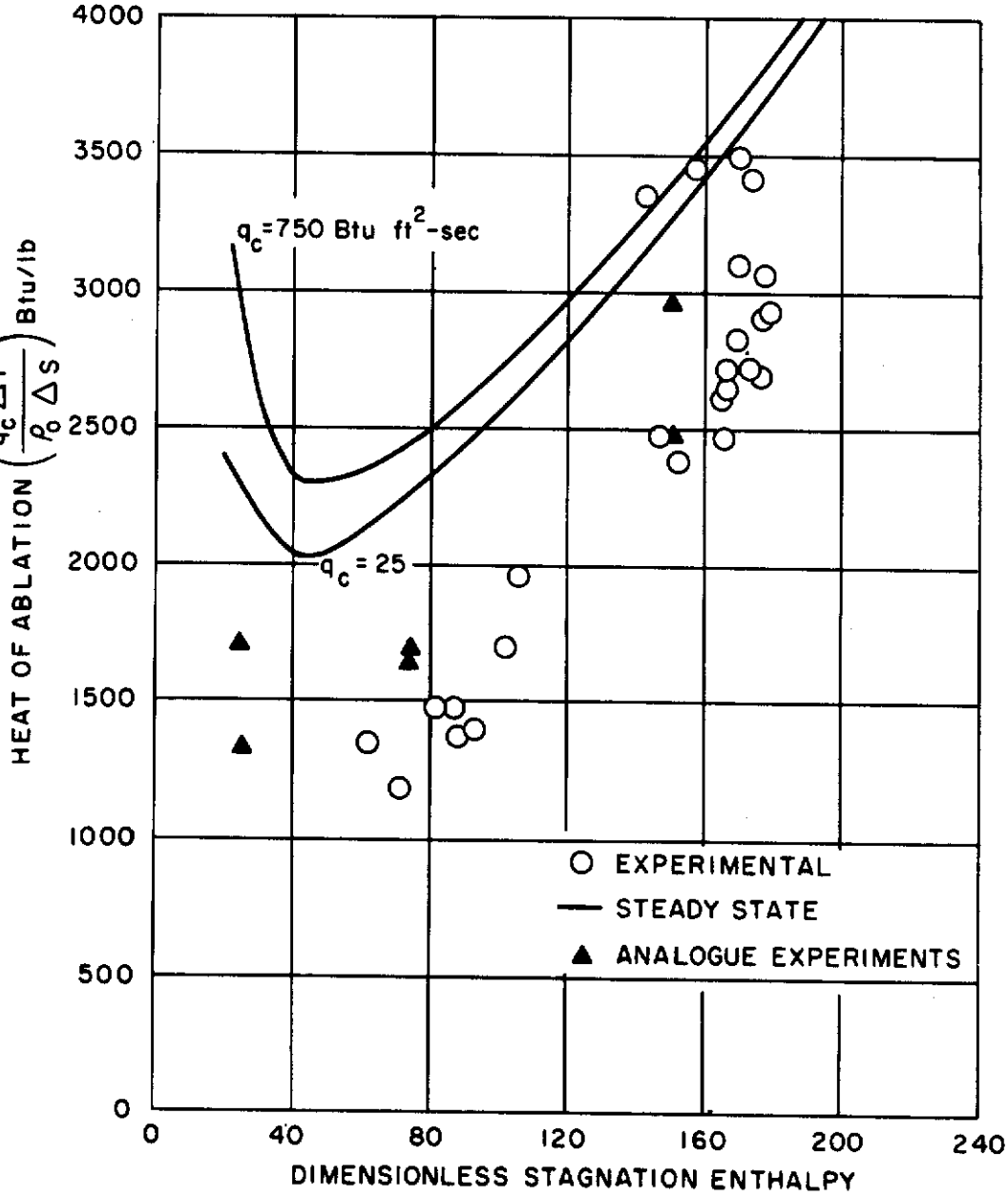

Figure V-2 TEFLON HEAT OF ABLATION

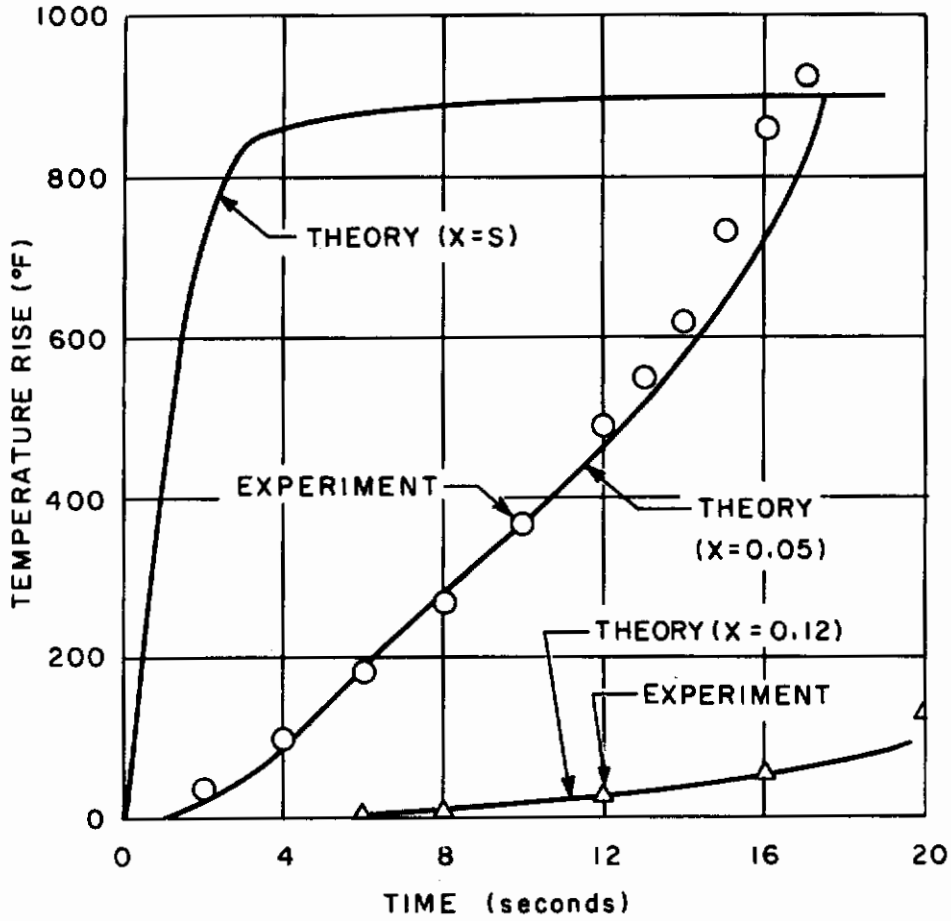

Figure V-3 EXPERIMENTAL AND THEORETICAL TEMPERATURE HISTORIES EPOXY VERSAMID MATERIAL

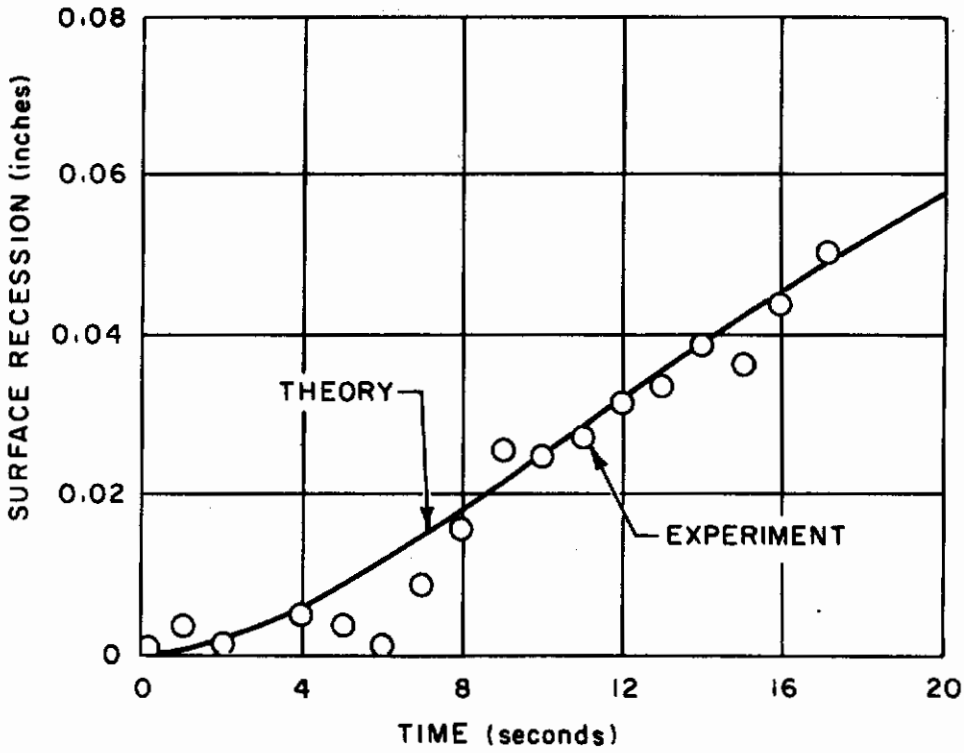

Figure V-4 EXPERIMENTAL AND THEORETICAL SURFACE RECESSION EPOXY VERSAMID MATERIAL

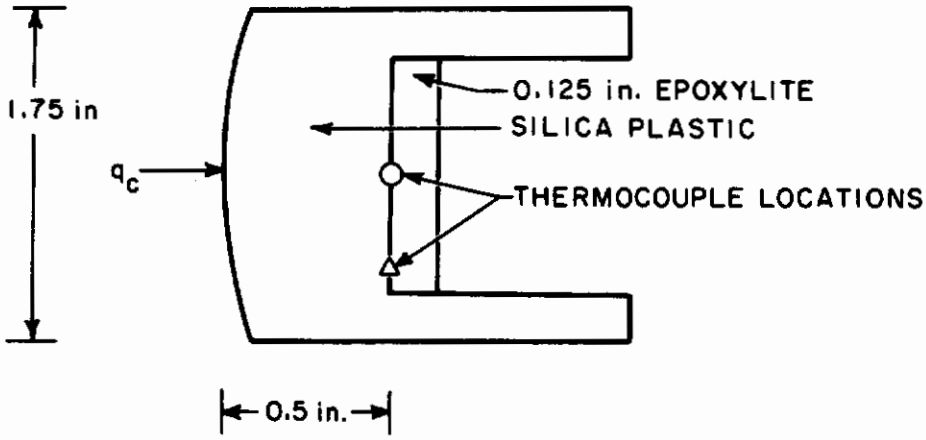

CONDITIONS:

COLD WALL HEAT FLUX	112 ± 8 Btu/ft^2-sec
STAGNATION ENTHALPY	6550 ± 300 Btu/lb
STAGNATION PRESSURE	0.023 ± 0.001 atm.
DURATION OF HEAT PULSE	118 seconds

Figure V-5 SILICA PLASTIC MODEL AND TEST CONDITIONS

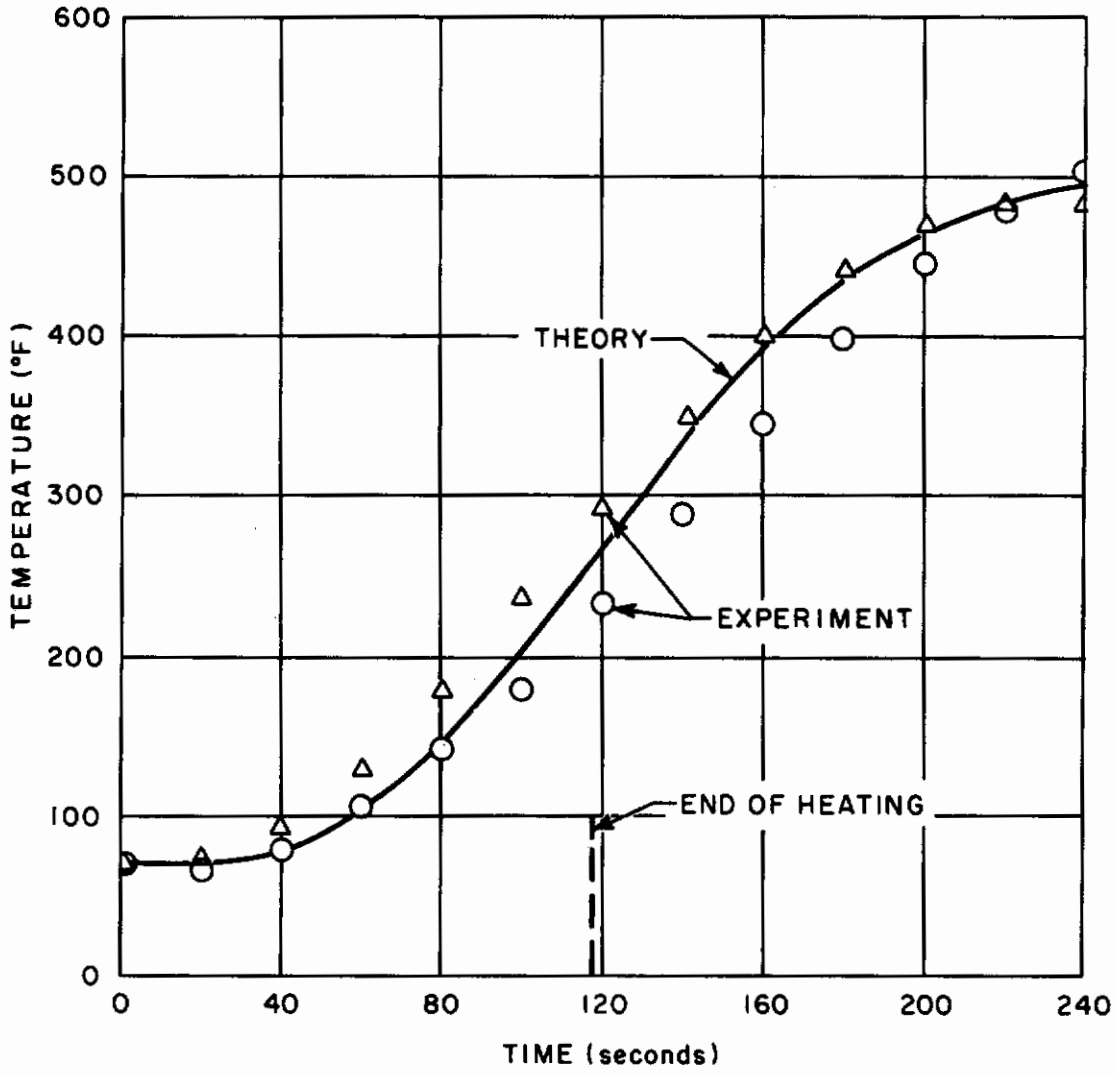

Figure V-6 EXPERIMENTAL AND THEORETICAL TEMPERATURE RESPONSE SILICA PLASTIC MATERIAL

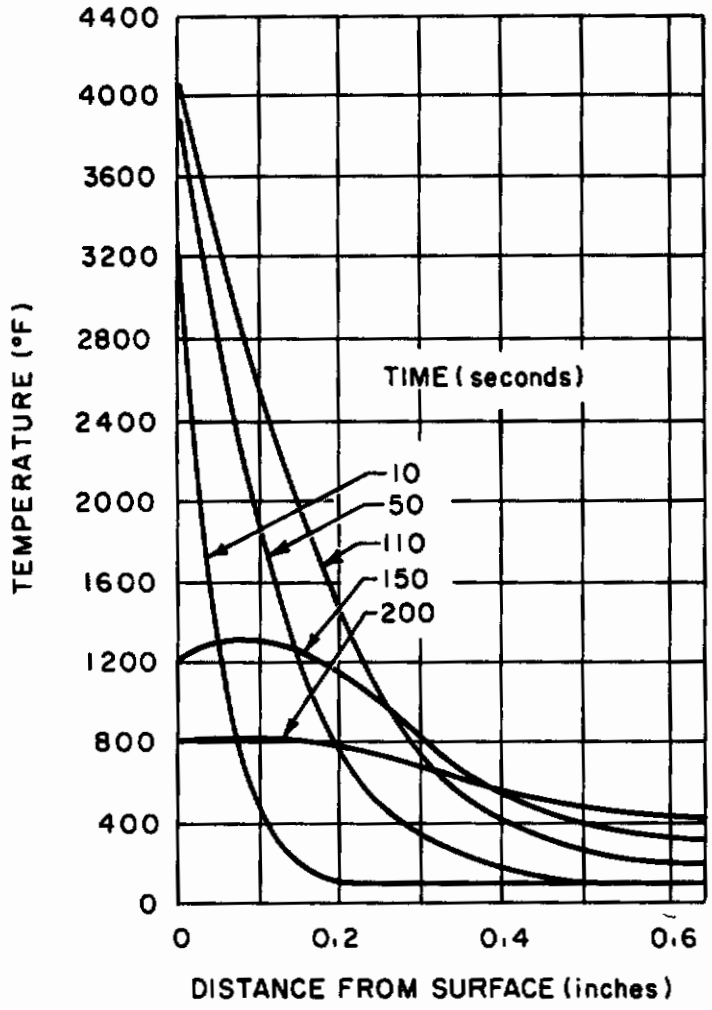

Figure V-7 THEORETICAL TEMPERATURE PROFILES SILICA PLASTIC MATERIAL

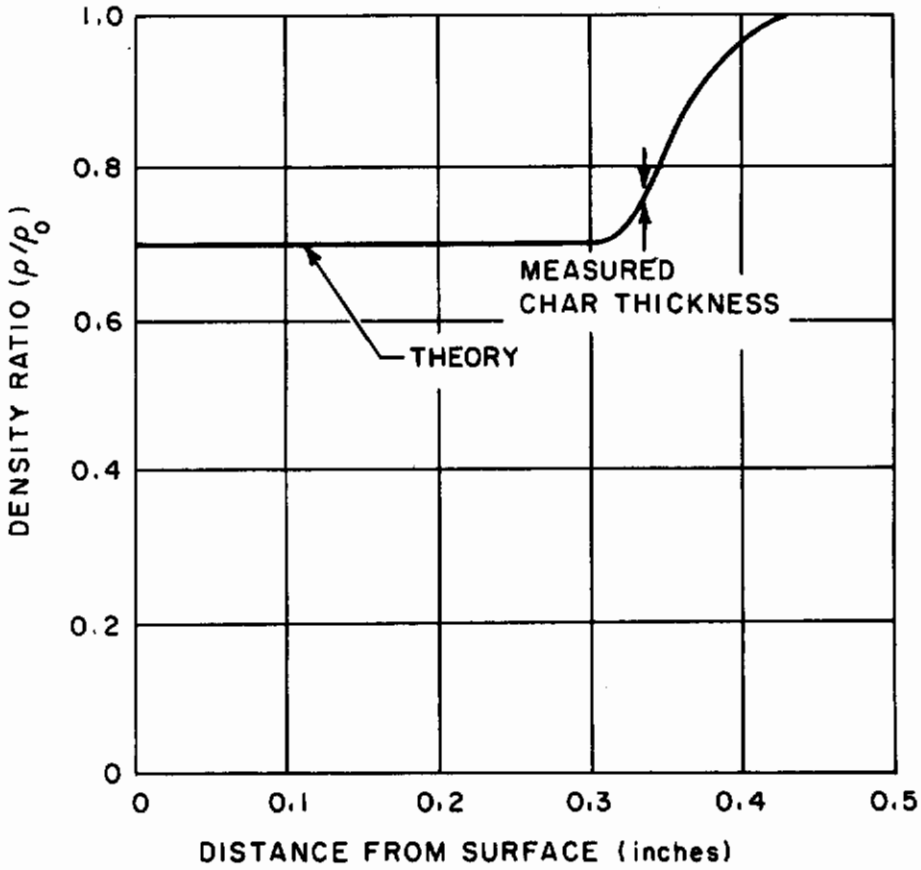

Figure V-8 FINAL DENSITY PROFILE SILICA PLASTIC MATERIAL

TABLE V-1

MATERIAL PROPERTIES

Property	Units	Teflon	Epoxy Versamid	Silica Plastic
A	1/sec	4.7×10^{18}	6.9×10^{9}	1×10^{6}
B	°R	72,900	31,700	20,000
β_1	in/sec-(°R)^2	-	-	0.11
β_2	-	-	-	2.0
β_3	°R	-	-	1×10^{5}
C_{po}	Btu/lb-°R	0.30	0.42	0.22
C_{p2}	Btu/lb-°R	0	0	0.18
C_g	Btu/lb-°R	0.28	0.30	0.4
ϵ	-	0.25	0.7	0.35
f	-	-	-	0.9
h_v	Btu/lb	-	-	5100
ΔH_c	Btu/lb	680	400	500
k_0	Btu/ft-hr-°R	0.14	0.114	0.18
k_2	Btu/ft-hr-°R	0	0	0.17
η	-	1	1	1
η_1	-	0.43	0.49	0.35
η_2	-	-	-	0.7
ρ_0	lb/ft^3	137.4	65.6	79.2
ρ_2	lb/ft^3	0	0	55.5

within 0.4 gram. After the experiment the model was sectioned and the "char thickness" measured as the distance from the surface to the point where the material was visably different from the virgin material. The result of this measurement is also shown in figure V-8. Of particular interest in connection with this experiment is the lack of appreciable surface recession, either experimental or theoretical. For this case, the only analysis possible is a transient one since steady state ablation can only be meaningfully defined for cases involving surface recession.

D. SUMMARY

A mathematical model has been presented for the transient behavior of materials which undergo thermal decomposition in depth. The model considers energy transfer by conduction, convection and radiation and is applicable to situations involving arbitrarily time varying heat inputs of both a convective and a radiative nature. Application of the model to several materials subjected to convective heating has been made by means of both analogue and digital computers. The results are compared with experiment and shown to provide

satisfactory agreement in certain cases which are far removed from steady state. It is concluded on the basis of the agreement between theory and experiment that the assumptions made in developing the model are justifiable at least for the materials considered.

E. LIST OF SYMBOLS

Symbols

A	Decomposition rate constant, equation (V-17)
A_1, A_2	Specific enthalpy constants, equation (V-13)
a	Attenuation coefficient for radiant flux, equation (V-24)
α	Volumetric optical absorption cross section
B	Decomposition rate constant, equation (V-17)
B_1,B_2	Conductivity constants, equations (V-15) and (V-16)
$\beta_1, \beta_2, \beta_3$	Empirical constants, equation (V-43)
C, C_p	Specific heat
ϵ	Surface emissivity
F, F_1, F_2	Radiant flux, equations (V-6), (V-19)
F_o	External radiant flux
f	Ratio of vaporizing to flowing surface material, equation (V-41)
H_o	Stagnation or recovery enthalpy, equation (V-41)
H_s	Boundary layer enthalpy at the receding surface, equation (V-41)
ΔH_c	Heat of decomposition, equation (V-5)
h	Specific enthalpy
J	Total radiant intensity
J_e	Function defined by equation (V-20)
k	Thermal conductivity

L, ℓ_1, ℓ_2	Coordinates of heat shield interfaces, figure V-1
m	Refractive index
n	Order of decomposition reaction, equation (V-17)
η	Blowing or transpiration factors, equation (V-41)
Q	Quantity of heat, equation (V-2)
q_c	Heat transfer to a cold, non-ablating wall, equation (V-41)
R_o, R_ℓ	Reflectivities associated with primary material boundaries
R_A	Apparent reflectivity, equation (V-25)
r	Space coordinate in equation (V-24)
ρ	Density
s	Coordinate of the receding surface, figure V-1
σ	Stephan-Boltzmann constant
T	Absolute temperature
t	Time
τ_A	Apparent transmissivity, equation (V-26)
w	Mass flow rate of gaseous products, equation (V-1)
x	Space coordinate, figure V-1

Subscripts (unless defined otherwise)

0	Refers to virgin material
1	Refers to decomposable or "active" material
2	Refers to inactive or fully degraded material
p	Refers to primary material
s1, s2	Refer to secondary materials
g	Refers to gaseous decomposition products
s	Refers to the receding surface

F. REFERENCES

1. Adams, M.C., Recent Advances in Ablation, ARS Journal, 29, 625 (1959).

2. Hidalgo, H., Ablation of Glassy Material Around Blunt Bodies of Revolution, ARS Journal, 30, 806 (1960).

3. Steg, L., Materials for Re-entry Heat Protection of Satellites, ARS Journal, 30, 815 (1960).

4. Barriault, R.J. and J. Yos, Analysis of the Ablation of Plastic Heat Shields that Form a Charred Surface Layer, ARS Journal, 30, 823 (1960).

5. Scala, S., A Study of Hypersonic Ablation, Conference on the Behaviour of Plastics in Advanced Flight Vehicle Environments, WADD TR 60-101 (September 1960).

6. Scala, S.M. and L.M. Gilbert, The Thermal Degradation of a Char Forming Plastic During Hypersonic Flight, Presented at ARS Space Flight Report to the Nation, New York (October 1961) Paper No. 2100-61.

7. Hurwicz, H., Aerothermochemistry Studies in Ablation, To be presented at the Fifth AGARD Combustion and Propulsion Colloquim, Braunschweig, Germany (April 1962).

8. Beecher, N. and R.E. Rosensweig, Ablation Mechanisms in Plastics with Inorganic Reinforcement, ARS Journal, 31, 532 (1961).

9. Lapple, C.E., A.P. Brady, and D.L. Chamberlain, Jr., Research on the Mechanism of Ablation of Polymeric Materials, ASD Technicial Report 61-204 (June 1961).

10. Kadanoff, L.P., Radiative Transport Within an Ablating Body, J. Heat Transfer, 83, 215 (1961), also Avco Everett Research Laboratory Research Report, No. 37(1958).

11. Spindler, R.J. and H. Hurwicz, Transient Heat Flow in Translucent Non-Gray Ablating Materials, Proceedings, Ballistic Missiles and Space Technology, Vol. II, Pergamon Press (1961) also Avco RAD-TR-9(7)-59-27 (October 1959).

12. Munson, T.R. and R.J. Spindler, Transient Thermal Behaviour of Decomposing Plastic Materials, Part I: General Theory and Application to Convective Heating, Avco RAD-TR-61-10 (3 May 1961).

13. Spindler, R.J. and T.R. Munson, Avco RAD report in preparation.

14. John, R.R. and J. Recesso, Ablation Characteristics of a Subliming Material Using Arc Heated Air, ARS Journal, 29, 663 (1959).

15. Hanst, P.L. and A.C. Walker, The Infrared Emission Spectra of Plastics Ablating in a Low Enthalpy Air Stream, Conference on the Behaviour of Plastics in Advanced Flight Vehicle Environments, WADD TR 60-101 (September 1960).

16. Jennings, R.L. and C.R. Easton, Surface Temperature of Ablating Teflon, Douglas Aircraft Company, Inc., Report No. SM-35759 (May 1959).

APPENDIX VI

A MODEL FOR ABLATION OF MATRICES IMPREGNATED WITH A PURE SUBSTANCE

by J. C. Boehringer

The problem under consideration concerns a model for heat transfer calculations of a composite material, part of which vaporizes at a lower temperature leaving a porous matrix that is also allowed to melt and vaporize into the boundary layer. The solution of the problem is related to the diffusion theory outlined in Appendix F (Ref. VI-1). Development on this work was ceased after its formulation because it is believed that similar problems can be solved by Avco RAD's programmed plastic ablation model. For this reason no numerical results were obtained. The work did, however, serve to provide some insight into the ablation process in such materials.

1. Assumptions

a. Matrix substance pores are filled with a material which vaporizes according to some relationship:

$$T_m = f(P_m) .$$

b. Any vaporizing material which condenses within the matrix material will be considered negligible.

c. The diffusing gas has constant density, and at any section, is in temperature equilibrium with the porous matrix material.

d. Diffusion of boundary-layer material toward vaporizing interface is negligible and Fick's Law type diffusion is small. This seems justified because a transpiration cooling effect is desired. Furthermore, inertial effects in diffusion processes are small.

e. There is no liquid transition in the vaporizing process. If one attempted to allow for presence of liquids in the flow, one would have "two-phase flow" which is unstable. This is consistent with assumption (a), and is true for materials with high triple-point pressure.

VI-1 RAD, Application Research of Materials Properties and Structure Concepts, Avco RAD-SR-23-60-94 (14 October 1960).

f. All material which vaporizes can find a path through which to flow toward the boundary layer. This is controlled by the manner in which the vaporizing material is distributed within the matrix material. This assumption is implicit when the matrix material is referred to as porous.

g. The flowing gas undergoes no chemical change.

h. The effective conductivity in the porous layer with flowing gas is in the ratio of volumes.

For $x \leq x_a$,

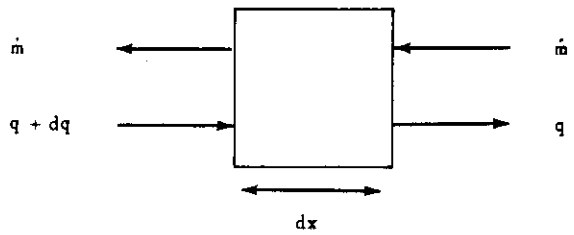

Control Volume 1

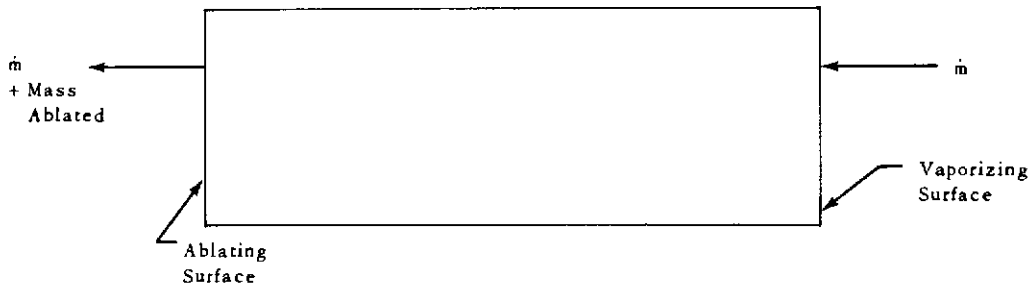

Control Volume 2

In view of the assumptions, one may postulate that

$$\frac{dm}{dt} = \alpha \frac{dp}{dx} . \qquad \text{(VI-1)}$$

By also postulating Fourier's Law of Heat Conduction and the First Law of Thermodynamics as applied to control volume 1, one obtains:

$$\alpha \frac{dp}{dx} C_{P_{gas}} \frac{\partial \theta}{\partial x} + \frac{\partial}{\partial x} \left\{ \left[\beta k_2 + (1-\beta) k_{gas} \right] \frac{\partial \theta}{\partial x} \right\} ,$$

$$- \left[(1-\beta) \rho_{gas} C_{P_{gas}} + \beta \rho_2 C_{P_2} \right] \frac{\partial \theta}{\partial t} = 0 . \qquad \text{(VI-2)}$$

Introducing the law of conservation of mass to the flowing substance in control volume 2, one observes that:

$$\alpha \frac{dp}{dx} = \text{constant} = \alpha \frac{P_m - P_s}{x_a - s} . \qquad \text{(VI-3)}$$

Substituting equation (VI-3) into equation (VI-2):

$$\alpha \frac{P_m - P_s}{x_a - s} C_{P_{gas}} \frac{\partial \theta}{\partial x} + \frac{\partial}{\partial x} \left\{ \left[\beta k_2 + (1-\beta) k_{gas} \right] \frac{\partial \theta}{\partial x} \right\}$$

$$- \left[(1-\beta) \rho_{gas} C_{P_{gas}} + \beta \rho_2 C_{P_2} \right] \frac{\partial \theta}{\partial t} = 0 . \qquad \text{(VI-4)}$$

Since both front and rear boundaries of control volume 2 can move relative to a fixed coordinate system when ablation of matrix material is permitted, the Landau transformation is introduced to cope with this. Let

$$\xi = \frac{x_a - x}{x_a - s} , \qquad \text{(VI-5)}$$

$$\theta(x,t) \rightarrow \tilde{\theta}(\xi, t) .$$

By substituting (VI-5) into (VI-4), one obtains:

$$\alpha \frac{P_s - P_m}{(x_a - s)^2} C_{P_{gas}} \frac{\partial \tilde{\theta}}{\partial \xi} + \frac{1}{(x_a - s)^2} \frac{\partial}{\partial \xi} \left\{ \left[\beta k_2 + (1-\beta) k_{gas} \right] \frac{\partial \tilde{\theta}}{\partial \xi} \right\}$$

$$= \left\{ (1-\beta) \rho_{gas} C_{P_{gas}} + \beta \rho_2 C_{P_2} \right\} \left\{ \frac{\partial \tilde{\theta}}{\partial t} + \frac{\partial \tilde{\theta}}{\partial \xi} \frac{\partial \xi}{\partial t} \right\} . \qquad \text{(VI-6)}$$

Now

$$\frac{d\xi}{dt} = \frac{\partial \xi}{\partial x_a} \frac{dx_a}{dt} + \frac{\partial \xi}{\partial s} \frac{ds}{dt} , \tag{VI-7}$$

and

$$\frac{\partial \xi}{\partial x_a} = \frac{1-\xi}{(x_a - s)} . \tag{VI-8}$$

Also,

$$\frac{\partial \xi}{\partial s} = \frac{\xi}{(x_a - s)} . \tag{VI-9}$$

Substituting (VI-8) and (VI-9) into (VI-7), one obtains:

$$\frac{d\xi}{dt} = \frac{1-\xi}{x_a - s} \frac{dx_a}{dt} + \frac{\xi}{x_a - s} \frac{ds}{dt} . \tag{VI-10}$$

By substituting (VI-10) into equation (VI-6),

$$\alpha \frac{P_s - P_m}{(x_a - s)^2} C_{P_{gas}} \frac{\partial \tilde{\theta}}{\partial \xi} + \frac{1}{(x_a - s)^2} \frac{\partial}{\partial \xi} \left\{ \left[\beta k_2 + (1-\beta) k_{gas} \right] \frac{\partial \tilde{\theta}}{\partial \xi} \right\}$$

$$= \left\{ (1-\beta) \rho_{gas} C_{P_{gas}} + \beta \rho_2 C_{P_2} \right\} \left\{ \frac{\partial \tilde{\theta}}{\partial t} + \frac{\partial \tilde{\theta}}{\partial \xi} \left(\frac{1-\xi}{x_a - s} \frac{dx_a}{dt} + \frac{\xi}{x_a - s} \frac{ds}{dt} \right) \right\} . \tag{VI-11}$$

The required boundary conditions for the solution of equation (VI-11) are as follows:

Front boundary, $\xi = 1$

$$P = P_s . \tag{VI-12}$$

Also,

$$q_c \left[1 - \frac{h_w}{h_g} \right] - \left[\alpha \frac{P_m - P_s}{x_a - s} \right] \eta_{gas} (h_g - h_{w_o})$$

$$- \beta \rho_2 f \frac{ds}{dt} \eta_2 (h_g - h_{w_o}) - \epsilon \sigma (\tilde{\theta} + 460)^4$$

$$- \left[\beta k_2 + (1-\beta) k_{gas} \right] \left. \frac{\partial \tilde{\theta}}{\partial \xi} \right|_{\xi=1} - \beta \rho_2 \left[f h_{v_2} + (1-f) h_{l_2} \right] \frac{ds}{dt} = 0 . \qquad \text{(VI-13)}$$

and, if $\frac{ds}{dt} \neq 0$

$$\tilde{\theta}(l_1, t) = \theta \text{ ablation of material 2} . \qquad \text{(VI-14)}$$

Rear boundary, $\xi = 0$

$$\tilde{\theta}(0, t) = \theta_m = f(p_m) . \qquad \text{(VI-15)}$$

and

$$- k_1 \left. \frac{\partial T}{\partial x} \right|_{x = x_a} = - \left[\beta k_2 + (1-\beta) k_{gas} \right] \left. \frac{\partial \theta}{\partial x} \right|_{x = x_a} - \alpha \frac{P_m - P_s}{x_a - s} h_{v_{gas}} \qquad \text{(VI-16)}$$

Time condition

$$\tilde{\theta}(\xi, 0) = \tilde{\theta} ; \qquad \text{(VI-17)}$$

and

$$x_a(t) \Big|_{t=0} = x_a' . \qquad \text{(VI-18)}$$

Now, consider the phenomena occurring for $x_a \leq x \leq x_b$ and $T \leq T_{MELT}$.

The phenomenological equation is:

$$\frac{\partial}{\partial x} \left(k_1 \frac{\partial T}{\partial x} \right) = \rho_1 C_{P_1} \frac{\partial T}{\partial t} . \qquad \text{(VI-19)}$$

Since the forward boundary of this problem, x_a, can be receding, one introduces the Landau transformation given by:

$$\phi = \frac{x_b - x}{x_b - x_a} \tag{VI-20}$$

$$T(x,t) \rightarrow \tilde{T}(\phi, t) .$$

Equation (VI-19) now becomes

$$\rho_1 C_{p_1} \left[\frac{\partial \tilde{T}}{\partial t} + \frac{\phi}{x_b - x_a} \frac{dx_a}{dt} \frac{\partial \tilde{T}}{\partial \phi} \right] = \frac{1}{(x_b - x_a)^2} \frac{\partial}{\partial \phi} \left(k_1 \frac{\partial \tilde{T}}{\partial \phi} \right) . \tag{VI-21}$$

The required boundary conditions are as follows:

Front boundary, $\phi = 1$

$$\tilde{T}(1, t) = f(C_{p_m}) , \tag{VI-22}$$

and

$$\frac{k_1}{x_b - x_a} \left. \frac{\partial \tilde{T}}{\partial \phi} \right|_{\phi=1} = \left[\beta k_2 + (1 - \beta\ k_{gas} \right] \left(\frac{1}{x_a - s} \right) \left. \frac{\partial \theta}{\partial \xi} \right|_{\xi=0} - \alpha \frac{P_m - P_s}{x_a - s} h_{v_{gas}} . \tag{VI-23}$$

Rear boundary, $\phi = 0$

$$\left. \frac{\partial T}{\partial \phi} \right|_{\phi=0} = 0 . \tag{VI-24}$$

Time boundary

$$\tilde{T}(\phi, 0) = \tilde{T} ; \tag{VI-25}$$

and

$$x_a(t)\big|_{t=0} = x_a' . \tag{VI-26}$$

One additional relationship is required. This is a relationship of compatibility for the system. The mass flowing through the system is:

$$\frac{dm}{dt} = a \frac{P_m P_s}{x_a - s} \quad . \tag{VI-27}$$

The rate of internal-gas generation is given by:

$$(\rho_1 - \rho_2 \beta) \frac{dx_a}{dt} \quad .$$

Therefore,

$$a \frac{P_m - P_s}{x_a - s} = (\rho_1 - \rho_2 \beta) \frac{dx_a}{dt} \quad . \tag{VI-28}$$

Hence,

$$\frac{dx_a}{dt} = \frac{a(P_m - P_s)}{(\rho_1 - \rho_2 \beta)(x_a - s)} \quad . \tag{VI-29}$$

2. Summary

The unknowns in the problem are $\tilde{\theta}$, $\tilde{T}$, s, and x_a. When supplied with the ablation temperature of the matrix material, it becomes possible to solve numerically equations (VI-11), (VI-13), (VI-21), and (VI-29) for the four unknowns. The required inputs are: x_b, a, $C_{p_{gas}}$, C_{p_2}, ρ_2, C_{p_1}, ρ_1, β, P_s, q_c, h_{w_o}, h_g, $T = f(C_p)$, f, η, ϵ, h_{v_2}, h_{v_1}, h_{f_2},

and initial temperature.

3. Symbols

$\frac{dm}{dt}$ mass flow of vaporized gas through porous matrix per unit area,

x space variable

x_a position of vaporizing interface (a function of time),

s ablated length of porous matrix material (a function of time),

a proportionality constant between mass rate of flow and pressure gradient,

θ temperature of porous matrix in x and t coordinates,

$\tilde{\theta}$	same as θ except coordinates are ξ and τ,
ρ_{gas}	average density of flowing gas,
k_2	conductivity of porous matrix material,
k_{gas}	conductivity of flowing gas,
$C_{p_{gas}}$	specific heat of flowing gas,
C_{p_2}	specific heat of porous matrix,
C_{p_1}	specific heat of original material,
k_1	conductivity of original material,
p_s	pressure on surface of porous matrix,
p_m	pressure at vaporizing interface,
p	pressure,
ξ	mapping variable (front),
ϕ	mapping variable (rear),
h_{w_o}	enthalpy of air at wall temperature
h	stagnation enthalpy
β	volume of matrix material per unit volume,
η	blowing factor, a constant dependent on transpired species and the type of flow,
ϵ	emissivity of porous material,
σ	radiation constant,
h_{v_2}	heat of vaporization of porous matrix,
$h_{v_{gas}}$	heat of vaporization of material which vaporizes internally,
f	fraction of matrix material which vaporizes
h_{f_2}	heat of liquefaction of matrix material,

T temperature in original material in x and t coordinates,

$\tilde{T}$ same as T except coordinates are ϕ and t,

t time.

APPENDIX VII

ELASTIC STRESS ANALYSIS AND BUCKLING OF SHELLS

by P. P. Radkowski

A. BASIC RELATIONS*

In general, the shape of a vehicle is determined by the following basic geometrical configurations: beams, plates, cylinders, cones, spheres, torus, and longitudinal sections of cylinders and cones. For analysis of single-layer beams and plates, we refer the reader to the numerous literature and texts on the subject matter, for instance the text by Boley and Weiner on "Theory of Thermal Stresses." For analysis of multi-layer beams and plates including a heat shield bonded onto sandwiches with honeycomb or corrugated cores, it is recommended that the analysis follow the procedure that is developed for shells of revolution. The solution for non-symmetric geometry such as longitudinal cylindrical, is being analyzed for programming onto a high-speed digital computer.

1. Geometric Definitions

The reference surface of a shell of revolution (that is, the surface**that experiences no circumferential bending stresses) prior to loading can be represented by

$$r = r(\xi) , \quad z = z(\xi) \quad ,$$

so that ξ together with the angle θ forms an orthogonal system and determines a point on the reference surface. (Here, ξ is the coordinate measured from the base of the shell along the longitudinal line.) The element of arc length on the reference surface is

$$ds^2 = a^2\, d\xi^2 + r^2\, d\theta^2 \quad ,$$

where a is defined by

$$a^2 = (r')^2 + (z')^2 \quad ,$$

where the primes (') designate differentiation with respect to ξ. Further, in what is to follow,

$$1/R_\xi = (z''r' - z'r'')/a^3 \quad ,$$

*This work was partially supported under contract AF04(694)-36, Mark II.

**A reference surface, with proper definition and interpretation, can be chosen to be other than the one chosen herein. The one chosen here is convenient and solves many practical shell problems.

and

$$1/R_\theta = z'/\alpha \ ,$$

where R_ξ and R_θ are the principal radii of curvature of the reference surface of the shell.

A point lying in the shell but not on the reference surface can be described relative to the reference surface by the coordinate ζ measured along the normal to the reference surface passing through the point. The origin of the coordinate ζ will be defined after the Stress-Moment Relations Section.

2. Deformation of an Element of the Reference Surface

a. Non-rotationally Symmetric Relations

The distortion of a shell is generally studied in terms of the bending and stretching of the reference surface. The stretching at a point is defined in terms of the strain components $\epsilon_{\xi m}$, $\epsilon_{\theta m}$, and $\gamma_{\xi\theta}$, while the bending of the reference surface in the ξ and θ directions is defined by the changes of curvature χ_ξ and χ_θ respectively. The relative angle of twist between two normals to the reference surface at a unit distance along the same longitudinal line, ξ , is defined by $\chi_{\xi\theta}$. In what is to follow, the primes (') and dots (·) designate differentiation with respect to ξ and θ , respectively. The strains and changes in curvature of the reference surface are written as functions of displacements as follows.*

1) Reference surface strains

$$\epsilon_{\xi m} = \frac{\bar{u}'}{a} + \frac{\bar{w}}{R_\xi} + \frac{1}{2}\left[\frac{\bar{u}^2}{R_\xi^2} + \frac{(\bar{u}')^2}{a^2} + \frac{\dot{\bar{u}}^2}{r^2}\right]$$

$$- \frac{r}{ar^2}\dot{\bar{u}}\bar{v} + \frac{\bar{u}'\bar{w} - \bar{u}\bar{w}'}{aR_\xi} + \frac{(r')^2}{2a^2r^2}\bar{v}^2 \frac{\bar{w}^2}{2R_\xi^2} \frac{(\bar{w}')^2}{2a^2} \ .$$

$$\epsilon_{\theta m} = \frac{\dot{\bar{v}}}{r} + \frac{r'}{ar}\bar{u} + \frac{\bar{w}}{R_\theta} + \frac{(r')^2}{2a^2r^2}\bar{u}^2 + \frac{r'}{ar^2}\bar{u}\dot{\bar{v}} + \frac{r'}{arR_\theta}\bar{u}\bar{w}$$

$$+ \frac{\bar{v}^2}{2R_\theta^2} + \frac{(\bar{v}')^2}{2a^2} + \frac{\dot{\bar{v}}^2}{2r^2} + \frac{\dot{\bar{v}}\bar{w}}{rR_\theta} + \frac{\bar{v}\dot{\bar{w}}}{rR_\theta} + \frac{\bar{w}^2}{2R_\theta^2} + \frac{\dot{\bar{w}}^2}{2r^2} \ .$$

$$\gamma_{\xi\theta} = \frac{\bar{v}'}{a} + \frac{u}{r} - \frac{r'}{ar}\bar{v} \ .$$

*These relations have been derived in reference VII-1.

2) Change in curvature

$$\chi_\xi = \frac{1}{ar}\left(\frac{r}{R_\xi}\right)'\bar{u} + \frac{2\bar{u}'}{aR_\xi} + \frac{\dot{\bar{v}}}{rR_\xi} + \frac{R_\xi + R_\theta}{R_\xi^2 R_\theta}\left(\bar{w} - \frac{1}{a^2}\bar{w}'' - \frac{a'\bar{w}'}{a}\right),$$

$$\chi_\theta = \frac{r'(R_\xi + R_\theta)}{arR_\xi R_\theta}\bar{u} + \frac{\bar{u}'}{aR_\theta} + \frac{2\bar{v}}{rR_\theta} + \frac{R_\xi + R_\theta}{R_\xi R_\theta^2}\bar{w} - \frac{\ddot{\bar{w}}}{r^2} - \frac{r'}{a^2 r}\bar{w}',$$

$$\chi_{\xi\theta} = \frac{\dot{\bar{u}}}{rR_\xi} - \frac{(rR_\theta)'}{arR_7^2}\bar{v} + \frac{\bar{v}}{aR_\theta} + \frac{r'}{ar^2}\dot{\bar{w}} - \frac{\dot{\bar{w}}'}{ar},$$

where $\bar{u}$, $\bar{v}/r$, and $\bar{w}$ are the increase in ξ, angle of rotation in the θ direction, and the displacement perpendicular to the reference surface of the undeformed shell, respectively.

Terms of the third or higher order in $\bar{u}$, $\bar{v}$, $\bar{w}$, and their derivatives with respect to ξ and θ are neglected in $\epsilon_{\xi m}$ and $\epsilon_{\theta m}$. Only the first-order terms are kept in $\gamma_{\xi\theta}$, χ_ξ, χ_θ, and $\chi_{\xi\theta}$.

b. Geometry of a Shell of Revolution Under Rotationally Symmetric Environment

In the elastic analysis of a shell of revolution under rotationally symmetric environment (here the θ derivative vanishes), the following coordinate system is used. Let u and w be the components of the displacement in the radical and axial direction, respectively; thus the deformed reference surface may be written in the form

$$r = r_o + u,$$

$$z = z_o + w,$$

where the subscript o refers to the undeformed reference surface. The difference between the angles of the tangent to the deformed and undeformed surface at the same material point is denoted by β; that is, the angle of rotation is

$$\beta = \phi_o - \phi .$$

The strain displacement relation in terms of u and w may be obtained by substituting

$$\bar{u} = u\cos\phi + w\sin\phi ,$$

$$\bar{w} = -u\sin\phi + w\cos\phi ,$$

into the reference surface strain relations.

The curvature-rotation relation is

$$K_\theta = \frac{r'}{ar} \beta ,$$

$$K_\xi = \frac{\beta'}{a} .$$

c. Compatibility Relations

The compatibility relations for displacement in the rotationally symmetric case is

$$(r \epsilon_{\theta m})' - r \epsilon_{\xi m} = a [\cos(\phi + \beta) - \cos\phi] .$$

The compatibility equation in addition to the equilibrium equations must be satisfied.

3. Elastic Stress-Strain Relations for Thin Shells and Reference Surface Definition

a. Non-isotropic Shells*

1) Stress-strain relations

In thin shells of revolution the stress normal to the reference surface is generally small in comparison to the other stresses and is generally small in comparison to the other stresses and is neglected only in the stress-strain relations.

The stress-strain relations for a thin shell are taken as follows:

$$\epsilon_\xi = \frac{\sigma_\xi}{E_\xi} - \frac{\sigma_\theta}{E_{\xi\theta}} + \bar{a}_\xi T ,$$

$$\epsilon_\theta = \frac{\sigma_\theta}{E_\theta} - \frac{\sigma_\xi}{E_{\theta\xi}} + \bar{a}_\theta T ,$$

where E_ξ, E_θ, $E_{\xi\theta}$, $E_{\theta\xi}$, $\bar{a}_\xi$, and $\bar{a}_\theta$ are functions of ξ, ζ, and T. Here, we assume from orthogonality considerations that $E_{\xi\theta} = E_{\theta\xi}$, and that $\bar{a}_\xi$ and $\bar{a}_\theta$ are average coefficient of thermal

*See also reference VII-2.

expansion over the temperature range considered. By inversion we have

$$\sigma_\xi = E^*_\xi \epsilon_\xi + E^*_{\xi\theta} \epsilon_\theta - (E^*_\xi \bar{\alpha}_\xi + E^*_{\xi\theta} \bar{\alpha}_\theta) T ,$$

$$\sigma_\theta = E^*_\theta \epsilon_\xi + E^*_{\theta\xi} \epsilon_\xi - (E^*_{\theta\xi} \bar{\alpha}_\xi + E^*_\theta \bar{\alpha}_\theta) T ,$$

where

$$E^*_\xi = \frac{E_\xi}{1-\nu^2} , \quad E^*_{\xi\theta} = E^*_{\theta\xi} = \frac{\nu^2 E_{\xi\theta}}{1-\nu^2} ,$$

$$E^*_\theta = \frac{E_\theta}{1-\nu^2} , \quad \nu^2 = \frac{E_\theta E_\xi}{E^2_{\xi\theta}} .$$

For an orthogonal system we have

$\frac{1}{E_{\xi\theta}} = \nu_{\xi\theta}/E_\xi$ and $\frac{1}{E_{\theta\xi}} = \frac{\nu_{\theta\xi}}{E_\theta}$, where $\nu_{\xi\theta}$ and $\nu_{\theta\xi}$ are Poisson's ratio.

The stress resultants - strain relations are

$$N_\xi = \int_\zeta \sigma_\xi \, d\zeta = A^*_\xi \epsilon_{\xi m} + A^*_{\xi\theta} \epsilon_{\theta m} + B^*_\xi K_\xi + B^*_{\xi\theta} K_\theta - N_{\xi T} ,$$

$$N_\theta = \int_\zeta \sigma_\theta \, d\zeta = A^*_\theta \epsilon_{\theta m} + A^*_{\theta\xi} \epsilon_{\xi m} + B^*_\theta K_\theta + B^*_{\theta\xi} K_\xi - N_{\theta T} .$$

The stress couples - strain relations are

$$M_\xi = \int_\zeta \zeta\, \sigma_\xi \, d\zeta = B^*_\xi \, \epsilon_{\xi m} + B^*_{\xi\theta} \, \epsilon_{\theta m} + C^*_\xi \, K_\xi + C^*_{\xi\theta} K_\theta - M_{\xi T} ,$$

$$M_\theta = \int_\zeta \zeta \sigma_\theta \, d\zeta = B^*_\theta \, \epsilon_{\theta m} + B^*_{\theta\xi} \, \epsilon_{\xi m} + C^*_\theta \, K_\theta + C^*_{\theta\xi} \, K_\xi - M_{\theta T} .$$

Here

$$A^*_\xi = \int_\zeta E^*_\xi \, d\zeta, \; A^*_\theta = \int_\zeta E^*_\theta \, d\zeta , \; A^*_{\xi\theta} = \int_\zeta E^*_{\xi\theta} \, d\zeta ,$$

$$B^*_\xi = \int_\zeta \zeta E^*_\xi \, d\zeta , \; B^*_\theta = \int_\zeta \zeta E^*_\theta \, d\zeta , \; B^*_{\theta\xi} = \int_\zeta \zeta E^*_{\theta\xi} \, d\zeta ,$$

$$C^*_\xi = \int_\zeta \zeta^2 \, E^*_\xi \, d\zeta, C^*_\theta = \int_\zeta \zeta^2 \, E^*_\theta \, d\zeta , C^*_{\theta\xi} = \int_\zeta \zeta^2 \, E^*_{\theta\xi} \, d\zeta,$$

$$N_{\xi T} = \int_\zeta (E^*_\xi \, \bar{\alpha}_\xi + E^*_{\xi\theta} \, \bar{\alpha}_\theta) \, T \, d\zeta ,$$

$$N_{\theta T} = \int_\zeta (E^*_\theta \, \bar{\alpha}_\theta + E^*_{\xi\theta} \, \bar{\alpha}_\xi) \, T \, d\zeta ,$$

$$M_{\xi T} = \int_\zeta \zeta \, (E^*_\xi \, \bar{\alpha}_\xi + E^*_{\xi\theta} \, \bar{\alpha}_\theta) \, T \, d\zeta,$$

$$M_{\theta T} = \int_\zeta \zeta \, (E^*_\theta \, \bar{\alpha}_\theta + E^*_{\theta\xi} \, \bar{\alpha}_\xi) \, T \, d\zeta .$$

Rewriting stress-strain relations we have the alternate form

$$\epsilon_{\xi m} = A_{\xi} N_{\xi} + A_{\xi\theta} N_{\theta} + B_{\xi} K_{\xi} + B_{\xi\theta} K_{\theta} + \epsilon_{\xi T} ,$$

$$\epsilon_{\theta m} = A_{\theta\xi} N_{\xi} + A_{\theta} N_{\theta} + B_{\theta\xi} K_{\xi} + B_{\theta} K_{\theta} + \epsilon_{\theta T} ,$$

$$M_{\xi} = C_{\xi} N_{\xi} + C_{\xi\theta} N_{\theta} + D_{\xi} K_{\xi} + D_{\xi\theta} K_{\theta} + M^{*}_{\xi T} ,$$

$$M_{\theta} = C_{\theta\xi} N_{\xi} + C_{\theta} N_{\theta} + D_{\theta\xi} K_{\xi} + D_{\theta} K_{\theta} + M^{*}_{\theta T} ,$$

where

$$H = 1/(A^{*}_{\xi} A^{*}_{\theta} - A^{*2}_{\xi\theta}) ,$$

and

$$A_{\xi} = A^{*}_{\theta} H , \quad A_{\theta} = A^{*}_{\xi} H , \quad A_{\xi\theta} = - A^{*}_{\xi\theta} H ,$$

$$B_{\xi} = (B^{*}_{\theta\xi} A^{*}_{\xi\theta} - B^{*}_{\xi} A^{*}_{\theta}) H ,$$

$$B_{\xi\theta} = (B^{*}_{\theta} A^{*}_{\theta\xi} - B^{*}_{\xi\theta} A^{*}_{\theta}) H ,$$

$$B_{\theta} = (B^{*}_{\theta\xi} A^{*}_{\xi\theta} - B^{*}_{\theta} A^{*}_{\xi}) H ,$$

$$\epsilon_{\xi T} = (A^{*}_{\theta} N_{\xi T} - A^{*}_{\xi\theta} N_{\theta T}) H ,$$

$$\epsilon_{\theta T} = (A^{*}_{\xi} N_{\theta T} - A^{*}_{\xi\theta} N_{\xi T}) H ,$$

$$C_{\xi} = B^{*}_{\xi} A_{\xi} + B^{*}_{\xi\theta} A_{\theta\xi} ,$$

$$C_{\xi\theta} = B^{*}_{\xi} A_{\xi\theta} + B^{*}_{\xi\theta} A_{\theta} ,$$

$$C_{\theta\xi} = B^{*}_{\theta} A_{\theta\xi} + B^{*}_{\theta\xi} A_{\xi} ,$$

$$C_{\theta} = B^{*}_{\theta} A_{\theta} + B^{*}_{\theta\xi} A_{\theta\xi} ,$$

$$D_{\xi} = B^{*}_{\xi} B_{\xi} + B^{*}_{\xi\theta} B_{\theta\xi} + C^{*}_{\xi} ,$$

$$D_{\xi\theta} = D_{\theta\xi} = B^{*}_{\xi} B_{\xi\theta} + B^{*}_{\xi\theta} B_{\theta} + C^{*}_{\xi\theta} ,$$

$$D_{\theta} = B^{*}_{\theta} B_{\theta} + B^{*}_{\theta\xi} B_{\xi\theta} + C^{*}_{\theta} ,$$

$$M^{*}_{\xi T} = B^{*}_{\xi} \epsilon_{\xi T} + B^{*}_{\xi\epsilon} \epsilon_{\theta T} - M_{\xi T} ,$$

$$M^{*}_{\theta T} = B^{*}_{\theta\xi} \epsilon_{\xi T} + B^{*}_{\theta} \epsilon_{\theta T} - M_{\theta T} .$$

2) Reference surface

It is observed in the stress-strain relations that if the B^*'s are chosen to be zero, then for a large class of shells used in practice we have chosen the reference surface as a surface experiencing no bending stress. This is possible if (a) the mechanical properties are the same in every direction at a material point (hence we have a multi-layer isotropic shell of revolution) and (b) the mechanical non-isotropic properties are constant or vary slightly through a cross section (although they may vary along the length).

The above two cases have been programmed for digital computer computation for stress analysis purposes. The remaining non-isotropic case, where the mechanical properties vary through the thickness, is still being programmed; the reference surface for the above two cases are:

$$x = \frac{\sum \frac{E_i}{1-\nu_i^2} Z_i}{\sum_{i=1}^{n} \frac{E_i}{1-\nu_i^2} h_i} ,$$

where

$$E_{\theta i} = E_{\xi i} = E_i, \text{ and } Z_i = \frac{h_i}{2}\left[h_i + 2 \sum_{j=1}^{i-1} h_i\right] ,$$

and $x = h/2$ where h is the total thickness, respectively. Here x is the distance, measured along a line normal to the outer surface, from the outer surface to the reference surface, $\zeta = 0$. The quantities $E_{\xi i}$, $E_{\theta i}$, $E_{\xi\theta i}$, and h_i ($i = 1, 2, \ldots, m$) are the elastic moduli and thickness of the i^{th} layer. The layers are numbered consecutively starting at the outer surface. Using the above definition for reference surface we find that the following cross sectional quantities are needed (although the B^*'s are set equal to zero in what is to follow, they are evaluated for cataloguing purposes only).

$$A^*_\xi = \sum_{i=1}^{m} E^*_{\xi i}\, h_i\,,\quad A^*_\theta = \sum_{i}^{m} E^*_{\theta i}\, h_i\,,\quad A^*_{\xi\theta} = \sum_{i}^{m} E^*_{\xi\theta i}\, h_i\ ;$$

$$H = 1/(A^*_\xi\, A^*_\theta - A^{*2}_{\xi\theta}),\ A_\xi = A^*_\theta\, H,\ A_\theta = A^*_\xi H,\ A_{\xi\theta} = -A^*_{\xi\theta}\, H\ ;$$

$$B^*_\theta = -A^*_\theta\, x + \sum_{1}^{m} E^*_{\theta i}\, Z_i\ ;$$

$$B^*_\xi = -A^*_\xi\, x + \sum_{1}^{m} E^*_{\xi i}\, Z_i\ ;$$

$$B^*_{\xi\theta} = -A^*_{\xi\theta}\, x + \sum_{1}^{m} E^*_{\xi\theta i}\, Z_i\ ;$$

$$C^*_\theta = \frac{1}{3} \sum_{i=1}^{m} E^*_{\theta i}\, Y_i,\ C^*_\xi = \frac{1}{3} \sum_{i=1}^{m} E^*_{\xi i}\, Y_i,\ C^*_{\xi\theta} = \frac{1}{3} \sum_{i=1}^{m} E^*_{\xi\theta_i}\, Y_i\ ;$$

$$Y_i = \Big(-x + \sum_{i=1}^{m} h_j\Big)^3 - \Big(-x + \sum_{i=1}^{i=1} h_j\Big)^3\ .$$

For our particular class of problems treated here we have

$$D_\xi = C^*_\xi\,,\quad D_\theta = C^*_\theta\,,\quad D_{\xi\theta} = D_{\theta\xi} = C^*_{\xi\theta}$$

3) Sandwich structures

In optimum designing of many structures the load carrying members should be designed so that their maximum strength should

be in the direction of the load. This is done in the form of stiffeners, corrugations, etc. In instability or bending analysis, the bending and extensional rigidities play an important role. This type of structure could be a sandwich (actually multi-layer) type shell. The mechanical properties (i.e., Young's modulus, Poisson's ratio, etc.) of the face sheets would be the same as that at the material point. The core of the sandwich would have average mechanical properties; this average could be determined experimentally or analytically. In this subsection we consider an example of orthotropic core.

For axial loads alone one generally would reinforce the vehicle by longitudinal stiffeners or longitudinal corrugations with or without skin or strips supporting the corrugation. Similarly, for lateral loads the reinforcements should go circumferentially with or without axial supporting elements. If a combined loading exists, i.e., a high longitudinal load as well as a large lateral load, then a combination of axial and circumferential reinforcements would be necessary.

The effective Young's modulus of the corrugation may be determined experimentally or analytically as illustrated:

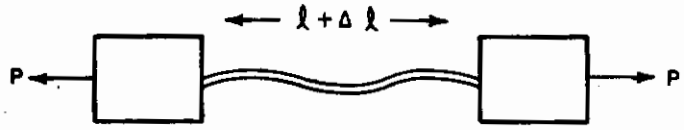

Here P (psi), ℓ, and $\Delta\ell$ are the loads, unstressed length, and change in length, respectively. Then by the simple formulae

$$P = E_1 \frac{\Delta\ell}{\ell} ,$$

one finds E_1 the effective modulus in the corrugated direction. The quantity $\Delta\ell$ can be determined analytically or experimentally. Similarly the effective modulus along the generatrix of the corrugation can be determined. Using these effective moduli along with those of the face sheets, we can determine the effective bending and extensional modulus.

b. Isotropic Multi-layer Shell

1) Stress-strain relations

Here

$$E_\xi = E_\theta = E, \quad \nu_{\xi\theta} = \nu_{\theta\xi} = \nu, \quad \bar{a}_\xi = \bar{a}_\theta = \bar{a},$$

$$E_{\xi\theta} = E/\nu,$$

and hence

$$\epsilon_\xi = \frac{1}{E}(\sigma_\xi - \nu\sigma_\theta) + \bar{a}T,$$

$$\epsilon_\theta = \frac{1}{E}(\sigma_\theta - \nu\sigma_\xi) + \bar{a}T.$$

Using the definitions of strains in terms of stress resultants and bending moments and then inventing the above stress-strain relations, we have

$$\sigma_\xi = \frac{E}{1-\nu^2}\left[\frac{1-\nu^2}{B}(N_\xi + (1+\nu)N_T) + \frac{\zeta}{D}(M_\xi + (1+\nu)M_T)\right] - \frac{E\bar{a}T}{1-\nu},$$

$$\sigma_\theta = \frac{E}{1-\nu^2}\left[\frac{1-\nu^2}{B}(N_\theta + (1+\nu)N_T) + \frac{\zeta}{D}(M_\theta + (1+\nu)M_T)\right] - \frac{E\bar{a}T}{1-\nu},$$

where B and D are the effective extensional and bending modulus, respectively. For a multi-layer isotropic structure, where Young's modulus and Poisson's ratio may vary through the thickness we have

$$B = \frac{K}{\sum_{i=1}^{m} B_i},$$

and

$$D = -\frac{1}{3}\sum_{i=1}^{m}\frac{B_i}{h_i}\left[\left(x-\sum_{j=1}^{i}h_j\right)^3-\left(x-\sum_{j=1}^{i-1}h_j\right)^3\right],$$

here

$$K = \left(\sum_{i=1}^{m}B_i\right)^2-\left(\sum_{i=1}^{m}\nu_i B_i\right)^2,$$

and

$$B_i = \frac{E_i h_i}{1-\nu_i^2}.$$

Here we assume that we have an m-layer structure. The quantity x is the distance from outer surface to inner surface and is defined as follows

$$x = \frac{1}{K}\left[\left(\sum_{i=1}^{m}B_i\right)\left(\sum_{i=1}^{m}B_i Z_i\right)-\left(\sum_{i=1}^{m}\nu_i B_i\right)\left(\sum_{i=1}^{m}\nu_i B_i Z_i\right)\right],$$

where

$$Z_i = h_i + 2\sum_{j=1}^{i-1}h_j.$$

Often ν_i is nearly constant through the thickness of the multi-layer shell or ν_i varies so slightly that it can be approximated by an equivalent $\bar{\nu}$, i.e.,

$$\nu = \frac{\sum \bar{\nu}_i B_i}{\sum B_i} .$$

For this case we have

$$x = \frac{\sum_1^m E_i h_i Z_i}{2\sum E_i h_i} ,$$

and then

$$B = \sum_1^m E_i h_i ,$$

$$D = -\frac{1}{3(1-\nu^2)} \sum_1^m E_i \left[\left(x - \sum_{j=1}^{i} h_j \right)^3 - \left(x - \sum_{j=1}^{i-1} h_j \right) \right]^3 .$$

It should be pointed out that if Poisson's ratio differs considerably then it is recommended that the value for each layer be used. As a rule of thumb the percentage of minimum error for an equivalent Poisson's ratio will be the difference between the maximum and minimum value of Poisson's ratio through the thickness.

2) Effective Modulus for Isotropic Sandwich Structure

As an illustration, let us assume that we have a heat shield bonded to a honeycomb back-up structure (see sketch below).

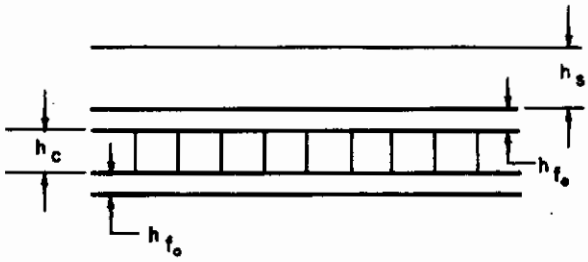

In practice we would divide the heat shield into layers in accordance to the variation of the properties of the material as a function of temperature. For simplicity let us assume that the temperature is constant through the thickness thus giving us a four-layer shell. We have the following table for each layer:

Mechanical Prop./Layer	Heat Shield	Face Sheet between Core and Heat Shield	Honeycomb Core	Inside Face Sheet
Young's Modulus	$E_s = E_1$	$E_{fo} = E_2$	$E_c = E_3$	$E_{fi} = E_4$
Poisson's Ratio	$\nu_s = \nu_1$	$\nu_{fo} = \nu_2$	$\nu_c = \nu_3$	$\nu_{fi} = \nu_4$
Thickness	$h_s = h_1$	$h_{fo} = h_2$	$h_c = h_3$	$h_{fi} = h_4$

These values would then be substituted into the expressions for cross-section properties given in the previous sections.

4. Equilibrium Equations

Assuming that there may exist a surface shear load r on either or both of the surfaces as well as a normal surface load, then every element of the shell is in equilibrium if

$$(r\,H)' - a\,N_\theta + r\,a\,p_H = 0\,,$$

$$(r\,V)' + r\,a\,p_V = 0\,,$$

$$(r\,M_\xi)' - a\cos\phi\,M_\theta - r\,a\,\theta + r\,a\,m = 0\,,$$

where H and V are the horizontal and vertical stress resultants and are related to N_ξ and Q (the transverse shear resultant) as follows

$$N_\xi = H\cos\phi + V\sin\phi\,,$$

$$Q = -H\sin\phi + V\cos\phi\,.$$

The quantity m is the moment portion of r and m is applied to the reference surface. Here p_H and p_V will contain the horizontal and vertical components, respectively, of the shear load r as well as the horizontal and vertical components of inertia loads and the other applied loads.

B. ELASTIC STRESS ANALYSIS AND BUCKLING

1. Load and Thermally Induced Stress Analysis of Isothropic or Non-isotropic Thin Multi-layer Shells of Revolution

The analysis and solution which was developed and programmed for high-speed computers, was initiated by the need to determine stress distributions in thin wall shell structures, where at a material point the elastic properties in the circumferential direction may be different from those in the meridional direction. These variances in properties at a material point is typical of orthotropical shells used in re-entry vehicle structures. These structures are subjected to arbitrarily varying axisymmetric pressures and temperatures and are usually multi-layer as well as having variable thickness. The analysis does reduce to the isotropic case when the properties at a material point are the same in every direction.

The generality, of the completed general analysis, computer program, and analytical results for particular geometries makes the results applicable to other types of axisymmetric shell structures such as rocket nozzles, space vehicles, pressure vessels, and as a first approximation to solutions of relatively "thick" shell problems. The analysis is restricted, however, to axisymmetric first order linear elastic shell theory.

The classical theory of thin elastic isotropic shells of revolution with small rotationally symmetric displacements is due to H. Reissner for spherical shells of uniform thickness and E. Meissner for the general shells of revolution. The symmetric bending of non-isotropic shallow shells of revolution has been analyzed by E. Reissner (Ref. VII-3). The derivation of the basic relations* presented herein is somewhat more general for the linear theory as it considers non-shallow as well as shallow shells of revolution.

The following basic equations assuming B*'s to be zero* are used in the analysis and are amendable to analytical solutions such as asymptotic integration.

$$\psi + \frac{\left(A_\theta \frac{r}{a}\right)'}{A_\theta \frac{r}{a}} \psi' + \left[\frac{\left(A_{\theta\xi} \frac{r'}{a}\right)'}{A_\theta \frac{r}{a}} - \frac{A_\xi}{A_\theta}\left(\frac{r'}{r}\right)^2 \right] \psi - \frac{az'}{rA_\theta} \beta = \frac{a\bar{X}}{rA_\theta} ,$$

and

$$\beta'' + \frac{\left(D_\xi r/a\right)'}{D_\xi r/a} \beta' + \left[\frac{\left(D_{\xi\theta} r'/a\right)'}{D_\xi r/a} - \frac{D_\theta}{D_\xi}\left(\frac{r'}{r}\right)^2 \right] \beta + \frac{az'}{rD_\xi} \psi = \frac{a\bar{Y}}{rD_\xi} ,$$

The A's and D's are effective elastic modulus. β is the rotation of reference surface and ψ (= r H) is directly proportional to the radial stress resultant. All of the terms including stress-strain relations are defined in the introduction of this section. In reference VII-4 the differential equations are solved numerically, and the procedure used makes possible solution of shells of revolution of arbitrary shape subjected to arbitrary pressures and temperature distributions, and it permits variation of non-isotropic material properties and temperature through the thickness by making appropriate subdivisions of each layer. In reference VII-5 a similar procedure has been set up for isotropic shells of revolution.

A procedure is set up to consider multi-regional shells, a region being defined as a portion of a shell which contains no load or geometrical discontinuities except at the boundaries. These regions are joined together by appropriate junction conditions.

Although not considered in this section, multi-layer shells are subject to shear stresses parallel to the interfaces. These shear stresses are generally large in magnitude in a narrow band of the order of one or two thickness at free ends and at stress concentrations of laminated structures.

The case where the B's do not vanish is still being programmed. (See reference VII-2)

A major portion of the present vehicles are determined geometrically by cylinders, steep cones, and shallow spherical shells. Here we present solutions of the above cases which may be used as preliminary design solutions for sizing of the vehicle. These solutions, except for the membrane solution for none-shallow shells, are specialized by the assumption of meridionally non-varying effective moduli. Further, a cone is replaced by an equivalent cylinder. Following this the general solution and a description of computer program is given.

a. Membrane Solution for Non-shallow Shells

A membrane solution for non-shallow shells of revolution is obtained from the second equation by assuming the D's to vanish. The solution is

$$\psi = \frac{1}{z'} Y = \frac{1}{z'} \left[-(r M^*_{\xi T})' + r' M^*_{\theta T} - r'(r' V) - r a m \right].$$

The corresponding membrane rotation is obtained by substituting the above quantity for ψ into the first basic differential equation and then solving for β.

The above solution may prove useful for points of shells sufficiently removed from ends and discontinuities in loads and geometries. As a rule of thumb this solution could be good for

$$z > \frac{\log_e 10}{2} \sqrt{ah} \sqrt{\frac{E_\xi}{3E_\theta}},$$

away from ends and discontinuities. Here a is the smallest radius of curvature and h = thickness. This inequality and a more general inequality is derived in the following section on cylindrical shells.

b. Cylindrical Shell

The general form of the differential equation for a cylinder, assuming meridionally non-varying properties, reduces to the single fourth order differential equation

$$\frac{d^4 \psi}{d \xi^4} + \psi k^4 \psi = S ;$$

where

$$r = a, z = a\xi, \alpha^2 = a^2$$

$$k^4 = \frac{\alpha^2}{A_\theta D_\xi} \quad , \quad S = \frac{a\overline{Y}}{A_\theta D_\xi} + \frac{1}{A_\theta} \frac{d^2\overline{X}}{d\xi^2}$$

The rotation is determined from

$$\beta = \frac{A_\theta}{a} \left(\psi'' - \frac{X}{a} \right) .$$

1) General solution

The solution to the above differential equation takes on the form

$$\psi = \psi_p + e^{-k\xi} [C_1 \cos k\xi + C_2 \sin k\xi]$$

$$+ e^{k\xi} [C_3 \cos k\xi + C_4 \sin k\xi] ,$$

and

$$\beta = \frac{A_\theta}{a} \frac{d^2 \psi_p}{d\xi^2} - \frac{\overline{X}}{a}$$

$$+ 2 \frac{k^2 A_\theta}{a} [e^{-k\xi} (C_1 \sin k\xi - C_2 \cos k\xi) + e^{k\xi} (-C_3 \sin k\xi + C_4 \cos k\xi)] .$$

The quantity ψ_p is a particular solution of the differential equation and can be determined in general by well-known methods. We now obtain several pertinent solutions for semi-infinite cylinders.

2) Semi-infinite cylinders

In what is to follow let, p_H = constant, $m = M^*_{\xi T} = p_V = \epsilon'_{\theta T} = 0$.

We now consider the following two basic problems: The first problem is defined by

(a) at $\xi = 0$, $\psi = aH_o$, $M_\xi = 0$,

at $\xi = \infty$, $M_\xi = M^*_{\xi T}$, $\psi = 0$,

and the second problem is defined by

(b) at $\xi = 0$, $M_\xi = M_0$, $\psi = 0$,

at $\xi = \infty$, $M_\xi = M^*_{\xi T}$, $\psi = 0$.

The particular solution ψ_p vanishes, for here $X = Y = 0$. From the condition at infinity we get $C_3 = C_4 = 0$, i.e.,

$$\psi = e^{-k\xi} (C_1 \cos k\xi + C_2 \sin k\xi),$$

and

$$\beta = \frac{2k^2 A_\theta}{a} e^{-k\xi} (C_1 \sin k\xi - C_2 \cos k\xi).$$

We now have

$$M_\xi = D_\xi \frac{\beta'}{a} + M^*_{\xi T}, M_\theta = D_{\theta\xi} \frac{\beta'}{a} + M^*_{\theta T},$$

$$N_\xi = 0, N_\theta = \frac{1}{a} \psi' + a p_H,$$

$$u = a A_\theta N_\theta + a \epsilon_{\theta T}.$$

For the first problem (a) we have

$$\psi(\xi = 0) = C_1 = a H_o,$$

$$M_\xi (\xi = 0) = \frac{2k^3 A_\theta D_\xi}{a^2} (C_1 + C_2) + M^*_{\xi T} = 0,$$

and

$$C_2 = - \frac{a^2 M^*_{\xi T}}{2k^3 A_\theta D_\xi} + a H_o .$$

Of particular interest for many practical problems is the change of slope, β, and the radius, u, for $\xi = 0$. We have

$$\beta(0) = \frac{2k^2 A_\theta}{a} e^{-k\xi} \left[\frac{a^2 M^*_{\xi T}}{2k^3 A_\theta D_\xi} + a H_o \right],$$

and

$$u(0) = a A_\theta \left[\frac{k}{a} (C_2 - C_1) + a p_H \right] + a \epsilon_{\theta T}.$$

For the second problem (b) we have

$$M_\xi(\xi=0) = M_o = \frac{2k^3 A_\theta D_\xi}{a^2}(C_1 + C_2) + M_{\xi T} \quad ,$$

$$\psi(\xi=0) = 0 \quad ,$$

and hence

$$C_1 = 0,$$

$$C_2 = \frac{a^2}{2k^3 A_\theta D_\xi}(M_o - M_{\xi T}) \quad .$$

The change of slope, β, at $\xi = 0$, is

$$\beta(0) = \frac{a}{kD_\xi}(M_{\xi T} - M_o),$$

and radial displacement u at $\xi = 0$ is

$$u = a^2 A_\theta \left[\frac{1}{2k^2 A_\theta D_\xi}(M_\theta - M_{\xi T}) + p_H\right] + a\epsilon_{\theta T} \quad .$$

3) Edge effects

The question that generally arises is when do the stresses, due to edge loads, decrease to an insignificant magnitude as ξ (or z) increases? Since the displacements and stress resultants depend on β and ψ, and since

$$\beta = \frac{A_\theta}{a}\psi'' \quad ,$$

we only have to discuss ψ. We have

$$\psi = e^{-k\xi}(C_1 \cos k\xi + C_2 \sin k\xi);$$

C_1 and C_2 are constant, $\cos k\xi$ and $\sin k\xi$ are bounded in magnitude by one. Hence ψ for relative maximums and minimums depend on on $e^{-k\xi}$.

Thus the stresses and deformation are insignificant in magnitude for values of ξ for which

$$e^{-k\xi} << 1 \ .$$

For convenience, let us assume

$$e^{-k\xi} < \frac{1}{10} \ ,$$

then

$$\xi > \frac{\log_e 19}{k} \ ,$$

but $z = a\xi$ and hence

$$z > \frac{a \log_e 10}{k} = \frac{a^4 \log_e 10}{\sqrt[4]{\frac{a^2}{4 A_\theta D_\xi}}}$$

or

$$z > \sqrt[4]{\frac{a^2 A_\theta D_\xi}{4}} \log_e 10 \ .$$

If the material is homogeneously orthotropic through the thickness, then

$$z > \frac{1}{2} \sqrt[4]{\frac{a^2 h^2 \nu_{\xi\theta}}{\nu_{\theta\xi} (1 - \nu_{\xi\theta} \nu_{\theta\xi})}} \log_e 10 \ .$$

If $\nu_{\xi\theta}$, $\nu_{\theta\xi}$ is sufficiently small, then

$$z > \frac{\log_e 10}{2} \sqrt[4]{\frac{a^2 h^2}{3} \frac{\nu_{\xi\theta}}{\nu_{\theta\xi}}}$$

or

$$z > \frac{\log_e 10}{2} \sqrt[4]{\frac{a^2 h^2}{3} \frac{E_\xi}{E_\theta}}$$

Thus the edge loading makes itself known only within the region of the end and depends on the order of magnitude of the effective extensional and bending modulus and radius to curvature of the

shell. It is interesting to note that for the homogeneously orthotropic material that if the meridional Young's modulus is significantly large compared to the circumferential then the edge is felt a greater distance than the case for the isotropic shell.

c. Shallow-Spherical Shell

For a shallow-spherical shell (Ref. VII-3) we now specialize the equation to the form

$$\psi'' + \frac{\psi'}{r} - \frac{A_\xi}{r^2 A_\theta}\psi - \frac{\beta}{R} = 0,$$

$$\beta'' + \frac{\beta'}{r} - \frac{D_\theta}{r^2 D_\xi}\beta + \frac{\psi}{R D_\xi} = \frac{1}{2} rp .$$

Here*

$$r = R \sin\xi \doteq R\xi$$

$$z = H - (R\cos\xi - R) = H - \frac{r^2}{2R} ,$$

$$M_\xi = -D_\xi \beta' - D_{\xi\theta}\frac{\beta}{r}, \quad M_\theta = -D_\theta \frac{\beta}{r} - D_{\theta\xi}\beta' ,$$

and the radial displacement u is given by

$$u = r\left[A_\theta \psi' + A_{\theta\xi}\frac{\psi}{r}\right] .$$

Reference VII-3 shows that on assuming $D_\xi = D_\theta = 0$ for a membrane solution we have

$$\psi = \frac{1}{2} pRr ,$$

and for membrane rotation we have

$$\beta = \frac{1}{2} pR^2 \frac{A_\theta - A_\xi}{r} .$$

*The shallow sphere is determined by a central angle ξ, base radius a, rise H, and curvature radius R. By letting $\frac{H}{a}$ be less than say $\frac{1}{5}$ we have $\sin\xi \approx \xi$ and $\cos\xi \approx 1 - \frac{\xi^2}{2}$.

As in reference VII-3 we see that β becomes infinite as r approaches zero, unless $A_\theta = A_\xi$ at $r = 0$. This implies that the membrane theory may not always be adequate to describe the state of stress due to continuous surface load distributions in the interior of a polar orthotropic shell of revolution.

The above membrane solution implies that it may be necessary to consider the complete differential equations to determine the actual solution of a practical problem. If we let

$$\frac{A_\xi}{A_\theta} = \frac{D_\theta}{D_\xi} = p^2 \ , \ u = \sqrt{\frac{A_\theta}{D_\xi}} \ , \ \lambda^2 = \frac{1}{R\sqrt{A_\theta D_\xi}} \ ,$$

and η a complex variable where

$$\eta = \beta + i u \psi \ ,$$

then the two differential equations for a shallow spherical shell reduces to

$$\eta'' + \frac{1}{r}\eta' - \left(i\lambda^2 + \frac{p^2}{r^2} \right) \eta = \frac{pr}{2 D_\xi} \ .$$

The solution of this equation is then

$$\eta = C_1 I_p (\sqrt{i}\,\lambda r) + C_2 K_p (\sqrt{i}\,\lambda r)$$

$$+ \frac{p}{2 D_\xi} \left[\int_0^r y^2 I_p (\sqrt{i}\,\lambda y)\, d\eta\, K_p (\sqrt{i}\,\lambda r) \right.$$

$$\left. + \int_r^a y^2 K_p (\sqrt{i}\,\lambda y)\, dy \right] .$$

Where I_p and K_p are modified Bessel function with a complex argument.

On specifying a realistic edge condition we can determine the complex constants C_1 and C_2. If no singularity in load or geometry exists at

the origin then $C_2 = 0$. For further discussion on the shallow shell the reader is referred to reference VII-3.

1) Form of general solution for a region and boundary conditions

If the point of discontinuities in loads and geometry are considered as boundary points of a region then a general solution for each region may be expressed as a linear combination of five so-called fundamental solutions as follows:

$$\beta(\xi) = \sum_{i=1}^{\psi} C_i \beta_i(\xi) + \beta_5(\xi),$$

$$\psi(\xi) = \sum_{i=1}^{\psi} C_i \psi_i(\xi) + \psi_5(\xi),$$

where the C_i's ($i = 1, 2, 3, 4$) are determined by the boundary and junction conditions between adjacent regions. The boundary conditions that are assumed for the fundamental solutions β_i and ψ_i ($i = 1, 2, \ldots, 5$) are given in the following table:

	Solution	Boundary Conditions	
I.	β_1	$\beta(0) = 1$	$\beta(\xi_{max}) = 0$
	ψ_1	$\psi(0) = 0$	$\psi(\xi_{max}) = 0$
II.	β_2	$\beta(0) = 0$	$\beta(\xi_{max}) = 0$
	ψ_2	$\psi(0) = 1$	$\psi(\xi_{max}) = 0$
III.	β_3	$\beta(0) = 0$	$\beta(\xi_{max}) = 0$
	ψ_3	$\psi(0) = 0$	$\psi(\xi_{max}) = 0$
IV.	β_4	$\beta(0) = 0$	$\beta(\xi_{max}) = 0$
	ψ_4	$\psi(0) = 0$	$\psi(\xi_{max}) = 1$
V.	β_5	$\beta(0) = 0$	$\beta(\xi_{max}) = 0$
	ψ_5	$\psi(0) = 0$	$\psi(\xi_{max}) = 0$

Continuity of slope and finite stress at $r = 0$ and $z' = 0$ is assured by setting $C_1 = C_2 = 0$. However, by this procedure everything but N_ξ, Q, K_θ and $E_{\theta m}$ takes on its correct value. So, by taking the limit of N_ξ as r approaches zero, we find

$$N_\xi = \lim_{r \to 0} \left[\frac{rH}{r} \frac{r'}{a} + \frac{z'}{ar} (rv) \right] = \frac{(rH)'}{a} ,$$

$$= \frac{\psi'}{a} .$$

Similar expressions may be determined for Q, K_θ and $E_{\theta m}$. Typical sets fo boundary and junction conditions could occur for multi-regional shells with at most three regions at a junction are:

a) two conditions at each boundary,

b) two equilibrium conditions at each junction,

c) a maximum of four continuity conditions at each junction,

d) one continuity condition and one finiteness condition at a singularity of the differentional equation.

2) Numerical solution and program procedure

a) Difference equations

The basic differential equations of the preceding section are transformed into difference equations for numerical integration. The derivatives are replaced by their appropriate central differences at the appropriate integration point. The basic equations after some algebraic manipulation reduce to the following basic difference equations.

$$a_1 \beta_{n+1} + a_2 \beta_n + a_3 \beta_{n-1} + a_4 \psi_n = f_1 ,$$

$$b_1 \psi_{n+1} + b_2 \psi_n + b_3 \psi_{n-1} + b_4 \beta_n = f_2 ,$$

$$a_1 = 1 + \frac{\Delta\xi}{2} \frac{(rD_\xi/a)'}{(rD_\xi/a)} ,$$

$$a_2 = -2 - (\Delta\xi)^2 \left[\frac{\left(D_{\xi\theta} \frac{r}{a} \right)}{D_\xi r/a} - \left(\frac{r'}{r} \right)^2 \frac{D_\theta}{D_\xi} \right] ,$$

$$a_3 = 1 - \frac{\Delta\xi}{2} \frac{\left(D_\xi \frac{r}{a} \right)}{D_\xi \frac{r}{a}} ,$$

$$a_4 = + (\Delta\xi)^2 \frac{z' a}{r D_\xi} ,$$

$$f_1 = (\Delta\xi)^2 \frac{a}{r D_\xi} \bar{Y} ,$$

$$b_1 = 1 + \frac{\Delta\xi}{2} \frac{(A_\theta r/a)'}{A_\theta r/a} ,$$

$$b_2 = -2 - (\Delta\xi)^2 \left[\frac{(A_{\theta\xi} r'/a)'}{A_\theta r/a} - \left(\frac{r'}{r} \right)^2 \frac{A_\xi}{A_\theta} \right] ,$$

$$b_3 = 1 - \frac{\Delta\xi}{2} \frac{(A_\theta r/a)'}{A_\theta r/a} ,$$

$$b_4 = -(\Delta\xi)^2 \frac{z' a}{r A_\theta} ,$$

$$f_2 = (\Delta\xi)^2 \frac{a}{r A_\theta} \bar{X} .$$

b) Numerical integration

The difference equations subject to the end conditions are solved by a scheme employing two by two coefficient matrices. A scheme developed by M.S. Potters and generalized by J.M. Hedgepath is used here. This generalization is as follows:

The difference equations for thin shells may be written in the matrix form

$$A_n y_{n+1} + \beta_n y_n + C_n y_{n-1} = f_n , \quad n = 1,\ldots, N-1 ,$$

with the corresponding boundary conditions

$$y_o + a y_1 = b ,$$

$$d y_{n-1} + y_n = e ,$$

where for our case

$$A_n = \begin{bmatrix} a_1 & 0 \\ 0 & b_1 \end{bmatrix} , \qquad \beta_n = \begin{bmatrix} a_2 & a_4 \\ b_4 & b_2 \end{bmatrix} ,$$

$$C_n = \begin{bmatrix} a_3 & 0 \\ 0 & b_3 \end{bmatrix} \qquad y_n = \begin{bmatrix} \beta_n \\ \psi_n \end{bmatrix} , \quad f_n = \begin{bmatrix} f_1 \\ f_2 \end{bmatrix} ,$$

$$a = P_o , \; b = q_o \quad d = \begin{bmatrix} d_1 & d_2 \\ d_3 & d_4 \end{bmatrix} , \quad e = \begin{bmatrix} e_1 \\ e_2 \end{bmatrix} ,$$

$$I = \begin{bmatrix} 1 & 0 \\ 0 & 1 \end{bmatrix} \text{ (unit matrix)} .$$

The method of solving the equations is as follows:
Let

$$y_n + P_n y_{n+1} = q_n , \quad n = 0,\ldots,N-1 ,$$

then

$$y_{n-1} = q_{n-1} - P_{n-1} y_n , \; n = 1,\ldots,N.$$

Substituting the last two relations into the basic difference equations yield

$$A_n P_n^{-1} (q_n - y_n) + \beta_n y_n + C_n (q_{n-1} - P_{n-1} y_n) = f_n , \; n = 1,..,N-1.$$

Now set

$$A_n P_n^{-1} q_n + C_n q_{n-1} = f_n \ , \qquad \text{(VII-8)}$$

or

$$q_n = P_n A_n^{-1} (f_n - C_n q_{n-1}), \ n = 1,\ldots,N-1 \ , \qquad \text{(VII-9)}$$

Also set

$$- A_n P_n^{-1} + B_n - C_n P_{n-1} = 0 \ , \qquad \text{(VII-10)}$$

or

$$P_n^{-1} = A_n^{-1} (B_n - C_n P_{n-1}) \ , \qquad \text{(VII-11)}$$

or

$$P_n = (B_n - C_n P_{n-1})^{-1} A_n, \ n = 1,\ldots,N-1 \ . \qquad \text{(VII-12)}$$

The procedure for obtaining the solution of the basic difference equation subject to the boundary conditions is as follows; Set

$$P_o = a \ , \ q_o = b \ , \qquad \text{(VII-13)}$$

hence from the last relation for P_n we find

$$P_1 = (B_1 - C_1 P_1)^{-1} A_1 = (B_1 - C_1 a)^{-1} A_1 \ , \qquad \text{(VII-14)}$$

and from the expressions for q_n and P_n we get

$$q_1 = P_1 A_1^{-1} (f_1 - C_1 q_o) = (B_1 - C_1 a)^{-1} (f_1 - C_1 b) \ . \qquad \text{(VII-15)}$$

By continuing this procedure and applying the relations for (VII-9) and (VII-12) the matrix quantities q_n and P_n for $n = 1$ $1, \ldots {}_D N-1$ can be easily obtained. Substituting the expression (VII-6) for $n = N$ into the second boundary condition gives

$$d (q_{N-1} - P_{N-1} y_n) + y_n = e \ . \qquad \text{(VII-16)}$$

Using I as the unit matrix $\begin{bmatrix} 1 & 0 \\ 0 & 1 \end{bmatrix}$ we get

$$(I - d P_{N-1}) y_N = e - d q_{N1} \ , \qquad \text{(VII-17)}$$

hence

$$y_N = (I - d\,P_{N-1})^{-1}\,(e - dq_{N-1}) \cdot$$

Substituting the matrix Y_N into relation (VII-6) for $n = N$ give

$$y_{N-1} = q_{N-1} - P_{N-1}\,y_N \cdot$$

Continuing this procedure, we can easily obtain the remaining quantities for the solution of the difference equation subject to the specified boundary conditions.

d. Computer Program for Isotropic and Orthotropic Shells of Revolution

1) Brief outline of their shell program

The program for the present analysis and reference (VII-5) is written in a very general form, which permits n regions and m layers to be considered. In each region, pressures, temperatures, thickness, and material properties can be specified at an arbitrarily chosen number and spacing of stations along the meridian. The information is specified in each layer for the corresponding station.

Curves are fitted to the specified data and used in the integration procedure. This permits the number of stations at which data are given to be independent of the integration interval. The number of integration intervals can be specified by the user as well as the degree of polynomials used to fit the input data.

After the integration is completed for each region, the junction and boundary conditions are satisfied. The solution is complete except for the calculation of the desired output data. The output data include such quantities as M_ξ, M_θ, N_ξ, N_θ, ϵ_ξ, ϵ_θ, K_ξ, K_θ, β, u, w, as well as σ_ξ and σ_θ at the inner and outer surface of each layer. The quantity x is also printed out, since for a multilayer shell it should be noted that the reference surface is not necessarily the middle surface.

2) One-dimensional analysis for preliminary design

A one-dimensional analysis (Ref. VII-6) solves the thermoelastic problem for a thick, multilayer infinite cylinder subjected to normal pressure and radial temperature gradients. The analysis is attached to a one-dimensional thermodynamic program so that the

resulting temperature gradients versus time are utilized directly by the stress program to compute the stresses.

The results obtained by this program are:

a) tangential stresses at the I. D. and O. D. of each material versus time,

b) the displacement of each material versus time,

c) radial stress for each material versus time.

The program is used to obtain stresses for preliminary evaluation and sizing of a vehicle. A complete description of this program is given in reference VII-6.

3. Bond Problem*

The bond is assumed to be thin and much more flexible than the bonded shells, that is, to have the elastic moduli, of the bonding material, small in comparison with the elastic moduli of the surrounding shell. The bond resists relative radial motion of the shells by developing normal stresses perpendicular to the middle surface and resists relative axial motion of the shells by developing shear stresses. Generally, in shell analysis the above stress components are the only stresses considered in analyzing the bond. For discussion purposes they are the only ones considered here.

If two dissimilar materials are bonded together by techniques, such as electroplating, the problem is the same as the above except that the bond thickness is zero and the shell may be considered as a multi-layer with an effective extensional and bending modulii.

Generally, within the elastic range the bond problem arises at boundaries (or edges) and at geometrical and loca discontinuities. (This is generally true for multi-layer shells with or without a flexible bond and a thermal environment.) The shear stresses are generally concentrated in a narrow band and, in general, can be analyzed as a boundary layer problem. The solutions can generally be approximated by an equivalent cylinder with radius of cylinder equal to the radius of curvature of the end of the shell or region in question. The usually first order linear theory of shells is used here. In addition, some detail of the assumptions on the bond are presented.

a. Assumptions of the Bond

For simplicity purposes, let us consider two equivalent isotropic plates of thickness h and length 2ℓ bonded together by a flexible bond of thickness t. The total energy in terms of the stresses is:

*Study conducted by P.P. Radkowski and R. Grief.

$$\int_{-\ell}^{\ell} \int_{o}^{h} \left\{ \frac{1-\nu^2}{E} \left[\sigma_x^2 + \sigma_y^2 - \frac{2\nu}{1-\nu} \sigma_x \sigma_y \right] + \frac{r_{xy}^2}{G} \right\} dx\, dy$$

$$+ \frac{t}{2} \int_{-\ell}^{\ell} \left[\frac{\sigma_b^2}{E_b} + \frac{r_b^2}{G_b} \right] dx \quad ,$$

where the first and second integrals represent the energy of the plate and bond, respectively. The plate normal stress σ_x is parallel to the plane of the bond, and σ_y is perpendicular to this plane. The shear stress acts in the planes determined by σ_x and σ_y. The bond stresses σ_y and r_{xy} act in similar directions to σ_x and r_{xy}, respectively.

We assume that the work of the stresses σ_y and r_{xy} in the plates is small in comparison to the work of the bond stresses. Further, in each plate we have

$$\int_{o}^{h} \frac{\sigma_y^2}{E}\, dy \approx \frac{h}{2E} \sigma_b^2 \quad ,$$

and

$$\int_{o}^{h} \frac{r_{xy}^2}{G}\, dy \approx \frac{h}{2G} r_b^2 \quad ,$$

then the flexibility of the plates may be neglected when

$$\frac{h}{E} \ll \frac{t}{E_b} \text{ and } \frac{h}{G} \ll \frac{t}{G_b} \quad .$$

(As a rule of thumb, the order of magnitude or h/E and h/G should be less than $1/10$ of t/E_b and t/G_b, respectively.)

b. Formulation of Basic Equations for Bond Problem

For generality, we assume that the shells are not necessarily isotropic and we use the basic relations given in Part B.1 of this Appendix. The

bonding forces will act on each layer as unknown external forces, with normal forces acting as normal forces to the reference surface of the adjacent layer and surface tangential forces being replaced by a couple and a meridional force acting on the reference surface. For simplicity, we assume only two layers with a bond of thickness t.

The stress-strain displacement relationships for the bond are:

$$\sigma_b = E_b \epsilon_b = \frac{E_b}{t} (\bar{w}_1 - \bar{w}_2) ,$$

$$\tau_b = G_p \gamma_b = \frac{G_b}{t} \left[\bar{u}_1 - \bar{u}_2 + \frac{h_1}{2} \left(\frac{\bar{u}_1}{R_{\xi 1}} + \bar{w}_1' \right) + \frac{h_2}{2} \left(\frac{\bar{u}_2}{R_{\xi 2}} + \bar{w}_2' \right) \right] ,$$

where $\bar{u}_i$ and $\bar{w}_i$ ($i = 1, 2$) are the meridional and normal displacements to the i^{th} layer, respectively. The quantities h_i and $R_{\xi *}$ are the thickness and the meridional curvature of the i^{th} layer. The loads for each layer are:

LAYER \ LOAD	SHEAR	NORMAL
1	$\tau^* - \tau_i$	$\sigma^* - \sigma_i$
2	$\tau_o - \tau^*$	$\sigma_o - \sigma^*$

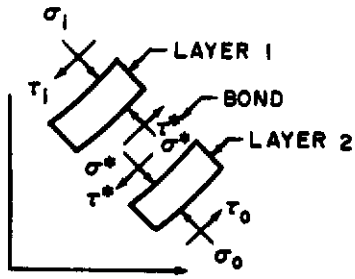

Using the above relations and the results of Part B. 1 in this appendix, we would have two sets of equations coupled through the meridional and normal displacements $\bar{u}_i$ and $\bar{w}_i$, respectively. The displacements could be written in terms of the rotation and resultant β and ψ, respectively; unfortunately, this form would not be convenient at this time. Therefore, the basic equations should be rewritten in terms of displacements. However, since many practical problems have only one bond layer and the region in question can be approximated by an equivalent cylinder, only the general equations in terms of displacements for a cylinder are considered in the following subsection.

c. Cylinder Solution

The basic equations* for a cylinder are:

*Here we assume that B^* is not necessarily zero.

$R_\theta = a,\ R_\xi = \infty$,

$$(A^*_{\xi 1}\ \bar{u}_1')' - \left(A^*_{\xi\theta 1}\ \frac{\bar{w}_1}{a_1}\right)' - (B^*_{\xi 1}\ \bar{w}_1'')' - N'_{\xi T1} + r_b - r_i = 0 ,$$

and

$$(B^*_{\xi 1}\ \bar{u}_1')'' - \left(B^*_{\xi\theta 1}\ \frac{\bar{w}_1}{a_1}\right)'' - (C^*_{\xi 1}\ \bar{w}_1'')'' - M''_{\xi T1} + A^*_{\theta\xi 1}\ \frac{\bar{u}_1'}{a_1}$$

$$- \frac{A^*_{\theta 1}\ \bar{w}_1}{a_1^2} - B^*_{\theta\xi 1}\ \frac{\bar{w}_1''}{a_1} - \frac{1}{a_1} N_{\theta T1} - \left(\frac{r_b - r_i}{2}\ h_1\right)'$$

$$+ \sigma_b - \sigma_i = 0 .$$

A similar set of two equations where 1) subscript 1 is replaced by subscript 2, and 2) $r^* - r_i$ and $\sigma^* - \sigma_i$ are replaced by $r_o - r^*$ and $\sigma_o - \sigma^*$, respectively. The coupling of the two sets of two equations each is done through the relations

$$\sigma_b = \frac{E_b}{t_b}\ (\bar{w}_1 - \bar{w}_2) ,$$

and

$$\tau_b = \frac{G_b}{t_b}\left[\bar{u}_1 - \bar{u}_2 + \frac{h_1}{2}\ \bar{w}_1' + \frac{h_2}{2}\ \bar{w}_2'\right] ,$$

with specified surface loads, edge restraints, material properties, temperature distribution. The problem solution of a semi-infinite cylinder under special loadings, along with a general to-be-programmed method will be forthcoming.

e. Pertinent Comments

The bonding problem is far from being solved mathematically or experimentally. (Such items as material properties are scarce.) Elastic, plastic, viscoelastic, and other analyses are highly desirable. However, in many problems, the above cylinder problem is extremely useful in preliminary investigation and as a solution if the design is to be within the linear elastic shell solution.

For stresses sufficiently removed from the small band of high shear stresses, one can use the multi-layer shell program with the bond considered as a layer of a multi-layer shell.

4. Buckling of Single and Multi-layer Shells of Revolution Subjected to Rotationally Symmetric Loads

A forthcoming report on "Buckling of Single and Multi-layer Shells of Revolution Subjected to Rotationally Symmetric Loads" will give a criteria for the determination of critical loads that could cause buckling of shells of revolution. This will include non-isotropic heat-shield materials and sandwich type back-up structure construction. For the special case of cones and cylinders see reference VII-7. All of the stability analyses are based on the strain-displacement relations and stress strain laws given in the basic relations of this appendix.

Criteria for the elastic instability of thin single-and multi-layer conical and cylindrical shells under combined axial load and external pressure are presented in reference VII-8. These criteria are based on theoretical results and correlation of the results with readily available experimental data.

C. REFERENCES

VII-1. Novozhilov, V. V., Foundations of the Non-Linear Theory of Elasticity, Graylock Press, London (1953).

VII-2. Radkowski, P. P., Stress Analysis of Orthotropic Thin Multi-Layer Shells of Revolution to be presented at AIAA Launch and Space Vehicle Shell Structures Conference, Palm Springs, Calif., Paper No. 2889-63 (April 1963).

VII-3. Reissner, E., Symmetric Bending of Shallow Shells of Revolution, Journal of Math. and Mech., 7, No. 2 (March 1958).

VII-4. Radkowski, P. P., Load and Thermally Induced Stress Analysis of Isotropic or Non-Isotropic Thin Multi-Layer Shells of Revolution (to be published).

VII-5. Radkowski, P. P., R. M. Davis and M. R. Bolduc, Numerical Analysis of Equations of Thin Shells of Revolution, ARS Journal, 32, No. 1 (January 1962).

VII-6. Daddario, A. S., Stress Analysis of Rocket Nozzle Sections Subjected to Pressure and Radial Temperature Gradients, Avco RAD-TM-60-46 (5 August 1960).

VII-7. Radkowski, P. P., Buckling of Thin Single- and Multi-Layer Conical and Cylindrical Shells with Rotationally Symmetric Stresses, Proceedings of the Third U.S. National Congress of Applied Mechanics, Brown Univ. Providence R.I. (June 1958).

VII-8. Radkowski, P. P. and D. R. Johnson, Buckling of Single- and Multi-Layer Conical and Cylindrical Shells Subjected to Axial Loads and Lateral Pressure, Avco RAD-TR-61-36 (December 1961).

APPENDIX VIII

CORRELATION OF THERMAL PROTECTION SYSTEM PERFORMANCE BY DIMENSIONAL ANALYSIS TECHNIQUES

The use of a dimensional analysis technique to derive correlation formulae for thermal protection system performance was initiated early in this study program. The basic equations for simplified thermal protection systems were analyzed, non-dimensional parameters were derived, and correlation models were postulated in an attempt to predict heat shield thicknesses. Non-ablating systems were considered first since the mechanisms are less complex and if attempts were successful with these systems, ablation would be investigated in later studies.

The non-ablating model consisted of a composite shield as shown in the sketch below:

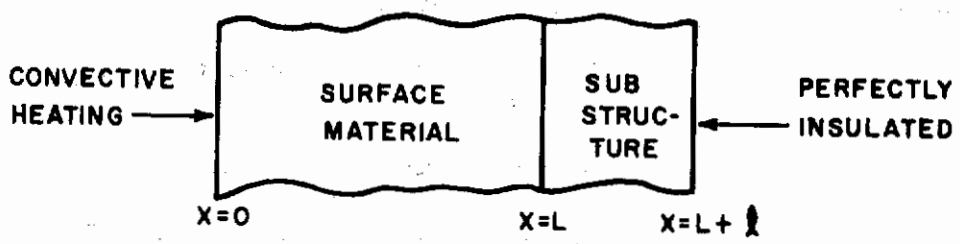

The substructure which is the load carrying member was assumed to be thin compared to the surface material and high enough thermal conductivity so that it acts as a pure capacitance, i.e., the thermal gradients across the substructure are negligible. In addition it was assumed that no heat is lost from the structure, thermal properties of both materials do not vary with temperature and the initial temperature is constant. The equations describing this system are as follows:

$$\frac{1}{\alpha}\frac{\partial T}{\partial t} = \frac{\partial^2 T}{\partial x^2} \; ; \quad 0 < x < L, \, t > 0 , \tag{VIII-1}$$

$$T(x, 0) = T_i = \text{constant.} \tag{VIII-2}$$

At the heated surface, $x = 0$

$$-k\frac{\partial T}{\partial x} = q_c(t)\left[1 - \frac{H_w}{H_s}\right] - \sigma\epsilon T^4 ,$$

$$= q_c(max)\,\phi\left(t, t_{q_c(max)}, t_f, \frac{Q_c}{q_c(max)}\right)\left[1 - \frac{H_w}{H_s}\right] - \sigma\epsilon T^4 . \qquad \text{(VIII-3)}$$

At the interface between the outer shield and substructure, $x = L$

$$-k\frac{\partial T}{\partial x} = \rho_s c_s \ell\frac{\partial T}{\partial t} , \qquad \text{(VIII-4)}$$

where

$T = T(x,t)$	= temperature, °R
$T_i = T(x,0)$	= initial temperature, °R
k	= thermal conductivity of surface material, Btu/sec-ft-°R
ρ	= density of surface material, lb/ft^3
C_p	= specific heat of surface material, Btu/lb-°R
α	= thermal diffusivity of surface material, ft^2/sec
ϵ	= emissivity of surface material,
L	= thickness of surface material, ft
ρ_s	= density of substructure, lb/ft^3
C_s	= specific heat of substructure, ft
	= thickness of substructure, ft
$q_c(t)$	= cold wall convective heat transfer rate at any time during re-entry, Btu/ft^2-sec
$q_c(max)$	= maximum cold wall heat transfer rate, Btu/ft^2-sec

t = time during re-entry, seconds

$t_{q_c(max)}$ = time at which maximum cold wall heat transfer rate occurs, seconds

t_f = impact time of the vehicle, seconds

$\phi\left(t, t_{q_c(max)}, t_f, \frac{Q_c}{q_{c(max)}}\right)$ = a normalized cold wall heat rate profile

$Q_c = \int_0^{t_f} q_c(t)\,dt$ = integrated cold wall heat rate, Btu/ft^2

H_w = enthalpy of hot gases next to the surface, Btu/lb

H_s = stagnation enthalpy, Btu/lb

σ = Stephan-Boltzmann radiation constant, Btu/ft^2-sec-° R^4

x = distance from hot surface, ft.

The non-dimensional heat rate profile $\phi\left(t, t_{q_c(max)}, t_f, \frac{Q_c}{q_{c(max)}}\right)$ is shown in the sketch below:

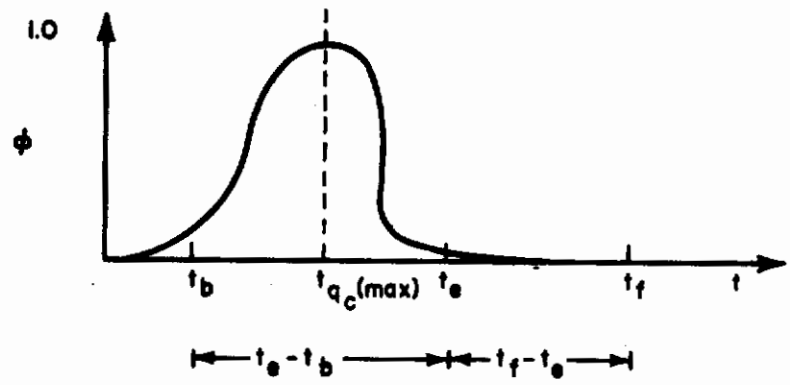

As indicated, the re-entry thermal environment is assumed to have a critical heating period of duration $t_e - t_b = 2Q_c/q_{c(max)}$ and a soak time of $t_f - t_e = t_f - t_{q_c(max)} - \frac{Q_c}{q_{c(max)}}$,

where t_e is the end of critical heating, $t_e = t_{q_c(max)} + \frac{Q_c}{q_{c(max)}}$. The above equations are next made dimensionless by setting

$$V(\xi,\tau) = \frac{Tk}{q_{c(max)}L}, \quad \xi = \frac{x}{L}, \quad \tau = \frac{\alpha t}{L^2},$$

$$V_i(\xi,\tau) = V(\xi,0) = \frac{T_i k}{q_{c(max)}L}; \quad R = \frac{\rho_s C_s \ell}{\rho C_p L},$$

$$\phi\left(t, t_{q_c(max)}, t_f, \frac{Q_c}{q_{c(max)}}\right) = \frac{q_c(t)}{q_{c(max)}},$$

$$\tau_{q_c(max)} = \frac{\alpha t_{q_c(max)}}{L^2}; \quad \tau_e = \frac{\alpha t_e}{L^2} = \frac{\alpha}{L^2}\left(t_{q_c(max)} + \frac{Q_c}{q_{c(max)}}\right),$$

$$\tau_f = \frac{\alpha t_f}{L^2}; \quad \bar{\epsilon} = \left(\frac{q_{c(max)}L}{k}\right)^3\left(\frac{\sigma\epsilon L}{k}\right),$$

$$\bar{H}_w = \frac{H_w}{RT_o}; \quad \bar{H}_s = \frac{H_s}{RT_o}.$$

Equations (VIII-1) through (VIII-3) become

$$\frac{\partial V}{\partial \tau} = \frac{\partial^2 V}{\partial \xi^2}; \quad 0 < \xi < 1, \quad \tau > 0 \tag{VIII-5}$$

at the heated surface, $\xi = 0$

$$-\frac{\partial V}{\partial \xi} = \phi\left(\tau, \tau_{q_c(max)}, \tau_f, \tau_e\right)\left[1 - \frac{\bar{H}_w}{\bar{H}_s}\right] - \bar{\epsilon} V^4. \tag{VIII-6}$$

At the interface $\xi = 1$

$$-\frac{\partial V}{\partial \xi} = R\frac{\partial V}{\partial \tau}. \tag{VIII-7}$$

Initally

$$V(\xi, 0) = V_i = \text{constant.} \tag{VIII-8}$$

Using the above analysis several correlation formulae were constructed and attempts were made to predict the maximum backface temperature for a given thermal environment, material properties, and geometry. One of the correlations attempted was

$$\left[V - V_i\right]_{\text{rear-max}} = \lambda \left[r_e - r_b \right]^a \left[\frac{r_f - r_e}{r_e - r_b}\right]^b \left[\bar{H}_s\right]^c \left[\bar{\tau}\right]^d \left[R\right]^e , \tag{VIII-9}$$

or in terms of the original variables

$$\Delta T_{r\text{-max}} = \lambda \left[\frac{q_c(\max) L}{k}\right] \left[\frac{\alpha Q_c}{L^2 q_c(\max)}\right]^a \left[\frac{(t_f - t_e) q_c(\max)}{Q_c}\right]^b \left[H_s\right]^c_{\text{p.h.}} \left[\bar{\tau}\right]^d \left[R\right]^e , \tag{VIII-10}$$

where the subscript on $\bar{H}_s$ indicates the evaluation is at peak heating, i.e., at $t = t_{q_c(\max)}$. In the above expression the unknown constants a, b, c, d, e, and λ were evaluated by substituting known results computated by finite differences using a digital computer. Since there were six unknowns, then six sets of known results were necessary to evaluate λ, a, b, c, d, and e. Numerous trials revealed that the values of constants obtained did not agree well with finite difference solutions over a wide range of thermal environment, material properties, and environment. As a result it was concluded that this investigation be dropped in favor of determining a short cut calculation method of computing thermal protection performance and then graphically presenting parametric studies covering a broad spectrum of material properties, geometry, and thermal environments.

APPENDIX IX

THE STRUCTURAL STRENGTH OF SANDWICH CYLINDRICAL AND CONICAL SHELLS SUBJECTED TO ROTATIONALLY SYMMETRIC LOADING

by Joseph C. Serpico

This appendix comprises previously reported Avco RAD-TR-61-35 under contract AF33(616)-7483, Project 0(7-7381), Task 73810, dated December 1961. It is repeated here, as requested, to form a part of this Final Report.

ABSTRACT

A strength analysis is presented for conical and cylindrical sandwich-shell structures subjected to combined axial load and lateral pressure distributions. The sandwich construction is assumed to consist of isotropic membrane facings separated by and bonded to a full-depth honeycomb core. Parametric curves are plotted to simplify the design approach and to establish optimum design points for the existing sandwich-shell construction.

LIST OF SYMBOLS

b = Marginal Depth

b_R = Width of Individual Core Ribbon

B, B_c, B_f = Extensional Rigidities of Composite Structure, Core, and Facing Sheet, Respectively

D, D_f = Bending Rigidities of Composite Structure and Cover Sheet

E_c, E_f = Moduli of Elasticity of Core and Facing Sheet

E_s, E_t = Secant and Tangent Moduli

$G_{Z\xi_c}, G_{Z\theta_c}$ = Shear Moduli of Core

$$H = \left[\frac{(2t_3 - \nu_f^2)/\lambda^4 k^2}{8 t_1 t_3 t_4}\right]\left(\frac{B}{D}\right)$$

$$\bar{H} = \left[(1 - \nu_f^2)/\lambda^4 R_o^2\right]\left(\frac{B}{D}\right)$$

$$k = R_o (1 - \beta/2)/\sin\alpha$$

$$\bar{k} = \frac{1}{\left(1 + \frac{R_i}{R_o}\right) - \frac{E_f (t - t_c) \ln\left(\frac{R_i}{R_o}\right)}{2 E_c R_o}}$$

$$K = \lambda k$$

$$K_1 = -\frac{2R_o (1 - \beta/2)}{L \sin^2\alpha} \int_0^L r \left(\frac{\bar{N}_\xi}{P}\right) \cos^2 \lambda\xi \, d\xi$$

LIST OF SYMBOLS (Cont'd)

$K_2 = -\frac{2 R_o (1 - \beta/2)}{L} \int_0^L \left(\frac{\bar{N}_\theta}{p}\right) \frac{\sin^2 \lambda \xi}{r} \, d\xi$

K_c = Foundation Modulus of Core

L = Slant-Length of Shell

m, n = Wave Numbers in the Longitudinal and Circumferential Directions

$M_\xi, M_\theta, M_{\xi\theta}$ = Moment Resultants

$N_\xi, N_\theta, N_{\xi\theta}$ = Axial, Circumferential, and Shear Stress Resultants

p = Reference Pressure for a Particular Loading Condition

$P_{cr}, \bar{P}_{cr}$ = Critical Pressures for Conical and Cylindrical Shells

$P = \left(\frac{32 t_1 t_3 \lambda^2 K_1^3}{k^5 K_2^2}\right) \left(\frac{1 - \nu_f^2}{2 t_3 - \nu_f^2}\right) \left(\frac{P_{cr}}{E_f}\right)$

$\bar{P} = \bar{y}^3 \lambda^2 R_o^2 \left(\frac{\bar{P}_{cr}}{E_f}\right)$

$P_B = \frac{P_{cr} K_2}{2 t_4 \lambda^2 D H^{1/4}}$

$\bar{P}_B = \frac{\bar{P}_{cr} K_2}{\lambda^2 D \bar{H}^{1/4}}$

LIST OF SYMBOLS (Cont'd)

$P_Y = \dfrac{2 R_o (1 - \beta/2)}{\left[3r^2 + \dfrac{R_o^4}{r^2}(1-\bar{\gamma})^2 (1-\beta)^4\right]^{1/2}} \left(\dfrac{\bar{\sigma}_y}{p_{cr}}\right)$

$\bar{P}_Y = \dfrac{2\left(\dfrac{\bar{\sigma}_y}{p_{cr}}\right)}{(\bar{\gamma} - 2\bar{\gamma} + 4)^{1/2}}$

r = Local Cross-Sectional Radius of Conical Shell

R_i, R_o = Inner and Outer Radii of Sandwich Shell

$S/2 = \dfrac{K_1}{k^2 K_2 H^{1/4}}$

$\bar{S}/2 = \left(\dfrac{K_1}{R_o^2 K_2} - 1\right) / \bar{H}^{1/4}$

t, t_c = Total Depth of Sandwich and Thickness of Core, Respectively

t_R = Thickness of an Individual Core Ribbon

u, v, w = Axial, Circumferential, and Radial Diplacements

α = Base Angle of Shell

$\bar{\alpha}$ = Geometric Shape Factor

$\beta = \dfrac{L}{R_o} \cos \alpha$

$\bar{\gamma}$ = Ratio of Axial to Lateral Pressure Distribution

$\lambda = \pi/L$

ν_c, ν_f = Poisson's Ratio for Core and Facing Sheet

LIST OF SYMBOLS (Concl'd)

$\phi = n^2 / H^{1/4} K^2 \sin^2 a$

$\bar{\phi} = \left(1 + \frac{n^2}{\lambda^2 R_o^2}\right) / \bar{H}^{1/4}$

$\phi_o = \cot^2 a / K$

NOTE: Terms that appear with a subscript i or o, refer to the inner or outer facing.

I. INTRODUCTION

Recent technological advances have permitted an increase in flight speeds and the operational life of re-entry vehicles. Associated with these increases has been the increased effect of the exit and re-entry environments of temperature, aerodynamic pressure, and inertial forces. In order to meet the demands of higher operating stresses and temperature, it is essential to develop and evaluate various structural configurations which will provide greater efficiency and reliability than previous conventional designs.

This report isconcerned with the structural strength of full-depth sandwich shells subjected to axisymmetrical loading conditions. The analysis is extended to cases involving steady-state elevated temperatures; however, no attempt is made to evaluate the detrimental effects of thermal stresses induced by transient heating conditions. The main purpose of the present investigation is to determine the structural efficiency of sandwich-shell structures and to provide sufficient understanding through stability and stress distribution studies for determining which structural applications are best suited for full-depth sandwich construction (Fig. IX-1).

In the problems to be considered, it is necessary to approximate the actual model by introducing some simplifying assumptions. Although these assumptions reduce the problems to an approximate analytic model, it is anticipated that the final results will serve as an indication of the strength characteristics of the proposed double-wall structure. Included under each phase of the investigation is a statement which defines the limits and justification of the assumptions and further, it is hoped the modifications of the results will be investigated if and when one or more of these assumptions are not warranted.

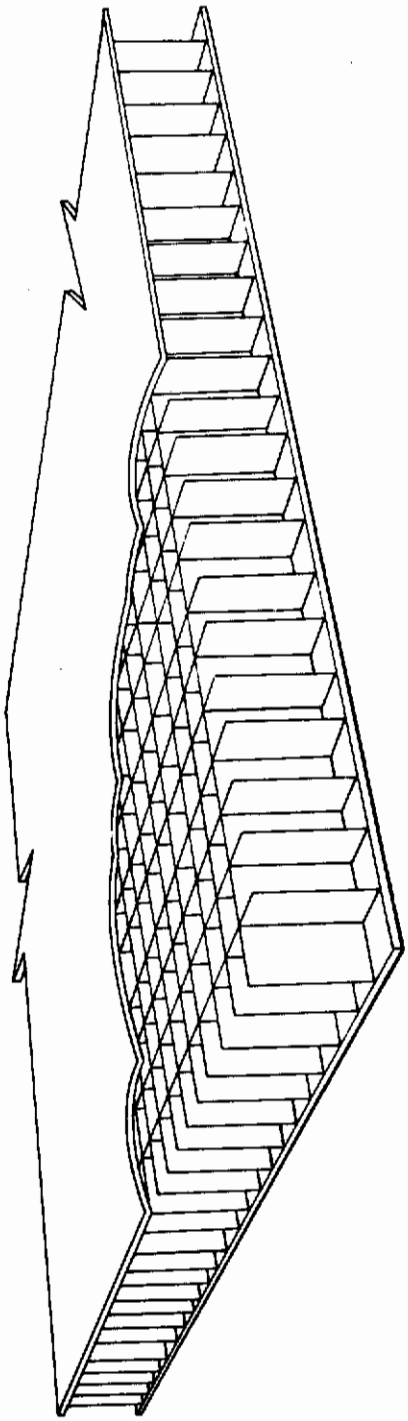

Figure IX-1 SECTION OF SQUARE CELLULAR CORE SANDWICH SHELL

II. CONCLUSIONS AND SUMMARY

A method has been presented for determining the structural strength of sandwich cylindrical and conical shells subjected to axisymmetric loading conditions. The basic modes of failure used in determining the strength of the sandwich construction include: 1) yielding of the cover sheets, 2) general instability of the composite structure, 3) wrinkling of the cover sheets, 4) compressive failure of the core resulting from induced crushing loads, and 5) local buckling of the facing into the core cell.

The results for the general instability modes of failure have been reduced to a form which contains two nondimensional parameters, one essentially dependent on a critical reference pressure and the other determined by the combined effect of shell geometry and ratio of axial-to-lateral loading. These parameters, as well as the parameters for the yield criterion, are graphically illustrated in figures 5a and 5b for various $\frac{k}{t - t_c}$ ratios. In applying the graphic results, it is reiterated that the transverse shear deformations of the core were neglected in simulating the general instability characteristics of full-depth sandwich construction. Although these additional deformations are slight for applications of aluminum or stainless steel honeycomb filler, their effect should be considered when the core is constructed of a soft material.

Finally, it is commented that the relationships (B-30 -33, -36) developed for the critical wrinkling stress represent a lower bound solution for the initially perfect sandwich cylindrical shell. This is accountable by the fact that the extensional energy stored in the cover sheets was neglected prior to formally minimizing equation (B-27).

III. STRENGTH ANALYSIS

The design of full-depth honeycomb shells is determined by the necessity of preventing yielding and buckling of the shell under the applied loading. Inasmuch as structural instability can occur as either a general buckling of the structure or as a local buckling within the structure, failure to predict both modes of instability can result in unconservative design and premature failure. For this reason the following analysis is presented in which combined axial-load and lateral-pressure loadings are considered. The basic modes of failure used in determining the strength of sandwich construction are:

1. Yielding of the cover sheets,

2. General instability of the composite structure,

3. Wrinkling of the cover sheets,

4. Compressive failure of the core resulting from induced crushing loads, and

5. Local buckling of the facing into the core cell (face dimpling).

A. ASSUMPTIONS

The following assumptions are made in order to more easily establish explicit results for sandwich-shell structures:

1. Applied loads are carried only by the facing sheets,

2. The facing sheets are plane; that is, the effects of manufacturing imperfections are negligible,

3. The bond layer is of sufficient strength to prevent slippage between the facing sheets and core material at elevated temperatures,

4. The core is homogeneous and provides continuous support to the cover sheets, and

5. The effect of shear deformation in the core is neglected in calculating the general instability load of the composite structure.

As mentioned previously, the analytic model used to simulate the general instability characteristics of full-depth honeycomb construction is independent of transverse shear deformations of the core. This condition is expected in cases where the stress distribution in the deformed shell differs only slightly from the stress distribution in the undeformed state; that is, the shell remains circular

and in a state of uniform compression until a critical pressure is obtained. If, however, the core is constructed of a soft material, it exhibits small deformations from the initially compressed, circular shape and additional radial and transverse shear stresses must be considered. The effects of these additional stresses are included in the present investigation for determining the critical wrinkling stress of sandwich-type structures, but they are neglected in the general instability considerations for applications of aluminum or stainless-steel honeycomb filler material.

B. DEFINITIONS

Prior to mathematically developing formulas, it is convenient to define certain parameters which often appear in describing the response of sandwich-shell construction to various loading conditions. These parameters are, at the outset:

1. Extensional Stiffness

The extensional rigidity of a sandwich shell is simply equal to the sum of the rigidities of the core and facing sheets; or,

$$B = \frac{E_f (t - t_c) + E_c t_c}{(1 - \bar{\nu}^2)} \quad , \tag{IX-1}$$

where E_f and E_c are the moduli of elasticity in the cover (facing) sheets and core respectively, t is the total depth of sandwich t_c is the core depth, and $\bar{\nu}$ is the effective Poisson's ratio, defined by

$$\bar{\nu} = \frac{\nu_f B_f + \nu_c B_c}{B_f + B_c} \quad , \tag{IX-2}$$

where

$$B_f = \frac{E_f (t - t_c)}{(1 - \nu_f^2)}$$

and,

$$B_c = \frac{E_c t_c}{(1 - \nu_c^2)} \quad .$$

Often, as mentioned previously, it is assumed that the applied loads are carried only by the facing sheets. In these instances, equation (IX-1) becomes (neglecting the last term of this expression)

$$B = \frac{E_f (t - t_c)}{(1 - \nu_f^2)} \quad . \tag{IX-3}$$

2. Bending Stiffness

The expression for the bending rigidity of a sandwich shell is given by

$$D = \frac{E_f}{12(1-\nu_f^2)}(t^3 - \rho t_c^3) \quad , \tag{IX-4}$$

where

$$\rho = \left[1 - \frac{E_c}{E_f}\frac{(1-\nu_f^2)}{(1-\nu_c^2)}\right] .$$

When the stiffness of the core is neglected, the formula for the bending rigidity becomes

$$D = \frac{E_f}{12(1-\nu_f^2)}(t^3 - t_c^3) \quad . \tag{IX-5}$$

C. YIELDING OF THE COVER SHEETS

In the present investigation, the Mises-Hencky yield criterion is used to determine the condition for yielding of the facings. For the plane stress problem, the criterion is expressed as

$$\bar{\sigma}_\xi^2 - \bar{\sigma}_\xi \bar{\sigma}_\theta + \bar{\sigma}_\theta^2 = \bar{\sigma}_y^2 \quad , \tag{IX-6}$$

where $\bar{\sigma}_\xi$ and $\bar{\sigma}_\theta$ are the membrane stresses in the axial and circumferential direction respectively, and $\bar{\sigma}_y$ is the yield stress of the selected material. In applying equation (6), it is only necessary, therefore, to determine the membrane stresses in the shell for each particular loading case. For example, the membrane stresses for a cylindrical shell (Fig. IX-2) under combined axial load and lateral pressure are approximately* given as

$$\bar{\sigma}_\xi = -\frac{\bar{\gamma} p_{cr} R_o}{2(t-t_c)} \quad ,$$

$$\bar{\sigma}_\theta = -\frac{p_{cr} R_o}{(t-t_c)} \quad . \tag{IX-7}$$

Substituting (IX-7) into (IX-6) and collecting in terms of the yield stress required of a selected material,

$$\bar{\sigma}_y = \frac{p_{cr} R_o}{2(t-t_c)}(\bar{\gamma}^2 - 2\bar{\gamma} + 4)^{1/2} \quad . \tag{IX-8}$$

*As will be shown in subsequent sections (appendix B) equation (IX-7) provides a valid approximation to the actual state of stress when the ratio R_i/R_o approaches unity.

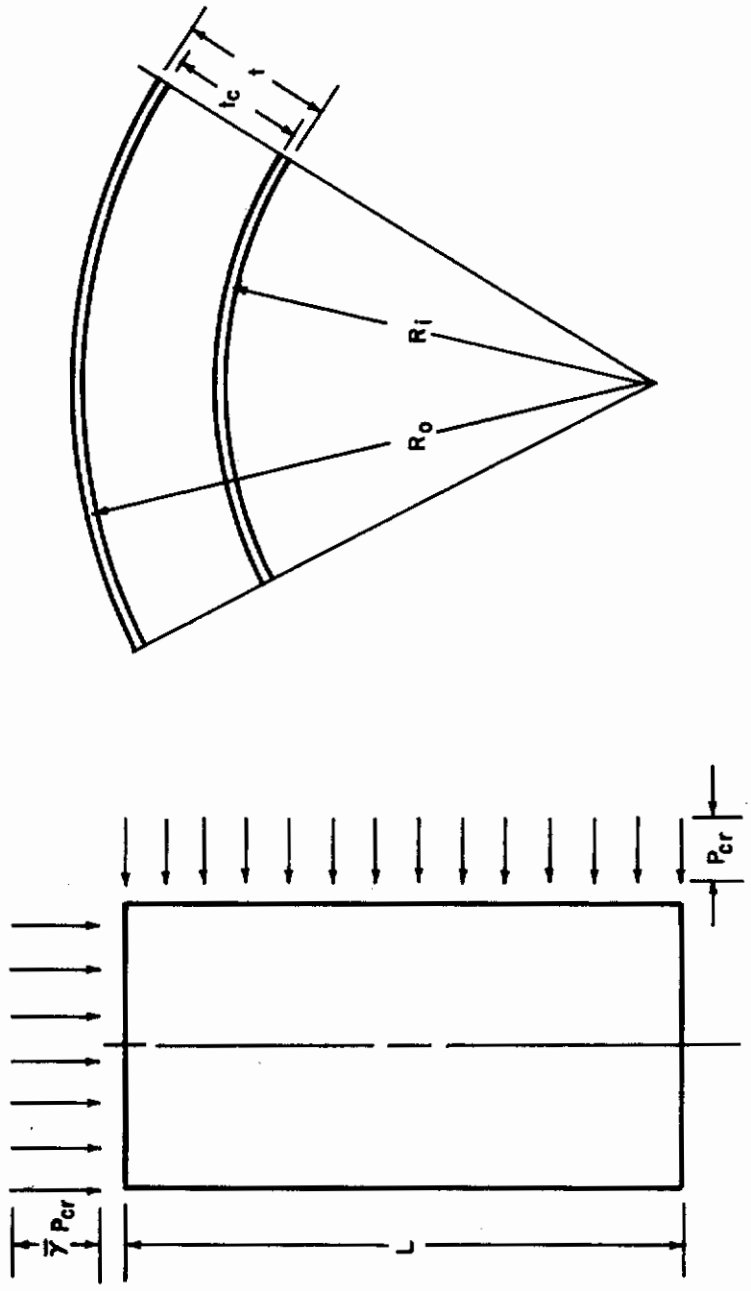

Figure IX-2 SECTION OF A CYLINDRICAL SANDWICH SHELL

For a conical shell subjected to a similar loading condition (Fig. IX-3), equation (IX-7) becomes

$$\bar{\sigma}_{\xi} = - \frac{P_{cr}}{2(t-t_c)\, r \sin\alpha} \left[r^2 - R_o^2 (1-\bar{y})(1-\beta)^2 \right]$$

$$\bar{\sigma}_{\theta} = - \frac{P_{cr}\, r}{(t-t_c) \sin\alpha} \qquad \text{(IX-9)}$$

Substituting equation (IX-9) into equation (IX-6), the value of the required yield stress of a selected material becomes

$$\bar{\sigma}_y = \frac{P_{cr}}{2(t-t_c)\sin\alpha} \left[3r^2 + \frac{R_o^4}{r^2} (1-\bar{y})^2 (1-\beta)^4 \right]^{1/2} . \qquad \text{(IX-10)}$$

In the above expression, the value of the local cross-sectional radius r which makes the required yield stress a maximum, is selected. This value is largely dependent upon the magnitudes of the geometric parameters, $\bar{y}$ and β, that is, the ratio of axial to lateral pressure distribution and the cone taper ratio, defined by

$$\beta = \frac{L}{R_o} \cos\alpha . \qquad \text{(IX-11)}$$

The yield stresses for other loading conditions, including lateral pressure distributions which vary along the generator of the shell, are obtained in a similar manner.

D. GENERAL INSTABILITY OF THE COMPOSITE STRUCTURE

Sandwich-shell construction consists of two thin facing sheets of high-strength material separated by a thick core layer of lightweight material. The function of the face layers is to withstand the design compressive stresses, whereas the core depth increases the bending rigidity of the cover sheets such that overall instability of the sandwich shell will not occur under the design load.

In the overall instability mode, both facings defect into a classical buckle pattern, with an accompanying distortion of the sandwich core. If the shear deformations of the core are assumed to be negligible, any displacement of the shell from the compressed, but unbuckled, state is tantamount to failure and the core depth is determined so as to prevent this mode of failure from occurring under the specified loading conditions.

The stability criterion for conical and cylindrical sheels is derived in appendix A by the principle of minimum potential energy and a Rayleigh-Ritz approximation. The criterion for the conical shell is expressed as

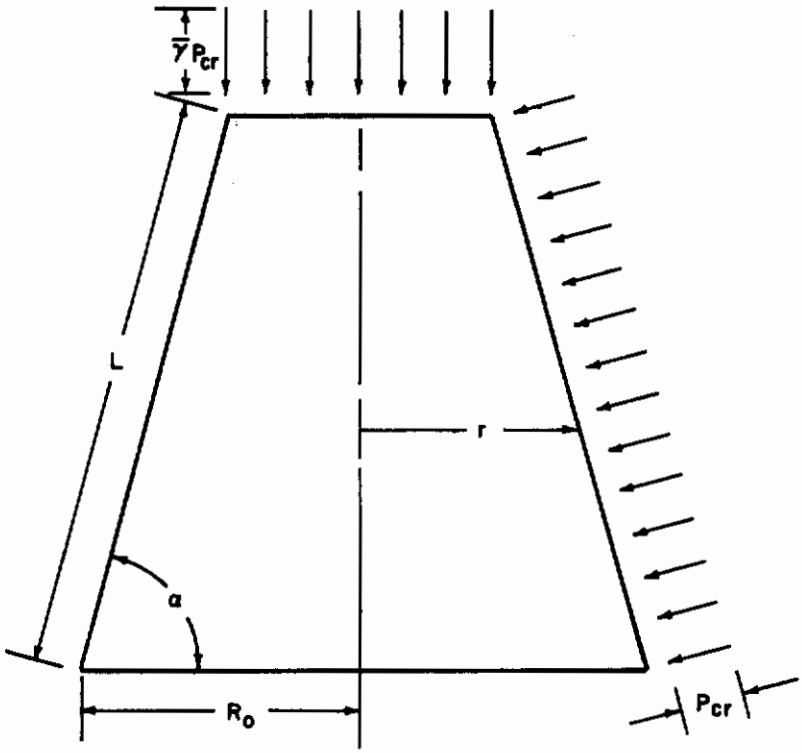

Figure IX-3 SECTION OF A CONICAL SANDWICH SHELL

$$P_B = \frac{\left(\frac{3+S}{1+S} + 1\right)}{\left(\frac{3+S}{1+S}\right)^{1/2}\left[\left(\frac{3+S}{1+S}\right)^{1/4} + S/2\right]} , \qquad \text{(IX-12)}$$

where,

$$P_B = \frac{P_{cr} K_2}{2t_4 \lambda^2 D H^{1/4}} , \quad S/2 = \frac{K_1}{k^2 K_2 H^{1/4}} , \quad H = \frac{(2t_3 - \nu_f^2)/\lambda^4 k^2}{8 t_1 t_3 t_4} \left(\frac{B}{D}\right) .$$

Equation (12) represents the results for the critical pressure of moderately long cones, defined by equation (A-18). The resulting expression for the critical pressure parameter of a cylindrical shell can be readily obtained from equation (12), with restriction (A-18) holding, by having α equal $\pi/2$. The result of removing condition (A-18) for the cylindrical sandwich shell is also given in appendix A; however, as discussed therein, a more exact correlation between the theoretical predictions and the experimental results is expected for the short cones and cylinders if equation (12) is applied in calculating the critical buckling parameter.

E. WRINKLING OF THE COVER SHEETS

For a given dimension of sandwich structure, failure under combined lateral pressure and axial compressive forces may occur by an antisymmetrical type of deformation of the shell or by a "wrinkling" of the cover sheets. The former mode of failure corresponds to an overall bowing of the structure similar to the Euler buckling of beams and is expected when the core depth is sufficiently thin.* If, however, the depth is increased such that this type of failure is not likely to occur, then the cover sheets wrinkle into a washboard pattern which is symmetric with respect to the central plane of the core (Fig. IX-4).

The wrinkling phenomenon involves the bending of the cover sheets and the compression or elongation of the core in a direction normal to the central plane of facings, the core behaving like independent springs fixed to this plane. Here, it is assumed that the buckling distortion in the core parallel to the direction of the applied axial loading is considered small when compared to the distortion in the transverse direction. Thus, the wrinkling of sandwich or solid-filled cylinders is regarded as the bukling of a cylindrical shell supported by an elastic foundation.

The expression for the critical wrinkling stress of a sandwich or a solid-filled cylindrical shell is obtained in appendix B. The expression is established by

*This failure mode was discussed in section III-D.

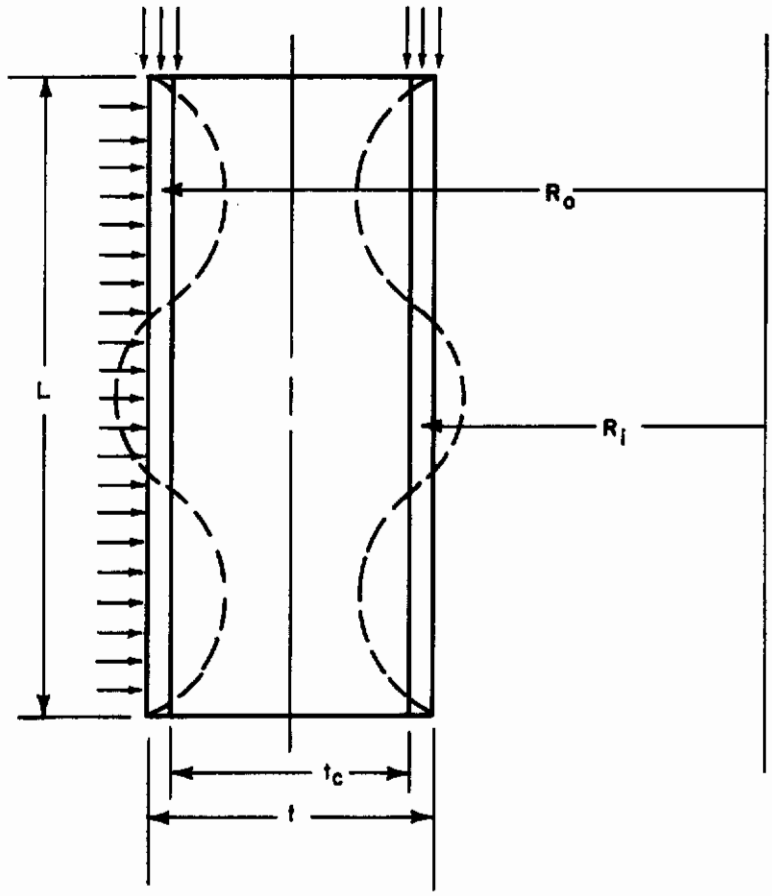

Figure IX-4 WRINKLING OF SANDWICH SHELL CONSTRUCTION

an application of the variational principle to the total potential energy of an equivalent, elastically supported cylinder.

The criterion is expressed as

$$\left[(-)N_{\xi_o}\frac{m^2\pi^2}{L^2}+(-)\,N_{\theta_o}\frac{n^2}{R_o^2}\right] = D_f\left(\frac{m^2\pi^2}{L^2}+\frac{n^2}{R_o^2}\right)^2 + \frac{\dfrac{B_f(1-\nu_f^2)}{R_o^2}\dfrac{m^4\pi^4}{L^4}}{\left(\dfrac{m^2\pi^2}{L^2}+\dfrac{n^2}{R_o^2}\right)^2}$$

$$+\frac{E_c}{b}+\frac{G_{Z\xi_c}}{3}\frac{m^2\pi^2}{L^2}\,b+\frac{G_{Z\theta_c}}{3}\frac{n^2}{R_o^2}\,b\,, \qquad \text{(IX-13)}$$

where b is a marginal zone adjacent to the facing sheet.

As discussed in Appendix B, the results for the critical wrinkling stress of a cylinderical sandwich shell under axial compressive load or lateral pressure distributions are given by

$$\sigma_{\xi_o} = \frac{0.91}{(1-\nu_f^2)^{1/3}}\,(E_f E_c G_{Z\xi_c})^{1/3}$$

$$\sigma_{\theta_o} = \frac{0.91}{(1-\nu_f^2)^{1/3}}\,(E_f E_c G_{Z\theta_c})^{1/3}\,. \qquad \text{(IX-14)}$$

For the rotationally symmetric loading case, it is suggested that the total combined stress should not exceed either of the values obtained in the above equations; that is,

$$\left(\sigma_{\xi_o}^2-\sigma_\xi\sigma_\theta+\sigma_\theta^2\right)^{1/2} \leq \frac{0.91}{(1-\nu_f^2)^{1/3}}(E_f E_c G_{Z\xi_o})^{1/3} \leq \frac{0.91}{(1-\nu_f^2)^{1/3}}\,(E_f E_c G_{Z\theta_o})^{1/3} \qquad \text{(IX-15)}$$

F. COMPRESSIVE FAILURE OF THE CORE RESULTING FROM INDUCED CRUSHING FORCE

As stated previously, a cylindrical or conical shell, prior to buckling, is in a state of uniform compression. The axial forces are carried by the facing sheets

and the lateral pressure loading is distributed as a uniform circumferential stress in the facings and as a uniform radial stress in the core. The radial stress, termed the induced crushing stress, tends to move the facings closer together and can result in a marked loss of compressive and shear stiffness of the core at incipient buckling. This reduction of stiffness is considered in determining the critical wrinkling stress of sandwich-type structures but is neglected in the general instability considerations, provided that the core elements undergo no compressive failure prior to incipient buckling.

The compressive stress for the individual elements of a tubular honeycomb cell is given by the familiar equation (IX-1),

$$\sigma_R = \bar{a} \frac{\pi^2 E_R}{12(1-\nu_R^2)} \left(\frac{t_R}{b_R}\right)^2 , \qquad \text{(IX-16)}$$

where t_R and b_R are respectively, the thickness and width of an individual core ribbon and $\bar{a}$ is a geometric shape factor.

For a square-cell core,

$$\bar{a} = 4 .$$

For a hexagonal-cell core,

$$\bar{a} = 6.3 .$$

Combining equation (IX-16) with equation (B-18), the expression for the critical compressive stress of a square-cell core, in terms of the applied lateral pressure loading, is

$$p = \frac{4}{3} \frac{\pi^2 E_R}{(1-\nu_R^2)\bar{k}} \left(\frac{R_i}{R_o}\right)\left(\frac{t_R}{b_R}\right)^3 . \qquad \text{(IX-17)}$$

The resulting expression for a hexagonal cell is

$$p = \frac{\sqrt{3}}{9} \frac{\bar{a}\pi^2 E_R}{(1-\nu_R^2)\bar{k}} \left(\frac{R_i}{R_o}\right)\left(\frac{t_R}{b_R}\right)^3 . \qquad \text{(IX-18)}$$

G. LOCAL BUCKLING OF THE FACING INTO THE CORE

The assumption that the core provides continuous support to the facing sheets is representative of sandwich structures which have solid cores. When the core is constructed of cellular material, it is necessary to select the core cell size such that the facing material contained within the bounds of the cell

walls is small enough to provide continuous support to the facing sheet and thus eliminate a premature failure of the structure.

An expression for the critical stress for local buckling of a facing into the core (face dimpling) is given in reference 2. The analysis presented therein is based on a consideration of the theoretical buckling stress of a facing sheet, the size of a honeycomb cell, and experimental values. The results are

$$\sigma_f = \left(\frac{E_f}{3}\right)\left(\frac{t - t_c}{d}\right)^{3/2} , \qquad \text{(IX-19)}$$

where d is the diameter of the inscribed circle of the honeycomb cell.

IV. PARAMETRIC STUDY FOR SANDWICH CYLINDERS AND CONES

Assuming that a design begins with a given loading and chosen design stresses, a cylindrical or conical sandwich shell under rotationally symmetric loading will be designed to comply with the following conditions:

1. The facing sheets will be thick enough to withstand the chosen design compressive stresses,

2. The core will be of sufficient depth to prevent overall buckling of the shell,

3. The core will have a shear modulus and modulus of elasticity, high enough to prevent wrinkling of either facing,

4. The core will have a flatwise compressive strength sufficient to prevent compressive failure of the core resulting from induced crushing loads, and

5. If the core is honeycomb, the cell size will be so determined that dimpling of either facing into the core cells will not occur.

The equations governing the condition for yielding of the cover sheets of a cylindrical or conical sandwich shell are expressed by equations (IX-8) and (IX-10). For convenience in further calculations, the yield stress is collected in the following nondimensionalized parameters:

$$P_Y = \left(\frac{k}{t - t_c}\right) , \qquad \text{(IX-20)}$$

where

$$P_Y = 2\left(\frac{\bar{\sigma}_y}{P_{cr}}\right) \frac{R_o (1 - \beta/2)}{\left[3 r^2 + \frac{R_o^4}{r^2} (1 - \bar{\gamma})^2 (1 - \beta)^4\right]^{1/2}}$$

For the cylindrical shell, P_Y is expressed as

$$\bar{P}_Y = \frac{2\left(\frac{\bar{\sigma}_y}{P_{cr}}\right)}{(\bar{\gamma}^2 - 2\bar{\gamma} + 4)^{1/2}} \qquad \text{(IX-21)}$$

The core depth required to prevent overall buckling of the shell is expressed by equation (IX-12). This equation is transformed for convenience into the following relationship. *

$$P = \left(\frac{t - t_c}{k}\right) \frac{S^3 \left(\frac{3+S}{1+S} + 1\right)}{\left(\frac{3+S}{1+S}\right)^{1/2} \left[\left(\frac{3+S}{1+S}\right)^{1/4} + S/2\right]} , \qquad \text{(IX-22)}$$

where

$$P = \left(\frac{32\, t_1\, t_3\, \lambda^2\, K_1^3}{k^5\, K_2^2}\right) \left(\frac{1 - \nu_f^2}{2\, t_3 - \nu_f^2}\right) \left(\frac{P_{cr}}{E_f}\right) ,$$

and

$$S/2 = \left(\frac{\lambda\, K_1\, t_c^{1/2}}{k^{3/2}\, K_2}\right) \left(\frac{2\, t_1\, t_3\, t_4}{2\, t_3 - \nu_f^2}\right)^{1/4} .$$

In the limiting case of a cylindrical shell under combined axial load and lateral pressure, the parameters reduce to the following:

$$\bar{P} = \bar{y}^3\, \bar{\lambda}^2\, R_o^2 \left(\frac{\bar{P}_{cr}}{E_f}\right)$$

$$S = \left(\frac{\bar{y}\, \lambda\, R_o^{1/2}\, t_c^{1/2}}{2}\right) \left(\frac{4}{1 - \nu_f^2}\right)^{1/4} . \qquad \text{(IX-23)}$$

Equations (IX-20) and (IX-22) represent the required relationship between the various nondimensionalized parameters which govern the required cover sheet thickness and core depth for conical and cylindrical shells under combined loading.

*Due to the transformation of equation (IX-12), the results for $K_1 = 0$ are not included in this parametric study. These results are, however, simply obtained by equating the geometric parameter, S, to zero, in equation (IX-12).

Design curves are obtained from appropriate plotting of these variables in figures IX-5a and b. The modes of failure and optimum design point for a selected material are readily obtainable from these parametric curves. Here, it is essential to emphasize that these curves constitute optimum design curves for a selected material when both modes of failure are considered. The optimization of the sandwich core can be more or less determined independently of these failure modes from the equations given previously for wrinkling, dimpling, and induced compressive failure of the core.

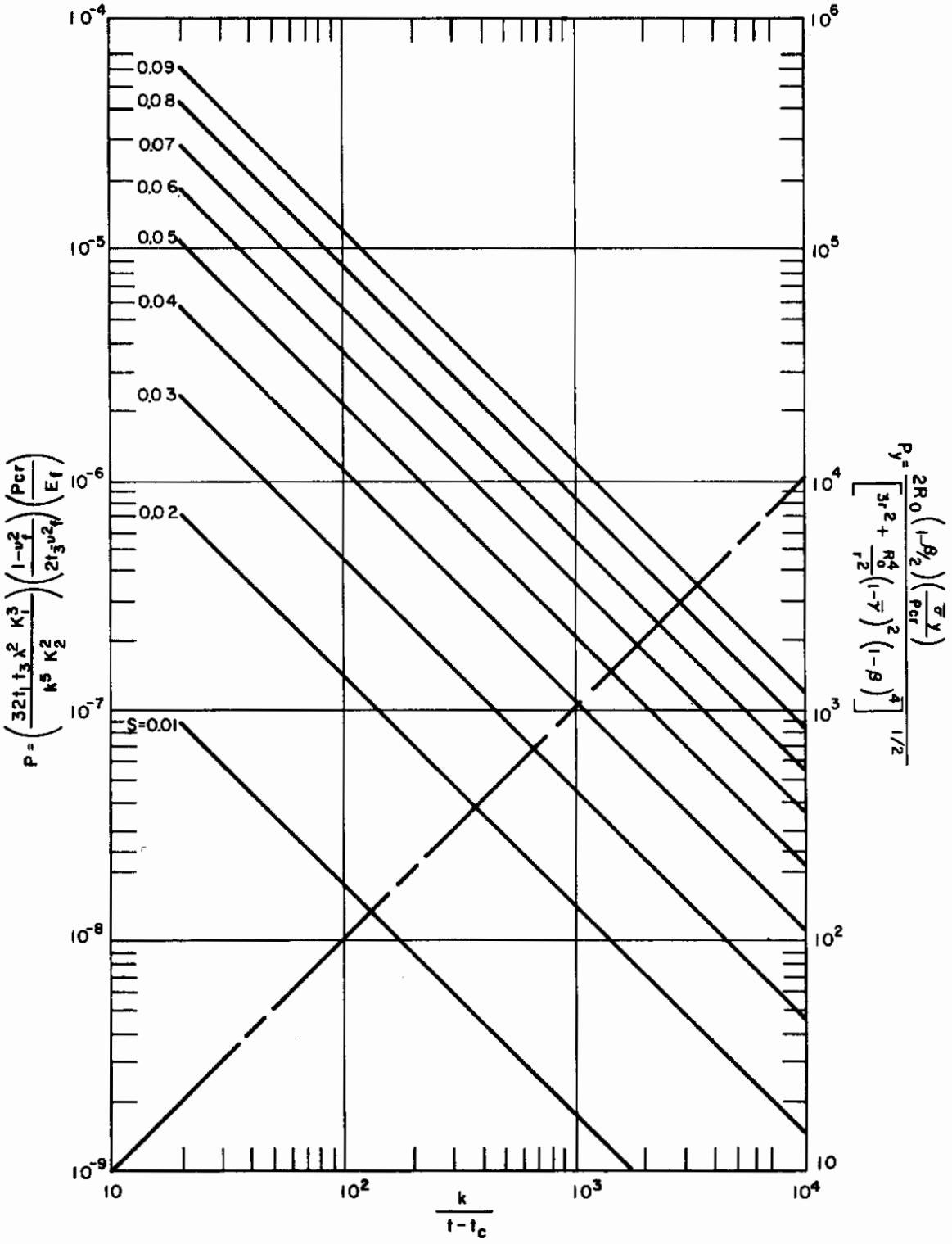

Figure IX-5a TYPICAL DESIGN CURVES FOR SANDWICH CYLINDRICAL AND CONICAL SHELLS

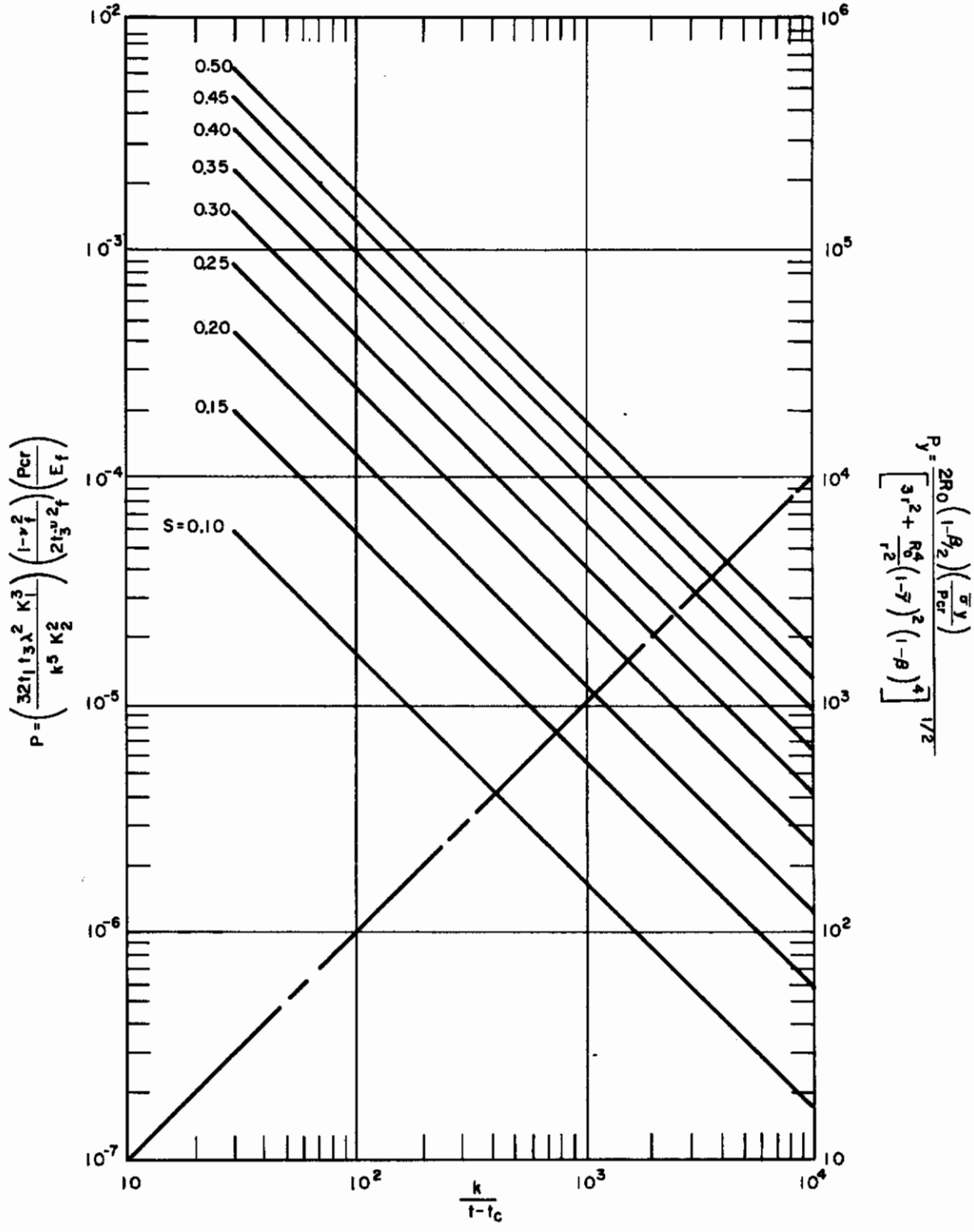

Figure IX-5b TYPICAL DESIGN CURVES FOR SANDWICH CYLINDRICAL AND CONICAL SHELLS

V. ACKNOWLEDGMENTS

The author wishes to thank S. R. Bodner (Consultation) and R. N. Kelly for their suggestions during the course of this investigation.

VI. REFERENCES

1. Bleich, H. H., Buckling Strength of Metal Structures, McGraw-Hill, New York (1952), ch. 9, p. 302-357.

2. Norris, C. B. and W. J. Kommers, Short-Column Compressive Strength of Sandwich Constructions as Affected by the Size of the Cells of Honeycomb Core Materials, Forest Prod. Lab. Rept. 1817 (August 1950).

3. Seide, P., [A]Donnell-type theory for asymmetrical bending and buckling of thin conical shells, J. Appl. Mech. 24, 547-552 (December 1957).

4. Serpico, J. C., Elastic Stability of Orthotropic Conical and Cylindrical Shells Subjected to Axisymmetric Loading Conditions, Avco RAD-TR-61-7 (April 1961).

5. Donnell, L. H., Stability of Thin-Walled Tubes under Torsion, NACA Rept. 479 (1933).

6. Raville, M. E., Analysis of Long Cylinders of Sandwich Construction under Uniform External Lateral Pressure, Forest Prod. Lab. Rept. 1844 (November 1954).

7. Hoff, N. J. and S. E. Mautner, [The]buckling of sandwich-type panels, J. Inst. Aeronaut. Sci. 12, 285-297 (July 1945).

8. Novozhilov, V. V., Foundations of the Nonlinear Theory of Elasticity, Graylock Press, Rochester, N. Y. (1953), p. 191-193.

APPENDIXES

A. DERIVATION OF EXPRESSIONS FOR THE GENERAL INSTABILITY LOAD OF CONICAL AND CYLINDRICAL SHELLS

B. DERIVATION OF EXPRESSIONS FOR THE CRITICAL WRINKLING STRESS OF CYLINDRICAL SHELLS

C. DERIVATION OF EXPRESSIONS FOR MIDDLE-SURFACE STRAINS AND DISPLACEMENTS

D. DEFINITION OF GEOMETRIC PARAMETERS

APPENDIX A

DERIVATION OF EXPRESSIONS FOR THE GENERAL INSTABILITY LOAD OF CONICAL AND CYLINDRICAL SHELLS

1. Middle-Surface Strains and Displacements

The expressions for the middle-surface strains and curvatures of a deformed conical shell are as follows (Fig. A-1):

$$\epsilon_\xi = u_{,\xi} + \tfrac{1}{2} w_{,\xi}^2$$

$$\epsilon_\theta = \frac{1}{r}(v_{,\theta} - u\cos\alpha + w\sin\alpha) + \frac{1}{2} w_{,\theta}^2/r^2$$

$$\epsilon_{\xi\theta} = v_{,\xi} + u_{,\theta}/r + v\cos\alpha/r + w_{,\xi} w_{,\theta}/r$$

$$\chi_\xi = -w_{,\xi\xi}$$

$$\chi_\theta = -\frac{1}{r}(w_{,\theta\theta}/r - w_{,\xi}\cos\alpha)$$

$$\chi_{\xi\theta} = -\frac{1}{r}(w_{,\xi\theta} + w_{,\theta}\cos\alpha/r) \quad . \qquad \text{(A-1)}$$

The above equations are Donnell-type relationships and are identical to the expressions developed by Seide[3] with the exception of a change in the coordinate system.

The strains and curvatures are related to the force and moment resultants by

$$N_\xi = B(\epsilon_\xi + \nu_f \epsilon_\theta)$$

$$N_\theta = B(\epsilon_\theta + \nu_f \epsilon_\xi)$$

$$N_{\xi\theta} = N_{\theta\xi} = \frac{1}{2}(1 - \nu_f) B \epsilon_{\xi\theta}$$

$$M_\xi = D(\chi_\xi + \nu_f \chi_\theta)$$

$$M_\theta = D(\chi_\theta + \nu_f \chi_\xi)$$

$$M_{\xi\theta} = M_{\theta\xi} = -(1 - \nu_f) D \chi_{\xi\theta} \quad . \qquad \text{(A-2)}$$

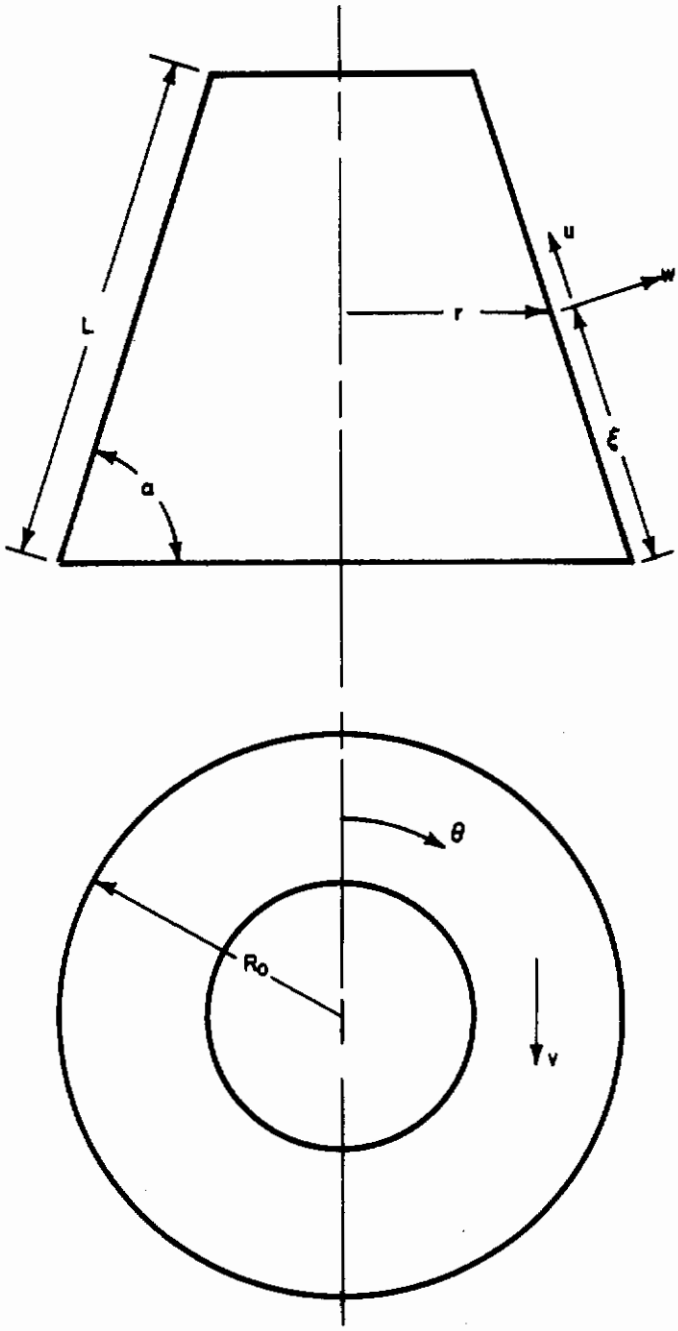

Figure A-1 NOTATION FOR A CONICAL SANDWICH SHELL

In applying equations (A-2) to sandwich-type structures, the values of the extensional and bending rigidities are taken as the relationships given by equations (IX-3) and (IX-5).

2. Energy Relations

The potential energy for an elastic system is governed by the relation

$$V = U + \Omega , \tag{A-3}$$

where U is the strain energy due to bending and stretching of the shell and Ω is the potential energy of the external force system.

The shell strain energy may be expressed as the surface integral

$$U = \frac{1}{2} \int_S (N_\xi \epsilon_\xi + N_\theta \epsilon_\theta + N_{\xi\theta} \epsilon_{\xi\theta} + M_\xi \chi_\xi + M_\theta \chi_\theta - 2M_{\xi\theta} \chi_{\xi\theta}) \, dS . \tag{A-4}$$

In this expression, the quantities N_ξ, N_θ, $N_{\xi\theta}$, M_ξ, M_θ, and $M_{\xi\theta}$ are the force and moment resultants.

The potential energy of the external-force system is equal to the product of the external load and the increase in volume enclosed by the shell. Thus, in the case of hydrostatic loading (p_o), the potential energy may be expressed as

$$\Omega = p_o(V_1 - V_o) , \tag{A-5}$$

where V_1 and V_o represent the volumes enclosed by the deformed and undeformed shells, respectively.

3. Infinitesimal Theory of Buckling

The infinitesimal theory of buckling requires that the variation of the change in potential energy of the system with respect to the allowable displacements must be zero. Expressed mathematically,

$$\delta(\Delta V) = 0 , \tag{A-6}$$

where

$$\Delta V = \Delta U + \Delta \Omega . \tag{A-7}$$

Assuming that the deformed shell, prior to buckling , is very close to its original shape, the expressions (A-1) for the strains and curvatures may be considered to represent the change in strains and curvatures after buckling occurs. Hence, the displacements u , v , and w and the force and moment resultants N_ξ , N_θ , $N_{\xi\theta}$, M_ξ , M_θ , and $M_{\xi\theta}$ are now taken as the additional displacements, forces, and moments in the shell after buckling, and equations (A-4) and (A-5) are taken as the changes in strain energy and potential energy of the external force system, respectively.

Since the middle-surface strains and curvatures are measured from the position of incipient buckling, the potential energy expression must be modified to include the energy stored by the shell in a compressed but unbuckled state. The term to be added to the potential energy expression is given by

$$\Delta U_M = \int_S (\bar{N}_\xi \epsilon_\xi + \bar{N}_\theta \epsilon_\theta + \bar{N}_{\xi\theta} \epsilon_{\xi\theta} + \bar{M}_\xi \chi_\xi + \bar{M}_\theta \chi_\theta - 2 \bar{M}_{\xi\theta} \chi_{\xi\theta}) \, dS , \qquad (A-8)$$

where $\bar{N}_\xi$, $\bar{N}_\theta$, $\bar{N}_{\xi\theta}$, $\bar{M}_\xi$, $\bar{M}_\theta$, and $\bar{M}_{\xi\theta}$ are the membrane stresses and moments existing in the shell prior to buckling.

The strain-energy relation (A-8) for the membrane stress resultants may be simplified appreciably, however, if the shell is assumed under rotationally symmetric loading and initial bending stresses are neglected. Omitting the terms $\bar{N}_{\xi\theta}$, $\bar{M}_\xi$, $\bar{M}_\theta$, and $\bar{M}_{\xi\theta}$, equation (A-8) reduces to the form

$$\Delta U_M = \int_S (\bar{N}_\xi \epsilon_\xi + \bar{N}_\theta \epsilon_\theta) \, dS . \qquad (A-9)$$

By substituting (A-1) and (A-2) into (A-4) and (A-9) and retaining all second-order terms, the total expression for the changes in strain energy of the shell becomes

$$\begin{aligned}
\Delta U_T = {} & \int_S \left\{ \bar{N}_\xi \left(u_{,\xi} + \frac{1}{2} w_{,\xi}^2 \right) + \bar{N}_\theta \left[\frac{1}{r} (v_{,\theta} - u \cos\alpha + w \sin\alpha) + \frac{1}{2} w_{,\theta}^2 / r^2 \right] \right\} dS \\
& + B/2 \int_S \left[u_{,\xi}^2 + 2\nu_f (v_{,\theta} - u\cos\alpha + w \sin\alpha)(u_{,\xi}/r) + \frac{1}{r^2} (v_{,\theta} - u\cos\alpha + w\sin\alpha)^2 \right. \\
& \left. + \frac{1}{2} (1 - \nu_f)(v_{,\xi} + u_{,\theta/r} + v\cos\alpha/r)^2 \right] dS \\
& + D/2 \int_S \left\{ \left[w_{,\xi\xi}^2 + 2\nu_f (w_{,\theta\theta}/r - w_{,\xi} \cos\alpha)(w_{,\xi\xi}/r) \right] + \frac{1}{r^2} (w_{,\theta\theta}/r - w_{,\xi} \cos\alpha)^2 \right. \\
& \left. + \frac{2}{r^2} (1 - \nu_f)(w_{,\xi\theta} + w_{,\theta} \cos\alpha/r)^2 \right\} dS \quad . \qquad (A-10)
\end{aligned}$$

The terms in the expression $\Delta\Omega$ for the change in potential energy of the external force system are not presented herein. However, it is noted that terms in $\Delta\Omega$ which are linear in u, v, and w cancel with similar terms in the strain-energy expression (A-10) by the principle of virtual work. Also, if the degree of approximation used in obtaining (A-10) is maintained, the nonlinear terms in $\Delta\Omega$ are of the same order of magnitude as those terms omitted from the strain displacement relations and are disregarded in what is to follow.

4. Upper Bound for the Critical Buckling Pressure

An upper bound for the critical buckling pressure of the shell will be determined by the Rayleigh-Ritz method. In applying this approximate method, it is necessary to determine a plausible set of displacements which accurately describe the deflected shape of the cone. In view of experimental observations for the monocoque conical shell, the following set of displacements has been selected. for the present investigation:

$$u = A_1 \cos(n\theta) \cos(m\pi\xi/L)$$

$$v = B_1 \sin(n\theta) \sin(m\pi\xi/L)$$

$$w = C_1 \cos(n\theta) \sin(m\pi\xi/L) \qquad \text{(A-11)}$$

where A_1, B_1, and C_1 are undetermined coefficients and m and n are the number of lobes in the axial and circumferential directions. Substituting these equations into the simplified energy relation (A-10) and integrating, yields a homogeneous quadratic function of A, B, and C:

$$\Delta V = a_{11} A_1^2 + a_{12} A_1 B_1 + a_{13} A_1 C_1 + a_{22} B_1^2 + a_{23} B_1 C_1 + a_{33} C_1^2 \quad . \qquad \text{(A-12)}$$

The coefficients in this expression are defined in appendix D.

The condition for the minimization of the potential energy of the system is obtained by setting the derivatives of (A-12) with respect to the unspecified coefficients equal to zero. This operation yields a set of linear homogeneous equations for the coefficients of the displacements, the determinant of which vanishes for nontrivial values of the critical load:

$$\begin{vmatrix} 2a_{11} & a_{12} & a_{13} \\ a_{12} & 2a_{22} & a_{23} \\ a_{13} & a_{23} & 2a_{33} \end{vmatrix} = 0 \qquad \text{(A-13)}$$

5. Membrane State of Stress

When initial bending stresses and the influence of boundary conditions are neglected, the resultant state of stress at incipient buckling is statically determined from the resultant forces per unit length N_ξ and N_θ. These quantities are collected in terms of the nondimensional parameters K_1 and K_2, defined by:

$$K_1 = -\frac{2R_o(1-\beta/2)}{L\sin^2\alpha}\int_0^L r\left(\frac{\bar{N}_\xi}{p}\right)\cos^2\lambda\xi\, d\xi$$

$$K_2 = -\frac{2R_o(1-\beta/2)}{L}\int_0^L \left(\frac{\bar{N}_\theta}{p}\right)\frac{\sin^2\lambda\xi}{r}\, d\xi \quad . \tag{A-14}$$

For illustrative purposes, the resultant forces for a conical shell subjected to combined vertical pressure ($\bar{\gamma}p$), applied at the small diameter of the cone, and subjected to a uniform lateral pressure (p) normal to the generator are given by

$$\bar{N}_\xi = -\frac{p}{2r\sin\alpha}\left[r^2 - R_o^2(1-\bar{\gamma})(1-\beta)^2\right]$$

$$\bar{N}_\theta = -\frac{pr}{\sin\alpha} \quad . \tag{A-15}$$

Substituting (A-15) into the expressions for K_1 and K_2 and integrating yields

$$K_1 = \frac{k^3\left[(1-\beta+\beta^2/3+\beta^2/2\pi^2)-(1-\bar{\gamma})(1-\beta)^2\right]}{2(1-\beta/2)^2} \tag{A-16}$$

$$K_2 = k \quad ,$$

where

$$\beta = (L/R_o)\cos\alpha \, , \quad k = R_o(1-\beta/2)/\sin\alpha \quad .$$

Other loading conditions, including rotationally symmetric pressure distributions which vary along the generator of the cone, can be treated in a similar manner.

6. Theoretical Results for Conical and Cylindrical Shells

a. Conical Shells

When the determinant (A-13) is expanded, the results for the conical shell can be approximately expressed as

$$P_{cr} = D\left[\left(1 + \frac{2t_1 \cot^2\alpha}{K^2}\right) K^4 + 4\,(2t_3 - t_1)\,\frac{K^2 n^2}{\sin^2\alpha} + 2t_4\, n^4/\sin^4\alpha\right] + \frac{B\,(2t_3 - \nu_f^2)\,K^4/k^2\,A_{mn}}{k^2(\lambda^2 K_1 + K_2\, n^2/\sin^2\alpha)}\,, \qquad \text{(A-17)}$$

where

$$A_{mn} = \frac{1}{k^4}\left[K^4 + \frac{2(2t_3 - \nu_f)}{(1-\nu_f)}\,\frac{K^2 n^2}{\sin^2\alpha} + 4t_1 t_3\,\frac{n^4}{\sin^4\alpha}\right].$$

In the limiting case of a cylindrical shell, t_1 given in appendix D and tabulated in Table A-1 is equal to one-half, and equation (A-17) reduces to a form which is obtainable from Donnell's equation for a cylindrical shell.

TABLE A-1

EVALUATION OF THE CONSTANTS $t_1 t_2 t_3$ AS A FUNCTION OF THE GEOMETRIC PARAMETER β

β	t_1	t_3	t_4
0.00	0.50000	0.50000	0.50000
0.10	0.50074	0.50018	0.50027
0.20	0.50334	0.50081	0.50470
0.25	0.50554	0.50134	0.50803
0.35	0.51242	0.50300	0.51621
0.40	0.51748	0.50417	0.52532
0.50	0.53223	0.50749	0.54946
0.55	0.54273	0.50985	0.56400
0.60	0.55625	0.51276	0.58430
0.65	0.57382	0.51638	0.61134
0.70	0.59704	0.52093	0.64769
0.75	0.62853	0.52670	0.69795

For the minimum value of the general instability load, it is necessary to minimize (A-17) with respect to m and n. However, as in the case of a monocoque shell(see reference 4), the minimum results are obtained either for $m = 1$ and arbitrary integer values of n or for $n = 2$ and $m = 1, 2, 3....$ In the present investigation, m is set equal to unity and n is allowed to vary continuously. This procedure assume that the axial wavelength extends over the entire length of the shell and that the core provides continuous support to the cover sheets such that local buckling of the facing into the core does not occur. The numerical value of the critical load parameter for $n = 2$ and arbitrary integer values of m is not presented herein, since equations (A-1) are simplified strain-displacement relations based on the assumption of a large number of circumferential waves.

Also in the dimensional ranges of greatest interest, defined as

$$\left(\frac{2t_3 - \nu_f^2}{8t_1 t_3 t_4}\right)^{1/2} \frac{L^2}{R_o}\left(\frac{B}{D}\right)^{1/2} > 100 \quad . \tag{A-18}$$

Equation (A-17) for all practical purposes becomes

$$\frac{P_{cr} K_2}{\lambda^2 D} = \frac{1}{(K_1/k^2 K_2 + n^2/K^2 \sin^2\alpha}\left[2t_4 \frac{n^4}{K^4 \sin^4\alpha} + \frac{(2t_3 - \nu_f^2)/\lambda^4 k^2}{4t_1 t_3 n^4/K^4 \sin^4\alpha}\left(\frac{B}{D}\right)\right]. \tag{A-19}$$

This expression was obtained by neglecting terms of the lowest order in $n^2/K^2 \sin^2\alpha$.

Using the notation

$$\phi = n^2/H^{1/4} K^2 \sin^2\alpha$$

$$P_B = \frac{P_{cr} K_2}{2t_4 \lambda^2 D H^{1/4}}, \quad S/2 = K_1/k^2 K_2 H^{1/4}, \quad H = \frac{(2t_3 - \nu_f^2)/\lambda^4 k^2}{8t_1 t_3 t_4}\left(\frac{B}{D}\right) ,$$

equation (A-19) can be rewritten as

$$P_B = \frac{\phi^2 + 1/\phi^2}{\phi + S/2} \quad . \tag{A-20}$$

Then, from

$$\frac{\partial P_B}{\partial \phi} = 0$$

$$\phi(\phi^4 - 3) + S(\phi^4 - 1) = 0 \quad . \tag{A-21}$$

The numerical value of a root of this equation can be approximated by

$$\phi = \left(\frac{3+S}{1+S}\right)^{1/4} \quad \text{for} \quad \phi > 0 \quad . \tag{A-22}$$

The approximate solution coincides with the root of (A-21) in the limiting cases $S \to 0, \infty$ and is graphically compared with the real root for all values of S in figure A-2 . Note that the maximum percentage deviation is of the order of magnitude of 1 percent.

Substituting (A-22) into (A-20), the final expression for the general instability load is

$$P_B = \frac{\left(\frac{3+S}{1+S} + 1\right)}{\left(\frac{3+S}{1+S}\right)^{1/2}\left[\left(\frac{3+S}{1+S}\right)^{1/4} + S/2\right]} \quad . \tag{A-23}$$

b. Cylindrical Shells

When the object of the investigation is confined to cylinders, it is possible of course to determine the critical buckling pressure from (A-23) subject to condition (A-18) by having α equal $\pi/2$. However, some interesting simple results can be found for cylinders with restriction (A-18) removed. In these instances, equation (A-17) is capable of further simplification and reduces to a form which is obtainable from Donnell's equation; namely,

$$\bar{P}_B = \frac{\bar{\phi}^2 + \frac{1}{\bar{\phi}^2}}{\bar{\phi} + \bar{S}/2} \tag{A-24}$$

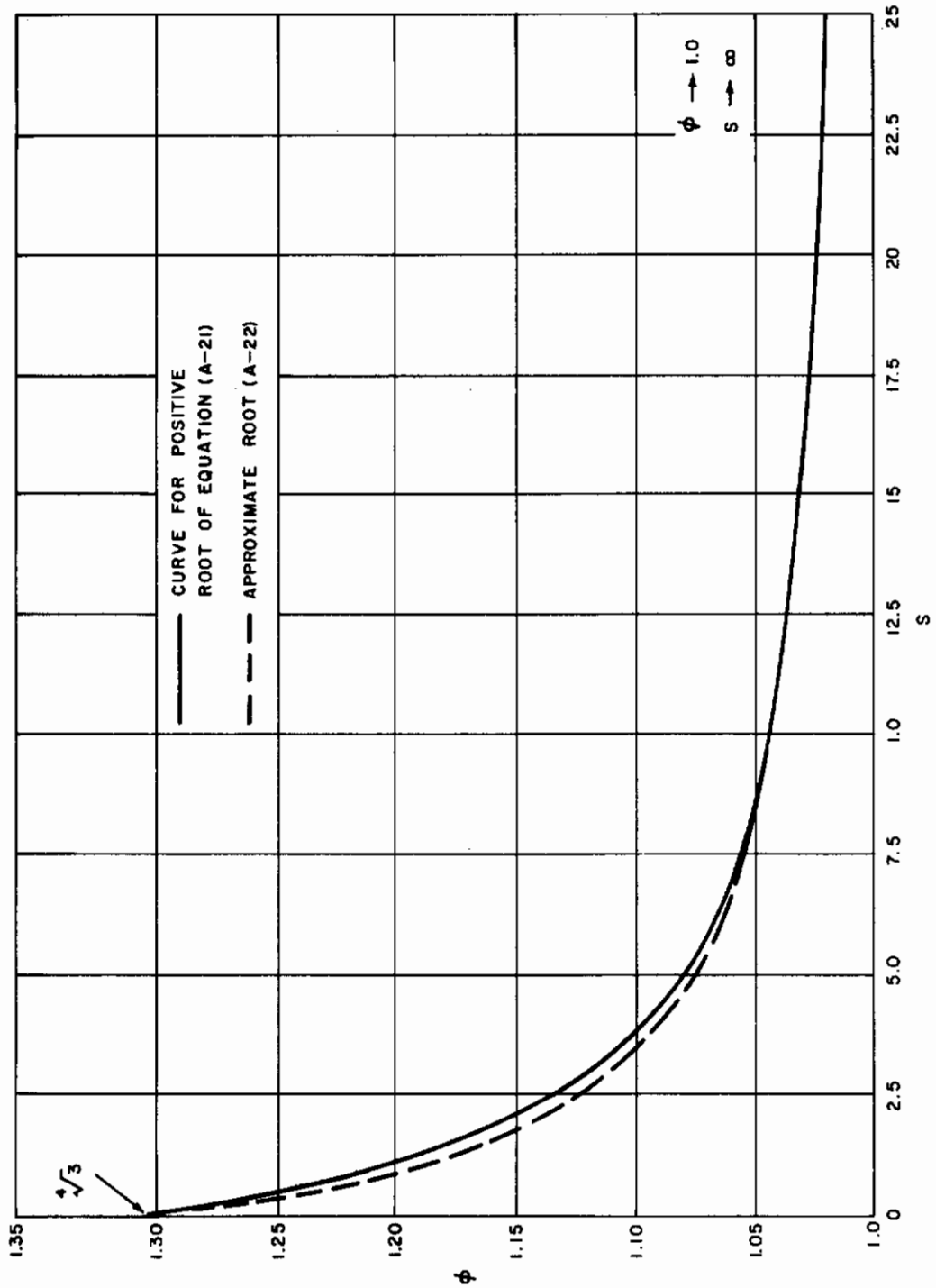

Figure A-2 GRAPHICAL COMPARISON OF THE APPROXIMATE ROOT (A-22) FOR A RANGE OF THE PARAMETER S

where

$$\bar{P}_B = \frac{\bar{P}_{cr} K_2}{\lambda^2 D \bar{H}^{1/4}}, \quad \bar{S}/2 = \left(\frac{K_1}{R_o^2 K_2} - 1 \right) / \bar{H}^{1/4}, \quad \bar{\phi} = \frac{\left(1 + \frac{n^2}{\lambda^2 R_o^2} \right)}{H^{1/4}},$$

$$\bar{H} = \left[(1 - \nu_f^2) / \lambda^4 R_o^2 \right] \left(\frac{B}{D} \right).$$

By formally minimizing equation (A-24) with respect to $\bar{\phi}$, the value of the critical pressure parameter, $\bar{P}_B$ becomes

$$\bar{P}_B = \frac{\left(\frac{3 + \bar{S}}{1 + \bar{S}} + 1 \right)}{\left(\frac{3 + \bar{S}}{1 + \bar{S}} \right)^{1/2} \left[\left(\frac{3 + \bar{S}}{1 + \bar{S}} \right)^{1/4} + \bar{S}/2 \right]} \quad \text{for } \bar{S} > (-1/4). \qquad \text{(A-25)}$$

From an inspection of equations (A-23) and (A-25), it is observed that the expression for the critical pressure parameter of moderately long cylinders and cones, defined by equation (A-18), is similar in form to the expression obtained for cylindrical shells with restriction (A-18) removed. In fact, the only dissimilarity in calculating the critical pressure for cylindrical shells by having α equal $\pi/2$ in equation (A-23) and obtaining the results from equation (A-25) appears in the geometric parameters S and $\bar{S}$. For large values of the curvature parameter H (likewise $\bar{H}$), the two expressions as expected, yield similar results; however, at low values of H this is not a valid approximation unless the ratio $K_1/R_o^2 K_2$ is large when compared to unity, the results obtained from (A-23) being below those obtained from (A-25) for small values of H. Further, since the experimental results are below the theoretical predictions at small values of the curvature parameter, a more exact correlation between the theoretical predictions and experimental results is achieved if equation (A-23) is applied in calculating the critical buckling parameter.

APPENDIX B

DERIVATION OF EXPRESSIONS FOR THE CRITICAL WRINKLING STRESS OF CYLINDRICAL SHELLS

1. Middle-Surface Strains and Displacements

The expressions for the middle-surface strains and curvatures of an elastically supported cylindrical shell are given as follows:

$$\epsilon_\xi = u_{,\xi} + \frac{1}{2} w_{,\xi}^2$$

$$\epsilon_\theta = \frac{1}{R_o} (v_{,\theta} + w) + \frac{1}{2} w_{,\theta}^2 / R_o^2$$

$$\epsilon_{\xi\theta} = v_{,\xi} + u_{,\theta}/R_o + w_{,\xi} w_{,\theta}/R_o$$

$$\chi_\xi = - w_{,\xi\xi}$$

$$\chi_\theta = - w_{,\theta\theta}/R_o^2$$

$$\chi_{\xi\theta} = - w_{,\xi\theta}/R_o \quad . \tag{B-1}$$

The strains and curvatures are related to the force and moment resultants by

$$N_\xi = B_f (\epsilon_\xi + \nu_f \epsilon_\theta)$$

$$N_\theta = B_f (\epsilon_\theta + \nu_f \epsilon_\xi)$$

$$N_{\xi\theta} = N_{\theta\xi} = \frac{1}{2}(1 - \nu_f) B_f \epsilon_{\xi\theta}$$

$$M_\xi = D_f (\chi_\xi + \nu_f \chi_\theta)$$

$$M_\theta = D_f (\chi_\theta + \nu_f \chi_\xi)$$

$$M_{\xi\theta} = - M_{\theta\xi} = - (1 - \nu_f) D_f \chi_{\xi\theta} \quad . \tag{B-2}$$

2. Energy Relations

Following the procedure given in appendix A, the expression for the change in potential energy of an elastically supported cylinder becomes

$$\Delta V_T = \int_S \left\{ \bar{N}_{,\xi_o} \left(u_{,\xi} + \frac{1}{2} w_{,\xi}^2 \right) + \bar{N}_{\theta_o} \left[\frac{1}{R_o} (v_{,\theta} + w) + \frac{1}{2} w_{,\theta}^2 / R_o^2 \right] \right.$$

$$\left. + \bar{N}_{\xi\theta_o} \left[v_{,\xi} + u_{,\theta}/R_o + w_{,\xi} w_{,\theta}/R_o \right] \right\} dS$$

$$+ \frac{B_f}{2} \int_S \left\{ \left[u_{,\xi}^2 + 2\nu_f (v_{,\theta} + w)(u_{,\xi}/R_o) \right] + \left[\frac{1}{R_o} (v_{,\theta} + w) \right]^2 \right.$$

$$\left. + \frac{1}{2} (1 - \nu_f) \left[v_{,\xi} + u_{,\theta}/R_o \right]^2 \right\} dS$$

$$+ \frac{D_f}{2} \int_S \left[w_{,\xi\xi}^2 + 2\nu_f (w_{,\theta\theta} w_{,\xi\xi}/R_o^2) + w_{,\theta\theta} w_{,\xi\xi}/R_o^2 + w_{,\theta\theta}^2/R_o^4 \right.$$

$$\left. + 2(1 - \nu_f) w_{,\xi\theta}^2/R_o^2 \right] dS \, . \qquad \text{(B-3)}$$

In the above expression, the relationship for the change in strain energy of the elastic spring system is represented by

$$\Delta U_S = \frac{1}{2} \int_S K_c w^2 \, dS \, , \qquad \text{(B-4)}$$

where K_c is the modulus of the foundation and is expressed in pounds per square inch per inch of deflection. As mentioned previously, the distortions in the elastic medium normal to the lateral pressure loading are considered small when compared to the transverse displacement and, therefore, are neglected in calculating the change in strain energy of the elastic spring system.

3. Differential Equations of the Elastically Supported Cylinder

The application of the variational principle to equation (B-3) leads to the equations of equilibrium and associated boundary conditions for the instability characteristics of an elastically supported cylinder. The following simultaneous equations in displacements u, v, and w define the conditions for the neutral equilibrium state:

$$u_{,\xi\xi} + \nu_f w_{,\xi}/R_o + \frac{(1+\nu_f)}{2R_o} v_{,\xi\theta} + \frac{(1-\nu_f)}{2R_o^2} u_{,\theta\theta} = 0$$

$$v_{,\theta\theta}/R_o^2 + w_{,\theta}/R_o^2 + \frac{(1-\nu_f)}{2} v_{,\xi\xi} + \frac{(1+\nu_f)}{2R_o} u_{,\theta\xi} = 0$$

$$D_f \left(w_{,\xi\xi\xi\xi} + \frac{2}{R_o^2} w_{,\xi\xi\theta\theta} + \frac{1}{R_o^4} w_{,\theta\theta\theta\theta} \right) + \frac{B_f}{R_o} (v_{,\theta}/R_o + w/R_o + \nu_f u_{,\xi}) + Kw$$

$$- \left(\bar{N}_{\xi_o} w_{,\xi\xi} + \frac{2\bar{N}_{\xi\theta_o}}{R_o} w_{,\xi\theta} + \frac{\bar{N}_{\theta_o}}{R_o^2} w_{,\theta\theta} \right) = 0 \quad . \tag{B-5}$$

For convenience in further calculations a single equation in the displacement, w, is obtained by operating on equations (B-5),

$$D_f \nabla^8 w + K\nabla^4 w + \frac{B_f(1-\nu_f^2)}{R_o^2} w_{,\xi\xi\xi\xi} - \nabla^4 \left(\bar{N}_{\xi_o} w_{,\xi\xi} + 2\bar{N}_{\xi\theta_o} w_{,\xi\theta} + \frac{\bar{N}_{\theta_o}}{R_o^2} w_{,\theta\theta} \right) = 0 \quad . \tag{B-6}$$

The relationships between u and w and between v and w are

$$\nabla^4 u = - \frac{\nu_f}{R_o} w_{,\xi\xi\xi} + \frac{1}{R_o^3} w_{,\xi\theta\theta}$$

$$\nabla^4 v = - \frac{(2+\nu_f)}{R_o^2} w_{,\xi\xi\theta} - \frac{1}{R_o^4} w_{,\theta\theta\theta} \quad . \tag{B-7}$$

The above equations reduce to the familiar eight-order Donnell equation[5] for the case of K_c equal to zero.

4. Solution of Differential Equations

The differential equation for the buckling of a cylindrical shell which is elastically supported and subjected to axisymmetric loading is given by equation (B-6). The associated boundary conditions corresponding to simply supported edges (no deflection and no moment along the edges) are

$$w(0,\theta) = w(\ell,\theta) = 0$$

$$w_{,\xi\xi}(0,\theta)\ w_{,\xi\xi}(\ell,\theta) = 0 \ . \tag{B-8}$$

If the shear-stress resultant, $\bar{N}_{\xi\theta_o}$, is omitted, a solution of equation (B-6) satisfying the boundary conditions for a simple support is

$$w = w_1 \cos(n\theta)\ \sin(m\pi\xi/L) \ , \tag{B-9}$$

where m and n are the wave numbers in the axial and circumferential directions, respectively.

Combining (B-6) and (B-9) yields the following equation:

$$\left[(-)\bar{N}_{\xi_o}\frac{m^2\pi^2}{L^2} + (-)\bar{N}_{\theta_o}\frac{n^2}{R_o^2}\right] = D_f\left(\frac{m^2\pi^2}{L^2}+\frac{n^2}{R_o^2}\right)^2 + \frac{\dfrac{B_f(1-\nu_f^2)}{R_o^2}\dfrac{m^4\pi^4}{L^4}}{\left(\dfrac{m^2\pi^2}{L^2}+\dfrac{n^2}{R_o^2}\right)^2} + K \ . \tag{B-10}$$

5. Membrane State of Stress Prior to Buckling

When initial bending stresses and the influence of boundary conditions are neglected, the resultant state of stress at incipient buckling is statically determined from the resultant forces per unit length $\bar{N}_\xi$ and $\bar{N}_\theta$. If it is assumed that the core can transmit only normal stress in the radial direction and transverse shear stresses, the only stress acting at incipient buckling is the normal radial stress[6].

Summing forces in the radial direction for the core gives (Fig. B-1)

$$\frac{\partial \sigma_{rc}}{\partial r} + \frac{\sigma_{rc}}{r} = 0 \ . \tag{B-11}$$

The equilibrium equation which pertains to the inner and outer facings of the sandwich is (from figure B-1),

$$\begin{aligned} \bar{N}_{\theta_i} &= R_i \, \sigma_r \\ \bar{N}_{\theta_o} &= R_o (p - \sigma_r) \ . \end{aligned} \tag{B-12}$$

Since

$$\sigma_r = \sigma_{rc}\big|_{r = R_i}$$

and

$$\sigma_r = \sigma_{rc}\big|_{r = R_o} \ ,$$

equation (B-12) becomes,

$$\bar{N}_{\theta_i} = R_i \, \sigma_{rc}\big|_{r = R_i}$$

$$\bar{N}_{\theta_o} = R_o \left(p - \sigma_{rc}\big|_{r = R_o}\right) . \tag{B-13}$$

The solution to equation (B-11) is

$$\sigma_{rc} = E_c \frac{A_o}{r} \ , \tag{B-14}$$

and from

$$\sigma_{rc} = E_c \, w_{,r} \ , \tag{B-15}$$

it follows that

$$w_c = A_1 \ln \frac{r}{R_o} + A_2 \ . \tag{B-16}$$

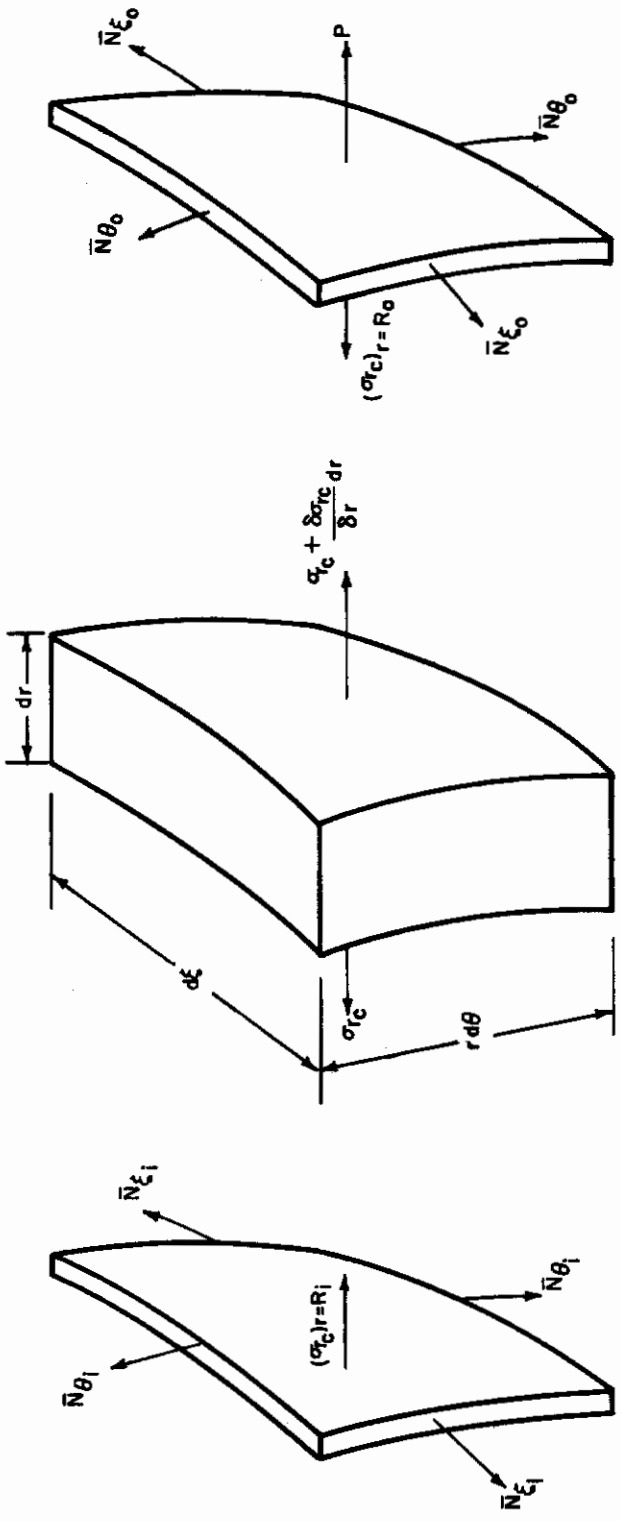

Figure B-1 DIFFERENTIAL ELEMENTS OF CORE AND FACINGS

From the conditions,

$$w_i = w_c|_{r=R_i}$$
$$w_o = w_c|_{r=R_o} \quad . \tag{B-17}$$

The constants of integration A_1 and A_2 are evaluated and substituted into equations (B-16, -15, and -13). The following expressions for the stresses in the cylinder are obtained:

$$\bar{N}_{\theta_i} = p^* R_o \bar{k}$$

$$\bar{N}_{\theta_o} = p R_o (1 - \bar{k})$$

$$\sigma_{rc} = p\left(\frac{R_o}{r}\right) \bar{k} \tag{B-18}$$

where,

$$\bar{k} = \frac{1}{\left(1 + \frac{R_i}{R_o}\right) - \frac{E_f(t-t_c) \ln (R_i/R_o)}{2 E_c R_o}} \quad .$$

The axial resultant forces $\bar{N}_{\xi_i}$ and $\bar{N}_{\xi_o}$, in terms of an applied load, P, are given by

$$2\pi R_i \bar{N}_{\xi_i} + 2\pi R_o \bar{N}_{\xi_o} = P \quad ; \tag{B-19}$$

or, if $\bar{N}_{\xi_i}$ is assumed equal to $\bar{N}_{\xi_o}$

$$\bar{N}_{\xi_i} = \frac{\bar{y} p}{2} \frac{R_o}{(1 + R_i/R_o)}$$

$$\bar{N}_{\xi_o} = \frac{\bar{y} p}{2} \frac{R_o}{(1 + R_i/R_o)} \quad , \tag{B-20}$$

*In the case of lateral compression, the pressure p is taken as negative.

where,

$$\bar{\gamma}_P = \left(\frac{P}{\pi R_o^2}\right) .$$

6. Correlation of Foundation Modulus to Core Properties

Equation (B-10) gives the critical wrinkling stress of an elastically supported cylinder under combined axial load and lateral pressure. The buckled mode shape corresponding to the deflected shell is governed by the values of the wave numbers, m and n. Prior to formally minimizing equation (B-10), it is necessary to correlate the foundation modulus in terms of the core properties; that is, the dependence of the core properties as a function of the wave numbers must be determined.

For the present study, the correlation between foundation modulus and core properties is obtained by equating the strain energy absorbed in the equivalent spring system for a given wave pattern equal to the strain energy absorbed by the core corresponding to the same wave pattern. Further, it is assumed that the displacements in the core are confined to a marginal zone of depth b adjacent to the facing sheets. This assumption is made since the amplitude of the wave pattern is sufficiently small when many waves are generated and, consequently, has little effect upon the material in the middle portion of the core. An expression for the transverse displacement which appropriately describes the physical model is illustrated in figure B-2 and is given by

$$W = W_1 \left(\frac{Z}{b}\right) \cos(n\theta) \sin \frac{m\pi\xi}{L} . \qquad \text{(B-21)}$$

The displacement is a maximum at the bonding surface and decreases linearly to zero when the full depth b is reached, the depth being less than or equal to one-half of the thickness of the core.

Equating the strain energy stored in the spring system to the sum of the extensional and shear strain energies stored in the core gives

$$U_S = U_\epsilon + U_\gamma \quad , \qquad \text{(B-22)}$$

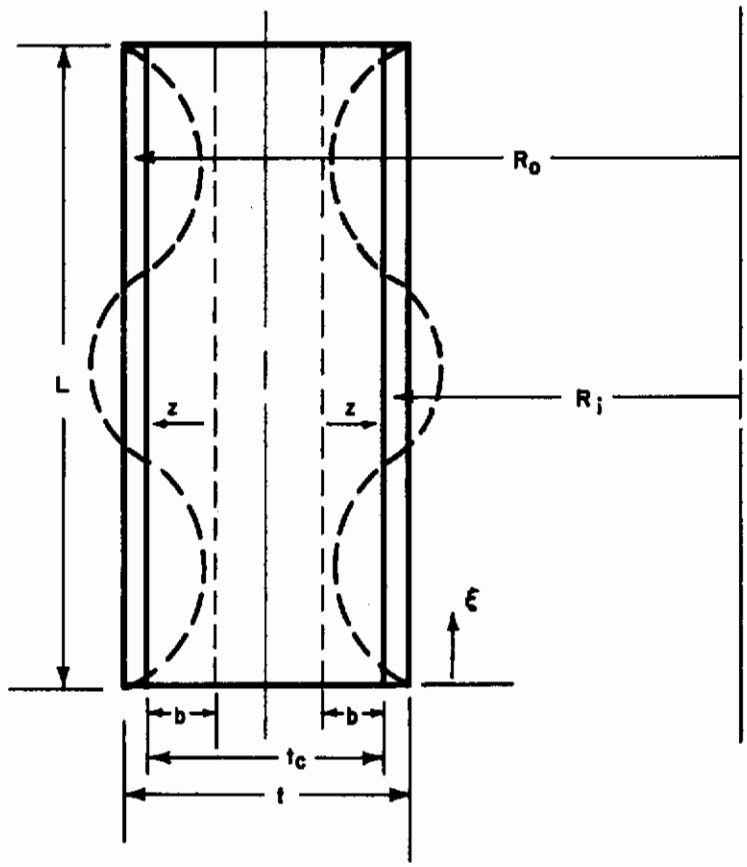

Figure B-2 ILLUSTRATION OF MARGINAL DEPTH FOR WRINKLING OF SANDWICH CONSTRUCTION

where

$$U_S = \frac{1}{2}\int_S K_c\, w^2|_{Z=b}\, dS$$

$$U_\epsilon = \frac{E_c}{2}\int_\gamma \epsilon_Z^2\, dV$$

$$U_\gamma = \frac{G_{Z\xi_c}}{2}\int_v \gamma_{Z\xi}^2\, dV + \frac{G_{Z\theta_c}}{2}\int_v \gamma_{Z\theta}^2\, dV\ , \qquad \text{(B-23)}$$

and

$$\epsilon_Z = w,_Z$$

$$\gamma_{Z\xi} = w,_\xi$$

$$\gamma_{Z\theta} = \frac{1}{[(R_o - b) + Z]}\, w,_\theta\ . \qquad \text{(B-24)}$$

As mentioned previously, it is assumed that w is the dominant displacement in the core, and the displacements, u and v, and their derivatives are small when compared to the derivatives of w.

Substituting (B-21) into (B-22, -23, and -24), the value of the foundation modulus corresponding to the elastic properties of the core becomes

$$K_c = \frac{E_c}{b}\left(1 - \frac{b}{2R_o}\right) + G_{Z\xi_c}\,\frac{m^2\pi^2}{L^2}\,b\left(1 - \frac{b}{4R_o}\right)$$

$$+ G_{Z\theta}\, n^2\,\frac{R_o}{b^2}\left[\left(\frac{3}{2}\,\frac{b}{R_o} - 1\right)\frac{b}{R_o} - \left(1 - \frac{b}{R_o}\right)^2 \ln\left(1 - \frac{b}{R_o}\right)\right]. \qquad \text{(B-25)}$$

If the expression $\ln\left(1-\frac{b}{R_o}\right)$ is expanded in a power series, and the condition $\frac{b}{R_o} << 1$ applied, equation (B-25) is approximately expressed as

$$K_c = \frac{E_c}{b} + \frac{G_{Z\xi_c}}{3}\frac{m^2\pi^2}{L^2}b + \frac{G_{Z\theta_c}}{3}\frac{n^2}{R_o^2}b \quad . \tag{B-26}$$

7. Theoretical Results for Wrinkling of Sandwich Cylindrical Shells

Substituting equation (B-26) into (B-10), the expression for the wrinkling stress becomes

$$\left[(-)N_{\xi_o}\frac{m^2\pi^2}{L^2} + (-)N_{\theta_o}\frac{n^2}{R_o^2}\right] = D_f\left(\frac{m^2\pi^2}{L^2}+\frac{n^2}{R_o^2}\right)^2 + \frac{\frac{B_f(1-\nu_f^2)}{R_o^2}\left(\frac{m^4\pi^4}{L^4}\right)}{\left(\frac{m^2\pi^2}{L^2}+\frac{n^2}{R_o^2}\right)^2}$$

$$+ \frac{E_c}{b} + \frac{G_{Z\xi_c}}{3}\frac{m^2\pi^2}{L^2}b + \frac{G_{Z\theta_c}}{3}\frac{n^2}{R_o^2}b \quad . \tag{B-27}$$

If equation (B-27) is considered as a continuous function of m and n, it can be shown that the only possibility of having many waves formed in the axial and circumferential directions occurs when the shear modulus and modulus of elasticity of the core are small. Since the range of core properties given by a formal minimization of (B-27) is somewhat less than those encountered in standard honeycomb design, the minimum results for two loading cases are obtained with $n = 0$ and arbitrary integer values of m, and with $m = 0$ and n continuously varying. The former case corresponds to a symmetric buckling of the cylinder under high compressive end load, and the latter represents the ring solution for lateral pressure distributions.

The results for high compressive end load are approximately expressed as*

$$\frac{L}{m} = \frac{1.65}{(1-\nu_f^2)^{1/3}}\left(\frac{t-t_c}{2}\right)\left(\frac{E_f^2}{E_c G_{Z\xi_c}}\right)^{1/6} \quad , \tag{B-28}$$

*Neglecting the extensional energy stored in the facing sheet.

$$b = \frac{0.91}{(1-\nu_f^2)^{1/3}} \left(\frac{t-t_c}{2}\right)\left(\frac{E_f E_c}{G_{Z\xi_c}^2}\right)^{1/3} , \tag{B-29}$$

and

$$\sigma_{\xi_o} = \frac{0.91}{(1-\nu_f^2)^{1/3}} (E_f E_c G_{Z\xi_c})^{1/3} . \tag{B-30}$$

The values for the ring solution are similarly given by

$$\frac{R_o}{n} = \frac{1.65}{(1-\nu_f^2)^{1/3}} \left(\frac{t-t_c}{2}\right)\left(\frac{E_f^2}{E_c G_{Z\theta_c}}\right)^{1/6} , \tag{B-31}$$

$$b = \frac{0.91}{(1-\nu_f^2)^{1/3}} \left(\frac{t-t_c}{2}\right)\left(\frac{E_f E_c}{G_{Z\theta_c}^2}\right)^{1/3} , \tag{B-32}$$

and,

$$\sigma_{\theta_o} = \frac{0.91}{(1-\nu_f^2)^{1/3}} (E_f E_c G_{Z\theta_c})^{1/3} . \tag{B-33}$$

The application of these formulas is correct only if the marginal depth b is equal to or smaller than one-half the core depth,

$$b \leq t_c/2 , \tag{B-34}$$

or

$$\frac{b}{\left(\frac{t-t_c}{a}\right)} = \frac{0.91}{(1-\nu_f^2)^{1/3}} \left(\frac{E_f E_c}{G_{Z\xi_c}^2}\right)^{1/3} = \frac{0.91}{(1-\nu_f^2)^{1/3}} \left(\frac{E_f E_c}{G_{Z\theta_c}^2}\right)^{1/3} \leq t_c/2 \tag{B-35}$$

Further, it is commented that the relationships developed above are similar to those given by Hoff[7] for sandwich-type panels subjected to axial compressive forces. Obviously, these approximate equations lead to a lower bound solution* for the sandwich cylindrical shell under either axial compressive forces or a lateral pressure distribution. For the rotationally symmetric loading case, it is suggested that the total combined stress should not exceed either of the values as obtained from equations (B-30) and (B-33); that is,

$$\left(\sigma_{\xi_o}^2 - \sigma_{\xi_o}\,\sigma_{\theta_o} + \sigma_{\theta_o}^2\right)^{1/2} \leq \frac{0.91}{(1-\nu_f^2)^{1/3}}\left(E_f\,E_c\,G_{Z\xi_c}\right)^{1/3} \leq \frac{0.91}{(1-\nu_f^2)^{1/3}}\left(E_f\,E_c\,G_{Z\theta_c}\right)^{1/3}$$

The suggestion for the above equation comes from the following consideration. When the ratios N_{ξ_o}/N_{θ_o} and $G_{Z\xi_c}/G_{Z\theta_c}$ are equated to unity in equation (B-27), the resulting expression for the wrinkling stress becomes, after neglecting the extensional energy stored in the facing sheet,

$$N_{\theta_o} = D_f\left(\frac{m^2\pi^2}{L^2} + \frac{n^2}{R_o^2}\right) + \frac{E_c}{b\left(\frac{m^2\pi^2}{L^2} + \frac{n^2}{R_o^2}\right)} + \frac{G_{Z\theta_c}}{3}\,b\,. \tag{B-37}$$

The critical stress in this equation depends upon the parameters, b, and $\left(\frac{m^2\pi^2}{L^2} + \frac{n^2}{R_o^2}\right)$. The actual values of these parameters are those which made the resultant force a minimum.

Consequently,

$$\frac{\partial N_{\theta_o}}{\partial b} = 0$$

$$\frac{\partial N_{\theta_o}}{\partial\left(\frac{m^2\pi^2}{L^2} + \frac{n^2}{R_o^2}\right)} = 0\,. \tag{B-38}$$

*Provided the initial shell imperfections are negligible in the case of high compressive end load.

Solution of the two resulting simultaneous equations gives

$$\frac{1}{\left(\frac{m^2\pi^2}{L^2}+\frac{n^2}{R_o^2}\right)^{1/2}} = \frac{0.525}{(1-\nu_f^2)^{1/3}}\left(\frac{t-t_c}{2}\right)\left(\frac{E_f^2}{E_c G_{Z\theta_c}}\right)^{1/6} ,$$

$$b = \frac{0.91}{(1-\nu_f^2)^{1/3}}\left(\frac{t-t_c}{2}\right)\left(\frac{E_f E_c}{G_{Z\theta_c}^2}\right)^{1/3} , \qquad \text{(B-39)}$$

and,

$$\sigma_{\theta_o} = \frac{0.91}{(1-\nu_f^2)^{1/3}} (E_f E_c G_{Z\theta_c})^{1/3} . \qquad \text{(B-40)}$$

The above expression is identical to the results suggested in (B-43), and shows that the number of waves into which the circumference subdivides during buckling is indefinite as long as, $\frac{m^2\pi^2}{L^2}$ and $\frac{n^2}{R_o^2}$ are large numbers. This accounts for the fact that the extensional energy stored in the cover sheets can be neglected prior to formally minimizing (B-37). When the quantity $\frac{m^2\pi^2}{L^2}+\frac{n^2}{R_o^2}$ is small (the magnitude of which is determined from (B-39)), the extensional energy stored by the cover sheets cannot be neglected, and the minimum results are obtained by fixing either m or n in equation (B-27) and allowing the remaining function to vary continuously.

APPENDIX C

DERIVATION OF EXPRESSIONS FOR MIDDLE-SURFACE STRAINS AND DISPLACEMENTS

A smooth surface is defined parametrically in a cartesian system by,

$$X = X(a_1, a_2) \quad Y = Y(a_1, a_2) \quad Z_1 = Z_1(a_1, a_2) , \tag{C-1}$$

where X, Y, and Z_1 are continuous, single-valued functions of the two surface parameters a_1 and a_2 (Fig. C-1). The three scalar equations (C-1) correspond to a single vector equation,

$$\bar{r} = \bar{i}X + \bar{j}Y + \bar{k}Z_1 , \tag{C-2}$$

where $\bar{i}, \bar{j}$, and $\bar{k}$ are the unit vectors along the X, Y, and Z_1 axes.

The quadratic differential form for the arc length between two points on the surface is given by the scalar product,

$$dS^2 = d\bar{r} \cdot d\bar{r} = E(da_1)^2 + 2F(da_1)(da_2) + G(da_2)^2 , \tag{C-3}$$

where,

$$E = \bar{r}_{,a_1} \cdot \bar{r}_{,a_1} = (X_{,a_1})^2 + (Y_{,a_1})^2 + (Z_{1,a_1})^2$$

$$F = \bar{r}_{,a_1} \cdot \bar{r}_{,a_2} = (X_{,a_1})(X_{,a_2}) + (Y_{,a_1})(Y_{,a_2}) + (Z_{1,a_1})(Z_{1,a_2})$$

$$G = \bar{r}_{,a_2} \cdot \bar{r}_{,a_2} = (X_{,a_2})^2 + (Y_{,a_2})^2 + (Z_{1,a_2})^2 . \tag{C-4}$$

The quantities E, F, and G are the scalar product of the vectors $\bar{r}_{,a_1}$ and $\bar{r}_{,a_2}$ and are called the first "fundamental magnitudes" for the surface.

If the surface parameters form an orthogonal curvilinear coordinate system on the surface

$$F = 0 , \tag{C-5}$$

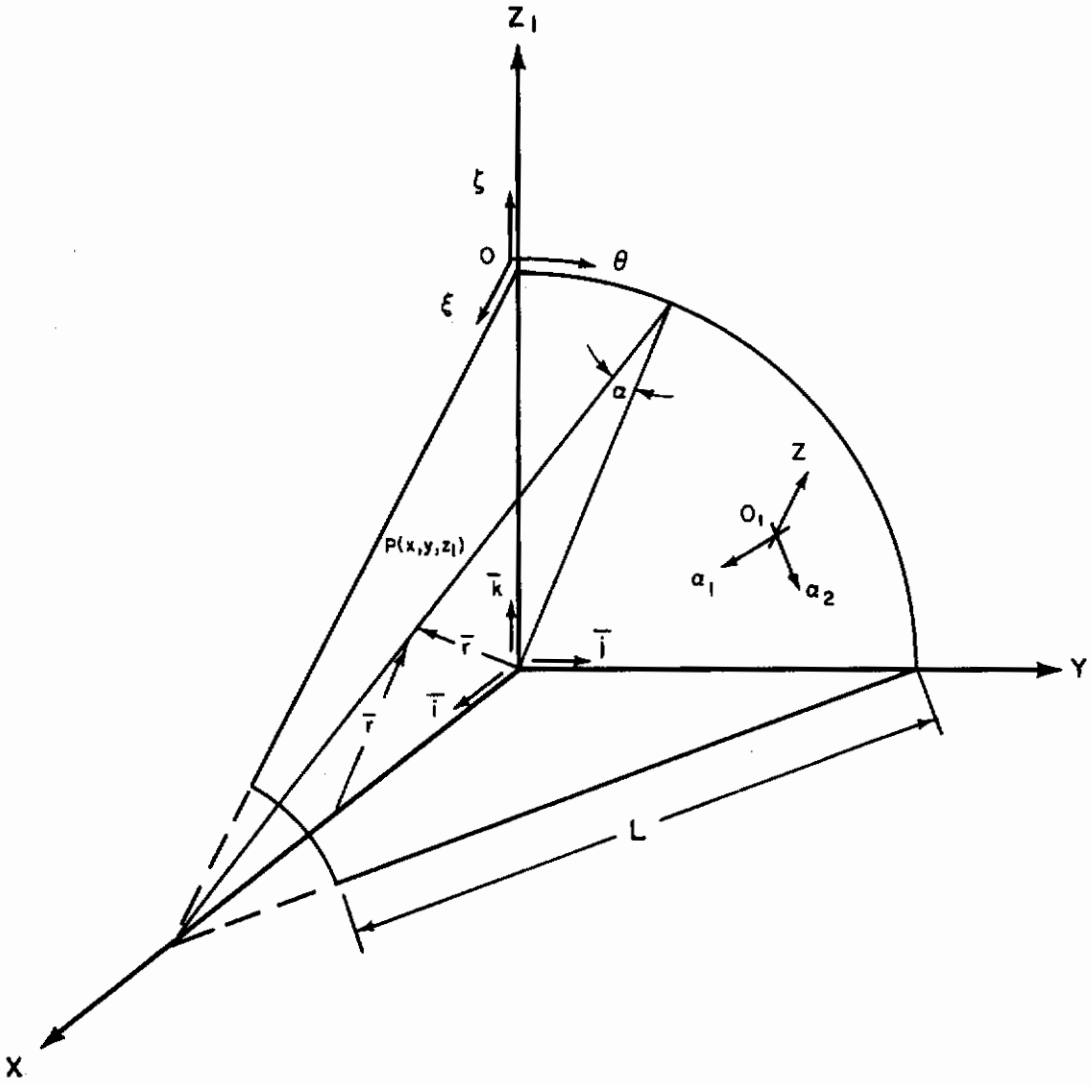

Figure C-1 REFERENCE COORDINATES FOR A SMOOTH, CONTINUOUS SURFACE

and equation (C-3) becomes

$$dS^2 = A_1^2 \, da_1^2 + A_2^2 \, da_2^2 \quad , \tag{C-6}$$

where

$$A_1 = \sqrt{E} \quad \text{and} \quad A_2 = \sqrt{G} \quad . \tag{C-7}$$

The unit vector in the direction of the a_1 coordinate line is given by

$$\bar{e}_1 = \bar{r}_{,a_1} \Big/ \left| \bar{r}_{,a_1} \right| = \bar{r}_{,a_1} \Big/ A_1 \quad . \tag{C-8}$$

Similarly the unit vector along the a_2 coordinate line is

$$\bar{e}_2 = \bar{r}_{,a_2} \Big/ \left| \bar{r}_{,a_2} \right| = \bar{r}_{,a_2} \Big/ A_2 \quad . \tag{C-9}$$

The unit normal to the surface in the z direction is perpendicular to $\bar{e}_1$, $\bar{e}_2$ and is defined by the vector product relation

$$\bar{e}_Z = (\bar{r}_{,a_1} \times \bar{r}_{,a_2}) \Big/ \left| \bar{r}_{,a_1} \times \bar{r}_{,a_2} \right| = (\bar{r}_{,a_1} \times \bar{r}_{,a_2}) \Big/ A_1 A_2 \quad . \tag{C-10}$$

Since the vector $\bar{r}_{,a_1}$ is tangent to the parametric curve $a_2 =$ constant at the point 0_1, it is perpendicular to the normal $\bar{e}_Z$. Hence,

$$\bar{e}_Z \cdot \bar{r}_{,a_1} = 0 \quad . \tag{C-11}$$

Similarly,

$$\bar{e}_Z \cdot \bar{r}_{,a_2} = 0 \quad . \tag{C-12}$$

If equations (C-11) and (C-12) are differentiated with respect to a_1 and a_2 respectively, the following relations are obtained,

$$\begin{aligned} \bar{e}_{Z,a_1} \cdot \bar{r}_{,a_1} &= -\bar{e}_Z \cdot \bar{r}_{,a_1 a_1} = -e \\ \bar{e}_{Z,a_1} \cdot \bar{r}_{,a_2} &= -\bar{e}_Z \cdot \bar{r}_{,a_1 a_2} = -f \\ \bar{e}_{Z,a_2} \cdot \bar{r}_{,a_2} &= -\bar{e}_Z \cdot \bar{r}_{,a_2 a_2} = -g \quad . \end{aligned} \tag{C-13}$$

The terms e, f, and g represent the projection of the vectors $\bar{r}_{,a_1 a_1}$, $\bar{r}_{,a_1 a_2}$ and $\bar{r}_{,a_2 a_2}$

in the direction of the normal to the surface and are referred to as the "fundamental magnitudes of second order."

In order to determine the principal curvatures of a surface, let $\bar{r}$ be a position vector to the surface at point P and R a principal radius of curvature in the direction of the unit normal $\bar{e}_Z$ (Fig. C-2). The distance from the reference point 0 to the center of curvature is given by

$$\bar{\rho} = \bar{r} - R\,\bar{e}_Z \quad . \tag{C-14}$$

If Q is a point adjacent to P along a line of curvature of the surface (Fig. C-3) then

$$d\bar{\rho} = d\bar{r} - d(R\bar{e}_Z) = (d\bar{r} - R\,d\bar{e}_Z) - \bar{e}_Z\,dR \quad . \tag{C-15}$$

The necessary condition for dr to lie on a line of curvature is that $d\bar{\rho}$ have the same line of action as the unit normal $\bar{e}_Z$. Therefore, from equation (C-15),

$$d\bar{r} - R\,d\bar{e}_Z = 0 \quad ,$$

or

$$\kappa\,dr - d\bar{e}_Z = 0 \quad , \tag{C-16}$$

where κ is the reciprocal of a principal radius of curvature and is defined as a principal curvature of the surface.

Substituting the relations

$$d\bar{r} = \bar{r}_{,a_1}\,da_1 + \bar{r}_{,a_2}\,da_2$$

and

$$d\bar{e}_Z = \bar{e}_{Z,a_1}\,da_1 + \bar{e}_{Z,a_2}\,da_2$$

into equation (C-16) and rearranging terms, gives

$$(\kappa\bar{r}_{,a_1} - \bar{e}_{Z,a_1})\,da_1 + (\kappa\bar{r}_{,a_2} - e_{Z,a_2})\,da_2 = 0 \quad . \tag{C-17}$$

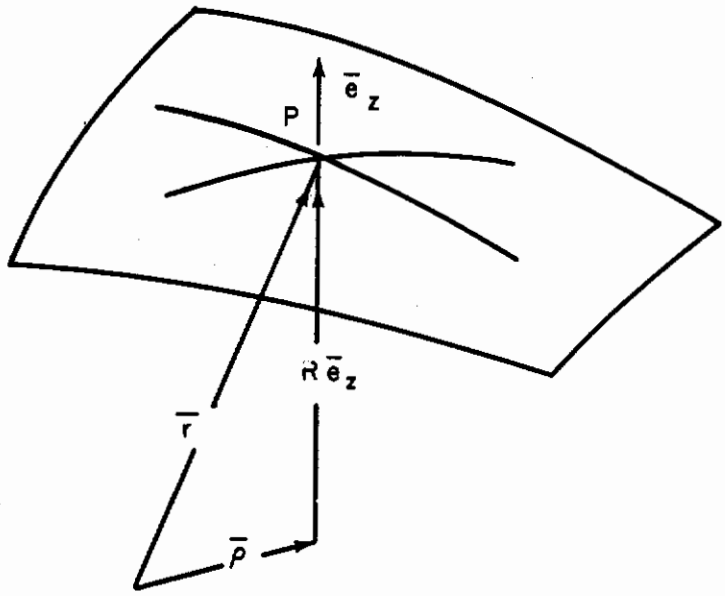

Figure C-2 PRINCIPAL RADIUS OF CURVATURE IN THE DIRECTION OF THE UNIT NORMAL

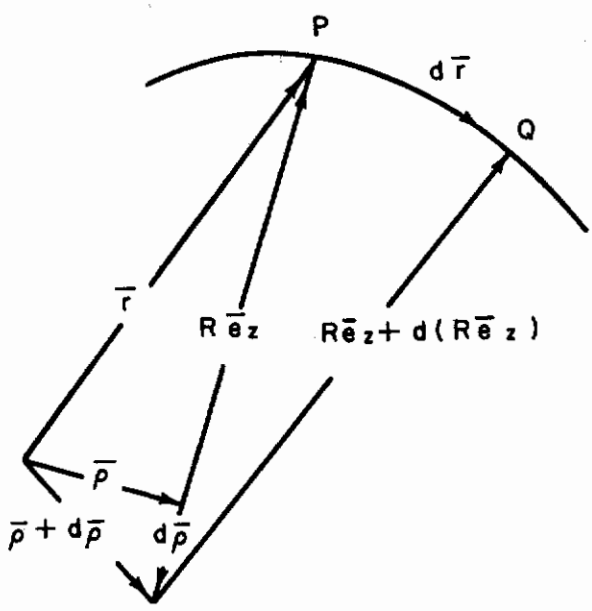

Figure C-3 LINE OF CURVATURE FOR THE SHELL SURFACE

If the scalar products of this equation are performed with respect to $\bar{r}_{,\alpha_1}$ and $\bar{r}_{,\alpha 2}$ the following equations are obtained:

$$(\kappa E + e)\, d\alpha_1 + (\kappa F + f)\, d\alpha_2 = 0$$
$$(\kappa F + f)\, d\alpha_1 + (\kappa G + g)\, d\alpha_2 = 0 \ . \qquad \text{(C-18)}$$

Eliminating $d\alpha_1/d\alpha_2$ and collecting terms,

$$(EG - F^2)\kappa^2 + (Eg - 2Ff + Ge)\kappa + (eg - f^2) = 0 \ . \qquad \text{(C-19)}$$

For an orthogonal curvilinear coordinate system,

$$F = f = 0 \ , \qquad \text{(C-20)}$$

and equation (C-19) becomes

$$(EG/eg)\kappa^2 + (E/e + G/g)\kappa + 1 = 0 \ . \qquad \text{(C-21)}$$

The two roots of this equation represent the principal curvature of the surface and are given by

$$\kappa_1 = 1/R_1 = -(e/E)$$

and

$$\kappa_2 = 1/R_2 = -(g/G) \ . \qquad \text{(C-22)}$$

The results to this point define the form of the middle surface and apply, generally, to all shell geometries. In specializing the results to conical shells, the following substitutions for the coordinates of a point on the median surface are made (Fig. C-1):

$$X = \xi \sin\alpha \ , \ Y = r \sin\theta \ , \ Z_1 = r\cos\theta \ , \qquad \text{(C-23)}$$

where

$$r = R_o [1 - \beta(\xi / L)]$$

$$\beta = (L/R_o) \cos \alpha$$

Substituting equation (C-23) into equations (C-2) through (C-22),

$$A_1 = \sqrt{E} = 1$$

$$A_2 = \sqrt{G} = r$$

$$\kappa_1 = 1/R_1 = 0$$

$$\kappa_2 = 1/R_2 = \sin \alpha / r \quad . \tag{C-24}$$

The expressions for the middle-surface deformations can be readily obtained in terms of these scalar functions from the equations given by Novozhilov[8]. In computing the relationships in this manner, all quadratic terms in the displacements (and their derivatives) which are multiplied by z are neglected. Also terms multiplied by z^2 are always negligible for small elongations and shears and are disregarded in the derivation. The resulting expressions for the middle-surface strains and curvatures (χ's) are

$$\epsilon_\xi = u_{,\xi} + 1/2 \left(u_{,\xi}^2 + v_{,\xi}^2 + w_{,\xi}^2 \right) ,$$

$$\epsilon_\theta = \frac{1}{r} (v_{,\theta} - u \cos \alpha + w \sin \alpha) + 1/2 \left[(u_{,\theta/r} + v \cos \alpha / r)^2 \right.$$

$$\left. + (v_{,\theta/r} - u \cos \alpha / r + w \sin \alpha / r)^2 + (w_{,\theta/r} - v \sin \alpha / r)^2 \right] ,$$

$$\epsilon_{\xi\theta} = v_{,\xi} + u_{,\theta/r} + v \cos \alpha / r + u_{,\xi} (u_{,\theta/r} + v \cos \alpha / r)$$

$$+ v_{,\xi} (v_{,\theta/r} - u \cos \alpha / r + w \sin \alpha / r) + w_{,\xi} (w_{,\theta/r} - v \sin \alpha / r) ,$$

$$\chi_\xi = - w_{,\xi\xi} ,$$

$$\chi_\theta = \frac{1}{r} (- w_{,\theta\theta/r} + v_{,\theta} \sin \alpha / r + w_{,\xi} \cos \alpha) ,$$

and

$$\chi_{\xi\theta} = \frac{1}{r} (- w_{,\xi\theta} - w_{,\theta} \cos \alpha / r + v_{,\xi} \sin \alpha + v \sin \alpha \cos \alpha / r) . \tag{C-25}$$

Many of the terms in these relations may be omitted, however, by considering that: (1) w is the dominant displacement, (2) quadratic terms containing derivatives of w are of a higher order of magnitude than the quadratic terms containing w as a factor, and (3) displacements u and v and their derivatives have a negligible effect on the bending energy of the shell. After omitting these terms, the expressions for middle-surface strains and curvatures reduce to the forms

$$\epsilon_\xi = u_{,\xi} + 1/2\, w_{,\xi}^2$$

$$\epsilon_\theta = \frac{1}{r}(v_{,\theta} - u\cos\alpha + w\sin\alpha) + 1/2\, w_{,\theta}^2/r^2$$

$$\epsilon_{\xi\theta} = v_{,\xi} + u_{,\theta/r} + v\cos\alpha/r + w_{,\xi}\, w_{,\theta/r}$$

$$\chi_\xi = -w_{,\xi\xi}$$

$$\chi_\theta = -\frac{1}{r}(w_{,\theta\theta/r} - w_{,\xi}\cos\alpha)$$

$$\chi_{\xi\theta} = -\frac{1}{r}(w_{,\xi\theta} + w_{,\theta}\cos\alpha/r)\ . \qquad \text{(C-26)}$$

The expressions for a cylindrical shell are obtained by having $\alpha = \pi/2$ in equation (C-26).

APPENDIX D

DEFINITION OF GEOMETRIC PARAMETERS

If a constant factor, multiplying each of the a_{ij} terms, is disregarded, the coefficients in equation (A-12) are defined as

$$a_{11} = B\left[\frac{K^2}{2} + t_1 K\phi_o + t_1 \frac{(1-\nu_f)}{2} \frac{n^2}{\sin^2\alpha}\right] ,$$

$$a_{12} = -\frac{B}{\sin\alpha}\left[\frac{(1+\nu_f)}{2} Kn + \frac{(1-\nu_f)}{2} n\phi_o\right] ,$$

$$a_{13} = -B(\nu_f K + t_2\phi_o)$$

$$a_{22} = B\left[t_3 \frac{n^2}{\sin^2\alpha} + \frac{(1-\nu_f)}{2} K(K/2 + t_3\phi_o)\right] ,$$

$$a_{23} = 2B t_3 \frac{n}{\sin\alpha} ,$$

and

$$a_{33} = -\frac{P}{2}\left(K_1\lambda^2 + K_2 \frac{n^2}{\sin^2\alpha}\right) + Bt_3 + \frac{D}{k^2}\left[\left(\frac{1}{2} + t_1 \cot^2\alpha/K^2\right) K^4 + 2(2t_3 - t_1) \frac{K^2 n^2}{\sin^2\alpha} + t_4 \frac{n^4}{\sin^4\alpha}\right] ,$$

where

$$t_1 = -\frac{\left(1 - \frac{\beta}{2}\right)}{2\beta}\left[\ln(1-\beta) + g_1(\beta)\right] ,$$

$$t_2 = -\frac{m\pi\left(1-\frac{\beta}{2}\right)^2}{\beta^2}\left[g_2(\beta)\right],$$

$$t_3 = -\left[t_1 + \frac{\left(1-\frac{\beta}{2}\right)}{\beta}\ln(1-\beta)\right],$$

$$t_4 = -\frac{m^2\pi^2}{\beta^3}\left[\left(1-\frac{\beta}{2}\right)^3 g_1(\beta)\right],$$

and

$$g_1(\beta) = \cos(2m\pi/\beta)\int_{2m\pi/\beta}^{2m\pi/\beta-2m\pi}\frac{\cos y}{y}\,dy + \sin(2m\pi/\beta)\int_{2m\pi/\beta}^{2m\pi/\beta-2m\pi}\frac{\sin y}{y}\,dy,$$

and

$$g_2(\beta) = \sin(2m\pi/\beta)\int_{2m\pi/\beta}^{2m\pi/\beta-2m\pi}\frac{\sin y}{y}\,dy - \cos(2m\pi/\beta)\int_{2m\pi/\beta}^{2m\pi/\beta-2m\pi}\frac{\sin y}{y}\,dy.$$

APPENDIX X

A STUDY OF CREEP COLLAPSE OF A LONG CIRCULAR CYLINDRICAL SHELL UNDER VARIOUS DISTRIBUTED FORCE SYSTEMS

by Joseph C. Serpico

An analysis is presented for determining the collapse of circular rings and long cylinders subjected to primary and secondary creep conditions at elevated temperatures. The types of loading considered for the present investigation are dead loading and hydrostatic pressure-type forces. The method of solution is based on an application of the variational theorem for creep described in reference X-1 with some additional terms being introduced for the pressure-type loading case. The general results are reduced to a relatively simple form for the theoretical predictions of collapse time and are graphically illustrated for a typical sample material.

I. INTRODUCTION

Recent advances in the technological field have permitted an increase in flight speeds and operational life of re-entry vehicles. Associated with these increases has been the increased effect of the exit and re-entry environments of temperature, aerodynamic pressure, and inertial forces. In order to meet the demands of higher operating stresses and temperature for extended flights, it is essential to evaluate the effects of new operating conditions such as creep, and to develop criteria for the time to failure mechanism associated with creep collapse.

Analytically, a rigorous study of the creep problem for shell structures is more complicated than its associated elastic counterpart as a result of the non-linearity in the creep stress-strain relationships. A consequence of this non-linearity is that the stress distributions across the thickness of the shell are not linear and that the stresses are varying with respect to both time and space. The study is complicated further by the great diversity of analytical expressions that have been advanced to describe the creep phenomenon. For this purpose, the mathematical analyses of shell structures have often been restricted to simplified models, that is, by assuming that the shell wall construction is of the ideal sandwich type and that the loading and temperature environments are such that the shell material exhibits only secondary creep deformations. The use of the elementary sandwich model eliminates the necessity of integrating the stress effects across the depth of the shell structure; whereas the assumption, that primary creep, as well as elastic deformations are absent in the shell material, permits the usage of an idealized form of the creep stress-strain relationships.

This paper is concerned with the creep collapse of circular rings and long cylinders subjected to dead loading and uniform pressure distributions. The

major purpose of the present investigation is to assess analytically the time to failure mechanism associated with creep collapse for a shell material which exhibits both primary and secondary creep, as well as elastic deformations; and, further, to demonstrate as in the static buckling of shell structures*, the sensitivity of various creep problems to the character of the loading system. The mathematical formulation of the problem for the dead-loading case is based on an application of the variational theorem for creep as described by Sanders, McComb, and Schlechte (Ref. X-1). The formulation for applications of pressure-type forces is similarly based on the previously stated variational theorem; however, additional terms are adjoined to appropriately describe the position change of the surface force vector.

In the problem to be considered, the cross-section of the shell is assumed to have some slight initial deviation from circularity; that is, quasi-elliptically cylindrical. This initial deviation is increased with time by the elastic and creep deformations until the normal displacement becomes indefinitely large and the cylinder collapses. During the course of the present study, as in previous investigations, some simplifying assumptions are introduced in order to obtain an explicit expression for the critical collapse time. Although these assumptions reduce the problems to a simplified analytical model, the final results represent an overall matching of the equations of equilibrium and stress-strain relations for the approximate model and should serve as an indication of the creep characteristics for the proposed shell structure.

II. THEORETICAL APPLICATION OF THE VARIATIONAL THEOREM TO RING PROBLEMS

The general variational theorem (X-1) for creep problems is expressed as

$$\delta \bar{I} = 0 \,, \tag{X-1}$$

in which,

$$\bar{I} = \int_V \left[\dot{\epsilon}_{ij}\, \dot{\sigma}_{ij} + \frac{1}{2}\, \dot{u}_{k,i}\, \dot{u}_{k,j}\, \sigma_{ij} - \frac{1}{2} (\dot{\epsilon}'_{ij} + 2\dot{\epsilon}''_{ij})\, \dot{\sigma}_{ij} \right] dV$$

$$\int_{S_s} \dot{\bar{T}}_i\, \dot{u}_i\, dS - \int_{S_d} (\dot{u}_i - \dot{\bar{u}}_i)\, \dot{T}_i\, dS \,. \tag{X-2}$$

*Load-type sensitivity has been previously examined for several elastic stability problems by Pearson (Ref. X-2), Boresi (Ref. X-3), and has been more recently discussed by Bodner (Ref. X-4). The various distributed force systems which were considered, are: 1) dead-loading, 2) hydrostatic pressure, and 3) centrally directed pressure loadings.

The variational theorem given above provides a powerful means of developing an appropriate theory for rings or long cylinders subjected to elastic and creep deformations. The analysis now is extended for the two types of loading of greatest practical importance; namely, dead loading, and hydrostatic pressure loading. In the dead loading case, the surface traction, $\overline{T}_i$, is considered to be produced by fixed loads which do not vary with respect to total magnitude or direction during a virtual displacement. For the hydrostatic pressure-type forces, the surface loading varies in such a manner as to remain always perpendicular to the shell surface while maintaining the same magnitude per unit area.

1. Analytical Condition for Dead Loading

a. Strain-Displacement Relations

As mentioned previously, some simplifying assumptions are introduced concerning the dependence of the shell displacements on the z-coordinate (measured normal to the middle surface, figure X-1). In particular, as in the elastic case, the Bernoulli-Euler hypothesis is retained; that is, the transverse shear stresses are negligible throughout the thickness of the shell in comparison to the inplane stresses. If the normal displacement, w , is assumed to be approximately independent of z , the Bernoulli-Euler hypothesis is expressed mathematically for the associated ring problem as,

$$u \approx U - \frac{z}{R}\left(\frac{\partial W}{\partial \theta} - U\right),$$

$$w \approx W , \qquad \text{(X-3)}$$

in which, U and W represent the middle-surface displacements.

The resulting expression for the circumferential strain can be readily obtained from the equations developed by Novozhilov (Ref. X-5). In computing the relationships in this manner, all quadratic terms in the displacements (and their derivatives) which are multiplied by z are neglected. Also, terms multiplied by z^2 are always negligible for small elongations and shears and are disregarded in the derivation. The resulting expression for the total circumferential strain is

$$\epsilon = \frac{1}{R}\frac{\partial U}{\partial \theta} + \frac{W}{R} + \frac{1}{2R^2}\left[\left(\frac{\partial U}{\partial \theta} + W\right)^2 + \left(\frac{\partial W}{\partial \theta} - U\right)^2\right] - \frac{z}{R^2}\left(\frac{\partial^2 W}{\partial \theta^2} - \frac{\partial U}{\partial \theta}\right). \qquad \text{(X-4)}$$

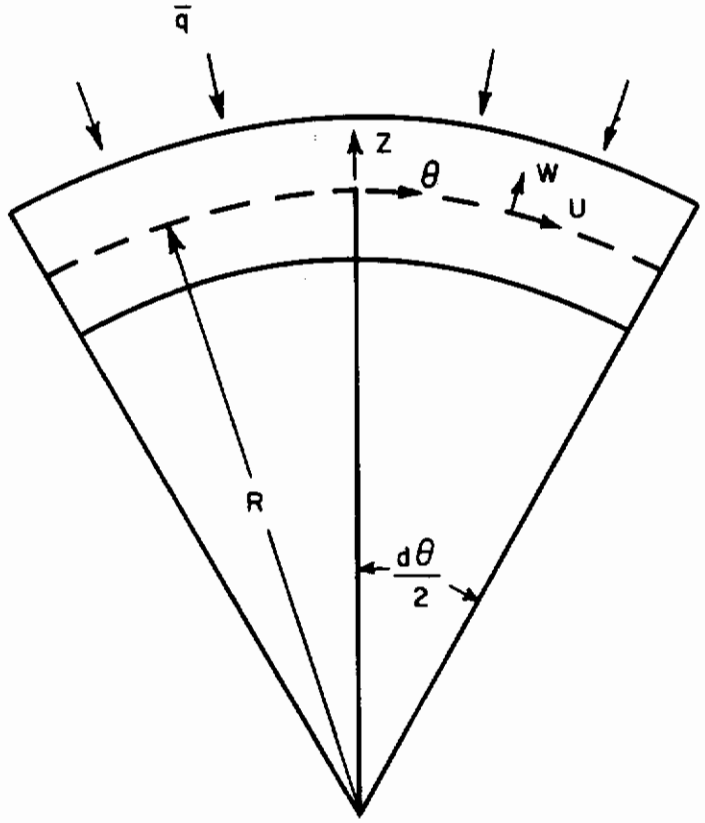

Figure X-1 REFERENCE COORDINATES FOR A DIFFERENTIAL SHELL ELEMENT

b. Stress-Strain Relations

A great majority of the theoretical analyses for creep problems are developed on the basis of stress-strain relations which are empirically formulated from uniaxial creep test specimens. An appropriate representation for the creep analysis of structures which exhibit a uniaxial state of stress has been discussed by Hoff (Ref. 6), and is mathematically expressed as

$$\epsilon'' = \lambda t^{p} \sigma^{m} \quad , \tag{X-5}$$

in which, ϵ'' is the creep strain, σ is the current stress, t represents time, and λ, p, and m are material constants obtained from creep tests at constant temperature.

For the creep analysis of shell structures subject to two or three dimensional states of stress, it has been common practice to base the relation on a general mathematical formulation of the uniaxial law since an empirical derivation from creep test data for the combined stress problem is extremely difficult. A simple example of the creep law for a triaxial state of stress as discussed by Hoff (X-6) is given in tensor notation as

$$\epsilon''_{ij} = C_o t^{p} J_2^{\eta_o} S_{ij} \quad , \tag{X-6}$$

where, ϵ''_{ij} is the creep strain tensor, $J_2 = \frac{1}{2} S_{ij} S_{ij}$, is the second invariant of the stress deviation tensor, defined by

$$S_{ij} = \sigma_{ij} - \frac{1}{3} \sigma_{kk} \delta_{ij} \quad . \tag{X-7}$$

From the requirement that the creep relations for the triaxial state of stress reduce to the uniaxial stress state, the following relationships exist between the material constants:

$$\eta_o = \frac{m-1}{2} \quad ,$$

and

$$C_o = \left(\frac{3^{\frac{m+1}{2}}}{2} \right) \lambda \tag{X-8}$$

With the preceding background, a simplified treatment of the problem for creep collapse of rings or long cylinders is investigated in the subsequent sections. The material of the shell is considered to be governed by equation (X-6); or for the present application to the associated one-dimensional ring problem, by equation (X-5). In addition, if elastic as well as creep deformations are included, equation (X-5) is rewritten as

$$\epsilon = \frac{\sigma}{E} + \lambda t^{p} \sigma^{m} , \tag{X-9}$$

with the constraining conditions, m odd and greater than unity;

$$m \geq 1 ,$$

and

$$0 < p \leq 1 .$$

In applying equation (X-9), it is implied that all inelastic deformations are time dependent and that the elastic deformations are linear and instantaneous.

c. Analytical Formulation

In the present case of dead loading the special form for $\bar{I}$ is obtained by substituting equations (X-4), (X-9) into (X-2). The resulting expression is given by

$$\bar{I} = \int_{V} \left\{ \frac{\dot{\sigma}}{R} \left[\frac{\partial \dot{U}}{\partial \theta} + \dot{W} + \frac{1}{R} \left(\frac{\partial U}{\partial \theta} + W \right) \left(\frac{\partial \dot{U}}{\partial \theta} + \dot{W} \right) + \frac{1}{R} \left(\frac{\partial W}{\partial \theta} - U \right) \left(\frac{\partial \dot{W}}{\partial \theta} - \dot{U} \right) \right.\right.$$

$$\left. - \frac{z}{R} \left(\frac{\partial^2 \dot{W}}{\partial \theta^2} - \frac{\partial \dot{U}}{\partial \theta} \right) \right] + \frac{\sigma}{2R^2} \left[\left(\frac{\partial \dot{U}}{\partial \theta} + \dot{W} \right)^2 + \left(\frac{\partial \dot{W}}{\partial \theta} - \dot{U} \right)^2 \right]$$

$$\left. - \frac{\dot{\sigma}^2}{2E} - \lambda p t^{p-1} \dot{\sigma} \sigma^{m} \right\} dV . \tag{X-10}$$

The boundary integral on the part S_s of the bounding surface is identically equal to zero since the prescribed surface traction for dead loading is independent of time and remains constant in both magnitude and direction during a virtual displacement.

When certain simplifying assumptions are made concerning the dependence of the stresses and displacements on the shell coordinates, the integrations with respect to these coordinates may be performed in equation (X-10). For simplicity, the variation of the stress, σ, in the z-direction is assumed to be linear and of the form

$$\sigma = \sigma_o^* + \frac{z}{h}\,\sigma_1^* \qquad \text{(X-11)}$$

where, the current membrane stress, $\sigma_o^* = -\frac{\bar{q}R}{h}$, is assumed to remain constant and independent of time.

Assuming inextensionable bending i.e.

$$\frac{\partial U}{\partial \theta} + W = 0 . \qquad \text{(X-12)}$$

The variation of the stresses and displacements in the θ-direction are taken as follows:

$$\sigma_1^* = \frac{\bar{q}R}{h}\,\sigma_1(t)\cos n\theta ,$$

$$W = h\,W_o(t)\cos n\theta ,$$

$$U = h\,U_o(t)\sin n\theta = -\frac{h\,W_o(t)}{n}\sin n\theta , \qquad \text{(X-13)}$$

in which, the dimensionless quantities $\sigma_1(t)$, $W_o(t)$, and $U_o(t)$ are functions of time only.

Using equations (X-11) and (X-13) and performing the integrations in $\bar{I}$, equation (X-10) becomes

$$\bar{I} = \frac{\pi \bar{q} R^3}{E h} \left\{ \frac{\bar{q}_{cr}}{\bar{q}} \left[\frac{(n^2-1)}{n^2} \dot{\sigma}_1(t) \dot{W}_o(t) - 6 \frac{(n^2-1)^2}{n^4} \dot{W}_o^2(t) \right] \right.$$

$$\left. - \frac{\dot{\sigma}_1^2(t)}{24} - \lambda p t^{p-1} E \left(\frac{\bar{q} R}{h} \right)^{m-1} \dot{\sigma}_1(t) \sum_{k=1}^{\frac{m+1}{2}} \frac{k m! \left[\frac{\sigma_1(t)}{4} \right]^{2k-1}}{(2k+1)[m-(2k-1)]!(k!)^2} \right\}, \qquad \text{(X-14)}$$

where, m is summed on odd integer values so as to be equally applicable in compressive as well as tensile stress states.

The condition that the variation of $\bar{I}$ vanish identically is obtained by setting the derivatives of (X-14) with respect to each of the dotted quantities equal to zero. This operation yields two simul-taneous differential equations for the coefficients of the stresses and displacement; namely,

$$\dot{\sigma}_1(t) - 12 \frac{(n^2-1)}{n^2} \dot{W}_o(t) = 0 ,$$

$$\frac{\bar{q}_{cr}}{\bar{q}} \frac{(n^2-1)}{n^2} \dot{W}_o(t) - \frac{\dot{\sigma}_1(t)}{12} - \lambda p t^{p-1} E \left(\frac{\bar{q} R}{h} \right)^{m-1} \sum_{k=1}^{\frac{m+1}{2}} \frac{k m! \left[\frac{\sigma_1(t)}{4} \right]^{2k-1}}{(2k+1)[m-(2k-1)]!(k!)^2} = 0. \qquad \text{(X-15)}$$

For convenience in further calculations, a single differential equation in terms of the dimensionless parameter, $W_o(t)$, is obtained by combining equations (X-15).

With n = 2, the result is

$$\left(\frac{\bar{q}_{cr}}{\bar{q}} - 1\right) \dot{W}_o(t) - \frac{4}{3} \lambda p t^{p-1} E \left(\frac{\bar{q} R}{h}\right)^{m-1} \sum_{k=1}^{\frac{m+1}{2}} \frac{k m! \left[\frac{9}{4} W_o(t)\right]^{2k-1}}{(2k+1)[m-(2k-1)]!(k!)^2} = 0 . \quad \text{(X-16)}$$

Integrating equation (X-16) for $m = 3$ and employing the initial condition that $W_o(t) = W_o(0)$ at $t = 0$, results in

$$t^p = \frac{\left(\frac{\bar{q}_{cr}}{\bar{q}} - 1\right)}{6\lambda E \left(\frac{\bar{q} R}{h}\right)^2} \log \left[\frac{W_o^2(t)}{1 + \frac{243}{80} W_o^2(t)}\right] \left[\frac{1 + \frac{243}{80} W_o^2(0)}{W_o^2(0)}\right] . \quad \text{(X-17)}$$

The condition for the critical collapse time is found by taking the limit as $W_o(t) \to \infty$, thus

$$t_{cr} = \left\{ \frac{\left(\frac{\bar{q}_{cr}}{\bar{q}} - 1\right)}{6\lambda E \left(\frac{\bar{q} R}{h}\right)^2} \log \left[1 + \frac{80}{243 W_o^2(0)}\right] \right\}^{1/p} . \quad \text{(X-18)}$$

It should be noted from an inspection of equation (X-18) that particular values for the critical collapse time are dependent upon the initial conditions assigned.

In the present investigation, the cross-section of the shell prior to loading is assumed to be quasi-elliptically cylindrical; that is, the initial displacement (Fig. X-2) is taken as,

$$w' = h f_o \cos 2\theta . \quad \text{(X-19)}$$

Under the application of the dead load, there is an additional distortion which amplifies the initial out-of-roundness of the shell. Denoting the corresponding radial displacement by $\bar{w}$, the differential equation for the equilibrium state immediately after the load is applied is given by, (see reference X-7)

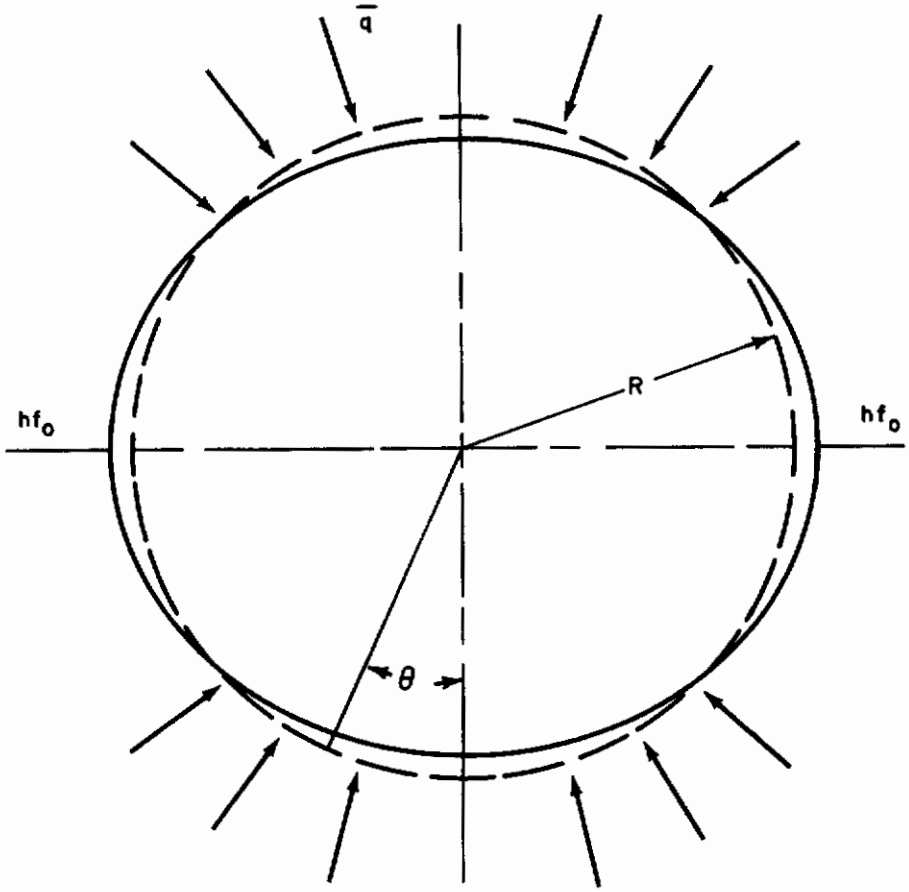

Figure X-2 GRAPHICAL ILLUSTRATION OF INITIAL SHAPE FACTOR AMPLITUDE

$$\frac{d^2\bar{w}}{d\theta^2} + \bar{w} = -\frac{MR^2}{EI} \quad , \tag{X-20}$$

where, M is the static bending moment at any cross-section and is expressed as

$$M = \bar{q}R\,(\bar{w} + hf_o \cos 2\theta) \quad . \tag{X-21}$$

The solution of equation (X-20) satisfying the conditions of continuity at points; $\theta = 1/4\pi, 3/4\pi, 5/4\pi, 7/4\pi$; is

$$\bar{w} = \frac{\bar{q}}{\bar{q}_{cr} - \bar{q}}\, hf_o \cos 2\theta \quad . \tag{X-22}$$

Furthermore, the relationship for the total shell displacement becomes

$$(w' + w) = \frac{1}{1 - \dfrac{\bar{q}}{\bar{q}_{cr}}}\, hf_o \cos 2\theta \quad , \tag{X-23}$$

which, from equation (X-12), is compatible with the original assumption for the radial displacement and is consistent with the following assignment for the initial conditions for the creep problem; namely

$$W_o(0) = \frac{f_o}{1 - \dfrac{\bar{q}}{\bar{q}_{cr}}} \quad . \tag{X-24}$$

Substituting (X-24) into (X-18), the final expression for the critical collapse time as a function of the shell irregularities is

$$t_{cr} = \left\{ \frac{\left(\dfrac{\bar{q}_{cr}}{\bar{q}} - 1\right)}{6\lambda E \left(\dfrac{\bar{q}R}{h}\right)^2} \log \left[1 + \frac{80}{243} \frac{\left(1 - \dfrac{\bar{q}}{\bar{q}_{cr}}\right)^2}{f_o^2} \right] \right\}^{1/p} \tag{X-25}$$

2. Analytical Condition for Hydrostatic Pressure Loading

A topic of considerable interest relates to the precise effects of different types of loading on the creep characteristics of shell structures. In the previous discussion, the effect of forces exerted by fixed constraints, i.e.,

dead loading, were examined by an application of variational techniques to equation (X-2). In applying similar techniques to hydrostatic pressure-type forces, it is recognized, as in the static buckling of the associated ring-problems, that some quadratic terms are essential in the boundary integrals; and, consequently, additional terms must be adjoined to equation (X-2). The physical reasoning of incorporating these terms is necessitated by the need of appropriately describing the position change of the surface force vector, for even though such forces maintain the same magnitude per unit area, their direction varies with time in such a manner as to remain always perpendicular to the shell surface.

The appropriate terms to be adjoined for constant prescribed surface tractions are of the form: (i.e., see Pearson, Ref. X-2)

$$\frac{q}{2} \int_{S_s} (n_i \dot{u}_{k,k} \dot{u}_i - n_k \dot{u}_{k,i} \dot{u}_i) \, dS \, , \tag{X-26}$$

or, considering the associated ring problem, as

$$\frac{q}{2} \int_0^{2\pi} \left(\dot{W}^2 + \dot{W} \frac{\partial \dot{U}}{\partial \theta} - \dot{U} \frac{\partial \dot{W}}{\partial \theta} + \dot{U}^2 \right) d\theta \, . \tag{X-27}$$

Combining equations (X-10) and (X-27), the resulting integral for $\bar{I}$ is given by

$$\bar{I} = \int_V \left\{ \frac{\dot{\sigma}}{R} \left[\frac{\partial \dot{U}}{\partial \theta} + \dot{W} + \frac{1}{R} \left(\frac{\partial U}{\partial \theta} + W \right) \left(\frac{\partial \dot{U}}{\partial \theta} + \dot{W} \right) + \frac{1}{R} \left(\frac{\partial W}{\partial \theta} - U \right) \left(\frac{\partial \dot{W}}{\partial \theta} - \dot{U} \right) \right.\right.$$

$$\left. - \frac{z}{R} \left(\frac{\partial^2 \dot{W}}{\partial \theta^2} - \frac{\partial \dot{U}}{\partial \theta} \right) \right] + \frac{\sigma}{2R^2} \left[\left(\frac{\partial \dot{U}}{\partial \theta} + \dot{W} \right)^2 + \left(\frac{\partial \dot{W}}{\partial \theta} - \dot{U} \right)^2 \right] - \frac{\dot{\sigma}^2}{2E}$$

$$\left. - \lambda p_t^{p-1} \dot{\sigma} \sigma^m \right\} dV + \frac{q}{2} \int_0^{2\pi} \left(\dot{W}^2 + \dot{W} \frac{\partial \dot{U}}{\partial \theta} - \dot{U} \frac{\partial \dot{W}}{\partial \theta} + \dot{U}^2 \right) d\theta \, . \tag{X-28}$$

Using the approximations (X-12) and performing the integrations in $\bar{I}$;

$$\bar{I} = \frac{\pi q^2 R^3}{Eh} \left\{ \frac{q_{cr}}{q} \left[\dot{\sigma}_1(t)\, \dot{W}_o(t) - 6\, \frac{(n^2-1)}{n^2}\, \dot{W}_o^2(t) - \frac{6}{n^2}\, \dot{W}_o^2(t) \right] \right.$$

$$\left. - \frac{\dot{\sigma}_1^2(t)}{24} - \lambda p t^{p-1} E \left(\frac{qR}{h}\right)^{m-1} \dot{\sigma}_1(t) \sum_{k=1}^{\frac{m+1}{2}} \frac{k\, m! \left[\frac{\sigma_1(t)}{4}\right]^{2k-1}}{(2k+1)[m-(2k-1)]!(k!)^2} \right\}. \quad \text{(X-29)}$$

The condition that the variation of $\bar{I}$ vanish identically results in the following set of differential equations:

$$\dot{\sigma}_1(t) - 12\, \frac{(n^2-1)}{n^2}\, \dot{W}_o(t) - \frac{12}{n^2}\, \dot{W}_o(t) = 0 ,$$

$$\frac{q_{cr}}{q}\, \dot{W}_o(t) - \frac{\dot{\sigma}_1(t)}{12} - \lambda p t^{p-1} E \left(\frac{qR}{h}\right)^{m-1} \sum_{k=1}^{\frac{m+1}{2}} \frac{k\, m! \left[\frac{\sigma_1(t)}{4}\right]^{2k-1}}{(2k+1)[m-(2k-1)]!(k!)^2} = 0 . \quad \text{(X-30)}$$

These equations, as in the previous section, are combined for a cubic form of the creep low to yield the critical time for creep collapse; namely;

$$t_{cr} = \left\{ \frac{\left(\frac{q_{cr}}{q} - 1\right)}{6\lambda E \left(\frac{qR}{h}\right)^2} \log \left[1 + \frac{5}{27 W_o^2(0)} \right] \right\}^{1/p} , \quad \text{(X-31)}$$

or, collected in terms of the initial shape factor, , for the shell cross-section, as

$$t_{cr} = \left\{ \frac{\left(\frac{q_{cr}}{q} - 1\right)}{6\lambda E \left(\frac{qR}{h}\right)^2} \log \left[1 + \frac{5}{27} \frac{\left(1 - \frac{q}{q_{cr}}\right)^2}{f_o^2} \right] \right\}^{1/p} . \qquad \text{(X-32)}$$

Here, it is essential to emphasize that the above results, as well as the previous results, for the dead loading case were determined for a cubic form of the creep law; that is, $m = 3$. Analytical results for other odd values of m are simply obtained by integrating equation (X-16) (or, the expression resulting from equations (X-30) for each of the prescribed values. Also, it is remarked that equation (X-32) is identical to the form established by Sanders (Ref. X-1) for the axially loaded column, viz.,

$$t_{cr} = \left\{ \frac{\frac{P_c}{P} - 1}{6\lambda E \left(\frac{P}{bh}\right)^2} \log \left[1 + \frac{5}{27} \frac{\left(1 - \frac{P}{P_c}\right)^2}{\Delta^2} \right] \right\}^{1/p} ,$$

in which, P_c represents the critical compressive stress for the column and Δ, the amplitude of the initial bow of the column divided by the column thickness.

Obviously, this correspondence, at least for a cubic form of the stress-strain relationship and for equal nominal stress states, is equivalent to replacing the shell structure by and axially loaded column whose length is $\frac{1}{2\sqrt{3}}$ times the circumference of the shell.

III. DISCUSSION

Equations (X-18), (X-31) represent the theoretical predictions for the time-to-failure mechanism associated with creep collapse for circular rings and long cylinders subjected to dead loading and pressure-type forces. A graphical illustration for the logarithmic behavior of these equations is shown in figure X-3 as a function of two non-dimensional parameters; one essentially dependent on the initial shape factor amplitude, $W_o(0)$, and the other determined by the combined effect of the critical collapse time, the mechanical properties of the material, and the shell geometry and loading.

Before proceeding with general discussion of figure X-3, it is worthwhile to consider a typical calculation for the mechanical properties of a sample material. In figure X-4, total stress-strain curves derived from constant creep

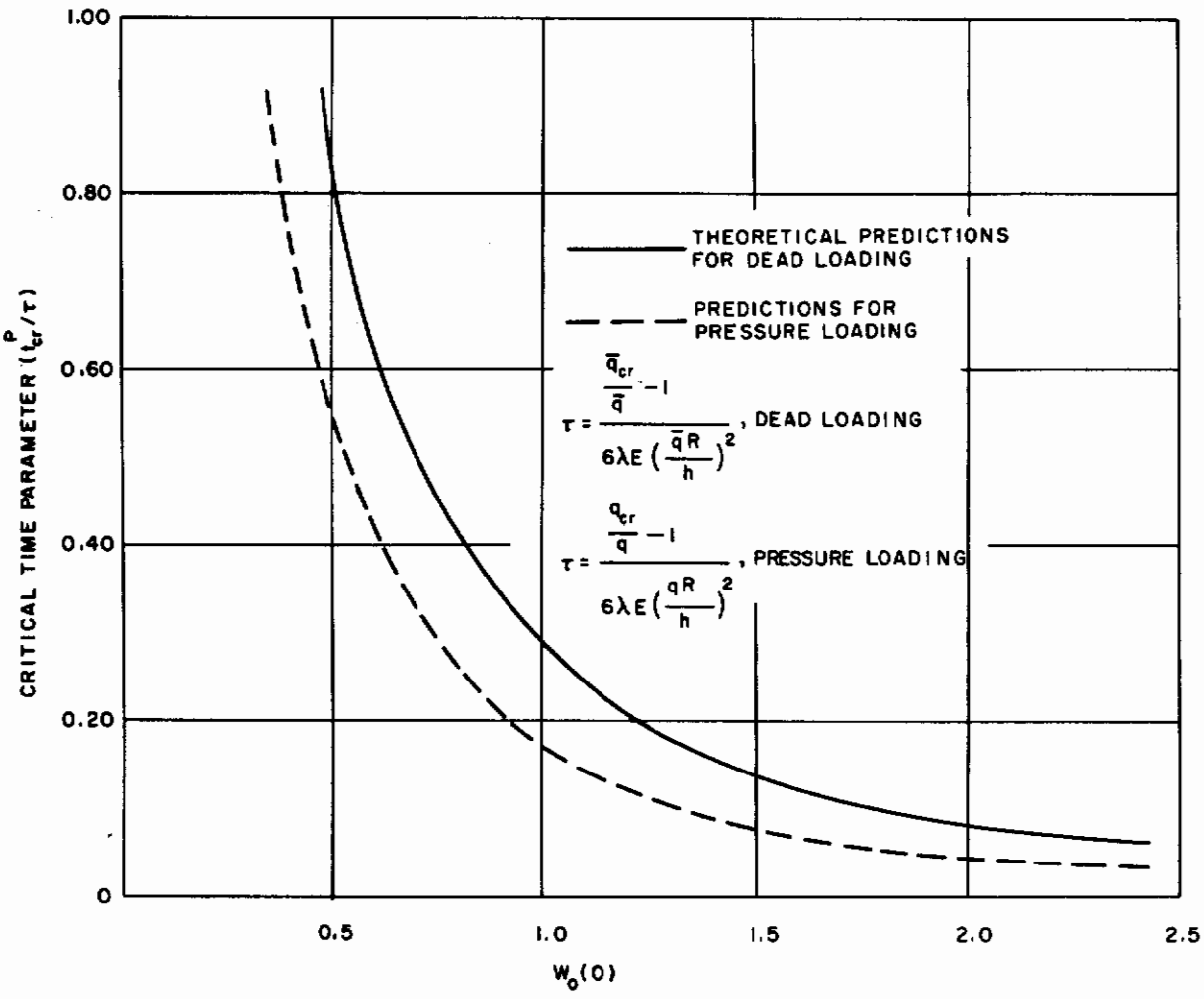

Figure X-3 CRITICAL TIME PARAMETER VERSUS INITIAL SHAPE FACTOR AMPLITUDE

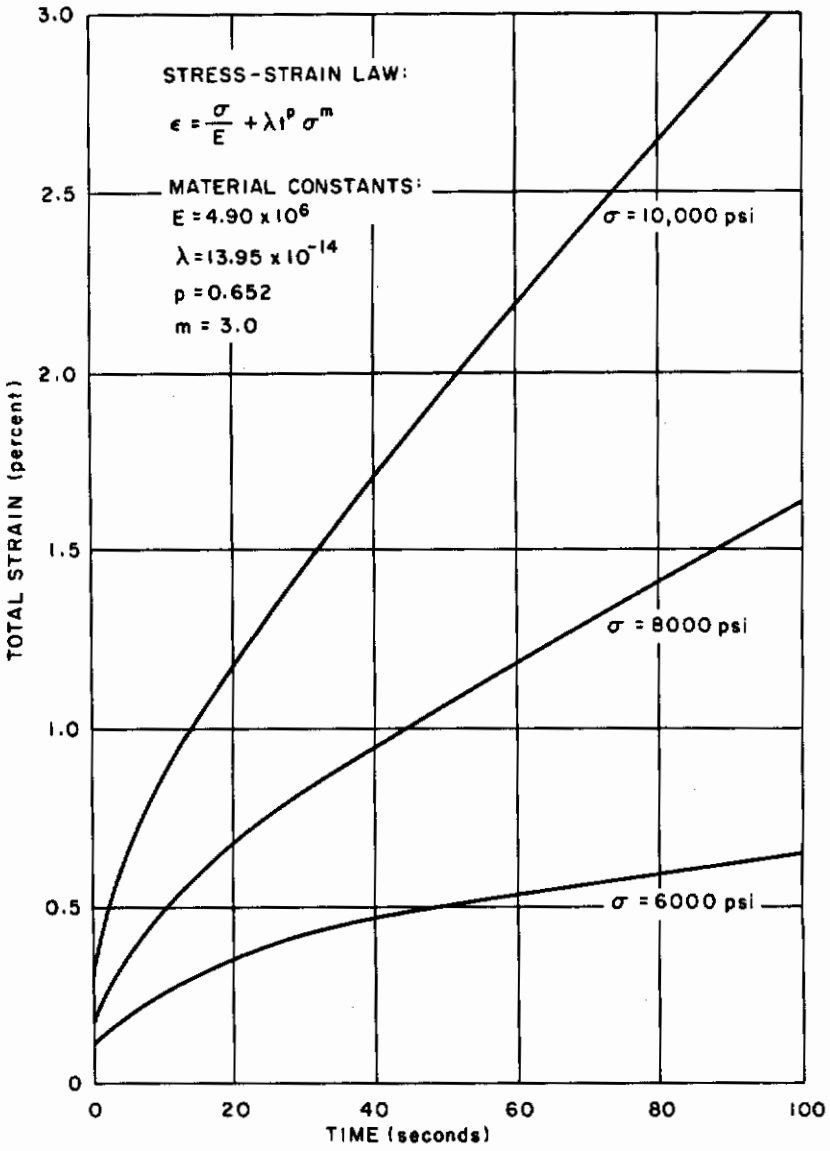

Figure X-4 TOTAL STRAIN AS A FUNCTION OF TIME FOR QQ-M-44H MAGNESIUM ALLOY AT 400°F

data (Ref. X-8) are given for QQ-M-44H magnesium alloy at a temperature of 400°F. As mentioned previously, the mechanical properties, including the elastic modulus, E, and creep constants λ, p, and m are determined in conjunction with the empirically formulated creep law (equation X-9) so as to appropriately describe the total stress-strain curves of a selected material.

For the present application, the values* which represent the best fit to the experimental data in both the transient and secondary regions are tabulated in figure X-4. These values are to be used in combination with equations (X-18), and (X-31) in determining numerical results for either the critical collapse time, the ratio of applied stress to the critical stress state, or the magnitude of the initial shape factor amplitude; the quantity determined, being dependent upon the values specified for a given design problem.

Returning now to the graphical illustration for the logarithmic behavior of equations (X-18), (X-31), it is observed that the values for the critical collapse times are subjected to relatively minor fluctuations for large values of the initial shape factor amplitude, $W_o(0)$. This characteristic, as previously shown by Hoff (Ref. X-9), is further exemplified when equation (X-18) or, (X-31) is differentiated to obtain the variation of the theoretically predicted collapse time as a function of the initial shape factor amplitude and a corresponding incremental deviation from this value.

Differentiating equation (X-18) and expressing the results as a ratio of the initially fixed critical collapse time,

$$p\left|\frac{\Delta t_{cr}}{t_{cr}}\right| = \frac{\frac{160}{243}\,\Delta W_o(0)}{W_o^3(0)\left[1+\frac{80}{243\,W^2(0)}\right]\log\left[1+\frac{80}{243\,W_o^2(0)}\right]}, \qquad \text{(X-33)}$$

in which, Δt_{cr} and $\Delta W_o(0)$ represent the incremental deviation from t_{cr} and $W_o(0)$, respectively. This ratio is shown plotted in figure X-5 as a function of the initial shape factor amplitude with uncontrollable deviations from this value ranging from 0.05 to 0.25.

As shown in figure X-5, the uncertainties in the theoretical predictions of collapse time are relatively insensitive for large values of the shape factor amplitude. If, however, a smaller value is selected, the uncertainties in predictions are subjected to radical fluctuations and increase very rapidly with each corresponding decrease in $W_o(0)$. For example, an uncontrollable deviation of 0.1

*The units for the elastic modulus are expressed in pounds per square inch and the creep constant, λ, as percent strain/$(psi)^m$ $(sec)^p$.

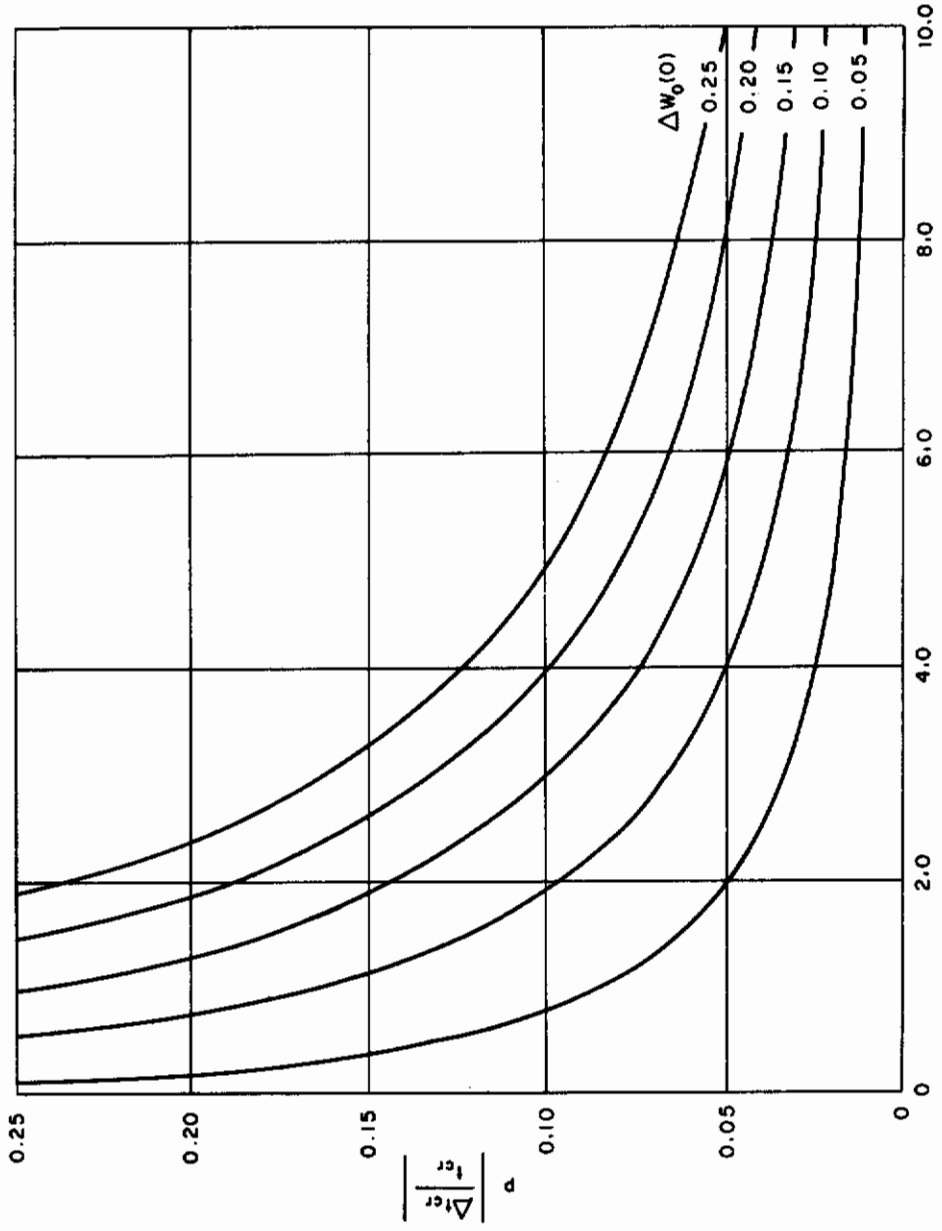

Figure X-5 UNCERTAINTIES OF CRITICAL COLLAPSE TIMES FOR A CORRESPONDING DEVIATION OF THE INITIAL SHAPE FACTOR AMPLITUDE

in $W_o(0)$, when $W_o(0) = 5.0$, produces only a 6 percent change in the critical time for QQ-M-44H magnesium alloy ($p = 0.652$); whereas, an initial shape factor amplitude of 0.6, with the same uncontrollable deviations, corresponds to an uncertainty in prediction for the critical time of 38 percent. Consequently, precise theoretical predictions of the critical collapse time for small values of the shape factor amplitude are obtained only if the deviation from circularity* of the shell is precisely measured. Less accurate information is required for large values of the initial shape factor amplitude.

Another topic of considerable interest, and one which is to be currently discussed; relates to the associated effects of the elastic and primary creep deformations on the theoretical predictions for collapse time. In the previous discussion, it is re-called that the relationships for the theoretical predictions were developed for a shell material which exhibited both primary and secondary creep as well as elastic deformations. If, now, the elastic strain rate is set identically equal to zero, the resulting expressions for the dead and pressure loading cases become

$$t'_{cr} = \left\{ \frac{\frac{\bar{q}_{cr}}{\bar{q}}}{6\lambda E \left(\frac{\bar{q}R}{h}\right)^2} \log \left[1 + \frac{80}{243 W_o^2(0)} \right] \right\}^{1/p} ,$$

and

$$t'_{cr} = \left\{ \frac{\frac{q_{cr}}{q}}{6\lambda E \left(\frac{qR}{h}\right)^2} \log \left[1 + \frac{5}{27 W_o^2 0} \right] \right\}^{1/p} . \qquad \text{(X-34)}$$

From an inspection of equations (X-18), (X-31), and (X-34), it is observed that the expressions previously developed for the critical times are similar in form to those obtained for the case in which the elastic deformations are neglected. In fact, the only dissimilarity in calculating the critical times by equations (X-18), (X-31) and obtaining the results from equation (X-34) appears in the critical stress ratio terms which multiply the logarithmic function for the initial shape factor amplitude.

For values of the critical stress ratios, $\frac{\bar{q}}{\bar{q}_{cr}}$, likewise, $\frac{q}{q_{cr}}$, which are small

*That is, the deviation from circularity of the shell immediately after the load is applied but prior to the primary creep phase, i.e., equation (X-24).

in comparison to one, and with the creep constant, p, of the order of unity; the expressions as expected for either case yield similar results. However, as the critical stress ratio is increased, it is apparent that for all values of p there exists a large discrepency between the theoretical predictions of equations (X-34) and those resulting from equations (X-18), (X-31). Consequently, a reasonable estimate for the collapse times can only be obtained by neglecting the elastic strain rate in instances where the critical stress ratio is small when compared to unity* while the creep constant, p, approaches one.**

In considering the effects associated with a shell material in which the primary creep deformations are assumed negligible, it is necessary to re-formulate the previously stated creep law so as to appropriately describe the elastic and steady (secondary) creep rates. An approximate representation of the elastic and secondary phase of creep as discussed by Hoff (Ref. X-3); and, one which will be employed in the present investigation for convenience in later calculations, is of the form:

$$\dot{\epsilon} = \frac{\dot{\sigma}}{E} + k'\left(\frac{\sigma}{\lambda'}\right)^{m'} \quad . \tag{X-35}$$

Comparing equation (X-35) with the expression previously developed for the creep rate; namely

$$\dot{\epsilon} = \frac{\dot{\sigma}}{E} + \lambda p t^{p-1} \sigma^{m} \quad , \tag{X-36}$$

it is seen that the extrapolation of results for the critical collapse times in the presence of elastic and steady secondary creep deformations is readily obtained from equations (X-18), (X-31) by equating:

$$p = 1 \ ,$$

$$m = m' \ ,$$

$$\lambda = k'\left(\frac{1}{\lambda'}\right)^{m'} \quad . \tag{X-37}$$

*The exception is naturally provided when the critical stress ratio is identically equal to unity; in which case, the shape factor amplitude becomes indefinitely large and the theoretical predictions for the collapse time in either case are zero.

**Since the creep constant, p, decreases with each corresponding decrease in temperature, it is implied that at low temperatures for which the normal stress is small, the elastic strain rate as in the relaxation phenomena is important and can not be neglected.

Substituting the above expressions into (X-18), the relationship for the dead loading case becomes

$$t''_{cr} = \frac{\left(\frac{\bar{q}_{cr}}{\bar{q}} - 1\right)}{6\left(\frac{k'E}{\lambda'^3}\right)\left(\frac{\bar{q}R}{h}\right)^2} \log\left[1 + \frac{80}{243 W_o^2(0)}\right] \quad . \tag{X-38}$$

Similarly, the results for hydrostatic pressure-type forces are given by

$$t''_{cr} = \frac{\left(\frac{q_{cr}}{q} - 1\right)}{6\left(\frac{k'E}{\lambda'^3}\right)\left(\frac{qR}{h}\right)^2} \log\left[1 + \frac{5}{27 W_o^2(0)}\right] \quad . \tag{X-39}$$

The current results, as expected, would indicate that at elevated temperatures and for constant stress states, a relatively accurate estimate for critical collapse times is obtained by treating the steady secondary creep rate problem. Further, it is interesting to demonstrate the correspondence between equation (X-39) and the results previously developed by Hoff (Ref. X-9) for an idealized sandwich shell under uniform external pressure and steady (secondary) creep conditions. The extension of equation (X-39) simply requires an interpretation of the parameters, q_{cr} and $W_o(0)$.

In equation (X-39), if one notes that, $\frac{h^3}{12}$, is the moment of inertia of the homogeneous shell, and is equivalent to, $\frac{b_s h_s^2}{4}$, for the sandwich shell; then

$$h = \sqrt{3}\, h_s \; ; \tag{X-40}$$

and, the resulting expression for the critical load, q_{cr}, becomes

$$q_{cr} = \frac{3E b_s h_s^2}{4(1-\nu^2)R^3} = \frac{3E A_s \rho_s}{(1-\nu^2)R^3} \quad , \tag{X-41}$$

where A_s represents the area of the facing sheets, and ρ_s the shell wall radius of gyration.

If, now, the initial shape factor amplitude, $W_o(0)$, is expressed in terms of the quantity previously defined by Hoff as a weighted shape factor of the cross

section, $\chi_o = \frac{\alpha R}{\rho_s}$, it is found that

$$W_o(0) = \frac{\chi_o}{2\sqrt{3}} \quad . \tag{X-42}$$

Substituting equations (X-41), (X-42) into (X-39), and neglecting any elastic effects

$$\frac{t'_{cr}}{\tau'} = \frac{1}{2} \log \left[1 + \frac{20}{9\chi_o^2} \right] \quad , \tag{X-43}$$

in which

$$(\tau')^{-1} = k'(1-\nu^2) \left(\frac{qR}{A_s \lambda'} \right)^3 \left(\frac{R}{\rho_s} \right)^2 \quad .$$

The above relationship is identical in form to the expression developed by Hoff from a continuous collocation method, except that the constant, 20/9 , is replaced by 9/2 in Hoff's analysis.

This discrepancy is difficult to explain in view of the different mathematical formulations and assumptions employed in both analyses. However, it can be demonstrated that the predictions indicated by Hoff would be more closely correlated with current predictions if the quadratic terms (X-27), which were adjoined to Equation (X-10), are omitted. For example, if the quadratic terms (X-27) are disregarded, and further, if the elastic strain effects are neglected, the resulting expression for the critical collapse time for the hydrostatic pressure loading becomes

$$\frac{t_{cr}}{\tau'} = \frac{1}{2} \log \left[1 + \frac{320}{81\chi_o^2} \right] \quad . \tag{X-44}$$

Although this relationship is seen to be in better qualitative agreement with the results obtained by Hoff, it is remarked that the omission of the second-order terms leads to a basic inconsistency within the context of the present analysis. That is, when the elastic strain rate effects are retained, the expression for the critical stress ratio term, i. e., see equations (X-30), which multiplies the logarithmic function for the initial shape factor amplitude is given by $\left(\frac{q_{cr}}{q} - \frac{3}{4} \right)$.

Since, in the usual results, and one which is naturally expected, the factor 3/4 is replaced by unity, it is apparent that the previous assumption regarding the quadratic terms has materially altered the theoretical predictions for collapse time.

It is also interesting to discuss the sensitivity of the various creep problems to the character of the loading . In the previous examples, the effects of the dead and hydrostatic pressure loadings were investigated for a shell material which exhibited (1) primary and secondary creep as well as elastic deformations (X-18), (X-31); (2) primary and secondary creep deformations (X-34); and (3) elastic and steady secondary creep deformations (X-38), (X-39). If, now, attention is drawn to the case of a centrally directed pressure loading, that is, the surface tractions during a virtual displacement remain constant in magnitude but directed toward a common pole, it is found that the resulting expressions for the theoretical predictions in the previously discussed deformation states are respectively given as:

$$t_{cr} = \left\{ \frac{\left(\frac{\bar{\bar{q}}_{cr}}{\bar{\bar{q}}} - 1 \right)}{6\lambda E \left(\frac{\bar{\bar{q}} R}{h} \right)^2} \log \left[1 + \frac{405}{972 W_o^2(0)} \right] \right\}^{1/p} , \tag{X-45}$$

$$t'_{cr} = \left\{ \frac{\frac{\bar{\bar{q}}_{cr}}{\bar{\bar{q}}}}{6\lambda E \left(\frac{\bar{\bar{q}} R}{h} \right)^2} \log \left[1 + \frac{405}{972 W_o^2(0)} \right] \right\}^{1/p} , \tag{X-46}$$

and

$$t''_{cr} = \frac{\frac{\bar{\bar{q}}_{cr}}{\bar{\bar{q}}} - 1}{6 \left(\frac{k'E}{\lambda'^3} \right) \left(\frac{\bar{\bar{q}} R}{h} \right)^2} \log \left[1 + \frac{405}{972 W_o^2(0)} \right] . \tag{X-47}$$

Thus, from an inspection of the above examples, as well as from the examples previously considered, it is observed that the theoretical collapse time for the centrally directed pressure loading is greater than that of the dead loading, which in turn, is greater than that obtained for hydrostatic pressure. It is remarked that these results for the various distributed force systems are quantitatively of the same order of sequence as the results attained in the elastic stability problem.

D. LIST OF SYMBOLS

$b_s/2$ = thickness of facing sheet for equivalent sandwich shell

E = Young's Modulus

f_o = Shape Factor of Shell Cross Section

h = Thickness of Homogeneous Shell

h_s = Distance between Facing Sheets for an Equivalent Sandwich Shell

$\bar{I}$ = Integral to be Varied

I = Moment of Inertia

J_2 = Second Invariant of Stress-Deviator Tensor

m = Empirical Constant in Creep Law

m', k' = Empirical Constants in Creep Law When Elastic and Primary Creep Deformation are Neglected

M = Bending Moment in Shell Wall

p = Empirical Constant in Creep Law

q, $\bar{q}$, $\bar{\bar{q}}$ = Compressive Loads for Hydrostatic Pressure, Constant Directional Pressure, and Centrally Directed Pressure, Respectively

$q_{cr} = \dfrac{3EI}{(1-\nu^2)R^3}$

$\bar{q}_{cr} = \dfrac{4EI}{(1-\nu^2)R^3}$

$\bar{\bar{q}}_{cr} = \dfrac{4.5EI}{(1-\nu^2)R^3}$

R = Radius of Shell

S_{ij} = Stress-Deviator Tensor

S = Surface of a Body

S_s = Surface Region where Stresses are Prescribed

S_d = Surface Region Where Displacements are Prescribed

t = Time

t_{cr} = Critical Time for Creep Collapse

t'_{cr}, t''_{cr} = Critical Time When Elastic and Primary Creep Deformations are Neglected, Respectively

Δt_{cr} = Deviation in Critical Time

T_i = Surface Traction

$\bar{T}_i$ = Prescribed Surface Traction On S_s

u = Displacement in the θ-Direction

u_i = Displacement Vector

$\bar{u}_i$ = Prescribed Displacement Vector on S_d

U = Displacement of Neutral Surface in the θ-Direction

U_o = Amplitude of Neutral Surface Displacement in the θ-Direction Divided by the Shell Thickness

w = Displacement in the z-Direction

w' = Initial Shell Irregularities Prior to Loading

W = Displacement of the Neutral Surface in the z-Direction

W_o = Amplitude of Neutral Surface Displacement in the z-Direction Divided by the Shell Thickness

$W_o(0)$ = Initial Shape Factor Amplitude

$\Delta W_o(0)$ = Uncertainties in the Initial Shape Factor Amplitude

z = Shell Coordinate

ϵ = Total Strain

ϵ_{ij} = Strain Tensor

ϵ'_{ij} = Noncreep Portion of Strain Tensor

ϵ''_{ij} = Creep Strain Tensor

θ = Angular Coordinate

λ, λ' = Empirical Creep Constant

ν = Poisson's Ratio

ρ, ρ_s = Radius of Gyration for the Homogeneous and Sandwich Shell, Respectively

σ_{ij} = Stress Tensor

r = Non-dimensionalized Parameter Defined in Figure X-3

r' = Non-dimensionalized Parameter Defined by Hoff (Ref. X-6)

Note: Dots over quantities represent differentiation with respect to time.

REFERENCES

1. Sanders, J. L., H. G. McComb, and F. R. Schlechte, A Variational Theorem for Creep with Applications to Plates and Columns, NACA Rept. 1342 (1958).

2. Pearson, C. E., General Theory of Elastic Stability, Quarterly of Applied Mathematics, 14, No. 2 (1956) p. 133.

3. Boresi, A. P., A Refinement of the Theory of Buckling of Rings Under Uniform Pressure, J. Appl. Mech., 22, No. 1 (1955) p. 95.

4. Bodner, S. R., On the Conservativeness of Various Distributed Force Systems, J. Aero Sciences, 25, No. 3 (1958)

5. Novozhilov, V. V., Foundations of the Nonlinear Theory Of Elasticity, Graylock Press, Rochester, New York (1953), p. 191-193.

6. Hoff, N. J., A Survey of the Theories of Creep Buckling, Department of Aeronautical Engineering, Stanford University, Sudaer No. 80 (1958).

7. Timoshenko, S., Theory of Elastic Stability, McGraw-Hill Book Company, New York, New York (1936), p. 222-224.

8. Baer, H. W., Prediction of Very Short Time Creep Buckling from Very Short Time Tensile - Creep Properties, Proceedings of the Second U. S. National Congress of Applied Mechanics (1954) p. 569-576.

9. Hoff, N. J., W. E. Jahsman, and W. Nachbar, A Study of Creep Collapse of a Long Circular Cylindrical Shell Under Uniform External Pressure, Journal of the Aerospace Sciences, 26, No. 10 (1959).

APPENDIX XI *

MULTI-DIMENSIONAL HEAT FLOW AND ABLATION DURING RE-ENTRY

by H. Hurwicz and T. Brady**

SUMMARY

Physical conditions (non-uniformities) and actual re-entry applications resulting in multi-dimensional heat flow and ablation are discussed. Mathematical formulation of problems arising in prediction of temperature response and surface recession is given for many commonly encountered multi-dimensional cases. Methods of programming of such problems for the electronic analogue computations are developed. Savings in equipment and computing ease are achieved by either appropriate mathematical transformations, or the complexity of the problem is reduced by physically justified simplified assumptions. The case of the wing leading edge of a re-entry glider is analyzed in detail while the calculated results were shown in the body of main report.

The concern about multi-dimensional heat and mass flow problem arises in many of the re-entry applications. Often, they are local of nature and restricted to componentry of the thermal protection system, however, on many occasions they do affect the design of major portions of the heat shield-structure composite.

In principle, all problems must be considered three-dimensional as they deal with three-dimensional bodies; in practice based on the uniformities of geometry or boundaries, they may be reduced to one- or two-dimensions. The design of the configuration may either eliminate the problem by fitting the shield geometry to the non-uniform boundary inputs, or take advantage of the two- or three-dimensionality inherent in the problem. In this latter case internal cooling of the hot spots is provided by conducting heat away from it to areas operating at lower temperature.

In either case, means have to be provided to evaluate the thermal protection system by computations considering more than one-dimension, or to estimate such effects. Transient problems involving more than one-dimensional effects become quite complex and require numerical machine solutions. Large computer facilities are required for even the simplest geometries and the attendant

*The general study was supported by AF33(616)-7483, AF04(647)-258, and AF04(647)-305. Only material directly applicable to AF33(616)-7483 is excerpted here.

**Dian Labs, Inc., 611 Broadway, New York, New York.

cost and time expenditures encourage the use of one-dimensional approximations or of their super-positions at the expense of accuracy, and may lead thus to unwarranted decisions concerning the protection system.

While two-dimensional solutions to the heat conduction problem exist, references XI-1 to XI-4, very few solutions are found to problems involving simultaneous mass transfer. Those which exist either assume one-dimensional conduction and specialize to flow of liquid layer (Refs. XI-5 to XI-8) or consider the mass transfer as (unidirectional) while two-dimensional heat conduction problem is solved. Reference XI-9 shows results of a two-dimensional ablation problem with two-dimensional heat conduction.

Cases involving both two-dimensional heat and mass transfers are much more complex and costly than when one of the mechanisms may be reduced to one-dimensionality, and thus solutions are more difficult to find. However, it is often difficult to resolve (Ref. XI-9) a priori which of the mechanisms may be treated one-dimensionally until complete solution is obtained. In the cases when it is possible, (Ref. XI-10 and Section VIII of the main report,) and even if the conduction effects are predominant but surface recession is involved, means are still required to handle them for design applications.

It was thus deemed of interest to review the circumstances under which multi-dimensional flow may affect the system operation and review or develop methods to simulate such effects, either by approximation based on geometry or boundary uniformities, or by programming of special and general cases where some (or all) of the approximations become not necessary. In programming, effort was aimed at the increase in speed, simplicity in formulation and thus decrease in costs. As a result means were to be provided to determine the accuracy of one-dimensional solutions and areas of their applicability for geometries commonly encountered in applications of interest.

A. MULTI-DIMENSIONAL FLOW EFFECTS

1. Physical Causes

Departure from uniform environmental boundary conditions, and/or from a flat plate geometry will usually create a situation where two- or three-dimensional flow effects must be at least considered, if not solved. In many areas of re-entry vehicle heat shield such is the case where a volume element may not be considered as insulated on the sides normal to the surface exposed to the environment.

Either or both of the two categories of non-uniformities creates the need for consideration of multi-dimensionality in practice as well as in the principle. The presence of surface recession, tends to aggravate the effects, as the non-uniformities initially absent may be generated as time progresses.

In terms of the re-entry variables local heat flux $q_{ir} = f(t)$ only, provides a uniform boundary condition. As long as the geometry of a flat plate subject to above mentioned restrictions may be considered and homogeneous materials exist around the body, one-dimensional flow may be assumed. If the flux varies some along the surface but relatively uniform surface temperature distribution is maintained throughout the cycle by proper adjustment of the shield thickness, the above assumption may still hold, since a compensating geometrical non-uniformity was introduced. A series of one-dimensional calculations to map isotherms will quickly indicate the validity of the assumption. The severity of the two-dimensional effects will vary with the thermal properties (k, ρ, C_p) of the shield material, duration of heating pulse,and the rate of change of the flux along the surface as now $q_{ir} = f(t, y)$.

The geometrical non-uniformity introduces similar problems when $q_{ir} = f(t)$ only and the effects will depend again on material properties as well as the degree of departure from the flat plate (or insulated cube) geometry. A combination of both non-uniformities may tend to accentuate or compensate the effects.

Each category causes a different source of difficulties (discussed in detail below) in formulating the solutions or in arriving on suitable simplification. Table XI-1 indicates schematically the various types of problems arising as a result of the common non-uniformities, and the required solutions when two- or three-dimensional effects (in cartesian coordinates) are obtained. It also indicates descriptively the type of geometrical simplifications which may be useful in obtaining a solution. Additional non-uniformities (e.g. $q = f(t, x, y, z)$) would complicate the input handling but would not affect significantly the internal network.

As a rule in design applications, one would deal with an arbitrary shape. However, in many cases a simplification of the problem may be made by reducing it to one of the geometrical symmetries of table XI-1. If no ablation is involved, a relatively straightforward formulation may be programmed for machine solution even for arbitrary shapes. Considerable savings may be realized, however, by solving special geometrical cases. Table XI-2 indicates that such solutions (digital or analogue) are available for two-dimensional problems or such three-dimensional problems in cartesian system which may be reduced to less dimensions in other coordinate system. If material decomposition and surface recession occur, considerably more equipment is required for machine solution. It may become prohibitive for practical purposes to obtain an arbitrary shape solution. Specialized geometries with attendant change in the coordinate system, however, and with additional assumptions concerning direction of recession may bring the problem within reach of practicability. Two such cases, (ba) and (ca) of table XI-1 were programmed during the course of this study.

TABLE XI-1

MULTI-DIMENSIONAL PROBLEMS
CAUSED BY NON-UNIFORMITIES

Geometry	Flow Mechanism	Heat Flux at the Boundary		
		$q = f(t)$ (a)	$q = f(t,y)$ $q = f(t,x,y)$ $q = f(t,\theta)_{etc.}$ (b)	$q = f(t,y,z)$ $q = f(t,x,y,z)$ $q = f(t,\theta,\phi)_{etc.}$ (c)
a. Thin Skin	-	Capacity Only	One-Dimensional	Two-Dimensional
b. Flat Plate	Conduction Only	Rectangular One-Dimensional x-Direction	Rectangular Two-Dimensional x - y Direction	Rectangular Three-Dimensional x - y - z Direction
(Insulated) Cube	With Ablation	Recession in x-Direction	Recession in Both x and y Direction	Recession in x - y - z Directions
c. Axisymmetric (r = Constant) Cylinder	Conduction Only	One-Dimensional Polar	Two-Dimensional Polar	Three-Dimensional Cylinder
	With Ablation	Uniform Recession In r-Direction	Non-Uniform Recession	Non-Uniform Recession
d. Spherical Symmetry	Conduction Only	One-Dimensional Spherical	Two-Dimensional Spherical	Three-Dimensional Spherical
	With Ablation	Uniform Recession In r-Direction	Non-Uniform Recession	Non-Uniform Recession
e. Axisymmetric [$r = f(z)$] Cylinder	Conduction Only	Two-Dimensional Cylindrical	Three-Dimensional Cylindrical	Three-Dimensional Cylindrical
	With Ablation	Uniform Recession With Respect to θ	Non-Uniform Recession	Non-Uniform Recession
f. Arbitrary Volume	Conduction Only	Three-Dimensional	Three-Dimensional	Three-Dimensional
	With Ablation	Non-Uniform Recession	Non-Uniform Recession	Non-Uniform Recession

TABLE XI-2

COMPUTER SOLUTIONS AVAILABLE FOR
PROBLEMS IN TABLE XI-1

Geometry	Flow Mechanism	Heat Flux at the Boundary		
		$q = f(t)$ (a)	$q = f(t,y)$, $q = f(t,x,y)$, $q = f(t,\theta)_{etc.}$ (b)	$q = f(t,y,z)$, $q = f(t,x,y,z)$, $q = f(t,\theta,\phi)_{etc.}$ (c)
a. Thin Skin	Conduction Only	Digital	-	-
b. Flat Plate (Insulated) Cube	Conduction Only	Digital and Analogue	Digital (Cylindrical with Large Radius) and Analogue	None
	With Ablation	Digital and Analogue	Analogue	Analogue by Superposition Only
c. Axisymmetric (r = Constant) Cylinder	Conduction Only	Digital and Analogue	Digital and Analogue	None
	With Ablation	Analogue	Analogue	None
d. Spherical	Conduction Only	Analogue	None	None
	With Ablation	Analogue	None	None
e. Axisymmetric [r = f(z)] Cylinder	Conduction Only	Digital	Digital	None
	With Ablation	None	None	None
f. Arbitrary Shape	Conduction Only	Digital	Digital	None
	With Ablation	None	None	None

The former, pertinent to the glider application, will be given in detail in this Appendix, while general formulation of other cases will be shown also.

2. Typical Problem Areas

Proper calculation of temperature distribution and of the external shape change of the re-entry vehicle is required for structural analysis and for feedback information used in determination of aerodynamic inputs. It is also needed in design and evaluation of performance limits of components attached internally or externally to the thermal protection system. It is in these three mutually dependent areas that the multi-dimensional flow effects may be of critical nature. Since the overall performance of the vehicle may be affected if not impaired, the problems generated may bear upon the thermal protection system selection, its design and choice of the materials. Consequently the system designer and materials man are directly concerned with such problems.

In many vehicle applications areas of high but localized heating exist, while the environment of the remainder is not severe. An opportunity thus presents itself in the system to either conduct or radiate the stored energy from the former toward the latter. Whether it is a natural phenomenon or a mechanism designed into the system, the problem cannot be treated by one-dimensional analysis. Such a situation may exist in the leading edges or nose cap of a re-entry glider, or in other re-entry application where the thermal properties of the shield are of orthotropic nature. The duration of the heating or soak times combined with a given set of properties may give rise to significant lateral flows.

Some control surfaces, fins or other stabilizing or spin inducing mechanisms external to the protection system may experience severe three-dimensional effects due to the many surfaces exposed to the non-uniform environment and often involved geometries. Similar problems may be created during testing of small samples in arc plasma jets.

Components attached to the structure provide local heat sinks. Instrumentation and sensors imbedded in shields, or voids and impurities may create "hot" or cold spots. Areas where dissimilar materials come in contact or where structural honeycombs or double-wall construction are used may also generate serious two-dimensional effects.

Finally, any sharp pointed shapes may undergo significant ablation or erosion which may affect in turn drag, heating,and other aerodynamic performance characteristics forming the input to the thermal protection system analysis. Such effects must be of necessity iterated with thermal and structural two- or three-dimensional analysis to assure reliability of system.

The neglect of such effects may either result in overdesign (or excessive safety factors due to ignorance) or failures of the components in performance of their basic functions either due to excessive erosion or thermal failure of the structure or of the sensing elements.

If one considers the possibility of surface recession due either to expected erosion or use of ablating materials, an overall at least two-dimensional program with a receding surface is required, in addition to heat conduction alone. Three conditions may be considered where:

a. There is no difference in shape change calculations by either one- or two-dimensional method, but internal heat flow is of multi-dimensional nature, due to configuration.

b. There is difference in shape change computation by the two methods, and while it may not affect the external flow characteristics, the recession rate does affect the internal flow over and above configuration effects.

c. The difference in external shape change calculation produces significant effects on the external as well as internal flows as per (a) and (b) above.

If a multi-dimensional computer program is not available, recession must be computed separately from the conduction problem. Such procedure while acceptable for short pulses breaks down for extended flight time applications. The absence of a computer program will often preclude analysis of two-dimensional effects, as no "yardstick" exists to gauge their significance. On the other hand, establishment of "one-dimensionality" of the problem will increase the design and analysis reliability even though no production calculations are required.

B. ANALOGUE SOLUTION OF ABLATION PROBLEMS

1. General Formulation

Mathematically, the problem consists of the heat conduction equation:

$$\rho c \frac{\partial T}{\partial t} = K \nabla^2 T \qquad \text{(XI-1)}$$

in a region R bounded by a surface C. The bounding surface moves, i.e., $C = C(t)$, and the normal derivatives are given on C. In the previous section some physical situations were described which give rise to such a problem. In some of such cases a fixed surface temperature may be prescribed at which the material starts to melt. If the decomposed material

is immediately blown away the region to which equation (XI-1) applies continuously shrinks in size.

Depending on the particular problem under consideration, the operator ∇ may be one, two- or three-dimensional and may be in rectangular, cylindrical or spherical coordinates. To obtain a numerical solution to such problems recourse must usually be made either to difference approximations to equation (XI-1), for solution by digital computers, or to difference-differential approximations to equation (XI-1), for solution by analogue computers. Emphasis here is on the latter type of approximation.

The reason for the emphasis on difference-differential schemes, and hence analogue computing methods, is that such methods are usually simpler. When equation (XL-1) is quantized in both time and space the computing procedure may very easily prove unstable. The art of determining whether a given computing procedure is stable or not is often difficult even for more basic problems (Ref. XI-12). With difference-differential methods however the time variable is kept continuous and only the space variables are quantized. On most analogue machines, in particular the electronic differential analyzer, time is usually a continuous independent variable so that such machines provide a natural setting for difference-differential systems. The electronic differential analyzer will be considered here as the analogue machine for which the systems are derived. For details of such machines the reader is referred to reference XI-13.

As noted before, in nature there is no such thing as a one-dimensional ablation problem. All problems are concerned with three-dimensional bodies. The reduction to a two- or one-dimensional problem is usually an approximation based on uniformities which the region R and boundary conditions may have. There is no one method for solving equation (XI-1) in all generality. Methods have been developed, however, for selected cases which are of practical significance. If the problem under consideration can be reduced or favorably approximated by one or some combination of these cases, worthwhile information may be obtained. In the following, difference-differential formulations will be presented for some cases and some indication given as to how they can be used to obtain information about more general problems.

Let $q(x, y, z, t)$ represent the normal flux (Ref. XI-14) at the surface of a body prior to any melting. That is

$$-K \frac{\partial T}{\partial n} = q(x,y,z,t), \qquad \text{(XI-2)}$$

where n is the unit vector normal to the surface. If the variation of q over the surface is quite small in comparison with the portion of the surface of

interest then the dimensions of prime interest will be that in the direction of the input flux. If the surface has little curvature it may be considered flat and equation (XI-1) becomes

$$\rho c \frac{\partial T}{\partial t} = K \frac{\partial^2 T}{\partial x^2} \quad , \tag{XI-3}$$

where x is measured perpendicular into the surface. If the curvature is significant in one direction cylindrical coordinates may be used whereby (XI-1) becomes

$$\rho c \frac{\partial T}{\partial t} = \frac{K}{r} \frac{\partial}{\partial r} \left(r \frac{\partial T}{\partial r} \right) \quad , \tag{XI-4}$$

where r is normal to the surface. And if curvature is significant in two normal directions spherical coordinates may be used giving

$$\rho c \frac{\partial T}{\partial t} = \frac{K}{r} \frac{\partial^2}{\partial r^2} (rT) . \tag{XI-5}$$

When the surface temperature reaches the temperature at which it melts the boundary condition (XI-2) must be replaced by one that takes into account the heat used in melting the material. If $\dot{s}$ is the velocity at which the surface moves in the direction of the normal and F is the heat of sublimation of the body then the more general expression of (XI-2) is

$$-K \frac{\partial T}{\partial n} = q - \rho F \dot{s} \quad , \tag{XI-6}$$

where ρ is the density of the material.

There are two basic ways of setting up difference-differential formulations for these problems. The first, and the most basic, allows for discrete removal, that is, the melting proceeds in steps. The second, and more sophisticated, method allows for continuous recession. While the second method is a more natural representation of the physical situation the first is a more flexible method and extends naturally to two- and three-dimensional problems. Both will be described for equation (XI-3) in the region $s \leq x \leq L_o$. The extension to other coordinate systems is fairly obvious.

Let the region $0 \leq x \leq L_o$ be considered as consisting of n sections of width Δx, where $n\Delta x = L_o$. Let x_i be the coordinate for the center of the i th cell. Let $f_{i-\frac{1}{2}}$ be the flux entering the cell over the area $\Delta y \Delta z$ at $x_{i-\frac{1}{2}}$, and $f_{i+\frac{1}{2}}$ be the flux leaving it at $x_{i+\frac{1}{2}}$ where $x_{i\pm\frac{1}{2}} = x_i \pm \frac{\Delta x}{2}$. Letting $T(x_i, t)$ be representative of the average temperature over Δx of the i th cell a heat balance for the cell can be written

$$\Delta x \Delta y \Delta z \rho c \dot{T}(x_i, t) = \Delta y \Delta z \left[f_{i-\frac{1}{2}} - f_{i+\frac{1}{2}} \right] . \tag{XI-7}$$

Approximating the flux terms $f_{i-\frac{1}{2}}$ by

$$f_{i-\frac{1}{2}} = K \frac{T_{i-1} - T_i}{\Delta x} \tag{XI-8}$$

and canceling out the common area term gives the standard difference-differential form

$$\rho c \dot{T}(x_i, t) = \frac{K}{\Delta x^2} \left[T(x_i - \Delta x, t) - 2\, T(x_i, t) + T(x_i + \Delta x, t) \right] , \tag{XI-9}$$

for interior cells and

$$\rho c \dot{T}(x_1, t) = \frac{1}{\Delta x} \left[\dot{q} - K \frac{T_1 - T_2}{\Delta x} \right] . \tag{XI-10}$$

for the first cell. For the last cell the flux at $x = L_o$ is usually taken as zero, and this is the case, although different conditions may be prescribed. Figure XI-1 illustrates the foregoing remarks.

When $T(x_1, t)$ reaches T_M, the ablation temperature, it is assumed that the entire first cell is at this temperature. Once it has reached the ablation temperature a specific amount of heat is required to ablate it, namely $\Delta x \rho F$, which is precisely the definition of F. If t_1 is the time at which $T(x_1, T)$ reaches T_M, then when

$$\int_{t_1}^{t} (q - F_{\frac{1}{2}})\, dt = \Delta x\, \rho F \tag{XI-11}$$

the first cell is completely melted. The removal of the first cell is accomplished by switching $\dot{q}$ to the face of the second cell and proceeding in a similar manner. In other words there are now $n-1$ cells and equation (XI-10) is replaced by

$$\rho c\, T(x_2, t) = \frac{1}{\Delta x} \left(\dot{q} - K \frac{T_2 - T_3}{\Delta x} \right) \quad t \geq t_2 , \tag{XI-12}$$

for the second cell. In this way ablation proceeds in Δx steps.

This is, admittedly, an approximate procedure. It may be improved to some degree but for one-dimensional problems a much better method is available, i. e., the so called shrinking coordinate method.

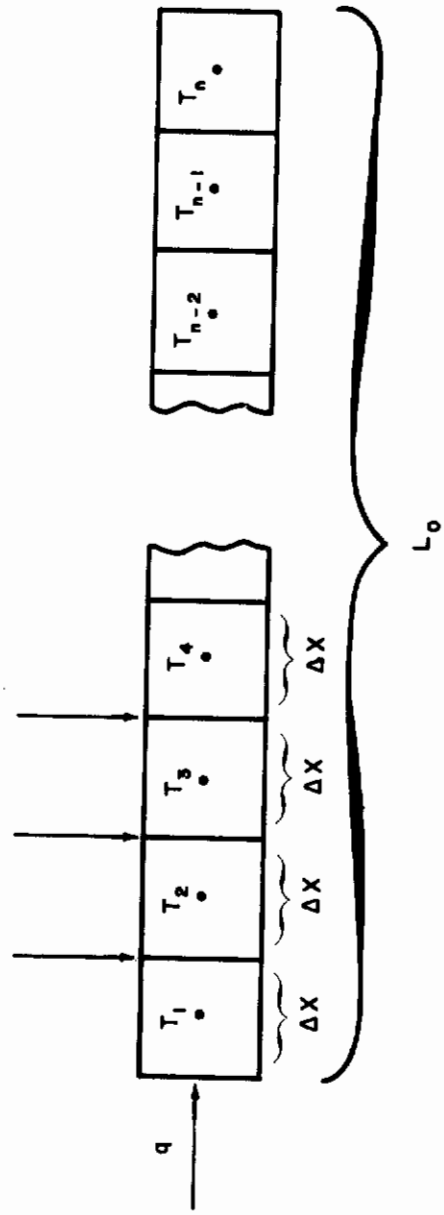

Figure XI-1 ONE-DIMENSION FINITE DIFFERENCE GRID

The transformation (Ref. XI-15)

$$\xi = (x - s)/(L_o - s) \tag{XI-13}$$

where s is the distance the boundary has moved, transforms the region $s \leq x \leq L$ into the region $0 \leq \xi \leq 1$. The convenience of this is that in the ξ, t plane the boundary condition is always applied at $\xi = 0$ and not at different points as was described for the discrete ablation method. Of course a price is paid for this convenience in that the system of difference-differential equations consists of much more complicated equations. The reason for referring to this as a shrinking coordinate method is that if a Δx is calculated for fixed ξ points from (XI-13) it will be seen that $\Delta x \to 0$ as $s \to L_o$.

Under transformation (XI-13) equation (XI-3) becomes

$$\rho c \frac{\partial T(\xi,t)}{\partial t} = \frac{K}{(L_o - S)^2} \frac{\partial^2 T(\xi,t)}{\partial \xi^2} + \rho c \frac{\dot{s}}{(L_o - S)} (1 - \xi) \frac{\partial T(\xi,t)}{\partial \xi}, \quad 0 \leq \xi \leq 1, \tag{XI-14}$$

and the boundary condition (XI-6) becomes

$$-K \frac{\partial T(0,t)}{\partial \xi} = (L_o - S)[q - \rho F \dot{s}], \tag{XI-15}$$

and if $x = L_o$ is considered insulated

$$-K \frac{\partial T(1,t)}{\partial \xi} = 0. \tag{XI-16}$$

There are many ways of expressing (XI-14) as a set of difference-differential equations. One check that may be applied to whatever representation is selected is that it satisfy the steady-state heat balance.

Let the heat input $\dot{q}$ be ≥ 0 for $0 \leq t \leq t_f$ and zero otherwise. If only a fraction of L_o ablates then the remaining part will eventually assume some steady state temperature T_{ss}. The total energy entering the bar $\int_0^{t_f} q\,dt$ must then account for the ablation and the heat content of the remaining bar in the steady state condition. If S_{ss} is the amount melted then a verbal equation describing the steady-state heat balance would be

$$\left\{\begin{array}{c}\text{total}\\ \text{heat}\\ \text{input}\end{array}\right\} = \left\{\begin{array}{c}\text{heat required}\\ \text{to raise S}\\ \text{to T}\end{array}\right\} + \left\{\begin{array}{c}\text{heat required}\\ \text{to melt S once}\\ \text{S reaches } T_A\end{array}\right\} + \left\{\begin{array}{c}\text{heat}\\ \text{content of}\\ L - S\end{array}\right\} \tag{XI-17}$$

This is quite obvious on physical grounds. It can be demonstrated mathematically and has been done so for the equation (XI- 3) in reference XI -15. The mathematical expression of (XI-17) is

$$\int_0^{t_{ss}} q\, dt = \rho c S_{ss} T_A + \rho F S_{ss} + T_{ss} \rho c (L_o - S_{ss}). \qquad \text{(XI-18)}$$

Thus a necessary, but not sufficient, condition that the difference-differential formulation chosen retains all the characteristics of the original problem is that it can be shown to satisfy (XI-18). Such formulations have been developed for rectangular, cylindrical, and spherical problems and are described in detail in reference XI-16.

A further check that may be made on the formulation is to let q be a constant and consider a semi-infinite bar. Under these conditions Landau (Ref. XI-15) has shown that the recession rate approaches a constant which can be determined.

When there is a significant variation of q over the surface in one direction the operator ∇ of (XI-1) must be represented in two dimensions. An example of such a case is shown in figure XI-2 for a rectangularly shaped body insulated on three sides and with a q variation in the y-direction. Because of the lack of variation of q in the z-direction the problem is two dimensional and may be described in the x - y plane. It should be noted that as shown in figure XI-2, the ablation proceeds essentially in one direction, i. e., the x-direction. This fact allows for the extension of transformation (XI-13) to such problems.

Consider first the method of discrete ablation applied to such a problem. A cross-section of the body is broken up into $\Delta x \Delta y$ cells. Let f denote, as before, flux in the x-direction and g the flux in the y-direction. Then, as illustrated in figure XI-3, a heat balance for the i , j th cell may be written as

$$\Delta x \Delta y \Delta z \rho c \dot{T}(\dot{x}_i, \dot{y}_j, t) = \Delta y \Delta z (f_{x_i - \Delta x/2} - f_{x_i + \Delta x/2}) + \Delta x \Delta z (g_{y_j - \Delta y/2} - g_{y + \Delta y/2}) \cdot \text{(XI-19)}$$

Expressing the fluxes in difference form as before gives

$$\rho c \dot{T}(x_i, y_j, t) = \frac{K}{\Delta x^2} [T_{i-1,j} - 2T_{i,j} + T_{i+1,j}] + \frac{K}{\Delta y^2} [T_{i,j-1} - 2T_{i,j} + T_{i,j+1}] \qquad \text{(XI-20)}$$

for the interior cells. The outer cells would have the appropriate boundary condition.

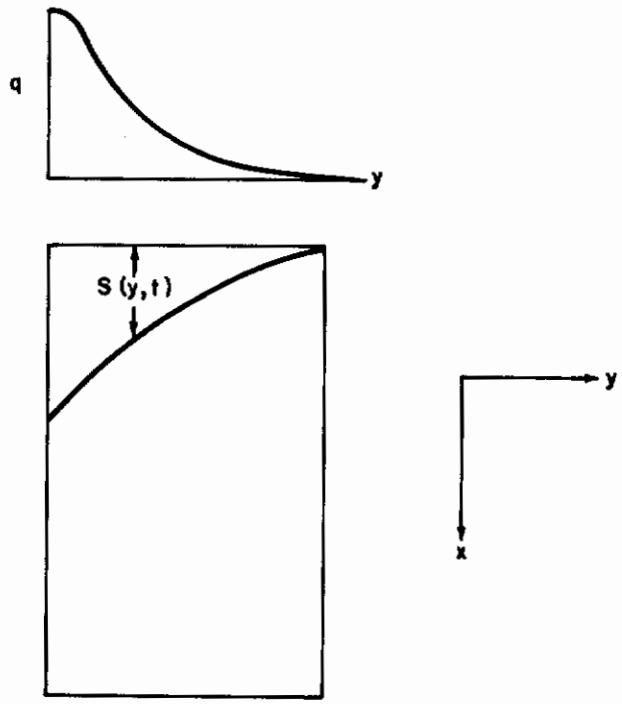

Figure XI-2 TWO-DIMENSIONAL ABLATION OF A RECTANGULAR PLATE WITH NON-UNIFORM HEATING ON ONE FACE

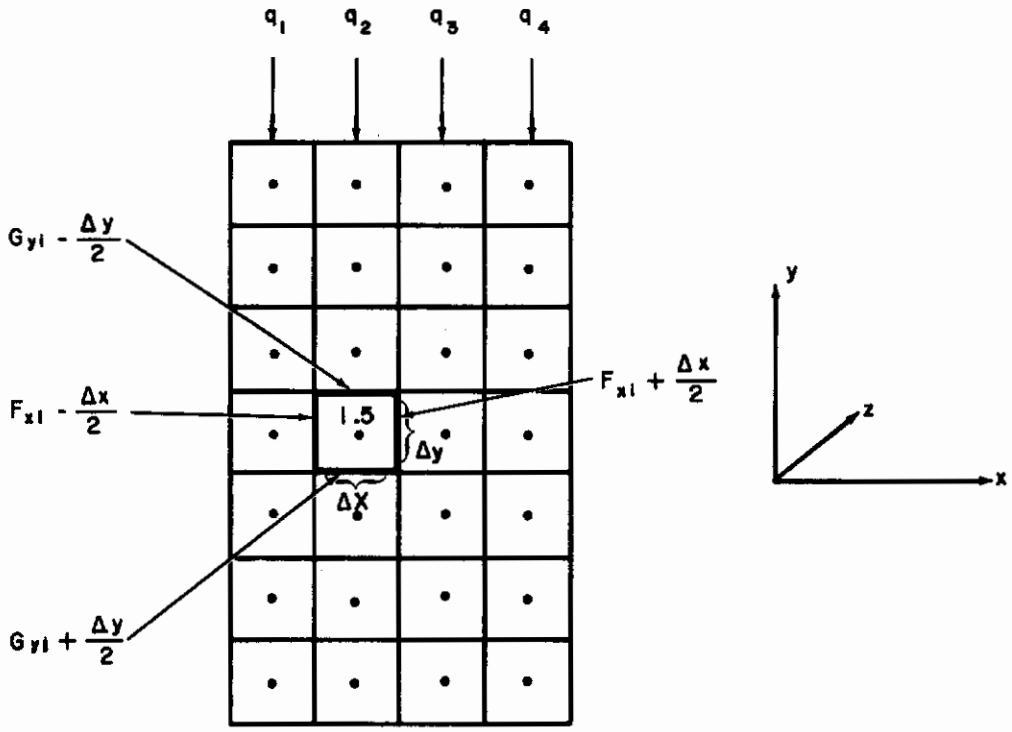

Figure XI-3 TWO-DIMENSIONAL FINITE DIFFERENCE GRID FOR HEAT CONDUCTION

In place of (XI-11) the expression which determines when a cell, e.g. the i, j th, is decomposed is

$$\int_{t_1}^{t} [(q - f_{i+\frac{1}{2}})\Delta y + (g_{j-\frac{1}{2}} - g_{j+\frac{1}{2}})\Delta x]\,dt = \Delta x \Delta y \rho F . \qquad \text{(XI-21)}$$

Thus when an outer cell reaches T_A it is held at this temperature until (XI - 21) is satisfied and then it is dropped and the boundary condition is applied to the next cell. If for a cell (XI-21) is never satisfied, although it reaches the melting temperature, then the fraction

$$\left\{ \int_{t_1} \left[(q - f_{i+\frac{1}{2}})\Delta y + (g_{j-\frac{1}{2}} - g_{j+\frac{1}{2}})\Delta x \right] dt \right\} / (\Delta x \Delta y \rho F) \qquad \text{(XI-22)}$$

is proportional to the portion of the cell that has melted.

To approximate continuous ablation for such a two-dimensional problem if there are n strips in the y-direction then there are n separate s's and thus n transformations of the type (XI-13). Applying these transformations results in a set of lattice points that move with time but not with the same velocity. The points in the strip that happened to be receding fastest would be shrinking together faster than the others. Thus a point which had neighbors to its left and right before ablation started may find that these neighbors have moved and there are no temperature stations to its left and right with which to calculate the fluxes in the y-direction. It is thus necessary to interpolate. Let the situation be as in figure XI-4b where the misalignment of the temperature stations is shown once ablation has started. Temperature station 3, 2 was originally next to 3, 1 and the y-flux into cell 3, 2 was calculated as

$$g = K \frac{T_{3,1} - T_{3,2}}{\Delta y} \qquad \text{(XI-23)}$$

At the moment during ablation shown, this is no longer true and $T_{3,2}$ corresponds to some temperature between $T_{4,1}$ and $T_{5,1}$. Interpolation between these two temperatures is required to find what is indicated in the figure as $T^*_{3,1}$.

The x-coordinate of $T_{3,2}$ at the moment shown in the figure is

$$x = (L_o - S_2)\xi_{3,2} + S_2 . \qquad \text{(XI-24)}$$

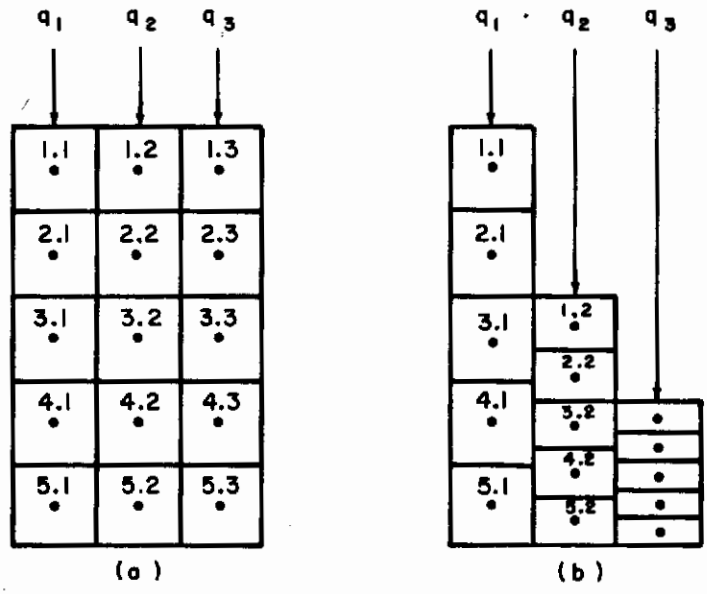

Figure XI-4 TWO-DIMENSIONAL FINITE DIFFERENCE GRID FOR HEAT CONDUCTION AND ABLATION IN A MOVING COORDINATE SYSTEM

In ξ coordinates for the 1st strip this is

$$\xi^*_{3,1} = [(L_o - S_2)\xi_{3,2} + S_2 - S_1] / (L_o - S_1) \qquad \text{(XI-25)}$$

and the interpolation formula is

$$T^*_{3,1} = \frac{T_{5,1} - T_{4,1}}{\Delta\xi} (\xi^*_{3,1} - \xi_{4,1}) + T_{4,1} \quad . \qquad \text{(XI-26)}$$

This is further complicated by the fact that some provision must be made to determine that $T_{4,1}$ and $T_{5,1}$ are the temperature stations to be used in the interpolation.

Thus associated with each point is not only a non-linear difference-differential equation but also some method for determining what its closest neighbors are and interpolation methods to be used with these neighbors.

To ease this situation somewhat, and make equipment requirements less formidable, a different transformation is used which restricts the number of points passing out of alignment to only a few in each strip near the boundary; let

$$S_m = \max_{i \le i \le n} (S_i) \qquad \text{(XI-27)}$$

and let δ be some small positive number. Then define

$$\xi^{(i)} = \frac{x - S_i}{S_m + \delta - S_i} \quad , \quad 0 \le \xi^{(i)} \le 1, \quad S_i \le x^i \le S_m + \delta \qquad \text{(XI-28)}$$

for each strip. Also

$$\eta^{(i)} = \frac{x^{(i)} - (S_m + \delta)}{L_o - (S_m + \delta)} \quad , \quad 0 \le \eta^{(i)} \le 1 \quad , \quad S_m + \delta \le x^{(i)} \le L_o \quad . \qquad \text{(XI-29)}$$

In this manner the η points are always aligned and only the ξ points can be misaligned as shown in figures XI-5a and XI-5b. This is convenient for some problems. For others it is not quite so good. One strip, that is, where $S_i = S_m$, has all its ξ points in the region $S_m + \delta$. The other regions however are larger, that is, the points in strip j, where $S_j \neq S_m$ instead of getting closer together get farther apart. For Δx in such a section is

$$\Delta x = \Delta\xi (S_m + \delta - S_i) \quad , \qquad \text{(XI-30)}$$

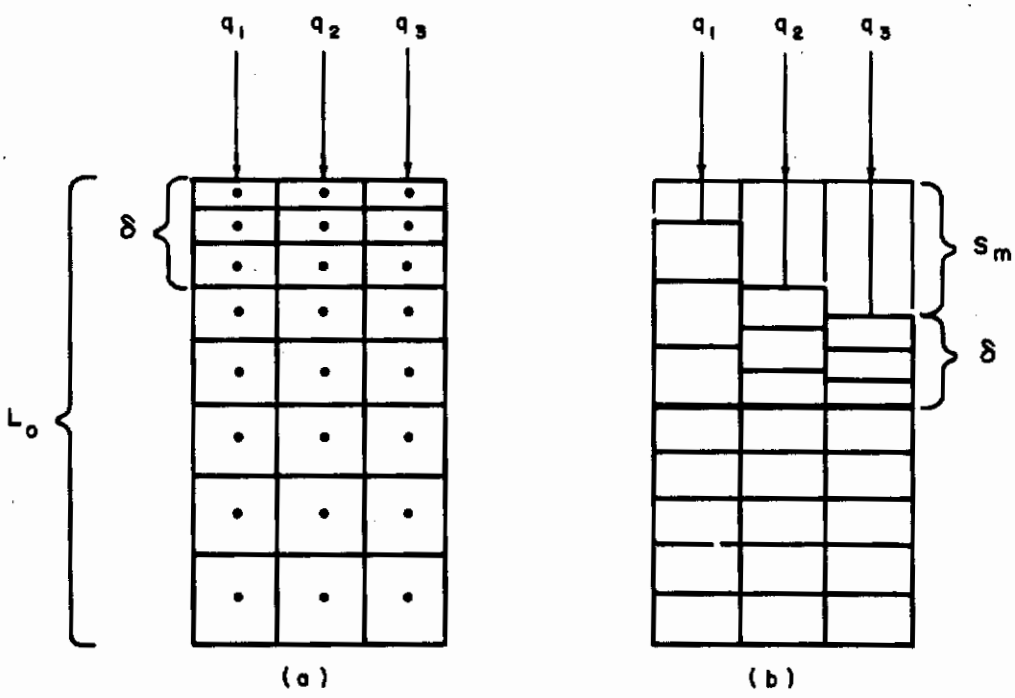

Figure XI-5 TWO-DIMENSIONAL FINITE DIFFERENCE GRID FOR HEAT CONDUCTION AND ABLATION IN A PARTIALLY MOVING COORDINATE SYSTEM

and in the section i where $S_i = S_m$ it is

$$\Delta x = \Delta\xi\delta \quad . \tag{XI-31}$$

Thus the difference approximations used become less accurate. The loss of accuracy is a function of the disparity in S_m and the minimum S_j.

Transformations similar in form and effect as (XI-28) and (XI-29) may also be applied to cylindrical and spherical coordinate problems.

These two methods, the discrete and continuous as described, constitute what may be considered two basic tools for solving ablation problems on analogue machines. Each has its strong points and weak points. The strong points of the discrete method are: 1) its simplicity; a linear conduction problem is solved, and 2) its flexibility; various geometries may be approximated by a modular type assembly of cubes with appropriate switching. Its weak points are: 1) the discontinuities produced by discrete ablation, and 2) the fact that when cells are melted, i.e., dropped off, the equipment associated with it is no longer used, so that the method doesn't use all the equipment available throughout the course of the problem. The continuous method for two-dimensional problems is characterized by the same advantages that it has for the one-dimensional one, among which are: the maximum use of computing equipment, a continuously moving boundary, and smooth temperature-time histories. The price paid for these desirable features is a sacrifice in simplicity and flexibility.

In the two specific problems illustrating the course of the study, these points were programmed and solved. The first is a two-dimensional problem in cylindrical coordinates and was solved with a shrinking coordinate transformation. As applicable to the wing leading edge it is described in the next section. The second was a three-dimensional problem in rectangular coordinates and was solved in fixed coordinates with discrete ablation. It is described in reference XI-8.

2. A Two-Dimensional Problem

In figure XI-6 is shown a cross section of the leading part of a wing structure composed of four different materials. The outer section is a radiation-ablation shield. Behind this is a substructure which is anisotropic (Ref. XI-3), i.e., the conductivities in the r and θ directions are different. Two insulating pieces are placed at the ends of the circular portion and the thin wing structure is molybdenum.

The heat input, normal to the surface, is illustrated by figure XI-7 as a function of time and θ. It will be noticed that the heat is highest at a point below the axis of symmetry, the stagnation point, and that it is of long duration heat input.

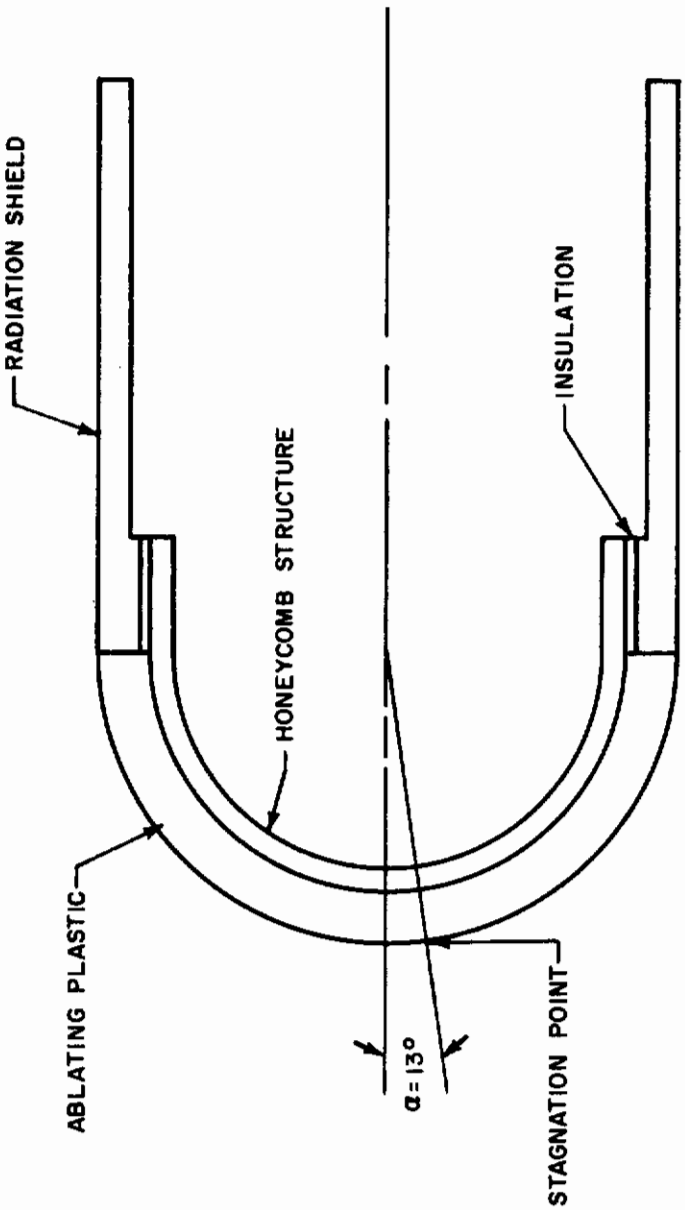

Figure XI-6 CROSS SECTION DIAGRAM OF A WING LEADING EDGE

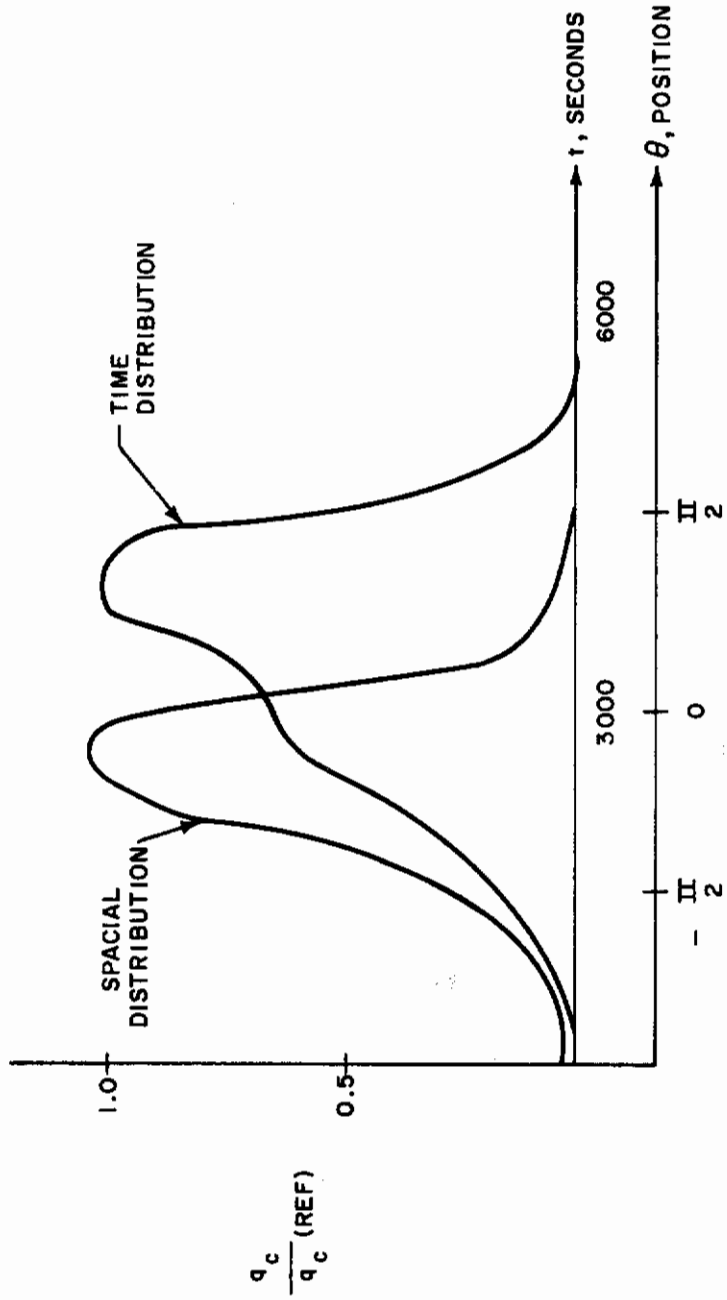

Figure XI-7 HEATING DISTRIBUTION FOR A WING LEADING EDGE

The problem is essentially a two-dimensional cylindrical coordinate problem for the radiation ablation shield, substructure, and a small portion of the other materials. Since the recession is assumed always in a direction normal to the surface it is possible to use a shrinking coordinate system in the ablation region for in cylindrical coordinates the ablation is one-dimensional although non-uniform on the periphery.

Preliminary to running the two-dimensional problem in its entirety a set of one-dimensional computations was made to obtain some rough estimates of the ablation depths and temperature gradients in the material. A cylindrical wedge was set up, as shown in figure XI-8, and it was assumed for the one-dimensional problem that the heat flux over the surface was uniform. To be on the conservative side 0.8-inch was allowed for the ablation region. The rest of the section was set up in fixed coordinates. Then this one dimensional problem was run a number of times using the different heat inputs around the wing leading edge. The transformation employed for the ablation section was

$$\xi = \frac{R_o - r - s}{R} \quad , \quad R = R_o - r - s \ , \tag{XI-32}$$

which when applied to

$$\rho c \frac{\partial T}{\partial t} = \frac{1}{r} \frac{\partial}{\partial r} \left(Kr \frac{\partial T}{\partial r} \right) \quad , \tag{XI-33}$$

results in

$$\rho c \frac{\partial T}{\partial t} = \frac{K}{R^2} \frac{\partial^2 T}{\partial \xi^2} - \frac{K}{R(R_o - s - \xi R)} \frac{\partial T}{\partial \xi} + \rho c \frac{\dot{s}}{R} (1 - \xi) \frac{\partial T}{\partial \xi} \quad , \tag{XI-34}$$

which is quantized in space in accordance with the model shown in figure XI-8 to give a system of difference-differential equations. For the fixed coordinate regions (XI-33) is quantized directly in space.

It was seen from one-dimensional calculations that in so far as a two-dimensional problem is concerned only a limited region must be capable of accommodating melting. And in this region the maximum depth of melting is approximately 0.2-inch. It means that the region of ablation, which as described in section 2 must be described by complicated equations, can be confined to a small fraction of the total material and thus the equipment requirements are such that an appreciable amount is left to represent the rest of the wing section in fixed coordinates.

The transformations used for each strip in the ablation section were

$$\xi^{(i)} = \frac{R_o - r - S_i}{R_i} \quad , R_i = R_o - r - S_i \ , \tag{XI-35}$$

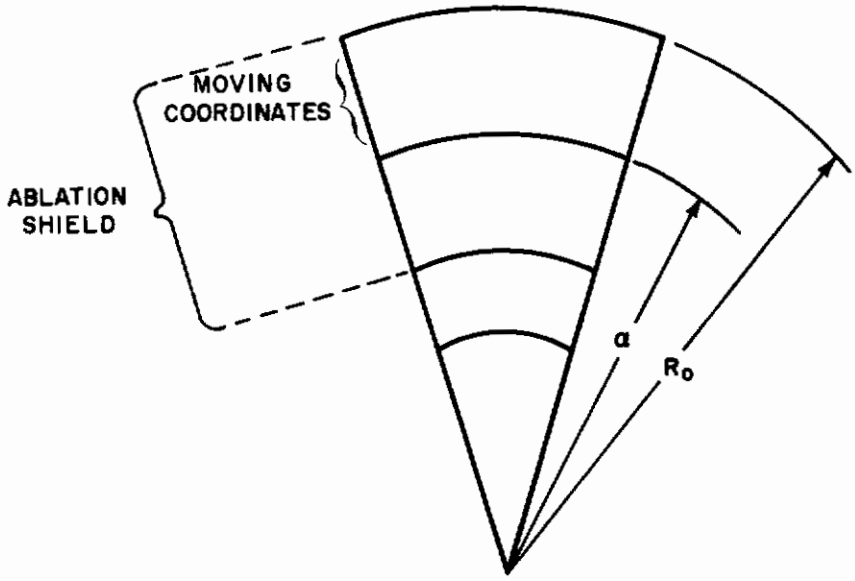

Figure XI-8 ONE-DIMENSIONAL RADIAL MODEL FOR ABLATION AND HEAT CONDUCTION

where S_i is the depth of melting of the ith strip. Transformation (XI-29) was not employed for this particular problem because the total depth of melting did not warrant it.

The equation which must now be used is

$$\rho c \frac{\partial T}{\partial t} = \frac{1}{r} \frac{\partial}{\partial r} \left(Kr \frac{\partial T}{\partial r} \right) + \frac{K}{r^2} \frac{\partial^2 T}{\partial \theta^2} \qquad \text{(XI-36)}$$

which in the ablation region becomes

$$\rho c \frac{\partial T}{\partial t} = \frac{K}{r_i^2} \frac{\partial^2 T}{\partial \xi^2} - \frac{K}{R_i (R_o - S_i - \xi R_i)} \frac{\partial T}{\partial \xi} + \frac{K}{(R_o - s - \xi R_i)^2} \frac{\partial^2 T}{\partial \theta^2} + \frac{\dot{S}_i}{R_i} (1 - \xi^{(i)}) \frac{\partial T}{\partial \xi} \rho c \, . \qquad \text{(XI-37)}$$

The boundary condition (XI-6) becomes in cylindrical coordinates

$$q_i = K \frac{\partial T}{\partial r} + \rho F \dot{S}_i \, . \qquad \text{(XI-38)}$$

The factor on q is a result of the cylindrical coordinate representation which for a normal flux input and a shrinking radius results in an increased density of flux. Under transformation (XI-32), (XI-38) becomes

$$- K \frac{\partial T}{\partial \xi} = R_i q_i - R_i \rho F \dot{S}_i \, . \qquad \text{(XI-39)}$$

There are many ways of applying finite difference methods to the space derivatives of (XI-37) and of using the boundary condition (XI 39). Purely formal approaches however can result in some formulations that are quite blatantly in contradiction to the physical situation being considered.

For example (XI-37) may be written

$$\rho c \frac{\partial T}{\partial t} = \frac{K}{R_i^2} \frac{\partial}{\partial \xi} \left(\frac{\partial T}{\partial \xi} \right) - \frac{K}{R_i (R_o - s - \xi R_i)} \frac{\partial T}{\partial \xi} + \frac{K}{(R_o - s - \xi R_i)^2} \frac{\partial^2 T}{\partial \theta^2} + \rho c \frac{\dot{S}_i}{R_i} (1 - \xi) \frac{\partial T}{\partial \xi} \, . \qquad \text{(XI-40)}$$

For boundary cells it would seem mathematically proper to insert (XI-39) into (XI-40) for the corresponding $\partial T / \partial \xi$ term. It can be shown that such a formal substitution will not result in a steady state heat balance, the reason being that not all the $\partial T / \partial \xi$'s of (XI-40) are flux terms. The last term with the s factor is a convection term due to moving coordinates. The first two terms on the right can be written

$$\frac{K}{R_i^2 (R_o - s - \xi R_i)} \quad \frac{\partial}{\partial \xi} \left([R_o - s - \xi_i R_i] \frac{\partial T}{\partial \xi} \right) . \qquad \text{(XI-41)}$$

This is the only term to which the boundary condition is applied since this is the only one involving fluxes in the ξ-direction.

The problem was programmed on the analogue computer and the results for the wing leading edge of a re-entry glider are shown and discussed in the body of the main report (Section VII C.-2).

C. REFERENCES

1. Hurwicz, H. and J. A. Collins, Thermal Analysis of the Shape 52 ICBM Re-entry Vehicle, Avco RAD-TR-9-59-10 (30 March 1959).

2. Beck, J., Axisymmetric Transient Heat Conduction In a Rocket Nozzle Calorimeter, Avco RAD-7(VIII)-TM-60-6 (7 April 1960).

3. Wolf, H., A Program Analysis For Two-Dimensional Heat Flow, Avco RAD-9-TM-59-1 (17 February 1959).

4. Baylor, R. N. and C. L. Conrey, The Calculation of the Effects of Internal Cross Radiation on Transient Temperature Distributions in Hypersonic Vehicles, Chance-Vought Report No. E9R-12456 (26 October 1959).

5. Fleddermann, R. G. and H. Hurwicz, Analysis of Transient Ablation and Heat Conduction Phenomena at a Vaporizing Surface, Chemical Engineering Symposium Series, 57 (32) 24 (1960) also Avco RAD-TR-9(7)-60-9 (April 1960).

6. Hurwicz, H. and R. G. Fleddermann, Computer Simulation of Transient Ablation and Heat Conduction Phenomena at a Vaporizing Surface, presented at the ARS Spaceflight Report to the Nation, New York (1961) Paper No. 2209-61.

7. Zlotnick, M. and B. Nordquist, Calculation of Transient Ablation, presented at International Heat Transfer Conference, September 1961, Boulder, Colorado.

8. Hurwicz, H. and T. Brady, On Two- and Three-Dimensional Ablation Simulation, Avco RAD technical report to be published.

9. Adams, E. W., Analysis of Quartz and Teflon Shields for a Particular Re-entry Mission, Proc. of 1961 Heat Transfer and Fluid Mech. Inst., Pasadena, California (June 1961).

10. Hurwicz, H., Aerothermochemistry Studies in Ablation, to be presented at the Fifth AGARD Combustion and Propulsion Colloquium (9-13 April 1962) Braunschweig, Germany.

11. Nolan, E. J. and S. M. Scala, The Aerothermodynamic Behavior of Pyrolytic Graphite During Sustained Hypersonic Flight, ARS Conference on Lifting Re-entry Vehicles, Palm Springs, Calif. (April 1961), Paper No. 1696-61.

12. Forsythe, G. and W. Wasow, Finite Difference Methods for Partial Differential Equations, John Wiley and Sons (1960).

13. Fifer, S., Analogue Computations, Vols. I-IV, McGraw-Hill Book Co., Inc. (1961).

14. Carslaw, H. S. and J. C. Jaegar, Conduction of Heat in Solids, Oxford at the Clarendon Press, 2nd Ed. (1959).

15. Landau, H. G., Heat Conduction in Melting Solids, Quarterly of Appl. Math., 8, 81 (1950).

16. Dian Laboratories, Private Communication to H. Hurwicz Avco RAD Wilmington, Mass.

APPENDIX XII

WORKING GRAPHS FOR PARAMETRIC STUDIES

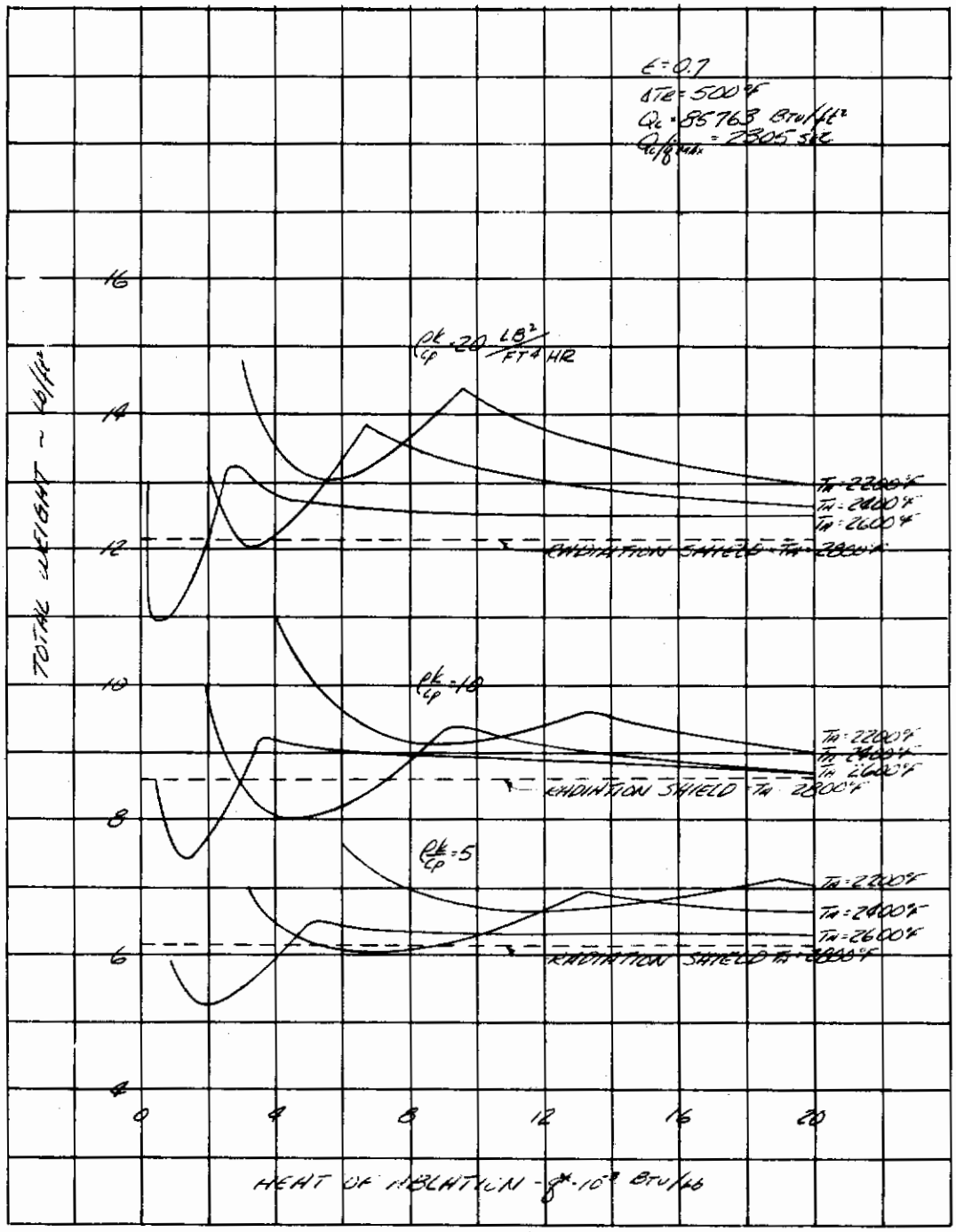

Figure XII-1 INFLUENCE OF HEAT OF ABLATION ON THE TOTAL SHIELD WEIGHT FOR VARIATION OF THE THERMAL PROPERTIES, Q_c = 85,763 BTU/FT^2, ΔT_R = 500 °F

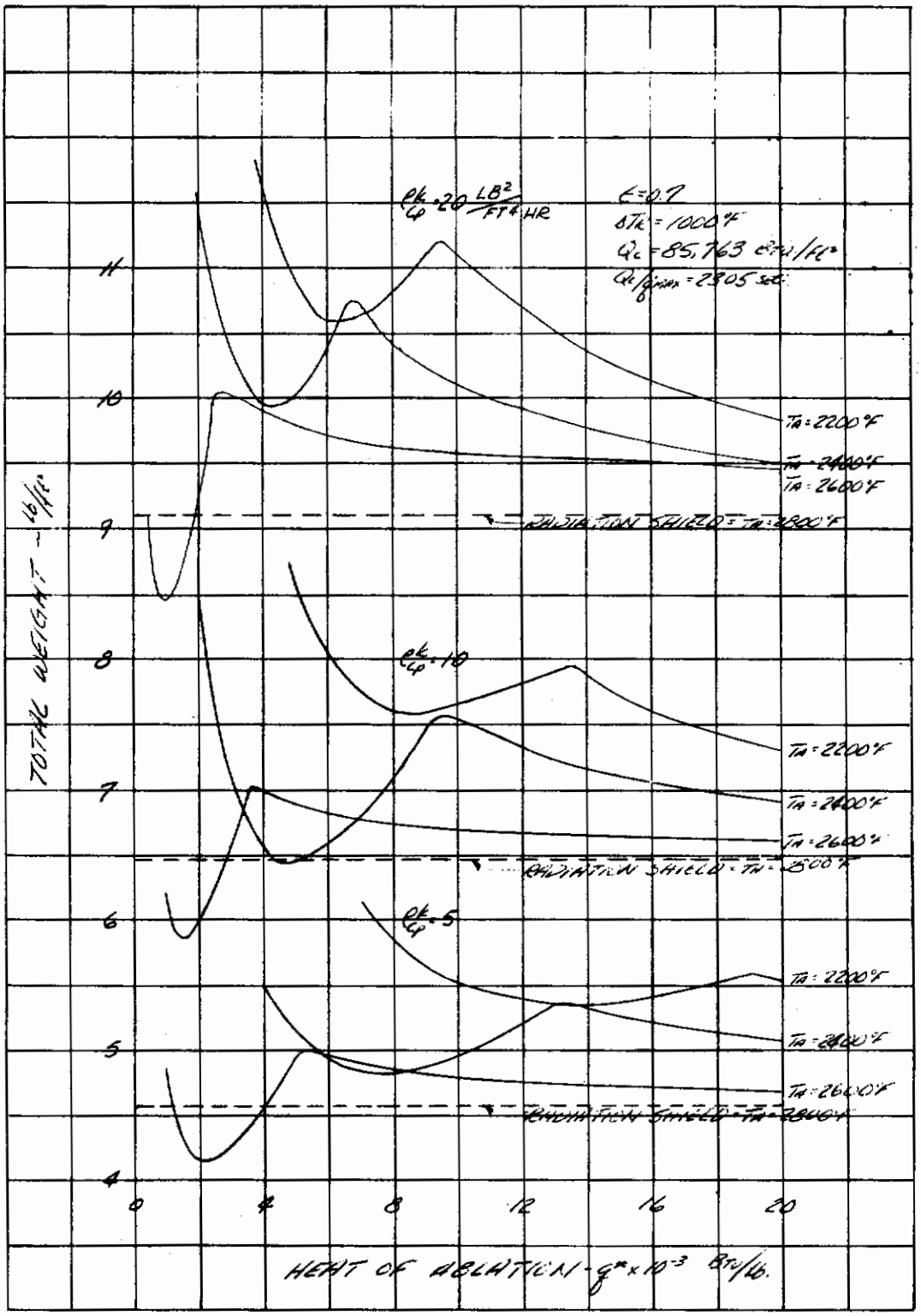

Figure XII-2 INFLUENCE OF HEAT OF ABLATION ON THE TOTAL SHIELD WEIGHT FOR VARIATION OF THE THERMAL PROPERTIES, $Q_c = 85,763$ BTU/FT^2, $\Delta T_R = 1000°F$

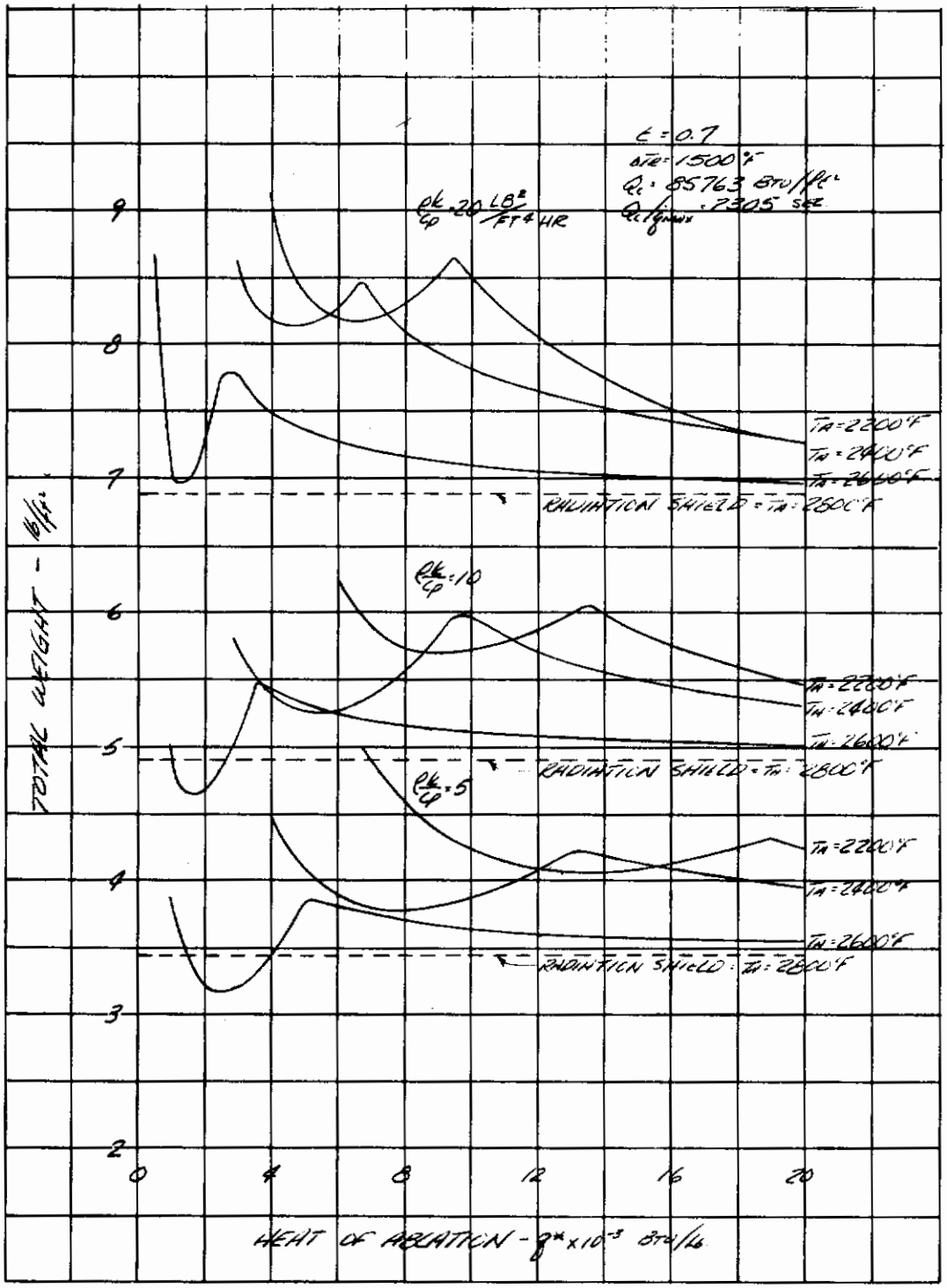

Figure XII-3 INFLUENCE OF HEAT OF ABLATION ON THE TOTAL SHIELD WEIGHT FOR VARIATION OF THE THERMAL PROPERTIES, Q_c = 85, 763 BTU/FT^2, ΔT_R = 1500 °F

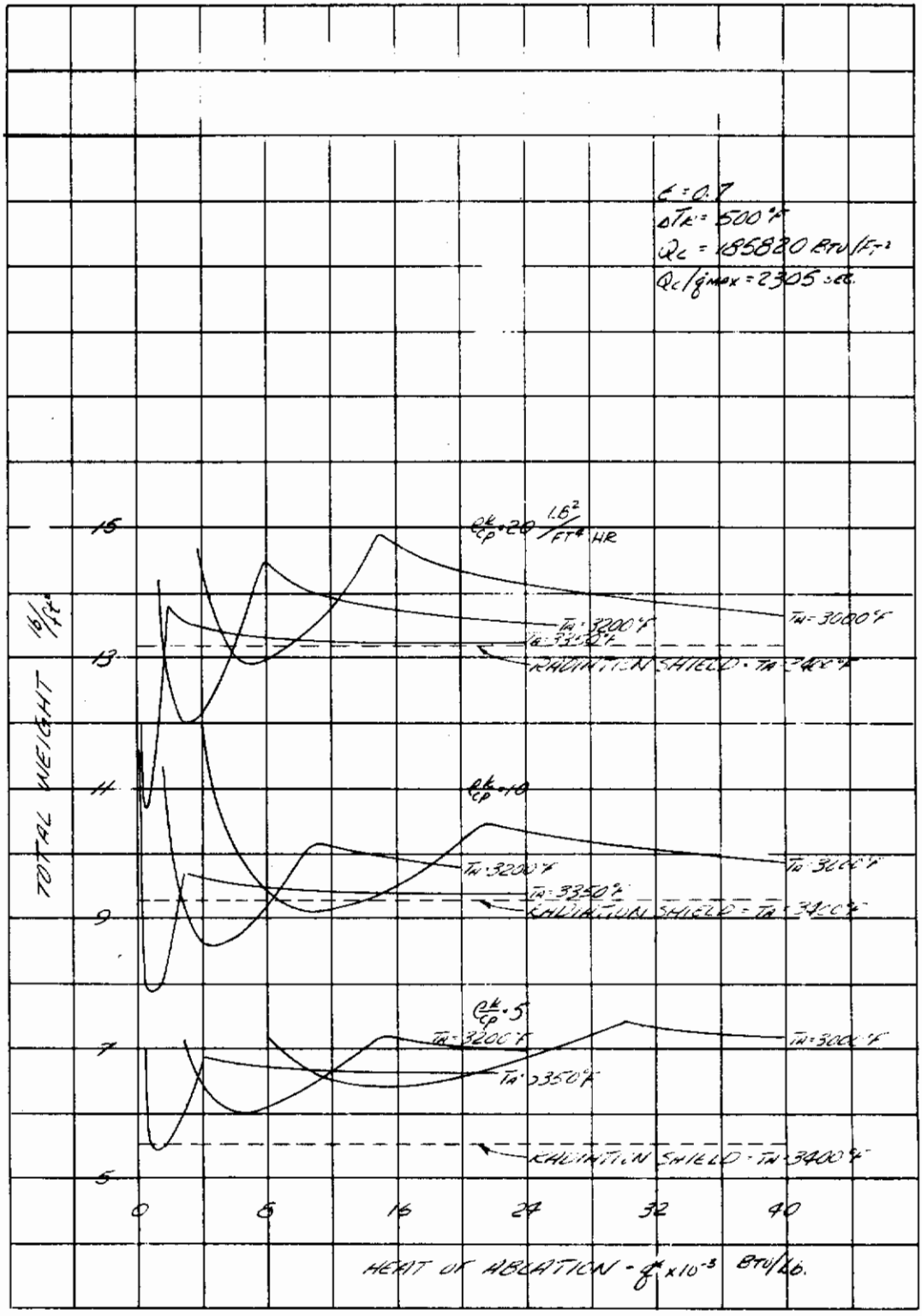

Figure XII-4 INFLUENCE OF HEAT OF ABLATION ON THE TOTAL SHIELD WEIGHT FOR VARIATION OF THE THERMAL PROPERTIES, Q_c = 185, 820 BTU/FT^2, ΔT_R = 500 °F

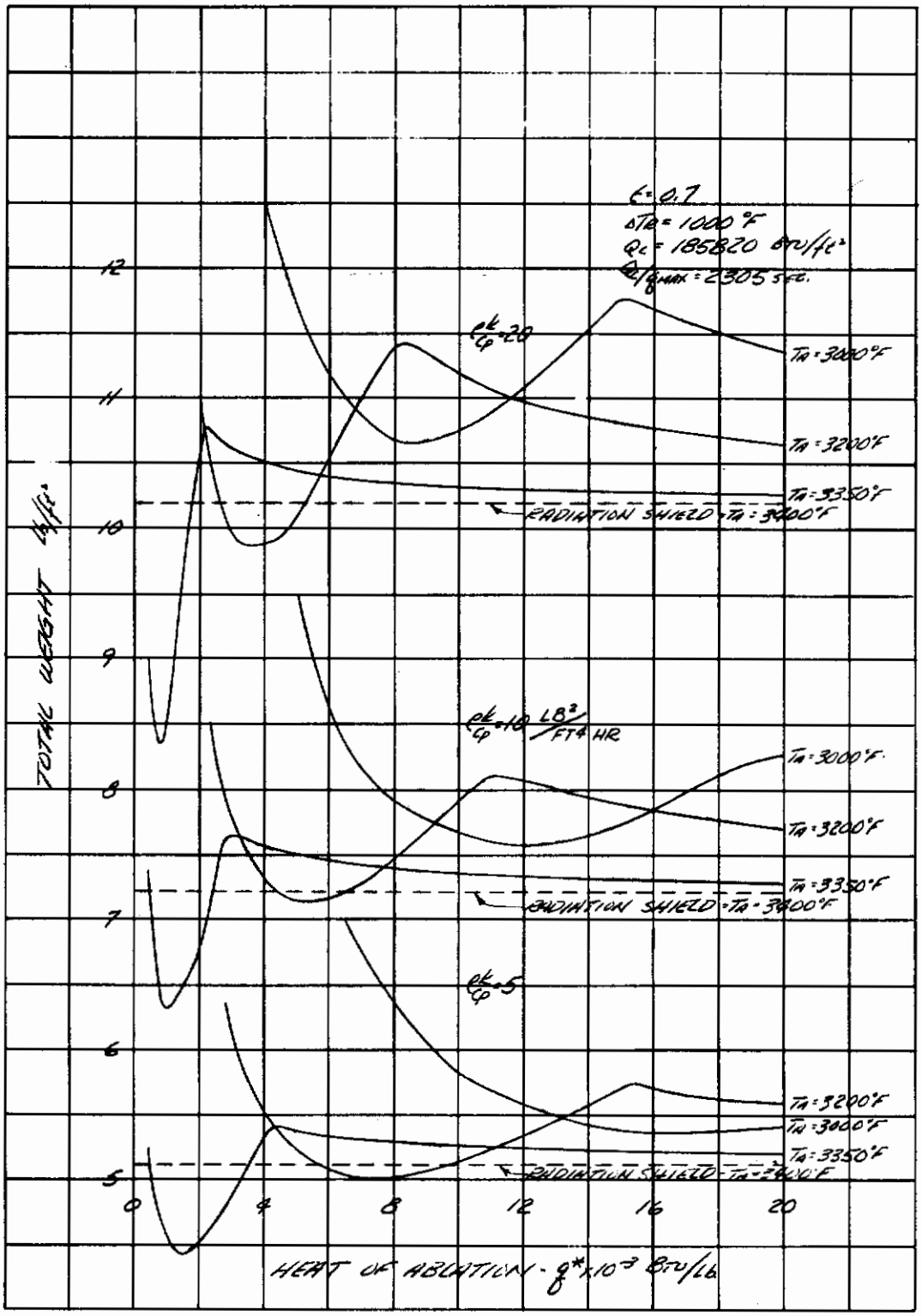

Figure XII-5 INFLUENCE OF HEAT OF ABLATION ON THE TOTAL SHIELD WEIGHT FOR VARIATION OF THE THERMAL PROPERTIES, Q_c = 185,820 BTU/FT^2, ΔT_R = 1000 °F

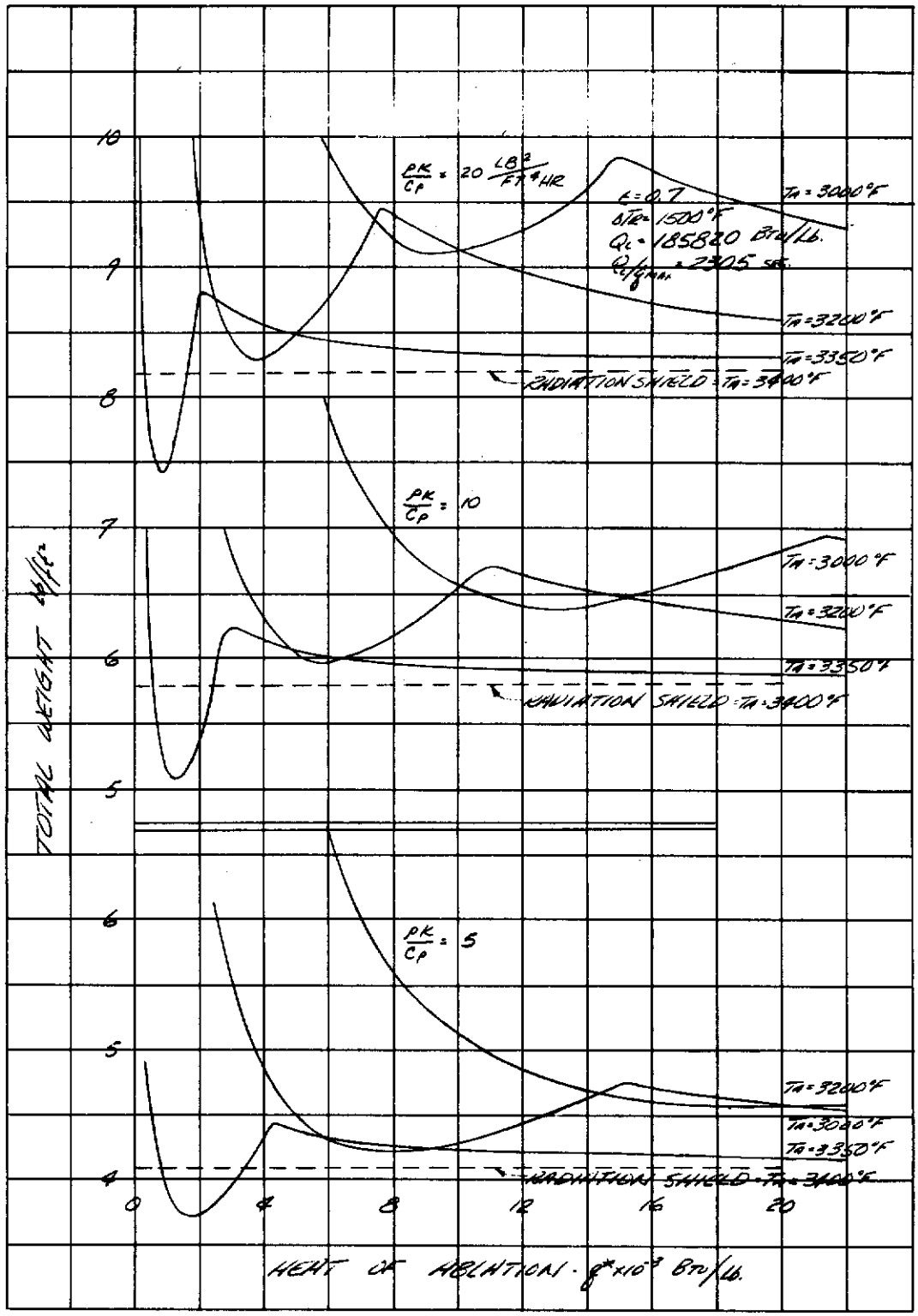

Figure XII-6 INFLUENCE OF HEAT OF ABLATION ON THE TOTAL SHIELD WEIGHT FOR VARIATION OF THE THERMAL PROPERTIES, Q_c = 185,820 BTU/FT^2, ΔT_R = 1500 °F

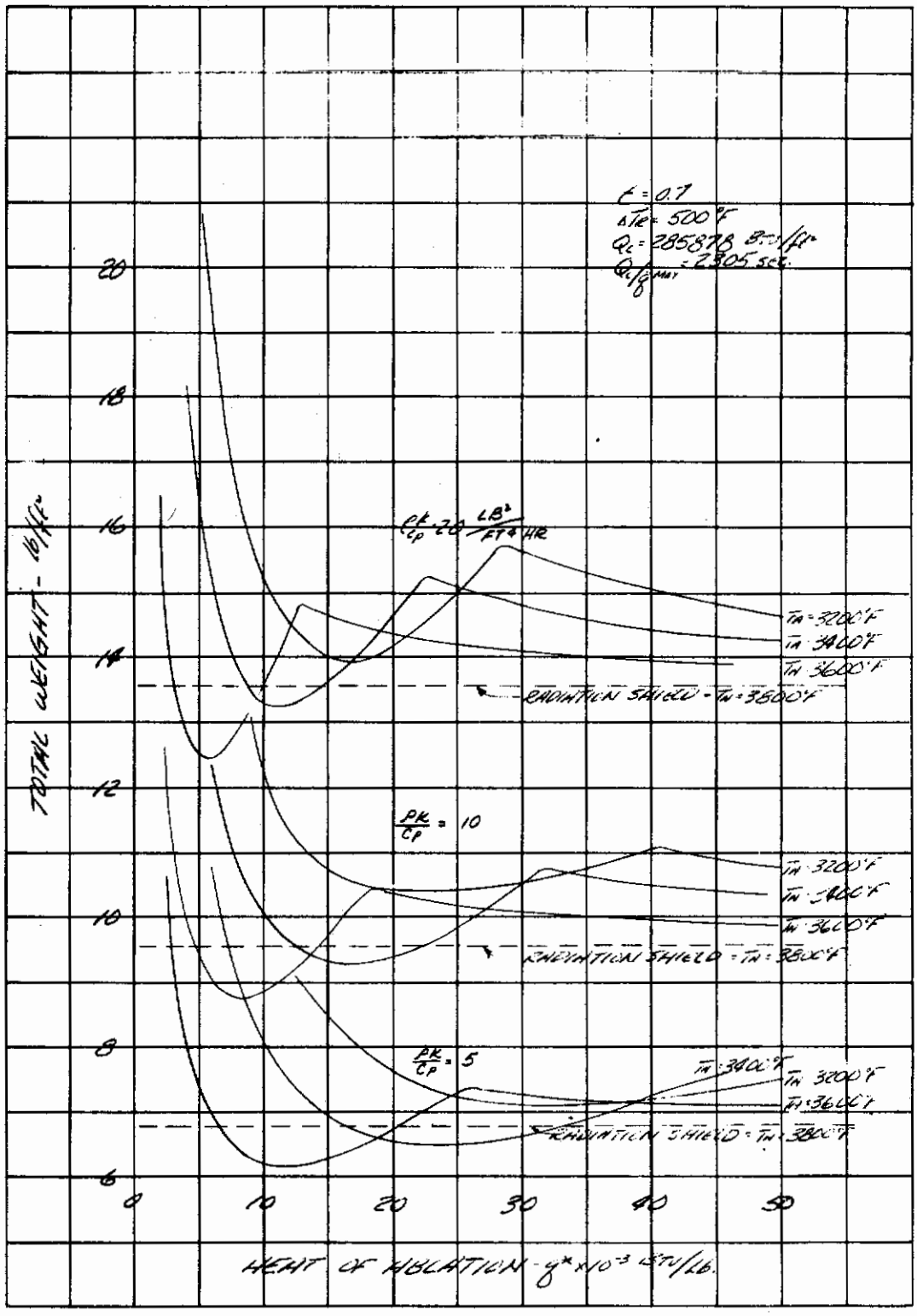

Figure XII-7 INFLUENCE OF HEAT OF ABLATION ON THE TOTAL SHIELD WEIGHT FOR VARIATION OF THE THERMAL PROPERTIES, Q_c = 285, 878 BTU/FT^2, ΔT_R = 500 °F

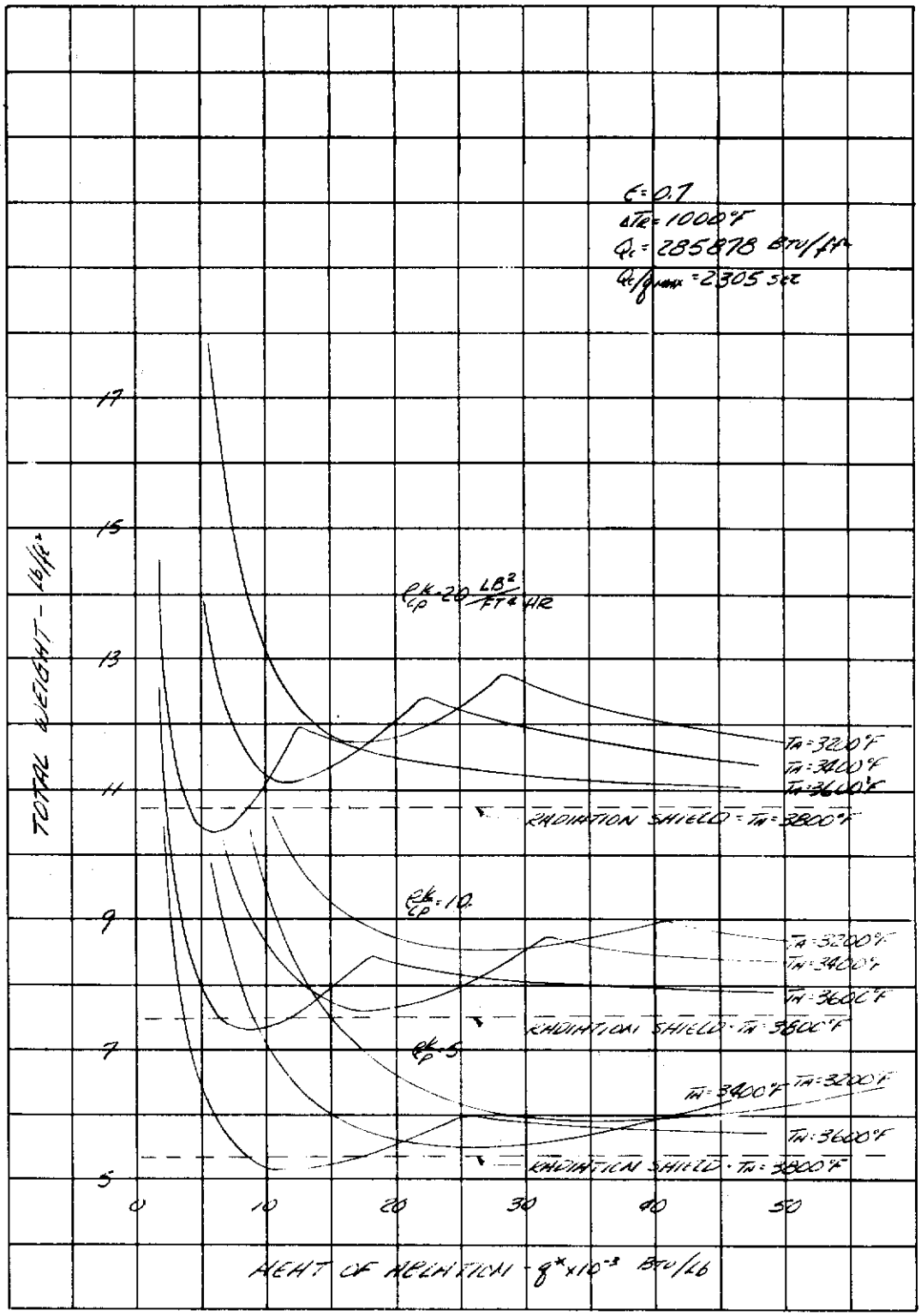

Figure XII-8 INFLUENCE OF HEAT OF ABLATION ON THE TOTAL SHIELD WEIGHT FOR VARIATION OF THE THERMAL PROPERTIES, Q_c = 285, 878 BTU/FT^2, ΔT_R = 1000 °F

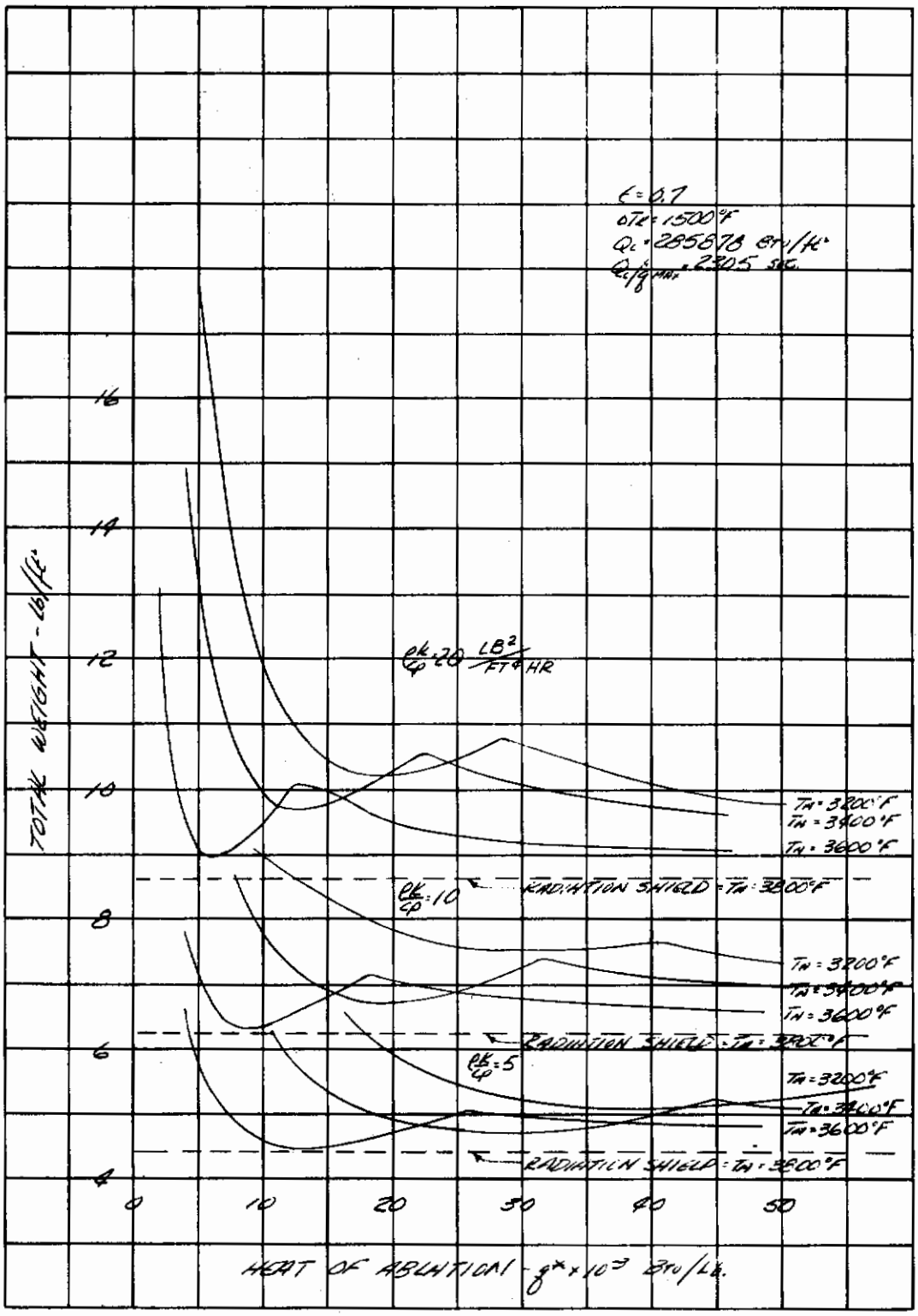

Figure XII-9 INFLUENCE OF HEAT OF ABLATION ON THE TOTAL SHIELD WEIGHT FOR VARIATION OF THE THERMAL PROPERTIES, Q_c = 285,878 BTU/FT^2, ΔT_R = 1500 °F

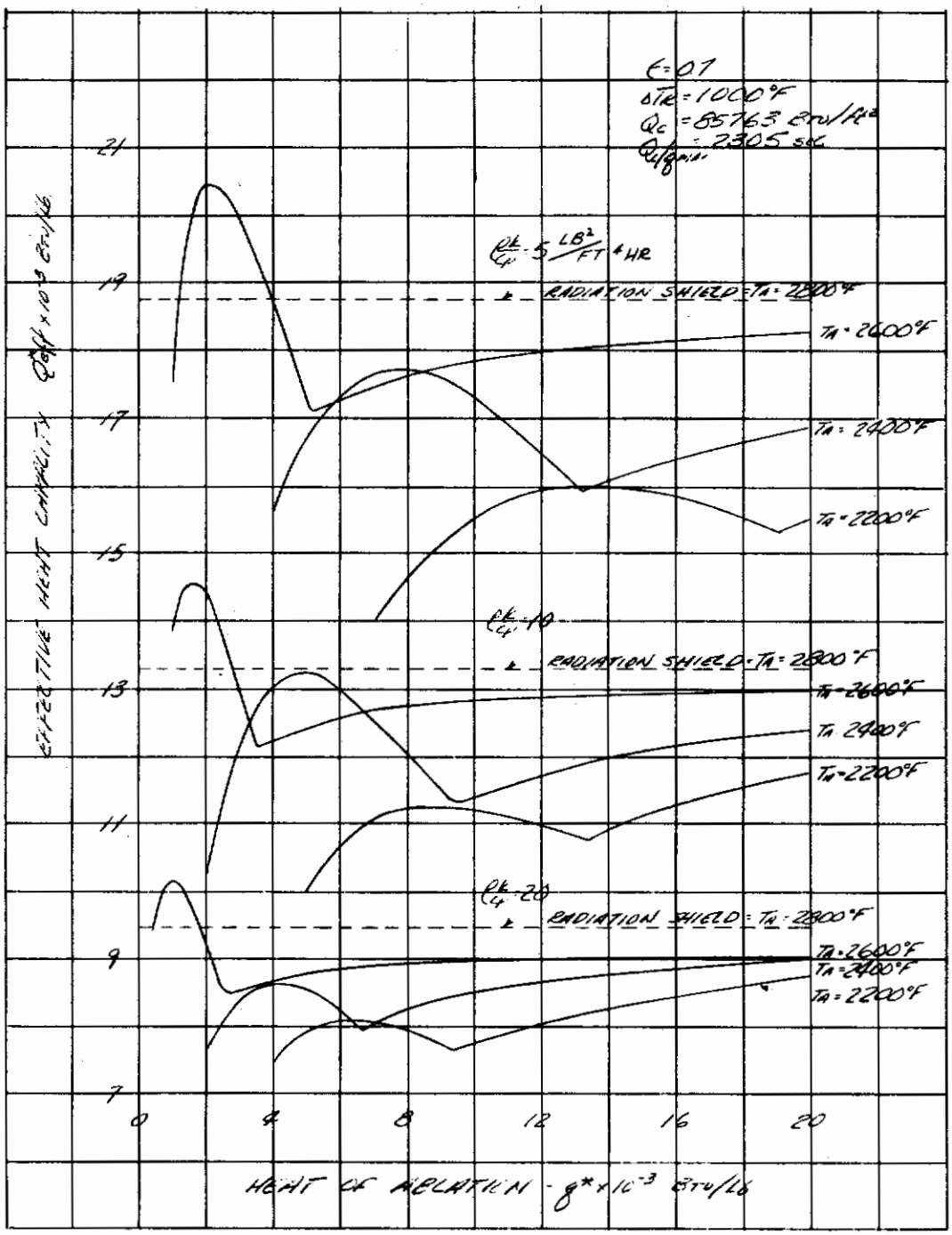

Figure XII-10 INFLUENCE OF HEAT OF ABLATION ON THE EFFECTIVE HEAT CAPACITY FOR VARIATION OF THE THERMAL PROPERTIES, Q_c = 85, 763 BTU/FT^2, ΔT_R = 1000 °F

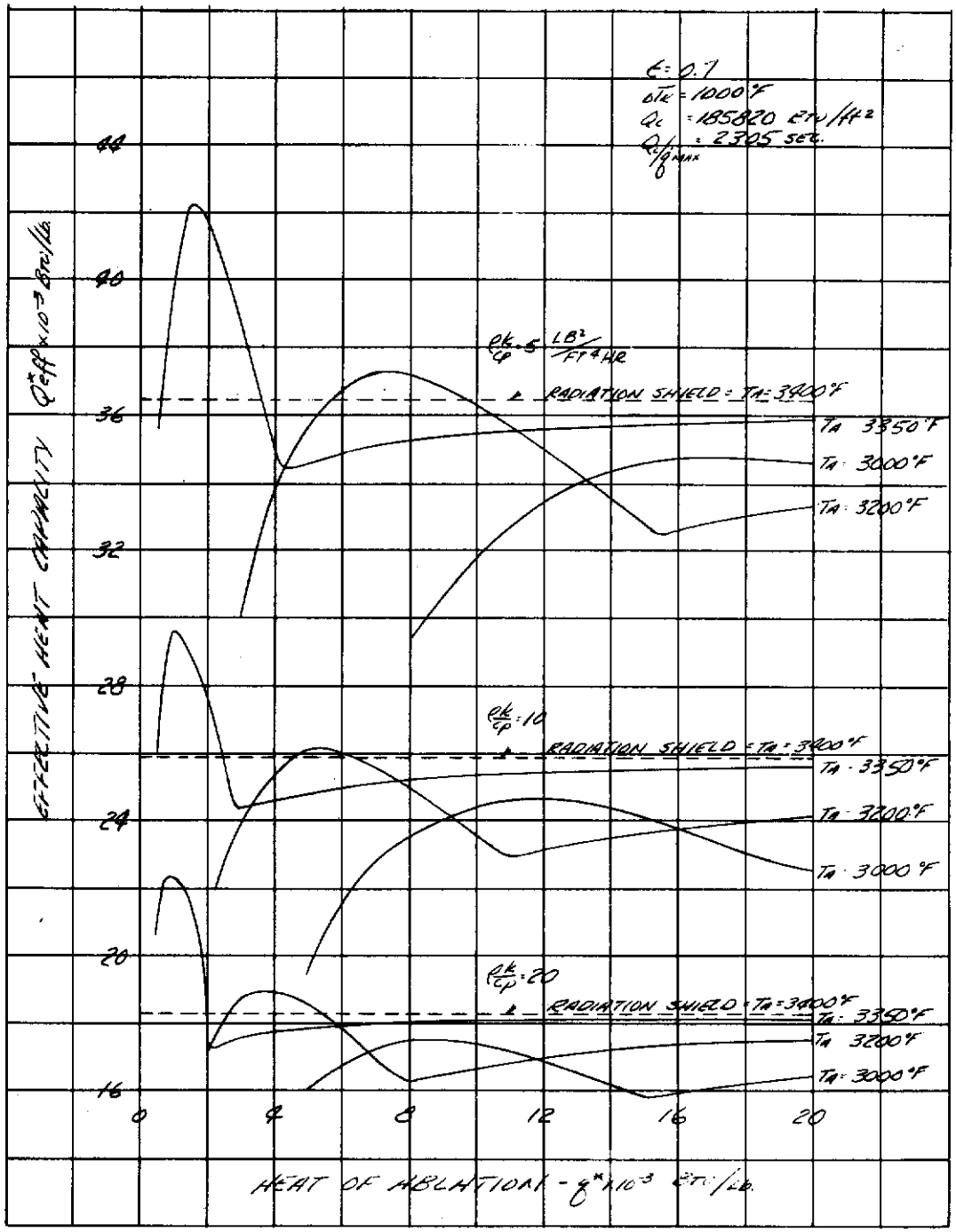

Figure XII-11 INFLUENCE OF HEAT OF ABLATION ON THE EFFECTIVE HEAT CAPACITY FOR VARIATION OF THE THERMAL PROPERTIES, Q_c = 185,820 BTU/FT^2, ΔT_R = 1000°F

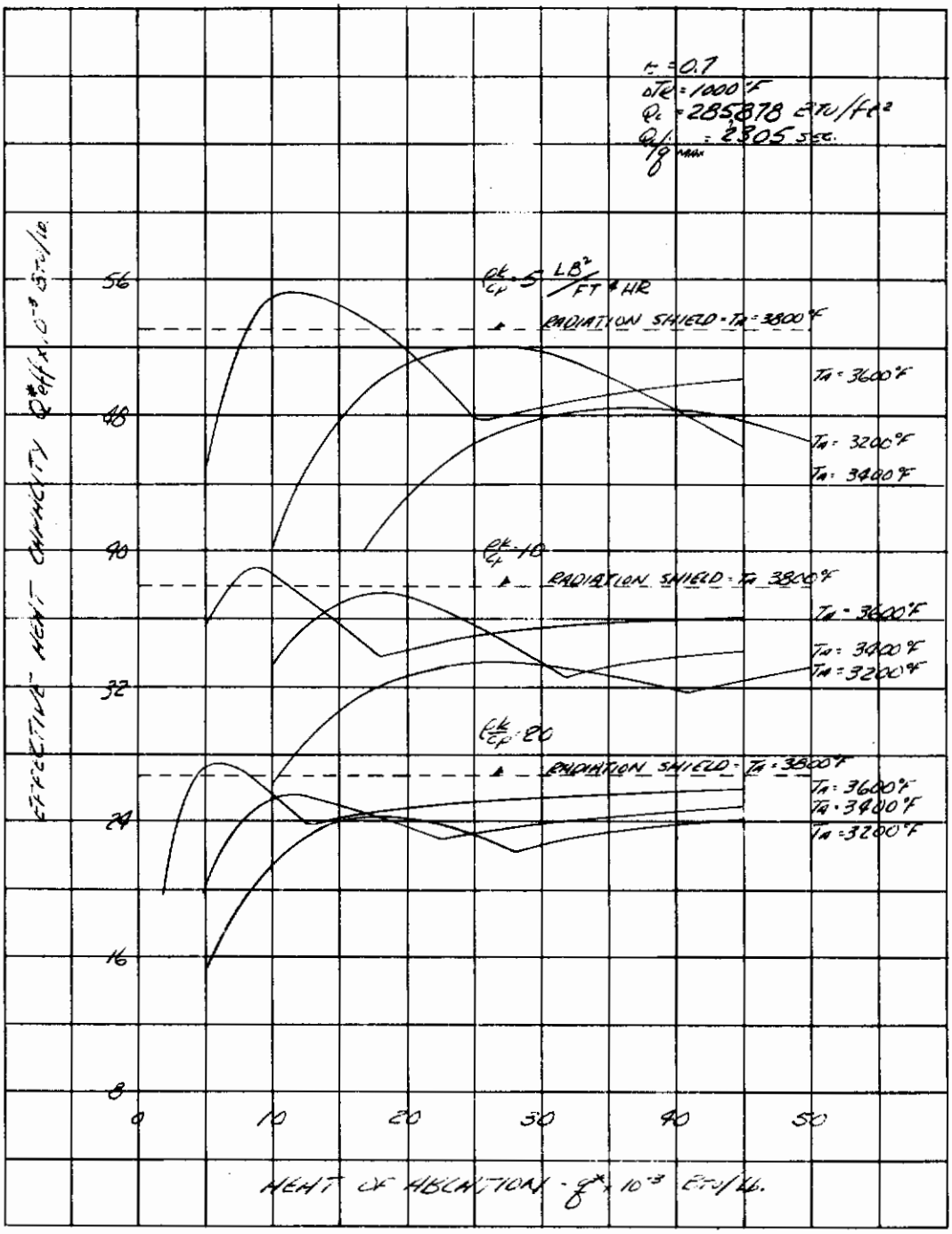

Figure XII-12 INFLUENCE OF HEAT OF ABLATION ON THE EFFECTIVE HEAT CAPACITY FOR VARIATION OF THE THERMAL PROPERTIES, Q_c = 285, 878 BTU/FT^2, ΔT_R = 1000 °F

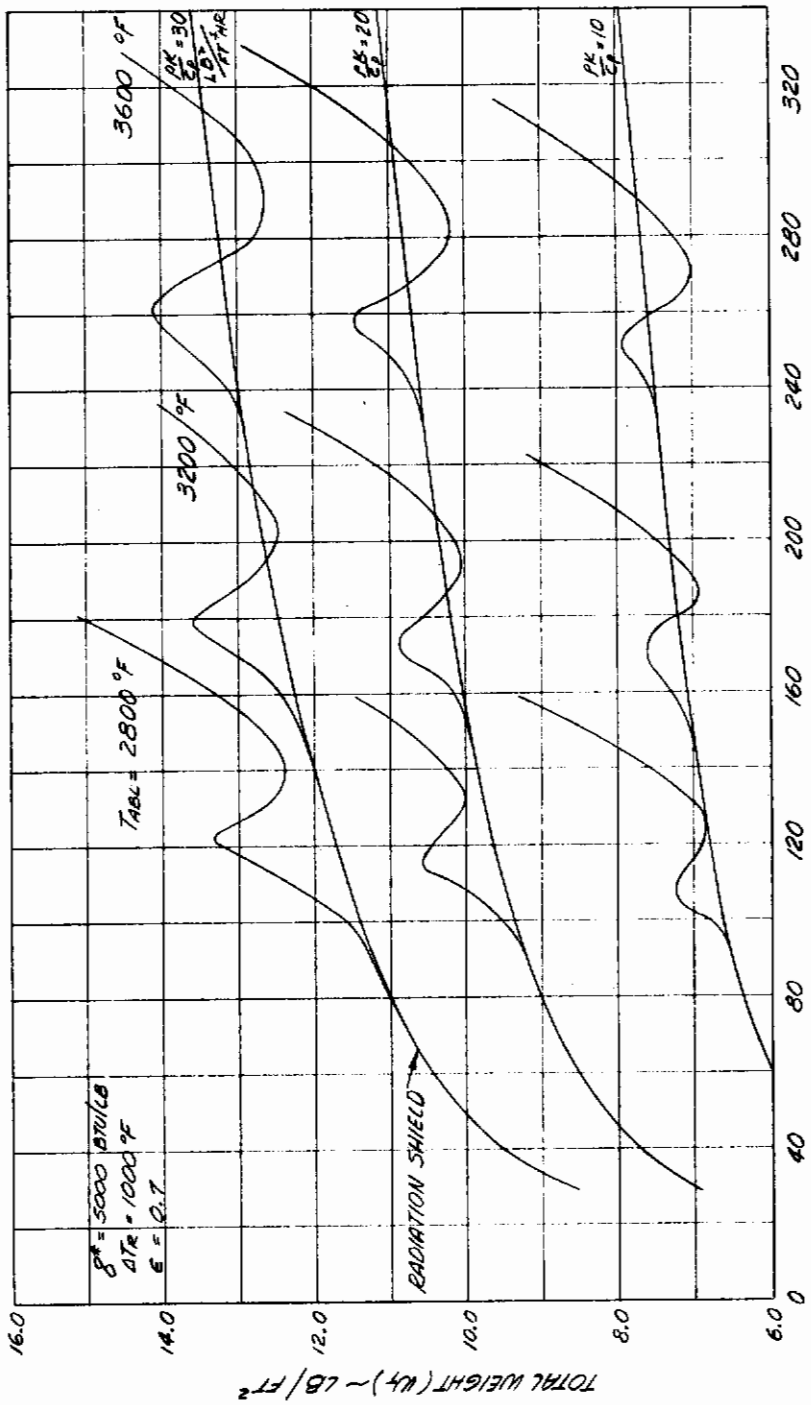

Figure XII-13 INTERACTION OF ABLATION TEMPERATURE AND HEAT OF ABLATION ON THE TOTAL WEIGHT $q^* = 5000$ BTU/LB

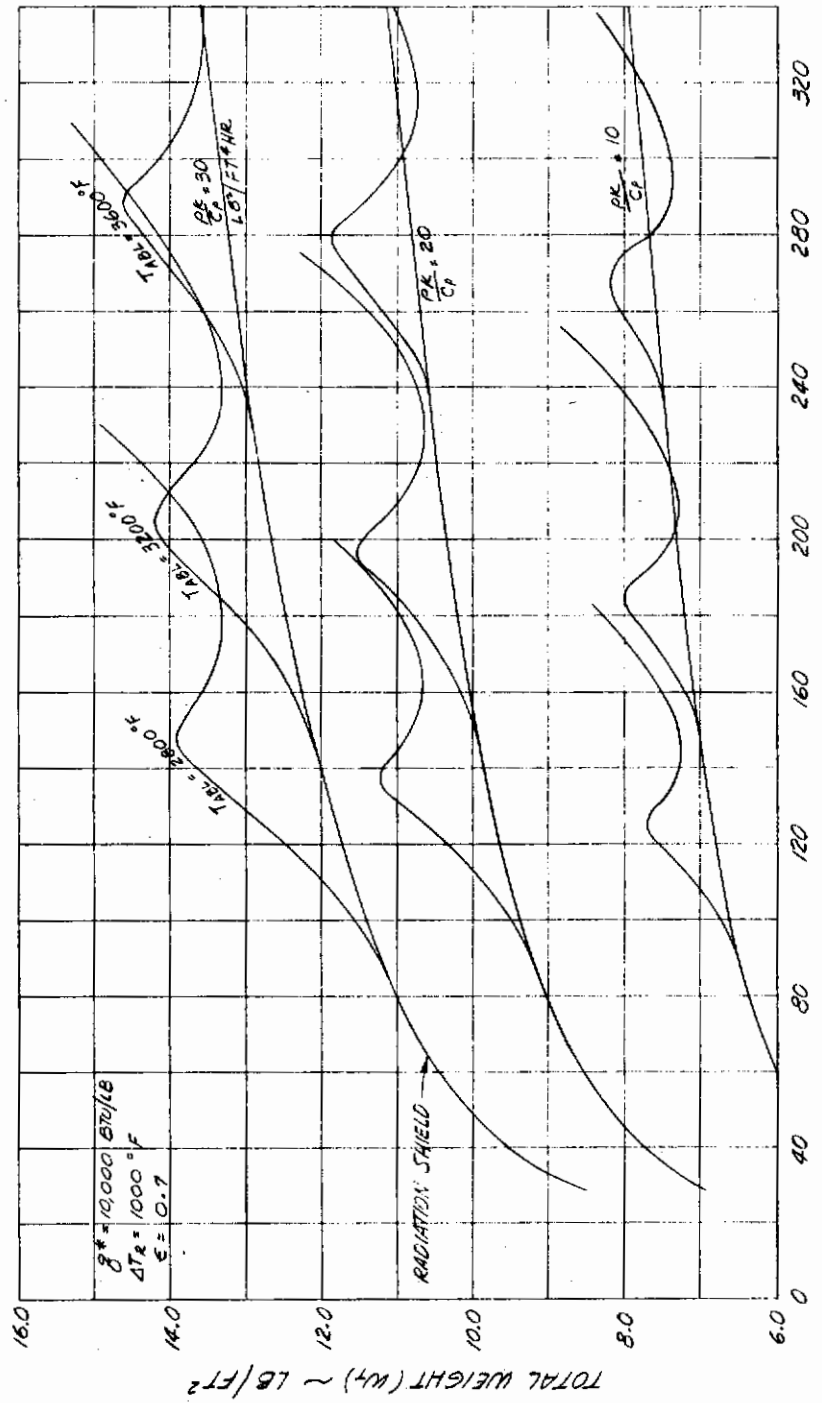

Figure XII-14 INTERACTION OF ABLATION TEMPERATURE AND HEAT OF ABLATION ON THE TOTAL WEIGHT $q^* = 10,000$ BTU/LB

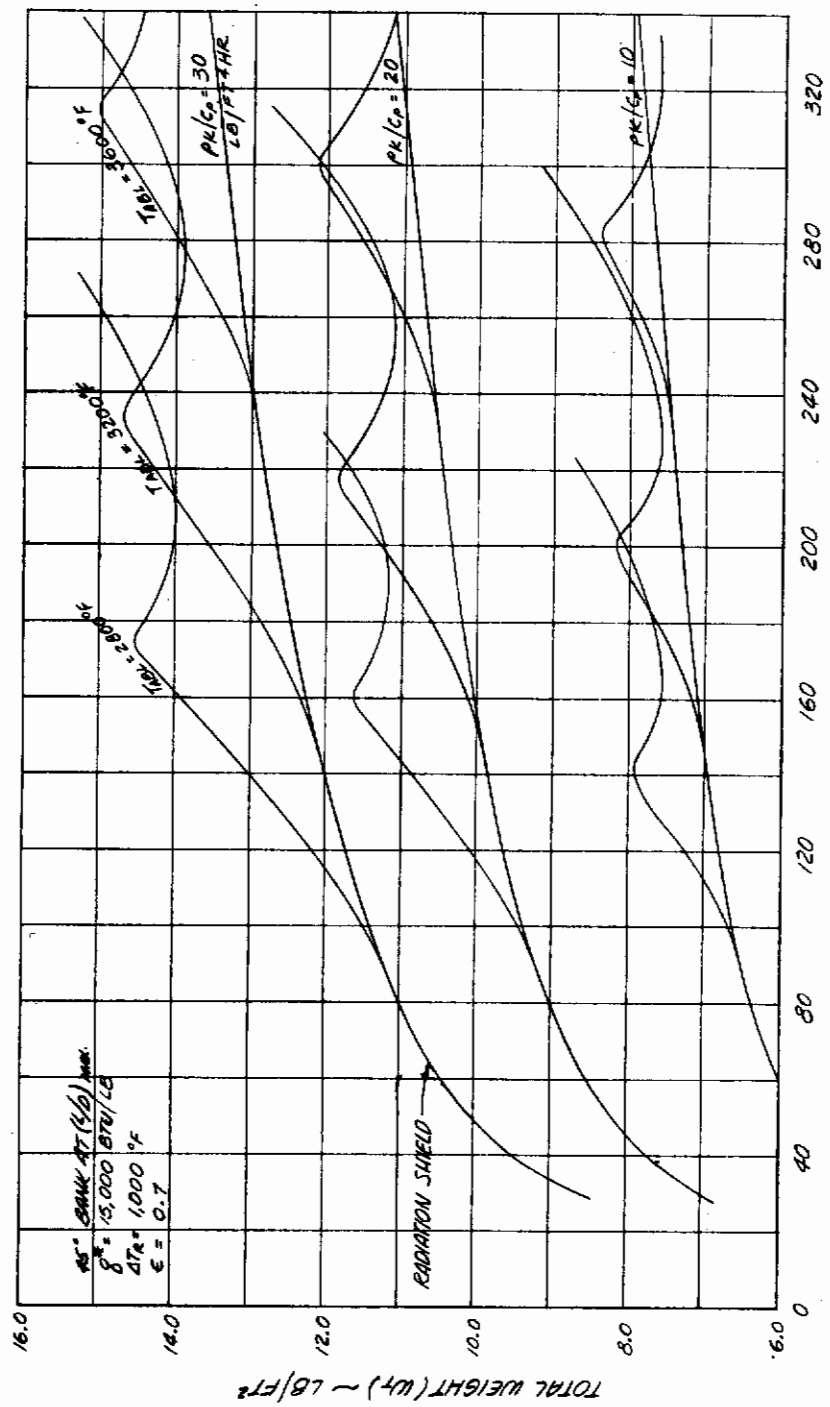

Figure XII-15 INTERACTION OF ABLATION TEMPERATURE AND HEAT OF ABLATION ON THE TOTAL WEIGHT $q^* = 15,000$ BTU/LB

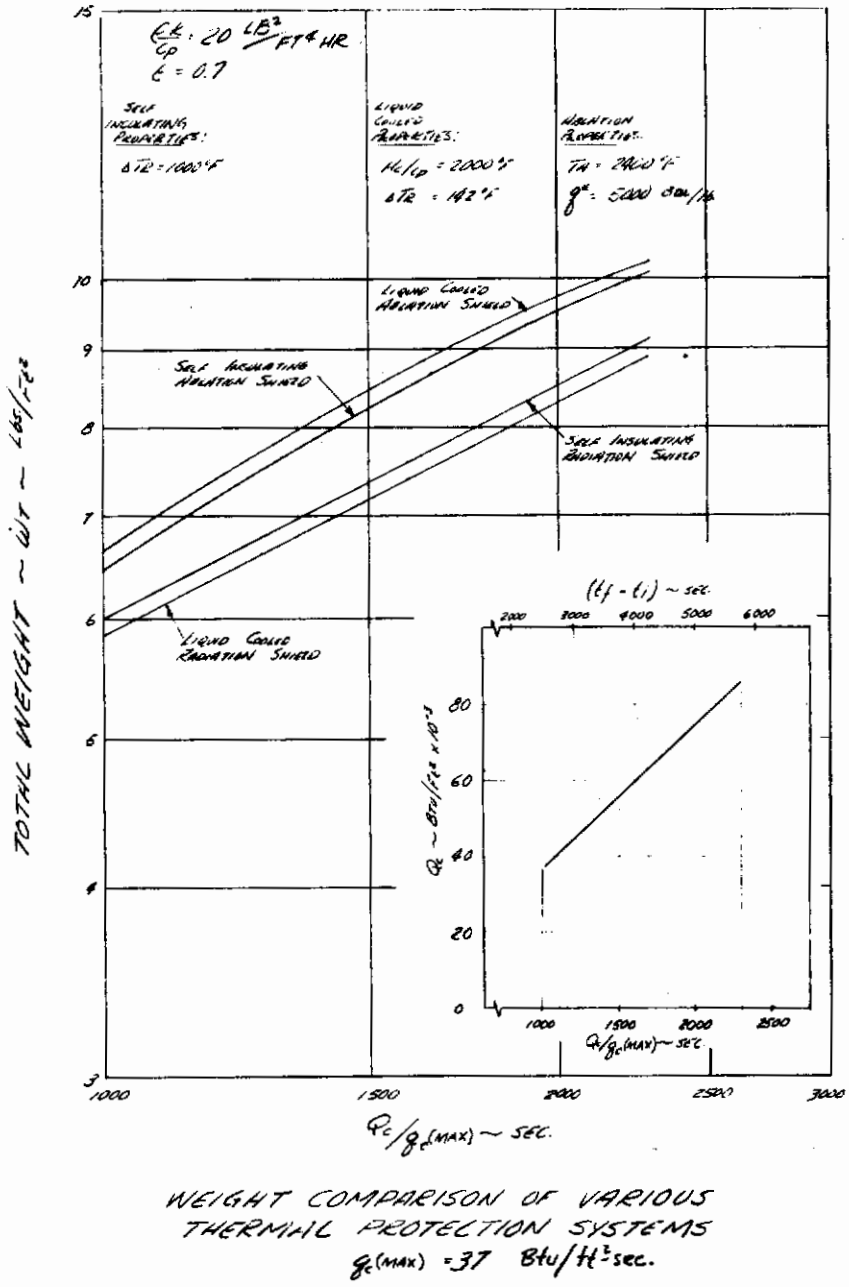

Figure XII-16 EFFECT OF THERMAL ENVIRONMENT ON THE WEIGHT OF RADIATION-ABLATION SHIELDS AND RADIATION SHIELDS
$q_{c(max)}$ = 37 BTU/FT^2-SEC

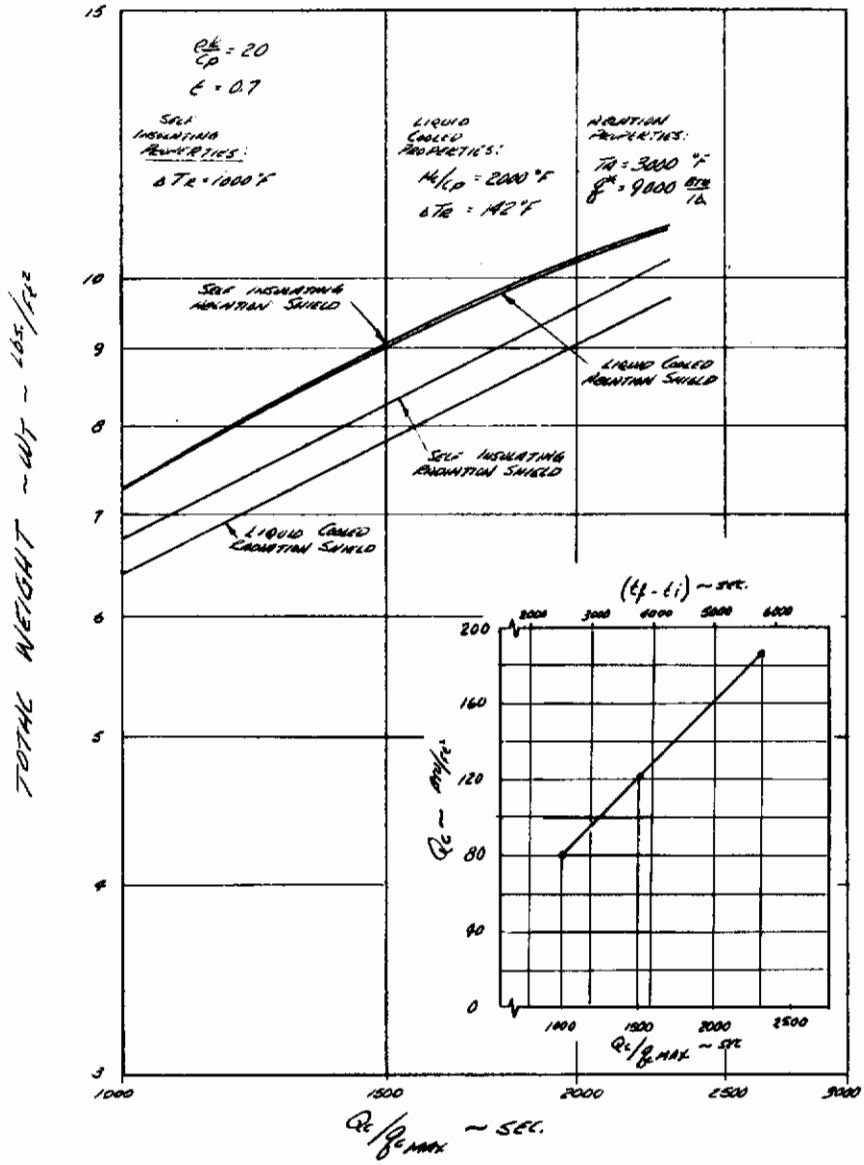

Figure XII-17 EFFECT OF THERMAL ENVIRONMENT ON THE WEIGHT OF RADIATION-ABLATION SHIELDS AND RADIATION SHIELDS
$q_{c(max)}$ = 81 BTU/FT^2-SEC

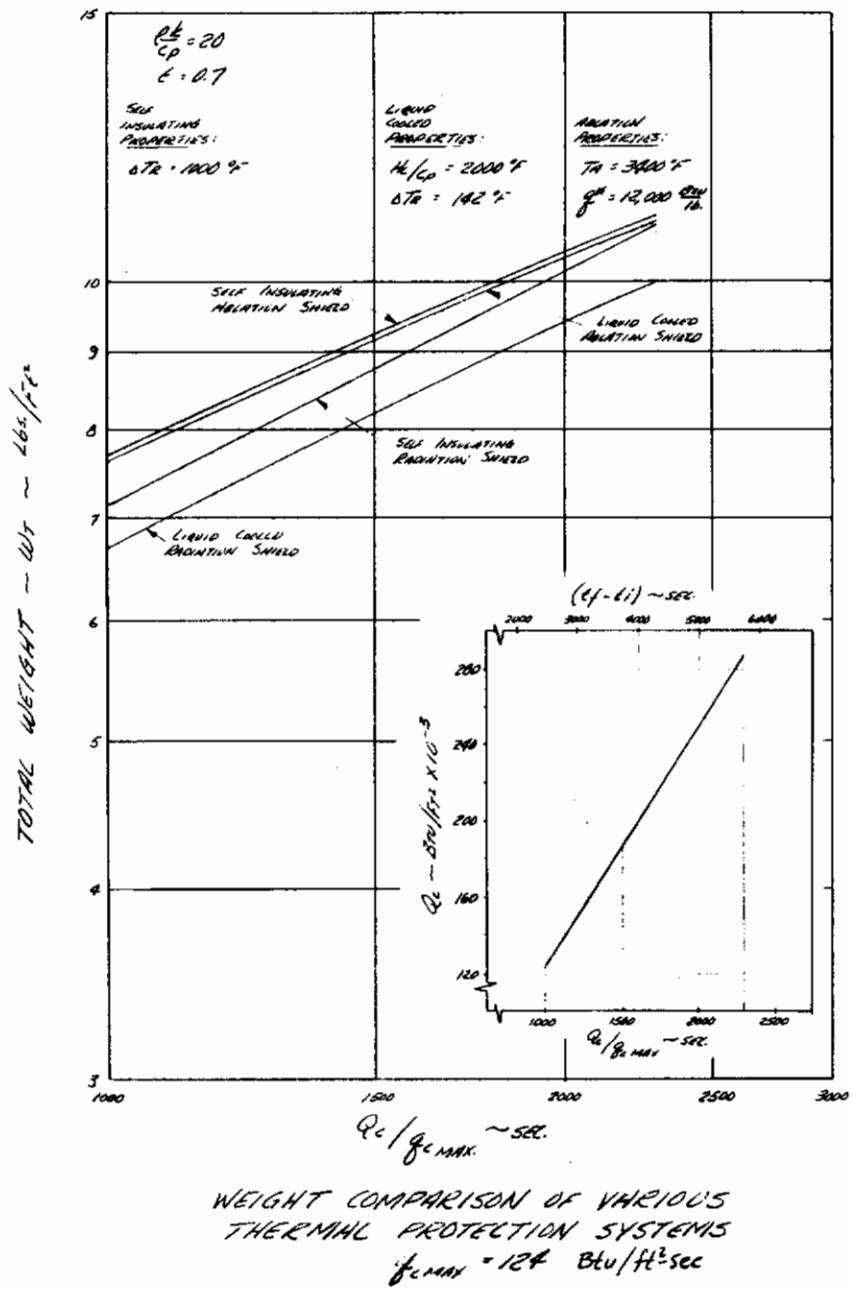

Figure XII-18 EFFECT OF THERMAL ENVIRONMENT ON THE WEIGHT OF RADIATION-ABLATION SHIELDS AND RADIATION SHIELDS
q_c(max) = 124 BTU/FT^2-SEC

APPENDIX XIII

SAMPLE PROBLEMS USING AN APPROXIMATE METHOD FOR DESIGN OF THERMAL PROTECTION SYSTEMS FOR GLIDE RE-ENTRY VEHICLES OR SYSTEMS IN WHICH THE PREDOMINANT THERMAL MECHANISM IS SURFACE RADIATION AND OR ABLATION

A. NECESSARY INFORMATION

1. Aerodynamic Heating

$q_{c_{max}}$ = 81.0 Btu/ft^2-sec

$Q_c/q_{c_{max}}$ = 2300 secs

t_o = 0 secs.

$t_{q_{max}}$ = 3300 secs.

t_f = 6000 secs.

q_c = as f(t) (from figure XIII-1)

2. Free-Stream Gas Enthalpy

$Hg/RT_o\Big|_{t_{q_{c_{max}}}}$ = 270

Hg/RT_o as f(t) (from figure XIII-1)

3. Initial Temperature

T_i = 70°F .

4. Design Maximum Temperature

T_R = 570° F (T_R = 70° F for liquid-cooled shields).

5. Radiation Shield Properties (Wins)

ρ = 100 lb/ft^3

k = 0.04 Btu/hr-ft^2-°F/ft

C_p = 0.2 Btu/lb-°F

ϵ = 0.7

T_A = too large for ablation (see step C.2)

6. Ablation Properties (Wa)

T_A = 3000° F

q^* = 10,000 Btu/lb.

7. Backup Structure Properties (Wst)

ρ = 120 lb/ft^3

L = 0.20 in.

C_p = 0.2 Btu/lb-° F

ϵ = 0.7

k = sufficiently high so that no appreciable temperature gradient will exist.

8. Liquid Coolant Properties (Wc)

H_c = 400 Btu/lf (this includes the thermal capacity of the structure).

9. Hot Radiating Skin (Wsk)

ρ = 125 lb/ft^3

L = 0.048 in.

C_p = 0.49 Btu/lb-° F

k = 0.23 Btu/hr-ft^2-° F/ft

ϵ = 0.9

T_A = 6600° F too large for ablation (See Step J.1).

B. SCHEMES

1. Self-Insulating Radiation Shield

2. Self-Insulating Ablation Shield

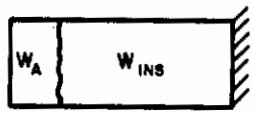

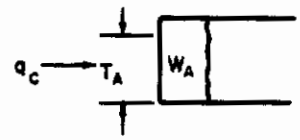

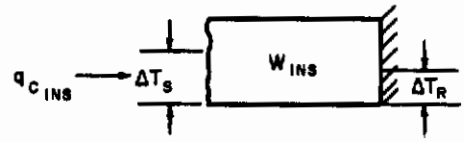

3. Radiation Shield and Structure

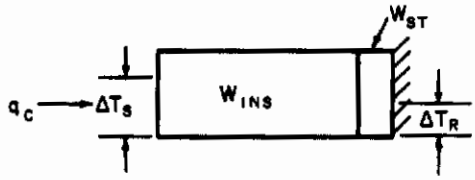

4. Ablation Shield and Structure

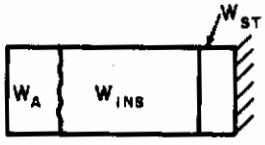

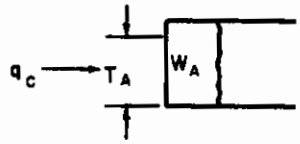

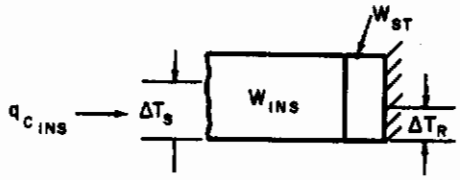

5. Liquid-Cooled Radiation Shield

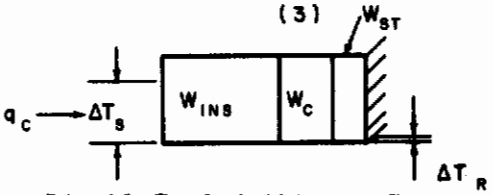

6. Liquid-Cooled Ablation Shield

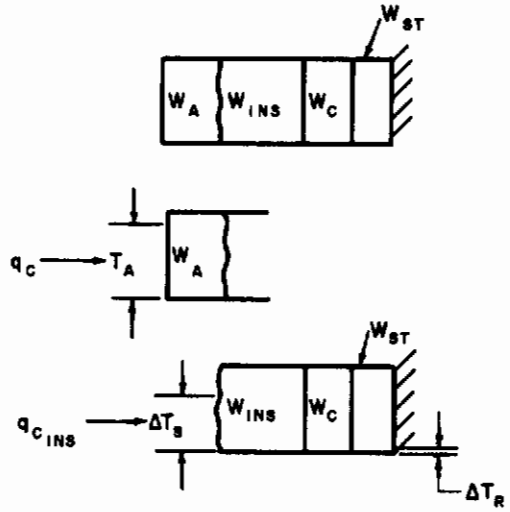

7. Hot Radiating Skin plus Insulation

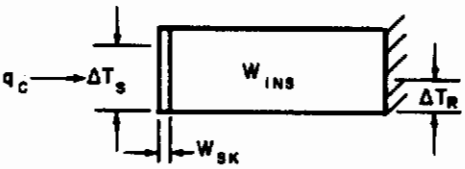

C. GENERAL CALCULATION PROCEDURE

1. Solve for the Initial Time of the Problem

$$t_i = t_{q_{c_{max}}} - \frac{2}{q_{c_{max}}} \int_{t_o}^{t_{q_{c_{max}}}} q_c \, dt$$

$$= 3300 - \frac{2}{81} (124{,}700) = 220 \text{ secs}$$

2. Check for Ablation

a. Let $T_s = T_A = 3390^\circ F$

$$\frac{h_w}{RT_o} = 0.0068 (T_s + 460) + 0.00000037 (T_s + 460)^2$$

$$= 0.0068 (3390 + 460) + 0.00000037 (3390 + 460)^2$$

$$= 26.2 + 5.50 = 31.7 ;$$

$$\left.\frac{Hg}{RT_o}\right|_{t_{q_{c_{max}}}} = 270 ; \qquad \text{(Fig. XIII-1)}$$

$$q_R = \frac{1.82 \sqrt{\frac{k\rho C_p}{2(t_{q_{c_{max}}} - t_i)}} \Delta T_s + \epsilon \left(\frac{T_s + 460}{1204}\right)^4}{\left(1 - \frac{h_w}{Hg}\right)}$$

$$= \frac{1.82 \sqrt{\frac{(.04)\,100\,(0.2)}{(3600)\,2\,(3300 - 220)}} (3390 - 70) + 0.7 \left(\frac{3390 + 460}{1204}\right)^4}{\left(1 - \frac{31.7}{270}\right)}$$

$$= \frac{1.15 + 73.2}{0.883} = 84 \text{ Btu/ft}^2\text{-sec}$$

Since $q_R > q_{c_{max}}$, ablation will occur only when $T_A < 3390°F$.

D. SCHEME 1 CALCULATION

1. Find the Duration of the Problem

Since $T_R = 570°F$

$$\frac{h_w}{RT_o} = 0.0068\,(570 + 460) + 0.00000037\,(560 + 460)^2$$

$$= 7.00 + 0.39 = 7.39 ,$$

$$\frac{H'_g}{RT_o} = \frac{1}{t_f - t_i} \int_{t_i}^{t_f} \frac{H_g}{RT_o}\,dt ,$$

$$= \frac{1}{(6000 - 220)}\,(1.237 \times 10^6) = 214 ,$$

$$Q'_c = \int_{t_o}^{t_f} q_c\,dt = 185{,}820 \text{ Btu/ft}^2 ,$$

$$t_R = \left(\frac{\sqrt{k\rho C_p \Delta T_R^2 + 4\epsilon \left(\frac{T_R + 460}{1204}\right)^4 Q'_c \left(1 - \frac{h_w}{H_g}\right)} - \sqrt{k\rho C_p \Delta T_R^2}}{2\epsilon \left(\frac{T_R + 460}{1204}\right)^4} \right)^2$$

$$= \left(\frac{\sqrt{\frac{(.04)}{3600}(100)(0.2)(500)^2 + 4(0.7)\left(\frac{570+460}{1204}\right)^4 185{,}820\left(1 - \frac{7.39}{214}\right)} - \sqrt{\frac{.04}{3600}(100)(0.2)(500)^2}}{2(0.7)\left(\frac{570+460}{1204}\right)^4} \right)^2$$

$$= \left(\frac{\sqrt{55.6 + 269{,}300} - \sqrt{55.6}}{0.75} \right)^2 = 4.65 \times 10^5 \text{ secs} .$$

Since, for this case, $t_R > t_f - t_i = 5780$,

$$t_D = t_f - t_i = 5780 \text{ secs} .$$

Note, however, if it were found that $t_R < t_f - t_i$, then the n^{th} convergent values of $\frac{H_g^N}{RT_o}$, Q_c^N, and t_R^N would have to be evaluated by an iterative process replacing t_f by $t_f^N = t_i + t_R^N$.

If $t_R^N \leq t_f - t_i$, we may solve for the required weight directly:

$$W^N = \sqrt{\frac{\rho k t_R}{C_p}} .$$

2. <u>Solve for the Average Free-Stream Gas Enthalpy</u>

$$\frac{H_g'}{RT_o} = \frac{1}{t_D} \int_{t_i}^{t_i + t_D} \frac{H_g}{RT_o} \, dt , \qquad \text{(Fig. XIII-1)}$$

$$= \frac{1}{5780} \int_{220}^{6000} \frac{H_g}{RT_o} \, dt = \frac{1}{5780}(1.237 \times 10^6) = 214 .$$

3. Solve for

$$\frac{Q_c}{\epsilon t_D} = \frac{185{,}820}{(0.7)\,5780} = 45.93 \text{ Btu/ft}^2\text{-sec}$$

4. Proceed to Find the Required Weight for this case

a. First Iteration

Assume $\frac{Q_k}{\epsilon t_D} = 0$

Read figure XVI-2 $T_s' = 2570°\text{F}$

$$\frac{\Delta T_R}{\Delta T_s'} = \frac{500}{2500} = 0.200$$

Read figure XIII-4 $B' = \frac{\alpha t}{L^2} = 0.185$ and $\frac{\Delta T_m'}{\Delta T_s'} = 0.485$

$$W' = \sqrt{\frac{\rho k t_D}{C_p B'}} = \sqrt{\frac{100\,(.04)\,5780}{(0.2)\,3600\,(0.185)}} = 13.19 \text{ lb/ft}^2$$

b. Second Iteration

$$\frac{Q_K'}{\epsilon t_D} = \frac{W' C_p \frac{\Delta T_m'}{\Delta T_s} \Delta T_s'}{\epsilon t_D}$$

$$= \frac{(13.19)(0.2)(0.485)\,2500}{(0.7)\,5780} = \frac{3199}{(0.7)\,5780} = 0.79 \text{ Btu/ft}^2\text{-sec}$$

Read figure XIII-3 $T_s'' = 2560°\text{F}$

$$\frac{\Delta T_R}{\Delta T_s''} = \frac{500}{2490} = 0.201$$

Read figure XIII-4 $B'' = \frac{\alpha t}{L^2} = 0.186$ and $\frac{\Delta T_m''}{\Delta T_s''} = 0.486$

$$W'' = \sqrt{\frac{(100)(.04)5780}{(0.2)\,3600\,(0.186)}} = 13.15 \text{ lb/ft}^2$$

For this case, W^N converges by the 2nd iteration to a value of 13.2 lb/ft^2; Thus

$$W_{ins} = \lim_{N \to \infty} W^N = 13.2 \text{ lb/ft}^2$$

This is the total weight required for Scheme 1.

E. SCHEME 2 CALCULATION

1. Verify existence of ablation by General Calculation, step C.2. This shows that ablation will occur for $T_A = 3000°F$.

2. Solve for the times at which ablation begins and ends

$$\left.\frac{H'_g}{RT_o}\right|_{t_{q_{c_{max}}}} = 270$$

Assume $\frac{Q_k}{\epsilon t_D} = 0$

Read figure XIII-2 using $T_s = T_A$, $\frac{Q_c}{\epsilon t_D} = 76.0$ Btu/ft^2-sec.

$$q_{c_A} = \frac{Q_c}{t_D} = (0.7)(76) = 53.2 \text{ Btu/ft}^2\text{-sec}.$$

Read figure XIII-1 - $t_{ia} = 2240$ secs.

$t_{fa} = 3890$ secs.

3. Solve for the amount of heat which enters into ablation

$$\int_{t_{ia}}^{t_{fa}} q_c \, dt = \int_{2240}^{3890} q_c \, dt = 118{,}000 \text{ Btu/ft}^2 \qquad \text{(Fig. XIII-1)}$$

$$\frac{h_w}{RT_o} = 0.0068\,(3000 + 460) + 0.00000037\,(3000 + 460)^2$$

$$= 23.53 + 4.43 = 27.96$$

$$\left.\frac{H_g}{RT_o}\right|_{t=\frac{t_{fa}+t_{ia}}{2}} = \left.\frac{H_g}{RT_o}\right|_{t=3065} = 297$$

$$Q_{oR_A} = \left(1 - \frac{h_w}{H_g}\right) \int_{t_{ia}}^{t_{fa}} q_c\, dt - \epsilon \left(\frac{T_A + 460}{1204}\right)^4 \left(t_{fa} - t_{ia}\right)$$

$$= \left(1 - \frac{27.96}{297}\right) 118{,}000 - 0.7 \left(\frac{3000 + 460}{1204}\right)^4 (3880 - 2240)$$

$$= 106{,}900 - 78{,}800 = 28{,}100 \text{ Btu/ft}^2 ,$$

4. Solve for the ablated weight

$$W_A = \frac{Q_{oR_A}}{q^*} = \frac{28{,}100}{10{,}000} = 2.81 \text{ lb/ft}^2 ,$$

5. Solve for the adjusted initial time of the insulation calculation

$$t_{adj} = t_{fa} - \frac{\rho k (t_{fa} - t_{ia})^2}{1.25 C_p W_A^2}$$

$$= 3890 - \frac{100\ (.04)\ (3890 - 2240)^2}{1.25\ (3600)\ (0.2)\ (2.81)^2}$$

$$= 3890 - 1530 = 2360 \text{ secs.}$$

Note: If t_{adj} were $\leq t_i$, then use $t_{adj} = t_i$ as obtained by general calculation step C.1.

6. Solve for the adjusted $\frac{H_g}{RT_o}$ for use in the insulation calculation

$$\left.\frac{H_g}{RT_o}\right|_{adj} = \frac{1}{t_f - t_{adj}} \int_{t_{adj}}^{t_f} \frac{H_g}{RT_o}\, dt$$

$$= \frac{1}{6000 - 2360} (5.26 \times 10^5) = 145 \ .$$

7. Solve for the total heat which is to be used for the insulation calculation

$$Q_{c_{ins}} = \int_{t_{adj}}^{t_f} q_c\, dt - Q_{oR_A} \ ,$$

$$= 129{,}300 - 28{,}100 = 101{,}200 \text{ Btu/ft}^2 \ .$$

8. Proceed now to find the insulation weight in the same manner as for scheme 1 except replace:

Q_c by $Q_{c_{ins}}$	Step E.7
t_i by t_{adj}	Step E.5
H_g by $H_{g_{adj}}$	Step E.6

9. Find the duration of the problem

Since $T_R = 570°F$

$\frac{h_w}{RT_o} = 7.39$ See Step D.1

$$\frac{H'_{g_{adj}}}{RT_o} = 145$$

$$Q'_{c_{ins}} = 101{,}200 \text{ Btu/ft}^2$$

$$t_R = \left(\frac{\sqrt{\frac{(.04)\,100\,(0.2)}{3600}(500)^2 + 4(0.7)\left(\frac{570+460}{1204}\right)^4 101{,}200\left(1 - \frac{7.39}{145}\right)} - \sqrt{\frac{(.04)100(0.2)}{3600}(500)^2}}{2\,(0.7)\left(\frac{570+460}{1204}\right)^4} \right)^2$$

$$= \left(\frac{379.5 - 7.46}{0.75}\right)^2 = 2.46 \times 10^5 \text{ secs} .$$

Since, for this case, $t_R > t_f - t_{adj} = 3640$, let

$$t_D = t_f - t_{adj} = 3640 \text{ secs} ,$$

10. Solve for

$$\frac{Q_c}{\epsilon t_D} = \frac{Q_{c_{ins}}}{\epsilon t_D} = \frac{101{,}200}{(0.7)\,3640} = 39.72 \text{ Btu/ft}^2 - \text{sec} .$$

11. Proceed to find the required insulation weight

a. First Interation

Assume $\frac{Q_k}{\epsilon t_D} = 0$

Read figure XIII-2 $T'_s = 2440°F$

$$\frac{\Delta T_R}{\Delta T'_s} = \frac{500}{2370} = 0.211$$

Read figure XIII-4 $-B' = \frac{\alpha t}{L^2} = 0.191$ and $\frac{\Delta T_m'}{\Delta T_s'} = 0.495$

$$W' = \sqrt{\frac{\rho k t_D}{C_p B'}} = \sqrt{\frac{(100)(.04)\,3640}{(0.2)\,3600\,(0.191)}} = 10.29 \text{ lb/ft}^2 .$$

b. Second Iteration

$$\frac{Q_k'}{\epsilon t_D} = \frac{W' C_p \frac{\Delta T_m'}{\Delta T_s'} \Delta T_s'}{\epsilon t_D}$$

$$= \frac{(10.29)(0.2)(0.495)\,2370}{(0.7)\,3640} = \frac{2414}{(0.7)\,3640} = 0.95 \text{ Btu/ft}^2 - \text{sec} .$$

Read figure XIII-3 $T_s'' = 2420°F$

$$\frac{\Delta T_R}{\Delta T_s''} = \frac{500}{2350} = 0.213 .$$

Read figure XIII-4 $-B'' = \frac{\alpha t}{L^2} = 0.192$ and $\frac{\Delta T_m''}{\Delta T_s''} = 0.496$

$$W'' = \sqrt{\frac{100\,(.04)\,3640}{(0.2)\,(3600)\,0.192}} = 10.26 \text{ lb/ft}^2 ;$$

Thus

$$W_{ins} = \lim_{n \to \infty} W^N = 10.3 \text{ lb/ft}^2 .$$

12. Solve for the total weight required for scheme 2.

$$W_T = W_A + W_{ins} = 2.81 + 10.3 = 13.11 \text{ lb/ft}^2$$

F. SCHEME 3 CALCULATION

1. Obtain Average T_s by scheme 1 calculation, step D.4. For this case $T_s = 2565°F$.

2. Obtain to by scheme 1 calculation, step. D.1 $t_D = 5780$ secs.

3. Obtain W^N by scheme 1 calculation, step D.4. $W^N = 13.2$ lb/ft^2.

4. Calculate:

$$W_{st} = \rho L = 120\left(\frac{0.20}{12}\right) = 2.0 \text{ lb/ft}^2$$

5. Arbitrarily select three or more values of

$$W_{ins} = W^N - aW_{st}, \text{ where } 0 \leq a \leq 1$$

$$W'_{ins} = 13.2 - (1.0)(2.0) = 11.2 \text{ lb/ft}^2,$$

$$W''_{ins} = 13.2 - (0.75)(2.0) = 11.7 \text{ lb/ft}^2,$$

$$W'''_{ins} = 13.2 - (0.50)(2.0) = 12.2 \text{ lb/ft}^2.$$

6. Solve for the capacitance ratios

$$R = \frac{(WC_p)_{st}}{(WC_p)_{ins}},$$

$$R' = \frac{(2.0)(0.2)}{(11.2)(0.2} = 0.179,$$

$$R'' = \frac{(2.0)(0.2)}{(11.7)(0.2)} = 0.171,$$

$$R''' = \frac{(2.0)(0.2)}{(12.2)(0.2)} = 0.164,$$

7. Solve for

$$\frac{\alpha t}{L^2} = \frac{\rho k t_D}{C_p W_{ins}^2} ,$$

$$\frac{\alpha t'}{L^2} = \frac{(100)(.04)\,5780}{(0.2)(3600)(11.2)^2} = \frac{32.11}{(11.2)^2} = 0.256 ,$$

$$\frac{\alpha t''}{L^2} = \frac{32.11}{(11.7)^2} = 0.235 ,$$

$$\frac{\alpha t'''}{L^2} = \frac{32.11}{(12.2)^2} = 0.216 .$$

8. Obtain the corresponding maximum rear temperatures:

$$\frac{\Delta T_R}{\Delta T_s} = f\left(R, \frac{\alpha t}{L^2}\right) .$$

Read figure XIII-5

$$\frac{\Delta T_R'}{\Delta T_s} = 0.242 ,$$

$$\frac{\Delta T_R''}{\Delta T_s} = 0.201 ,$$

$$\frac{\Delta T_R'''}{\Delta T_s} = 0.181 .$$

9. Solve for the weight corresponding to the design temperature

For this case we wish $\frac{\Delta T_R}{\Delta T_s} = \frac{500}{2495} = 0.200.$

An interpolation of a plot of $\frac{\Delta T_R^N}{\Delta T_s}$, step F.8 vs. W_{ins}^N, step F.5 yields:

$W_{ins} = 11.7$ lb/ft^2.

10. Solve for the total weight required for scheme 3.

$W_T = W_{ins} + W_{st} = 11.7 + 2.0 = 13.7$ lb/ft^2.

G. SCHEME, 4 CALCULATION

1. Obtain W_A by scheme 2 calculation, step E.4

$W_A = 2.81$ lb/ft^2

2. Obtain average T_s by scheme 2 calculation, step E.11

$T_s = 2420°F$.

3. Obtain W_{ins} by scheme 2 calculation, step E.11

$W_{ins} = 10.3$ lb/ft^2.

4. Obtain t_D by scheme 2 calculation, step E.9

$t_D = 3640$ secs.

5. Calculate

$$W_{st} = \rho L = 120 \left(\frac{0.2}{12}\right) = 2.0 \text{ lb/ft}^2 .$$

6. Proceed as in scheme 3 calculation, steps F.5, F.6, F.7, F.8, and F.9.

a.

$$W'_{ins} = 10.3 - (1.0)(2.0) = 8.3 \text{ lb/ft}^2 ,$$

$$W''_{ins} = 10.3 - (0.75)(2.0) = 8.8 \text{ lb/ft}^2 ,$$

$$W'''_{ins} = 10.3 - (0.50)(2.0) = 9.3 \text{ lb/ft}^2 .$$

b.

$$R' = \frac{(2)(0.2)}{(8.3)(0.2)} = 0.241 ,$$

$$R'' = \frac{2}{8.8} = 0.227 ,$$

$$R''' = \frac{2}{9.3} = 0.215 .$$

c.

$$\frac{\alpha t'}{L^2} = \frac{(100)(0.04)\ 3640}{(0.2)(3600)(8.3)^2} = \frac{20.22}{(8.3)^2} = 0.294 ,$$

$$\frac{\alpha t''}{L^2} = \frac{20.22}{(8.8)^2} = 0.261 ,$$

$$\frac{\alpha t'''}{L^2} = \frac{20.22}{(9.3)^2} = 0.234 .$$

d.

$$\frac{\Delta T'_R}{\Delta T_s} = 0.24 ,$$

$$\frac{\Delta T''_R}{\Delta T_s} = 0.20 ,$$

$$\frac{\Delta T'''_R}{\Delta T_s} = 0.18 .$$

e. For $\frac{\Delta T_R}{\Delta T_s} = \frac{500}{2350} = 0.213$,

$$W_{ins} = 8.56 \text{ lb/ft}^2 .$$

7. Solve for the total weight required for scheme 4.

$$W_T = W_A + W_{ins} + W_{st}$$

$$= 2.81 + 8.56 + 2.0 = 13.37 \text{ lb/ft}^2 .$$

H. SCHEME 5 CALCULATION

1. Solve for the initial time of the problem

$$t_b = t_{q_{c_{max}}} - \frac{Q_c}{q_{c_{max}}} = 3300 - 2300 = 1000 \text{ secs.}$$

2. Solve for final time of the problem

$$t_f = t_{q_{c_{max}}} + \frac{Q_c}{q_{c_{max}}} = 3300 + 2300 = 5600 \text{ secs.}$$

3. Solve for duration of the problem

$$t_D = t_f - t_b = 5600 - 1000 = 4600 \text{ secs.}$$

4. Solve for the average gas enthalpy

$$\frac{H_g'}{RT_o} = \frac{1}{t_D} \int_{t_b}^{t_f} \frac{H_g}{RT_o} dt = \frac{1}{4600} (9.9 \times 10^5) = 215 .$$

5. Solve for

$$\frac{Q_c}{\epsilon t_D} = \frac{q_{c_{max}}}{2\epsilon} = \frac{81}{2(0.7)} = 57.86 \text{ Btu/ft}^2\text{-sec.}$$

6. Proceed to find the required weights for this case.

a. First Iteration

Assume $\frac{Q_k}{\epsilon t_D} = 0$

Read figure XIII-2 $T_s' = 2740°F$

$$\frac{\Delta T_m'}{\Delta T_s'} = \frac{1}{2}\left(\frac{\Delta T_s' + \Delta T_R}{\Delta T_s'}\right) = \frac{1}{2}\left(\frac{2670+0}{2670}\right) = 0.500 .$$

Read figure XIII-4 $B' = \frac{\alpha t}{L^2} = 0.195$

$$\frac{H_c}{C_p(T_s' - T_R)} = \frac{400}{(0.2)(2740-70)} = 0.749 .$$

Read figure XIII-6

$$\left(\frac{2W_s^2 C_p}{\rho k t_D}\right) = 3.58$$

Solve for:

$$W_s' = \sqrt{\frac{100(0.04)4600}{(0.2)(3600)^{(2)}}\,(3.58)}$$

$$= 3.575\sqrt{3.58} = 6.76 \text{ lb/ft}^2$$

$$\left(\frac{2W_T^2 C_p}{\rho k t_D}\right) = 7.80$$

Solve for:

$$W_T' = 3.575\sqrt{7.80} = 9.98 \text{ lb/ft}^2$$

b. Second Iteration

$$\frac{Q'_k}{\epsilon t_D} = \frac{1}{\epsilon}\,\frac{k(T'_s - T_R)}{x'_s} = \frac{1}{\epsilon}\,\frac{\rho k(T'_s - T_R)}{W'_s}$$

$$= \frac{100(0.04)(2740-70)}{(0.7)(3600)6.76} = 0.63 \text{ Btu/ft}^2\text{-sec.}$$

Read figure XIII-3 $T''_s = 2730°F$

$$\frac{\Delta T''_m}{\Delta T''_s} = \frac{1}{2}\left(\frac{2660+0}{2660}\right) = 0.500 .$$

Read figure XIII-4 $B'' = \frac{\alpha t}{L^2} = 0.195$

$$\frac{H_c}{C_p(T''_s - T_R)} = \frac{400}{(0.2)(2730-70)} = 0.752 .$$

Read figure XIII-6

$$\left(\frac{2W_s^2 C_p}{\rho k t_D}\right)'' = 3.55 .$$

Solve for:

$$W''_s = 3.757\sqrt{3.55} = 6.74 \text{ lb/ft}^2$$

$$\left(\frac{2W^2 C_p}{\rho k t_D}\right)'' = 7.76$$

$$W''_T = 3.575\sqrt{7.76} = 9.96 \text{ lb/ft}^2$$

It is seen that the weights converge to:

$$W_{ins} = W_s^N = 6.75 \text{ lb/ft}^2 ,$$

$$W_{ins+c} = W_T^N = 9.97 \text{ lb/ft}^2 .$$

7. The coolant weight may be obtained if desired

$$W_c = W_{ins+c} - W_{ins} = 9.97 - 6.75 = 3.22 \text{ lb/ft}^2 .$$

8. Since the thermal effect of the structure has been included in H_c, the total system weight required for scheme 5 is:

$$W_T = W_{ins} + W_c + W_{st}$$

$$= 6.75 + 3.22 + 2.0 = 11.97 \text{ lb/ft}^2 .$$

I. SCHEME 6 CALCULATION

1. Obtain W_A by scheme 2 calculation, step E.4

$$W_A = 2.81 \text{ lb/ft}^2 .$$

2. Obtain t_{adj} by scheme 2 calculation, step E.5

$$t_{adj} = 2360 \text{ secs.}$$

Note if t_{adj} were $\leq t_b = t_{q_{c_{max}}} - \dfrac{Q_c}{q_{c_{max}}}$

then use $t_{adj} = t_b$.

3. Obtain $Q_{c_{ins}}$ by scheme 2 calculation, step E.7

$$Q_{c_{ins}} = 101{,}200 \text{ Btu/ft}^2 .$$

4. Solve for the final time of the problem

$$t_f = t_{q_{c_{max}}} + \frac{Q_c}{q_{c_{max}}} = 3300 + 2300 = 5600 \text{ secs}$$

5. Solve for the duration of the problem

$$t_D = t_{q_{c_{max}}} + \frac{Q_c}{q_{c_{max}}} - t_{adj} = 5600 - 2300 = 3240 \text{ secs.}$$

6. Solve for the average gas enthalpy

$$\frac{H_g'}{RT_o} = \frac{1}{t_D} \int_{t_{adj}}^{t_f} \frac{H_g}{RT_o}\, dt = \frac{1}{3240} (5.26 \times 10^5) = 162 .$$

7. Solve for

$$\frac{Q_c}{\epsilon t_D} = \frac{Q_{c_{ins}}}{\epsilon t_D} = \frac{101,200}{(0.7)3240} = 44.62 \text{ Btu/ft}^2\text{-sec.}$$

8. Proceed to find the weights required for this case.

   a. First Interation

   Assume $\frac{Q_k}{\epsilon t_D} = 0$

   Read figure XIII-2 $T_s' = 2530°F$

$$\frac{\Delta T_m'}{\Delta T_s'} = \frac{1}{2}\left(\frac{\Delta T_s' + \Delta T_R}{\Delta T_s'}\right) = \frac{1}{2}\left(\frac{2460 + 0}{2460}\right) = 0.500 .$$

   Read figure XIII-4 $B' = \frac{\alpha t}{L^2} = 0.195$

$$\frac{H_c}{C_p(T_s' - T_R)} = \frac{400}{(0.2)(2530 - 70)} = 0.813 .$$

Read figure XIII-6

$$\left(\frac{2W_s^2 C_p}{\rho k t_D}\right)' = 3.28 .$$

Solve for:

$$W_s' = \sqrt{\frac{100(0.04)3240}{(0.2)(3600)2}\ (3.28)} = 3.00\sqrt{3.28} = 5.43 \text{ lb/ft}^2 ,$$

$$\left(\frac{2W_T^2 C_p}{\rho k t_D}\right)' = 7.43 ,$$

$$W_T' = 3.00\sqrt{7.43} = 8.18 \text{ lb/ft}^2 .$$

b. Second Iteration

$$\frac{Q_k'}{\epsilon t_D} = \frac{1}{\epsilon}\ \frac{\rho k(T_s' - T_R)}{W_s'} = \frac{100(0.04)(2530-70)}{(0.7)(3600)\ 5.43} = 0.72 \text{ Btu/ft}^2\text{-sec} .$$

Read figure XIII-3 $T_s'' = 2515°F$

$$\frac{\Delta T_m''}{\Delta T_s''} = \frac{1}{2}\left(\frac{2445+0}{2445}\right) = 0.500 .$$

Read figure XIII-4 $B'' = \frac{\alpha t}{L^2} = 0.195$

$$\frac{H_c}{C_p(T_s'' - T_R)} = \frac{400}{(0.2)(2515-70)} = 0.818$$

Read figure XIII-6

$$\left(\frac{2W_s^2 C_p}{\rho k t_D}\right)'' = 3.26 ,$$

$$W_s'' = 3.00\sqrt{3.26} = 5.42 \text{ lb/ft}^2 ,$$

$$\left(\frac{2W_T^2 C_p}{\rho k t_D}\right)'' = 7.40 ,$$

$$W_T'' = 3.00\sqrt{7.40} = 8.16 \text{ lb/ft}^2 .$$

It is seen that the weights converge to:

$$W_{ins} = W_s^N = 5.42 \text{ lb/ft}^2 ,$$

$$W_{ins+c} = W_T^N = 8.17 \text{ lb/ft}^2 .$$

9. The coolant weight may be obtained

$$W_c = W_{ins+c} - W_{ins} = 8.17 - 5.42 = 2.75 \text{ lb/ft}^2$$

10. Since the thermal effect of the structure has been included in H_c, the total system weight required for scheme 6 is:

$$W_T = W_A + W_{ins} + W_c + W_{st}$$

$$= 2.81 + 5.42 + 2.75 + 2.0 = 12.98 \text{ lb/ft}^2 .$$

J. SCHEME 7 CALCULATION

1. Verify that no ablation will occur

Let $T_s = T_A = 6600°F$,

$\epsilon = 0.9$,

$$\frac{h_w}{RT_o} = 0.0068\,(6600 + 460) + 0.00000037\,(6600 + 460)^2 \quad ,$$

$$= 48.0 + 18.4 = 66.4$$

$$\left.\frac{H_g'}{RT_o}\right|_{t_{q_{c_{max}}}} = 270$$

$$q_R = \frac{1.82\sqrt{\dfrac{k\rho C_o}{2(t_{q_{c_{max}}} - t_i)}}\,\Delta T_s + \epsilon\left(\dfrac{T_s + 460}{1204}\right)^4}{\left(1 - \dfrac{h_w}{H_g'}\right)} \quad ,$$

$$= \frac{1.82\sqrt{\dfrac{(0.04)(100)(0.2)}{(3600)(2)(3300 - 220)}}\,(6600 - 70) + 0.9\left(\dfrac{6600 + 460}{1204}\right)^4}{\left(1 - \dfrac{66.4}{270}\right)} \quad ,$$

$$= \frac{7.14 + 1064}{0.754} = 1420\ \text{Btu/ft}^2\text{-sec}\,.$$

Since $q_R > q_{c_{max}}$, no ablation will occur.

2. Calculate a self-insulating radiation shield system weight required using the insulation material, except replace its emissivity by that of the skin material ($\epsilon = 0.9$).

a. Obtain by scheme 1 calculation, step D.1

$$\frac{h_w}{RT_o} = 7.39 \ ,$$

$$\frac{H'_g}{RT_o} = 214 \ ,$$

$$Q'_c = 185{,}820 \text{ Btu/ft}^2 \ ,$$

$$t_R > 5780 \text{ secs} \ ,$$

$$t_D = 5780 \text{ secs.}$$

b. Solve for

$$\frac{Q_c}{\epsilon t_D} = \frac{185{,}820}{(0.9)\,5780} = 35.72 \text{ Btu/ft}^2\text{-sec.}$$

c. Proceed as in scheme 1 calculation, step D.4

1) First Iteration

Assume $\frac{Q_k}{\epsilon t_D} = 0$.

Read figure XIII-2 $T'_s = 2400°F$

$$\frac{\Delta T_R}{\Delta T'_s} = \frac{500}{2330} = 0.215 \ .$$

Read figure XIII-4 $B' = \frac{at}{L^2} = 0.193$ and $\frac{\Delta T'_m}{\Delta T'_s} = 0.497$,

$$W' = \sqrt{\frac{100(0.04)\,5780}{(0.2)(3600)\,0.193}} = 12.90 \text{ lb/ft}^2 \ .$$

2) Second Iteration

$$\frac{Q'_k}{\epsilon t_D} = \frac{(12.90)(0.2)\,0.497\,(2330)}{0.9(5780)} = 0.574 \text{ Btu/ft}^2\text{-sec.}$$

Read figure XIII-3 $T_s'' = 2390°F$

$$\frac{\Delta T_R}{\Delta T_s''} = \frac{500}{2320} = 0.216$$

Read figure XIII-4 $B'' = \frac{\alpha t}{L^2} = 0.193$ and $\frac{\Delta T_m''}{\Delta T_s''} =$

$$W'' = \sqrt{\frac{(100)(0.04)5780}{(0.2)(3600)(0.193)}} = 12.90 \text{ lb/ft}^2 ,$$

Thus $W^N = 12.90 \text{ lb/ft}^2$.

3. Solve for the weight W'_{ins} of insulation material thermally equivalent to the given weight of hot skin material

$$W'_{ins} = W_{sk} \sqrt{\frac{(\rho k/C_p)_{ins}}{(\rho k/C_p)_{sk}}} = \frac{0.048}{12} (125) \sqrt{\frac{\frac{100(0.04)}{0.2}}{\frac{125(0.23)}{0.49}}} ,$$

$$= 0.5 \sqrt{\frac{20}{58.7}} = 0.29 \text{ lb/ft}^2 .$$

4. Solve for the required insulation weight of the system

$$W_{ins} = W^N - W'_{ins} = 12.90 - 0.29 = 12.61 \text{ lb/ft}^2 .$$

5. Solve for the total weight required for scheme 7

$$W_T = W_{sk} + W_{ins} = 0.50 + 12.61 = 13.11 \text{ lb/ft}^2 .$$

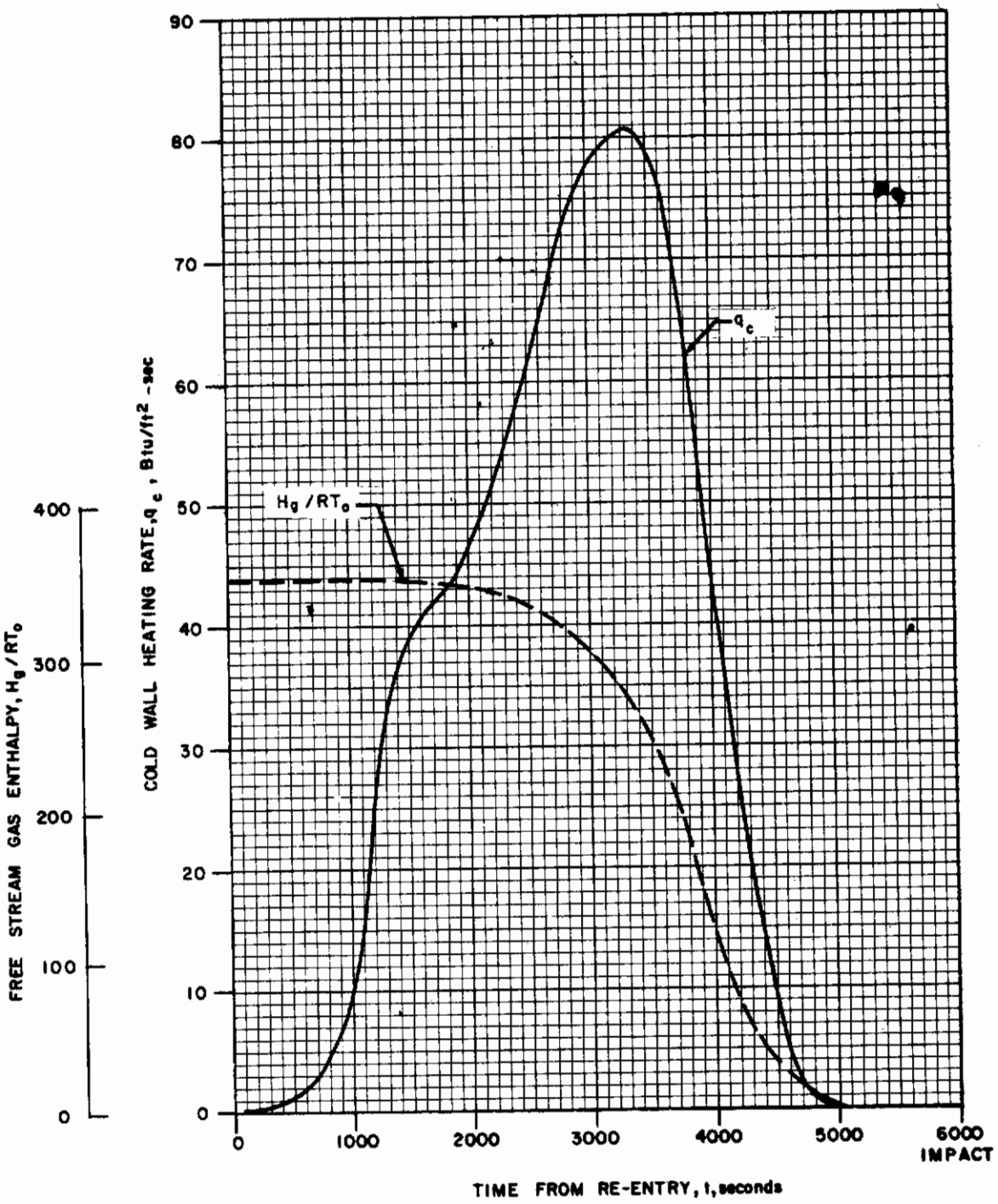

Figure XIII-1 AERODYNAMIC ENVIRONMENT

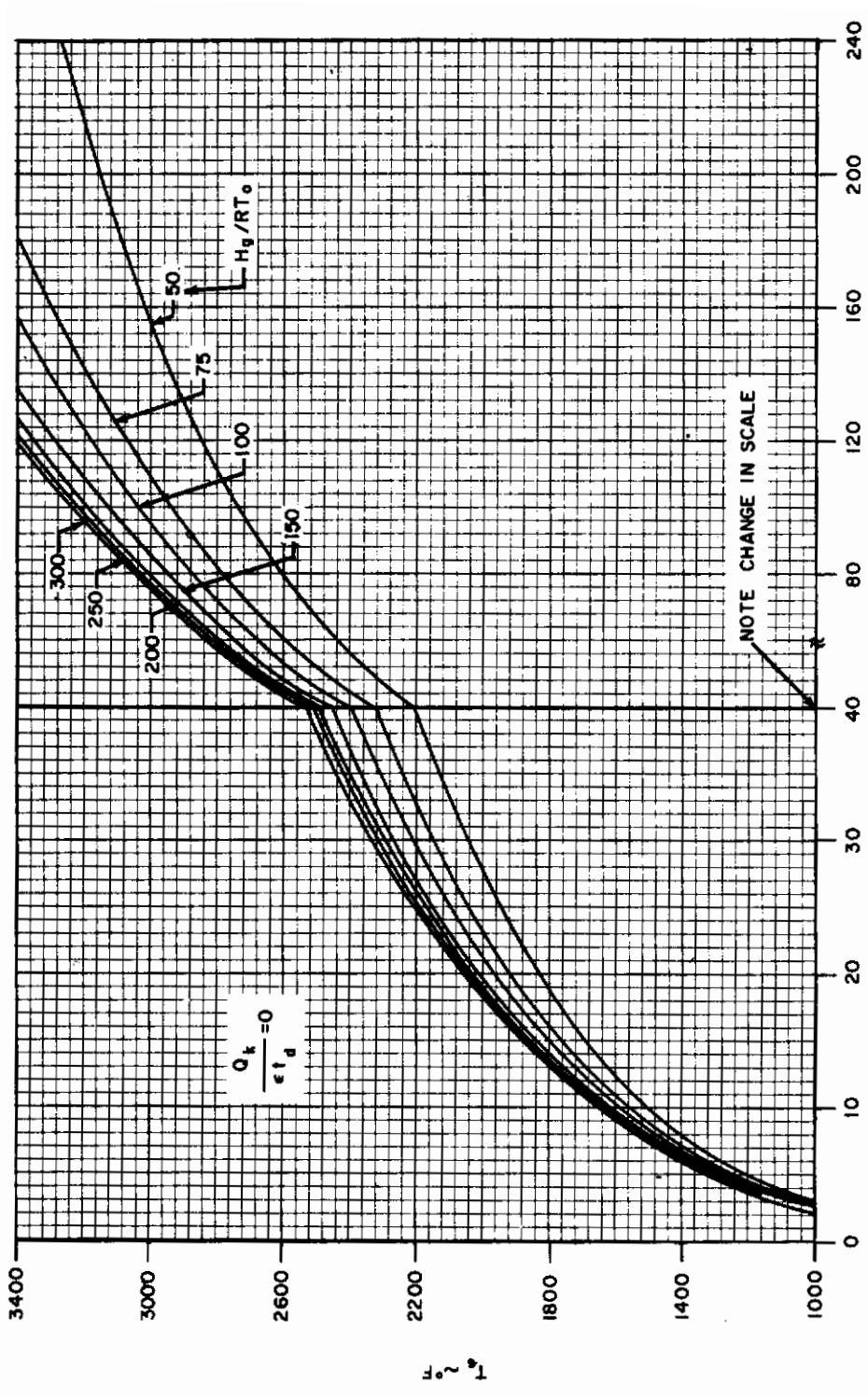

Figure XIII-2 STEADY STATE ENERGY BALANCE - $\frac{Q_k}{\epsilon t_D} = 0$

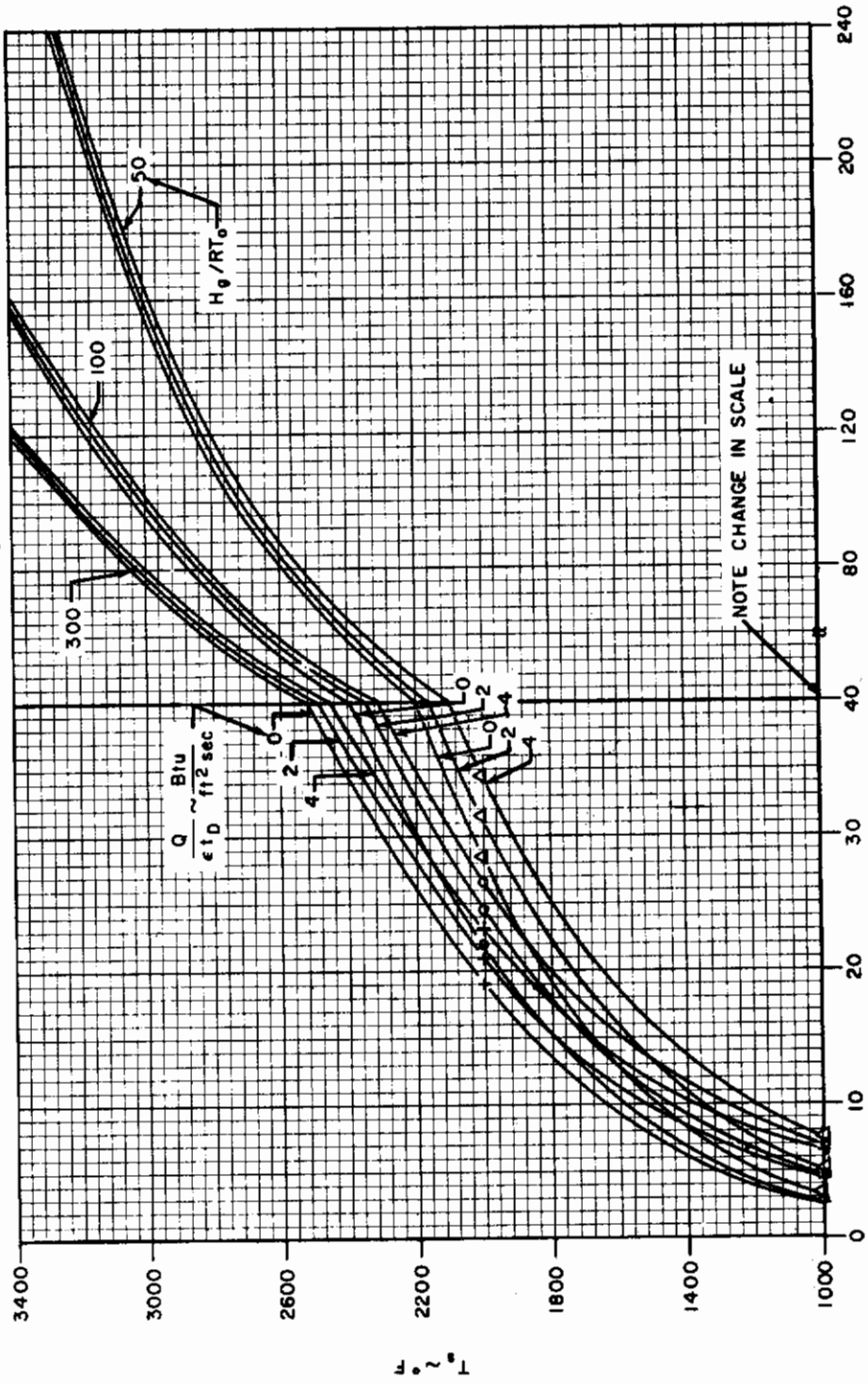

Figure XIII-3 STEADY STATE ENERGY BALANCE $\frac{Q_k}{\epsilon t_D} \neq 0$

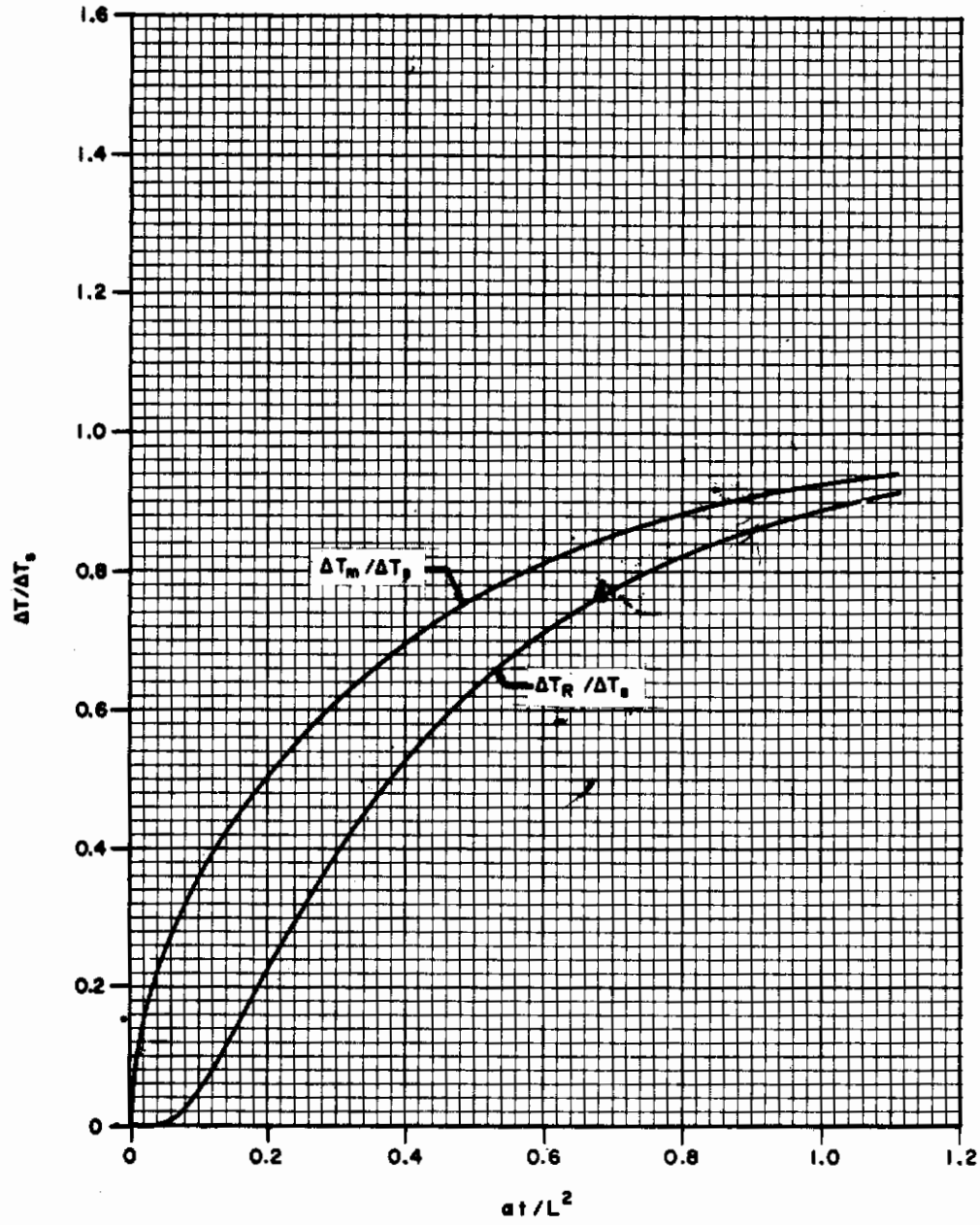

Figure XIII-4 REAR AND MEAN TEMPERATURE RISE IN A FINITE MEDIUM WITH CONSTANT SURFACE TEMPERATURE (T_s) AND INSULATED REAR BOUNDARY

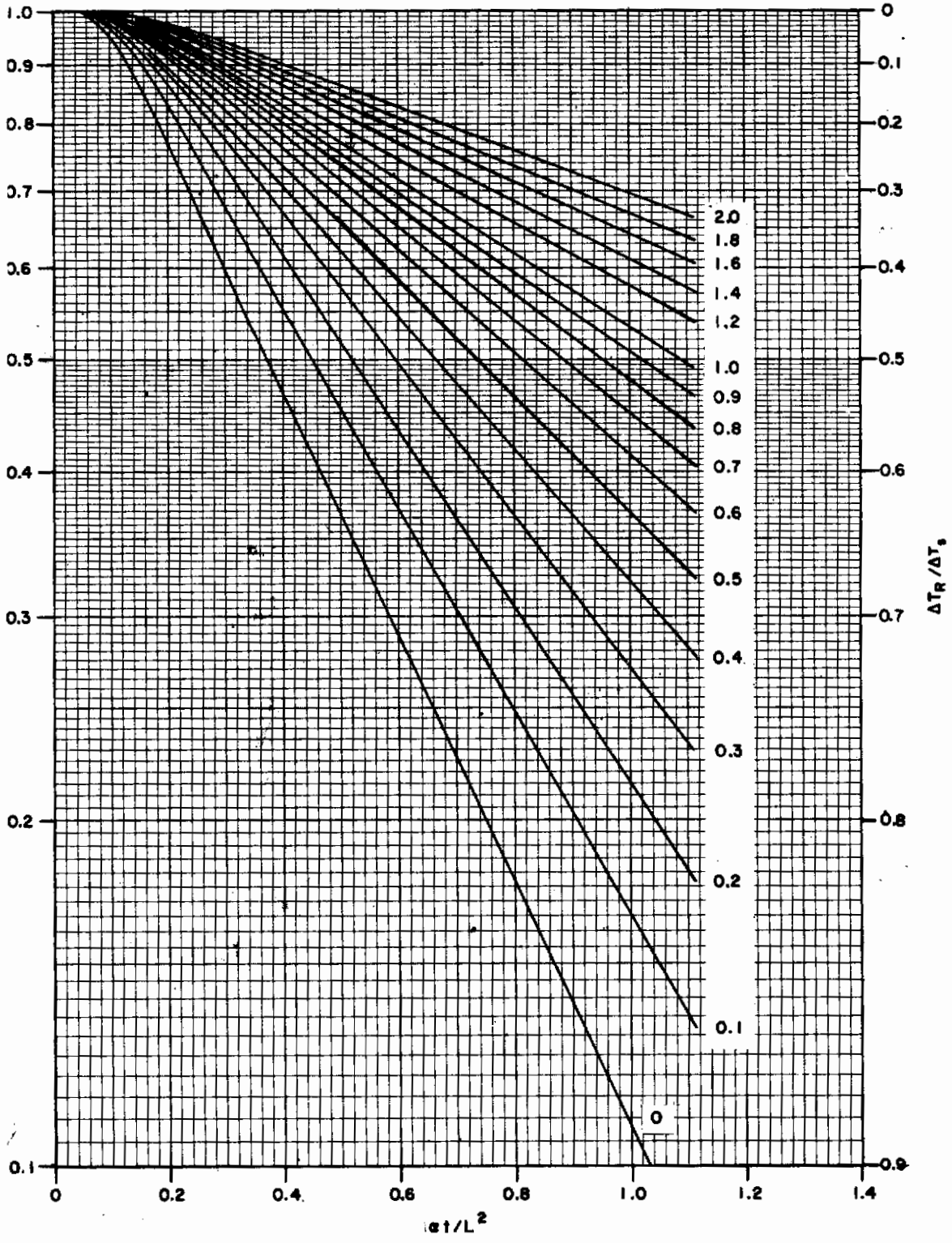

Figure XIII-5 REAR TEMPERATURE RISE IN A FINITE SLAB WITH A CONSTANT SURFACE TEMPERATURE (T_s) AND A PERFECTLY CONDUCTING SUBSTRUCTURE

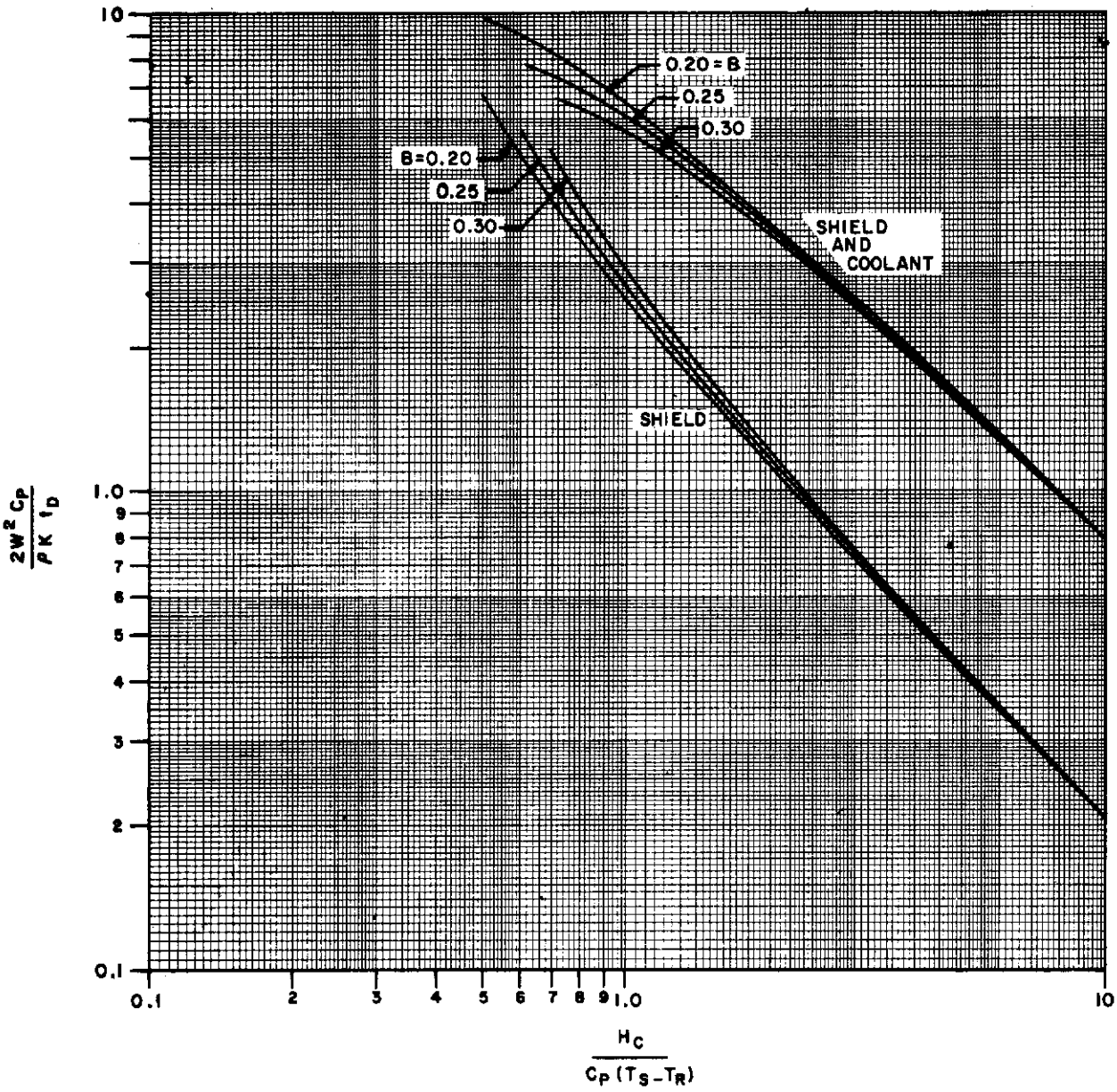

Figure XIII-6 REQUIRED WEIGHT FOR A LIQUID COOLED RADIATION SHIELD

APPENDIX XIV

SOLUTION OF LAMINAR COMPRESSIBLE BOUNDARY LAYER WITH DISCRETE INJECTION (FOR AIR IN CHEMICAL EQUILIBRIUM)

by A. Pallone

A. BASIC EQUATIONS

Equations (XIV-1) through (XIV-4) describe the boundary-layer flow over two-dimensional or axisymmetric bodies for dissociated air in chemical equilibrium with Lewis number of unity and a constant Prandtl number.

Momentum equation in x direction:

$$\rho u u_x + \rho v u_y = - p_x + \left(\mu u_y\right)_y \quad . \tag{XIV-1}$$

Continuity equation:

$$(\rho u)_x + (\rho v)_y + \frac{\rho u r_x \cdot j}{r} = 0 \qquad j = \begin{array}{l} 1 \text{ for axisymmetric,} \\ 0 \text{ for two-dimensional.} \end{array} \tag{XIV-2}$$

Energy equation:

$$\rho u H_x + \rho v H_y = \left(\frac{\mu}{Pr} H_y\right)_y + \left[\mu \left(1 - \frac{1}{Pr}\right)\left(\frac{u^2}{2}\right)_y\right]_y \quad . \tag{XIV-3}$$

The analysis of the injection region can be made of immediate practical interest by adding to the preceding equations the following heat-balance relation:

$$\left(K \frac{\partial T}{\partial y}\right)_w = (\rho v)_w (H_w - H_c) \, . \tag{XIV-4}$$

The boundary conditions applicable to equations (XIV-1) through (XIV-5) are at $y = \delta$; $u = u_1$; $H = H_1$; at $y = 0$; $u = 0$; in addition two of the following quantities must be specified as a function of ξ:

$$H_w\,,\ H_c\,,\ (\rho v)_w \quad \text{and} \quad \left(\frac{\partial H}{\partial y}\right)_w \quad . \qquad \text{(XIV-5)}$$

B. ANALYSIS

Gas properties:

Solutions of the boundary-layer equations are dependent upon the physical properties of the fluid considered. In the past, many methods have been employed to account for the variation of fluid properties throughout the flow field. While these methods provide sufficient accuracy for most computational purposes, an exact set of fluid properties would be desirable for any theoretical analysis.

Several methods of obtaining fluid properties have been used in the present analysis. The standard thermodynamic variables (i.e., ρ, T, S, H) have been obtained from polynomial curve fits to the Mollier Diagram for Air in Chemical Equilibrium (set 13). These curvefits, as programmed on a digital computer, are accurate to within one percent of the Mollier Diagram values.

Analytic expressions for certain gas properties have been needed in addition to the Mollier curve fits. In particular, the energy balance and matching conditions at the boundaries required the derivatives of certain properties to be evaluated. The inherent difficulty of finding derivatives on a digital computer necessitated use of an analytic expression.

The governing equations are cast in the form of ordinary first-order differential equations by following the procedure developed earlier (Ref. XIV-1).

The boundary-layer region is divided into N curvilinear strips. Equations (XIV-1) and (XIV-3) are integrated from $y = 0$ to the boundary of each strips, and v is replaced by equation (XIV-2). Finally, the Howarth-Doronitzien

$$f = \int_0^y \frac{\rho}{\rho_1}\, dy\,, \qquad \text{(XIV-6)}$$

is introduced.

XIV-1 Pallone, A., Non-similar Solutions of the Compressible Laminar Boundary Layer Equations with Applications to the Upstream Transpiration Cooling Problem, Avco RAD-TR-9-60-8 (10 May 1960).

The following set of equations are obtained:

$$\frac{F_{1k}\lambda'}{2} + \lambda F_{1k}' + \lambda F_{1k}\left[\left(\ln \rho_1 u_1 \mu_1\right)^{1/2}\right)' + (\ln u_1)'\Big] + \frac{\lambda j}{r_o}\frac{dr_o}{d\xi} F_{2k} - \frac{u_k}{u_1}(\lambda Re_L)^{1/2}\frac{(\rho v)_w}{\rho_1 u_1} - \lambda F_{2k}\left(\frac{u_k}{u_1}\right)' + \lambda F_{3k}(\ln u_1)' - r_w - r_k = 0 , \qquad \text{(XIV-7)}$$

and

$$\frac{F_{4k}\lambda'}{2} + \lambda F_{4k}' + \lambda F_{4k}\left[\ln (\rho_1 u_1 \mu_1)^{1/2}\right]' - \lambda F_{2k}\left(\frac{H_k}{H_1}\right)' + \frac{j}{r_o}\frac{dr_o}{d\xi}\lambda F_{4k} + \frac{H_w - H_k}{H_1}(\lambda Re_L)^{1/2}\frac{(\rho v)_w}{\rho_1 u_1} = \left[\frac{l}{Pr}\left(\frac{H}{H_1}\right)_\eta\right]_w - \left[\frac{l}{Pr}\left(\frac{H}{H_1}\right)_\eta\right]_k - \left[\frac{l}{Pr}(Pr-1)\frac{u_1^2}{2H_1}\frac{\partial}{\partial\eta}\left(\frac{u}{u_1}\right)^2\right]_k , \qquad \text{(XIV-8)}$$

where

$$F_{1k} = \int_0^{\eta_k} \left(\frac{u}{u_1} \frac{u_k}{u_1} - \frac{u^2}{u_1^2} \right) d\eta \ ,$$

$$F_{2k} = \int_0^{\eta_k} \frac{u}{u_1} \, d\eta \ .$$

$$F_{3k} = \int_0^{\eta_k} \left(\frac{\rho_1}{\rho} - \frac{u_k}{u_1} \frac{u}{u_1} \right) d\eta$$

$$= \int_0^{\eta_k} \frac{\rho_1}{\rho} \, d\eta - \frac{u_k}{u_1} F_{2k} \ ,$$

$$F_{4k} = \int_0^{\eta_k} \frac{u}{u_1} \left(\frac{H_k}{H_1} - \frac{H}{H_1} \right) d\eta \ ,$$

$$\lambda = \frac{\rho_1 u_1}{\mu_1} \frac{L \delta_t^2}{L^2} \ ; \quad r \equiv \left(\ell \frac{\partial}{\partial \eta} \left(\frac{u}{u_1} \right) \right) \ ,$$

$$\eta \equiv \frac{t}{\delta_t} \ ; \quad k = 1 \ldots N \ ,$$

$$\eta_k = \frac{N - (k-1)}{N} \ ,$$

and where ($\quad$)′ denotes differentiation in the respect to $\xi = \frac{x}{L}$.

Polynomials in η are assumed for $\frac{u}{u_1}$ and $\frac{H}{H_1}$. The coefficients of these polynomials are selected so that appropriate boundary and compatibility conditions are satisfied, while the remaining unknowns are determined so that equations (XIV-7) and (XIV-8) are satisfied.

Polynomials of degree $N+n$ are assumed for $\frac{u}{u_1}$, and of degree $N+n+1$ are assumed for H/H_1:

$$\frac{u}{u_1} = \sum_{m=0}^{N+n} a_m \eta^m \quad ; \quad \frac{H}{H_1} = \sum_{m}^{N+n+1} b_m \eta^m \ .$$

The additional coefficient in the thermal profile is assumed to serve as an unknown in place of a separate thermal boundary thickness. n will depend on the number of compatibility conditions at the wall and at the outer edge that may be applied.

A program has been constructed for solving the system of equations (XIV-7) and (XIV-8), and is presently being checked out.

C. NOMENCLATURE

Symbols

c_f local skin-friction coefficient $\left(\frac{\tau_w}{\frac{1}{2}\rho_1 u_1^2}\right) = \left(\frac{\rho_1 u_1 x}{\mu_1 c}\right)^{-1/2} 2a_1 \left(\frac{\xi}{\bar{\lambda}}\right)^{1/2} \frac{\ell}{c}$,

c_p specific heat at constant pressure,

$f(0)$ variable proportional to the blowing rate,

$F_{1,2,3,4,5}$ integrals defined after equation (XIV-8),

G functions of ρ_1 , u_1 , and μ_1 ,

H stagnation enthalpy $= (u^2/2) + c_p T$,

K conductivity,

ℓ nondimensional ratio $(\rho\mu/\rho_1\mu_1)$,

L	reference length,
M	Mach number,
N	number of strip in which viscous region is divided,
P	Static pressure,
Pr	Prandtl number $(c_p \mu/K)$,
Q	Surface heat-transfer rate,
r	Cylindrical radius,
R	gas constant,
$\bar{R}$	gas constant of mixture,
Re_x	Reynolds number based on properties at outer edge of, the boundary layer $\frac{u_1 \times \rho_1}{\mu_1}$,
S	Sutherland constant 216° R for air,
t	transformed variable,
T	absolute temperature,
$\bar{T}$	an average temperature $\frac{(T_{L_1} + T_a)}{2}$,
u	velocity component in x direction,
v	velocity component in y direction,
x	coordinate along the surface,
y	coordinate normal to the surface.

Greek:

γ	ratio of specific heats,
η	transformed variable,

δ boundary-layer thickness,

λ nondimensional boundary-layer thickness $\left(\lambda = \frac{\rho_1 u_1 L}{\rho_1} \frac{\delta_t^2}{L^2}\right)$,

μ coefficient of viscosity

ξ nondimensional space coordinate $\xi = \frac{x}{L}$,

ρ mass density,

τ $= -\left[\mu \frac{\partial}{\partial \eta} \frac{u}{u_1}\right]$.

Subscripts:

a adiabatic wall,

L value at the end of porous region,

r reference value,

s stagnation values,

t value in the $x-t$ or $\xi-\eta$ plane,

w value at the surface, $y = 0$, for any value,

1 value at the outer edge of the boundary,

∞ value at free stream,

k index,

n index.

APPENDIX XV

THE STAGNATION POINT FLOW OF NON-EQUILIBRIUM AIR, WITH AND WITHOUT INJECTION

by A. Pallone

A. SUMMARY

This appendix, the laminar boundary layer flow of dissociated air in chemical non-equilibrium is studied at the stagnation point. The influence of injecting a variety of foreign gas is also investigated. The air is treated as a mixture of five components (O, O_2, N, N_2, NO) with the molecular internal degrees of freedom in equilibrium with the translational mode. The best presently available reaction rates for the pertinent gas phase reactions are employed. A new set of transport and thermodynamic properties is utilized. The analysis is restricted to temperatures below 8000°K.

The equations expressing conservation of chemical species, energy, and momentum are transformed to a set of linear ordinary differential equations which may be solved by an iteration procedure on the Philco 2000 automatic digital computer.

B. NOTATION

$C_{v\alpha}$ = Specific heat per unit mass, at constant volume, of species α,

$C_{p\alpha}$ = Specific heat per unit mass, at constant pressure, of species α,

$\bar{C}_v$ = Average specific heat per unit mass, at constant volume, of the frozen gas mixture $= \sum_{\alpha} Y_\alpha C_{v\alpha}$,

$\bar{C}_p$ = Average specific heat per unit mass, at constant pressure, of the frozen gas mixture $= \sum_{\alpha} Y_\alpha C_{p\alpha}$,

$\mathcal{D}_{\alpha\beta}$ = Binary diffusion coefficient,

$D_{\alpha\beta}$ = Multicomponent diffusion coefficient, defined by equation (17),

$G_{\alpha\beta}$ = Defined by equation (XV15),

H_β = Enthalpy (chemical and thermal) per unit mass of species β, as referred to O_2 and N_2 at 0 °K,

H = Enthalpy (chemical and thermal) per unit mass of the gas mixture, as referred to 0_2 and N_2 at 0 °K $= \sum_\alpha Y_\alpha H_\alpha$

$\overset{I}{k_\alpha}, \overset{II}{k_\alpha}, \overset{III}{k_\alpha}$ = Chemical reaction rate constants for species α, referred to reaction I, II, or III, defined in Table II,

$\overset{IV}{k}, \overset{V}{k}$ = "Global" chemical reaction rate constants for the reactions IV and V; defined in Table XV-2,

$\overset{I}{K_N} \ldots \overset{V}{K_N}$ = Equilibrium constants for reactions I through V, defined by equation (27),

$|K|$ = Determinant of $K_{\alpha\beta}$,

$K_{\alpha\beta}$ = Defined by equation (18),

$K^{\alpha\beta}$ = Minor of $K_{\alpha\beta}$ in determinant $|K|$,

L = Characteristic body length,

M_γ = Molecular weight of a species γ,

$\bar{M}$ = Average molecular weight of the gas mixture $= \sum_\gamma X_\gamma M_\gamma$

$M_{\alpha\beta}$ = Reduced molecular weight of species α and β $= \dfrac{M_\alpha M_\beta}{M_\alpha + M_\beta}$,

n = Coordinate normal to the surface,

N_α = Number of moles of species α per unit volume,

N = Number of moles of gas mixture per unit volume $= \sum_\alpha N_\alpha$,

P = Hydrostatic pressure,

r = Local cylindrical body radius,

R = Non-dimensional local cylindrical body radius = r/L

R_0 = Universal gas constant = $1.987 \frac{\text{cal}}{\text{GM-mole } ^\circ\text{K}}$

Re_1 = Reynolds number based on the local properties at the outer edge of the boundary layer = $\frac{\rho_1 u_1 L}{\mu_1}$,

s = Coordinate along the surface,

t = Time,

T = Absolute temperature,

u = s-component of the mass average velocity of the gas mixture,

v = n-component of the mass average velocity of the gas mixture,

V_α = n-component of the average diffusion velocity of species α,

W_α = Mass rate of formation of species α per unit volume due to chemical reactions, defined by equations (XC-22) through (XV-26),

X_α = Mole fraction of species $\alpha = \frac{N_\alpha}{N}$,

Y_α = Mass fraction of species $\alpha = \frac{\rho_\alpha}{\rho}$,

γ_α = Ratio of psecific heats for species $\alpha = C_{p\alpha}/C_{v\alpha}$,

γ = Ratio of average specific heats of the gas mixture $= \bar{C}_p/\bar{C}_v$,

δ = Boundary layer thickness in the (s–n) plane,

ϵ = Exponent of the functions r and R; unity for axisymmetric bodies and zero for two-dimensional bodies,

η = Transformed variable, defined by equation (XV-28),

λ_β = Thermal conductivity of species , defined by equation (XV-11),

λ = Thermal conductivity of the gas mixture, defined by equation (XV-16),

μ_α = Coefficient of viscosity of species α,

μ = Coefficient of viscosity of the gas mixture, defined by equation (XV-14),

ξ = Transformed variable, defined by equation (XV-29),

ρ_a = Mass density of species $a = N_a M_a$,

ρ = Mass density of the gas mixture = $N\bar{M}$

Subscripts

1 = Value at the outer edge of the boundary layer,

∞ = Value at infinity,

a = Species subscript for N_2,

b = Species subscript for N ,

c = Species subscript for O_2,

d = Species subscript for O ,

e = Species subscript for NO ,

S = Stagnation value,

w = Value at the body surface,

α,β,γ = Generalized subscripts referring to species a, b, c, d, and e.

C. INTRODUCTION

The flow of dissociating gases has been the subject of considerable research in recent years. Detailed knowledge of the flow field around bodies is of great importance from the point of view of hypersonic vehicle design, communication, and detection.

The qualitative phenomena of "real" gas flows is rather well understood for temperatures below 8000 °K and flow regimes where the continuum assumption is applicable. However, quantitative analyses are confined to various simplified models. Examples of these models are: idealized gas composition, limiting cases of infinitely slow or infinitely fast reaction rates, "global" reaction rates, small perturbations from either equilibrium or frozen flow, simplified thermodynamics and transport properties, and simplified flow fields. In this connections, the work of Rosner (Ref. XV-1) provides an excellent review of the status up to 1958 of the general theories of a viscous dissociating gas. A more detailed discussion of the boundary layer theories for the limiting cases of "frozen" and

equilibrium reaction rates has been presented by Hayes and Probstein (Ref. XV-2). On the other hand, a good indication of the present state of knowledge of the inviscid flow problem involving dissociative reactions is given by the recent works of Li (Ref. XV-3), Bloom and Steiger (Ref. XV-4), and Clarke (Ref. XV-5).

In recent months more work concerning simple shear and boundary layer flows has appeared in the literature. Lighthill (Ref. XV-6) has published a study on the quasiequilibrium theory of dissociating gases, including the effects of radiative heat transfer. The paper presents a lucid account of the basic equations and of the physical mechanism involved. Clarke (Ref. XV-7) has studied Couette flow of an "ideal" dissociating gas" and has examined in detail the effects of the limiting, very fast and very slow, reaction rates in the gas phase, including the influence of wall catalysis on the energy transfer. He has, moreover, obtained a parameter which defines the regime of validity of the "frozed" and "equilibrium' flow assumptions for a specified reaction rate constant. Chung (Ref. XV-8) has presented an approximate analysis of the Couette and flat plate laminar boundary layer flow with fluid injection and oxygen dissociation. Chung and Anderson, (Ref. XV-9) have examined the non-equilibrium laminar boundary layer flow around blunt bodies with non-catalytic surfaces, for air considered as a mixture of molecules, oxygen atoms and nitrogen atoms. The analysis has been carried out by means of an integral method and is subject to several restrictive assumptions.

The laminar boundary layer flow of dissociated air in chemical non-equilibrium is studied at the stagnation point. The aim is to obtain high order approximate solutions to a generalized model of the non-equilibrium boundary layer which will permit more exact determination of the boundary layer characteristics* (including concentration, velocity, and temperature profiles), and also serve to check results obtained by simpler, cruder methods. The main emphasis of this study will be on dissociation non-equilibrium; related phenomena, such as vibration-dissociation coupling, ionization, etc. will be neglected. Radiative heat transfer** and viscous-inviscid interaction will also be neglected at this time.

In particular, the following model is adopted: the air is treated as a mixture of five components (O, O_2, N, N_2, NO) with the molecular internal degrees of freedom in equilibrium with the translational mode. The best presently available reaction rates for the pertinent gas phase reactions are employed. A new set of transport and thermodynamic properties is utilized. The analysis is restricted to temperatures below 8000 °K.

*For example, the heat transfer to a non-catalytic wall is, at present, only known within a factor of 2.

**The radiative heat transfer becomes of importance at very high speed and low altitudes. An estimate of this effect can be obtained from reference XV-10.

In order to understand the precise nature and limitations of the present approach to the problem of chemical non-equilibrium, it may be instructive to briefly discuss non-equilibrium effects in general.

When a collection of molecules experiences a rapid increase in energy, the statistical equilibrium between the various degrees of freedom of the gas molecules is temporarily destroyed. The "relaxation" process of these molecules to an equilibrium state at the higher energy level can be considered to follow the following idealized sequence of events. First, the translational degrees of freedom will arrive at equilibrium within only a few collisions, (e.g. Jeans Ref. XV-11) and molecular rotation will approach equilibrium with the translational mode in the order of 10 collisions.* Disregarding electronic excitation, the last step in equilibrating the molecular degrees of freedom is the transfer of energy to the vibrational mode. The relaxation time for this mode is usually the longest; requiring, in some cases, on the order of 10^4 collisions at high temperatures.**

The final step is, of course, the dissociation and subsequent ionization of the molecule or atom. Even at relatively high temperatures an impact which can supply the requisite dissociation energy is relatively rare; implying a large value for the ratio of dissociative to vibrational relaxation times. Under such conditions it can be assumed, as it is here, that local thermal equilibrium is maintained among the various molecular degrees of freedom during "chemical" relaxation.***

D. BASIC EQUATIONS

1. Laminar Boundary Layer Equations

Considering the steady flow over two-dimensional or axisymmetric bodies, the general governing equations for the continuum flow of a chemically reacting multicomponent gas mixture (Ref. XV-16-18) can be simplified to the following expressions by employing the boundary layer approximations.

a. Conservation of Mass

$$\frac{\partial(\rho u r^{\epsilon})}{\partial s} + \frac{\partial(\rho v r^{\epsilon})}{\partial n} = 0 \quad , \qquad \text{(XV-1)}$$

*Experimental values for the average number of collisions required for rotational relaxation, in the vicinity of 300°K, varies from 3.6 to 20 for N_2 and 3 to 40 for O_2, (Ref. XV-12).

**Both experiment (Ref. XV-13) and (Ref. XV-14) demonstrate that at 3000°K the average number of collisions required to de-excite the first vibrational level, in a pure gas, is of the order of 10^3 for the O_2 molecule and 10^4 for the N_2 molecule.

***It should be noted that at very high temperatures vibration and dissociation often become inseparable events. For example, the vibrational and dissociative relaxation times for oxygen become comparable at temperatures approaching 8000°K; resulting in a decrease by a factor of 2 in the dissociation rate (Ref. XV-15).

where

$$\epsilon = \begin{cases} 1 \text{ for an axisymmetric body} \\ 0 \text{ for a two-dimensional body.} \end{cases}$$

b. Conservation of Chemical Species

$$\rho u \frac{\partial Y_a}{\partial s} + \rho v \frac{\partial Y_a}{\partial n} = -\frac{\partial}{\partial n}(\rho Y_a \mathcal{V}_a) + \dot{W}_a \quad , \tag{XV-2}$$

where

$$\sum_{\beta=a}^{e} Y_\beta = 1 \tag{XV-3}$$

and

$$Y_a \mathcal{V}_a = \sum_{\beta=a}^{e} D_{a\beta}\left[\left(\frac{M_a}{\bar{M}}\right)\frac{\partial Y_\beta}{\partial n} - Y_\beta \frac{\partial}{\partial n}\left(\frac{M_a}{\bar{M}}\right)\right] - \frac{D_a^T}{\rho T}\frac{\partial T}{\partial n} \quad . \tag{XV-4}$$

c. Conservation of Momentum

$$\rho u \frac{\partial u}{\partial s} + \rho v \frac{\partial u}{\partial n} = -\frac{\partial P}{\partial s} + \frac{\partial}{\partial n}\left(\mu \frac{\partial u}{\partial n}\right) \quad , \tag{XV-5}$$

$$\frac{\partial P}{\partial n} = 0 \quad . \tag{XV-6}$$

d. Conservation of Energy

$$\rho u \frac{\partial H}{\partial s} + \rho v \frac{\partial H}{\partial n} = u \frac{\partial P}{\partial s} + \mu\left(\frac{\partial u}{\partial n}\right)^2 + \frac{\partial}{\partial n}\left(\lambda \frac{\partial T}{\partial n}\right) - \frac{\partial}{\partial n}\left(\sum_{\beta=a}^{e} \rho Y_\beta \mathcal{V}_\beta H_\beta\right) . \tag{XV-7}$$

e. Thermal Equations of State

The gas mixture is postulated to be sufficiently dilute to allow each chemical species to be treated as an ideal gas. That is:

$$P_\beta = \rho_\beta \frac{R_0}{M_\beta} T \quad , \tag{XV-8}$$

and for the mixture:

$$P = \rho \frac{R_0}{\bar{M}} T \quad , \tag{XV-9}$$

where

$$\bar{M} = \sum_{a=a}^{e} X_a M_a = \left(\sum_{a=a}^{e} Y_a / M_a \right)^{-1} \quad . \tag{XV-10}$$

2. Transport Properties of High-Temperature Air*

Calculations of the transport properties of high temperature air have been performed utilizing the kinetic theory of gases in the approximation originated by Chapman and Enskog (Ref. XV-16). Intermolecular force potentials for the pair interactions among the species N_2, O_2, N and O, which became available only recently (Ref. XV-19-23), were fitted by employing four basic types of functions: (1) exponential repulsion, (2) rigid sphere, (3) attractive power law, and (4) modified Buckingham Exp. -6 potential. The requisite collision integrals were than calculated by employing tables and formulas existing in the literature (Ref. 16, 24-26).

The complete multicomponent formalism, was employed for computing the behavior of the mixture of N_2, O_2, NO, N, and O, but a number of simplifying approximations were used in calculating properties of the pure species and the binary systems.

Specifically:

a. The viscosity-temperature relations were considered only for pure N_2 and pure N. The viscosities of pure O_2 and NO were assumed to be equal to that for N_2, and the viscosity of pure O was assumed to be equal to that for N. That is:

* The transport property calculations were performed by Dr. W. L. Bade, to whom the authors are greatly indebted.

$$\mu_a = \mu_c = \mu_e \quad ,$$

and

$$\mu_b = \mu_d \quad .$$

b. The (chemically frozen) thermal conductivity for each pure species was computed from the corresponding viscosity using the Euken relation:

$$\lambda_a = 1/4\ (9\gamma_a - 5)\ C_{va}\ \mu_a \quad , \qquad \text{(XV-11)}$$

with the values of γ_a and C_{va} given by the thermodynamic calculations.

c. The binary diffusion coefficients were calculated only for the systems N_2 - O_2, N - O, and N - N_2. The diffusion coefficients for N_2 - NO and O_2 - NO were estimated from that for N_2 O_2 by assuming the interaction potentials to be the same in all three cases, using a simple reduced molecular weight correction. That is:

$$\mathcal{D}_{a\beta} = \mathcal{D}_{ac} \left(\frac{M_{ac}}{M_{a\beta}} \right)^{1/2} \quad , \qquad \text{(XV-12)}$$

for the molecular - molecule systems. Diffusion coefficients for O - N_2, O - O_2, O - NO, N - O_2 and N - NO, the atom-molecule systems, were estimated from that for N - N_2 in the following similar manner:

$$\mathcal{D}_{a\beta} = \mathcal{D}_{ab} \left(\frac{M_{ab}}{M_{a\beta}} \right)^{1/2} \quad . \qquad \text{(XV-13)}$$

The computations are summarized in Table XV-1 for temperatures up to 8000 °K only; since, at higher temperatures, ionization effects modify the transport properties to an appreciable extent (Ref. XV-27).

The viscosity of the five-component mixture was calculated using Wilke's (Ref. XV-28) approximate formula:

$$\mu = \sum_{a=a}^{e} \mu_a \left[1 + \sum_{\substack{\beta=a \\ \beta \neq a}}^{e} G_{a\beta} \frac{X_\beta}{X_a} \right]^{-1} \quad , \qquad \text{(XV-14)}$$

TABLE XV-1

SUMMARY OF RESULTS

T	$\mu_{N_2} \times 10^4$*	$\mu_N \times 10^4$	pD_{N-N_2}	$pD_{N_2-O_2}$	pD_{N-O}	$(\alpha_T)_{N-N_2}$		
°K	poise	poise	atm cm^2/sec	atm cm^2/sec	atm cm^2/sec	$X_N = 0$	$X_N = 1/2$	$X_N = 1$
500	2.6			0.50		0.11	0.15	0.21
1000	4.0	(4.6)	(2.4)	1.56	(3.3)	0.11	1.14	0.20
1500	5.2	(6.2)	(4.9)	3.1	(6.7)	0.10	0.13	0.19
2000	6.3	(7.7)	(8.1)	4.9	(11)	0.09	0.13	0.18
3000	8.5	10.5	16.5	9.6	23	0.09	0.12	0.17
4000	10.7	13	28	15.5	38	0.08	0.11	0.16
5000	13	16	41	22	57	0.08	0.10	0.15
6000	15	18	57	30	79	0.07	0.10	0.14
7000	17	20	75	39	100	0.07	0.09	0.13
8000	19	22	95	49	130	0.06	0.09	0.13

* Viscosity values for N_2 from Amdur and Mason.[14]

** Values in parentheses are extrapolated, or depend significantly upon portions of the interaction potential which are not accurately known.

where

$$G_{a\beta} = \frac{1}{2\sqrt{2}} \left(1 + \frac{M_a}{M_\beta}\right)^{-1/2} \left[1 + \left(\frac{\mu_a}{\mu_\beta}\right)^{1/2} \left(\frac{M_\beta}{M_a}\right)^{1/4}\right]^2 \quad . \qquad \text{(XV-15)}$$

The thermal conductivity of the mixture was calculated using a similar formula, (Ref. XV-29);

$$\lambda = \sum_{a=a}^{e} \lambda_a \left[1 + \sum_{\substack{\beta=a \\ \beta \neq a}}^{e} G_{a\beta} \frac{X_\beta}{X_a}\right]^{-1} \quad . \qquad \text{(XV-16)}$$

The multicomponent diffusion coefficients, $D_{a\beta}$ were computed using Equation (8. 2-49) or Hirschfelder, Curtiss, and Bird (Ref. XV-16);

$$D_{a\beta} = \frac{1}{M_\beta} \left(\sum_{\gamma=a}^{e} X_\gamma M_\gamma\right) \frac{K^{\beta a} - K^{aa}}{|K|} \quad , \qquad \text{(XV-17)}$$

where

$$K_{aa} = 0 \quad ,$$

$$K_{a\beta} = \frac{X_a}{\mathcal{D}_{a\beta}} + \frac{M_\beta}{M_a} \sum_{\substack{\gamma=a \\ \gamma \neq a}}^{e} \frac{X_\gamma}{\mathcal{D}_{a\gamma}} \quad (a \neq \beta) \quad , \qquad \text{(XV-18)}$$

and $K^{\beta a}$ is the minor of the element $K_{a\beta}$ in the determinant $|K|$.

The coefficient of thermal diffusion was considered for the air mixture only (i.e., without injection and, thus, for the five component air mixture) on the basis of a "pseudo-binary" system. That is, for the atoms O or N, (i.e., $a = b, d$);

$$D_a^T = \left(\frac{Y_a}{Y_b + Y_d}\right) \rho \, (Y_b + Y_d) \, \mathcal{D}_{ab} \, (\alpha_T)_{atom} \, (Y_a + Y_c + Y_e) \quad , \qquad \text{(XV-19)}$$

and for the molecules O_2, N_2 or NO; (i.e., $a = a, c, e$);

$$D_a^T = -\left(\frac{Y_a}{Y_a + Y_c + Y_e}\right) \rho \, (Y_a + Y_c + Y_e) \mathcal{D}_{ab} \, (\alpha_T)_{atom} \, (Y_b + Y_d) \quad . \qquad \text{(XV-20)}$$

These formulas being a slight generalization of the true binary relation;

$$D_1^T = \rho \, Y_1 Y_2 \mathcal{D}_{12} \, (\alpha_T)_1 = - D_2^T \quad .$$

The thermal diffusion factor α_T was computed using the formula;

$$(\alpha_T)_{atoms} = (6C^*_{ab} - 5) \frac{X_{atoms} \delta_b - X_{molec.} \delta_a}{X^2_{atoms} Q_b + X_{atoms} X_{molec.} Q_{ab} + X^2_{molec.} Q_a} \quad , \qquad \text{(XV-21)}$$

where the quantities C^*_{ab}, δ_a, δ_b, Q_a, Q_b, and Q_{ab} are computed on the basis of an N-N_2 system only. The thermal diffusion factor for various N-N_2 mixtures is given in table XV-1.

3. Chemical Reaction Rates

The five significant gas phase reactions for high temperature air are taken to be the following (Refs. XV-30, 31):

I $\quad O_2 + (X) + 5.1$ e.v. $\rightleftharpoons O + O + (X)$

II $\quad N_2 + (X) + 9.8$ e.v. $\rightleftharpoons N + N + (X)$

III $\quad NO + (X) + 6.5$ e.v. $\rightleftharpoons N + O + (X)$

IV $\quad NO + O + 1.4$ e.v. $\rightleftharpoons O_a + N$

V $\quad N_a + O + 3.3$ e.v. $\rightleftharpoons NO + N$

It is assumed that the net rate of production of each chemical species is dictated by the (phenomenological) Law of Mass Action, with the rate constants being determined by experiment. The rate constants employed here are those given by Wray et al (Ref. XV-31) (see table XV-2). Thus, the species "source" equations may be written as follows:

TABLE XV-2

REACTION RATE CONSTANTS

Reaction	Third Body (X)	Exothermic Rate Constants	Units
I	N_2, N, NO	$k_a^I = k_b^I = k_e^I = 2/3 \times 10^{14} \times (4500/T)^{1.5}$	$\frac{cm^6}{mole^2\ sec}$
	O_2	$k_c^I = 2 \times 10^{14} \times (4500/T)^{1.5}$	
	O	$k_d^I = 1 \times 10^{15} \times (4500/T)^{1.5}$	
II	N_2	$k_a^{II} = 1/2 \times 10^{15} \times (4500/T)^{1.5}$	$\frac{cm^6}{mole^2\ sec}$
	N	$k_b^{II} = 5/2 \times 10^{15} \times (4500/T)^{1.5}$	
	O_2, O, NO	$k_c^{II} = k_d^{II} = k_e^{II} = 1/6 \times 10^{15} \times (4500/T)^{1.5}$	
III	N_2, N, O_2, O, NO	$k^{III} = 2 \times 10^{15} \times (4500/T)^{1.5}$	$\frac{cm^6}{mole^2\ sec}$
IV	N_2, N, O_2, O, NO	$k^{IV} = 1 \times 10^{12}\ T^{0.5}\ \exp(-3120/T)$	$\frac{cm^3}{mole\ sec}$
V	N_2, N, O_2, O, NO	$k^V = 1.3 \times 10^{13}$	$\frac{cm^3}{mole\ sec}$

$$\frac{W_c}{M_c} = \left(\frac{\partial N_c}{\partial t}\right)_{\rho,T} = \left(\sum_a {}^{I}k_a N_a\right)\left(N_d^2 - N_c\, {}^{I}K_N\right) - {}^{IV}k\left(N_c N_b - N_e N_d\, {}^{IV}K_N\right), \quad \text{(XV-22)}$$

$$\frac{W_a}{M_a} = \left(\frac{\partial N_a}{\partial t}\right)_{\rho,T} = \left(\sum_a {}^{II}k_a N_a\right)\left(N_b^2 - N_a\, {}^{II}K_N\right) + {}^{IV}k\left(N_e N_b - N_a N_d\, {}^{V}K_N\right), \quad \text{(XV-23)}$$

$$\frac{W_e}{M_e} = \left(\frac{\partial N_e}{\partial t}\right)_{\rho,T} = \left(\sum_a {}^{III}k_a N_a\right)\left(N_b N_d - N_e\, {}^{III}K_N\right) + {}^{IV}k\left(N_c N_b - N_e N_d\, {}^{IV}K_N\right) \quad \text{(XV-24)}$$

$$+ {}^{V}k\left(N_e N_b - N_c N_d\, {}^{V}K_N\right),$$

and, from conservation of atomic species,

$$\frac{W_b}{M_b} = \left(\frac{\partial N_b}{\partial t}\right)_{\rho,T} = -2\left(\frac{\partial N_a}{\partial t}\right)_{\rho,T} - \left(\frac{\partial N_c}{\partial t}\right)_{\rho,T}, \quad \text{(XV-25)}$$

$$\frac{W_d}{M_d} = \left(\frac{\partial N_d}{\partial t}\right)_{\rho,T} = -2\left(\frac{\partial N_c}{\partial t}\right)_{\rho,T} - \left(\frac{\partial N_e}{\partial t}\right)_{\rho,T} \quad \text{(XV-26)}$$

where the equilibrium constants ${}^{I\ldots V}K_N$ are the following known functions of temperature;

$${}^{I}K_N = \left(\frac{N_d^2}{N_c}\right)_{\text{equil.}} \quad {}^{II}K_N = \left(\frac{N_b^2}{N_c}\right)_{\text{equil.}} \quad {}^{III}K_N = \left(\frac{N_b N_d}{N_e}\right)_{\text{equil.}}$$

$${}^{IV}K_N = \frac{{}^{III}K_N}{{}^{I}K_N} \qquad {}^{V}K_N = \frac{{}^{II}K_N}{{}^{III}K_N}. \quad \text{(XV-27)}$$

Two limiting cases of surface activity will be treated; non-catalytic and fully-catalytic. The latter corresponds to allowing only a relatively small number of atoms (for computational purposes this number is taken to be identically zero) to survive after impinging on the wall; the rest having recombined.

D. ANALYSIS

Introducing the following transformation proposed by Levy (Ref. XV-32) as modified by Lee's (Ref. XV-33),

$$\eta = \frac{u_1}{(2\xi)^{1/2}} \int_0^n r^\epsilon \rho \, dn \quad , \tag{XV-28}$$

$$\xi = \int_0^s \rho_1 \mu_1 u_1 r^{2\epsilon} \, ds \quad , \tag{XV-29}$$

Equations (XV-2), (XV-4), (XV-5), and (XV-7) transform, when specialized to the stagnation point, to the set of ordinary non-linear differential equations given below;

1. Species Continuity Equation

$$f \frac{dY_\alpha}{d\eta} + \frac{W_\alpha}{\rho(\epsilon+1)\left(\frac{du_1}{ds}\right)_S}$$

$$= -\frac{d}{d\eta}\left\{\left(\frac{\rho}{\rho_1}\right)^2 \sum_\beta \frac{D_{\alpha\beta}}{\nu_1}\left[\left(\sum_\gamma Y_\gamma \frac{M_\alpha}{M_\gamma}\right)\frac{dY_\beta}{d\eta} - Y_\beta\left(\sum_\gamma \frac{M_\alpha}{M_\gamma}\frac{dY_\gamma}{d\eta}\right)\right] - \frac{\rho}{\rho_1}\frac{D_\alpha^T}{\rho_1\nu_1}\frac{1}{\theta}\frac{d\theta}{d\eta}\right\} . \tag{XV-30}$$

2. Momentum Equation

$$f\frac{d^2f}{d\eta^2}+\frac{d}{d\eta}\left(\frac{\rho}{\rho_1}\frac{\mu}{\mu_1}\frac{d^2f}{d\eta^2}\right)+\frac{1}{\epsilon+1}\left[\left(\frac{\rho}{\rho_1}\right)^{-1}-\left(\frac{df}{d\eta}\right)^2\right]=0 \quad . \qquad \text{(XV-31)}$$

3. Energy Equation

$$f\frac{dg}{d\eta}=\frac{d}{d\eta}\left[\sum_\alpha\frac{H_\alpha}{H_{S1}}\left\{\left(\frac{\rho}{\rho_1}\right)^2\sum_\beta\frac{D_{\alpha\beta}}{\nu_1}\left[\left(\sum_\gamma Y_\gamma\frac{M_\alpha}{M_\gamma}\right)\frac{dY_\beta}{d\eta}-Y_\beta\left(\sum_\gamma\frac{M_\alpha}{M_\gamma}\frac{dY_\gamma}{d\eta}\right)\right]\right.\right.$$

$$\left.\left.-\frac{\rho}{\rho_1}\frac{D_\alpha^T}{\rho_1\nu_1}\frac{1}{\theta}\frac{d\theta}{d\eta}\right\}\right]-\frac{T_1\lambda_1}{H_{S1}\mu_1}\frac{d}{d\eta}\left[\frac{\rho}{\rho_1}\frac{\lambda}{\lambda_1}\frac{d\theta}{d\eta}\right] \quad ,$$

where, by definition;

$$\theta\equiv T/T_1 \quad , \quad g\equiv\frac{H_S}{H_{S1}} \quad ,$$

$$f=\int_0^\eta\frac{u}{u_1}\,d\eta \quad . \qquad \text{(XV-33)}$$

Finally, the following variables are introduced;

$$\tau = \left(\frac{\rho}{\rho_1}\,\frac{\mu}{\mu_1}\right)\,\frac{d^2f}{d\eta^2} = N_1\,\frac{d^2f}{d\eta^2} \quad ,$$

$$\sigma = \left(\frac{\rho}{\rho_1}\,\frac{\lambda}{\lambda_1}\right)\,\frac{d\theta}{d\eta} = N_2\,\frac{d\theta}{d\eta} \quad ,$$

$$\zeta = \frac{df}{d\eta} \quad , \quad \Gamma_a = \frac{dY_a}{d\eta} \quad , \tag{XV-34}$$

and we set, at the stagnation point;

$$\frac{dg}{d\eta} = \frac{\bar{C}_{p1}\,T_1}{H_{S1}}\left(\frac{\bar{C}_p}{\bar{C}_{p1}}\right)\,\frac{d\theta}{d\eta} + \sum_a \frac{H_a}{H_{S1}}\,\Gamma_a \tag{XV-35}$$

Equations (XV-30), (XV-31), and XV-32) can now be resolved to a set of first order linear differential equations in the variable τ, σ and Γ_a. That is, after some manipulation;

4. Species Continuity Equation

$$\left[\frac{2\sigma}{N_2\theta}\left(\frac{\rho}{\rho_1}\right)^2 + 2\theta\left(\frac{\rho}{\rho_1}\right)^3\left(\sum_a \frac{\bar{M}_1}{M_a}\,\Gamma_a\right)\right]\sum_\gamma \frac{D_{\beta\gamma}}{\nu_1}\left(\frac{M_\beta}{\bar{M}_1}\right)$$

$$\times \left[\frac{\Gamma_\gamma}{\theta}\left(\frac{\rho}{\rho_1}\right)^{-1} - Y_\gamma\left(\sum_a \frac{\bar{M}_1}{M_a}\,\Gamma_a\right)\right]$$

$$-\left(\frac{\rho}{\rho_1}\right)^2 \sum_\gamma \frac{D_{\beta\gamma}}{\nu_1}\left(\frac{M_\beta}{\bar{M}_1}\right)\left[\frac{1}{\theta}\left(\frac{\rho}{\rho_1}\right)^{-1}\,\frac{d\Gamma_\gamma}{d\eta} - Y_\gamma\left(\sum_a \frac{\bar{M}_1}{M_a}\,\frac{d\Gamma_a}{d\eta}\right)\right]$$

$$-\left(\frac{\rho}{\rho_1}\right)^2 \sum \frac{dD_{\beta\gamma}}{d\eta} \frac{1}{\nu_1}\left(\frac{M_\beta}{\bar{M}_1}\right)\left[\frac{\Gamma_\gamma}{\theta}\left(\frac{\rho}{\rho_1}\right)^{-1} - Y_\gamma\left(\sum_\alpha \frac{\bar{M}_1}{M_\alpha}\,\Gamma_\alpha\right)\right]$$

$$-\frac{D_\beta^T}{\rho_1\nu_1}\left[\frac{2\sigma^2}{N_2^2\theta^2}\left(\frac{\rho}{\rho_1}\right) + \frac{\sigma}{N_2}\left(\frac{\rho}{\rho_1}\right)^2\left(\sum_\alpha \frac{\bar{M}_1}{M_\alpha}\,\Gamma_\alpha\right) - \left(\frac{\rho}{\rho_1}\right)\left(\frac{1}{\theta N_2}\frac{d\sigma}{d\eta} - \frac{\sigma}{\theta N_2^2}\frac{dN_2}{d\eta}\right)\right]$$

$$+\frac{\sigma}{N_2\theta}\left(\frac{\rho}{\rho_1}\right)\frac{1}{\rho_1\nu_1}\frac{dD_\beta^T}{d\eta} + f\,\Gamma_\beta + W_\beta = 0 \quad , \qquad \text{(XV-36)}$$

where

$$W_\beta \equiv \frac{\mathbb{W}_\beta}{\rho(\epsilon+1)\left(\frac{du_1}{ds}\right)_S} \qquad \text{(XV-37)}$$

5. Momentum Equation

$$\frac{d\tau}{d\eta} + \frac{f}{N_1}\,\tau = -\frac{1}{\epsilon+1}\left[\left(\frac{\rho}{\rho_1}\right)^{-1} - \zeta^2\right] \qquad \text{(XV-38)}$$

6. Energy Equation

$$f\left[\left(\frac{\bar{C}_{p1}T_1}{H_{S1}}\right)\frac{\bar{C}_p}{\bar{C}_{p1}}\frac{\sigma}{N_2}\right] + \left(\frac{T_1\lambda_1}{H_{S1}\mu_1}\right)\frac{d\sigma}{d\eta}$$

$$= \sum_{a} \left[\frac{H_a}{H_{S1}} \left(W_a \right) + \left(\frac{\bar{C}_{p1} T_1}{H_{S1}} \right) \left(\frac{\rho}{\rho_1} \right)^2 \frac{C_{pa}}{\bar{C}_{p1}} \frac{\sigma}{N_2} \right. \quad \times$$

$$\left. \sum_{\beta} \left\{ \frac{D_{a\beta}}{\nu_1} \left(\frac{M_a}{\bar{M}_1} \right) \left[\frac{\left(\frac{\rho}{\rho_1} \right)^{-1}}{\theta} \Gamma_\beta - Y_\beta \left(\sum_{\gamma} \frac{\bar{M}_1}{M_\gamma} \Gamma_\gamma \right) \right] - \left(\frac{\rho}{\rho_1} \right)^{-1} \frac{D_a^T}{\rho_1 \nu_1} \left(\frac{\sigma}{\theta N_2} \right) \right\} \right] \quad \text{(XV-39)}$$

These equations have been programmed on the Philco 2000 automatic technical computer. Some preliminary results are presented in figure XV-1. The analytical and numerical techniques which were employed and final results will be described in a future technical report.

REFERENCES

XV-1. Rosner, D.E., Recent Advances in Convective Heat Transfer with Dissociation and Atom Recombination, Jet Propulsion, 28, No. 7, (July 1958) p. 445-451.

XV-2. Hayes, W.D. and R.F. Probstein, Hypersonic Flow Theory, Academic Press, New York (1959) p. 284-316.

XV-3. Li, T.Y., Nonequilibrium Flow in Gas Dynamics, American Rocket Society Preprint No. 852-59 (June 1959).

XV-4. Bloom, M.H. and M.H. Steiger, Inviscid Flow with Nonequilibrium Molecular Dissociation for Pressure Distributions Encountered in Hypersonic Flight, Journal of the Aero/Space Sciences, 27, No. 11, (November 1960) p. 82-1835.

XV-5. Clarke, J.F., The Linearized Flow of a Dissociating Gas, Journal of Fluid Mechanics, 7, Part 4 (April 1960) p. 577-595.

XV-6. Lighthill, M.J., Dynamics of a Dissociating Gas, Part 2. Quasi-Equilibrium Transfer Theory, Journal of Fluid Mechanics, 8, Part 2, (June 1969) p. 161-182.

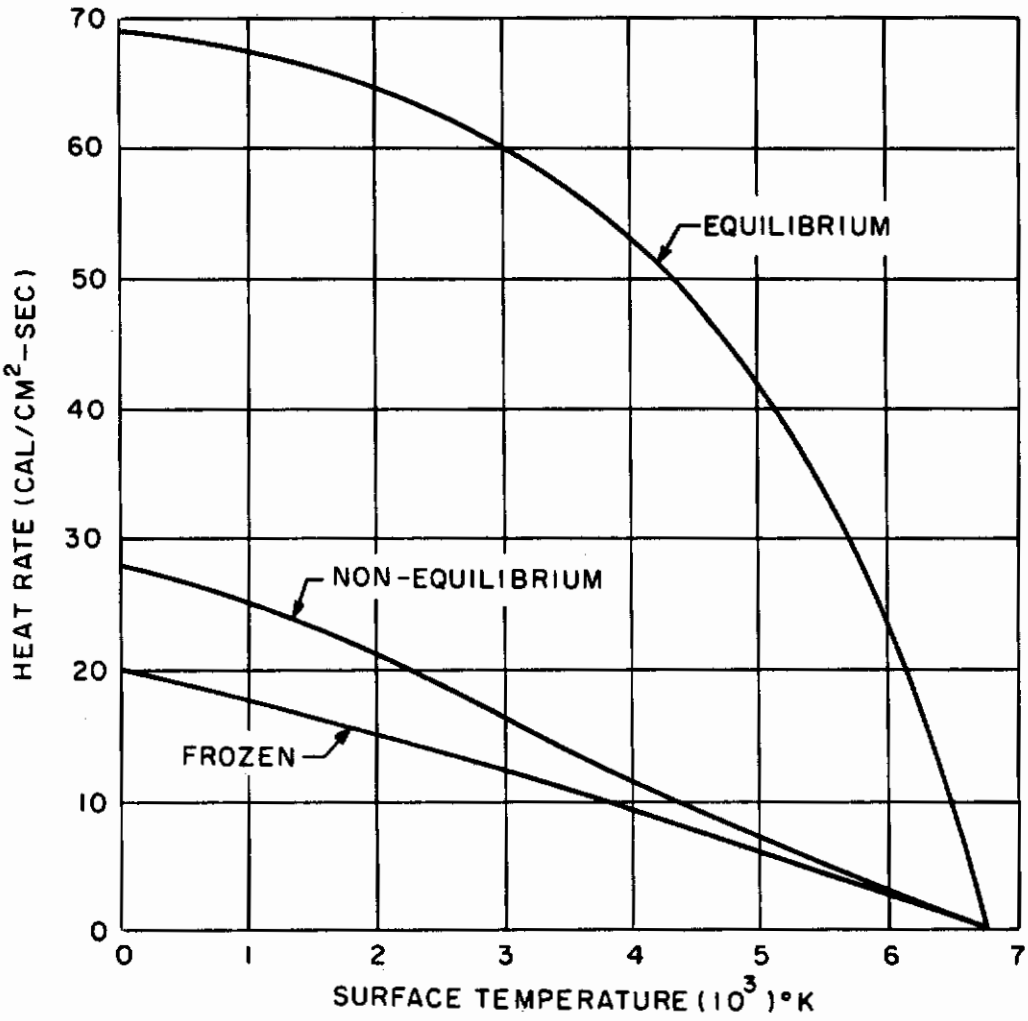

Figure XV-1 STAGNATION POINT HEAT TRANSFER, M = 25, ALTITUDE = 2×10^{-5} FEET

7-7. Clarke, J.F., Energy Transfer Through a Dissociated Diatomic Gas in Couette Flow, Journal of Fluid Mechanics, 4, Part 5, (September 1958) p. 441-465.

7-8. Chung, P.M., A Simplified Study on the Nonequilibrium Couette and Boundary-Layer Flows with Air Injection, NASA Technical Note D-306, (February 1960).

7-9. Chung, P.M. and A.D. Anderson, Heat Transfer Around Blunt Bodies with Nonequilibrium Boundary Layers, Proceedings of the 1960 Heat Transfer and Fluid Mechanics Institute, Stanford University Press (June 1960) p. 150-163.

-10. Kivel, B., Radiation From Hot Air and Stagnation Heating, Avco Everett Research Laboratory Research Report 79 (October 1959).

-11. Jeans, J.H., An Introduction to the Kinetic Theory of Gases, Cambridge University Press (1952) p. 233-239.

-12. Herzfeld, K.F. and T.A. Litovitz, Absorption and Dispersion of Ultrasonic Waves, Academic Press, New York (1959) p. 239.

-13. Blackman, V., Vibrational Relaxation in Oxygen and Nitrogen, Journal of Fluid Mechanics, 1, Part 1, (May 1956) p. 61-85.

-14. Schwartz, R.N. and K.F. Herzfeld, Vibrational Relaxation Times in Gases (Three-Dimensional Treatment), The Journal of Chemical Physics, 22, No. 5 (May 1954) p. 767-773.

-15. Camac, M. and A. Vaughan, Oxygen Vibration and Dissociation Rates in Oxygen-Argon Mixtures, Avco Everett Research Laboratory Research Report 83, (December 1959).

16. Hirschfelder, J.O., C.F. Curtiss, and R.B. Bird, Molecular Theory of Gases and Liquids, Wiley, New York (1954).

17. Penner, S.S., Chemistry Problems in Jet Propulsion, Pergamon Press, New York (1957) p. 234-251.

18. Von Karman, T., Fundamental Equations in Aerothermochemistry, Selected Combustion Problems, II, 2nd AGARD Combustion Colloquim, Liege, Belgium, Butterworths Scientific Publications, London (1956) p. 167-184.

19. Vanderslice, J.T., E.A. Mason and E.R. Lippincott, Interactions Between Ground State Nitrogen Atoms and Molecules. The N-N, N-N_2, and N_2-N_2 Interactions, The Journal of Chemical Physics, 30, No. 1, (January 1959) p. 129-136.

XV-20. Vanderslice, J.T., E.A. Mason, and W.G. Maisch, Interactions Between Oxygen and Nitrogen: O-N, O-N_2, and O_2-N_2, The Journal of Chemical Physics, 31, No. 3 (March 1959) p. 738-748.

XV-21. Vanderslice, J.T., E.A. Mason, and W.G. Maisch, Interactions Between Ground State Oxygen Atoms and Molecules: O-O and O_2-O_2, The Journal of Chemical Physics, 32, No. 2 (February 1960) p. 515-524.

XV-22. Vanderslice, J.T. and E.A. Mason, Quantum Mechanical Calculations of Short-Range Intermolecular Forces, Reviews of Modern Physics, 32, No. 2 (February 1960) p. 417-421.

XV-23. Vanderslice, J.T., E.A. Mason, W.G. Maisch, and E.R. Lippincott, Potential Curves for N_2, NO, and O_2, The Journal of Chemical Physics, 33, No. 2 (February 1960) p. 614-615.

XV-24. Monchick, L., Collision Integrals for the Exponential Repulsive Potential, Physics of Fluids, 2, No. 6, (November-December 1959) p. 695-700.

XV-25. Kihara, T., M.H. Taylor, and J.O. Hirschfelder, Transport Properties for Gases Assuming Inverse Power Intermolecular Potentials, Physics of Fluids, 3, No. 5 (September-October 1960) p. 715-720.

XV-26. Mason, E.A., Transport Properties of Gases Obeying a Modified Buckingham (Exp. - 6) Potential, The Journal of Chemical Physics, 22, No. 2, (February 1954) p. 169-186.

XV-27. Hansen, C.F., Approximations for the Thermodynamic and Transport Properties of High Temperature Air, NACA TN-4150 (March 1958).

XV-28. Wilke, C.R., A Viscosity Equation for Gas Mixtures, The Journal of Chemical Physics, 18, No. 4, (April 1959) p. 517-519.

XV-29. Mason, E.A. and S.C. Saxena, Approximate Formula for the Thermal Conductivity of Gas Mixtures, Physics of Fluids, 1, No. 5, (September-October 1958) p. 361-369.

XV-30. Davidson, W., Selected Reactions Involving Nitrogen and Oxygen, Avco-Everett Research Laboratory Report No. 32 (June 1958).

XV-31. Wray, K., J.D. Teare, B. Kivel, and P. Hammerling, Relaxation Processes and Reaction Rates Behind Shock Fronts in Air and Component Gases, Avco-Everett Research Laboratory Report No. 83 (December 1959).

XV-32. Levy, S., Effect of Large Temperature Changes (including Viscous Heating) upon Laminar Boundary Layers with Variable Free-Stream Velocity, Journal of the Aeronautical Sciences, 21, No. 7 (July 1954) p. 459-474.

XV-33. Lees, L., Laminar Heat Transfer Over Blunt-Nosed Bodies at Hypersonic Flight Speeds, Jet Propulsion, 26 No. 4 (April 1956) p. 259-269.